

5-20-2011

Numerical Modeling of River Diversions in the Lower Mississippi River

Joao Miguel Faisca Rodrigues Pereira
University of New Orleans

Follow this and additional works at: <https://scholarworks.uno.edu/td>

Recommended Citation

Pereira, Joao Miguel Faisca Rodrigues, "Numerical Modeling of River Diversions in the Lower Mississippi River" (2011). *University of New Orleans Theses and Dissertations*. 1309.
<https://scholarworks.uno.edu/td/1309>

This Dissertation is protected by copyright and/or related rights. It has been brought to you by ScholarWorks@UNO with permission from the rights-holder(s). You are free to use this Dissertation in any way that is permitted by the copyright and related rights legislation that applies to your use. For other uses you need to obtain permission from the rights-holder(s) directly, unless additional rights are indicated by a Creative Commons license in the record and/or on the work itself.

This Dissertation has been accepted for inclusion in University of New Orleans Theses and Dissertations by an authorized administrator of ScholarWorks@UNO. For more information, please contact scholarworks@uno.edu.

Numerical Modeling of River Diversions in the Lower Mississippi River

A Dissertation

Submitted to the Graduate Faculty of the
University of New Orleans
in partial fulfillment of the
requirements for the degree of

Doctor of Philosophy
in
Engineering and Applied Science

by

João Miguel Faísca Rodrigues Pereira

B.S. Technical University of Lisbon, Portugal, 2002
M.S. Technical University of Lisbon, Portugal, 2007

May 2011

© 2011, João Miguel Faísca Rodrigues Pereira

ACKNOWLEDGEMENTS

I would like to thank Dr. J. Alex McCorquodale for his guidance, advising and support during this study. Without Dr. McCorquodale's kindness, patience and wisdom this document would not have been possible. It was a great privilege to work under his supervision.

I would also like to thank the Lake Pontchartrain Basin Foundation and Dr. John Lopez. The Lake Pontchartrain Basin Foundation funded part of the research herein. Dr. John Lopez gave important technical assistance throughout this study.

I wish to thank the Science and Technology Fund (Louisiana Federal Support) for funding part of this research.

The FVCOM simulations were performed using computational resources (higher performance computing - HPC) provided by the Louisiana Optical Network Initiative (LONI).

Dr. Ehab Meselhe deserves special thanks. Dr. Meselhe is probably the main responsible for me coming to Louisiana. I also thank Dr. Meselhe for the semester I spent at the University of Louisiana at Lafayette working under his supervision and all the technical assistance throughout this Mississippi River study.

I would like to express my gratitude to Dr. Ioannis Georgiou for all the help and support throughout my research. His availability to spend numerous sessions transmitting to me some of his vast knowledge of the numerical models ECOMSED and FVCOM as well as pre-processing and post-processing tools is deeply appreciated.

I would also like to thank the rest of the committee members, Dr. Donald Barbé and Dr. Martin Guillot for their help and suggestions.

I would like to thank Dr. Changsheng Chen and the FVCOM group for allowing me to use their code throughout this study.

I wish to thank Dr. Forrest Holly for several reasons. First of all, for starting the chain of contacts that eventually led me to the University of New Orleans. I also thank Dr. Holly for having the kindness of allowing me to use CHARIMA in my dissertation research. Finally, I thank Dr. Holly for all of the help throughout the modeling process, the technical assistance, the availability to answer all possible questions, and the words of encouragement.

I would like to express my gratitude to Dr. Mead Allison for making available field data that was key to the execution of this research project.

Dr. Gabriel Retana deserves special thanks for the help with the FVCOM modeling and, most recently, the help given on the ECOMSED post-processing scripts.

Dr. João Rego deserves special thanks for sharing some his work and scripts that helped me during the FVCOM preliminary modeling and testing.

I wish to thank Ms. Mallory Davis for making available her modeling results for use in this study. Her M.Sc. Thesis results are the starting point of part of the research presented herein. I would also like to thank Mallory for her patience and constant availability to answer questions about her work.

I wish to thank my other coworkers at the University of New Orleans during this period: Ms. Rachel Roblin, Mr. Marc Ischen, Ms. Jenni Schindler and Mr. Jeevan Neupane. I also wish to thank Ms. Lynn Brien, Dr. Matthew Bethel, Dr. Sarah Fearnley, Ms. Nathallie Tejada, Ms. Diane Maygarden and Ms. Heather Gordon-Egger for their precious help with environmental sciences coursework.

I wish to thank all the good friends who helped and encouraged me along the way. In particular, I would like to thank Mr. Boone Larson and Mrs. Brenna Larson, Dr. Gustavo Ferreira, Mr. João Abecasis and Dr. Claes Eskilson for making it easier for me to adapt to a new country and a new reality.

I would like to thank my friends back home for their support along the way and for always finding time to email me. I would like to thank Dr. José Matos Silva in particular for all the encouragement and, for years ago, opening the door for me to enter the hydraulics and numerical modeling world.

Finally, I would like to thank my family for all the unconditional love and support. I thank my parents and my brother for helping me in all possible ways to achieve my goals and for always believing in me. I would like to thank my grandmother for all the love and for all the prayers.

TABLE OF CONTENTS

LIST OF FIGURES.....	viii
LIST OF TABLES	xxi
NOMENCLATURE.....	xxiii
ABSTRACT.....	xxx
1) INTRODUCTION.....	1
1.1 Background	1
1.2 Statement of the Problem.....	2
1.3 Objectives	4
1.4 General Methodology and Research Plan	4
2) LITERATURE REVIEW.....	6
2.1 General	6
2.2 Conservativeness.....	7
2.3 Sigma-Coordinate and Pressure Gradient	8
2.4 Boundary Conditions	9
2.5 Sediment Transport.....	9
2.5.1 Non-Cohesive Sediment - Bed Load	10
2.5.2 Non-Cohesive Sediment - Suspended Bed Material.....	13
2.5.3 Non-Cohesive Sediment - Total Bed-Material Load	15
2.5.4 Bed Roughness/Friction Relationships	16
2.5.5 Cohesive Sediment – Wash Load	17
2.6 Flow of Density Current	19
2.7 Consistency of External and Internal Modes	20
2.8 Analytical Solutions for Model Testing.....	20
2.9 Classification of Models	20
2.9.1 Mathematical Models.....	21
2.9.2 Analogue or Physical Model.....	21
2.10 One-dimensional Modeling Options	23
2.10.1 HEC-RAS	23
2.10.2 CHARIMA.....	24
2.11 Three-dimensional Modeling Options	24
2.11.1 Finite-Volume Coastal Oceanographic Model (FVCOM).....	24
2.11.2 Estuarine, Coastal and Ocean Modeling System with Sediments (ECOMSED).....	25
3) RESEARCH PLAN	26
3.1 Selection Criteria	27
4) MODELS DEVELOPMENT.....	28
4.1 Rationale for Models Choice	28
4.2 Model Description CHARIMA.....	28
4.2.1 Governing Equations	29
4.2.2 The Sediment Transport Formulations	31
4.2.3 The Program structure.....	35

4.3 Model Description ECOMSED	36
4.3.1 Dynamic and Thermodynamic Equations	37
4.3.2 Composition of the grid	40
4.3.3 The turbulent closure models	41
4.3.4 The Sediment (SED) Model	41
4.5.5 The Program structure	48
4.5.6 Mode Splitting	49
4.5.7 Modifications and Additions to the Original ECOMSED Code	50
5) MODEL TESTING	56
5.1 Rectangular Channel Test	56
5.2.1 Boundary Conditions	58
5.2.2 Initial Conditions	58
5.2.3 Model Results	59
5.2 Trapezoidal Channel Test	63
5.3 Short Mississippi River Reach Test	65
5.3.1 Boundary Conditions	68
5.3.2 Model Results	69
6) ONE-DIMENSIONAL MODELING	79
6.1 Existing Outflows	80
6.1.1 Boundary Conditions	80
6.1.2 Results	86
6.2 Myrtle Grove + Existing Outflows	124
6.2.1 Boundary Conditions	125
6.2.2 Results	126
6.3 Belair + Existing Outflows	137
6.3.1 Boundary Conditions	138
6.3.2 Results	138
7) THREE-DIMENSIONAL ECOMSED MODELING	150
7.1 Computational Grid Domain	150
7.2 Existing Outflows	150
7.2.1 Boundary Conditions	151
7.2.2 Results	154
7.3 Myrtle Grove + Existing Outflows	190
7.4 Belair + Existing Outflows	215
7.5 Proposed MLODS Diversions + Existing Outflows	241
8) DISCUSSION	266
8.1 One-Dimensional Modeling	266
8.2 Three-Dimensional Modeling	275
8.3 Results	280
9) CONCLUSIONS	289
9.1 One-Dimensional Studies	289
9.2 Three-Dimensional Studies	290

9.3 General	292
10) RECOMMENDATIONS	293
11) REFERENCES	294
APPENDIX A: 1-D Modeling Boundary Conditions	300
APPENDIX B: Flow Roughness Coefficients (Ks and n) used in the 1-D Modeling	305
APPENDIX C: Changes Made to the Original ECOMSED Code	342
VITA	346

LIST OF FIGURES

Figure 1.1 – Plan View of the Mississippi River Study Area (<i>Source: Visible Earth 2001</i>).....	2
Figure 4.1 – Flow chart for solution strategy in one time-step for CHARIMA (<i>Source: Holly et al. 1990</i>)	36
Figure 4.2 – The sigma coordinate system (<i>Source: HydroQual 2002</i>)	39
Figure 4.3 – The locations of the variables on the finite difference grid (<i>Source: HydroQual 2002</i>)	40
Figure 4.4 – Schematic of the sediment bed model	45
Figure 4.5 – ECOMSED Modeling Framework (<i>Source: HydroQual 2002</i>)	49
Figure 4.6 – Simplified Illustration of the interaction between the External and the Internal Mode in ECOMSED (<i>Source: HydroQual 2002</i>).....	50
Figure 5.1 – ECOMSED Model – Downstream Boundary Mesh.....	57
Figure 5.2 – FVCOM Model – Downstream Boundary Mesh.....	57
Figure 5.3– ECOMSED Model – Stage after 24 h	59
Figure 5.4– FVCOM Model – Stage after 24 h	60
Figure 5.5 – ECOMSED Model – Depth Averaged Velocity near the D/S Boundary after 24h.	61
Figure 5.6 – FVCOM Model – Depth Averaged Velocity near the D/S Boundary after 24 h.....	61
Figure 5.7– ECOMSED Model – Surface Sand Concentration after 10 h.....	62
Figure 5.8– ECOMSED Model – Bottom Sand Concentration after 10 h.....	63
Figure 5.9 – ECOMSED Trapezoidal Channel Cross-Sectional Geometry	63
Figure 5.10 – ECOMSED Trapezoidal Channel Model – Depth Averaged Velocity in an intermediate section after 24h	64
Figure 5.11 – ECOMSED Trapezoidal Channel Model – Depth Averaged Velocity near the D/S Boundary after 24h.....	65
Figure 5.12– Short Mississippi River Reach Test Domain.....	66
Figure 5.13– Short Mississippi River Reach Test Grids.....	68
Figure 5.14– Longitudinal Profile of the Main Channel Water Discharge - Short Mississippi River Reach Test.....	70
Figure 5.15– Longitudinal Profile of the Main Channel Stage - Short Mississippi River Reach Test.....	70
Figure 5.16– Longitudinal Profile of the Main Channel Sand Concentration - Short Mississippi River Reach Test.....	71
Figure 5.17– Longitudinal Profile of the Main Channel Sand Load - Short Mississippi River Reach Test.....	71
Figure 5.18– Short Mississippi River Reach Test - Surface Velocity at a Bend	74
Figure 5.19– Short Mississippi River Reach Test - Bottom Velocity at a Bend	76
Figure 5.20– Surface Speed Profile on a Bend - Short Mississippi River Reach Test	77
Figure 5.21– Bottom Speed Profile on a Bend - Short Mississippi River Reach Test	78
Figure 6.1 – Schematic diagram of the Existing Outflows Topology.....	81
Figure 6.2 – Stage at Belle Chasse for the 1-D Hydrodynamics Calibration – 2008.....	87
Figure 6.3 – Stage at West Pointe-À-La-Hache for the 1-D Hydrodynamics Calibration – 2008	87
Figure 6.4 – Stage at Scofield North for the 1-D Hydrodynamics Calibration – 2008.....	88

Figure 6.5 – Stage at Scofield South for the 1-D Hydrodynamics Calibration – 2008.....	88
Figure 6.6 – Outflow at Bohemia Spillway Upstream for the 1-D Hydrodynamics Calibration – 2008.....	90
Figure 6.7 – Outflow at Bayou Lamoque North for the 1-D Hydrodynamics Calibration – 2008 90	
Figure 6.8 – Outflow at Bohemia Spillway Intermediate for the 1-D Hydrodynamics Calibration – 2008.....	91
Figure 6.9 – Outflow at Bayou Lamoque South for the 1-D Hydrodynamics Calibration – 2008 91	
Figure 6.10 – Outflow at Bohemia Spillway Downstream for the 1-D Hydrodynamics Calibration – 2008.....	92
Figure 6.11 – Outflow at Fort St. Philip for the 1-D Hydrodynamics Calibration – 2008	92
Figure 6.12 – Outflow at Baptiste Collette for the 1-D Hydrodynamics Calibration – 2008	93
Figure 6.13 – Outflow at Tiger Pass for the 1-D Hydrodynamics Calibration – 2008	93
Figure 6.14 – Outflow at Grand Pass for the 1-D Hydrodynamics Calibration – 2008.....	94
Figure 6.15 – Outflow at West Bay for the 1-D Hydrodynamics Calibration – 2008	94
Figure 6.16 – Outflow at Main Pass for the 1-D Hydrodynamics Calibration – 2008	95
Figure 6.17 – Total Outflow Quadratic Function adjusted to field measurements (<i>Based on Data from Pratt 2009</i>)	97
Figure 6.18 – Stage at Belle Chasse for the 1-D Hydrodynamics Validation – 2007	97
Figure 6.19 – Stage at West Pointe-À-La-Hache for the 1-D Hydrodynamics Validation – 2007 98	
Figure 6.20 – Stage at Scofield North for the 1-D Hydrodynamics Validation – 2007.....	98
Figure 6.21 – Stage at Scofield South for the 1-D Hydrodynamics Validation – 2007	99
Figure 6.22 – Outflow at Bohemia Spillway Upstream for the 1-D Hydrodynamics Validation – 2007.....	100
Figure 6.23 – Outflow at Bayou Lamoque North for the 1-D Hydrodynamics Validation – 2007	100
Figure 6.24 – Outflow at Bohemia Intermediate for the 1-D Hydrodynamics Validation – 2007	101
Figure 6.25 – Outflow at Bayou Lamoque South for the 1-D Hydrodynamics Validation – 2007	101
Figure 6.26 – Outflow at Bohemia Downstream for the 1-D Hydrodynamics Validation – 2007	102
Figure 6.27 – Outflow at Fort St. Philip for the 1-D Hydrodynamics Validation – 2007	102
Figure 6.28 – Outflow at Baptiste Collette for the 1-D Hydrodynamics Validation – 2007	103
Figure 6.29 – Outflow at Tiger Pass for the 1-D Hydrodynamics Validation – 2007	103
Figure 6.30 – Outflow at Grand Pass for the 1-D Hydrodynamics Validation – 2007	104
Figure 6.31 – Outflow at West Bay for the 1-D Hydrodynamics Validation – 2007.....	104
Figure 6.32 – Outflow at Main Pass for the 1-D Hydrodynamics Validation – 2007.....	105
Figure 6.33 – Stage at Belle Chasse for the 1-D Mobile-Bed Calibration – 2008.....	106
Figure 6.34 – Stage at West Pointe-À-La-Hache for the 1-D Mobile-Bed Calibration – 2008..	106
Figure 6.35 – Stage at Scofield North for the 1-D Mobile-Bed Calibration – 2008.....	107
Figure 6.36 – Stage at Scofield South for the 1-D Mobile-Bed Calibration – 2008.....	107

Figure 6.37 – Outflow at Bohemia Spillway Upstream for the 1-D Mobile-Bed Calibration – 2008.....	108
Figure 6.38 – Outflow at Bayou Lamoque North for the 1-D Mobile-Bed Calibration – 2008 ..	108
Figure 6.39 – Outflow at Bohemia Intermediate for the 1-D Mobile-Bed Calibration – 2008 ..	109
Figure 6.40 – Outflow at Bayou Lamoque South for the 1-D Mobile-Bed Calibration – 2008 ..	109
Figure 6.41 – Outflow at Bohemia Spillway Downstream for the 1-D Mobile-Bed Calibration – 2008.....	110
Figure 6.42 – Outflow at Fort St. Philip for the 1-D Mobile-Bed Calibration – 2008	110
Figure 6.43 – Outflow at Baptiste Collette for the 1-D Mobile-Bed Calibration – 2008	111
Figure 6.44 – Outflow at Tiger Pass for the 1-D Mobile-Bed Calibration – 2008	111
Figure 6.45 – Outflow at Grand Pass for the 1-D Mobile-Bed Calibration – 2008.....	112
Figure 6.46 – Outflow at West Bay for the 1-D Mobile-Bed Calibration – 2008	112
Figure 6.47 – Outflow at Main Pass for the 1-D Mobile-Bed Calibration – 2008	113
Figure 6.48 – 1-D Existing Outflows – Suspended Sand Concentration at Low Flows – Calibration.....	114
Figure 6.49 – 1-D Existing Outflows – Suspended Sand Concentration at Intermediate Flows – Calibration.....	115
Figure 6.50 – 1-D Existing Outflows – Suspended Sand Concentration at Peak Flows – Calibration.....	115
Figure 6.51 – Suspended Sand Concentration at Belle Chasse for the 1-D Mobile-Bed Calibration – 2008.....	116
Figure 6.52 – Suspended Sand Concentration at Myrtle Grove for the 1-D Mobile-Bed Calibration – 2008.....	117
Figure 6.53 – Suspended Sand Concentration at Scofield North for the 1-D Mobile-Bed Calibration – 2008.....	117
Figure 6.54 – Suspended Sand Concentration at Scofield Intermediate for the 1-D Mobile-Bed Calibration – 2008.....	118
Figure 6.55 – Suspended Sand Concentration at Scofield South for the 1-D Mobile-Bed Calibration – 2008.....	118
Figure 6.56 – Suspended Sand Load at Belle Chasse for the 1-D Mobile-Bed Calibration – 2008	119
Figure 6.57 – Suspended Sand Load at Myrtle Grove for the 1-D Mobile-Bed Calibration – 2008	120
Figure 6.58 – Suspended Sand Load at Scofield North for the 1-D Mobile-Bed Calibration – 2008.....	120
Figure 6.59 – Suspended Sand Load at Scofield Intermediate for the 1-D Mobile-Bed Calibration – 2008.....	121
Figure 6.60 – Suspended Sand Load at Scofield South for the 1-D Mobile-Bed Calibration – 2008.....	121
Figure 6.61 – 1-D Simulations - Existing Outflows – Outflows Suspended Sand Concentration at Peak Flows	122

Figure 6.62 – 1-D Simulations - Existing Outflows – Outflows Suspended Sand Concentration at Intermediate Flows.....	123
Figure 6.63 – Schematic diagram of the Myrtle Grove Case Topology	124
Figure 6.64 –Myrtle Grove Outflow – Myrtle Grove Case - 1-D Hydrodynamics Calibration – 2008.....	126
Figure 6.65 – Stage at Belle Chasse – Myrtle Grove - 1-D Hydrodynamics Calibration – 2008	127
Figure 6.66 – Stage at West Pointe-Á-La-Hache - Myrtle Grove - 1-D Hydrodynamics Calibration – 2008.....	128
Figure 6.67 – Stage at Scofield North – Myrtle Grove – 1-D Hydrodynamics Calibration 2008	128
Figure 6.68 – Stage at Scofield South – Myrtle Grove 1-D Hydrodynamics Calibration – 2008	129
Figure 6.69 – Stage at Belle Chasse – Myrtle Grove 1-D Mobile-Bed Calibration – 2008.....	131
Figure 6.70 – Stage at West Pointe-Á-La-Hache - Myrtle Grove 1-D Mobile-Bed Calibration – 2008.....	131
Figure 6.71 – Stage at Scofield North – Myrtle Grove 1-D Mobile-Bed Calibration – 2008.....	132
Figure 6.72 – Stage at Scofield South – Myrtle Grove 1-D Mobile-Bed Calibration – 2008.....	132
Figure 6.73 – Suspended Sand Concentration at Myrtle Grove for the 1-D Mobile-Bed Calibration – 2008.....	133
Figure 6.74 – Suspended Sand Concentration at Scofield North for the 1-D Mobile-Bed Calibration – 2007/08	134
Figure 6.75 – Suspended Sand Concentration at Scofield Intermediate for the 1-D Mobile-Bed Calibration – 2007/08	134
Figure 6.76 – Suspended Sand Concentration at Scofield South for the 1-D Mobile-Bed Calibration – 2007/08	135
Figure 6.77 – 1-D Simulations – Myrtle Grove – Outflows Suspended Sand Concentration at Peak Flows	136
Figure 6.78 – 1-D Simulations – Myrtle Grove – Outflows Suspended Sand Concentration at Intermediate Flows.....	136
Figure 6.79 – Schematic diagram of the Belair Case Topology	137
Figure 6.80 – Belair Outflow – Belair Case - 1-D Hydrodynamics Calibration – 2008.....	139
Figure 6.81 – Stage at Belle Chasse – Belair - 1-D Hydrodynamics Calibration – 2008	140
Figure 6.82 – Stage at West Pointe-Á-La-Hache - Belair - 1-D Hydrodynamics Calibration – 2008.....	140
Figure 6.83 – Stage at Scofield North – Belair – 1-D Hydrodynamics Calibration 2008.....	141
Figure 6.84 – Stage at Scofield South – Belair - 1-D Hydrodynamics Calibration – 2008	141
Figure 6.85 – Stage at Belle Chasse – Belair 1-D Mobile-Bed Calibration – 2008.....	144
Figure 6.86 – Stage at West Pointe-Á-La-Hache - Belair 1-D Mobile-Bed Calibration – 2008	144
Figure 6.87 – Stage at Scofield North – Belair 1-D Mobile-Bed Calibration – 2008.....	145
Figure 6.88 – Stage at Scofield South – Belair 1-D Mobile-Bed Calibration – 2008.....	145
Figure 6.89 – Suspended Sand Concentration at Myrtle Grove for the Belair 1-D Mobile-Bed Calibration – 2008.....	146
Figure 6.90 – Suspended Sand Concentration at Scofield North for the Belair 1-D Mobile-Bed Calibration – 2008.....	146

Figure 6.91 – Suspended Sand Concentration at Scofield Intermediate for the Belair 1-D Mobile-Bed Calibration – 2008	147
Figure 6.92 – Suspended Sand Concentration at Scofield South for the Belair 1-D Mobile-Bed Calibration – 2008.....	147
Figure 6.93 – 1-D Simulations – Belair – Outflows Suspended Sand Concentration at Peak Flows	148
Figure 6.94 – 1-D Simulations – Belair – Outflows Suspended Sand Concentration at Intermediate Flows.....	149
Figure 7.1 – Sample of Existing ECOMSED Mesh, Bathymetry and Mask at Myrtle Grove (RM 59, RK 94).....	151
Figure 7.2 – Variation of Bed Shear Stress for the Lower Mississippi River Miles 0 to 300 (<i>Source: El Kheishy 2007</i>)	153
Figure 7.3 – Variation of Bed Form Height for the Lower Mississippi River Miles 0 to 300 (<i>Source: El Kheishy 2007</i>)	153
Figure 7.4 – Stage at Belle Chasse for the ECOMSED Hydrodynamics Calibration at High Flows (2008).....	154
Figure 7.5 – Stage at West Pointe-À-La-Hache for the ECOMSED Hydrodynamics Calibration at Low Flows (2008).....	155
Figure 7.6 – Stage at Scofield North for the ECOMSED Hydrodynamics Calibration at High Flows (2008)	155
Figure 7.7 – Stage at Scofield South for the ECOMSED Hydrodynamics Calibration at High Flows (2008)	156
Figure 7.8 – Stage at Belle Chasse for the ECOMSED Hydrodynamics Calibration at Intermediate Flows (2008)	156
Figure 7.9 – Stage at West Pointe-À-La-Hache for the ECOMSED Hydrodynamics Calibration at Intermediate Flows (2008)	157
Figure 7.10 – Stage at Scofield North for the ECOMSED Hydrodynamics Calibration at Intermediate Flows (2008)	157
Figure 7.11 – Stage at Scofield South for the ECOMSED Hydrodynamics Calibration at Intermediate Flows (2008)	158
Figure 7.12 – Stage at Belle Chasse for the ECOMSED Hydrodynamics Calibration at Low Flows (2008)	158
Figure 7.13 – Stage at West Pointe-À-La-Hache for the ECOMSED Hydrodynamics Calibration at Low Flows (2008)	159
Figure 7.14 – Stage at Scofield North for the ECOMSED Hydrodynamics Calibration at Low Flows (2008)	159
Figure 7.15 – Stage at Scofield South for the ECOMSED Hydrodynamics Calibration at Low Flows (2008)	160
Figure 7.16 – Velocity Vectors at Myrtle Grove (RM 59, RK 94)	161
Figure 7.17 – Bottom Shear Stress at Myrtle Grove (RM 59, RK 92) for Peak Flows	162
Figure 7.18 – Main Channel Water Discharge at Peak Flows for the Existing Outflows Case..	164
Figure 7.19 – Main Channel Stage at Peak Flows for the Existing Outflows Case.....	164

Figure 7.20 – Main Channel Total Energy of the Flow at Peak Flows for the Existing Outflows Case.....	165
Figure 7.21 – Main Channel Kinetic Energy of the Flow at Peak Flows for the Existing Outflows Case.....	165
Figure 7.22 – Main Channel Total Energy Flux of the Flow at Peak Flows for the Existing Outflows Case.....	166
Figure 7.23 – Main Channel Potential Energy Flux of the Flow at Peak Flows for the Existing Outflows Case.....	167
Figure 7.24 – Main Channel Kinetic Energy Flux of the Flow at Peak Flows for the Existing Outflows Case.....	167
Figure 7.25 – Main Channel Water Discharge at Intermediate Flows for the Existing Outflows Case.....	168
Figure 7.26 – Main Channel Total Stage at Intermediate Flows for the Existing Outflows Case.....	169
Figure 7.27 – Main Channel Total Energy of the Flow at Intermediate Flows for the Existing Outflows Case.....	169
Figure 7.28 – Main Channel Kinetic Energy of the Flow at Intermediate Flows for the Existing Outflows Case.....	170
Figure 7.29 – Main Channel Total Energy Flux of the Flow at Intermediate Flows for the Existing Outflows Case.....	170
Figure 7.30 – Main Channel Potential Energy Flux of the Flow at Intermediate Flows for the Existing Outflows Case.....	171
Figure 7.31 – Main Channel Kinetic Energy Flux of the Flow at Intermediate Flows for the Existing Outflows Case.....	171
Figure 7.32 – Suspended Sand Concentration at Peak Flows – Calibration.....	173
Figure 7.33 – Suspended Sand Concentration at Low Flows – Validation	173
Figure 7.34 – Suspended Sand Concentration at Intermediate Flows – Validation.....	174
Figure 7.35 – Scofield North (RM 24) Sand Concentration Vertical Profile in the Center of the Channel at Peak Flows.....	174
Figure 7.36 – Modeling versus Field Data (Source: Allison 2010)	175
Figure 7.37 – Depth Average Suspended Sand Concentration for ECOMSED Mobile-Bed Calibration at Peak Flows (2008)	176
Figure 7.38 – Depth Average Suspended Sand Concentration for ECOMSED Mobile-Bed Calibration at Intermediate Flows (2008)	177
Figure 7.39 – Main Channel Suspended Sand Load at Peak Flows for the Existing Outflows Case.....	178
Figure 7.40 – Main Channel Suspended Sand Concentration at Peak Flows for the Existing Outflows Case.....	178
Figure 7.41 – Main Channel Suspended Sand Load at Intermediate Flows for the Existing Outflows Case.....	179
Figure 7.42 – Main Channel Suspended Sand Concentration at Intermediate Flows for the Existing Outflows Case.....	179

Figure 7.43 – Existing Outflows – Model Domain - Bed Sediment Thickness Change after 1 day at Peak Flows. Positive values indicate deposition and negative values indicate erosion.....	180
Figure 7.44 – Existing Outflows – Model Domain - Bed Sediment Thickness Change after 10 days at Peak Flows. Positive values indicate deposition and negative values indicate erosion..	181
Figure 7.45 – Existing Outflows – Belair Area (RM 65) - Bed Sediment Thickness Change after 1 day at Peak Flows. Positive values indicate deposition and negative values indicate erosion	182
Figure 7.46 – Existing Outflows – Myrtle Grove Area (RM 59) - Bed Sediment Thickness Change after 1 day at Peak Flows. Positive values indicate deposition and negative values indicate erosion	182
Figure 7.47 – Existing Outflows – Belair Area (RM 65) - Bed Sediment Thickness Change after 10 days at Peak Flows. Positive values indicate deposition and negative values indicate erosion	183
Figure 7.48 – Existing Outflows – Myrtle Grove Area (RM 59) - Bed Sediment Thickness Change after 10 days at Peak Flows. Positive values indicate deposition and negative values indicate erosion	183
Figure 7.49 – Existing Outflows – Model Domain - Bed Sediment Thickness Change after 1 day at Intermediate Flows. Positive values indicate deposition and negative values indicate erosion	184
Figure 7.50 – Existing Outflows – Model Domain - Bed Sediment Thickness Change after 10 days at Intermediate Flows. Positive values indicate deposition and negative values indicate erosion.....	185
Figure 7.51 – Existing Outflows – Belair Area (RM 65) - Bed Sediment Thickness Change after 1 day at Intermediate Flows. Positive values indicate deposition and negative values indicate erosion.....	186
Figure 7.52 – Existing Outflows – Myrtle Grove Area (RM 59) - Bed Sediment Thickness Change after 1 day at Intermediate Flows. Positive values indicate deposition and negative values indicate erosion	186
Figure 7.53 – Existing Outflows – Belair Area (RM 65) - Bed Sediment Thickness Change after 10 days at Intermediate Flows. Positive values indicate deposition and negative values indicate erosion.....	187
Figure 7.54 – Existing Outflows – Myrtle Grove Area (RM 59) - Bed Sediment Thickness Change after 10 days at Intermediate Flows. Positive values indicate deposition and negative values indicate erosion	187
Figure 7.55 – Existing Outflows – Outflows Suspended Sand Concentration at Peak Flows....	189
Figure 7.56 – Existing Outflows – Outflows Suspended Sand Concentration at Intermediate Flows.....	189
Figure 7.57 – Existing Outflows + Myrtle Grove ECOMSED Mesh and Mask at Myrtle Grove (RM 59, RK 94)	190
Figure 7.58 – Existing Outflows + Myrtle Grove (RM 59, RK 94) – Main Channel Kinetic Energy of the Flow at Peak Flows	191
Figure 7.59 – Existing Outflows + Myrtle Grove (RM 59, RK 94) – Main Channel Total Energy of the Flow at Peak Flows.....	191

Figure 7.60 – Existing Outflows + Myrtle Grove (RM 59, RK 94) – Main Channel Total Energy Flux of the Flow at Peak Flows	192
Figure 7.61 – Existing Outflows + Myrtle Grove (RM 59, RK 94) – Main Channel Potential Energy Flux of the Flow at Peak Flows	192
Figure 7.62 – Existing Outflows + Myrtle Grove (RM 59, RK 94) – Main Channel Kinetic Energy Flux of the Flow at Peak Flows	193
Figure 7.63 – Existing Outflows + Myrtle Grove (RM 59, RK 94) – Main Channel Suspended Sand Concentration at Peak Flows	194
Figure 7.64 – Existing Outflows + Myrtle Grove (RM 59, RK 94) – Main Channel Suspended Sand Load at Peak Flows	194
Figure 7.65 – Existing Outflows + Myrtle Grove (RM 59, RK 94) – Main Channel Kinetic Energy of the Flow at Intermediate Flows	195
Figure 7.66 – Existing Outflows + Myrtle Grove (RM 59, RK 94) – Main Channel Total Energy of the Flow at Intermediate Flows	196
Figure 7.67 – Existing Outflows + Myrtle Grove (RM 59, RK 94) – Main Channel Total Energy Flux of the Flow at Intermediate Flows	196
Figure 7.68 – Existing Outflows + Myrtle Grove (RM 59, RK 94) – Main Channel Potential Energy Flux of the Flow at Intermediate Flows.....	197
Figure 7.69 – Existing Outflows + Myrtle Grove (RM 59, RK 94) – Main Channel Kinetic Energy Flux of the Flow at Intermediate Flows.....	197
Figure 7.70 – Existing Outflows + Myrtle Grove (RM 59, RK 94) – Main Channel Suspended Sand Concentration at Intermediate Flows	198
Figure 7.71 – Existing Outflows + Myrtle Grove (RM 59, RK 94) – Main Channel Sand Load at Intermediate Flows.....	199
Figure 7.72 – Myrtle Grove Area (RM 59) - Bed Sediment Thickness Change after 1 day at Peak Flows. Positive values indicate deposition and negative values indicate erosion	200
Figure 7.73 – Myrtle Grove Area (RM 59, RK 94) - Bed Sediment Thickness Change after 10 days at Peak Flows. Positive values indicate deposition and negative values indicate erosion..	201
Figure 7.74 – Model Domain - Bed Sediment Thickness Change after 1 day at Peak Flows. Positive values indicate deposition and negative values indicate erosion	203
Figure 7.75 – Model Domain - Bed Sediment Thickness Change after 10 days at Peak Flows. Positive values indicate deposition and negative values indicate erosion	205
Figure 7.76 – Model Domain – Difference between Existing and Myrtle Grove Test Bed Sediment Thickness Change after 10 days at Peak Flows. Positive values indicate that the addition of the Myrtle Grove Diversion increased deposition. Negative values indicate that the addition of the Myrtle Grove Diversion Myrtle Grove (RM 59, RK 94) increased erosion.....	206
Figure 7.77 – Myrtle Grove Area (RM 59, RK 94) - Bed Sediment Thickness Change after 1 day at Intermediate Flows. Positive values indicate deposition and negative values indicate erosion	207
Figure 7.78 – Myrtle Grove Area (RM 59, RK 94) - Bed Sediment Thickness Change after 10 days at Intermediate Flows. Positive values indicate deposition and negative values indicate erosion.....	208

Figure 7.79 – Model Domain - Bed Sediment Thickness Change after 1 day at Intermediate Flows. Positive values indicate deposition and negative values indicate erosion	210
Figure 7.80 – Model Domain - Bed Sediment Thickness Change after 10 days at Intermediate Flows. Positive values indicate deposition and negative values indicate erosion	212
Figure 7.81 – Existing Outflows + Myrtle Grove (RM 59, RK 94) – Outflow Suspended Sand Concentrations at Peak Flows	213
Figure 7.82 – Existing Outflows + Myrtle Grove (RM 59, RK 94) – Outflow Suspended Sand Concentrations at Intermediate Flows.....	214
Figure 7.83 – Existing Diversions + Belair ECOMSED Mesh and Mask at Belair (RM 65, RK 105)	215
Figure 7.84 – Existing Diversions + Belair (RM 65, RK 105)– Main Channel Kinetic Energy of the Flow at Peak Flows	216
Figure 7.85 – Existing Diversions + Belair (RM 65, RK 105)– Main Channel Total Energy of the Flow at Peak Flows	216
Figure 7.86 – Existing Diversions + Belair (RM 65, RK 105)– Main Channel Total Energy Flux of the Flow at Peak Flows.....	217
Figure 7.87 – Existing Diversions + Belair (RM 65, RK 105)– Main Channel Potential Energy Flux of the Flow at Peak Flows	217
Figure 7.88 – Existing Diversions + Belair (RM 65, RK 105)– Main Channel Kinetic Energy Flux of the Flow at Peak Flows	218
Figure 7.89 – Existing Diversions + Belair (RM 65, RK 105) – Main Channel Sand Concentration at Peak Flows	219
Figure 7.90 – Existing Diversions + Belair (RM 65, RK 105) – Main Channel Sand Load at Peak Flows.....	219
Figure 7.91 – Existing Diversions + Belair (RM 65, RK 105)– Main Channel Kinetic Energy of the Flow at Intermediate Flows.....	220
Figure 7.92 – Existing Diversions + Belair (RM 65, RK 105)– Main Channel Total Energy of the Flow at Intermediate Flows.....	220
Figure 7.93 – Existing Diversions + Belair (RM 65, RK 105)– Main Channel Total Energy Flux of the Flow at Intermediate Flows	221
Figure 7.94 – Existing Diversions + Belair (RM 65, RK 105) – Main Channel Potential Energy Flux of the Flow at Intermediate Flows	221
Figure 7.95 – Existing Diversions + Belair (RM 65, RK 105)– Main Channel Kinetic Energy Flux of the Flow at Intermediate Flows	222
Figure 7.96 – Existing Diversions + Belair (RM 65, RK 105)– Main Channel Suspended Sand Concentration at Intermediate Flows	223
Figure 7.97 – Existing Diversions + Belair (RM 65, RK 105) – Main Channel Suspended Sand Load at Intermediate Flows.....	223
Figure 7.98 – Existing Diversions + Belair (RM 65, RK 105)- Bed Sediment Thickness Change after 1 day at Peak Flows. Positive values indicate deposition and negative values indicate erosion.....	225

Figure 7.99 – Existing Diversions + Belair (RM 65, RK 105) - Bed Sediment Thickness Change after 10 days at Peak Flows. Positive values indicate deposition and negative values indicate erosion.....	226
Figure 7.100 – Model Domain - Bed Sediment Thickness Change after 1 day at Peak Flows. Positive values indicate deposition and negative values indicate erosion	228
Figure 7.101 – Model Domain - Bed Sediment Thickness Change after 10 days at Peak Flows. Positive values indicate deposition and negative values indicate erosion	230
Figure 7.102 – Model Domain – Difference between Existing and Belair Test Bed Sediment Thickness Change after 10 days at Peak Flows. Positive values indicate that the addition of the Belair Diversion increased deposition. Negative values indicate that the addition of the Belair (RM 65, RK 105) Diversion increased erosion.....	231
Figure 7.103 – Belair Area (RM 65, RK 105) - Bed Sediment Thickness Change after 1 day at Intermediate Flows. Positive values indicate deposition and negative values indicate erosion .	232
Figure 7.104 – Belair (RM 65, RK 105)- Bed Sediment Thickness Change after 10 days at Intermediate Flows. Positive values indicate deposition and negative values indicate erosion .	233
Figure 7.105 – Belair (RM 65, RK 105) - Bed Sediment Thickness Change after 1 day at Intermediate Flows. Positive values indicate deposition and negative values indicate erosion .	235
Figure 7.106 – Model Domain - Bed Sediment Thickness Change after 10 days at Intermediate Flows. Positive values indicate deposition and negative values indicate erosion	237
Figure 7.107 – Existing Outflows + Belair (RM 65, RK 105) Diversion – Outflows Suspended Sand Concentration at Peak Flows	239
Figure 7.108 – Existing Outflows + Belair (RM 65, RK 105) – Outflows Suspended Sand Concentration at Intermediate Flows	240
Figure 7.109 – Existing Outflows + Proposed Diversions – Main Channel Water Discharge at Peak Flows. <i>Proposed Diversions: Jesuit Bend (RM 68, RK 109), Belair (RM 65, RK 105), Myrtle Grove (RM 59, RK 94), Deer Range (RM 54, RK 87) and Buras (RM 25, RK 40).</i>	242
Figure 7.110 – Existing Outflows + Proposed Diversions – Main Channel Total Energy of the Flow at Peak Flows. <i>Proposed Diversions: Jesuit Bend (RM 68, RK 109), Belair (RM 65, RK 105), Myrtle Grove (RM 59, RK 94), Deer Range (RM 54, RK 87) and Buras (RM 25, RK 40).</i>	243
Figure 7.111 – Existing Outflows + Proposed Diversions – Main Channel Kinetic Energy of the Flow at Peak Flows. <i>Proposed Diversions: Jesuit Bend (RM 68, RK 109), Belair (RM 65, RK 105), Myrtle Grove (RM 59, RK 94), Deer Range (RM 54, RK 87) and Buras (RM 25, RK 40).</i>	243
Figure 7.112 – Existing Outflows + Proposed Diversions – Main Channel Total Energy Flux of the Flow at Peak Flows. <i>Proposed Diversions: Jesuit Bend (RM 68, RK 109), Belair (RM 65, RK 105), Myrtle Grove (RM 59, RK 94), Deer Range (RM 54, RK 87) and Buras (RM 25, RK 40).</i>	244
Figure 7.113 – Existing Outflows + Proposed Diversions – Main Channel Potential Energy Flux of the Flow at Peak Flows. <i>Proposed Diversions: Jesuit Bend (RM 68, RK 109), Belair (RM 65, RK 105), Myrtle Grove (RM 59, RK 94), Deer Range (RM 54, RK 87) and Buras (RM 25, RK 40).</i>	245

Figure 7.114 – Existing Outflows + Proposed Diversions – Main Channel Kinetic Energy Flux of the Flow at Peak Flows. <i>Proposed Diversions: Jesuit Bend (RM 68, RK 109), Belair (RM 65, RK 105), Myrtle Grove (RM 59, RK 94), Deer Range (RM 54, RK 87) and Buras (RM 25, RK 40).</i>	245
Figure 7.115 – Existing Outflows + Proposed Diversions – Main Channel Suspended Sand Concentration at Peak Flows. <i>Proposed Diversions: Jesuit Bend (RM 68, RK 109), Belair (RM 65, RK 105), Myrtle Grove (RM 59, RK 94), Deer Range (RM 54, RK 87) and Buras (RM 25, RK 40).</i>	246
Figure 7.116 – Existing Outflows + Proposed Diversions – Main Channel Sand Load at Peak Flows. <i>Proposed Diversions: Jesuit Bend (RM 68, RK 109), Belair (RM 65, RK 105), Myrtle Grove (RM 59, RK 94), Deer Range (RM 54, RK 87) and Buras (RM 25, RK 40).</i>	247
Figure 7.117 – Existing Outflows + Proposed Diversions – Main Channel Water Discharge at Intermediate Flows. <i>Proposed Diversions: Jesuit Bend (RM 68, RK 109), Belair (RM 65, RK 105), Myrtle Grove (RM 59, RK 94), Deer Range (RM 54, RK 87) and Buras (RM 25, RK 40).</i>	248
Figure 7.118 – Existing Outflows + Proposed Diversions – Main Channel Kinetic Energy of the Flow at Intermediate Flows. <i>Proposed Diversions: Jesuit Bend (RM 68, RK 109), Belair (RM 65, RK 105), Myrtle Grove (RM 59, RK 94), Deer Range (RM 54, RK 87) and Buras (RM 25, RK 40).</i>	248
Figure 7.119 – Existing Outflows + Proposed Diversions – Main Channel Total Energy of the Flow at Intermediate Flows. <i>Proposed Diversions: Jesuit Bend (RM 68, RK 109), Belair (RM 65, RK 105), Myrtle Grove (RM 59, RK 94), Deer Range (RM 54, RK 87) and Buras (RM 25, RK 40).</i>	249
Figure 7.120 – Existing Outflows + Proposed Diversions – Main Channel Total Energy Flux of the Flow at Intermediate Flows. <i>Proposed Diversions: Jesuit Bend (RM 68, RK 109), Belair (RM 65, RK 105), Myrtle Grove (RM 59, RK 94), Deer Range (RM 54, RK 87) and Buras (RM 25, RK 40).</i>	250
Figure 7.121 – Existing Outflows + Proposed Diversions – Main Channel Potential Energy Flux of the Flow at Intermediate Flows. <i>Proposed Diversions: Jesuit Bend (RM 68, RK 109), Belair (RM 65, RK 105), Myrtle Grove (RM 59, RK 94), Deer Range (RM 54, RK 87) and Buras (RM 25, RK 40).</i>	250
Figure 7.122 – Existing Outflows + Proposed Diversions – Main Channel Kinetic Energy Flux of the Flow at Intermediate Flows. <i>Proposed Diversions: Jesuit Bend (RM 68, RK 109), Belair (RM 65, RK 105), Myrtle Grove (RM 59, RK 94), Deer Range (RM 54, RK 87) and Buras (RM 25, RK 40).</i>	251
Figure 7.123 – Existing Outflows + Proposed Diversions – Main Channel Suspended Sand Concentration at Intermediate Flows. <i>Proposed Diversions: Jesuit Bend (RM 68, RK 109), Belair (RM 65, RK 105), Myrtle Grove (RM 59, RK 94), Deer Range (RM 54, RK 87) and Buras (RM 25, RK 40).</i>	252
Figure 7.124 – Existing Outflows + Proposed Diversions – Main Channel Suspended Sand Load at Intermediate Flows. <i>Proposed Diversions: Jesuit Bend (RM 68, RK 109), Belair (RM 65, RK 105), Myrtle Grove (RM 59, RK 94), Deer Range (RM 54, RK 87) and Buras (RM 25, RK 40).</i>	252

Figure 7.125 – Proposed Diversions – Belair Area (RM 65, RK 105) - Bed Sediment Thickness Change after 1 day at Peak Flows. Positive values indicate deposition and negative values indicate erosion	254
Figure 7.126 – Proposed Diversions – Myrtle Grove Area (RM 59, RK 94) - Bed Sediment Thickness Change after 1 day at Peak Flows. Positive values indicate deposition and negative values indicate erosion	255
Figure 7.127 – Proposed Diversions – Belair Area (RM 65, RK 105) - Bed Sediment Thickness Change after 10 days at Peak Flows. Positive values indicate deposition and negative values indicate erosion	256
Figure 7.128 – Proposed Diversions – Myrtle Grove Area (RM 59, RK 94) - Bed Sediment Thickness Change after 10 days at Peak Flows. Positive values indicate deposition and negative values indicate erosion	257
Figure 7.129 – Model Domain – Difference between Existing and Proposed Test Bed Sediment Thickness Change after 10 days at Peak Flows. Positive values indicate that the addition of the Proposed Diversions increased deposition. Negative values indicate that the addition of the Proposed Diversions increased erosion.....	259
Figure 7.130 – Proposed Diversions – Belair Area (RM 65, RK 94) - Bed Sediment Thickness Change after 1 day at Intermediate Flows. Positive values indicate deposition and negative values indicate erosion	260
Figure 7.131 – Proposed Diversions – Myrtle Grove Area (RM 59, RK 94) - Bed Sediment Thickness Change after 1 day at Intermediate Flows. Positive values indicate deposition and negative values indicate erosion	261
Figure 7.132 – Proposed Diversions – Belair Area (RM 65, RK 105) - Bed Sediment Thickness Change after 10 days at Intermediate Flows. Positive values indicate deposition and negative values indicate erosion	262
Figure 7.133 – Proposed Diversions – Myrtle Grove Area (RM 59, RK 94) - Bed Sediment Thickness Change after 10 days at Intermediate Flows. Positive values indicate deposition and negative values indicate erosion	263
Figure 7.134 – Existing Outflows + Proposed Diversions – Outflows Suspended Sand Concentration at Peak Flows	265
Figure 7.135 – Existing Outflows + Proposed Diversions – Outflows Suspended Sand Concentration at Intermediate Flows	265
Figure 8.1 – Rectangular Channel Longitudinal Profile with 1-D Models	267
Figure 8.2 – Stage at Scofield North with different time-steps.....	268
Figure 8.3 – Outflow at the Main Pass with different time-steps	269
Figure 8.4 – Bed-load concentration for different time-steps (Mobile-Bed)	270
Figure 8.5 – Suspended Load concentration for different time-steps (Mobile-Bed)	270
Figure 8.6 – Cumulative Degradation for different time-steps (Mobile-Bed)	271
Figure 8.7 – Volume out of a reach in one-time step for different time-steps (Mobile-Bed)	272
Figure 8.8 – Suspended Load Concentration with for different time-steps (Rigid Bed)	273
Figure 8.9 – 2008 Hourly Stage Data at Several Lower River Stations.....	277

Figure 8.10 – 2008 Hourly Stage Data - Examples of Inconsistent Measurements.....	278
Figure 8.11 – 1-D Modeling – Main Channel Suspended Sand Concentration at Myrtle Grove (RM 59) for the Tested Scenarios – 2008 Calibration	283
Figure 8.12 – 1-D Modeling - Main Channel Suspended Sand Concentration at Scofield Intermediate (RM 20) for the Tested Scenarios – 2008 Calibration	283
Figure 8.13 – 3-D Modeling - Comparison of Total Energy Line for Existing River alone, with an Intermediate Diversion and with a Large Diversion at High River Flows. <i>Tested Diversions: Belair (RM 65, RK 105 and Myrtle Grove (RM 59, RK 94)</i>	285
Figure 8.14 – 3-D Modeling - Comparison of Kinetic Energy Line for Existing River alone, with an Intermediate Diversion and with a Large Diversion at High River Flows. <i>Tested Diversions: Belair (RM 65, RK 105 and Myrtle Grove (RM 59, RK 94)</i>	285
Figure 8.15 - 3-D Modeling - Comparison of Suspended Sand Load for Existing River alone, with an Intermediate Diversion and with a Large Diversion at High River Flows. <i>Tested Diversions: Belair (RM 65, RK 105 and Myrtle Grove (RM 59, RK 94)</i>	286
Figure 8.16 – 3-D Modeling - Outflows Suspended Sand Concentration at Peak Flows for the Tested Scenarios	287
Figure 8.17 – 3-D Modeling – Main Channel Suspended Sand Concentration at Peak Flow for the Tested Scenarios. <i>Proposed Diversions: Jesuit Bend (RM 68, RK 109), Belair (RM 65, RK 105), Myrtle Grove (RM 59, RK 94), Deer Range (RM 54, RK 87) and Buras (RM 25, RK 40).</i>	288

LIST OF TABLES

Table 5-1 – Time-Steps and Split for the Short Mississippi River Test	68
Table 5-2 – Boundary Conditions for the Short Mississippi River Test.....	69
Table 5-3 – Short Mississippi River Reach Test - Water discharge and Sand concentration in the Diversions.....	69
Table 6-1 – Flow Boundary Conditions - Existing Outflows Case – 1-D Calibration - /2008.....	81
Table 6-2 – Stage Boundary Conditions - Existing Outflows Case – 1-D Calibration - 2008	82
Table 6-3 – Sand Load Boundary Condition - Existing Outflows Case – 1-D Calibration - 2008.....	82
Table 6-4 – Weirs Parameters - Existing Outflows Case – 1-D Hydrodynamics Calibration - 2008	83
Table 6-5 – Gates Parameters - Existing Outflows Case – 1-D Hydrodynamics Calibration - 2007/2008	83
Table 6-6 – Weirs Parameters - Existing Outflows Case – 1-D Mobile-Bed Calibration - 2007/2008	84
Table 6-7 – Gates Parameters - Existing Outflows Case – 1-D Mobile-Bed Calibration - 2007/2008	84
Table 6-8 – Bed load diameters used in the 1-D CHARIMA Model.....	85
Table 6-9 – Flow Boundary Conditions - Existing Outflows Case – 1-D Validation - 2007	85
Table 6-10 – Stage Boundary Conditions - Existing Outflows Case – 1-D Validation - 2007	86
Table 6-11 – RMSE and Coefficient of Efficiency for the Stage – 2008 Calibration	89
Table 6-12 – RMSE and Coefficient of Efficiency for the Outflows – 2008 Calibration	95
Table 6-13 – Inflows and Outflows for the Existing Outflows Case – 1-D Calibration – 2008...	96
Table 6-14 – RMSE and Coefficient of Efficiency for the Stage – 2007 Validation	99
Table 6-15 – RMSE and Coefficient of Efficiency for the Outflows – 2007 Validation	105
Table 6-16 – Observed versus Modeled – 1-D Mobile-bed Simulations	114
Table 6-17 – Stage Boundary Condition – Myrtle Grove Case – 1-D Calibration - 2008.....	125
Table 6-18 – Gates Parameters – Myrtle Grove Case – 1-D Hydrodynamics Calibration - 2008	125
Table 6-19 – Gates Parameters – Myrtle Grove Case – 1-D Mobile-Bed Calibration - 2008	126
Table 6-20 – Inflows and Outflows for the Myrtle Grove Case – 1-D Calibration - 2008.....	129
Table 6-21 – Change in the average flow with the introduction of the Myrtle Grove Diversions – 1-D Calibration - 2008	130
Table 6-22 – Stage Boundary Condition – Belair Case – 1-D Calibration - 2008.....	138
Table 6-23 – Gate Parameters – Belair Case – 1-D Hydrodynamics and Mobile-Bed Calibrations - 2008	138
Table 6-24 – Inflows and Outflows for the Belair Case – 1-D Calibration - 2008.....	142
Table 6-25– Change in the average flow with the introduction of the Belair Diversion – 1-D Calibration - 2008	143
Table 7-1 – Inflows and Outflows for the Existing Outflows Modeling	151
Table 7-2 – Roughness Coefficients used in the ECOMSED Model	152
Table 7-3 – Observed versus Modeled – 3-D Mobile-bed Simulations	172

Table 7-4 – Water Discharge, Suspended Sand Concentration and Suspended Sand Load at Outflows – Existing Outflows Case Study – Peak Flows	188
Table 7-5 – Water Discharge, Suspended Sand Concentration and Suspended Sand Load at Outflows – Myrtle Grove Myrtle Grove (RM 59, RK 94) Case Study	213
Table 7-6 – Water Discharge, Suspended Sand Concentration and Suspended Sand Load at Outflows – Belair (RM 65, RK 105) Case Study – Peak Flows	238
Table 7-7 – Outflows for the Proposed Diversions Modeling	241
Table 7-8 – Water Discharge, Suspended Sand Concentration and Suspended Sand Load at Outflows.....	264
Table 8-1 – Rectangular Channel Flow Depth Results with 1-D Models	267
Table 8-2 – Observed versus Modeled – 1-D Mobile-bed Simulations using the New Formulation	275
Table 8-3 – Change in the average flow with the introduction of the Myrtle Grove and the Belair Diversions – 1-D Calibration - 2008.....	282

NOMENCLATURE

Symbol	Description	Units
\bar{C}	Mean sediment concentration of suspended sediment	M/L^3
\bar{C}_T	Sediment flux concentration (sediment mass flux per unit mass flow rate)	$M/L^3/M$
R_0^*	Parameter for initiation of sediment transport in Iwagaki Formulation	Dimensionless
R_e^*	Particle Reynolds Number	Dimensionless
\bar{u}_i	Mean flow velocity	L/T
\tilde{W}	Wall proximity function	Dimensionless
∇	Divergence operator	
∂	Partial differential operator	
A	Cross-sectional Area	L^2
a	Reference level above the bed	L
a	Empirical constant for Power equations	Dimensionless
a_0	Constant depending upon bed properties for resuspension of cohesive sediment	Dimensionless
a_0, a_1, a_2, a_3	Empirical coefficients for TLTM modified formulation	Dimensionless
A_H	Horizontal mixing coefficient for heat and salinity	Dimensionless
A_M	Horizontal mixing coefficient for momentum	Dimensionless
A_p	Peak orbital amplitude	L
B	Width of the section affected by bedload transport	L
b	Empirical constant for Power equations	Dimensionless
b_1, b_2	Coefficient calibrations for Karim's Hiding Factor Equation	Dimensionless
b_s		
C	Suspended load concentration; Constant used for determination of reference level above the bed	M/L^3 Dimensionless
c'	Fluctuating component of sediment concentration	M/L^3

C_0	Shallow water wave speed; Maximum volumetric bed sediment concentration	L/T
C_1	Cohesive suspended sediment concentration near the sediment-water interface	M/L ³
c_1, c_2, c_3, c_4	Coefficients in Ackers-White Total-Load Predictor	Dimensionless
C_2	Near-bed suspended sediment concentration	M/L ³
c_5, c_6, c_7	Empirical coefficients in Karim and Kennedy flow resistance equation	Dimensionless
C_D	Drag coefficient	Dimensionless
C_f	Drag (friction) coefficient	Dimensionless
c_s	Vertical concentration of the suspended particles	M/L ³
$C_s(i,j,k)$	Sediment Concentration in element (i,j) for level k	M/L ³
C_{sa}	Sediment concentration at reference level a	M/L ³
C_z	Concentration of suspended sediment in the lowest σ layer	M/L ³
d	Particle diameter	L
D	Total water column depth	L
d^*	Dimensionless grain diameter	Dimensionless
D^*	Non-dimensional particle parameter	Dimensionless
D_1	Depositional Flux	M/L ² /T
D_2	Non-cohesive sediment depositional flux	
D_{50}	Median diameter of sediment	L
d_{gr}	Dimensionless grain diameter	Dimensionless
D_j	Sediment diameter for particle size j	L
D_k	Effective particle diameter	L
$dQ(i,j,k)$	Water discharge for level k in element (i,j)	L ³ /T
$dQ_s(i,j,k)$	Sediment load for level k in element (i,j)	M/T
D_u	Representative diameter of bed material	L
$DZ(k)$	Fraction of flow depth attributed to level k	Dimensionless

E	Resuspension flux;	L
	Total energy head	
E_k	Resuspension rate of sediment of class k	$M/L^2/T$
E_{tot}	Total resuspension rate	$M/L^2/T$
f	Coriolis Parameter	T^{-1}
F	F-factor	Dimensionless
F_{gr}	Sediment mobility number	Dimensionless
F_H	Hydrodynamic force	$M/L/T^2$
f_k	Fraction of class k sediment in the cohesive bed	Dimensionless
F_s	Horizontal diffusion for salinity	
F_x	Horizontal viscosity	
F_y	Horizontal diffusion	
F_θ	Horizontal diffusion for temperature	
G	Water column shear stress	$M/L/T^2$
g	Acceleration of gravity	L/T^2
g_s	Bed-material discharge in weight per unit width	M/L
H	Total Energy Head	L
H	Bottom depth relative to $z = 0$	L
h	Mean Flow depth;	L
	Flow depth	L
h_m	Mean flow depth	L
H_s	Wave height	L
K	Conveyance	L^3/T
k_e	Kinetic energy term	L
K_H	Vertical eddy diffusivity for turbulence mixing of heat and salt	L^2/T
K_M	Vertical eddy diffusivity of turbulent momentum mixing	L^2/T
K_s	Manning-Strickler Coefficient	L^3/T
k_s	Nikuradse roughness height	L
L	Wave length	L
ℓ	turbulence macroscale	L
$L(i,j)$	Space-step of element (i,j) normal to the direction of the flow	L
m	Constant dependent upon the depositional environment	Dimensionless

n	Manning's coefficient; Porosity of bed material; Constant dependent upon the depositional environment	$L^{1/3}/T$ Dimensionless Dimensionless
n'	Manning's coefficient component due to particle roughness	$L^{1/3}/T$
$n'(i,j)$	Manning's coefficient for element (i,j)	$L^{1/3}/T$
n''	Manning's coefficient component due to bed forms	$L^{1/3}/T$
n_i	Manning's coefficient for a certain sub-section i	$L^{1/3}/T$
P	Pressure; Power	$M/L/T^2$ ML^2/T
P_I	Probability of deposition	Dimensionless
P_i	Wetted Perimeter for a certain sub- section i	L
P_{ke}	Kinetic Energy Power	ML^2/T
Pt_j	Proportion of size fraction j in the bed material	Dimensionless
Q	Water discharge	L^3/T
q	Lateral inflow; Water discharge per unit width	$L^3/T/L$ $L^3/T/L$
q^2	Turbulent kinetic energy	L^2/T^2
q_d	Sediment flux due to deposition	M/L^2
q_e	Sediment flux due to erosion	M/L^2
Q_s	Volumetric bedload sediment discharge;	L^3/T
	Sediment load	M/T
Q_{ss}	Volumetric suspended load sediment discharge;	L^3/T
	Suspended sediment load	M/T
q_s	Total bed-material load; Sediment discharge per unit width;	$L^3/T/L$
	Suspended load flux	
q_{sb}	Bed load; Volumetric solid discharge per unit width	M/L^2 L^2/T
q_{ss}	Suspended load	L^2/T
q_{sw}	Wash load	L^2/T
q_{sw}	Total sediment discharge for particle size j	L^2/T

R	Hydraulic Radius	L
$r(I,J)$	Roughness factor for element (I,J)	Dimensionless
R_h	Hydraulic Radius	L
R_h'	Hydraulic Radius component for the particle roughness	L
R_h''	Hydraulic Radius component for the bed forms	L
S	Sediment source or sink within the solution domain other than the boundaries;	M/L ³ /T
	Salinity	M/M [ppt]
s	Specific gravity of the particles	Dimensionless
S_f	Steady-State Energy or Friction Slope	Dimensionless
T	Wave period;	T
	Transport Stage parameter	Dimensionless
t	Time	T
T_d	Time after deposition	T
U	Mean flow velocity	L/T
u	Velocity component in the xx direction;	L/T
	Near bed velocity	L/T
u^*	Shear Velocity	L/T
u^*	Shear Velocity due to particle roughness	L/T
$u^{*''}$	Shear Velocity due to bedforms	L/T
$u^{*cr\ bed}$	Critical shear velocity near the bed	L/T
$u^{*cr\ sus}$	Critical shear velocity for resuspension	L/T
U_c	Critical Velocity for beginning of sediment motion	L/T
u_i	Instantaneous flow velocity	L/T
U_p	Near bed orbital velocity	L/T
$V(i,j,k)$	Component of velocity normal to the face of the element (i,j) through which water is flowing for level k	L/T
V_b	Velocity in the grid point nearest the bottom	L/T
v_{ss}	Settling velocity of suspended particles	L/T
w	Vertical velocity component in the zz direction	L/T
w'	Fluctuating velocity component in the vertical direction	L/T
W_j	Karim's hiding factor	Dimensionless

W_p	Submerged weight of a particle	ML/T ²
W_s	Settling velocity of the sediment particles	L/T
$W_{s,1}$	Settling velocity of cohesive suspended sediment flocs	L/T
$W_{s,2}$	Settling velocity of non-cohesive suspended sediment particles	L/T
x	Abscissa measured along the river; Spatial component;	L
y	Water surface elevation Spatial component	L
Z	Rouse Exponent	Dimensionless
z	Bed Elevation; Spatial Vertical Component; Flow depth at the center of the bottom layer	L
Z'	Suspension Parameter	Dimensionless
Z_0	Bottom Friction	L
z_b	Grid point nearest the bottom	L
α	Coefficient in Smagorinsky Parameterization	Dimensionless
β	<i>B-factor</i>	Dimensionless
γ	Specific weight of water	ML/T ² /M ³
γ_f	Specific weight of a fluid	ML/T ² /M ³
γ_s	Specific weight of sediment	ML/T ² /M ³
Δt	Time-step	T
Δx	Horizontal grid spacing in the xx direction	L
Δy	Horizontal grid spacing in the yy direction	L
$\Delta \sigma$	Vertical Increment which varies with thickness	L
ε	Resuspension Potential	M/L ²
ε_j	Exposure correction factor	Dimensionless
ε_s	Diffusivity of the suspended particles	L ² /T
η	Free surface elevation relative to $z = 0$	L
θ	Potential Temperature (or in situ temperature) for shallow water equations; Wave direction	°C
θ_c	Current direction	
θ_{cr}	Critical mobility parameter	Dimensionless

κ	Prandtl Number	Dimensionless
ν	Kinematic Viscosity;	L^2/T
	Velocity component in the yy direction	L/T
ρ	Fluid Density	L/M^3
ρ_o	Reference Density	L/M^3
ρ_s	Sediment Density	L/M^3
τ	Bottom Shear stress	$M/L/T^2$
τ_*	Dimensionless shear stress	Dimensionless
τ_{*cr}	Critical Dimensionless shear stress	Dimensionless
τ'	Bottom Shear stress due to particle roughness	$M/L/T^2$
τ''	Bottom Shear stress due to bedforms	$M/L/T^2$
τ_0	Total Bottom Shear Stress;	$M/L/T^2$
	Average bed level shear stress	$M/L/T^2$
τ_{0c}	Critical Total Bottom Shear Stress	$M/L/T^2$
τ_b	Bottom Shear Stress	$M/L/T^2$
τ_c	Critical shear stress for erosion	$M/L/T^2$
τ_d	Critical shear stress for deposition	$M/L/T^2$
τ_{zx}	Dispersivity	$M/L/T^2$
ψ	Dimensionless intensity of shear stress applied upon the solid particles	Dimensionless
ω	Dummy variable for Partheniades formulation	Dimensionless
Γ_s	Diffusion coefficient	L^2/T
Φ	Intensity of sediment discharge;	Dimensionless
	Difference between wave direction and current direction;	
	Φ -Factor	Dimensionless

ABSTRACT

The presence of man-made levees along the Lower Mississippi River (MR) has significantly reduced the River sediment input to the wetlands and much of the River's sediment is now lost to the Gulf of Mexico. The sediment load in the River has also been decreased by dams and river revetments along the Upper MR. Freshwater and sediment diversions are possible options to help combat land loss. Numerical modeling of hydrodynamics and sediment transport of the MR is a useful tool to evaluate restoration projects and to improve our understanding of the resulting River response. The emphasis of this study is on the fate of sand in the river and the distributaries.

A 3-D unsteady flow mobile-bed model (ECOMSED; HydroQual 2002) of the Lower MR reach between Belle Chasse (RM 76) and downstream of Main Pass (RM 3) was calibrated using field sediment data from 2008 – 2010 (Nittrouer *et al.* 2008; Allison, 2010). The model was used to simulate River currents, diversion sand capture efficiency, erosional and depositional patterns with and without diversions over a short period of time (weeks). The introduction of new diversions at different locations, e.g., Myrtle Grove (RM 59) and Belair (RM 65), with different geometries and with different outflows was studied. A 1-D unsteady flow mobile-bed model (CHARIMA; Holly *et al.* 1990) was used to model the same Lower MR reach. This model was used for longer term simulations (months).

The simulated diversions varied from $28 \text{ m}^3/\text{s}$ (1,000 cfs) to $5,700 \text{ m}^3/\text{s}$ (200,000 cfs) for river flows up to $35,000 \text{ m}^3/\text{s}$ (1.2×10^6 cfs). The model showed that the smaller diversions had little impact on the downstream sand transport. However, the larger diversions had the following effects: 1) reduction in the slope of the hydraulic grade line downstream of the diversion; 2) reduction in the available energy for transport of sand along distributary channels; 3) reduced sand transport capacity in the main channel downstream of the diversion; 4) increased shoaling downstream of the diversion; and 5) a tendency for erosion and possible head-cutting upstream of the diversion.

Keywords: 3-D numerical modeling, 1-D numerical modeling, river diversions, mobile-bed, sediment transport, Lower Mississippi River

1) INTRODUCTION

1.1 Background

The Mississippi River (MR) has been, since the 1800s, a major natural, economic, and industrial resource for the United States. Historically, the MR was a major source of sediment, freshwater, and nutrients to the Louisiana coast. However, the installation of the levee system, along with the dams, and navigation works, prevents the replenishment of the sediment to the delta. The Louisiana's coastal wetlands have been deprived of most of their historic sediment load (about 120 million tons annually), which the river is now transporting to the Gulf of Mexico (Allison and Meselhe, 2010; Parker and Sequeiros 2006).

In order to restore the delta, or at least re-direct part of the sediment being lost, several options are available. One of the most attractive options is the use of river diversions to create new areas of deposition (Parker and Sequeiros 2006). The numerical modeling of hydrodynamics and sediment transport of the MR can be very useful in assessing the potential impacts and behavior of this type of restoration projects for the Louisiana coast (Meselhe *et al.* 2005).

This study includes the one-dimensional and three-dimensional modeling of the Lower MR reach from Belle Chasse, LA (RM 76, RK 121) to downstream of the Main Pass, LA (RM 3, RK 5) as shown in Figure 1.1. Due to the presence of flood protection levees, there are no significant inflows along the reach. There are several existing diversions, e.g. White Ditch, Naomi, West Bay and Bayou Lamoque. The east bank of the River downstream of Bohemia (RM 48, RK 77) has a natural levee, which overtops during high flow periods.

In 2008 and 2009, Pereira *et al.* (2009) used HEC-RAS (USACE 2008), a 1-D quasi-unsteady flow model, to model the bed material transport of the studied MR reach. Davis (2010) developed a HEC-RAS hydrodynamics unsteady flow application from Tarbert Landing (RM 306, KM 492) to the Gulf of Mexico. A 3-D model is now needed to estimate dredging river currents, depositional patterns, tides and salinity intrusion.

The focus of this study is to develop a 3-D numerical model that predicts the sediment transport on the Lower MR and other alluvial rivers and study the effect of river diversions in the system. ECOMSED (HydroQual 2002), a public domain 3-D finite volume, orthogonal curvilinear grid, hydrodynamic and sediment transport code will be prepared to be used for the 3-D modeling of river diversions. The model will support projects that pursue the goal of rebuilding land and inducing the development of a new delta.



Figure 1.1 – Plan View of the Mississippi River Study Area (Source: Visible Earth 2001)

1.2 Statement of the Problem

The interaction between sediment and flow has been extensively studied since the 1940s. Vito Vanoni, Hans Albert Einstein, John Kennedy, Hunter Rouse, and Daryl Simons are among the prominent researchers in this field (Barkdoll and Duan 2008).

The modeling of sediment transport is challenging because of the large number of variables and different time-scales involved in the process. Watershed variables such as precipitation, infiltration, evaporation, and the groundwater table interact with hydraulic variables such as riverbed slope, depth, velocity, turbulence, and bed forms. Due to the complex nature of sediment transport, research studies on the topic, e.g., on predicting bed and suspended load or quantifying the effect of

turbulence on sediment movement, require further experimental, field, and numerical studies (Barkdoll and Duan 2008).

Since the 1980s, a large number of computational hydrodynamic/sediment transport models have been developed. With the rapid developments in numerical methods for fluid mechanics, 3-D sediment computational modeling has become a much more attractive tool for studying the sediment transport in such different environments as rivers, lakes, and coastal areas (Papanicolaou *et al.* 2008). Unlike physical models, computational models are adaptable to different physical domains and are not subject to distortion effects.

The Lower Mississippi River is a very particular environment. During lower flows, it is mostly dominated by the presence of cohesive sediment, requiring the use of cohesive sediment formulations when performing the numerical modeling of the system. Under high flow conditions, when most of the coarser sediments are transported, the river bed behaves essentially like a non-cohesive sediment bed, requiring very different formulations for the calculation of erosion and deposition rates. This unique setting makes the Lower MR both an interesting and extremely difficult environment for the multidimensional numerical modeling of the sediment transport.

In the last few decades, several modeling efforts have been devoted to the Lower Mississippi River. The United States Army Corps of Engineers (USACE) used TABS-MD (Donnel and Letter 1991) to model a portion of the Lower MR that includes the Head of Passes and 10 miles of the main channel and used CH3D-SED to evaluate dredging and channel evolution issues in the Lower MR. Spasojevic and Holly (1994) incorporated a 2-D mobile bed technique into the CH3D model to simulate the sediment transport at the Old River Structure. Barbé, Fagot and McCorquodale (2000) applied HEC-6 to the Lower MR to determine the sensitivity of dredging requirements to flow and relative sediment diversions (Meselhe *et al.* 2005). Meselhe *et al.* (2006) used the 1-D model Mike11 (DHI 2004) to model the Lower MR bed-material transport from Tarbert Landing, MS (RM 306) to Venice, LA (RM 11). Pereira *et al.* (2009) used HEC-RAS (USACE 2008) to model the bed material transport of the studied MR reach. Davis (2010) used HEC-RAS (USACE 2008) for the 1-D unsteady flow modeling of the hydrodynamics of the Lower MR from Tarbert Landing to the Gulf of Mexico.

A review of various publications concerned with the river hydrologic characteristics and several river-modeling applications, e.g. Demuren (1993) and Corti and Pennati (2000), indicated that complex flow patterns of three-dimensional nature characterize the hydrodynamics of the Lower MR. Therefore, a 3-D model is required to provide information on the river's secondary motion, the sediment distribution in the water column and the modeling of the salt water wedge (Meselhe *et al.* 2005).

ECOMSED (HydroQual. 2002), a 3-D finite volume numerical model, will be used for the modeling of sediment transport in the Lower MR. ECOMSED sediment module has been tested and used in numerous applications for modeling both cohesive and non-cohesive sediment transport.

ECOMSED will serve as a tool to study the non-cohesive sediment transport, which will be done by using the van Rijn (1984) entrainment function.

1.3 Objectives

The main objective of this study is to develop a three-dimensional hydrodynamic and non-cohesive sediment transport model for the Lower MR.

The specific objectives of the study are:

- To determine the distribution of non-cohesive sediment for the Lower MR under the existing conditions and with the introduction of new river diversions proposed by the MLODS Study (Lopez and LPBF 2008). Four different scenarios will be tested:
 1. Existing Conditions
 2. Existing Conditions plus a medium size diversion (850 m³/s; 30,000 cfs) at Myrtle Grove (RM59)
 3. Existing Conditions plus a large size diversion (5,700 m³/s; 200,000 cfs) at Belair (RM65)
 4. Existing Conditions plus the multiple diversions proposed in the MLODS Study (Lopez and LPBF 2008) with modification to the existing passes.
- To develop a three-dimensional model for simulating the non-cohesive sediment transport in the Lower MR.
- To develop a one-dimensional model for simulating the non-cohesive sediment transport in the Lower MR.
- To investigate with the aid of numerical models in the large scale diversion of water and sediment in a low energy environment.
- To quantify the impact of river diversions in the flow, energy and sediment available in the system.

1.4 General Methodology and Research Plan

The proposed methodology will be followed to meet the objectives:

1. A literature review will be conducted.
2. A selection criterion will be applied to choose the appropriate one-dimensional and the three-dimensional numerical models. A description of both the one-dimensional and three-dimensional models, and its capabilities will be provided
3. A three-dimensional, finite-volume, sigma-layer, numerical model capable of simulating hydrodynamics and dynamics of sediment transport will be selected and set up for some simplified tests (rectangular channel; trapezoidal channel; grid dependency study).
4. The code of the three-dimensional model will be extended to include the calculation of specific hydrodynamic and sediment transport variables and the sediment transport

formulation will be adapted to allow its application to the Lower MR.

5. Calibration and verification of longer term one-dimensional simulations for the MR will be performed to obtain boundary conditions for the three-dimensional model.
6. The three-dimensional model will be calibrated with base on the available data from the United States Army *Corps* of Engineers (USACE) and the United States Geological Survey (USGS) stations and field data collected by Nittrouer *et al.* (2008) and by Allison (2010).
7. The three-dimensional model will be applied to the Lower MR (Belle Chasse, LA (RM 76, RK 121) to downstream of Main Pass, LA (RM 3, RK 5)) with existing conditions and with the introduction of possible diversions in the MLODS Report (Lopez and LPBF, 2008).

2) LITERATURE REVIEW

2.1 General

Computational fluid dynamics (CFD) is the analysis of systems involving fluid flow, heat transfer and associated phenomena by means of computer-based simulation. The recent advance on high-performance computing hardware and the introduction of user-friendly interfaces have contributed for a broader use of CFD (Versteeg and Malalasekera 2006).

CFD codes are structured around the numerical algorithms that can tackle fluid flow problems. The codes include a pre-processor, a solver and a post-processor (Versteeg and Malalasekera 2006).

The pre-processing stage involves: a) definition of the geometry of the region of interest, the computational domain; b) the sub-division of the domain into a number of smaller, non-overlapping sub-domains, called grid or mesh of cells; c) the selection of the phenomena that need to be modeled; d) the definition of fluid properties and; e) the specification of appropriate boundary conditions (Versteeg and Malalasekera 2006).

There are three numerical solution techniques: finite difference, finite elements and spectral methods. The finite volume method is a special finite difference formulation. The control volume integration distinguishes the finite volume method from the other CFD techniques. The resulting statements express the (exact) conservation of relevant properties for each finite size cell, making its concepts easier to understand by engineers than the finite elements and spectral methods (Versteeg and Malalasekera 2006). Finite volume formulations can be obtained either by a finite difference basis or a finite element basis. The results are identical for one-dimensional problems (Chung 2002).

The finite difference method has the advantage of allowing a simple code structure and computational efficiency. However, it is limited because of the difficulty in accurately fitting irregular geometry. (Chen *et al.* 2007).

Geometry flexibility is the main advantage of the finite elements method. The use of unstructured grids allows the possibility of easily discretizing computational domains corresponding to very complex flow geometries (Kobayashi *et al.* 1998). However, the traditional finite elements method is computationally very expensive and does not provide an explicit way to check the mass conservation in individual cells during the computation (Chen *et al.* 2007).

In the finite volume approach, the integral form of the governing equations is discretized. Since these integral equations can be solved numerically by flux calculation used in the finite difference method over arbitrarily sized triangular meshes, the finite volume approach is better at guaranteeing mass conservation. The finite volume formulation combines the best attributes of finite

difference methods for simple discrete computational efficiency and finite element methods for geometry flexibility (Chen *et al.* 2007).

Post-processing tools usually include: a) domain geometry and grid display; vector plots; b) line and shaded contour plots; c) 2D and 3D surface plots; d) particle tracking; e) view manipulation (translation, rotation, scaling, etc.) and; f) color PostScript output (Versteeg and Malalasekera 2006).

CFD is a very powerful problem additional solving tool but it is no substitute for experimentation (Versteeg and Malalasekera 2006). Any CFD code must be validated by comparison with either experimental test work and/or field measurements.

2.2 Conservativeness

The governing equations of fluid mechanics are mathematical statements of physical conservation laws. In fluid mechanics, any given process must conserve mass, momentum (Newton's second law) and energy (first law of thermodynamics) (Versteeg and Malalasekera 2006). Conservation statements are usually based on the time rate of change of the conserved quantity Φ , which is related to the physical processes occurring within the system and/or its boundaries (Guillot 2009).

In theory, if the grid resolution is high enough, numerical results can be indistinguishable from an exact analytical solution. However, due to computational and time constraints, in practical situations, the numerical results will only be accurate when the discretization scheme possesses certain fundamental properties, namely conservativeness, boundedness and transportiveness (Versteeg and Malalasekera 2006).

In order to assure conservation of a certain transported property Φ for the whole solution domain, the flux of Φ leaving a control volume across a certain face must be equal to the flux of Φ entering the adjacent control volume through the same face. To achieve this, the flux through a common face must be represented in a consistent manner – by one and the same expression – in adjacent control volumes (Versteeg and Malalasekera 2006).

There are several methods to derive the equations of fluid mechanics. The most common procedures are the derivation through the use of a finite control volume or an infinitesimal control volume. The first approach leads to the integral form of the equations, while the second leads to the differential form of the equations (Guillot 2009). The finite volume formulation solves the integral form of the governing equations to be solved numerically by flux calculation, guaranteeing mass conservation in each grid cells and the entire computational domain (Chen *et al.* 2006)).

The basic idea of finite volume or control volume methods is to obtain a system of algebraic equations for a discretized control volume and the control surfaces that envelop this control volume. The conservation of all variables is enforced across the control surfaces, which means that there is no

artificial creation or destruction of a conserved variable. In addition, in the finite volume approach the discretized governing equations retain their physical interpretation (Chung 2002).

2.3 Sigma-Coordinate and Pressure Gradient

The traditional x,y,z coordinate system used in z-level models is often considered to lack flexibility and not be able to describe large bathymetric variations (HydroQual 2002). In the sigma coordinate system, the water column is divided into the same number of grid cells independent of depth, dealing better with bottom topography (Mellor *et al.* 1993).

The sigma-coordinates or terrain-following ocean models started being developed around 30 years ago with the purpose of modeling the turbulent processes in surface and bottom boundary layers and to simulate flows in estuaries and coastal regions. The Blumberg-Mellor model and later the Princeton Ocean Model (POM) (Mellor 2003) are examples of the models developed during the last three decades (Ezer *et al.* 2002).

While sigma-coordinate models allow a smooth representation of topography and are able to simulate interactions between flows and topography, the traditional z-level models have difficulties in simulating overflow processes and bottom boundary layer dynamics because of the step-like representation of topography (Ezer *et al.* 2002).

In the last few years there has been a concern about the errors associated to the use of sigma-coordinate models when modeling areas of steep topography. Mellor *et al.* (1998) point two kinds of sigma coordinate errors: i) “sigma errors of the first kind” (SEFK) and ii) “sigma errors of the second kind” (SESK).

SEFK is a velocity error that occurs in 2-D applications. It is associated with the evaluation of horizontal density or pressure gradients. The error prognostically disappears and leaves a small and physically distortion in the density field. In a finite difference calculation the SEFK always decays (Mellor *et al.* 1998). This type of error cannot be completely eliminated as long as the grid does not follow geopotential or isopycnal surfaces but there are methods to reduce it to an acceptable level below other numerical errors (Ezer *et al.* 2002).

SESK is a 3-D error dependent on the curvature of the topography (Ezer *et al.* 2002). It is a vorticity error and does not vanish prognostically. SESK is smaller than the SEFK before decay and it is nil for 2-D flows. Contrarily to the SEFK, the SESK does not always decay in a finite difference formulation. This type of error doesn’t vanish but it is small and can be reduced by subtracting a horizontally averaged initial density before computing the baroclinic integrals (Mellor *et al.*, 1998).

Smoothing the topography or using a curvilinear grid to better describe the bathymetric contours are two possible ways of reducing the sigma-coordinate pressure gradient errors (Mellor *et al.*, 1998). Retana (2008) presents a benchmark model for an idealized estuary in which the FVCOM pressure gradient error was studied.

2.4 Boundary Conditions

CFD problems are defined in terms of initial and boundary conditions. Correct definitions and implementations of boundary and initial conditions are fundamental in obtaining acceptable and accurate solutions in fluid mechanics. According to (Versteeg and Malalasekera 2006), the most common boundary conditions are: (i) inlet; (ii) outlet; (iii) wall; (iv) prescribed pressure; (v) symmetry; (vi) periodicity (or cyclic boundary conditions).

The definition of boundary conditions depends on the types of partial differential equations used and the physical process dominating the studied flows, e.g., compressibility and turbulence. Partial differential equations are classified as either hyperbolic, parabolic, elliptic, or some combination (Chung 2002; Guillot 2009).

It is important to note that not all types of boundary conditions are appropriate to every boundary and they cannot be arbitrarily specified (Guillot 2009). The boundary conditions should be specified in a way that a problem is well-posed, i.e., satisfies the following conditions: (i) the solution exists; (ii) the solution is unique; and (iii) the solution depends continuously on the initial and boundary conditions.

In a way, the results obtained inside a CFD solution domain are an interpolation of the defined boundary conditions based on the governing equations. The modeling results are no more than a function of the prescribed boundary condition. Thus, physically realistic and well-posed boundary conditions are needed for obtaining accurate and physically relevant solutions (Versteeg and Malalasekera 2006).

2.5 Sediment Transport

In the last few decades, a large number of 1-D, 2-D and 3-D, computational transport models have been developed. The processes simulated in these models can include bed aggradation and degradation, bank failure, local scour around structures, formation of river bends, fining, coarsening and armoring of streambeds, transport of pollutants, settling, deposition, bed consolidation, and wave or current induced sediment transport (Papanicolaou *et al.* 2008).

Traditionally, the motion of a non-cohesive sediment particle is classified in three different modes: i) rolling and sliding motion; ii) saltation motion; and iii) suspended motion. Rolling and sliding occur when the bed-shear velocity is only slightly higher than the critical bed-shear velocity for initiation of movement. Suspension of the particles happens when the bed-shear velocity is high

enough when compared with the critical value to allow the transport without any contact with the bed. Saltation occurs when the bed-shear velocity is high enough to allow the particle to travel for some distance without hitting the bed but not high enough for the particle to be kept in suspension.

Based on the type of particle motion, the materials transported in a stream can be classified as (Graf 1998):

- i) bed load, q_{sb} : the volumetric discharge per unit width of rolling and sliding particles;
- ii) suspended load, q_{ss} : the volumetric discharge per unit width of saltating particles;
- iii) total bed-material load, q_s , (bed load + suspended load): $q_s = q_{sb} + q_{ss}$; and
- iv) wash load, q_{sw} : the particles travel in suspension (are “washed” by the flow); mostly includes the fine cohesive sediment particles.

The transport of sediments by the water flow is a very complex problem. It involves many physical processes, such as turbulence, and cannot be accurately represented by a restricted number of independent variables. Although theoretical formulations can only be used for very simplified cases, they can provide valuable insights into trends. The quantitative determination of sediment transport usually relies on empirical formulas, developed from experimental or field data, which, in general, should not be applied under different conditions from the ones in which they were established.

According to Graf (1998), there are three possible ways of estimating the amount of sediment being transported in a stream: i) using existing formulae; ii) obtaining field measurements with adequate instruments; and iii) performing physical models.

2.5.1 Non-Cohesive Sediment - Bed Load

In bed-load transport, the sediments travel very close to the bed although they may leave it temporarily. In this type of transport the random concept of turbulence plays an important role (Graf 1998). Experimental studies indicate that bed load transport is a function of the surplus shear stress beyond the one needed for incipient motion ($\tau_* - \tau_{*critical}$) (McCorquodale 2006).

Bed load equations can be organized in three different classes: i) DuBoys-Shields type or shear based equations; ii) discharge based equations; or iii) Probability equations, e.g. Einstein. Many of the bed-load methods are of empirical nature, but it is common for the equations to include dimensionless numbers. This type of approach allows the use of the formulas for different conditions from the ones in which they were developed.

The steady and uniform motion of a single particle, isolated and without cohesion, is governed by the following two forces (Graf 1998):

- the hydrodynamic force:
$$F_H \propto f \left(\frac{u_* d}{\nu} \right) \rho d^2 u_*^2 \quad (2.1)$$

- the submerged weight of the particle: $W_p \propto g(\rho_s - \rho)d^3$ (2.2)

The 7 components of the water/sediment flow are (Graf 1998):

- the fluid density, ρ , and viscosity, ν ;
- the solid material density, ρ_s , and a characteristic diameter, d ;
- the flow depth, h or the hydraulic radius, R_h , the slope, S_f , and the gravity, g ; and the friction velocity, $u_* = \sqrt{\rho g R_h S_f}$, which characterizes the turbulence.

The transport of sediments can be expressed as a function of 4 dimensionless quantities, functions of the 7 components referred (Graf 1998):

$$\Phi = f(d_*, \tau_*, R_h / d, \rho_s / \rho) \quad (2.3)$$

where d_* is the dimensionless particle diameter given by:

$$d_* = d \left((s_s - 1) \frac{g}{\nu^2} \right)^{1/3} \quad (2.4)$$

τ_* is a dimensionless shear stress given by:

$$\tau_* = \frac{\rho u_*^2}{(\gamma_s - \gamma)d} = \frac{\tau_0}{(\gamma_s - \gamma)d} = \frac{\gamma R_h S_f}{(\gamma_s - \gamma)d} \quad (2.5)$$

R_h/d is a relative depth and ρ_s/ρ is a relative density.

Using the Π -theorem, one obtains an expression for a dimensionless intensity of the solid discharge as the bed load, or (Graf 1998):

$$\Phi = q_{sb*} = \frac{q_{sb}}{\sqrt{(s_s - 1)gd^3}} \quad (2.6)$$

with q_{sb} [m^2/s] as the volumetric solid discharge per unit width

Since R_h/d and ρ_s/ρ , are included in the term of τ_* , and taking $\tau_* = f(Re_*)$, the following relation can be stated:

$$\Phi = f(\tau_*) \quad \text{or} \quad \frac{q_{sb}}{\sqrt{(s_s - 1)gd^3}} = f\left(\frac{\tau_0}{(\gamma_s - \gamma)d}\right) \quad (2.7)$$

which is often written as (Graf 1998):

$$\Phi = f(\psi) \quad (2.8)$$

where $\tau_* \equiv \psi^{-1}$ and Ψ is called the dimensionless intensity of shear stress, applied upon the solid particles.

The previous expression links the solid transport, q_{sb} , to the shear stress, τ_* . An increase in τ_* - passing by τ_{*cr} , where erosion begins – is responsible for an increase in q_{sb} (Graf 1998).

Function Φ will vary with the case being studied. Its specific formulation is given by the formulae of bed-load transport used.

Function Φ is often expressed in form of a power law, as follows:

$$\Phi = \alpha(\tau_*)^\beta \quad (2.9)$$

Making use of the ratio, which defines the coefficient of friction:

$$\frac{U}{\sqrt{\tau_0 / \rho}} = \sqrt{\frac{8}{f}} \quad (2.10)$$

one can formulate the following proportionalities:

$$U^2 \propto \tau_0 \propto \tau_* \quad (2.11)$$

Thus it is possible to express the power law equation in the form of (Graf 1998; Holly *et al.* 1990):

$$q_{sb} = a_s U^{b_s} \quad (2.12)$$

where a_s , α and $b_s = 2\beta$ are empirical coefficients, essentially dependent on the granulometry of the sediment.

Computational models such as CHARIMA (Holly *et al.* 1990; Holly 2009), allow the use of a power law in sediment transport calculations.

At present, the available bed load formulas give only reasonably satisfying results within a domain of the parameters for which the chosen formula has been established. The application of these formulas requires extreme care and usually a more careful calibration and validation than those based on the equations of physics.

2.5.2 Non-Cohesive Sediment - Suspended Bed Material

In suspended-load transport, the sediments travel by saltation, i.e., they make large jumps and occasionally contact with the bed, and with the bed load. Suspended load transport can be considered as an advanced stage of bed load transport. It consists of the transport of material usually available on the bed, bed-material load, but it increases as a fraction of the total bed material load as the shear stress increases. There are no analytical methods that allow a description of the two modes of transport with the same relationship (Graf 1998).

The concept of diffusion-convection can be used to describe the transport of sediments in suspension. Assuming steady-state and uniform flow, the vertical distribution of the concentration of the suspended particles, $c_s(z)$, in the fluid, can be given by the 1-D diffusion-convection equation (Graf 1998):

$$0 = v_{ss} \frac{\partial c_s}{\partial z} + \frac{\partial}{\partial z} \left(\varepsilon_s \frac{\partial c_s}{\partial z} \right) \quad (2.13)$$

where $c_s(z)$ is the local volumetric concentration, ε_s is the diffusivity of the suspended particles, whose units are $[L^2/T]$, and v_{ss} is the settling velocity of the particles.

Equation 2.13 relates the vertical exchange of solid particles due to the turbulence (upwards) with the gravitational motion (downwards), expressed with the settling velocity, v_{ss} . It is applicable only for low sediment concentrations, namely for $(1 - c_s) \cong 1$ or $c_s < 0.1\%$, meaning that the concentration at the water surface is assumed to be 0 (zero) (Graf 1998).

The integration of Eq. 2.13:

$$v_{ss} c_s + \varepsilon_s \frac{dc_s}{dz} = Constant = 0 \quad (2.14)$$

where the constant of integration is taken to be constant and equal to 0 (zero), implying that $c_s = 0$ at the water surface for $\varepsilon_s = 0$.

For higher concentrations of sediment, the following equation should be applied:

$$v_{ss}c_s(1-c_s) + \varepsilon_s \frac{dc_s}{dz} = 0 \quad (2.14a)$$

where ε_s is the diffusivity of suspended particles in the fluid and ε_t , the turbulent diffusivity of a (soluble) substance in the fluid, related by (Graf 1998):

$$\varepsilon_s = \beta_s \varepsilon_t$$

where $\beta_s \sim 0.5$ to 1 is the Prandtl-Schmidt Number

For weak concentrations it is usually assumed that:

$$\varepsilon_s = \varepsilon_t$$

thus $\beta_s = 1$.

For the case, where the diffusivity is independent of the level, $\varepsilon_s = \text{Constant}$, integrating Eq. 2.14, we obtain:

$$\frac{c_s}{c_{sa}} = \exp\left[-\frac{v_{ss}}{\varepsilon_s}(z-a)\right]$$

where c_{sa} is the concentration at a reference level, a .

Assuming linear shear distribution from the water surface to the bed we can obtain the diffusivity by:

$$\varepsilon_s = \kappa u_*' \frac{z}{h} (h-z) \quad (2.15)$$

and the dispersivity will be given by:

$$\tau_{zx} = \tau_0 \left(\frac{h-z}{h} \right)$$

Combining equations 2.15 and 2.14, and separating the variables, yields:

$$\frac{dc_s}{c_s} = -\frac{v_{ss}}{\kappa u_*'} \left(\frac{h}{h-z} \right) \frac{dz}{z} \quad (2.16)$$

Eq. 2.16, can now be integrated by parts, within the limits of $a < z < h$ and yields:

$$\frac{c_s}{c_{sa}} = \left(\frac{h-z}{z} \cdot \frac{a}{h-a} \right)^Z \quad (2.17)$$

where c_{sa} is the concentration at a reference level, a , an Z is the *Rouse* exponent, defined as:

$$Z = \frac{v_{ss}}{\kappa u_*'} \quad (\text{or } Z' = \frac{v_{ss}}{\beta_s \kappa u_*'}) \quad (2.18)$$

Eq. 2.18, gives the distribution of the relative concentration, c_s/c_{sa} , for one single particle size, v_{ss} and Z (Graf 1998).

There are many different methods for the calculation of the suspended-load transport. Einstein (1950) is probably the most popular one.

2.5.3 Non-Cohesive Sediment - Total Bed-Material Load

Total-load transport (or bed-material load) transport includes the transport of both bed load and suspended load. It can be equated as (Graf 1998):

$$q_s = q_{sb} + q_{ss} \quad (2.19)$$

In same formulations, the transport as wash load, q_{sw} , is also included as part of q_s .

According to Graf (1998), the methods used to determine total load transport can be direct or indirect. In direct methods, the total load is calculated directly, while in indirect methods, bed load and suspended load are calculated separately taking into account the different hydromechanics of the two modes of transport.

Total-load formulae, like bed-load and suspended-load formulae, are based on empirical coefficients and usually give only reasonable results in the domain of their established parameters. The results obtained with such formulae should only be seen as guide-lines. It is always advisable to run tests with several different formulae (Graf 1998).

A verification of these formulae accuracy with base on field measurements is a complicated task. The error margin associated to sediment discharge measurements is high and the distinction of the zones corresponding to each mode of transport is not clear (Graf 1998).

Einstein (1950) proposed a unified total bed material method by converting his computed bed load, q_b , to a reference concentration at a level z above the bed equal to 2 particle diameters (McCorquodale 2006). Many other formulae have been developed since then, including Engelund-Hansen (1967) and Ackers-White (1973) that have been used by the author in previous 1-D HEC-RAS Lower MR studies. These two formulas are among the most used in the world.

2.5.4 Bed Roughness/Friction Relationships

Estimation of friction or roughness coefficients for a fixed bed is a complicated task. Even harder is to estimate the coefficients for flows over a mobile bed. Bed roughness is a function of many parameters, e.g., the bed sediment size and concentration, the available vegetation and the water flow. Thus, while doing numerical modeling, the friction coefficients used are many times determined through calibration instead of being obtained from field measurements.

The Manning-Strickler equation is possibly the most popular uniform flow resistance formula. This formula is available in most of the 1-D numerical models, including CHARIMA and HEC-RAS, and is as follows:

$$U = \frac{1}{n} R_h^{2/3} S_f^{1/2} \text{ (in SI Units)} \quad (2.20)$$

where U is the cross-sectional average velocity, R_h is the hydraulic radius, S_f is the friction slope and n is Manning's friction coefficient. This relationship should be applied only for turbulent, rough flow (large Reynolds numbers) when the coefficient of Manning, n , can assumed to be constant for a given roughness.

In sections where the wetted perimeter is not homogeneous, the bed and the side walls roughnesses will be different. In this case, an equivalent coefficient of friction can be determined as (Chang 1988):

$$n = \left[\frac{\sum_{i=1}^N (P_i n_i^{3/2})}{P} \right]^{2/3} \quad (2.21)$$

where P_i is the wetted perimeter for a certain sub-section i , P is the wetted perimeter of the whole cross-section, N is the total number of sub-sections and n_i is the Manning's n coefficient for a certain sub-section.

The nature of sediment transport in a stream is a function of both the shear flow and the type of bed material (McCorquodale 2006). Flow resistance increases with appearance of bed forms and

subsequently with the increase of bed form size. The total shear stress on the bed, τ_0 , includes the contribution of the roughness due to the particles, τ' , and the one due to the bed forms, τ'' :

$$\tau_0 = \tau' + \tau'' \Leftrightarrow \gamma R_h S_f = \gamma (R_h' + R_h'') S_f \quad (2.22)$$

where R_h' and R_h'' are the hydraulic radius due to the particle roughness and to the bed forms, respectively.

Using the definition of the friction velocity and of the coefficient of friction, one can write:

$$u_*^2 = (u_*')^2 + (u_*'')^2 \quad (2.23)$$

and according to the Cowan formula (Chow 1959):

$$n = n' + n'' \quad (2.24)$$

The total shear stress, τ_0 , varies as a function of the Froude number, Fr .

The most commonly used uniform-flow formulas are the Manning formula, the Chézy formula, and the Darcy-Weisbach formula. Many flow resistance equations for mobile-bed streams have been developed in order to obtain Manning's, Chézy or Darcy-Weisbach friction coefficients as function of hydraulic parameters, usually the average flow depth or the hydraulic radius, and the sediment size. Limerinos (1970), Hey (1979) and Bray (1979) are examples of this type of equations. Among the available methods, some consist on the determination of the entire coefficient of friction, while others include separate calculations to determine the coefficient of friction due to the grain roughness and the coefficient of friction due to the bed forms, f' or n' (Chang 1988).

2.5.5 Cohesive Sediment – Wash Load

2.5.5.1 Overview

Typically particles of size less than 0.06 mm are considered to be fine grained, cohesive sediment. However, according to Torfs (1997), sand as large as 120 μm can exhibit cohesion in salt water. The effect of salinity on the settling of cohesive sediments has been the focus of several studies in the last five decades (Kim and Nestmann 2009).

Modeling the transport of cohesive sediments is, in general, harder than modeling the transport of non-cohesive sediments. The main difference between the transport processes is the way the particles interact. While coarse-grained particles behave as individual particles, fine-grained sediments can form agglomerates of particles called flocs. Water chemistry, organic matter, electrolyte concentration and pH play a major role on flocculation. Chemical and biological effects

play an important role in flocculation but their quantitative effects are hard to determine (Mehta *et al.* 1987; Burban *et al.* 1990).

According to Willis and Krishnappan (2004), the bed shear stress is the most important flow property for modeling cohesive sediment transport. They add that the settling velocity is the most important property of cohesive sediment to be modeled. These two statements seem to be consensual. The author found that most of the studies have the purpose of creating accurate tools to estimate or measure the settling velocity of flocs and the bed shear stress.

The settling velocity is a strong function of the individual particle and the aggregate sizes (Lau and Krishnappan, 1992; Burban *et al.* 1990; Hawley 1982), the pH (Kim and Nestmann 2009; Tambo and Hozumi 1979) and the sediment concentration. Kim and Nestmann (2009) state that the flocculation process is strongly dependent on salinity and Burban *et al.* (1990) show that the settling velocity of flocs specifically is a weak function of salinity. The settling velocity is probably a function of the concentration of Ca^{++} and Mg^{++} ions.

Mehta (1989) finds appropriate to consider the existence of a fluid mud layer that separates the flow from the cohesive bed instead of relying on an erosion/deposition approach like the one used to describe sand transport. Willis and Krishnappan (2004) add that most of the complexity of numerical models for cohesive bed sediments comes from the bookkeeping of layers of sediment below the bed surface, when there is formation of fluid mud. The same authors state that the modeling of fluid mud requires a coupled 3-D or 2-D layered hydraulic model, due to the fact that the fluid behaves as a non-Newtonian fluid.

Maa *et al.* (2008) found that the average-bed-shear stress is not significantly influenced by the present of secondary currents as revealed in comparing their results with those obtained by Mehta (1973). While Mehta obtained values of around 0.18 Pa for the average shear stress without the presence of secondary circulation, Maa *et al.* (2008) results were of around 0.16 Pa for an experimental setting similar to the one used by Mehta (1973) but with significant secondary flow currents.

2.5.5.2 Mathematical Formulation

According to Willis and Krishnappan (2004), the transport characteristics of cohesive sediment in a flow field can be described in terms of a mass balance equation as follows:

$$\frac{\partial \bar{c}}{\partial t} + u_i \frac{\partial \bar{c}}{\partial x_i} + v_i \frac{\partial \bar{c}}{\partial y_i} + w_i \frac{\partial \bar{c}}{\partial z_i} = -\frac{\partial(u'_j c')}{\partial x_i} + S(x, y, z) \quad (2.25)$$

$x_i = x, y, z$ and $u_i = u, v, w$

where \bar{c} is the mean concentration of sediment in suspension; t is the time; \bar{u}_i and u_i are the mean and instantaneous flow velocities, respectively; u'_i and c' are the fluctuating velocity components and fluctuating sediment concentration, respectively; w is the vertical velocity component; w_s is the settling velocity of the sediment particle; and $S(x, y, z)$ is the sediment source or sink within the solution domain other than the boundaries, where x and y are the horizontal spatial components and z is the vertical spatial component.

The boundary conditions are given by the following equations:

$$(w - w_s)\bar{c} + \overline{w'c'} = 0 \text{ (at the free surface)} \quad (2.26)$$

$$-w_s\bar{c} + \overline{w'c'} = q_d + q_e \text{ (at the bed)} \quad (2.27)$$

where q_d and q_e are fluxes due to deposition and erosion, respectively; and w' is the fluctuating velocity component in the vertical direction.

The turbulent flux of sediment can be determined using the eddy diffusivity concept:

$$\overline{u'_i c'} = -\Gamma_{si} \frac{\partial \bar{c}}{\partial x_i} \quad (2.28)$$

where Γ_s is the diffusion coefficient.

For a decoupled approach, in which it is assumed that the sediment transport does not affect the properties of the flow field, the difference between cohesive and non-cohesive sediment transport equations relies in the values of parameters w_s , q_e and q_d , for the two types of sediments (Willis and Krishnappan 2004).

2.6 Flow of Density Current

Under low flow conditions a salt wedge can be observed in the Lower MR traveling several dozens of miles upstream the Head of Passes. In this situation, the salt water, being denser than the fresh water, flows upstream in the bottom of the water column, while fresh water flows downstream in the layers closer to the water surface.

Retana (2008) studied the lock-exchange flow using a physical model and the 3-D finite volume numerical model FVCOM. An overview of density currents can be found in this reference.

2.7 Consistency of External and Internal Modes

The 3-D models FVCOM and ECOMSED use the mode-splitting technique that allows for external wave mode (volume transport) and internal mode (vertical velocity shear) calculations to be solved separately, saving some computational time. Some of the calculations are performed for every internal time-step but others are only performed for every external time-step reducing the frequency of some of the calculations and consequently the computational time.

Retana (2008) describes in some detail the purpose of using the mode-splitting technique and how it is implemented.

2.8 Analytical Solutions for Model Testing

While using numerical models it is always necessary to determine how precise they are and what are the errors associated with the schemes implemented. A comparison between the models results and available analytical solutions is a good way to determine the accuracy of numerical models (Retana 2008).

Retana (2008) used the *quarter-annular case*, an idealization of a tidal coastal domain, developed by the ADCIRC Development Group (2005) to assess the hydrodynamic performance of FVCOM finite volume formulation. The analytical solutions were obtained using the formulation by Lynch and Gray (1978). ECOMSED hydrodynamics model has a similar the finite volume formulation to that used in FVCOM. Thus, Retana (2008) results validate both FVCOM and ECOMSED models for coastal environments.

The purpose of this study is the application of numerical tools in fluvial environments, not in coastal areas. Thus, a simple rectangular channel (width of 500 m and flow depth of 20m) will be set to run with both ECOMSED and FVCOM for a constant flow equal of 15,000 m³/s. The selected dimensions are based in field data, so that flow variables have a MR order of magnitude. This channel will be used for hydrodynamics and sediment transport testing.

2.9 Classification of Models

Models can be classified in two different types: mathematical models and analogue (physical) models. In mathematical models the real phenomena are represented by mathematical relationships. In physical models the real phenomena are represented by another process such as flow in a smaller scale reproduction of the full scale (McCorquodale and Georgiou 2006).

Traditionally physical models were used for three-dimensional flow simulations, particularly when involving sediment transport. With the evolution in computational modeling that occurred in the last twenty years, numerical models have become a much more attractive tool for studying flow and sediment transport in environments such as lakes and rivers (Papanicolaou *et al.* 2008).

The decision of using a physical or a mathematical model relies on the nature of the problem to be solved, the available resources, and the overall cost associated with the problem solution. In some cases a combination of both physical and numerical models can be used to better understand the process being investigated (Papanicolaou *et al.* 2008).

According to Bamgboye and De Vries (1986), the design of a river diversion is so complicated from a hydraulic standpoint, that it is advisable the use of both physical and mathematical models.

2.9.1 Mathematical Models

Mathematical models are called “numerical” or “computational” models, since they are usually solved by digital computers (McCorquodale and Georgiou 2006). Based on the complexity and accuracy of the formulations used, mathematical models can be classified in three classes: (i) black box, (ii) glass box and opaque or (iii) grey box, described as follows.

2.9.1.1 Black Box

This class of models includes the simplest mathematical functions that are fitted to known inputs and outputs. The application of such models is limited to the calibration conditions used in setting it up (McCorquodale and Georgiou 2006).

2.9.1.2 Glass Box

The most complex form of mathematical models attempt to represent all of important processes in the system by solving the differential equations of continuity, momentum, energy, mass transport and other physical, chemical or biological reactions subject to realistic boundary conditions (McCorquodale and Georgiou 2006). Contrarily to black box models, these models can be applied outside of the range of calibration, but with caution (McCorquodale and Georgiou 2006).

2.9.1.3 Opaque or Grey Box

This class includes models that are based on gross simplifications of physical laws, e.g., flux theory, plug flow and diffusion reactor models (McCorquodale and Georgiou 2006).

2.9.2 Analogue or Physical Model

As stated before, when the hydraulic problem to be solved is too complex, it may be necessary to use physical models. A major advantage of physical models is their capacity to reproduce complex flow situations (Ettema *et al.* 2000).

Possibly the biggest limitation of physical modeling is due to scale effects. According to Ettema *et al.* (2000), scale effects can be defined as the incomplete satisfaction of a full set of similitude criteria associated with a particular situation and typically increase in severity as the ratio of prototype to model increases or the number of physical properties to be replicated simultaneously increases.

Physical models can be classified based on their geometric scaling as being undistorted or distorted. The differences are as follows.

2.9.2.1 Undistorted Model

The geometric dimensions are exactly scaled by a constant scaling factor (McCorquodale and Georgiou 2006).

2.9.2.2 Distorted Model

In this case, the dimensions in one of the direction, usually the vertical, is distorted with respect to the other two direction (McCorquodale and Georgiou 2006).

Mathematical models can also be classified on the basis of the range of their applications (e.g., suspended load versus bed-load), their spatial resolution (e.g., one-dimensional (1-D) model; two-dimensional (2-D) model; or three-dimensional model (3-D)), and their temporal resolution (steady and unsteady flow models) (Papanicolaou *et al.* 2008).

The following classification based on spatial-temporal capabilities is presented in McCorquodale and Georgiou (2006):

- 0-D. These models represent the system by a single cell which is usually assumed to be fully mixed.
Box Model e.g. Completely Mixed Reactor
Steady state or unsteady state flows
Steady state or unsteady state mass computations
- 1-D. Models with one spatial dimension, e.g. along a stream or along a water column.
Depth and Width averaged
Steady state or unsteady state flows
Steady state or unsteady water quality computations
Dispersion models like QUAL-2E, which has steady state flows but unsteady state water quality computations, is used where lateral and vertical mixing are not required.
- 2-D. Models with variation in two spatial directions:
Lateral averaged, e.g. Reservoir models, e.g. 2Dc
Depth averaged, e.g. RMA 2 and RMA 4
Steady state or unsteady state flows
Steady state or unsteady state mass computations

- 3-D. Models with variation in three spatial directions:
Advanced mechanistic models that solve in some way the variables in x, y, z space, e.g. ECOMSED
Steady state or unsteady state flows; however, most of these models are unsteady.
Steady state or unsteady state mass computations; however, most of these models are unsteady.

2.10 One-dimensional Modeling Options

2.10.1 HEC-RAS

HEC-RAS is a 1-D numerical model (USACE, 2008). It calculates water surface elevation and the longitudinal profile of the riverbed. The program permits the simulation of tributaries and complex networks. HEC-RAS operates in both steady and unsteady flows over a fixed bed and can simulate steady and quasi-steady flows over a mobile-bed.

The recently released HEC-RAS 4.0 and 4.1 (USACE, 2008) includes a version of HEC-6 (USACE, 1993) for bed material transport. There are fewer transport/entrainment options than in HEC-6. The options available are: (i) Ackers-White; (ii) Engelund-Hansen; (iii) Yang; (iv) Laursen; (v) Toffaleti; (vi) Wilcock. In addition to these entrainment options, there are the following settling velocity equations: (i) Toffaleti; (ii) van Rijn; (iii) Rubey; (iv) the default formulation used in HEC-6. The cohesive sediment modeling can be performed using Krone (1962) and Partheniades (1992) methods.

The sediment option in HEC-RAS runs in the quasi-unsteady mode, i.e. it computes the unsteady hydraulics as a series of steady state events. The sediment transport in HEC-RAS is based on shear stresses computed from these ‘steady’ state events. However, the interaction of the bed profile with the entrainment and transport equations is quasi-dynamic in that the bed is adjusted for erosion or deposition by the Exner Equation. The quasi-steady state hydraulics has to be calibrated separately from the HEC-RAS unsteady hydraulics. Manning’s roughness coefficient, n , is the primary parameter for this calibration. The value of this coefficient can be varied laterally in a cross-section or vertically by making it a function of the flow (Pereira *et al.* 2009).

Although HEC-RAS is a public domain model, it is not an open source code. The calibration of the sediment model in HEC-RAS is somewhat limited, e.g. none of the coefficients, parameters and exponents in the various entrainment functions can be changed by the user. The calibration options include: selection of the best entrainment option to satisfy observed data; selection of the best settling velocity option to satisfy observed data; selection of the best erosion/deposition pattern option; modification of the input temperature and/or grain size distribution. There are obvious constraints on these changes since the inputs still must be consistent with field observations (Pereira *et al.* 2009).

2.10.2 CHARIMA

CHARIMA (Holly *et al.* 1990, Holly 2009) is a one-dimensional unsteady state computational model prepared for the simulation of steady or unsteady water, sediment, and contaminant movement in simple or complex systems of channels.

The model is prepared to simulate bedload and/or suspended-load transport of mixtures of non-cohesive or cohesive sediment, along with the associated short- or long-term bed-level changes (aggradation and degradation), bed-sediment sorting, and armoring. Subsurface layering is also included (*from www.iuhr.uiowa.edu/projects/charima/index.html*).

The Preissmann four-point implicit finite-difference scheme is used for the hydrodynamic computation. Mobile-bed dynamics, e.g., bed erosion and aggradation, rely on the modified Exner equation with a suspended-sediment source/sink term. The model formulation accommodates reverse unsteady flow (*from www.iuhr.uiowa.edu/projects/charima/index.html*).

The four total-load predictors adopted for use in CHARIMA are: (i) Modified TLTM method (Karim 1985); (ii) Modified Ackers-White Method (Proffitt and Sutherland 1983); (iii) Engelund-Hansen Method (1967); (iv) Power-law Method. In CHARIMA, Karim and Kennedy (1982) formula is used for the friction-factor predictor. In alternative, the Strickler coefficient (K_s) or the friction factor (f) can also be given as inputs (Holly *et al.* 1990).

CHARIMA is based on a decoupling procedure, whose validity is based on the hypotheses that the changes experienced by a variable in each time-step are small enough so that its effect in other variables can be ignored. In a single-channel model, CHARIMA uses the double sweep method (Liggett and Cunge 1975), first solving the de St. Venant equations, “freezing” the river bed, and then solving Exner equation, a sediment discharge equation and other mobile-bed sorting and armoring equations to obtain the new bed elevations z (*from www.iuhr.uiowa.edu/projects/charima/index.html*).

2.11 Three-dimensional Modeling Options

2.11.1 Finite-Volume Coastal Oceanographic Model (FVCOM)

FVCOM (Chen *et al.* 2003) is a 3-D finite volume model and uses the hydrostatic approximation for the vertical momentum. FVCOM was developed for coastal and ocean modeling applications and it has its origin in the Princeton Ocean Model (POM). It has been successfully applied to tidal estuaries and tidal channels (Xue *et al.*, 2009; Retana, 2008; Zheng and Chen, 2000). Some features of the model include a finite-volume formulation, which ensures mass conservation in the transport equations, and the use of unstructured triangular elements, which allows a better fitting of the geometry and better resolution in key-areas. FVCOM can be run in serial or parallel modes.

While FVCOM has been used in numerous applications, it has not been extensively applied to riverine modeling. As a result, it is yet to be used for non-cohesive sediment transport. Additionally, the original code only includes the Meyer-Peter and Müller (1948) total load formula as a transport/entrainment option. Due to this fact, FVCOM is basically limited to be used for hydrodynamics modeling.

The FVCOM code was modified in this study to allow the use of variable roughness coefficients in time, given as an input file. This feature allows a better calibration of river hydrodynamics, where water discharges and elevations vary widely in time.

2.11.2 Estuarine, Coastal and Ocean Modeling System with Sediments (ECOMSED)

ECOMSED (HydroQual 2002) is a 3-D finite volume hydrodynamic and sediment transport model that allows the computation of water circulation, temperature, salinity, and mixing and the transport of cohesive and non-cohesive sediments. The complete ECOMSED model consists of several modules which can be linked internally or externally. These are hydrodynamic module, sediment transport module, wind induced wave module, heat flux module and particle tracking module. The ECOMSED is also coupled with HydroQual's quality model, RCA. This code runs in serial mode only.

The sediment transport module can calculate temporal and spatial distributions of: (1) suspended sediment concentrations (cohesive and non-cohesive); (2) sediment bed elevation changes; (3) fluxes at sediment-water interface; and (4) changes in sediment bed composition (HydroQual 2002).

In ECOMSED, the suspended transport of non-cohesive sediments is calculated using van Rijn procedures (van Rijn 1984). Similarly to HEC-RAS, the deposition of cohesive materials can be simulated using Krone (1962) and Partheniades (1992) approaches. A one-dimensional Mike11 (DHI 2004) application to the Lower MR developed by Meselhe *et al.* (2006) shows that the van Rijn formulation is a good option.

3) RESEARCH PLAN

This chapter gives an overview of the methodology used to select and develop a model to accurately simulate the sediment transport on a Lower MR reach. In order to simulate secondary currents and sediment distribution in the water column, a three-dimensional model will be selected for this purpose. A one-dimensional model will be used to provide boundary conditions and longer term sediment simulations. The following steps will be taken:

1. Selection Criteria

Capabilities such as the type of grid or the numerical solution technique and the models applicability for the modeling of sediment transport in alluvial rivers are among the considered model attributes. Section 3.1 gives a detailed description of the selection criteria.

2. Model Development

Details of how the selected models met the criteria are given in Chapter 4. An overview of numerical river modeling physical and mathematical principles used, its advantages and disadvantages, as well as theoretical basis, skills and weaknesses is shown.

3. Model Testing and Sensitivity Analysis

After selecting an appropriate model/tool, the next step is to set up the model to be applied to the Lower MR. Data collection, grid design and definition of boundary conditions are part of the model development. The three-dimensional model was initially tested against standard or benchmark datasets with well defined solutions (analytical or experimental) e.g., the hydrodynamics of a relatively short reach (15 miles) and the bed-material transport on a rectangular channel. Preliminary tests with the one-dimensional model included hydrodynamic simulation with a rectangular channel, simulations with the main stem of the river and hydrodynamic and sediment transport steady-state simulations.

4. Model Calibration, Validation

Both one-dimensional and three-dimensional models were used to model the bed-material transport of the Lower Mississippi River reach from Belle Chasse (RM 76) to Downstream of the Main Pass (RM 3). Short-term (10 days) three-dimensional simulations and longer-term (several months to a year) one-dimensional simulations were performed.

The models were first calibrated and validated for hydrodynamics using existing conditions. Sediment calibration followed hydrodynamic calibration and validation. 2007 and 2008 data was used. The ECOMSED code had to be adapted for sediment calibration to be possible. The main changes and additions to the original ECOMSED code are described in Chapter 4.

5. Model Application

After calibrating and validating the models for existing conditions, the following scenarios were tested: 1) Existing Outflows; 2) Introduction of a medium size diversion (peak flow of 850 m³/s) on the West bank of the main channel at Myrtle Grove; 3) Introduction of a large size diversion

on the East bank at Belair (peak flow of 5,700 m³/s); 4) Introduction of several small, medium and large size diversions proposed in the MLOD Study (Lopez and LPBF 2008).

The one-dimensional model was used to estimate the sand loads and concentrations in both main channel and the diversions over a longer time period while the three-dimensional model was used for the same purpose but under close to steady-state condition for peak flows (34,000 m³/s) and Intermediate Flows (23,000 m³/s).

The three-dimensional model was necessary for determination of deposition and erosion patterns with focus on localized changes, particularly in the vicinity of river diversions.

3.1 Selection Criteria

The selection of a model to solve a specific problem is based on the nature and complexity of the problem, the questions that the model should be able to answer, the type and amount of data available for both model calibration and verification, and the available time and budget for solving the problem (Papanicolaou *et al.*, 2008, McCorquodale and Georgiou, 2006).

In agreement with McCorquodale and Georgiou (2006), the following attributes are used for model selection in the present study:

- Availability of the model
- Dimensionality of the model
- Processes included in the model
- Model assumptions and limitations
- Cost of obtaining and implementing the code
- Access to the source code, e.g. proprietary versus public domain
- Hardware and software requirements
- Type of grid, e.g. structured or unstructured and sigma versus z-level
- Order of accuracy of numerical schemes that are used
- Formulation, e.g. finite volume or finite element
- Mass conservation characteristics
- Execution efficiency
- Precedence for using this model at the site or similar site and the quality of the outcome
- Site specific requirements, e.g. branching or hydraulic structures
- Expertise needed to learn and apply the model
- Data requirements for calibration, validation and application of the model

4) MODELS DEVELOPMENT

4.1 Rationale for Models Choice

Pereira *et al.* (2009) applied HEC-RAS to study the sand transport in the main stem of the Lower River. Davis (2010) used HEC-RAS for the hydrodynamics of the Lower River including confluences and flow split; however, HEC-RAS does not have the capability to model sand transport at confluences and flow splits. The possible 1-D and 3-D models for the Lower Mississippi River were presented in Chapter 2. All the models proved to be useful for some aspects of the study. Nonetheless, the final simulations of the sand transport were made with a 1-D model, CHARIMA and a 3-D model, ECOMSED. The downstream boundary conditions and the distributary boundary conditions for ECOMSED were obtained from Davis (2010) HEC-RAS simulations.

CHARIMA was selected over HEC-RAS for three main reasons: 1) allows the simulation of sediment transport with fully unsteady flow; 2) it computes the sediment exchanges at junctions; and 3) allows the user to input/change more parameters than HEC-RAS, which permits a better calibration. In addition, Dr. Forrest Holly provided access to the source code of CHARIMA.

ECOMSED and FVCOM are both 3-D models which are based on the original Princeton Ocean Model (POM) code (Mellor 2003). FVCOM has the advantages of running in parallel mode, using an unstructured grid formulation and having a wetting and drying scheme implemented in the code. However, the FVCOM sediment module is still being developed, meaning that it is not parallelized and has not been applied for non-cohesive sediment, while ECOMSED has a functional sediment module that has been used and tested for both cohesive and non-cohesive sediment transport. For this reason, ECOMSED was selected for the three-dimensional sediment study.

4.2 Model Description CHARIMA

CHARIMA (Holly *et al.* 1990, Holly 2009) is a one-dimensional code that can simulate steady and unsteady-flow regimes, sediment, and contaminant movement in simple channels or fluvial networks. Mobile-bed capabilities include bedload and/or suspended-load transport of mixtures of non-cohesive or cohesive sediment, along with the associated short or long-term bed level changes, bed sediment sorting, armoring and subsurface layering (*from www.iuhr.uiowa.edu/projects/charima/index.html*).

4.2.1 Governing Equations

The de St. Venant (1871) equations for unsteady flow are based on the following series of assumptions: a) the flow is one-dimensional, i.e. the velocity is uniform over the cross section and the water level across the section is horizontal; b) the streamline curvature is small and vertical accelerations are negligible hence the pressure is hydrostatic; c) the effects of boundary friction and turbulence can be accounted for through resistance laws analogous to those used for steady state flow; d) the average channel bed slope is small so that the cosine of the angle it makes with the horizontal may be replaced by unity.

There are many formulations expressing the interrelation of the sediment transport and water flow in unsteady situations; the simplest acceptable mathematical description is summarized by the following system of equations:

Water-Continuity Equation

$$\frac{\partial A}{\partial t} + \frac{\partial Q}{\partial x} = q \quad (4.1)$$

Momentum Equation

$$\frac{\partial Q}{\partial t} + \frac{\partial}{\partial x} \left(\alpha \frac{Q^2}{A} \right) + gA \frac{\partial y}{\partial x} + gA = \frac{Q|Q|}{K^2} = 0 \quad (4.2)$$

Continuity equation for solid discharge (modified Exner)

$$(1 - n) \tilde{B} \frac{\partial z}{\partial t} + \frac{\partial Q_s}{\partial x} = S \quad (4.3)$$

The suspended-sediment transport formula

$$\frac{\partial C}{\partial t} + \frac{\partial}{\partial x} \left(\frac{QC}{A} \right) = \frac{1}{A} \frac{\partial}{\partial x} \left(AK_x \frac{\partial C}{\partial x} \right) + \frac{S}{A} \quad (4.4)$$

where Q = water discharge; A = cross-sectional area; y = water surface elevation; g = gravitational acceleration; x = abscissa measured along the river; α = momentum correction factor; t = time; q = lateral inflow; z = bed elevation; S_f = steady state energy slope; Q_s = volumetric bedload sediment discharge; \tilde{B} = water surface width of the section affected by bed load transport; n = porosity of the bed material; K = conveyance; S represents symbolically the source-sink exchange of solid material between the bed layer and suspension, and C = suspended-load concentration.

The modified Exner and the suspended-sediment transport formulas are symbolic, representing a summation over all sediment classes, each class being transported all or partly as suspended load or bedload, the allocation being variable in space and time. Holly and Rahuel (1990) present a more detailed description of the equations and their terms of reference.

Equations (4.1)-(4.4) form a non-linear partial differential system that can be solved by numerical methods of integration. The equations are complemented by empirical relations for bedload transport capacity, near-bed equilibrium suspended-sediment concentration, and bedload-suspended load allocation factors depending on local shear stress, for each size class.

CHARIMA is based on a decoupling procedure, whose validity is based on the hypotheses that the changes suffered by a variable in each time-step are small enough so that its effect in other variables can be ignored. In a single-channel model, CHARIMA uses the double sweep method (Liggett and Cunge 1975), first solving the de St. Venant equations (4.1.) and (4.2), “freezing” the river bed, and then solving equations (4.3) and (4.4) and other mobile-bed sorting and armoring equations to obtain the new bed elevations z .

The Preissmann four-point implicit finite-difference scheme is used for the hydrodynamics computation. Mobile-bed dynamics, including bed elevation changes, sorting and armoring, are based on the modified Exner equation with a suspended-sediment source/sink term. Subsurface layering is included. All equations and their numerical solution procedures accommodate reversing unsteady flow, e.g. in estuaries (*from www.iihr.uiowa.edu/projects/charima/index.html*).

To simulate the presence of weirs in fluvial networks, CHARIMA, includes among its non-fluvial links a special “weir-type” link. Two distinct weir regimes are available: free flowing and flooded. The simulation of gated structures is also done through the use of a “gate-type” link. In these links special boundary conditions, appropriate for the hydraulic structure being represented, are applied.

In CHARIMA, the friction calculations can be performed using three different approaches: a) Karim and Kennedy (1982) formula can be used for the friction-factor predictor; b) the Strickler coefficient (K_s) can be given as an input for each cross-section; c) the Darcy-Weisbach friction factor (f) can be given as an input for each cross-section.

Karim and Kennedy (1982) formulation is as follows:

$$\frac{U}{\sqrt{g(s-1)D_{50}}} = c_5 \left[\frac{q}{\sqrt{g(s-1)D_{50}^3}} \right]^{c_6} (10^3 C_f)^{c_7} \quad (4.5)$$

where q = unit water discharge; c_5 , c_6 and c_7 are the coefficients determined with base on regression analysis of 615 flow measurements by Karim and Kennedy (1982), with values of $c_5 = 0.33$, $c_6 = 0.376$ and $c_7 = 0.310$.

4.2.2 The Sediment Transport Formulations

The critical shear stress for initiation of sediment motion can be calculated by the use of two different formulations: Rouse (1939), which is an adaptation of the Shields Curve, and Iwagaki (1956).

Iwagaki formulation is as follows:

$$R_0^* = \frac{\sqrt{(s-1)gD_{50}^3}}{\nu} \quad (4.6)$$

$$\frac{\tau_{oc}}{(\gamma_s - \gamma_f)D_{50}} = 0.05 \quad R_0^* \geq 671.0 \quad (4.7)$$

$$\frac{\tau_{oc}}{(\gamma_s - \gamma_f)D_{50}} = 8.45 \times 10^{-3} (R_0^*)^{3/11} \quad 162.7 \leq R_0^* \leq 671.0 \quad (4.8)$$

$$\frac{\tau_{oc}}{(\gamma_s - \gamma_f)D_{50}} = 0.034 \quad 54.2 \leq R_0^* \leq 162.7 \quad (4.9)$$

$$\frac{\tau_{oc}}{(\gamma_s - \gamma_f)D_{50}} = 0.195 (R_0^*)^{-7/16} \quad 2.14 \leq R_0^* \leq 54.2 \quad (4.10)$$

$$\frac{\tau_{oc}}{(\gamma_s - \gamma_f)D_{50}} = 0.14 \quad R_0^* \leq 2.14 \quad (4.11)$$

4.2.2.1 The cohesive sediment formulation

The erosion and deposition of cohesive sediments is calculated using the formulation proposed in Mehta (1987).

4.2.2.2 The non-cohesive sediment formulation

The four total-load predictors adopted for use in CHARIMA are: i) Modified TLTM method (Karim 1985); ii) Modified Ackers-White Method (Proffitt and Sutherland 1983); iii) Engelund-Hansen Method (1967); iv) Power-law Method.

TLTM Method

The TLM method was developed by Karim and Kennedy (1982) and later modified by Karim (1985). The sediment discharge per unit width is obtained as follows:

$$\log \left(\frac{q_s}{\sqrt{g(s-1)D_{50}^3}} \right) = a_0 + a_1 \log V_1 + a_2 \log V_1 \log V_3 + a_3 \log V_2 \log V_3 \quad (4.12)$$

where

$$V_1 = \frac{U}{\sqrt{g(s-1)D_{50}}} ; V_2 = \frac{h_m}{D_{50}} ; V_3 = \frac{u_* - u_{*c}}{\sqrt{g(s-1)D_{50}}}$$

where q_s = total sediment discharge per unit width; U = average velocity; h_m = mean flow depth; a_0, a_1, a_2, a_3 are coefficients determined from linear regression ($a_0 = -2.278$; $a_1 = 2.972$; $a_2 = 1.06$; $a_3 = 0.299$) for 615 flow measurements analyzed by Karim and Kennedy (1982); u_* = bottom shear velocity; and u_{*c} = critical bottom shear velocity.

The total sediment load by size fraction is calculated with the formulation:

$$q_{sj} = q_s(D_j)W_jPt_j \quad (4.13)$$

where q_{sj} = total sediment discharge for particle size j ; $q_s(D_j)$ = sediment discharge computed from equation (4.13) by the use of D_j instead of D_{50} ; Pt_j = proportion of size fraction j in the bed material; W_j is Karim's hiding factor.

The hiding factor proposed by Karim is given by:

$$W_j = b_1 \left(\frac{D_j}{D_u} \right)^{b_2} \quad (4.14)$$

where b_1 and b_2 are calibration coefficients and D_u is a representative size of the bed material, usually taken as D_{50} .

Ackers-White Formulation

The Ackers-White (1973) total-load predictor was developed for uniform sediments and has been expanded by Proffitt and Sutherland (1983) to calculate the sediment transport for non-uniform sediments. The original Ackers-White (1973) formula for uniform sediments is:

$$\bar{C}_T = \frac{\gamma_s D c_2 \left(\frac{F_{gr}}{c_3} - 1 \right)^{c_4}}{(u_* / U)^{c_1} \gamma_f d} \quad (4.15)$$

with the sediment mobility number, F_{gr} , given by:

$$F_{gr} = \left(\frac{u_*^{c_1}}{\sqrt{(s-1)gD_{35}}} \right) \left(\frac{U}{\sqrt{32 \log(10d / D_{35})}} \right)^{1-c_1} \quad (4.16)$$

and the dimensionless grain diameter, d_{gr} , is:

$$d_{gr} = ((s-1)g / \nu^2)^{1/3} D_{35} \quad (4.17)$$

for $1.0 < d_{gr} < 60.0$:

$$c_1 = 1.0 - 0.56 \log d_{gr}; c_2 = 10^{(2.86 \log d_{gr} - (\log d_{gr})^2 - 3.53)}; c_3 = 0.23 / d_{gr}^{1/2} + 0.14; c_4 = 9.66 / d_{gr} + 1.34$$

for $d_{gr} > 60.0$:

$$c_1 = 0.0; c_2 = 0.025; c_3 = 0.17; c_4 = 1.5$$

where, \bar{C}_T = sediment flux concentration (sediment mass flux per unit mass flow rate). To apply this formulation for nonuniform sediments, D_{35} must be replaced by each size fraction diameter and F_{gr} must be corrected by an exposure correction factor, ε_j , given as follows:

$$\varepsilon_j = \frac{F_{gr}(\text{To satisfy the measured data})}{F_{gr}(\text{for uniform sediments with } D = D_j)} \quad (4.18)$$

Proffitt and Sutherland (1983) give ε_j as follows:

$$\varepsilon_j = 1.3 \quad D_j / D_u > 3.7 \quad (4.19)$$

$$\varepsilon_j = 0.53 \log (D_j / D_u) + 1.0 \quad 0.075 < D_j / D_u < 3.7 \quad (4.20)$$

$$\varepsilon_j = 0.4 \quad D_j/D_u < 0.075 \quad (4.21)$$

The diameter D_u can be determined by a formula defined by Proffitt and Sutherland (1983):

$$\frac{D_u}{D_{50}} = f \left[\frac{U_*^2}{g(s-1)D_{50}} \right] \quad (4.22)$$

or D_u can simply be taken as D_{50} .

Engelund-Hansen Formulation

The Engelund-Hansen (1967) formulation for the total bed-material load is:

$$g_s = 0.05 \gamma_s U^2 \sqrt{\frac{D_{50}}{g \left(\frac{\gamma_s}{\gamma} - 1 \right)}} \left[\frac{\tau_0}{(\gamma_s - \gamma) D_{50}} \right]^{3/2} \quad (4.23)$$

where g_s = the bed material discharge in weight per unit width; U = mean flow velocity; D_{50} = median fall diameter of bed sediment; γ = specific weight of water; $\gamma_s = \gamma S_s$ = specific weight of sediment where $S_s = 2.65$; $\tau_0 = \gamma h S_f$ = average bed level shear stress; h = mean flow depth; q_s

(discharge per unit width) = $\frac{g_s}{\gamma_s}$

This formula was calibrated from flume data obtained with a 2.4 m wide and 45 m long channel. Sediment diameters ranging from 0.19 mm to 0.93 mm were used (Holly *et al.* 1990).

According to Garde and Raju (2000), the Engelund-Hansen formulation does not adequately describe the suspended sediment transport and there is no method to calculate the sediment load per size-fraction. However, the equation has produced reasonable results for alluvial rivers. The author has used this formulation in a CHARIMA application to the Mondego River in Portugal (Pereira *et al.* 2007; Pereira 2007) and in a preliminary application of HEC-RAS to the Lower Mississippi River reach from Tarbert Landing (RM 306) to Venice (RM 11) presented in Pereira *et al.* (2009) and Meselhe *et al.* (2010).

Power-Law

The model allows the user to give an empirical power-law relation between the sediment transport rate and a know flow parameter such as the discharge. According to Holly *et al.* (1990) the

most reasonable way is to select the effective velocity (difference between flow velocity and critical velocity) as the flow parameter to be used:

$$q_s = a(U - U_c)^b \quad (4.24)$$

in which q_s = sediment discharge per unit width (L^3/TL); a , b = regression constants from available data; U = mean flow velocity; U_c = critical velocity for sediment motion.

4.2.3 The Program structure

CHARIMA is written in FORTRAN 77. The model can run in both Windows and LINUX/UNIX environments. The code consists of a main program (NEWMAIN.f) and other 85 files. A simplified flowchart of the solution strategy in one time-step including water and sediment calculations is presented in Figure 4.1. A user-friendly interface, developed in Visual Basic, for Windows environments has recently been released. This interface doesn't yet allow the creation of new input files but it allows the user to update the input files and check their formatting as well as running the application making the model more user-friendly.

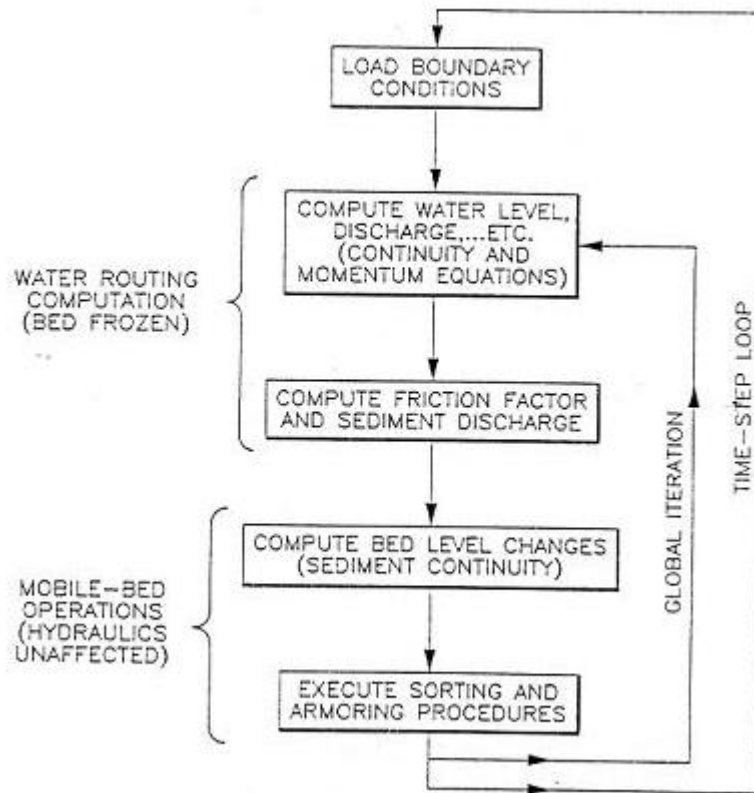


Figure 4.1 – Flow chart for solution strategy in one time-step for CHARIMA (Source: Holly et al. 1990)

4.3 Model Description ECOMSED

ECOMSED is a fully integrated 3-D hydrodynamic, wave and sediment transport model. The model has the purpose of simulating time-dependent distributions of water levels, currents, temperature, salinity, tracers, cohesive and non-cohesive sediments in both fresh and saltwater environments (HydroQual 2002).

ECOMSED uses a finite volume formulation and an orthogonal curvilinear computation grid structure in the horizontal plane. Although the model doesn't allow the use of unstructured grids, the curvilinear grid option allows a good description of a meandering river and permits some refinement in key-areas.

The model is composed of several modules: hydrodynamic module, sediment transport module, wind induced wave module, heat flux module and particle tracking module. In this section, the focus will be on the hydrodynamic and sediment transport modules.

4.3.1 Dynamic and Thermodynamic Equations

Consider a system of orthogonal Cartesian coordinates with x increasing eastward, y increasing northward, and z increasing vertically upwards. The free surface is located at $z = \eta(x, y, t)$ and the bottom is at $z = -H(x, y)$. If \vec{V} is the horizontal velocity vector with components (U, V) and ∇ the horizontal gradient operator, the continuity equation is:

$$\nabla \cdot \vec{V} \frac{\partial W}{\partial z} = 0 \quad (4.25)$$

In Cartesian coordinates, the Reynolds Averaged Navier-Stokes (RANS) equations to describe the fluid momentum equations are:

$$\frac{\partial U}{\partial t} + \vec{V} \nabla U + W \frac{\partial U}{\partial z} - fV = -\frac{1}{\rho_o} \frac{\partial P}{\partial x} + \frac{\partial}{\partial z} \left(K_m \frac{\partial U}{\partial z} \right) + F_x \quad (4.26)$$

$$\frac{\partial V}{\partial t} + \vec{V} \nabla V + W \frac{\partial V}{\partial z} - fU = -\frac{1}{\rho_o} \frac{\partial P}{\partial y} + \frac{\partial}{\partial z} \left(K_M \frac{\partial V}{\partial z} \right) + F_y \quad (4.27)$$

$$\rho g = -\frac{\partial P}{\partial z} \quad (4.28)$$

with ρ_0 the reference density, ρ the in situ density, g the gravitational acceleration, P the pressure, K_M the vertical eddy diffusivity of turbulent momentum mixing. A latitudinal variation of the Coriolis parameter, f , is introduced by use of the β plane approximation (HydroQual 2002).

For Cartesian coordinates the conservation equations for Temperature and Salinity come:

$$\frac{\partial \theta}{\partial t} + \vec{V} \Delta \theta + W \frac{\partial \theta}{\partial z} = \frac{\partial}{\partial z} \left(K_M \frac{\partial \theta}{\partial z} \right) + F_\theta \quad (4.29)$$

$$\frac{\partial S}{\partial t} + \vec{V} \Delta S + W \frac{\partial S}{\partial z} = \frac{\partial}{\partial z} \left(K_M \frac{\partial S}{\partial z} \right) + F_s \quad (4.30)$$

where θ is the potential temperature (or in situ temperature for shallow water equations), and S is the salinity. The vertical eddy diffusivity for turbulent mixing of heat and salt is denoted as K_H . The vertical eddy diffusivity for turbulent mixing of heat and salt is denoted as K_H .

Using the temperature and salinity, the density is computed according to an equation given by Fofonoff (1962) (HydroQual 2002):

$$\rho = \rho(\theta, S) \quad (4.31)$$

In which ρ is the potential density, (density evaluated as a function of potential temperature and salinity, but at atmospheric pressure).

The bottom shear stress is determined by matching velocities with the logarithmic wall, as follows:

$$\bar{\tau}_b = \rho_0 C_D |V_b| V_b \quad (4.32)$$

where C_D is the drag coefficient and is given by:

$$C_D = \max \left(\left[\frac{1}{\kappa} \ln(H + z_b) / z_0 \right]^{-2}, C_f \right) \quad (4.33)$$

In which z_b and V_b are the grid point and corresponding velocity in the grid point nearest the bottom, κ is the von Karman constant taken to be equal to 0.4, and C_f is the drag coefficient given by the user, with a default value of 0.0025 set by the model.

In ECOMSED, to better describe large bathymetric irregularities, the vertical calculations are performed using the sigma-coordinate system instead of the Cartesian coordinate system. Figure 4.2 illustrates the sigma coordinate system. The conversion between Cartesian and sigma-coordinate system consists of a definition of σ as a function of z :

$$\sigma = \frac{z - \eta}{H + \eta} = \frac{z - \eta}{D} \quad (4.34)$$

where D is the total water column, H is the bottom depth relative to $z = 0$, and η is the free water surface elevation relative to $z = 0$.

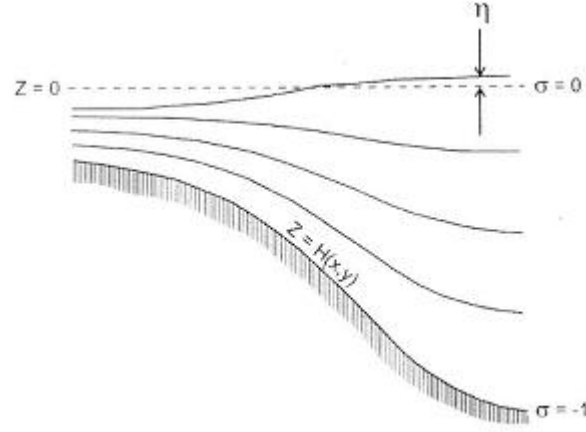


Figure 4.2 – The sigma coordinate system (Source: HydroQual 2002)

The transformation of coordinates gives the following changes in the derivatives for Equations (4.25) to (4.30):

Water Continuity

$$\frac{\partial \eta}{\partial t} + \frac{\partial UD}{\partial x} + \frac{\partial VD}{\partial y} + \frac{\partial \omega}{\partial \sigma} = 0 \quad (4.35)$$

RANS momentum equations

$$\begin{aligned} & \frac{\partial UD}{\partial t} + \frac{\partial U^2 D}{\partial x} + \frac{\partial UVD}{\partial y} + \frac{\partial U\omega}{\partial \sigma} - fVD + gD \frac{\partial \eta}{\partial x} \\ &= \frac{\partial}{\partial \sigma} \left(\frac{K_M}{D} \frac{\partial U}{\partial \sigma} \right) \frac{gD^2}{\rho_0} \frac{\partial}{\partial x} \int_{\sigma}^{\sigma_0} \rho d\sigma + \frac{gD}{\rho_0} \frac{\partial D}{\partial x} \int_{\sigma}^{\sigma_0} \sigma \frac{\partial \rho}{\partial \sigma} d\sigma + F_x \end{aligned} \quad (4.36)$$

$$\begin{aligned} & \frac{\partial VD}{\partial t} + \frac{\partial UVD}{\partial x} + \frac{\partial V^2 D}{\partial y} + \frac{\partial V\omega}{\partial \sigma} + fUD + gD \frac{\partial \eta}{\partial y} \\ &= \frac{\partial}{\partial \sigma} \left(\frac{K_M}{D} \frac{\partial V}{\partial \sigma} \right) \frac{gD^2}{\rho_0} \frac{\partial}{\partial y} \int_{\sigma}^{\sigma_0} \rho d\sigma + \frac{gD}{\rho_0} \frac{\partial D}{\partial y} \int_{\sigma}^{\sigma_0} \sigma \frac{\partial \rho}{\partial \sigma} d\sigma + F_y \end{aligned} \quad (4.37)$$

Conservation of Temperature and Salinity

$$\frac{\partial \Theta D}{\partial t} + \frac{\partial \Theta UD}{\partial x} + \frac{\partial \Theta VD}{\partial y} + \frac{\partial \Theta \omega}{\partial \sigma} = \frac{\partial}{\partial \sigma} \left(\frac{K_H}{D} \frac{\partial \Theta}{\partial \sigma} \right) + F_{\Theta} \quad (4.38)$$

$$\frac{\partial SD}{\partial t} + \frac{\partial SUD}{\partial x} + \frac{\partial SVD}{\partial y} + \frac{\partial S\omega}{\partial \sigma} = \frac{\partial}{\partial \sigma} \left(\frac{K_H}{D} \frac{\partial S}{\partial \sigma} \right) + F_s \quad (4.39)$$

where: F_x = horizontal viscosity; F_y = horizontal diffusion; F_s = horizontal diffusion coefficient for salinity; and F_θ = horizontal diffusion coefficient for temperature.

4.3.2 Composition of the grid

The governing equations require numerical computational methods using discretized equations on a grid. To insure that certain integral constraints are maintained by the differencing, the governing equations have been cast into their flux form.

In ECOMSED, a structured grid formulation is used. Figure 4.3 shows the locations of the variables on the finite difference grid. The staggered arrangement uses U at points to the east and west of the point where η and H are defined and V at points to the north and south of the η and H points. The Δx and Δy are the constant horizontal grid spacings and $\Delta \sigma$ is the vertical increment which varies in thickness to accommodate more resolution near the surface and bottom (HydroQual 2002).

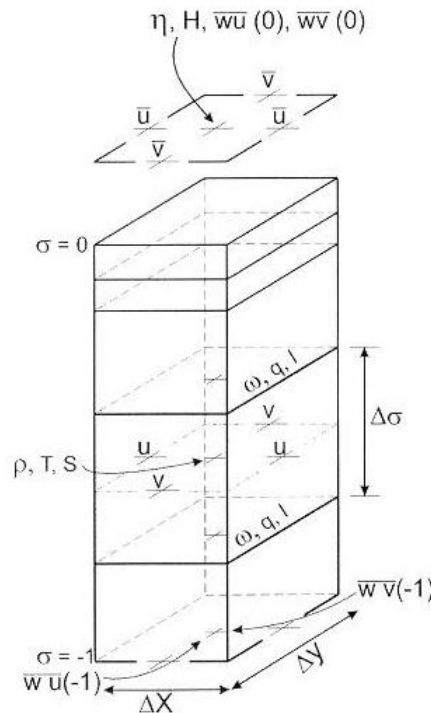


Figure 4.3 – The locations of the variables on the finite difference grid (Source: HydroQual 2002)

4.3.3 The turbulent closure models

4.3.3.1 The horizontal closure treatment

For the horizontal diffusion calculations, the model uses the parameterization suggested by Smagorinsky (1963), dependent on the horizontal grid spacing. The formulation, in Cartesian coordinates, is as follows:

$$A_M = \alpha \Delta x \Delta y \left[\left(\frac{\partial U}{\partial x} \right)^2 + \left(\frac{\partial V}{\partial y} \right)^2 + \frac{1}{2} \left(\frac{\partial U}{\partial y} + \frac{\partial V}{\partial x} \right)^2 \right]^{1/2} \quad (4.40)$$

The parameter α is typically equal to 0.10 and has ranged from 0.01 to 0.5 in various applications (HydroQual 2002). The model assumes $A_H = A_M$ by default.

4.3.3.2 The vertical closure treatment

The vertical mixing coefficients, K_M and K_H are calculated by using the Mellor-Yamada level 2.5 model. This is a second order scheme that characterizes the turbulence kinetic energy, $q^2/2$, and a turbulence macroscale, ℓ . The formulation is below.

$$\begin{aligned} \frac{\partial q^2}{\partial t} + \vec{V} \cdot \nabla q^2 + W \frac{\partial q^2}{\partial z} = \\ \frac{\partial}{\partial z} \left(K_q \frac{\partial q^2}{\partial z} \right) + 2K_M \left[\left(\frac{\partial U}{\partial z} \right)^2 + \left(\frac{\partial V}{\partial z} \right)^2 \right] + \frac{2g}{\rho_0} K_H \frac{\partial \rho}{\partial z} - \frac{2q^3}{B_1 \ell} + F_q \end{aligned} \quad (4.41)$$

$$\begin{aligned} \frac{\partial (q^2 \ell)}{\partial t} + \vec{V} \cdot \nabla (q^2 \ell) + W \frac{\partial (q^2 \ell)}{\partial z} = \\ \frac{\partial}{\partial z} \left(K_q \frac{\partial}{\partial z} (q^2 \ell) \right) + \ell E_1 K_M \left[\left(\frac{\partial U}{\partial z} \right)^2 + \left(\frac{\partial V}{\partial z} \right)^2 \right] + \frac{\ell E_1 g}{\rho_0} K_H \frac{\partial \rho}{\partial z} - \frac{q^3}{B_1} \tilde{W} + F_\ell \end{aligned} \quad (4.42)$$

where \tilde{W} is a wall proximity function.

4.3.4 The Sediment (SED) Model

The SED module can run in conjunction with both the hydrodynamic and the wave models. It uses the same numerical grid structure and computational framework as the hydrodynamic and transport models. The model allows the calculation of sediment resuspension, transport and deposition of cohesive and non-cohesive sediments. The code is prepared to deal with cohesive

sediments with particle diameters smaller than 75 μm (clays and silts) and non-cohesive sediments with particle sizes between 75 μm and 500 μm (fine and medium sands) (HydroQual 2002).

Bedload transport for particles diameters higher than 500 μm is not covered by the van Rijn formulation that was used; however, bed load can be assumed to be part of the load in the bottom σ -layer. The Lower MR reach covered in this study sediment-size distributions for non-cohesive sediment of the order are of 200 to 300 μm (Nittrouer *et al.* 2008). These values fall in the range of applicability of ECOMSED.

The calculations of deposition and resuspension of both cohesive and non-cohesive sediments are based on the shear stress induced at the sediment-water interface. The bed shear stress is calculated as follows:

$$\tau = \rho u_*^2 \quad (4.43)$$

Where ρ is the density of the suspending medium; and u_* is the shear velocity.

For currents only, the shear velocity is obtained by the Prandtl-von Karman logarithmic velocity profile:

$$u_* = \frac{\kappa u}{\ln\left(\frac{z}{z_0}\right)} \quad (4.44)$$

where κ is the von Karman constant, assumed to be approximately equal to 0.4; u is the resultant near-bed velocity; z is the depth at the center of the bottom layer; and z_0 is the bottom roughness (friction) specified as input to the model (HydroQual 2002).

For wave-current induced bottom shear stress computations, ECOMSED uses an alternative formulation. In this case, the hydrodynamic model predicts the near bottom current velocity (U), direction of current (θ_c), and the total water depth (h) and the wave model predicts the significant wave height (H_s), period (T) and direction (θ). Linear wave theory is used to translate the wave parameters (H_s and T) into a near-bed peak orbital velocity (U_p) and peak orbital amplitude (A_p) (HydroQual 2002). The formulation is below.

$$U_p = \frac{\pi H_s}{T \sinh\left(2\pi \frac{h}{L}\right)} \quad (4.45)$$

$$A_p = \frac{H_s}{2 \sinh\left(2\pi \frac{h}{L}\right)} \quad (4.46)$$

where the wave length (L) is given by:

$$L = C_0 T \quad (4.47)$$

and the shallow water wave speed (C_0) is:

$$C_0 = \sqrt{gh} \quad (4.48)$$

in which g is the gravitational acceleration.

The bottom shear stresses due to currents and waves are calculated using the Grant-Madsen wave-current model (Grant and Madsen, 1979) with base on the following inputs:

- U = magnitude of the near bottom current velocity
- $\Phi = \theta - \theta_c$, the difference between wave and current direction
- U_p = near-bed peak orbital velocity
- A_p = near-bed peak orbital amplitude
- z_0 = effective bottom roughness height

The final output from the Grant-Madsen model is the bottom shear velocity to be used in the shear stress calculation.

4.3.4.1 The cohesive sediment formulation

The resuspension of cohesive sediments is given by Gailani *et al.* (1991):

$$\varepsilon = \frac{a_0}{T_d^m} \left(\frac{\tau_b - \tau_c}{\tau_c} \right)^n \quad (4.49)$$

where ε is the resuspension potential (mg cm^{-2}); a_0 is a constant depending upon the bed properties; T_d is the time after deposition (days); τ_b = bed shear stress (dynes cm^{-2}); τ_c is the critical shear stress for erosion (dynes cm^{-2}); and m, n are constants dependent upon the depositional environment.

The resuspension rate is given by:

$$E_{tot} = \frac{\varepsilon}{3600 \text{ seconds}} \quad (4.50)$$

in which E_{tot} is assumed to be constant until all available sediment is eroded. Once the amount ε has been resuspended, E_{tot} is set to zero until additional sediment is deposited and available for resuspension or until the shear stress increases. The resuspension of sediments of class k (E_k), which given by

$$E_k = f_k E_{tot} \quad (4.51)$$

where f_k = fraction of class k sediment in the cohesive bed.

The deposition rate for cohesive sediment is given by the formulation of Krone (1962) as follows:

$$D_1 = -W_{s,1} C_1 P_1 \quad (4.52)$$

in which D_1 is the depositional flux ($\text{g cm}^{-2} \text{s}^{-1}$); $W_{s,1}$ is the settling velocity of the cohesive sediment flocs (cm s^{-1}); C_1 is the cohesive suspended sediment concentration (g cm^{-3}) near the sediment-water interface; and P_1 is the probability of deposition.

The settling velocity of the flocs is obtained by:

$$W_{s,1} = \alpha (C_1 G)^\beta \quad (4.53)$$

in which $W_{s,1}$, C_1 and G are expressed in m day^{-1} , mg L^{-1} , and dynes cm^{-2} , respectively.

The water column shear stress (G) is computed from the hydrodynamic output (current velocity and vertical velocity) by the following equation:

$$G = \rho K_M \left[\left(\frac{\partial u}{\partial z} \right)^2 + \left(\frac{\partial v}{\partial z} \right)^2 \right]^{1/2} \quad (4.54)$$

where K_M = vertical eddy viscosity, and ρ = density of the suspending medium.

The probability of deposition can be given by two different formulations: a) Krone (1962); or b) Partheniades (1992).

Krone (1962) formulation is:

$$P_1 = \begin{cases} 1 - \frac{\tau_b}{\tau_d}, & \tau_b \leq \tau_d \\ 0, & \tau_b > \tau_d \end{cases} \quad (4.55)$$

where τ_b is the bottom shear stress (dynes cm^{-2}), and τ_d is the critical shear stress for deposition (dynes cm^{-2}).

Partheniades (1992) formulation is:

$$P_1 = 1 - \frac{1}{\sqrt{2\pi}} \int_{-\infty}^{\omega} e^{-\frac{\omega^2}{2}} d\omega \quad (4.56)$$

where ω is a dummy variable, and

$$Y = 2.04 \log \left[0.25 \left(\frac{\tau_b}{\tau_{b,\min}} - 1 \right) e^{1.27 \tau_{b,\min}} \right] \quad (4.57)$$

In the code, the probability integral in Equation (4.56) is approximated by a cubic equation.

To simulate deposition and erosion of cohesive sediments as well as changes in bed properties such as thickness and erodibility characteristics, ECOMSED uses a 7-layer vertically segmented model. Each layer is described by a dry density, a critical shear stress for erosion and an initial thickness. A schematic of the sediment bed model is shown in Figure 4.4.

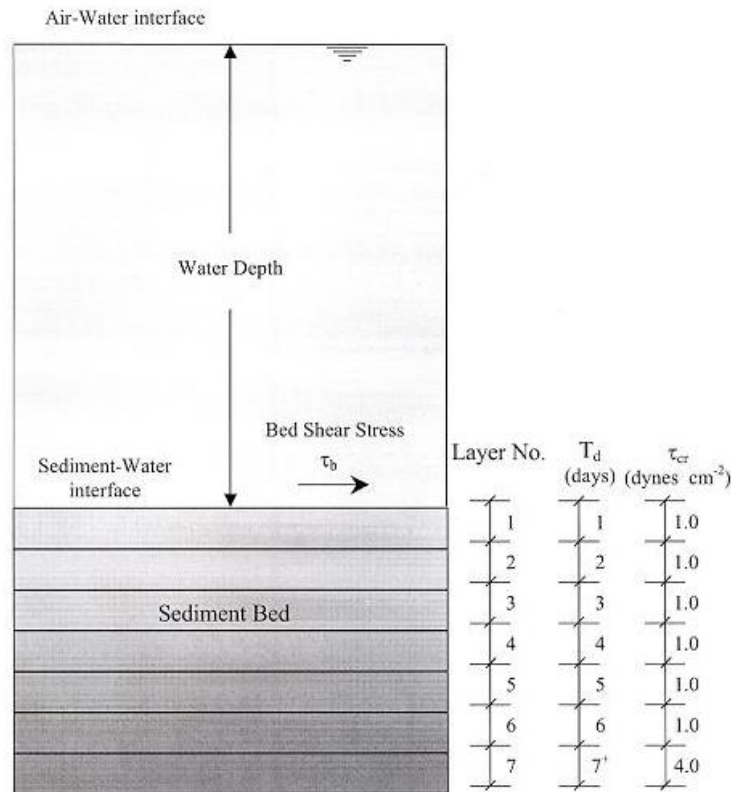


Figure 4.4 – Schematic of the sediment bed model

4.3.4.3 The non-cohesive transport formulation

The non-cohesive sediment transport calculations are based on the procedure for the calculation of suspended load transport given by van Rijn (1984). This procedure is described below.

The first step consists of determining the non-dimensional particle parameter:

$$D_* = \left[\frac{(s-1)g}{\nu^2} \right]^{1/3} D_{50} \quad (4.58)$$

where s = specific gravity of the particles; g = gravitational acceleration; ν = kinematic viscosity; and D_{50} = median particle diameter in the bed.

The critical bed shear velocity for initiation of bed motion is then determined by the Shields criteria:

$$u_{*,crbed} = [(s-1)gD_{50}\theta_{cr}]^{1/2} \quad (4.59)$$

where θ_{cr} = critical mobility parameter which is a function of D_* .

The critical shear velocity for resuspension is calculated by assuming that:

$$u_{*,crsus} = W_{s,2} \quad (4.60)$$

where $W_{s,2}$ = settling velocity of the non-cohesive suspended sediment. The settling velocity is given as an input and is computed from the median particle diameter (D_k) of the suspended sediment using the formulation of Cheng (1997):

$$W_{s,2} = \frac{\nu}{D_k} [(25 + 1.2D_*^2)^{0.5} - 5]^{1.5} \quad (4.61)$$

where D_* = non-dimensional particle diameter parameter with effective particle diameter D_k .

The near-bed shear velocity due to the flow is computed using the Prandtl-von Karman logarithmic approach presented in Section 4.3.4.

Deposition of sediment will occur if the bed shear velocity (u_*) is less than the threshold for motion ($u_{*,crbed}$) or less than the critical shear velocity for resuspension ($u_{*,crsus}$).

If u_* exceeds $u_{*,crbed}$ and $u_{*,crsus}$, the sediment flux will be from the bed to the lower layer of the water column. In this case, the suspended load transport is computed using the following set of equations:

Transport stage parameter Equation

$$T = \frac{u_*^2}{u_{*crbed}^2} - 1 \quad (4.62)$$

Reference Level above the bed Equation

$$a = \max(0.01h, k_s) \quad (4.63)$$

where h = water depth, and k_s = effective Nikuradse roughness height.

$$C_a = \frac{0.015 D_k T^{1.5}}{a D_*^{0.3}} \quad (4.64)$$

β -factor Equation

$$\beta = 1 + 2 \left(\frac{W_s}{u_*} \right)^2 \text{ for } 0.1 < \frac{W_s}{u_*} < 1 \quad (4.65)$$

Φ -factor Equation

$$\beta = 2.5 \left(\frac{W_s}{u_*} \right)^{0.8} \left(\frac{C_a}{C_0} \right)^{0.4} \text{ for } 0.1 < \frac{W_s}{u_*} < 1 \quad (4.66)$$

where C_0 = maximum volumetric bed concentration = 0.65.

Suspension parameter Equation

$$Z' = Z + \phi = \frac{W_s}{\beta k u_*} + \phi \quad (4.67)$$

F-factor Equation

$$F = \frac{\left(\frac{a}{h} \right)^{Z'} - \left(\frac{a}{h} \right)^{1.2}}{\left(1 - \frac{a}{h} \right)^{Z'} (1.2 - Z')} \quad (4.68)$$

Suspended load transport Equation

$$q_s = F_z u C_a \quad (4.69)$$

where z = depth of the lowest σ -layer.

Resuspension flux Equation

$$E = \frac{(s q_s - q_z C_z) \Delta t}{\Delta x \Delta y} \quad (4.70)$$

where C_z = concentration of suspended sediment in the lowest σ layer; s = specific gravity of the sediment; Δt = time step; and $\Delta x \Delta y$ = surface area of bottom.

The resuspension flux is the difference between the total suspended load transport and the existing sediment flux in the lowest σ -layer. If this difference is greater than zero erosion occurs; if the difference is lower than zero deposition occurs. Deposition can occur even if u^* is higher than u^*_{crbed} and u^*_{crsus} .

When the bed shear velocity (u^*) is less than the critical value (u^*_{crbed} or u^*_{crsus}), the sediment from the water column will be deposited in the bed. The deposition flux is obtained by:

$$D_2 = W_{s,2} C_2 \quad (4.71)$$

where D_2 = non-cohesive sediment depositional flux; $W_{s,2}$ = settling velocity; and C_2 = near-bed suspended sediment concentration.

4.5.5 The Program structure

ECOMSED is written in FORTRAN 77. The model can run in both Windows and LINUX/UNIX environments. The code consists of a main program (ecom3d.f) and a set of subroutines, totaling approximately 15,000 lines. The file “comdeck” contains the information for the number of nodes, elements and vertical levels used (HydroQual 2002). The code is not parallelized.

As stated before, the model is composed by several modules. The central module, corresponding to the main program ecom3d.f, is the hydrodynamic module. The heat flux, sediment-transport, particle tracking, water quality and wave modules can be linked internally or externally to the hydrodynamic module. Figure 4.5 shows the modeling framework of ECOMSED.

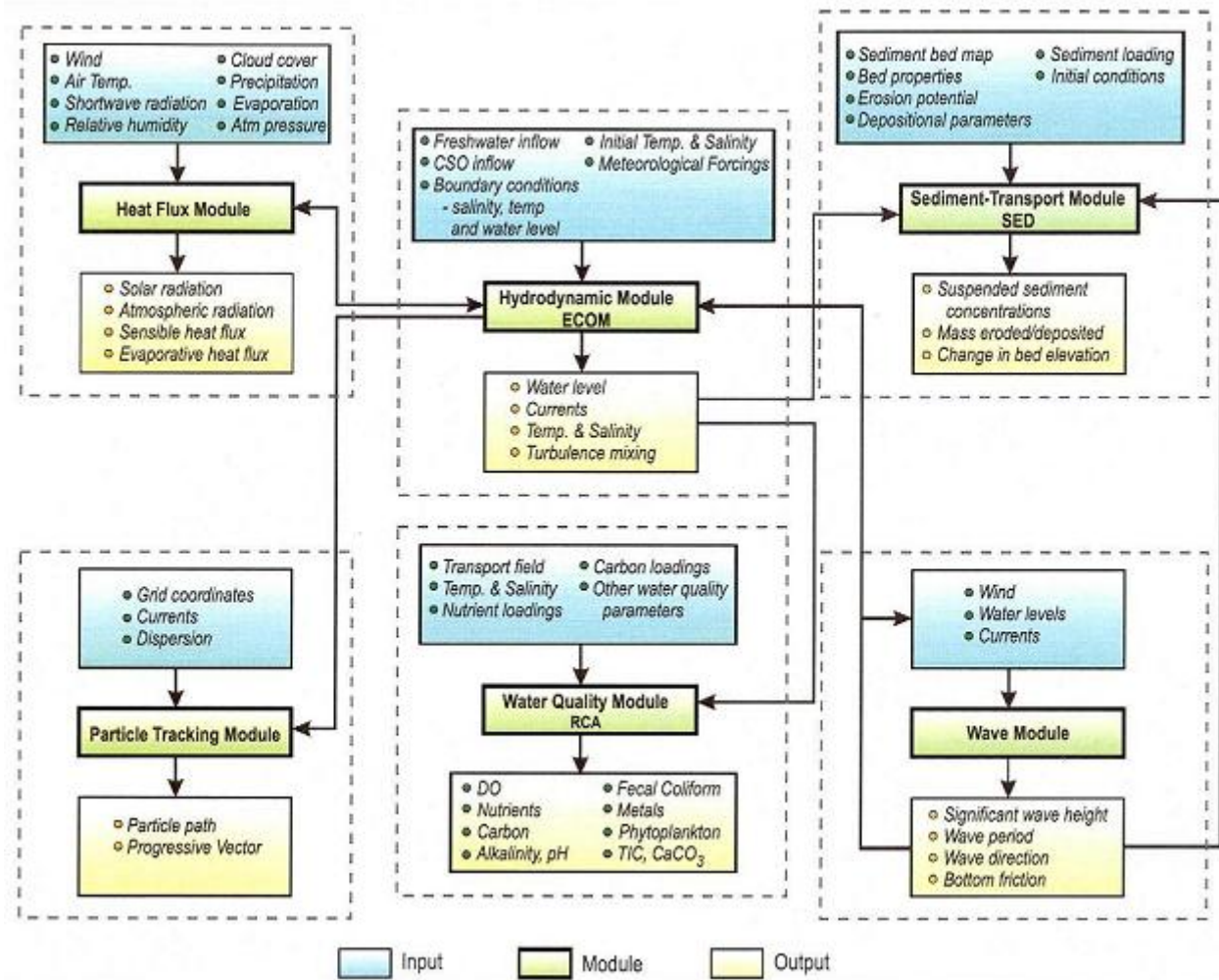


Figure 4.5 – ECOMSED Modeling Framework (Source: HydroQual 2002)

4.5.6 Mode Splitting

The use of the mode splitting technique allows the model to compute the free surface elevation prognostically. In the technique used, the volume transport (external mode) and vertical velocity shear (internal mode) are solved separately. This separation allows some computational economy. Figure 4.6 illustrates the interaction of the External and the Internal Mode. ECOMSED uses the leap-frog approach which is a second order time-marching formulation.

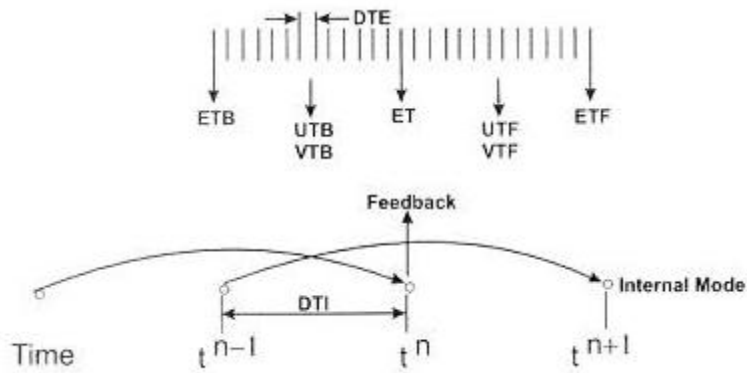


Figure 4.6 – Simplified Illustration of the interaction between the External and the Internal Mode in ECOMSED (Source: HydroQual 2002)

4.5.7 Modifications and Additions to the Original ECOMSED Code

The ECOMSED original code has been applied mainly for coastal and estuarine modeling and has been tested in the past for both cohesive and non-cohesive sediment transport. However, it has not been as extensively applied for riverine or fluvial modeling and, particularly, it has not been applied to the Lower MR. Thus, during this study, it was necessary to adapt the original ECOMSED source code to be applied to the study area. This section presents a description of the modifications made to the code.

4.5.7.1 Hydrodynamic Module

The ECOMSED original code was modified to allow the use of the Manning's formulation and user defined spatially variable roughness coefficients, given as an input file. The latter feature was necessary for calibration of river hydrodynamics and also to accurately reproduce and maintain the observed flow and transport trends near the deep holes throughout the domain. These changes are also necessary to account for the additional energy loss and generation due to bends and the flow expansions of turbulent kinetic energy.

The original ECOMSED formulation allows the user to input a constant friction coefficient (C_f) or a constant roughness (Z_0) for the whole domain. The shear stress is obtained as a function of this friction coefficient as follows:

$$\tau = C_f \rho V^2 \quad (4.72)$$

where τ = bottom shear stress, C_f = friction coefficient, ρ = density of water, and V = flow velocity.

In river modeling, it is common to use the Manning's n value as the reference friction coefficient. It was decided to adapt the code in order for the user to be able to give a reference Manning's n as an input.

The shear stress can be given as:

$$\tau = \gamma R S_f \quad (4.73)$$

where γ = specific weight of water, R = hydraulic radius, and S_f = friction slope which is given by:

$$S_f = \frac{V^2 n^2}{R^{4/3}} \quad (4.74)$$

Substituting S_f by Eq. (4.74), Eq. (4.73) becomes:

$$\tau = \gamma \frac{V^2 n^2}{R^{1/3}} \quad (4.75)$$

Equating Eq. (4.72) to Eq. (4.75), it is possible to express C_f as a function of n :

$$C_f = g \frac{n^2}{R^{1/3}} \quad (4.76)$$

where g = acceleration of gravity taken as constant and equal to 9.81 m/s^2 .

Approximating the hydraulic radius to the flow depth ($R \cong D$) we obtain:

$$C_f = g \frac{n^2}{D^{1/3}} \quad (4.77)$$

To obtain spatially variable friction, a new input file was coded, which contains the roughness factor attributed to each element. The final Manning's n per element is obtained as follows:

$$n'(I, J) = r(I, J)n \quad (4.78)$$

where n = reference Manning's n value constant for the whole domain, $n'(I, J)$ = Manning's n for the element (I,J), and $r(I, J)$ = roughness factor for the element (I, J).

Finally, the C_f per element is obtained as follows:

$$C_f(I, J) = g \frac{(r(I, J)n)^2}{D(I, J)^{1/3}} = g \frac{(n')^2}{D(I, J)^{1/3}} \quad (4.79)$$

where $C_f(I, J)$ = friction coefficient for the element (I,J), and $D(I, J)$ = flow depth for the element (I,J).

4.5.7.2 Sediment Module

Initial tests with the Lower Mississippi River showed exaggerated erosion and bottom sand concentrations that caused numerical instabilities and/or unrealistic sediment transport results. To calibrate the model, the code was modified to guarantee a minimum active layer volume of $1.0 \times 10^{-5} \text{ m}^3$ and a maximum of 1% change on bed-thickness in one time-step.

The original formulation was also changed to set the reference height (Z_0) equal to 3% of the flow depth instead of the original 1%. This change is justified by the dimensions of the Lower Mississippi River bedforms as described by El Kheishy (2007). The original formulation uses Eq. (4.63) as follows:

$$a = \max(0.01h, k_s) \quad (4.63)$$

where a = reference level above the bed, h = water depth, and k_s = Nikuradse roughness height.

In the new formulation, Eq. (4.63) is replaced by:

$$a = Ch \quad (4.80)$$

where C = constant equal to 0.03.

This change is intended to make the code applicable to the Lower MR, meaning that for a different fluvial environment C may have to take a different value.

The bottom layer non-cohesive sediment concentration was limited to a maximum of 500 mg/L, which is considerably higher than the near bed concentrations measured by Nittrouer *et al.* (2008) and Allison (2010). This was introduced to prevent an uncontrolled feedback that resulted in unrealistic bed elevation changes. The introduction of this limit, generally resulted in near bed concentrations below this limit.

4.5.7.3 Post-Processing

To aid in the analysis of the model results, several new variables had to be derived from the existing variables through an added post-processing subroutine. The subroutine used for this purpose was initially developed by Chilmakuri (2005) and was adapted here to include variables relevant in riverine and sediment transport studies. It was necessary to include the calculation of water discharge (Q), sediment load (Q_s), depth averaged sediment concentration (C_s), total energy (E) and kinetic energy of the flow (ke), for both the main channel cross-sections and the River diversions. The subroutine produces output files in ASCII format. Some of the outputs are formatted for Tecplot® visualization.

The first derived variable to be determined is the water discharge (Q) over a cross-section. To obtain it, it is necessary to first calculate the water discharge for each layer of each element of the cross-section, which is given by:

$$dQ(i, j, k) = V(i, j, k) L(i, j) [DZ(k) DT(i, j)] \quad (4.81)$$

where, $dQ(i, j, k)$ = water flow in the element (i,j) for level k; $V(i, j, k)$ = component of velocity normal to the face of the element (i,j) for level k; $L(i, j)$ = space-step of the element (i,j) to be used in the calculation (equal to Δy for flows in the i direction and Δx for flows in the j direction); $DZ(k)$ = fraction of flow depth attributed to level k; $DT(i, j)$ = total flow depth for element (i,j).

The total water discharge over a cross-section with flow in the j direction is obtained by:

$$Q(i) = \sum_{j=1}^{JM} \sum_{k=1}^{KM} dQ(i, j, k) \quad (4.82)$$

where, $Q(i)$ = water discharge over a cross-section with a certain i value, JM = the highest value taken by j, and KM = highest value taken by k.

By analogy, the water discharge over a cross-section with flow in the I direction is given by:

$$Q(j) = \sum_{i=1}^{IM} \sum_{k=1}^{KM} dQ(i, j, k) \quad (4.83)$$

where, $Q(j)$ = water discharge over a cross-section with a certain j value, IM = the highest value taken by i, and KM = highest value taken by k.

In the ECOMSED grids used for the Lower MR, the main channel flow is defined in the i direction and the diversions flow in the j direction.

The depth-averaged velocities over cross-sections i and j are obtained by the formulas:

$$V(i) = \frac{Q(i)}{\sum_{j=1}^{JM} \sum_{k=1}^{KM} L(i, j) [DZ(k) DT(i, j)]} \quad (4.84)$$

$$V(j) = \frac{Q(j)}{\sum_{i=1}^{IM} \sum_{k=1}^{KM} L(i, j) [DZ(k) DT(i, j)]} \quad (4.85)$$

where, $V(i)$ = depth-averaged velocity over a cross-section with a certain i value, and $V(j)$ = depth-averaged velocity over a cross-section with a certain j value.

The sediment load (Q_s) calculation is treated in a similar way to the water flow calculation. To obtain it, it is necessary to first calculate the sediment load for each layer of each element of the cross-section, which is given by:

$$dQ_s(i, j, k) = C_s(i, j, k)dQ(i, j, k) \quad (4.86)$$

where, $dQ_s(i, j, k)$ = sediment load in the element (i,j) for level k, and $C_s(i, j, k)$ = sediment concentration in the element (i,j) for level k.

The total sediment loads over cross-sections i and j are obtained by the formulas:

$$Q_s(i) = \sum_{j=1}^{JM} \sum_{k=1}^{KM} dQ_s(i, j, k) \quad (4.87)$$

$$Q_s(j) = \sum_{i=1}^{IM} \sum_{k=1}^{KM} dQ_s(i, j, k) \quad (4.88)$$

where, $Q_s(i)$ = sediment load over a cross-section with a certain i value, and $Q_s(j)$ = sediment load over a cross-section with a certain j value.

The depth-averaged sediment concentrations over cross-sections i and j are given by:

$$C_s(i) = \frac{Q_s(i)}{Q(i)} \quad (4.89)$$

$$C_s(j) = \frac{Q_s(j)}{Q(j)} \quad (4.90)$$

where, $C_s(i)$ = depth-averaged sediment concentration over a cross-section with a certain i value, and $C_s(j)$ = depth-averaged sediment concentration over a cross-section with a certain j value.

One of the main resources available in the Lower Mississippi River is the energy of the flow which is also included in the post-processing subroutine. The kinetic energy and the total energy over a cross-section equations are as follows:

$$ke(i) = \alpha \frac{V(i)^2}{2g} \quad (4.91)$$

$$ke(j) = \alpha \frac{V(j)^2}{2g} \quad (4.92)$$

$$E(i) = h + ke(i) = h + \alpha \frac{V(i)^2}{2g} \quad (4.93)$$

$$E(i) = h + ke(i) = h + \alpha \frac{V(i)^2}{2g} \quad (4.94)$$

where $ke(i)$ = the cross-sectional averaged kinetic energy term over a cross-section with a certain i value; $ke(j)$ = the cross-sectional averaged kinetic energy term over a cross-section with a certain j value; where $E(i)$ = the cross-sectional energy of the flow over a cross-section with a certain i value; $E(j)$ = the cross-sectional energy of the flow over a cross-section with a certain j value; g = acceleration of gravity which is assumed constant and equal to 9.81 m/s^2 ; α = kinetic energy correction factor which is assumed constant and equal to 1.0; and h = water surface stage in the center of the desired cross-section.

5) MODEL TESTING

This Chapter presents some tests performed with the ECOMSED model using simpler grids than the one developed for the final Lower Mississippi River Simulations. The following tests are presented:

1. Rectangular Channel Test
2. Trapezoidal Channel Test
3. Short Mississippi River Reach Test

The Rectangular Channel Test was performed using the original ECOMSED code with geometric dimensions of the same order of magnitude of those found in the Lower Mississippi River. The purpose of this exercise was the assessment of the behavior of the model with main focus on the hydrodynamic module. The hydraulic gradient, surface and bottom velocity patterns were evaluated and compared with the ones obtained with an FVCOM model. The ECOMSED sediment module was tested for non-cohesive sediment transport. Bottom and surface sediment concentrations were obtained.

The Trapezoidal Channel Test includes a hydrodynamic simulation with the original ECOMSED code. The purpose of the case was to evaluate the model using a cross-sectional shape closer to the one found in Natural Rivers such as the Mississippi River. The effect of the channel shape on the velocity profile is tested.

The Short Mississippi River Reach Test includes the simulation of both hydrodynamics and sand transport for about 14 miles of the main channel of the study area; the study reach includes a diversion. This part of the study investigates grid-dependency. Four different grid resolutions were used. This setup was also used to test modifications to ECOMSED. These modifications were needed in order to allow the model to be applied to the Lower Mississippi River. Most of the changes or additions to the original code are related to the non-cohesive sediment transport formulation or involve the calculation of new derived variables which are necessary for river modeling purposes, e.g., water discharge over a cross-section or the depth averaged sediment concentration over an element. These changes were presented in Section 4.5.7.

5.1 Rectangular Channel Test

A simple rectangular sections channel was set to run with both ECOMSED and FVCOM. The selected dimensions were based on Lower MR field data so that the flow variables would have the same order of magnitude as those in the MR. With ECOMSED both hydrodynamic and sand transport simulations were performed. FVCOM was used for hydrodynamic simulations only.

A horizontal channel with a length of 20 km and prismatic rectangular shaped cross-sections was used. The width of 500 m and the water depth of 20 m were approximately mean values calculated from existing river bed data from Tarbert Landing, MS (RM 306, RK 492) to Venice, LA (RM 11, RK 18).

In both models, the channel geometry was described by 10 layers, corresponding to a vertical space-step (Δz) of 2 m and a Δy of 50 m was used. Δx was 200 m in ECOMSED and 50 m in FVCOM. The ECOMSED mesh is a structured grid and was prepared in Tecplot[®] 10, while the unstructured FVCOM mesh was prepared in SMS[®] 9.2 and Tecplot[®] 10. Figure 5.1 and Figure 5.2 show respectively the ECOMSED mesh and the FVCOM mesh close to the downstream end of the domain.

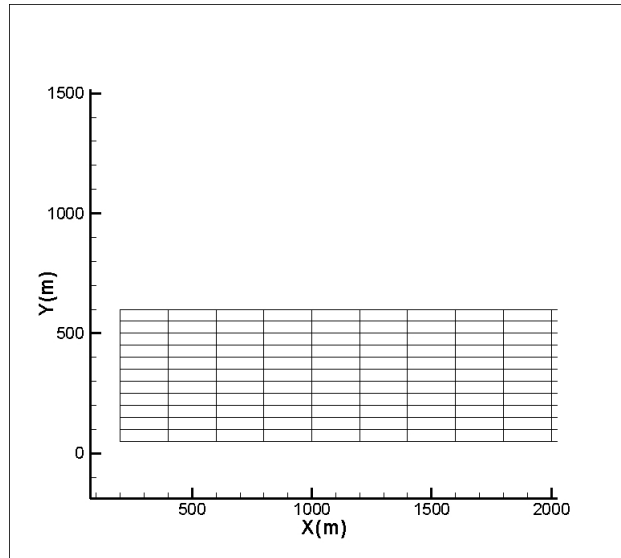


Figure 5.1 – ECOMSED Model – Downstream Boundary Mesh

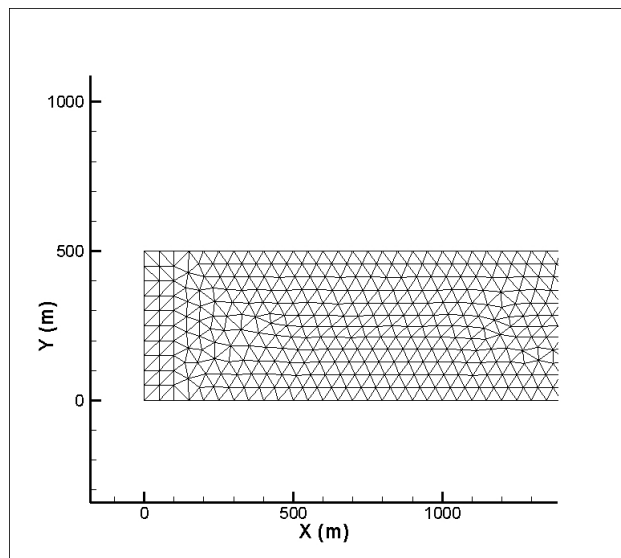


Figure 5.2 – FVCOM Model – Downstream Boundary Mesh

After preliminary runs with FVCOM, an external time-step of 0.4 seconds was selected. It allowed stable runs and minimized computational time. THE ISPLIT (number of time-steps between internal and external modes) was set to 4. These conditions correspond to an internal time-step of 1.6 seconds.

Both ECOMSED and FVCOM models ran with a friction coefficient (C_f) equal to 0.0045 so that the results would be comparable.

5.2.1 Boundary Conditions

A constant water discharge equal to 15,000 m³/s and a constant water depth of 20 m were given as upstream and downstream boundary conditions, respectively, in all the simulations. These values were based on existing measurements at Tarbert Landing, MS (RM 306, RK 492) and Venice, LA (RM 11, RK 18) for the last half-century and on the MR characteristics.

ECOMSED sand transport tests were performed for the same hydrodynamic boundary conditions. A constant concentration of 70 mg/L was defined as the upstream boundary condition. The model ran with an armoring coefficient equal to 0.0, basically meaning that there is no erosion from the bed and the only sediment available for transport is that being input at the upstream boundary.

In the ECOMSED model, two types of boundary formulations were tested for the open boundary downstream: CLAMPED and RANDB. The first one is a rigid boundary and does not allow long wave energy (tides or storm surges) to enter or radiate out of the model domain. The second, Reid and Bodine (1968), is an open-boundary condition allowing long wave energy to radiate through the boundary (HydroQual 2002). For the present study, CLAMPED proved to be the appropriate option and the performed simulations confirmed it.

5.2.2 Initial Conditions

In all simulations a ramping period was used to allow the model to adapt and minimize possible initial stability problems. A value of 10,000 internal time-steps was used, corresponding to a warm-up period of 4.5 hours over a total period of 24 hours.

The channel has no sediment when the simulations start. This means that an initial concentration of 0 mg/L is assumed in the model domain for the ECOMSED test.

5.2.3 Model Results

Figure 5.3 and Figure 5.4 represent the final water surface elevation profile after 24 hours, respectively for ECOMSED and FVCOM. Both models gave a hydraulic gradient close to 0.5 m, which is reasonable.

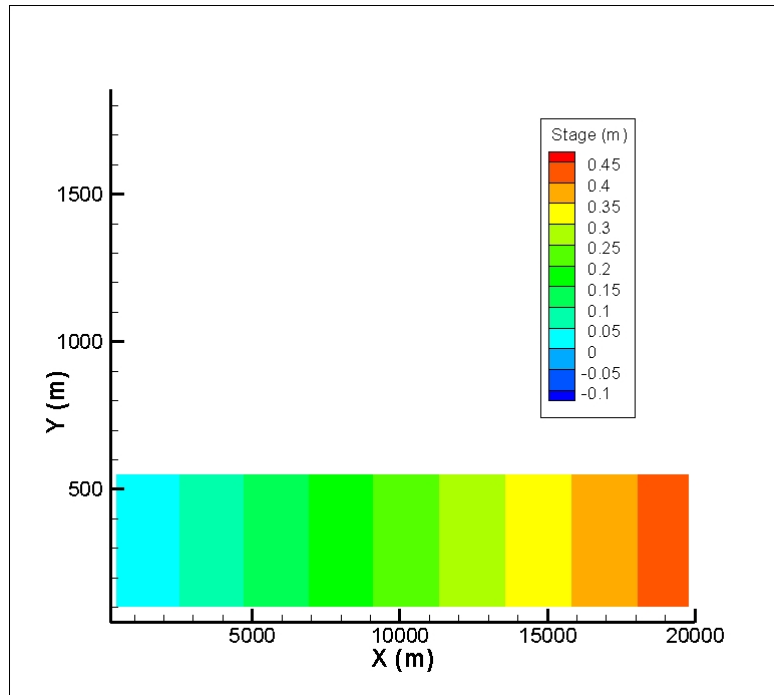


Figure 5.3– ECOMSED Model – Stage after 24 h

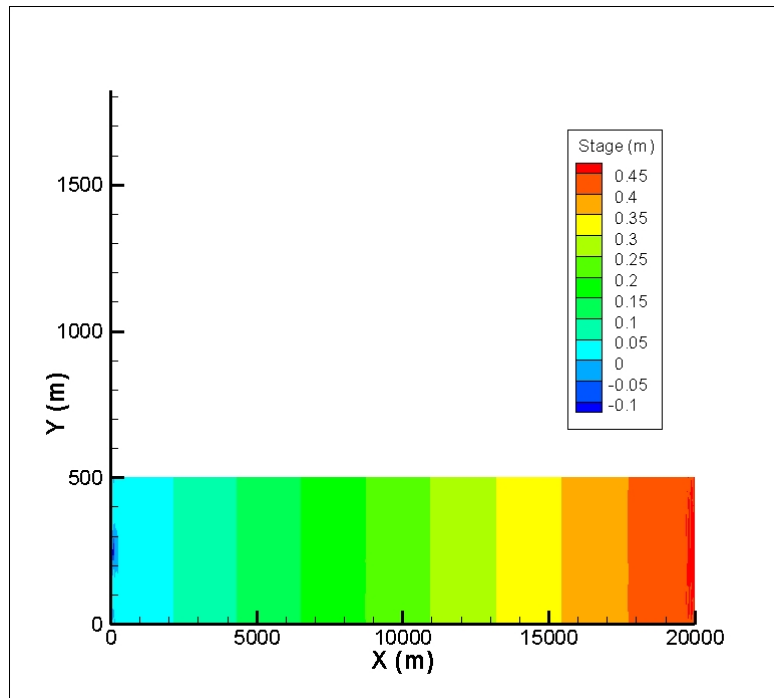


Figure 5.4– FVCOM Model – Stage after 24 h

Figure 5.5 and Figure 5.6 show the depth averaged velocity propagation after 24 hours for ECOMSED and FVCOM. The FVCOM solution shows some instability caused by the transition between internal cells of the model and the isosceles triangular cells in the rows at the boundary.

The results indicated that both ECOMSED and FVCOM hydrodynamics modules are working properly, i.e. they are stable and yield similar gradients. However, the velocity vectors are uniform along a cross-section, which is not realistic. The lateral velocity distribution should exhibit a nearly parabolic profile near the banks. In part, the unrealistic velocity distribution is caused by the full-slip formulation on vertical cell surfaces the code. In this simplified case, the velocity is ultimately a function of the flow depth and for equal flow depths equal velocities are obtained. Natural river cross-sectional shapes are not rectangular but closer to trapezoidal which results in more realistic profiles. To test the model behavior trapezoidal channel test was performed and the results obtained can be seen in Section 5.3. The code was also tested with a partial slip condition on the vertical faces but this tended to introduce a local spike in the velocity profile.

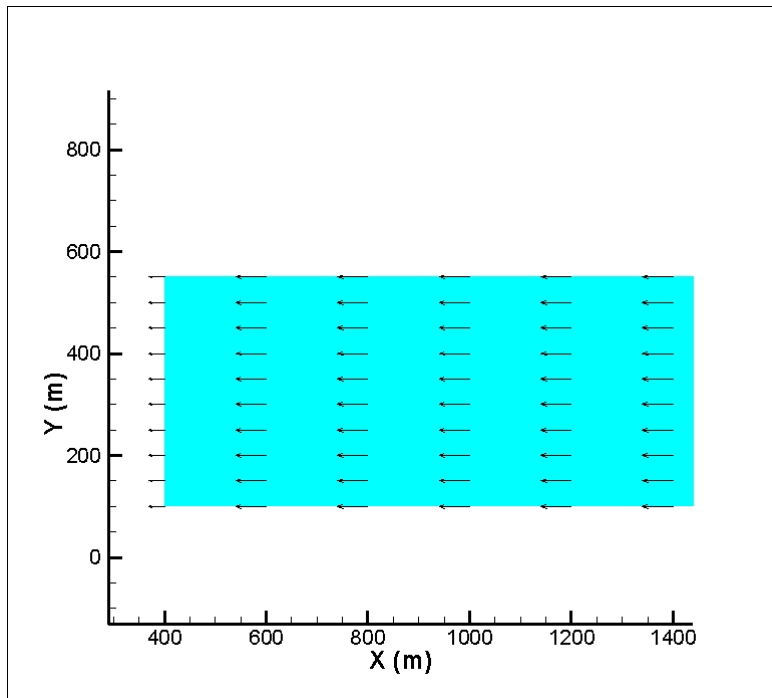


Figure 5.5 – ECOMSED Model – Depth Averaged Velocity near the D/S Boundary after 24h

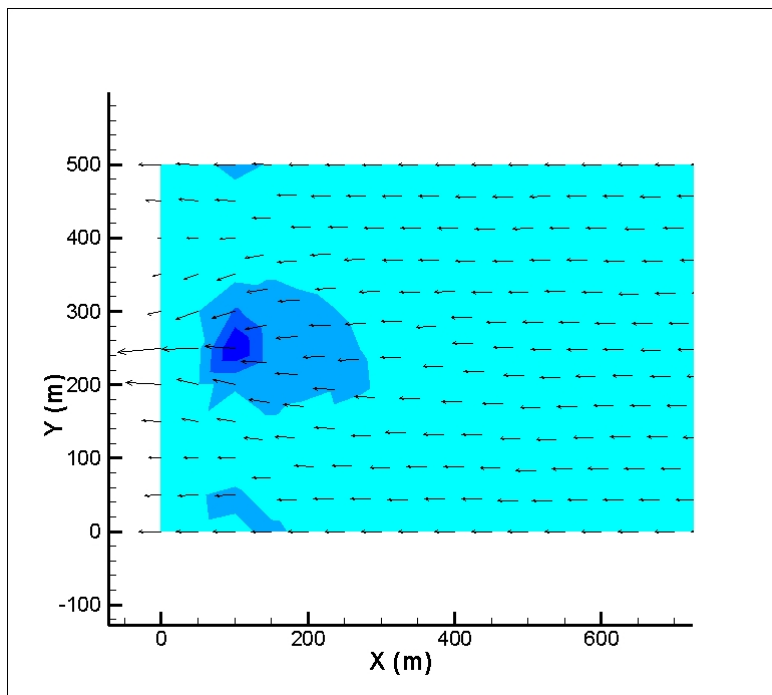


Figure 5.6 – FVCOM Model – Depth Averaged Velocity near the D/S Boundary after 24 h

The surface and bottom sand concentration distribution after 10 hours for the runs performed with ECOMSED can be seen in Figure 5.7 and Figure 5.8. It is evident that the sediment propagates faster at the surface than at the bottom and that the concentrations are much higher at the bottom. The order of magnitude of the results are reasonable with a maximum of around 300 mg/L at the bottom as observed by in the field data (Nittrouer *et al.* 2008; Allison 2010).

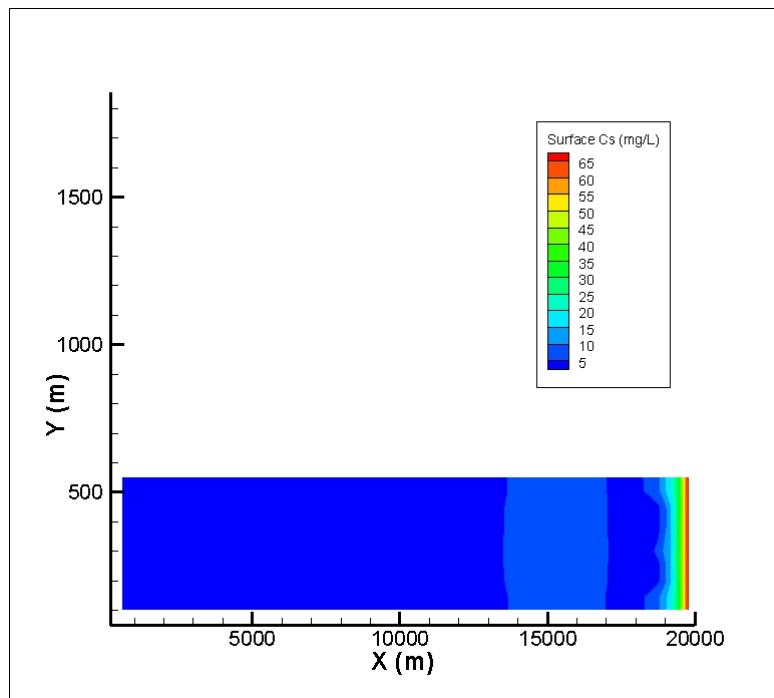


Figure 5.7– ECOMSED Model – Surface Sand Concentration after 10 h

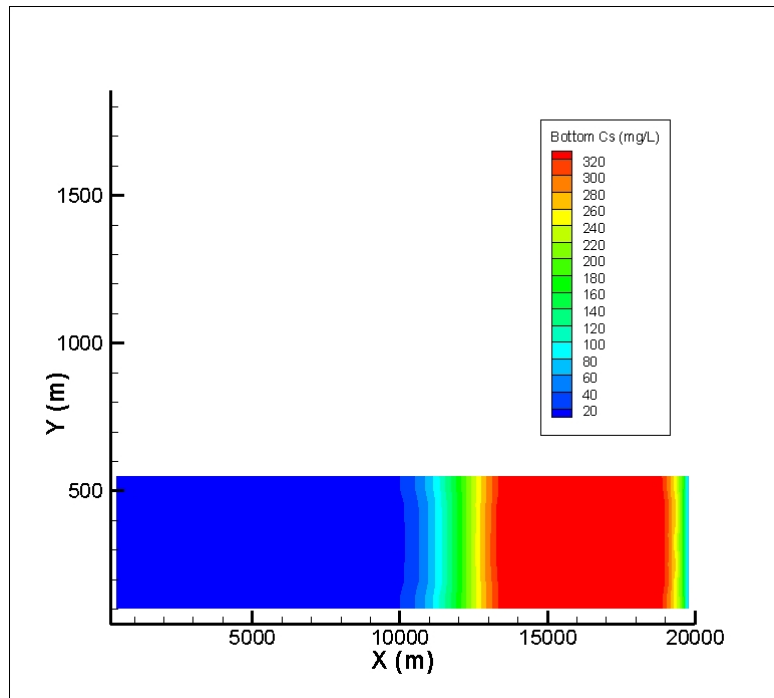


Figure 5.8– ECOMSED Model – Bottom Sand Concentration after 10 h

5.2 Trapezoidal Channel Test

A trapezoidal channel with a length of 20 km was set to run with ECOMSED to test the hydrodynamic module. The cross-sectional geometry is shown in Figure 5.9. A constant water discharge equal of $15,000 \text{ m}^3/\text{s}$ was used as the upstream boundary condition. A constant 15 m depth was used as the downstream boundary condition.

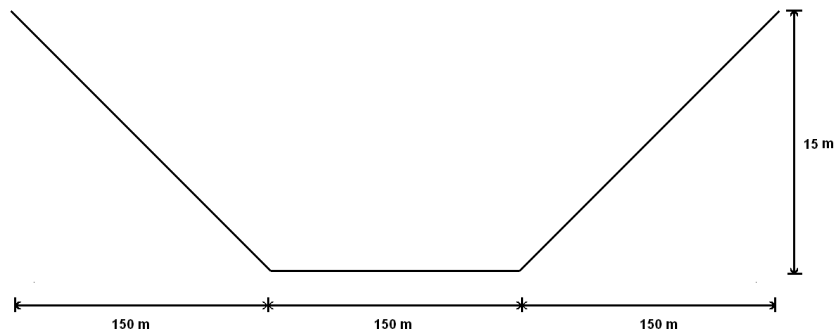


Figure 5.9 – ECOMSED Trapezoidal Channel Cross-Sectional Geometry

The time-step, ISPLIT and other coefficients used in this test are equal to those used in the rectangular channel simulations. The model was stable with these values.

The channel geometry was described by 10 layers, corresponding to a vertical space-step (Δz) of 2 m, a Δy of 50 m was and a Δx of 200 were used which are the same as those used in the rectangular tests.

The goal of this test was to confirm that for a trapezoidal channel, the ECOMSED code would be able to display a more realistic lateral velocity profiles with the highest speed being observed in the center of the channel. Plots of the velocity vectors and speed distribution near the downstream boundary and in an intermediate section of the channel are shown in Figure 5.10 and Figure 5.11. It is evident that the results are more realistic than those obtained with the rectangular channel case. The velocities in the center of the channel have higher values than the ones closer to the boundaries. Also the effect of the downstream boundary is limited to a few hundreds of meters even though we are working with a coarse grid.

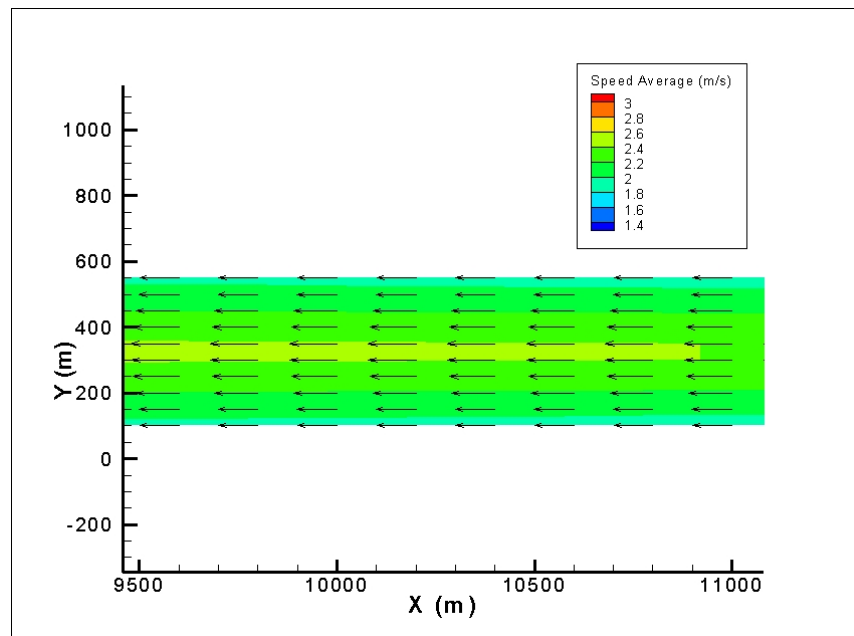


Figure 5.10 – ECOMSED Trapezoidal Channel Model – Depth Averaged Velocity in an intermediate section after 24h

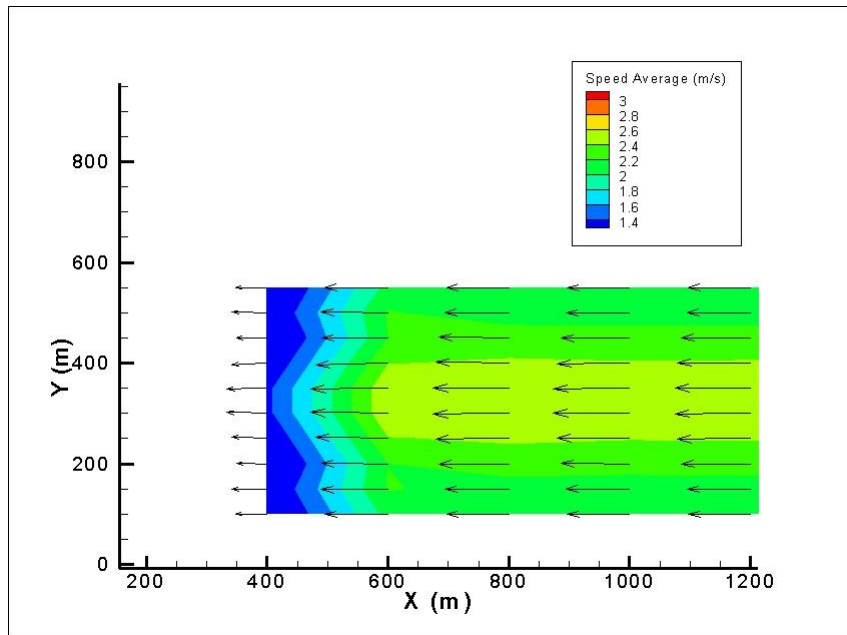


Figure 5.11 – ECOMSED Trapezoidal Channel Model – Depth Averaged Velocity near the D/S Boundary after 24h

5.3 Short Mississippi River Reach Test

A 14-mile Lower Mississippi River reach located approximately between RM64 and RM51 on the Myrtle Grove area was used to perform a grid dependency study with the modified ECOMSED code. The following resolutions were used:

- 100 m by 50 m
- 50 m by 50 m
- 50 m by 25 m
- 25 m by 25 m

The model domain is shown in Figure 5.12. To analyze the influence of the grid in the sediment and water diversion results, one diversion was included at Myrtle Grove (RM 59). The diversion is 100 m wide and has depths that vary from 10 m at the main channel to 5 m at the outflow area.

The coarser grid (100 m by 50 m) includes 10,250 elements while the finer grid (25 m by 25 m) includes 78,850 elements. Zoomed plots of the diversion area for the four different grids are shown in Figure 5.13.

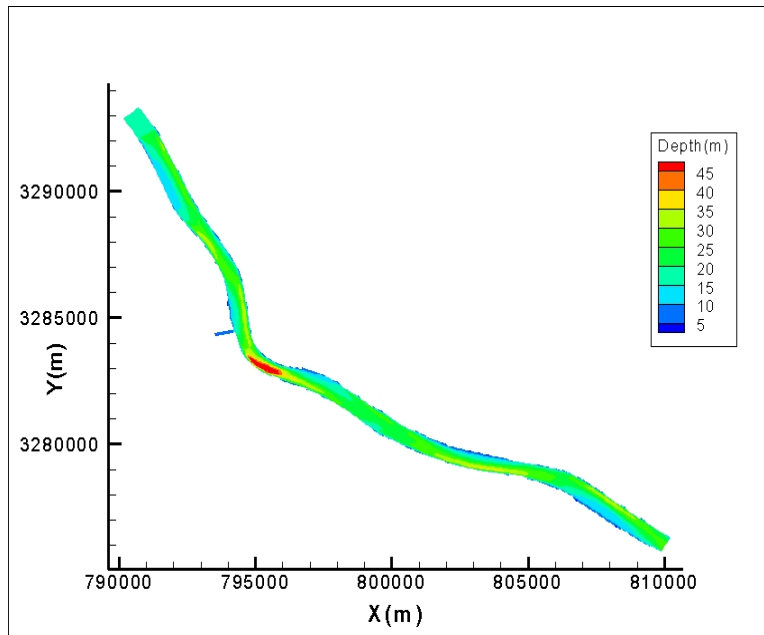
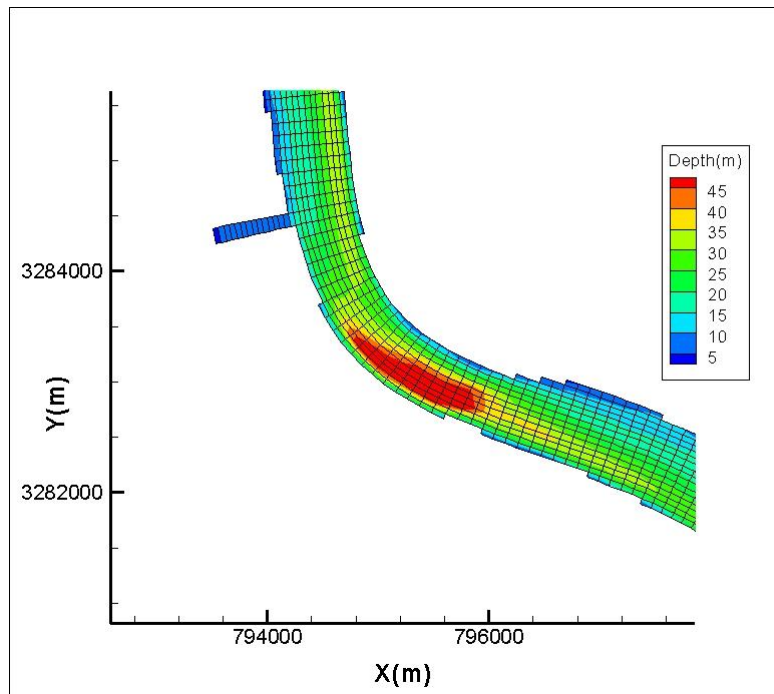
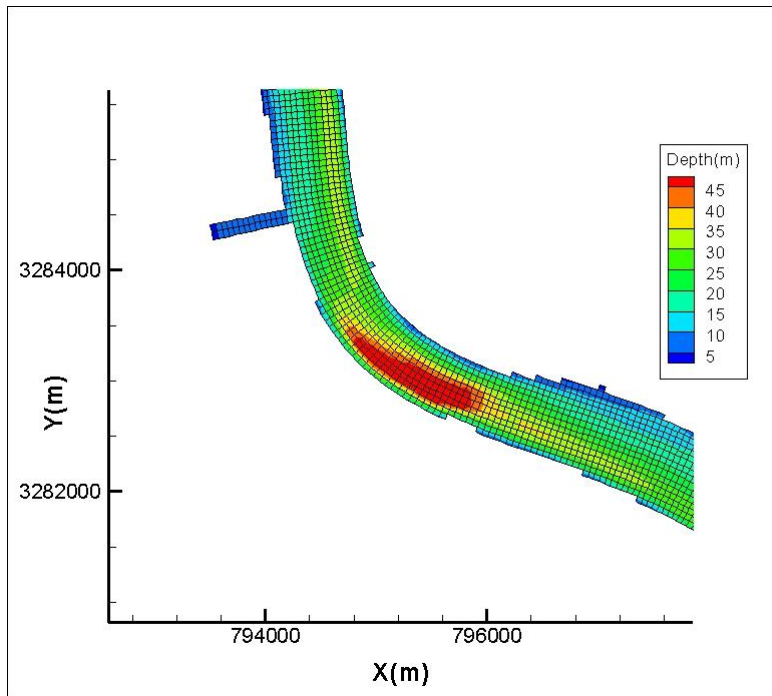


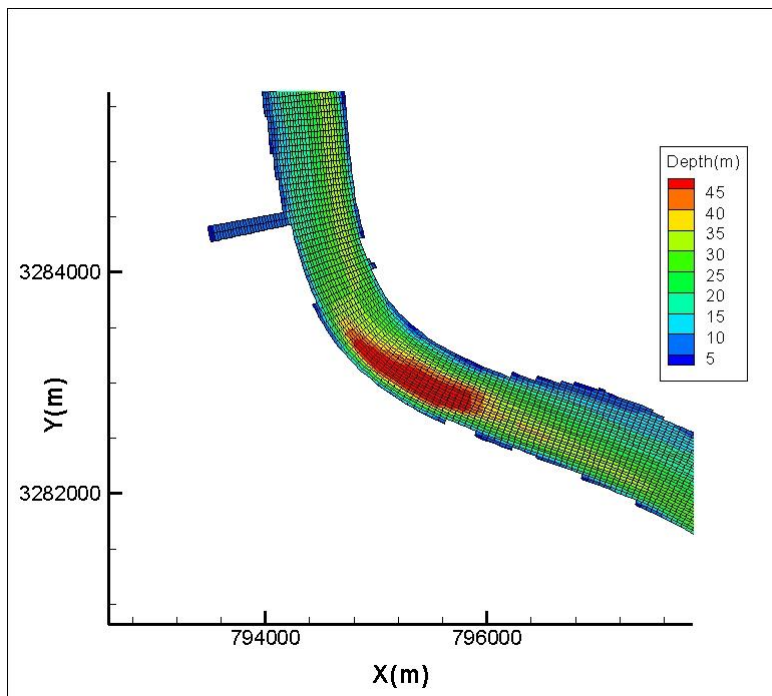
Figure 5.12– Short Mississippi River Reach Test Domain



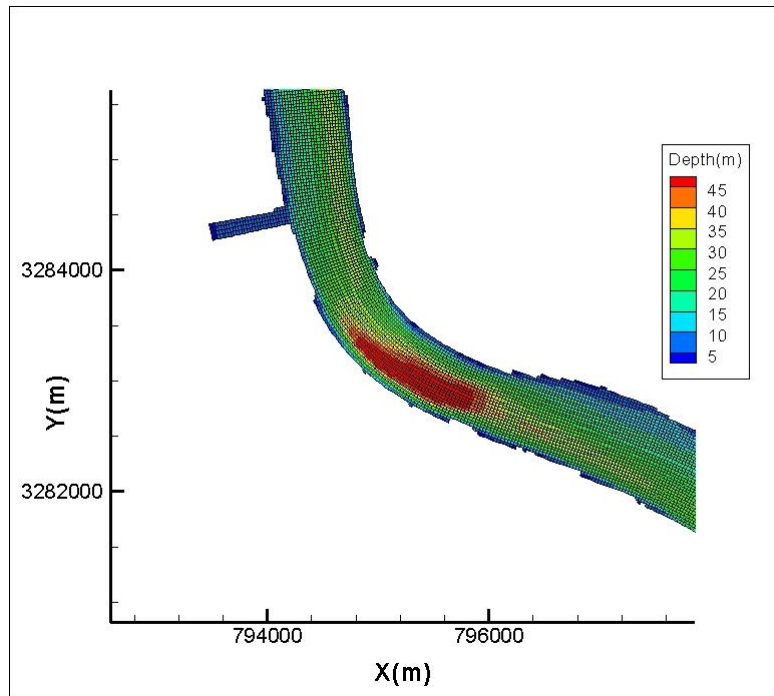
a) 100 m by 50 m Grid



b) 50 m by 50 m Grid



c) 50 m by 25 m Grid



d) 25 m by 25 m Grid

Figure 5.13– Short Mississippi River Reach Test Grids

For the different resolutions, different time-steps had to be used to maintain stability. The finer is the resolution of a grid, the lower the time-step (Δt) will have to be for the model to give a stable solution. Table 5-1 shows the Δt and Split values used for each grid resolution.

Table 5-1 – Time-Steps and Split for the Short Mississippi River Test

	Grid Resolution			
	100 m by 50 m	50 m by 50 m	50 m by 50 m	50 m by 50 m
Δt (s)	1.20	0.60	0.30	0.12
Split	3	3	3	3

5.3.1 Boundary Conditions

The model was run until there were steady state conditions which required one-day simulations. The goal was to compare the results under a steady-state condition, which would take around 8 hours to be reached. Thus, constant peak flow water discharges, stage and sand concentrations were used as boundary conditions. These boundary conditions were obtained from a calibrated and validated 1-D model developed for the Belle Chasse (RM 76) to downstream Main Pass (RM 3) reach.

Table 5-2 – Boundary Conditions for the Short Mississippi River Test

Q_{u/s} RM 63		Q_{out} RM 59		Stage_{d/s} RM 56		Cs_{u/s} RM 63	Cs_{d/s} RM 56
m³/s	cfs	m³/s	cfs	m	ft	mg/L	mg/L
32,500	1.15x10 ⁶	820	28,944	2.37	7.78	120	80

Uniform sand with a diameter $D_m=0.20$ mm was used for both suspended and bed sediments. This diameter represents a good estimate of the material available in the Lower Mississippi River based on measurements (Nittrouer *et al.*, 2008; Allison *et al.* 2010). A sediment control depth of 30 m was used.

A reference Manning's n value of 0.0290 was used for the whole reach. Roughness multiplication factors of 1.2 for depths higher or equal than 30 m and of 0.95 for depths lower than 30 m were used.

5.3.2 Model Results

Table 5-3 shows the water discharge and sand concentration results obtained in the Myrtle Grove diversion with different resolutions. It can be noticed that the water flows obtained are very similar but that the sand concentration values for the two finer grids is about 60% of those values obtained for the two coarser grids. These results may lead to the conclusion that the sand concentration significantly depends on the grid resolution. However, that is probably not the case. The cross-sectional averaged sediment concentration is particularly hard to estimate when compared to the water discharge. The sediment concentration is first calculated for each element (or node) and after that averaged over the cross-section. In addition, the formulation used in this study assumes that the water is flowing along the I-direction. Thus, if there is some small recirculation, cross-flow or reversed flow in the cross-section where the calculation is performed, the water discharge result may not be significantly influenced but the sand concentration might be, especially in the case where a small reversed flow occurs in an element with very high sediment concentration, e.g., at the bottom of the channel. The fine grid model captures more of these features.

Table 5-3 – Short Mississippi River Reach Test - Water discharge and Sand concentration in the Diversion

Grid Resolution	Q_{out} RM 59		Cs_{out} RM 59
	m³/s	cfs	mg/L
100 m by 50 m	811	28,640	32
50 m by 50 m	811	28,640	30
50 m by 25 m	821	28,993	18
25 m by 25 m	812	28,675	18

Figure 5.14 through Figure 5.17 show the water discharge, the stage, the sand concentration and the sand load longitudinal profiles for the main channel. The results were smoothed by the use of a 5-point filter. The results obtained with the four different grid resolutions are close. In general, the

results obtained with the finest grid are the highest and the ones with the coarser grid the lowest. Nonetheless, the maximum difference in the sand concentration values is of 8 mg/L.

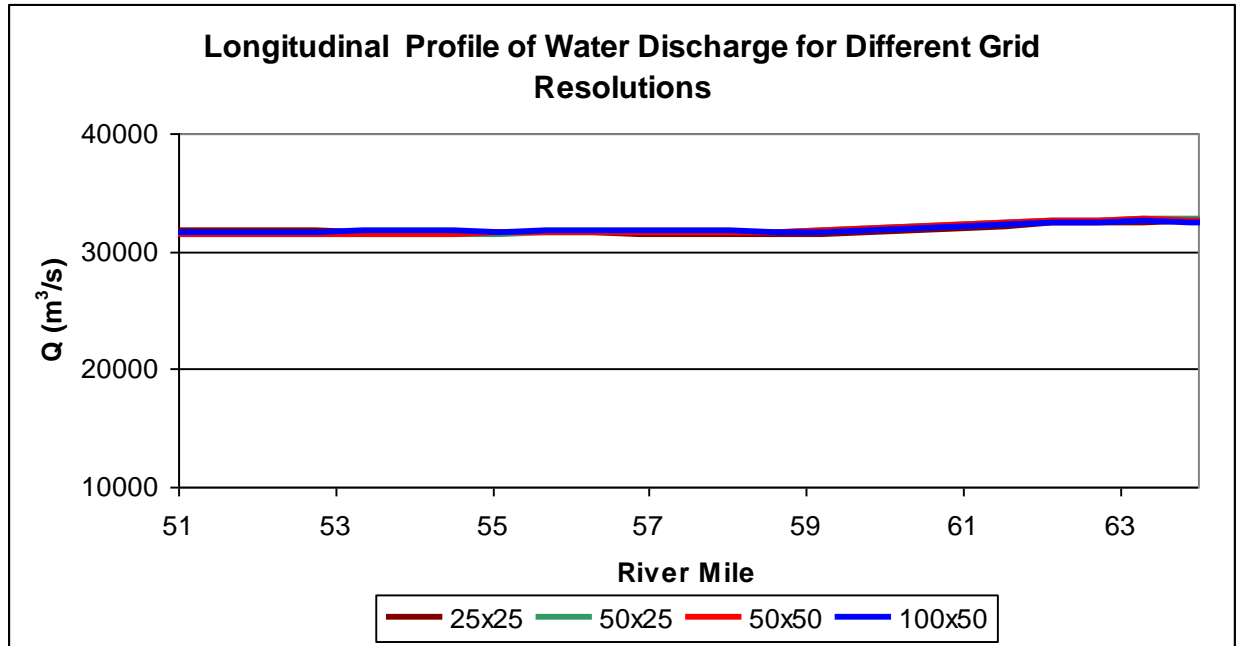


Figure 5.14– Longitudinal Profile of the Main Channel Water Discharge - Short Mississippi River Reach Test

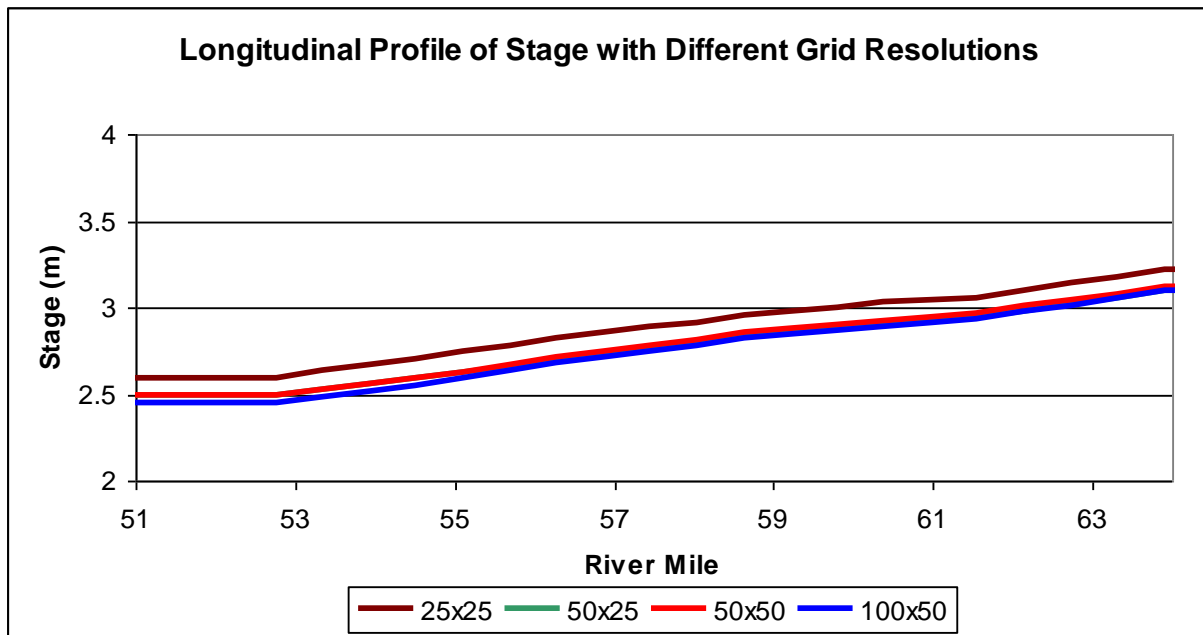


Figure 5.15– Longitudinal Profile of the Main Channel Stage - Short Mississippi River Reach Test

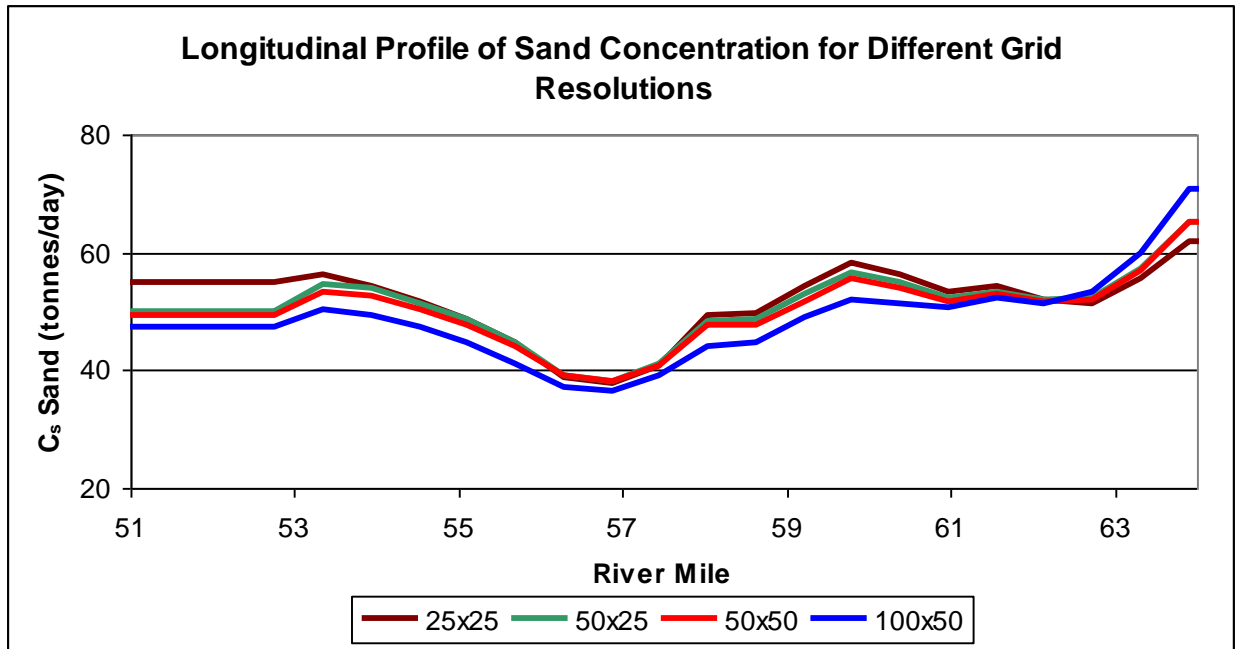


Figure 5.16– Longitudinal Profile of the Main Channel Sand Concentration - Short Mississippi River Reach Test

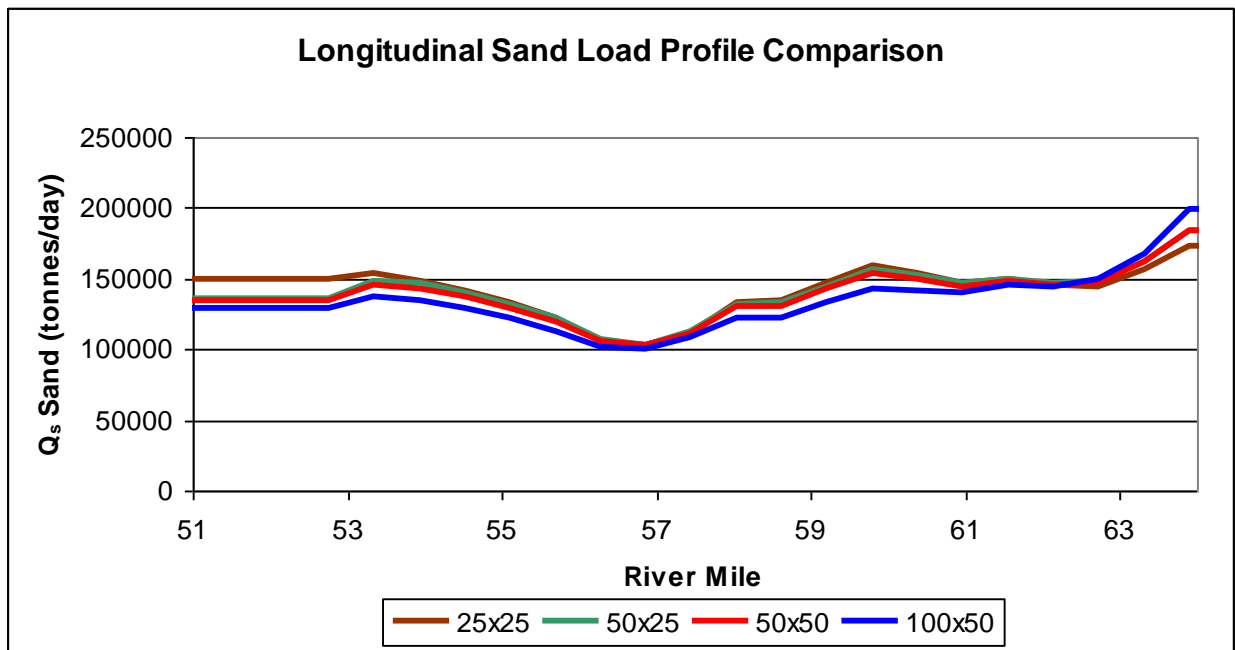
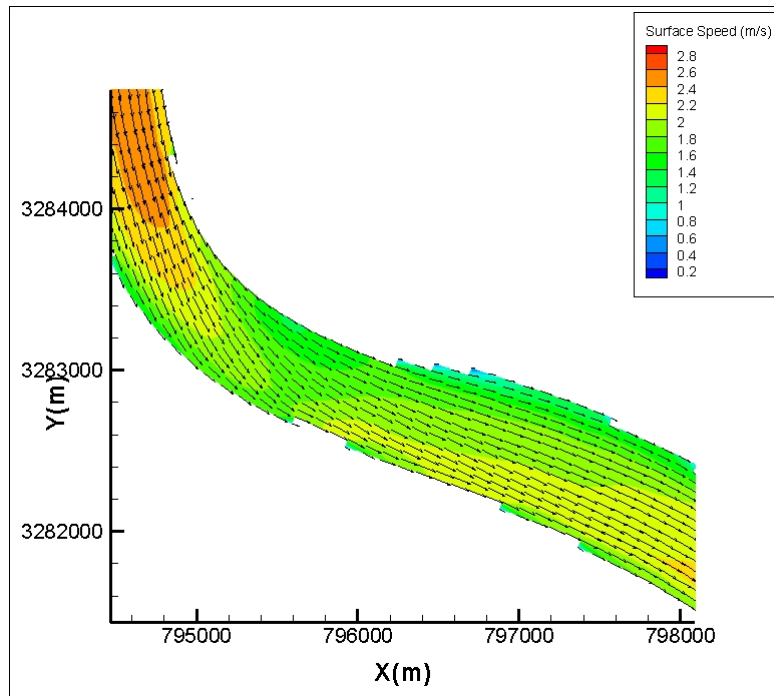
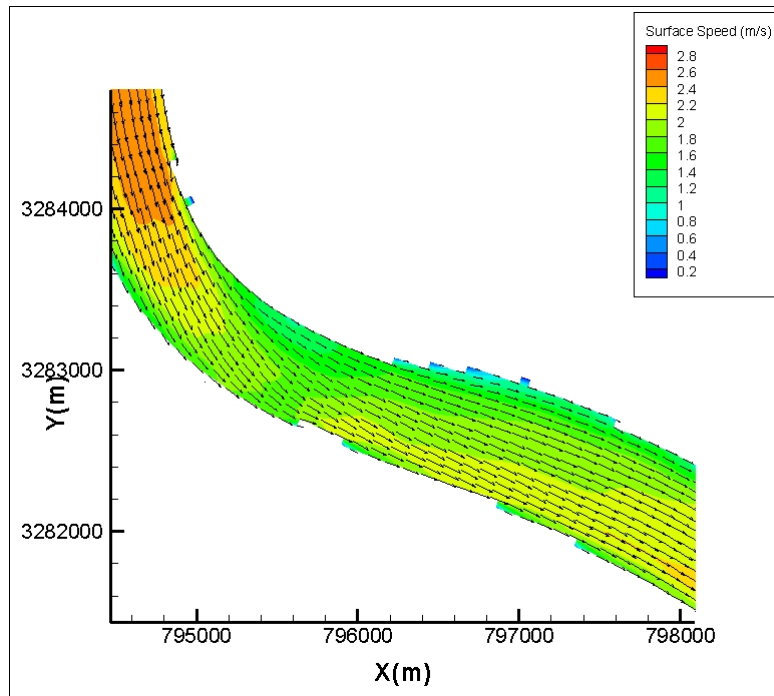


Figure 5.17– Longitudinal Profile of the Main Channel Sand Load - Short Mississippi River Reach Test

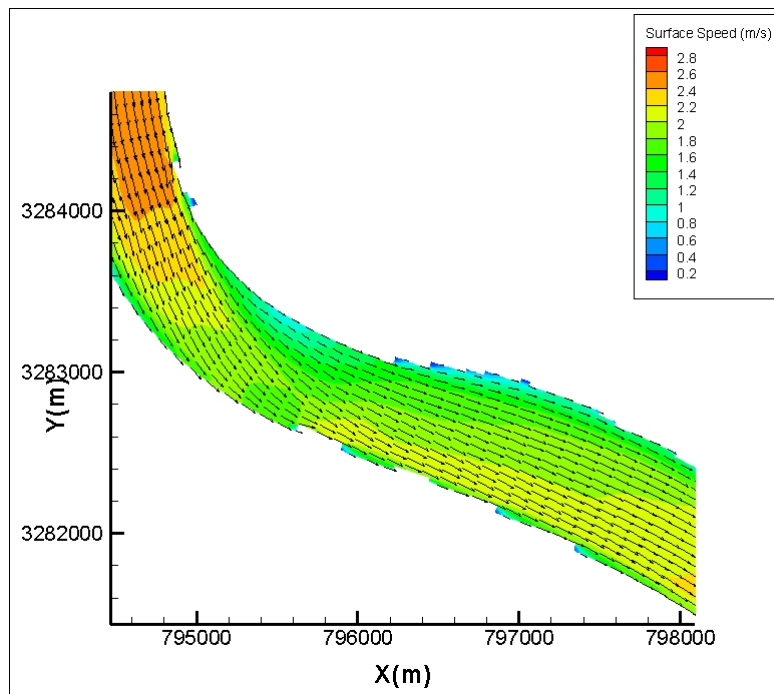
The velocity distributions at the surface and at the bottom in the vicinity of a bend in the main channel are presented in Figure 5.18 and in Figure 5.19. The results obtained are realistic. The model is able to reproduce the existence of secondary flow and the patterns are similar for the different grid resolutions. It is noted that there is a more pronounced propagation downstream of the highest velocities at the bottom with the refinement of the grid but overall the behavior of the model with the different resolutions is close.



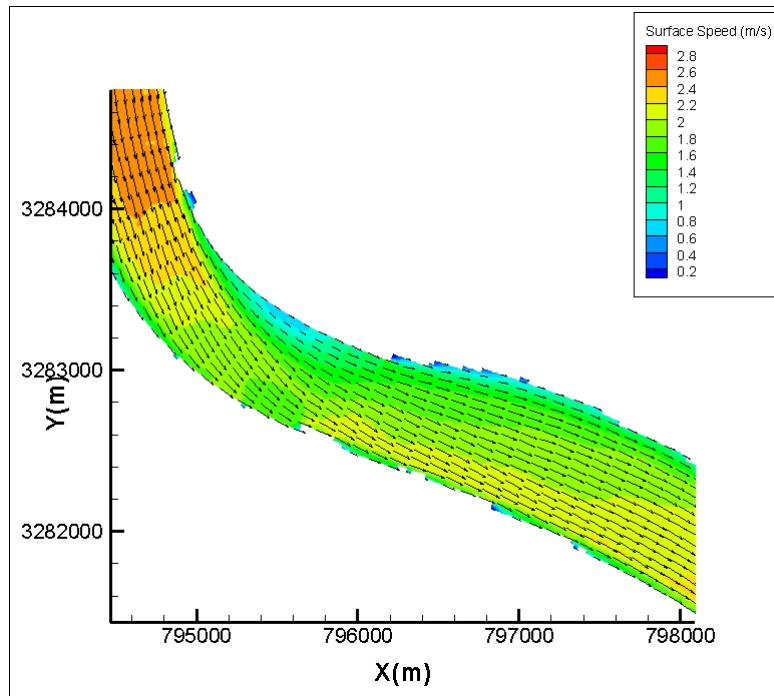
a) 100 m by 50 m Grid



b) 50 m by 50 m Grid

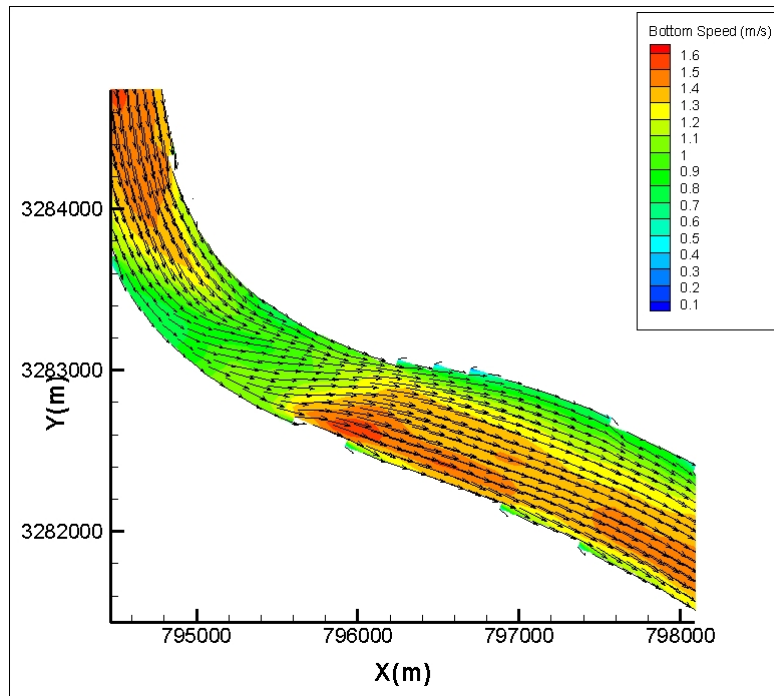


c) 50 m by 25 m Grid

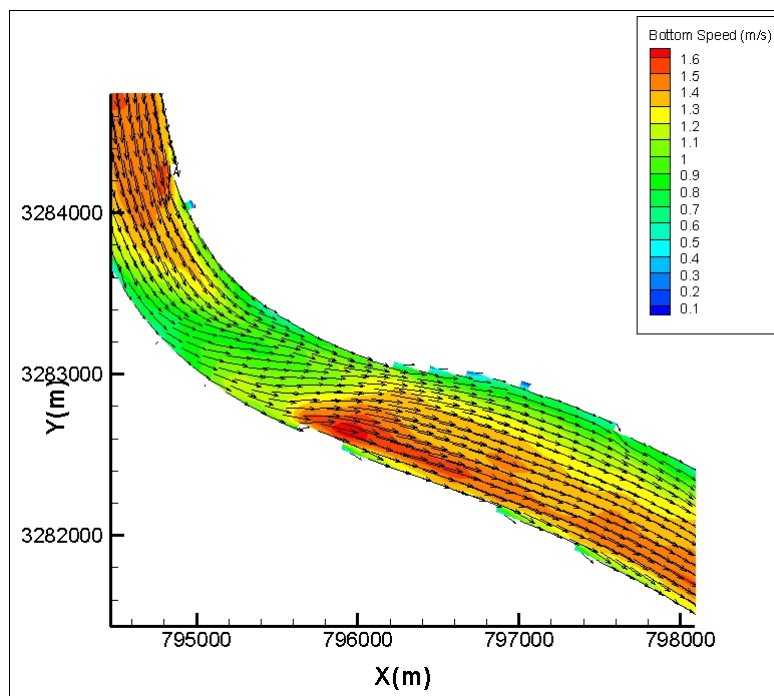


d) 25 m by 25 m Grid

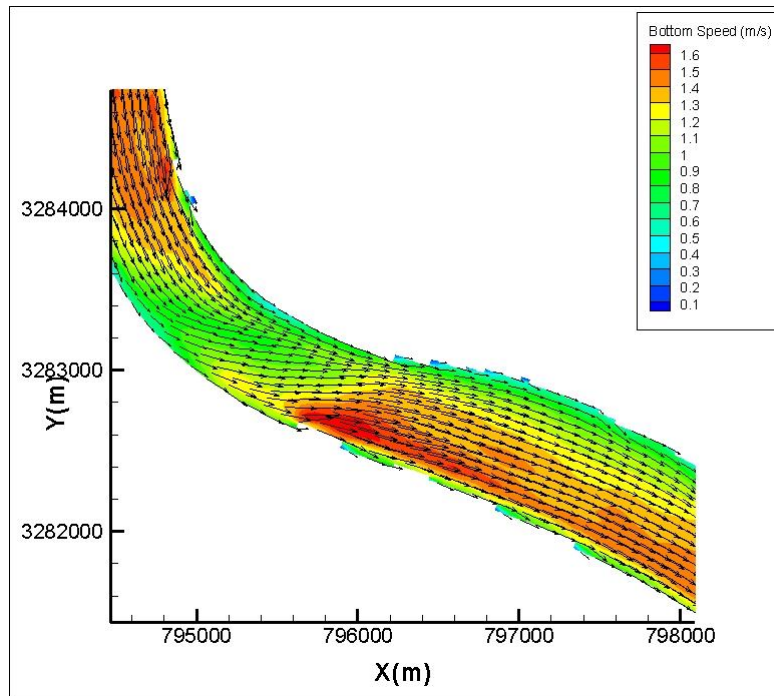
Figure 5.18– Short Mississippi River Reach Test - Surface Velocity at a Bend



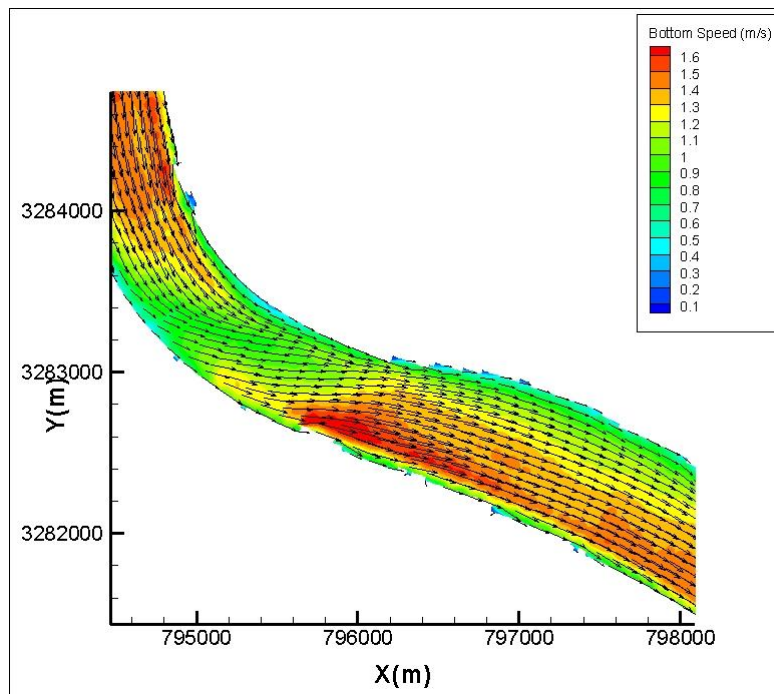
a) 100 m by 50 m Grid



b) 50 m by 50 m Grid



c) 50 m by 25 m Grid



d) 25 m by 25 m Grid

Figure 5.19– Short Mississippi River Reach Test - Bottom Velocity at a Bend

The bottom and surface velocity and speed plots allow a good visualization of the model's behavior but are not enough to compare the effect of the mesh in the results. More information is given by the cross-sectional speed distribution. Figure 5.20 and Figure 5.21 present the surface and bottom speed distributions for a cross-section on a bend for the several grids tested. Once again the results are close, particularly in the center of the channel. The boundary effect is influenced by the grid, as the results indicated that a lateral grid size of between 25 and 50 m is needed to best resolve the near bank effects.

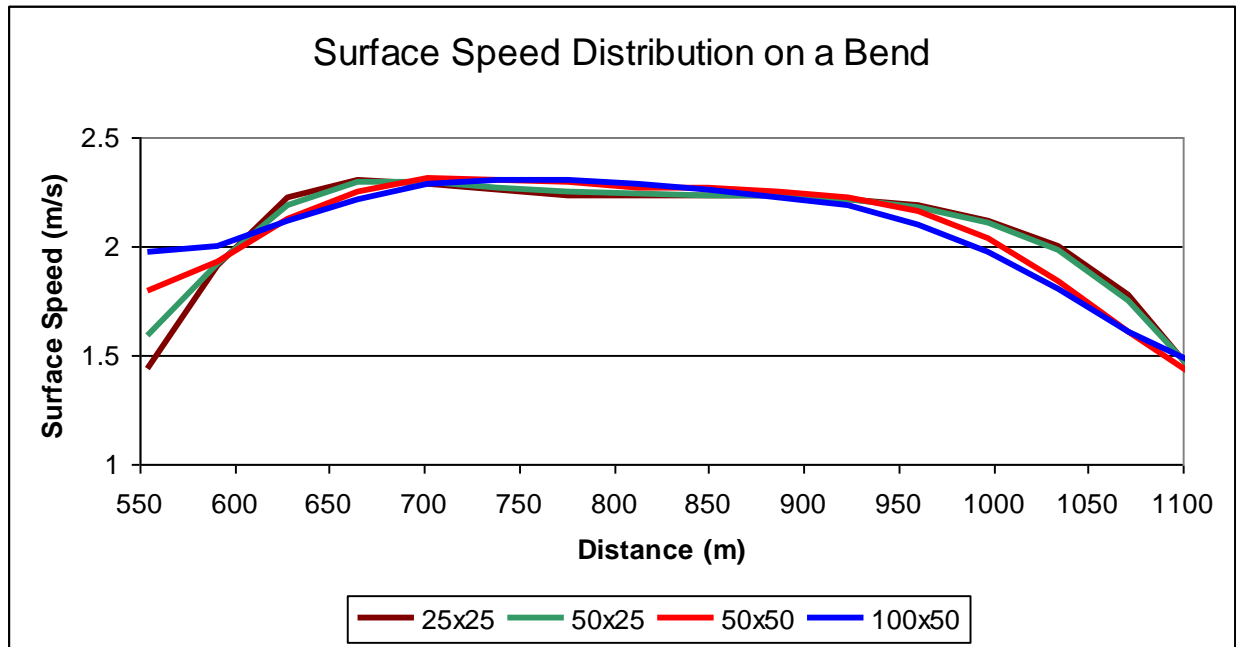


Figure 5.20– Surface Speed Profile on a Bend - Short Mississippi River Reach Test

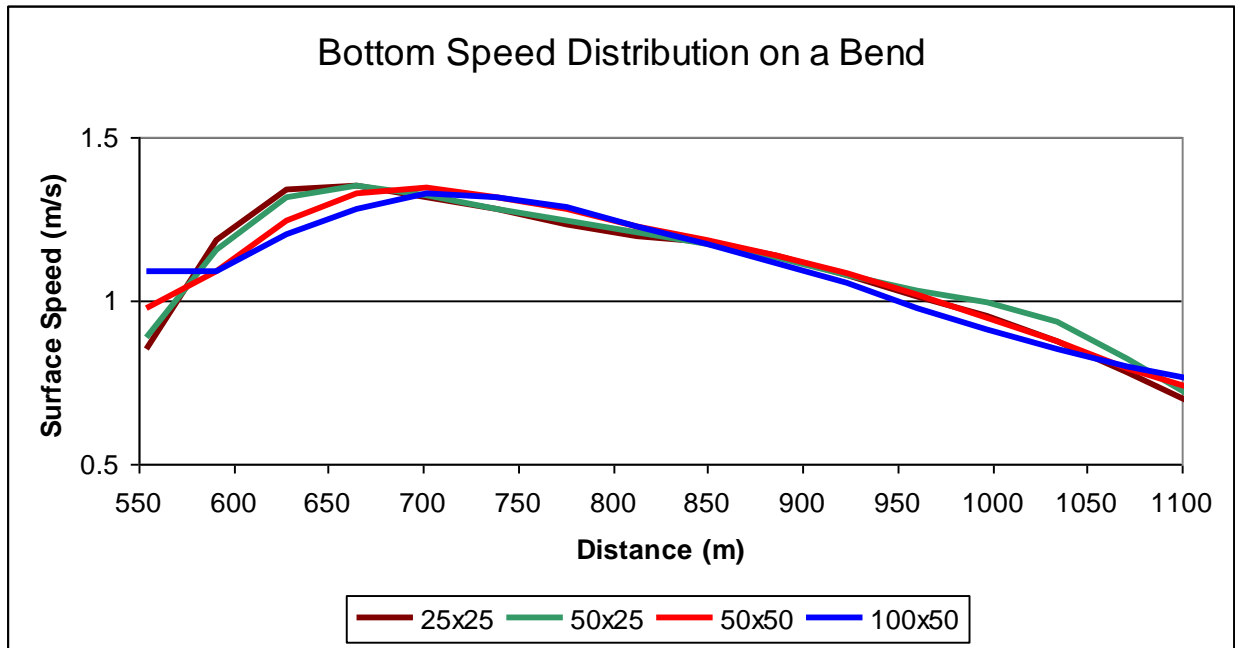


Figure 5.21– Bottom Speed Profile on a Bend - Short Mississippi River Reach Test

6) ONE-DIMENSIONAL MODELING

The 1-D CHARIMA model (Holly *et al.* 1990, Holly 2009) was applied to the Lower Mississippi River Reach from Belle Chasse (RM 76, RK 121) to downstream of Main Pass (RM3, RK 5). Both hydrodynamics and mobile-bed simulations were performed. The period of 01/01/2008 to 06/05/2008 was used for calibration of hydrodynamics and suspended sand transport. The calendar year of 2007 was used for validation of hydrodynamics. Sediment data was obtained from Nittrouer *et al.* (2008) and Allison (2010). Hydrodynamics data was obtained from the Davis (2010) study in which HEC-RAS was applied to model the Lower Mississippi River from Tarbert Landing (RM 306, RK 492) to the Gulf of Mexico.

Three different cases are presented herein: i) Existing outflows; ii) Myrtle Grove Diversion + Existing outflows; iii) Belair Diversion + Existing outflows. The existing case includes 13 outflows divided into 5 distributaries and 8 man-made diversions. White Ditch and Naomi (RM 65) and West-Pointe-À-La-Hache (RM 49) are treated as simple flow extractions meaning that the amount of flow to be extracted is prescribed directly to the model as a boundary condition. The rest of the outflows are modeled as distributaries and the stage at the Gulf of Mexico is given as the downstream boundary condition for these reaches. The Myrtle Grove tests include 14 outflows (existing plus the diversion being tested) while the Belair test includes 13 outflows (Belair replaces White Ditch & Naomi in the existing outflows scenario).

The computational domain includes 538 different types of cross-sections organized in a structure of 37 nodes and 37 links for the existing outflows scenario and 40 nodes and 40 links for both the Myrtle Grove and the Belair scenarios.

The Bathymetric data used herein has been used in previous studies (Pereira *et al.* 2009; Meselhe *et al.* 2010; Davis 2010). The main channel bathymetry from Belle Chasse (RM 76, RK 121) to Venice (RM 11, RK 18) was obtained from Pereira *et al.* (2009) and is derived from 2003 data. The main channel bathymetry downstream of Venice (RM 11, RK 18) through downstream of Main Pass (RM 3, RK 5) was obtained from Davis (2010). The geometry for the outflows and diversions was also obtained from Davis (2010). According to Davis (2010), the cross-sections downstream of Venice, as well as Baptiste Collette, Grand Pass and Tiger Pass were taken from the Hydrographic Survey (USACE NOD, 2007) while the Wilkinson Canal geometry was extracted for 2003 LIDAR/bathymetry for the Barataria Basin available in Tecplot® 10 (Georgiou *et al.* 2010). Due to insufficient survey data, Bayou Lamoque, Fort St Philip, Main Pass, Grand Pass and Tiger Pass equivalent channels were dimensioned based on Google Earth Imagery and/or the Lacey Regime Equations. The West Bay Sediment Diversion was extended beyond the design length, using wide equivalent cross-sections, to help the flow transition into open water (Davis 2010).

Several hydraulic structures were included in the model. The geometries of these structures are different from the ones used in Davis (2010) HEC-RAS study. However, they were calibrated to allow similar flow extractions in the CHARIMA model. The Bohemia Spillway is represented by three weirs, all of them lateral to the main channel and located approximately at RM 31 (Bohemia

Spillway Downstream (D/S)), RM 32.5 (Bohemia Spillway Intermediate) and RM 34 (Bohemia Spillway Upstream (U/S)). Bayou Lamoque North (RM 33) and Bayou Lamoque South (RM 32) channels include each one a gated structure. The Myrtle Grove (RM 59) diversion consists on the application of a gated structure to the Wilkinson Canal reach. The Belair (RM 65) diversion is simulated through the use of a weir structure lateral to the main channel. Both weirs and gates are simulated with the use of special types of links in which the de St.Venant equations are replaced by particular equations for treatment of weirs or gates. In these links, boundary conditions, e.g. the weir-crest elevation or the gate width, must be prescribed.

6.1 Existing Outflows

The first step of the 1-D modeling was the calibration and validation of a model that included only the existing diversions and distributaries within the domain. The Existing Outflows case includes 13 outflows: White Ditch & Naomi, West Pointe-A-La-Hache, Bohemia Spillway U/S, Bohemia Spillway Intermediate, Bohemia Spillway D/S, Bayou Lamoque N, Bayou Lamoque S, Fort St. Philip, Baptiste Collette, Tiger Pass, Grand Pass, Main Pass and West Bay. Figure 6.1 shows the topology of the fluvial network for this case.

6.1.1 Boundary Conditions

Mean daily hydrographs were used for both upstream (flow), and downstream and tributaries (water level) hydrodynamic boundary conditions. The 01/01/2008 to 06/05/2008 period was simulated for both hydrodynamics and sediment transport calibration. The Belle Chasse inflow, the outflow water discharges and the downstream stage boundary conditions were obtained from the 1-D HEC-RAS model developed by Davis (2010) that extends from Tarbert Landing (RM 306, RK 492) to the Gulf of Mexico. Table 6-1 and Table 6-2 show the hydrodynamics boundary conditions maximum, minimum and average values used for the calibration period. The complete hydrographs are given in Appendix A.

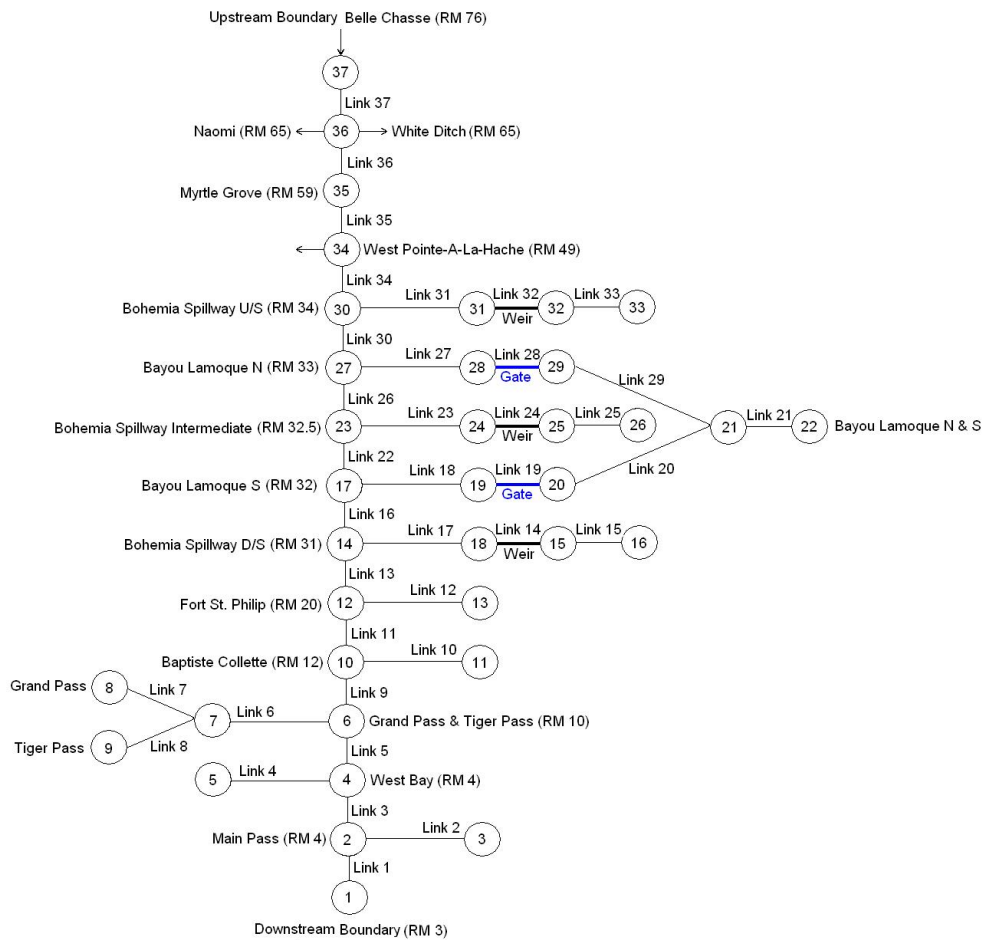


Figure 6.1 – Schematic diagram of the Existing Outflows Topology

Table 6-1 – Flow Boundary Conditions - Existing Outflows Case – 1-D Calibration - /2008

Site	Q maximum (m ³ /s, cfs)		Q minimum (m ³ /s, cfs)		Q average (m ³ /s, cfs)	
Belle Chasse* (RM 76)	33,830	1.19x10 ⁶	10,332	364,850	23,269	821,720
White Ditch and Naomi (RM 65)	-42	-1500	-42	-1500	-42	-1500
West-Pointe-A-La-Hache (RM 49)	-14	-500	-14	-500	-14	-500

*Upstream Boundary

Table 6-2 – Stage Boundary Conditions - Existing Outflows Case – 1-D Calibration - 2008

Site	Stage maximum (m, ft)		Stage minimum (m, ft)		Stage average (m, ft)	
Downstream of Main Pass* (RM 3)	0.71	2.33	0.12	0.39	0.48	1.57
Bohemia Spillway U/S (RM 34)	0.01	0.03	-0.04	-0.12	-0.01	-0.03
Bohemia Spillway Int. (RM 32.5)	0.01	0.03	-0.04	-0.12	-0.01	-0.03
Bohemia Spillway D/S (RM 31)	0.01	0.03	-0.04	-0.12	-0.01	-0.03
Bayou Lamoque N & S (RM 33)	0.01	0.03	-0.04	-0.12	-0.01	-0.03
Fort St. Philip** (RM 20)	0.01	0.03	-0.04	-0.12	-0.01	-0.03
Baptiste Collette** (RM 12)	0.01	0.03	-0.04	-0.12	-0.01	-0.03
Grand Pass** (RM 10)	0.01	0.03	-0.04	-0.12	-0.01	-0.03
Tiger Pass** (RM 10)	0.01	0.03	-0.04	-0.12	-0.01	-0.03
West Bay (RM 4)	0.01	0.03	-0.04	-0.12	-0.01	-0.03
Main Pass** (RM 4)	0.01	0.03	-0.04	-0.12	-0.01	-0.03

*Downstream Boundary **Natural Outflows (Distributaries)

The Belle Chasse inflow suspended sand loads were based on the field data obtained by Nittrouer *et al.* (2008) and the Belle Chasse water discharge given by HEC-RAS, similarly to what was done by Pereira *et al.* (2009). There was no need to give sand concentrations or loads as boundary conditions for the outflows. The formulation in CHARIMA allows the calculation of the balance of not only the water but also the sediment that is extracted at each diversion. Table 6-3 shows the maximum, minimum and average values of the sand load series given as upstream boundary condition for the 2008 simulations. The complete sand load is given in Appendix A.

Table 6-3 – Sand Load Boundary Condition - Existing Outflows Case – 1-D Calibration - 2008

Site	Q _s maximum (metric tons/day, cfs)		Q _s minimum (metric tons/day, cfs)		Q _s average (metric tons/day, cfs)	
Belle Chasse* (RM 76)	282,211	43.63	810	0	140,943	21.75

*Upstream Boundary

The initial hydrodynamic calibration was performed in fixed-bed mode by matching the results obtained in CHARIMA with the results obtained by Davis (2010), namely the outflow hydrographs for the distributaries and the stage hydrographs at Belle Chasse (RM 76), West-Pointe-A-La-Hache (RM 49), Scofield North (RM 24) and Scofield South (RM 16). The inconsistency of the available stage data for the modeled reach was the main reason to rely on Davis (2010) results as the reference for calibration instead of using available data directly. The model developed by Davis (2010) was calibrated for the New Orleans – Carrollton station (RM 102.8) which has reliable data, and used as boundary conditions the flows at Tarbert Landing (RM 306) and the stage at the Gulf of Mexico, both also considered to be reliable.

The main parameter used for the hydrodynamics calibration was the inverse of Manning's n , the Manning-Strickler coefficient ($K_s = 1/n$), which in CHARIMA can be given for each different cross-section. The other parameters used for calibration were the width and crest of the modeled weirs and the width and sill elevation of the simulated gates.

For hydrodynamics calibration, K_s values between 4.70 and 100.00 were used. In the main channel, values between 41.67 and 100.00 were used. The values above 60.00 are not very realistic but they were necessary to guarantee a good calibration. For most of the diversions, the Manning-Strickler coefficients ranged from 35.00 to 55.00. The exceptions were the West Bay (4.70), some cross-sections of the Bohemia Spillway D/S reach (5.00) and the Fort St. Philip channel (6.00). Such low values are unrealistic but were necessary to guarantee the desired flows in those channels. A full description of the roughness coefficients used in hydrodynamics calibration is given in Appendix B.

In the Existing Outflows scenario five hydraulic structures are included in the model: three weirs, that simulate the Bohemia Spillway and two gates, which represent Bayou Lamoque. The parameters used in the hydrodynamics simulations for the weirs are presented in

Table 6-4 and the gates parameters used in the same simulations are presented in Table 6-5. Although CHARIMA allows the use of time-variable weir-crest elevations, constant values were used for all three weirs.

Table 6-4 – Weirs Parameters - Existing Outflows Case – 1-D Hydrodynamics Calibration - 2008

Site	Weir Crest Width (m, ft)		Weir Crest Elevation (m, ft)		Discharge Coefficients (submerged, free-flow)	
Bohemia D/S (Link 14)	1,372	4,500	0.19	4.00	1.0	1.0
Bohemia Intermediate (Link 24)	128	420	0.30	1.00	1.0	1.0
Bohemia U/S (Link 32)	3,109	10,200	0.19	4.00	1.0	1.0

Table 6-5 – Gates Parameters - Existing Outflows Case – 1-D Hydrodynamics Calibration - 2007/2008

Site	Gate Sill Width (m, ft)		Gate Sill Elevation (m, ft)		Discharge Coefficients (submerged, free-flow)	
Bayou Lamoque South (Link 19)	1.62	5.3	-3.66	-12.00	1.0	1.0
Bayou Lamoque North (Link 28)	3.05	10.00	-2.90	-9.50	1.0	1.0

After the calibration with a fixed-bed for the hydrodynamics, the model was calibrated in mobile-bed mode for the sand transport. The starting point for this calibration was the calibrated fixed-bed model. Nonetheless, due to the erosion and deposition phenomena, there was a need to re-adjust some of the K_s values as well as some of the weirs and gates parameters to obtain a calibrated model simultaneously for hydrodynamics and sediment transport.

For mobile-bed calibration, K_s values between 4.80 and 65.00 were used. In the main channel, values between 41.67 and 65.00 were defined. Once again, for most of the diversions the Manning-Strickler coefficients ranged from 35.00 to 55.00. As before, the exceptions were the West Bay (4.80), some cross-sections of the Bohemia Spillway D/S reach (5.00) and the Fort St. Philip channel (6.20). A full description of the roughness coefficients used in hydrodynamics calibration is given in Appendix B.

As stated before, for mobile-bed calibration there was the need to re-adjust the hydraulic structures parameters. The values used in the mobile-bed simulations for the weirs are presented in Table 6-6 and the gates parameters used in the same simulations are presented in Table 6-7. Once again, time-constant weir-crest elevation values were used for all three weirs.

Table 6-6 – Weirs Parameters - Existing Outflows Case – 1-D Mobile-Bed Calibration - 2007/2008

Site	Weir Crest Width (m, ft)		Weir Crest Elevation (m, ft)		Discharge Coefficients (submerged, free-flow)	
Bohemia D/S (Link 14)	1,311	4,300	0.19	4.00	1.0	1.0
Bohemia Intermediate (Link 24)	128	420	0.30	1.00	1.0	1.0
Bohemia U/S (Link 32)	3,353	11,000	0.19	4.00	1.0	1.0

Table 6-7 – Gates Parameters - Existing Outflows Case – 1-D Mobile-Bed Calibration - 2007/2008

Site	Gate Sill Width (m, ft)		Gate Sill Elevation (m, ft)		Discharge Coefficients (submerged, free-flow)	
Bayou Lamoque South (Link 19)	1.62	5.3	-3.66	-12.00	1.0	1.0
Bayou Lamoque North (Link 28)	3.05	10.00	-2.90	-9.50	1.0	1.0

For all mobile-bed simulations, a sediment control volume depth of 30 m (maximum scour depth), and a uniform $D_m = 0.100$ mm for the suspended sand inflow were used. Initially, bed materials with a uniform $D_m = 0.200$ mm were defined for the whole domain, which is reasonable for the Lower MR, according to Nittrouer *et al.* (2008). However, in order to accurately calibrate the model, these needed some adjustments. Thus, in areas where the model gave unrealistic computational erosion, specifically in the vicinity of West Pointe-Á-La-Hache (RM 49) and Myrtle Grove (RM 59), a bed material with $D_m = 0.600$ mm was used to account for the local unrealistically high shear stress which was originated from the low K_s values.

Table 6-8 – Bed load diameters used in the 1-D CHARIMA Model

Channel	River Mile			
	76.2-75.5	75.5-52.2	52.2-45.9	45.9-3.0
	D ₅₀ (mm)			
Mississippi River* (RM 76 to RM 3)	0.200	0.200	0.600	0.200
Bohemia Spillway U/S (RM 34)	0.200	0.200	0.200	0.200
Bohemia Spillway Int. (RM 32.5)	0.200	0.200	0.200	0.200
Bohemia Spillway D/S (RM 31)	0.200	0.200	0.200	0.200
Bayou Lamoque N & S (RM 33)	0.200	0.200	0.200	0.200
Fort St. Philip** (RM 20)	0.200	0.200	0.200	0.200
Baptiste Collette** (RM 12)	0.200	0.200	0.200	0.200
Grand Pass** (RM 10)	0.200	0.200	0.200	0.200
Tiger Pass** (RM 10)	0.200	0.200	0.200	0.200
West Bay (RM 4)	0.200	0.200	0.200	0.200
Main Pass** (RM 4)	0.200	0.200	0.200	0.200

*Main Channel **Natural Outflows (Distributaries)

The hydrodynamics validation was performed for the calendar year of 2007. Similarly to what was done for the calibration period, the Belle Chasse inflow, the outflow water discharges and the downstream stage boundary conditions were obtained from the 1-D HEC-RAS model developed by Davis (2010) that extends from Tarbert Landing (RM 306, RK 492) to the Gulf of Mexico.

Table 6-9 and

Table 6-10 show the hydrodynamic boundary conditions (maximum, minimum and average) values used for the validation period. The complete hydrographs are given in Appendix A.

Table 6-9 – Flow Boundary Conditions - Existing Outflows Case – 1-D Validation - 2007

Site	Q maximum (m ³ /s, cfs)		Q minimum (m ³ /s, cfs)		Q average (m ³ /s, cfs)	
Belle Chasse* (RM 76)	25,674	906,668	4,639	163,829	12,593	444,700
White Ditch and Naomi (RM 65)	-42	-1500	-42	-1500	-42	-1500
West-Pointe-À-La-Hache (RM 49)	-14	-500	-14	-500	-14	-500

*Upstream Boundary

Table 6-10 – Stage Boundary Conditions - Existing Outflows Case – 1-D Validation - 2007

Site	Stage maximum (m, ft)		Stage minimum (m, ft)		Stage average (m, ft)	
Downstream of Main Pass* (RM 3)	0.50	1.66	0.09	0.28	0.28	0.93
Bohemia Spillway U/S (RM 34)	0.04	0.12	-0.04	-0.12	0.01	0.02
Bohemia Spillway Int. (RM 32.5)	0.04	0.12	-0.04	-0.12	0.01	0.02
Bohemia Spillway D/S (RM 31)	0.04	0.12	-0.04	-0.12	0.01	0.02
Bayou Lamoque N & S (RM 33)	0.04	0.12	-0.04	-0.12	0.01	0.02
Fort St. Philip** (RM 20)	0.04	0.12	-0.04	-0.12	0.01	0.02
Baptiste Collette** (RM 12)	0.04	0.12	-0.04	-0.12	0.01	0.02
Grand Pass** (RM 10)	0.04	0.12	-0.04	-0.12	0.01	0.02
Tiger Pass** (RM 10)	0.04	0.12	-0.04	-0.12	0.01	0.02
West Bay (RM 4)	0.04	0.12	-0.04	-0.12	0.01	0.02
Main Pass** (RM 4)	0.04	0.12	-0.04	-0.12	0.01	0.02

*Downstream Boundary **Natural Outflows (Distributaries)

6.1.2 Results

The model was calibrated for stage at four locations in the main channel and for ten existing outflow channels. The hydrodynamics stage calibration results are shown from Figure 6.2 to Figure 6.5. A visual inspection of the results shows that the model appears to be well calibrated.

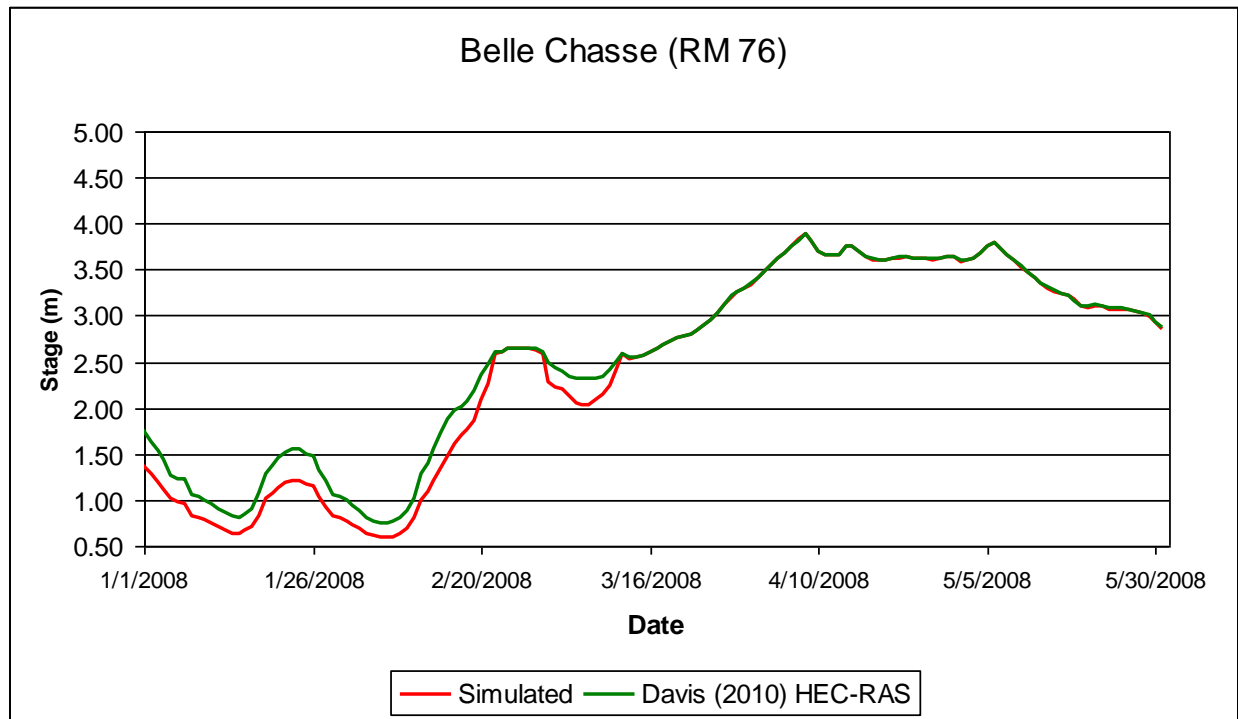


Figure 6.2 – Stage at Belle Chasse for the 1-D Hydrodynamics Calibration – 2008

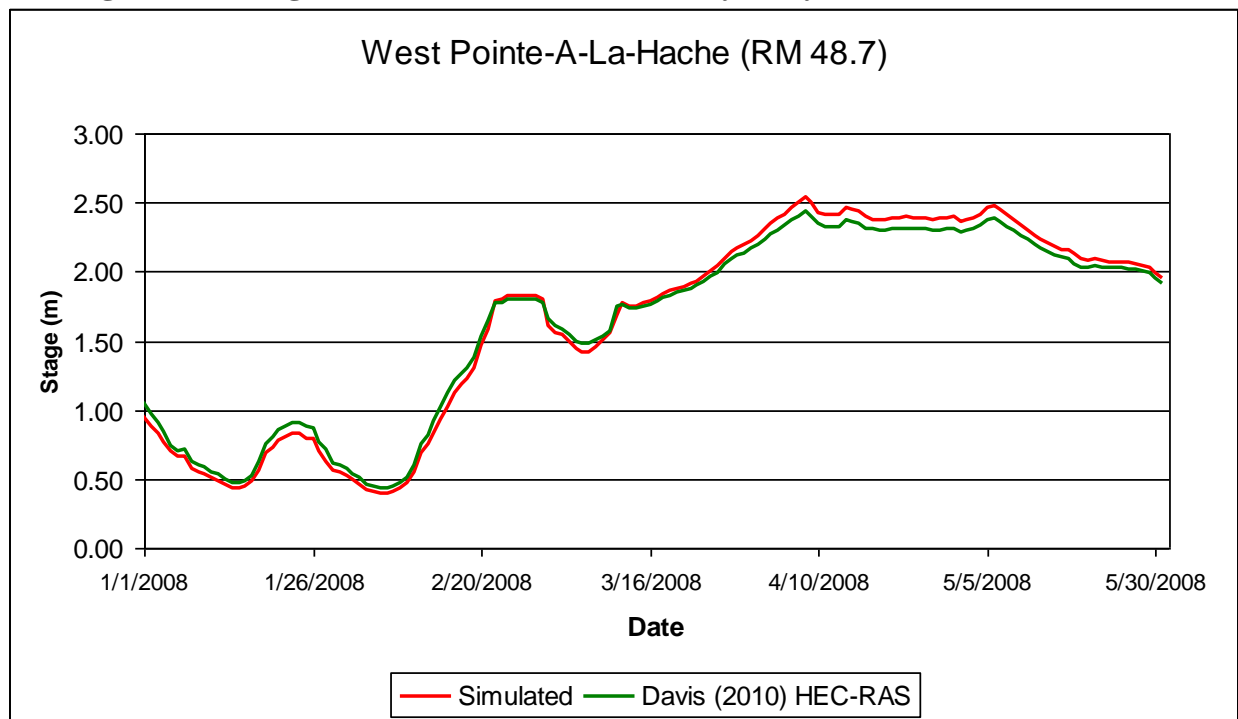


Figure 6.3 – Stage at West Pointe-A-La-Hache for the 1-D Hydrodynamics Calibration – 2008

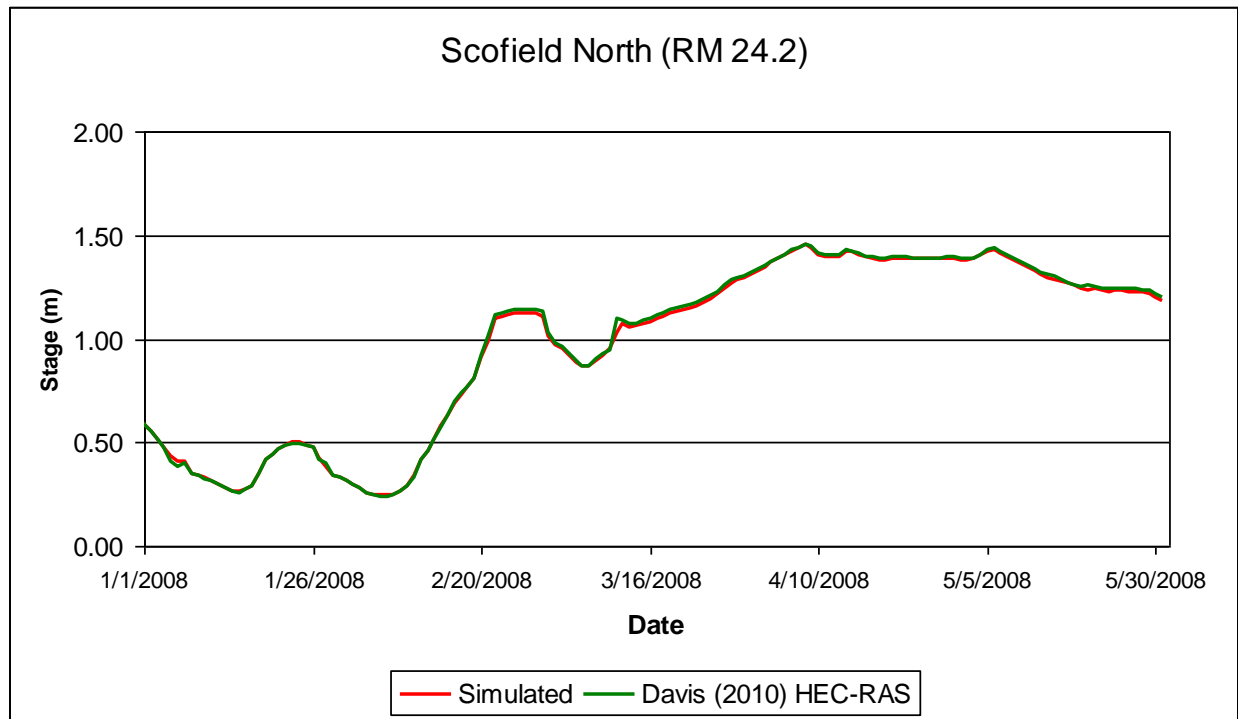


Figure 6.4 – Stage at Scofield North for the 1-D Hydrodynamics Calibration – 2008

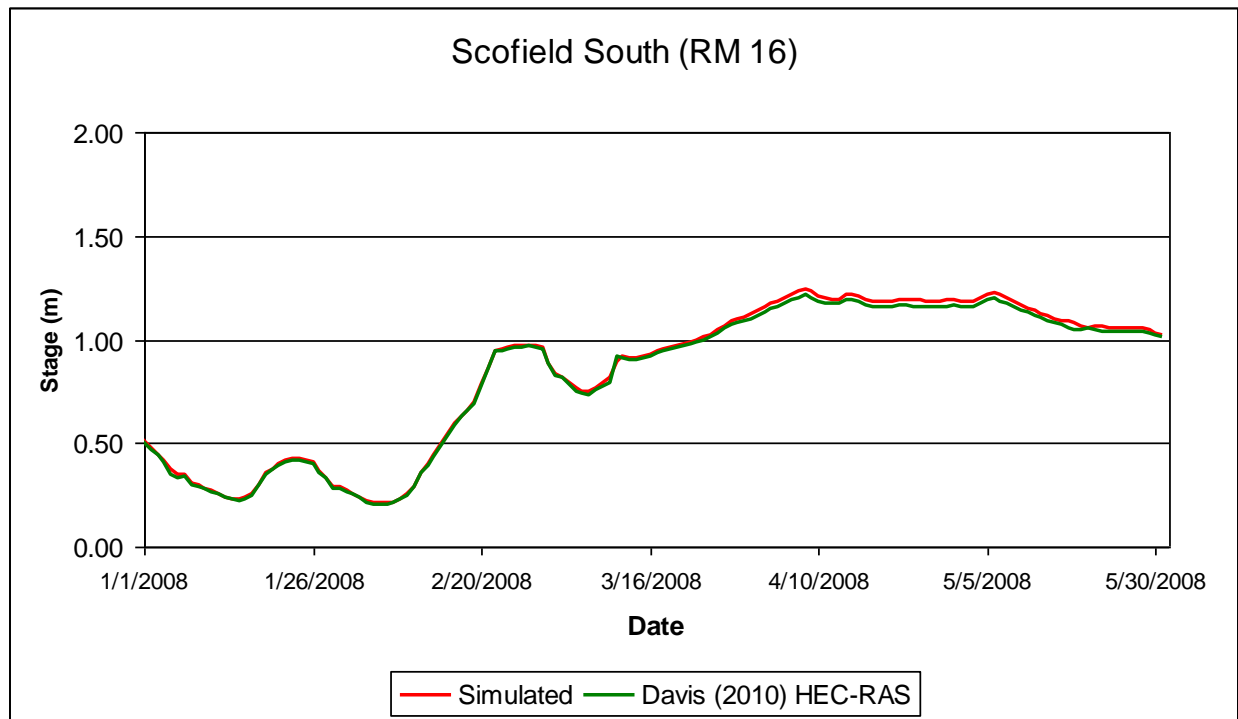


Figure 6.5 – Stage at Scofield South for the 1-D Hydrodynamics Calibration – 2008

The root mean square error (RMSE), the coefficient of efficiency and the bias of the results obtained during the hydrodynamics stage calibration were determined using the following equations:

$$\text{Root Mean Square Error (RMSE)} = \sqrt{\frac{\sum_{i=1}^N (O_i - P_i)^2}{N}} \quad (6.1)$$

$$\text{Coefficient of Efficiency} = 1.0 - \frac{\sum_{i=1}^N (O_i - P_i)^2}{\sum_{i=1}^N (O_i - \bar{O})^2} \quad (6.2)$$

$$\text{Bias Error} = 1.0 - \frac{\sum_{i=1}^N (O_i - P_i)}{N} \quad (6.3)$$

where O_i is the observed value, in this case taken as the result obtained by Davis (2010); P_i is the model predicted value; \bar{O} is the average of the observed value, in this case taken as the result obtained by Davis (2010); N is the number of observations.

Table 6-11 shows the coefficient of efficiency and the RMSE obtained for the hydrodynamics stage calibration. These results confirm a good agreement between the simulations and the Davis (2010) modeling.

Table 6-11 – RMSE and Coefficient of Efficiency for the Stage – 2008 Calibration

Mississippi River Location	RMSE (m)	RMSE (ft)	Efficiency	Bias Error (m)	Bias Error (ft)
Belle Chasse (RM 76)	0.20	0.65	0.963	0.137	0.449
West Pointe-À-La-Hache (RM 49)	0.07	0.22	0.991	0.001	0.003
Scofield North (RM 24)	0.01	0.03	0.999	0.005	0.017
Scofield South (RM 16)	0.02	0.05	0.998	-0.013	-0.043

The outflows calibration results are presented from Figure 6.6 to Figure 6.16. The RMSE and coefficient of efficiency were also calculated for the outflow calibration and the results obtained can be seen in Table 6-12. The results show the model is well calibrated for flow.

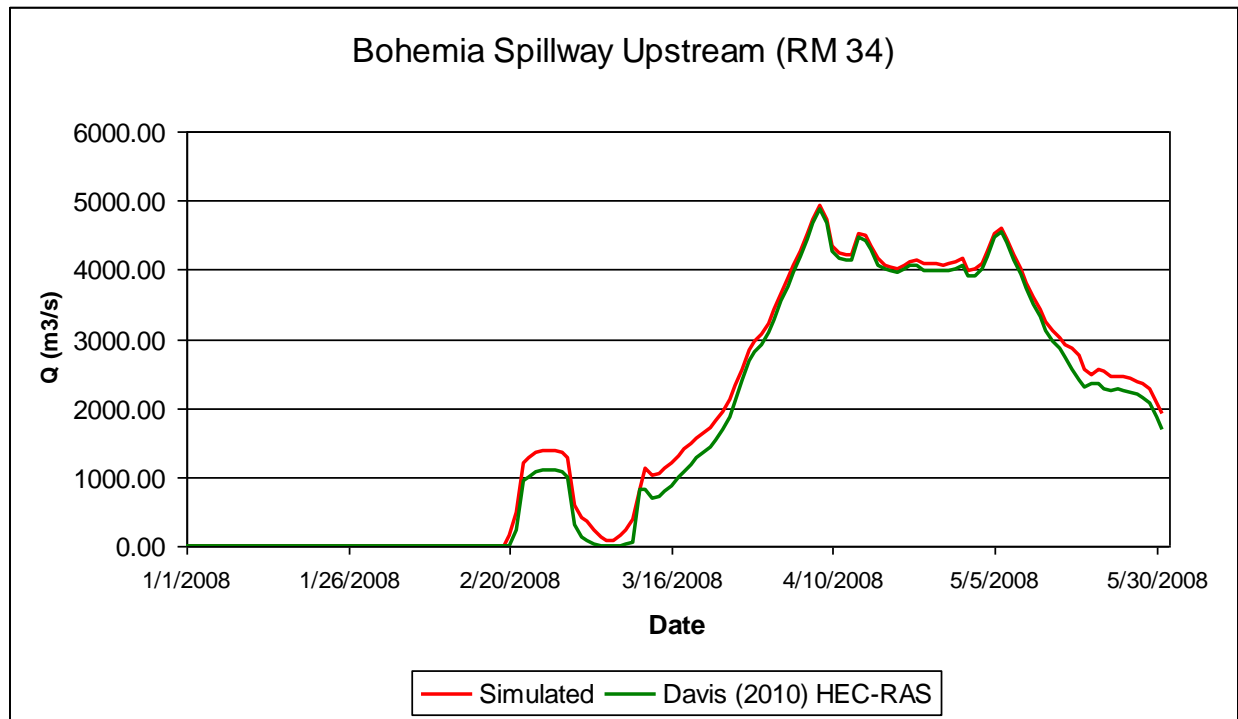


Figure 6.6 – Outflow at Bohemia Spillway Upstream for the 1-D Hydrodynamics Calibration – 2008

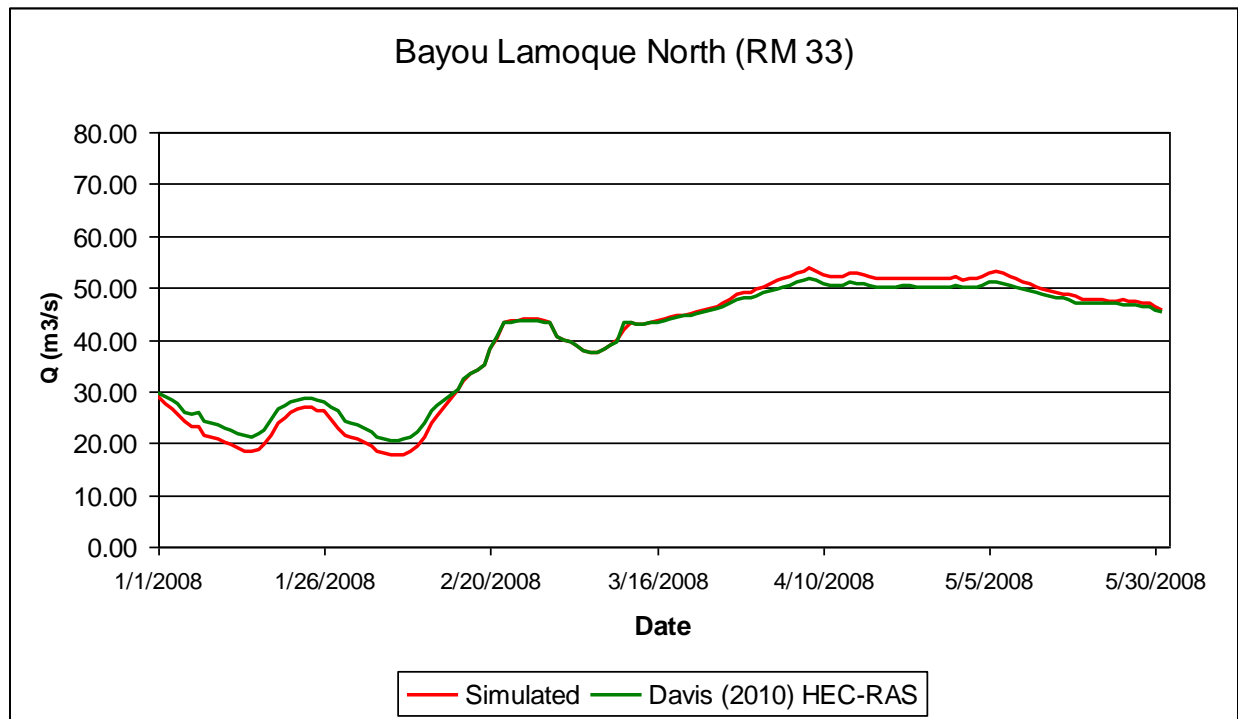


Figure 6.7 – Outflow at Bayou Lamoque North for the 1-D Hydrodynamics Calibration – 2008

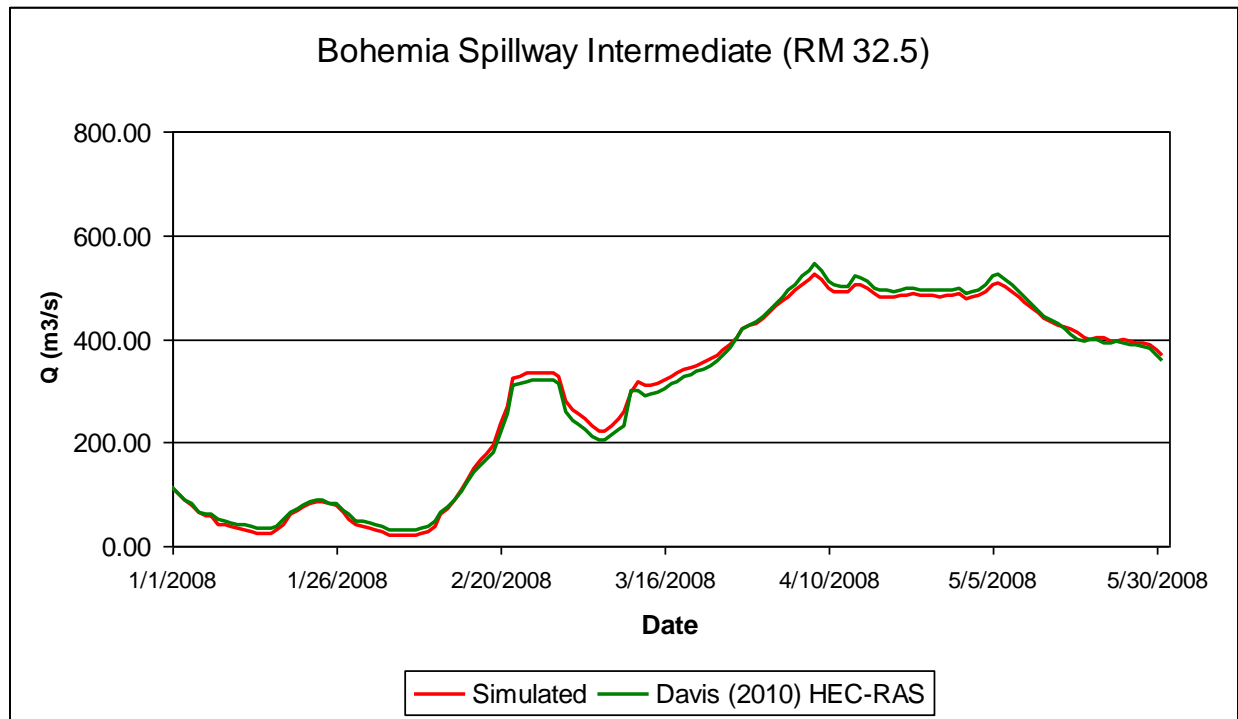


Figure 6.8 – Outflow at Bohemia Spillway Intermediate for the 1-D Hydrodynamics Calibration – 2008

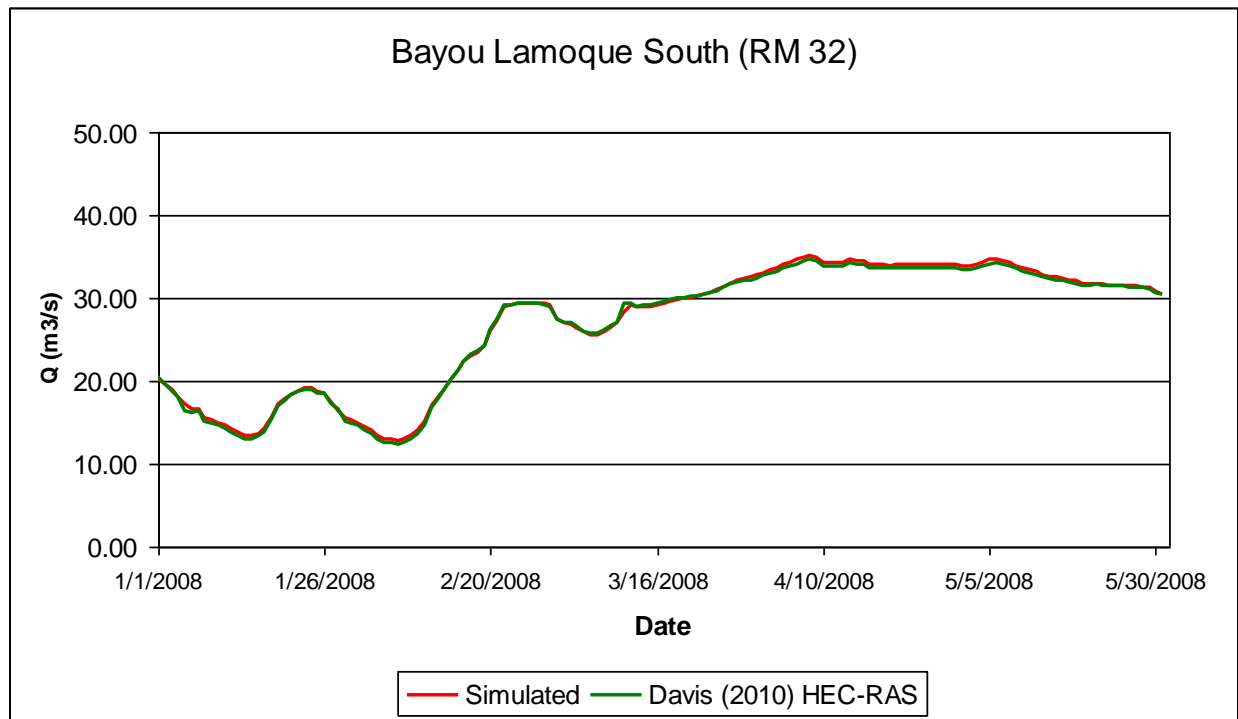


Figure 6.9 – Outflow at Bayou Lamoque South for the 1-D Hydrodynamics Calibration – 2008

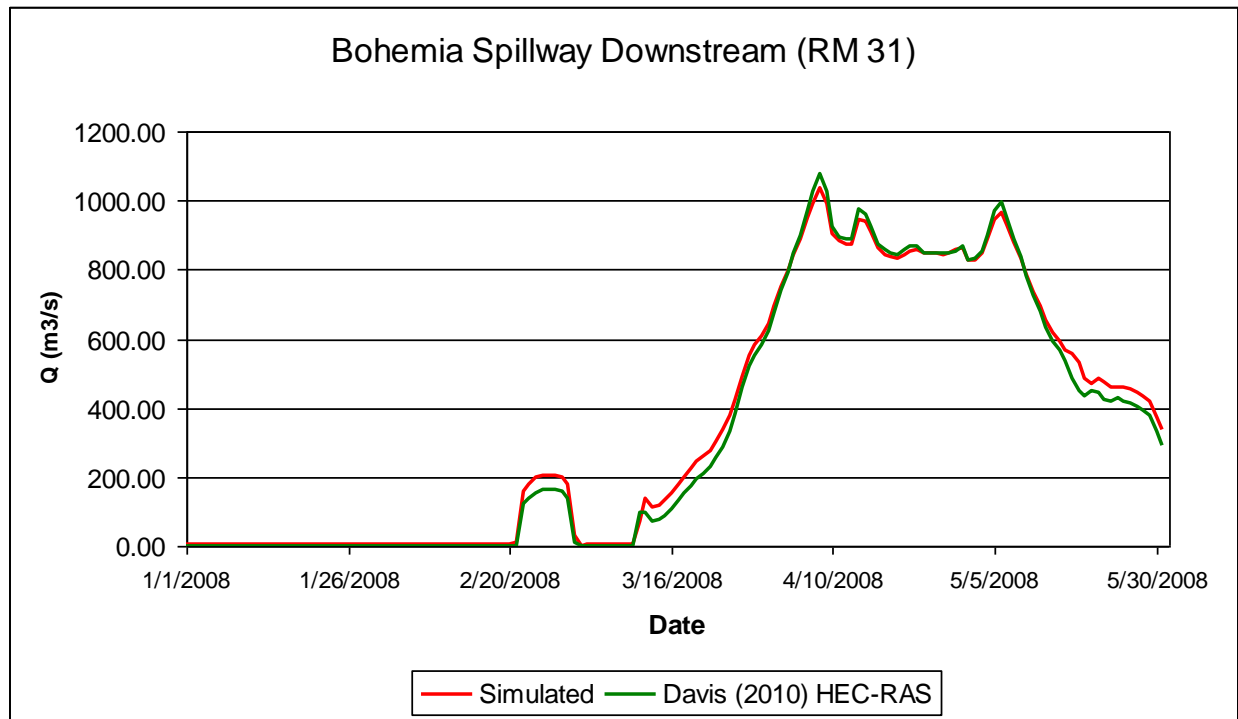


Figure 6.10 – Outflow at Bohemia Spillway Downstream for the 1-D Hydrodynamics Calibration – 2008

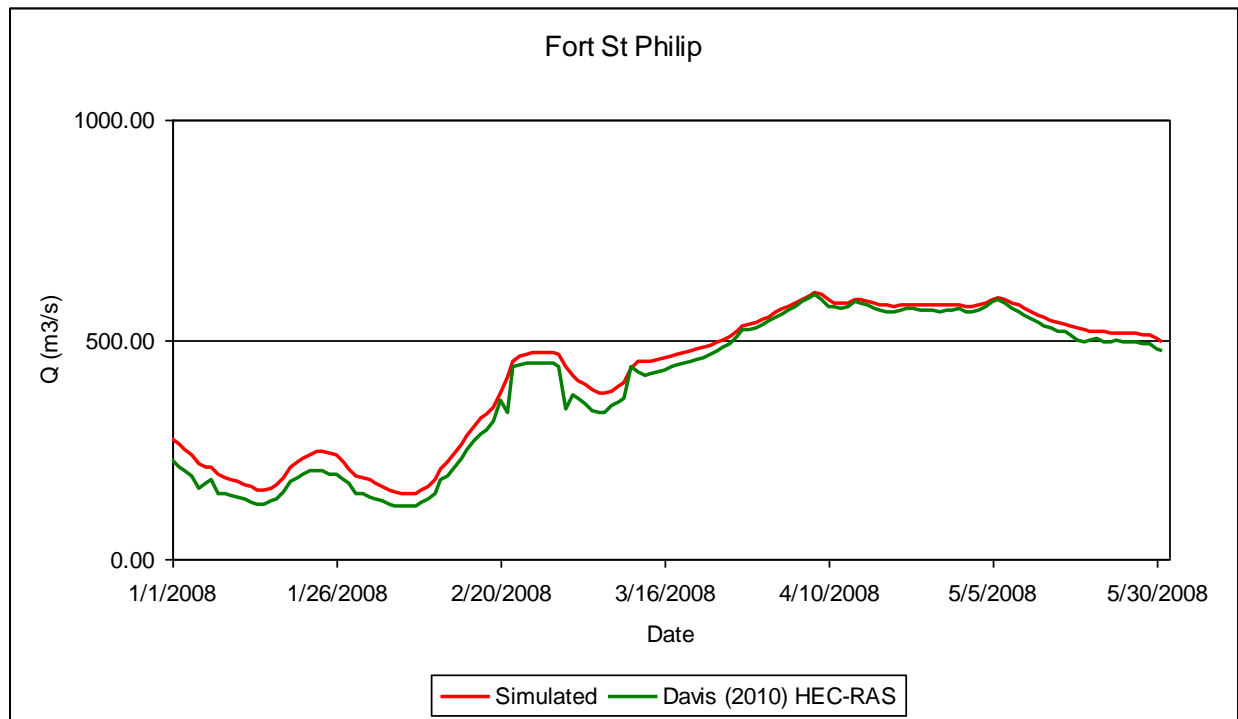


Figure 6.11 – Outflow at Fort St. Philip for the 1-D Hydrodynamics Calibration – 2008

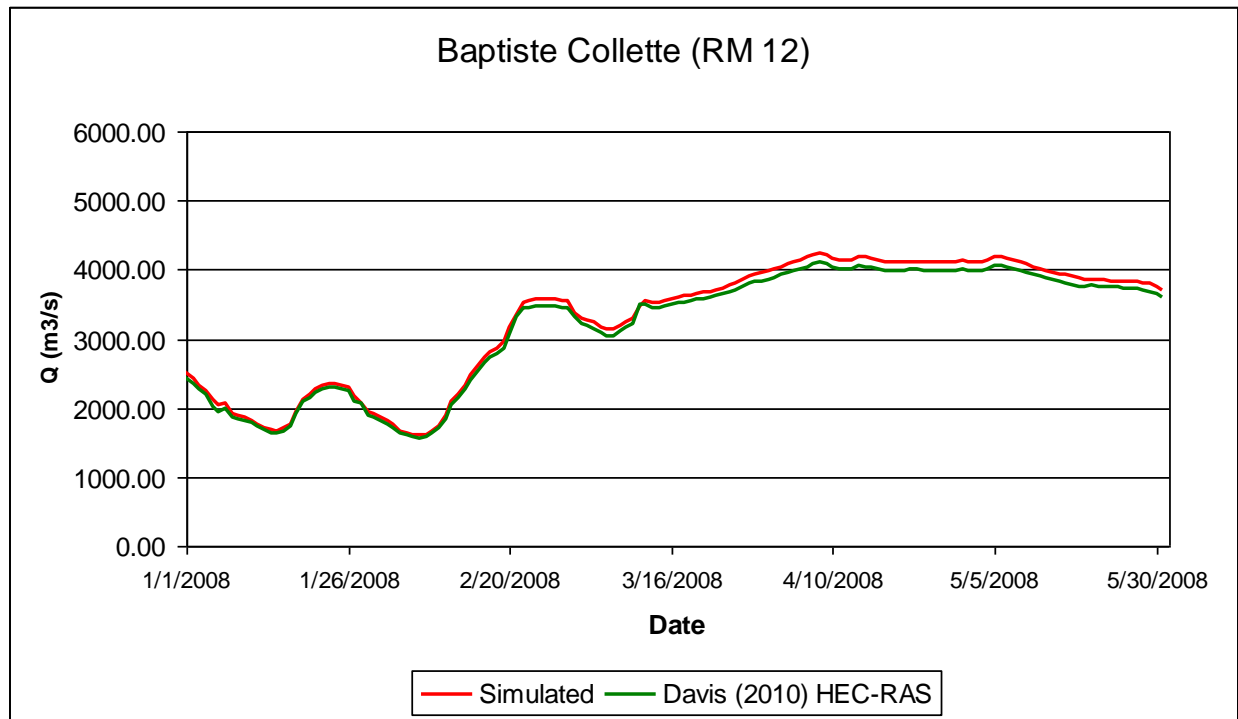


Figure 6.12 – Outflow at Baptiste Collette for the 1-D Hydrodynamics Calibration – 2008

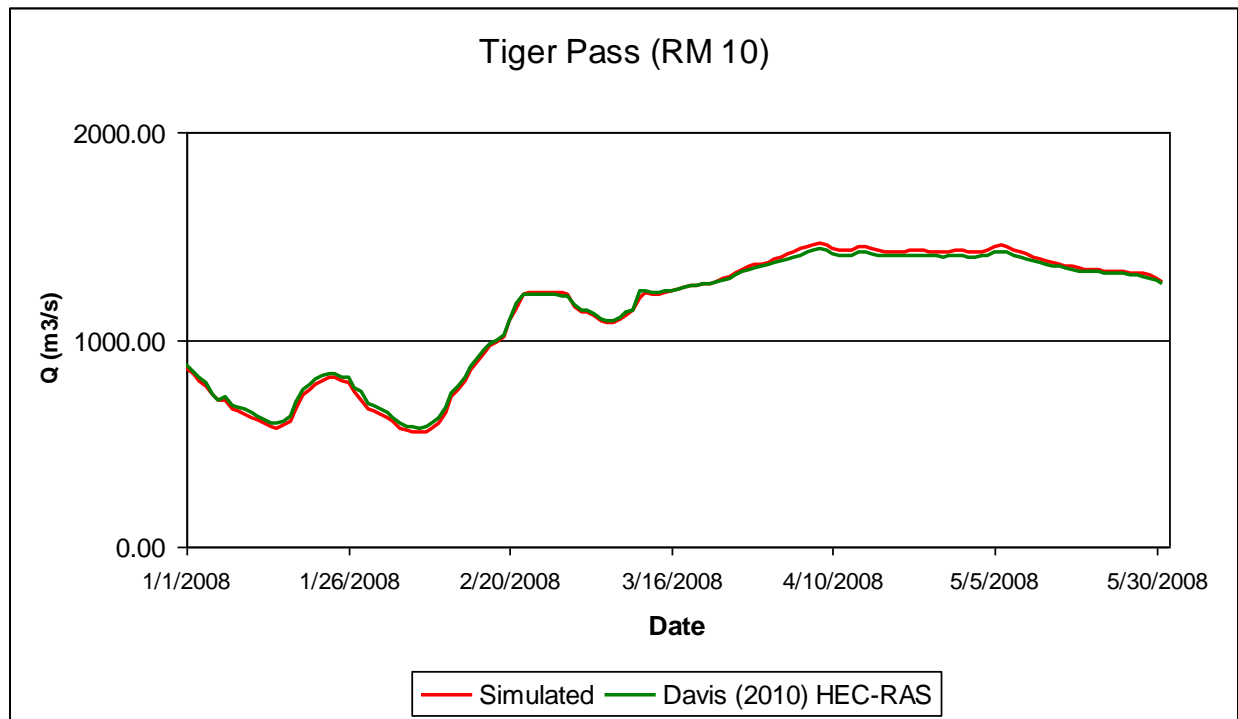


Figure 6.13 – Outflow at Tiger Pass for the 1-D Hydrodynamics Calibration – 2008

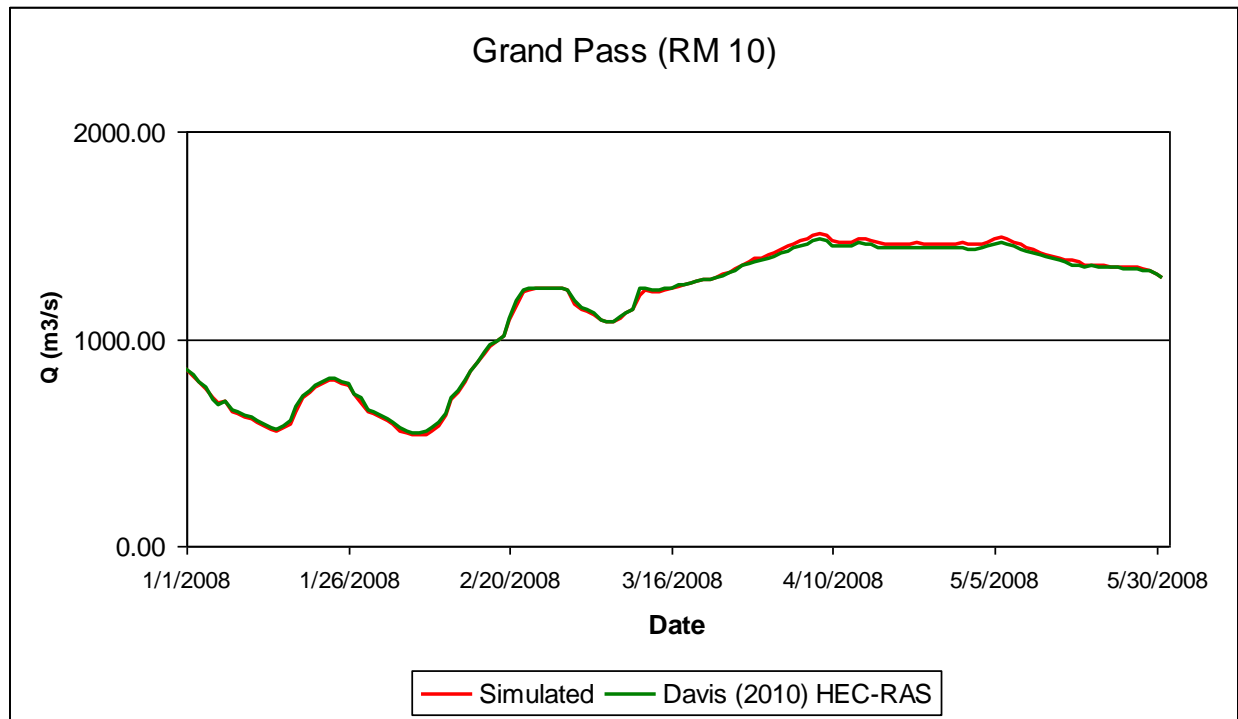


Figure 6.14 – Outflow at Grand Pass for the 1-D Hydrodynamics Calibration – 2008

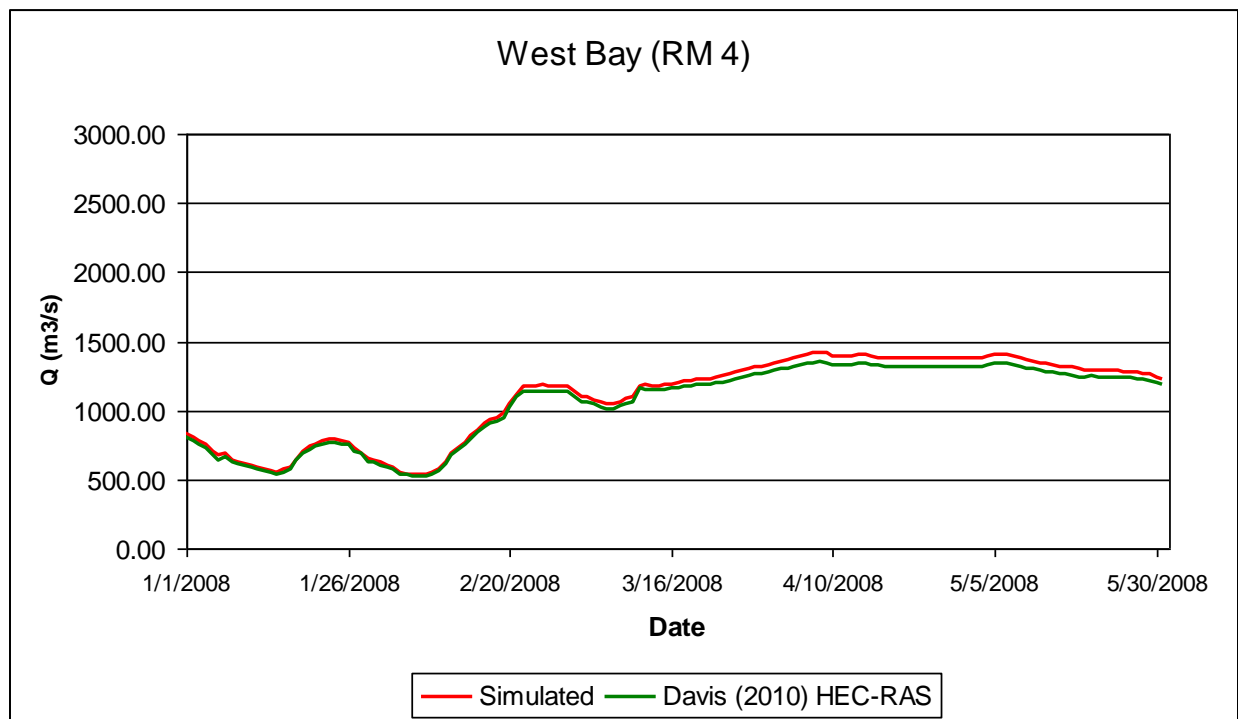


Figure 6.15 – Outflow at West Bay for the 1-D Hydrodynamics Calibration – 2008

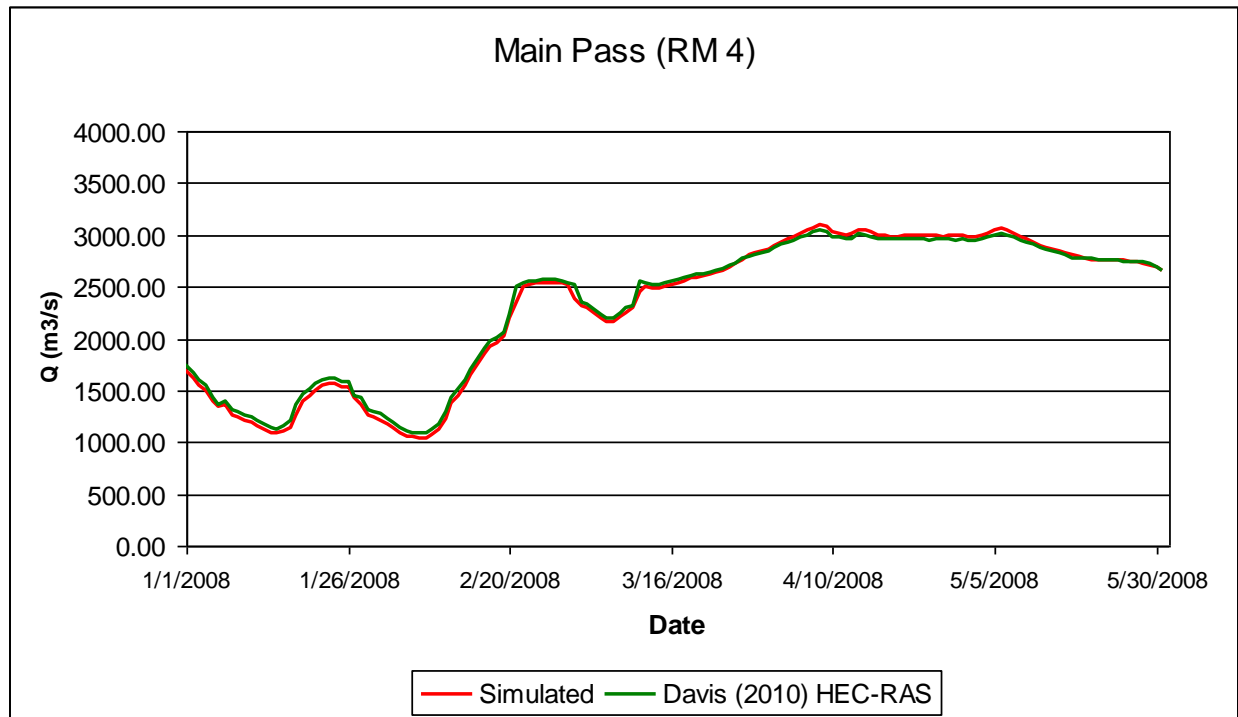


Figure 6.16 – Outflow at Main Pass for the 1-D Hydrodynamics Calibration – 2008

Table 6-11 shows the coefficient of efficiency and the RMSE obtained for the hydrodynamics stage calibration. These statistics confirm a good agreement between the simulations and the Davis (2010) modeling.

Table 6-12 – RMSE and Coefficient of Efficiency for the Outflows – 2008 Calibration

Site	RMSE (m ³ /s)	RMSE (cfs)	Efficiency	Bias (m ³ /s)	Bias (cfs)
Bohemia U/S (RM 34)	151	5,326	0.992	-107	-3,775
Bayou Lamoque North (RM 33)	5	167	0.849	0	-5
Bohemia Spillway Intermediate (RM 32.5)	11	400	0.996	1	31
Bayou Lamoque South (RM 32)	3	115	0.855	0	-16
Bohemia Spillway D/S (RM 31)	25	875	0.995	-12	-407
Fort St. Philip (RM 20)	29	1,042	0.969	-26	-911
Baptiste Collette (RM 12)	94	3,314	0.988	-88	-3093
Tiger Pass (RM 10)	19	668	0.996	-2	-63
Grand Pass (RM 10)	14	493	0.998	-4	-146
West Bay (RM 4)	44	1,555	0.976	-40	-1411
Main Pass (RM 4)	42	1,501	0.996	14	508

The magnitude of the flows being extracted at each outflow can now be reviewed with the calibrated model. The maximum, minimum and average water inflows and outflows (values with a

negative sign) for the 2008 period are shown in Table 6-13. It can be seen that at peak flows more than 60% of the main channel flow is diverted, that at average flow about 50% is diverted and that at low flow only around 40% is extracted in the reach. These results match what would be expected with base on available data for the Belle Chasse-Venice reach which is shown in Figure 6.17. According to these data a maximum of 45% of the main channel flow can be extracted just for the reach between Belle Chasse and Venice.

Table 6-13 – Inflows and Outflows for the Existing Outflows Case – 1-D Calibration – 2008

Site	Q maximum (m ³ /s, cfs)		Q minimum (m ³ /s, cfs)		Q average (m ³ /s, cfs)	
Belle Chasse* (RM 76)	33,830	1177000	10,331	364,850	22,556	796,549
White Ditch & Naomi (RM 65)	-42	-1500	-42	-1500	-42	-1500
West-Pointe-À-La-Hache (RM49)	-14	-500	-14	-500	-14	-500
Bohemia U/S (RM 34)	-4,922	-173,833	-11	-389	-1,817	-64,163
Bohemia Int. (RM 32.5)	-524	-18,508	-19	-669	-292	-10,304
Bohemia D/S (RM 31)	-1,037	-36,619	-2	-69	-355	-12,521
Bayou Lamoque N (RM 33)	-54	-1,897	-18	-621	-40	-1,401
Bayou Lamoque S (RM 32)	-35	-1,240	-13	-453	-27	-944
Fort St. Philip** (RM 20)	-605	-21,366	-149	-5,251	-417	-14,733
Baptiste Collette** (RM 12)	-4,235	-149,567	-1,604	-56,651	-3,258	-115,064
Grand Pass** (RM 10)	-1,506	-53,176	-535	-18,897	-1,136	-40,107
Tiger Pass** (RM 10)	-1,468	-51,831	-552	-19,478	-1,125	-39,729
West Bay (RM 4)	-1,421	-50,189	-532	-18,789	-1,088	-38,437
Main Pass** (RM 4)	-3,096	-109,326	-1,036	-36,603	-2,300	-81,220
D/S of Main Pass*** (RM 3)	14,871	507,448	5,804	204,980	10,645	375,926

*Upstream Boundary

**Natural Outflows (Distributaries)

***Downstream Boundary

As stated before, following the hydrodynamics 2008 calibration, validation for the 2007 calendar year was performed. The stage validation results can be seen in Figure 6.18 to Figure 6.21. The RMSE and coefficient and efficiency results are shown in Table 6-16. There is a good agreement between the simulation results and the Davis (2010) results showing that the model is validated for stage.

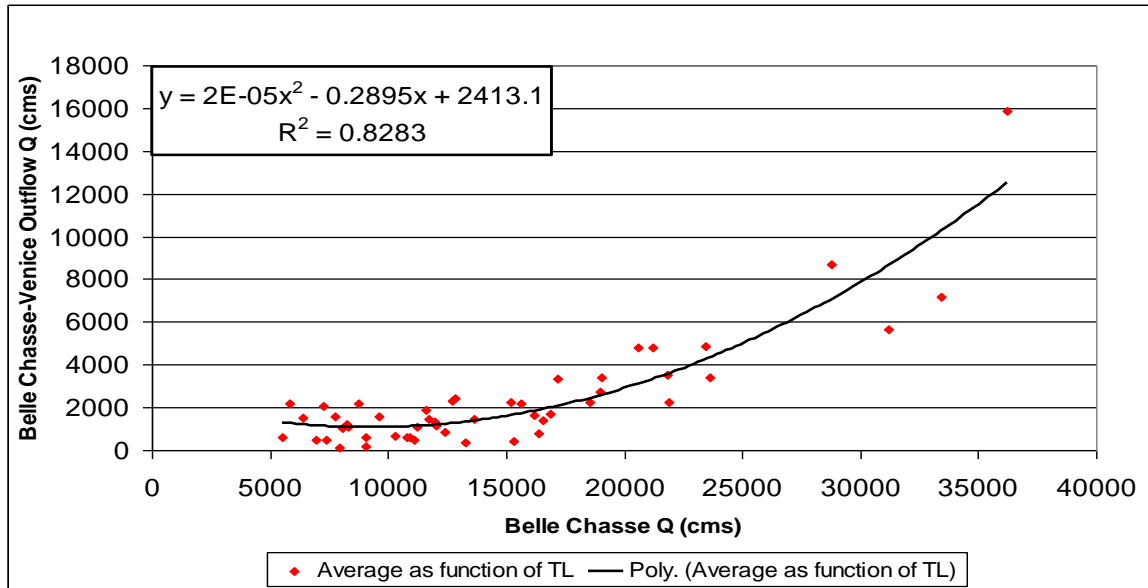


Figure 6.17 – Total Outflow Quadratic Function adjusted to field measurements (*Based on Data from Pratt 2009*)

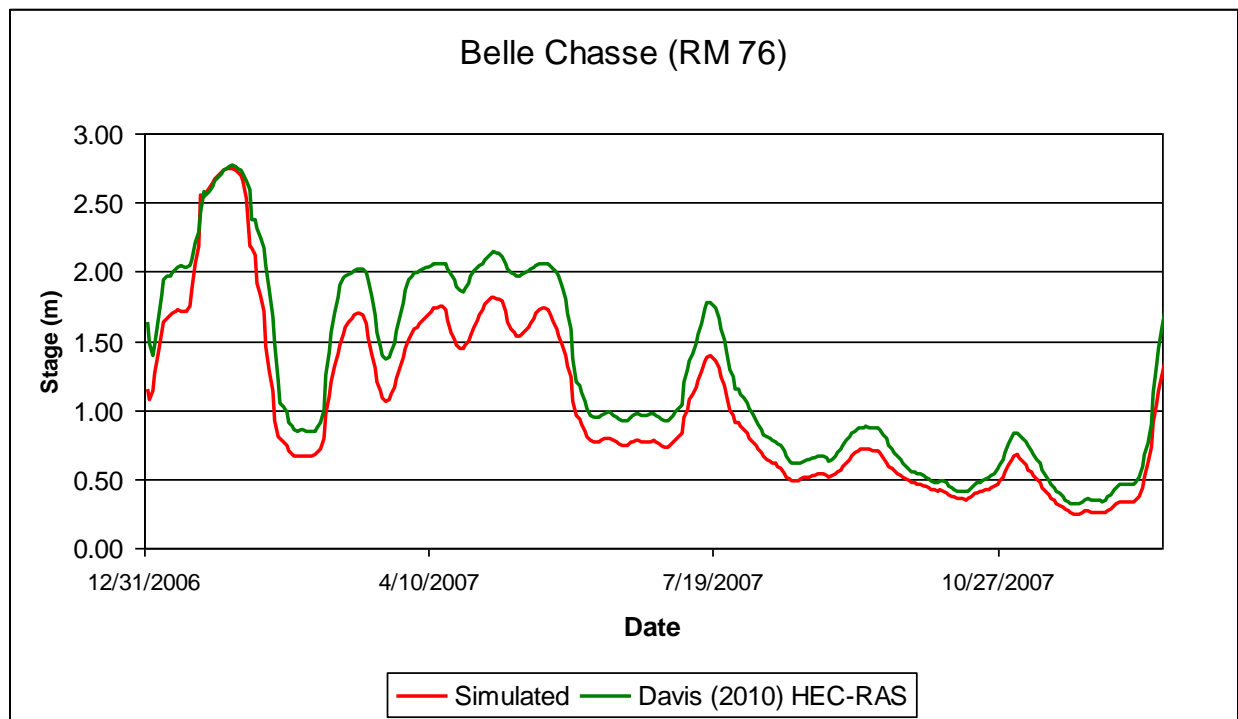


Figure 6.18 – Stage at Belle Chasse for the 1-D Hydrodynamics Validation – 2007

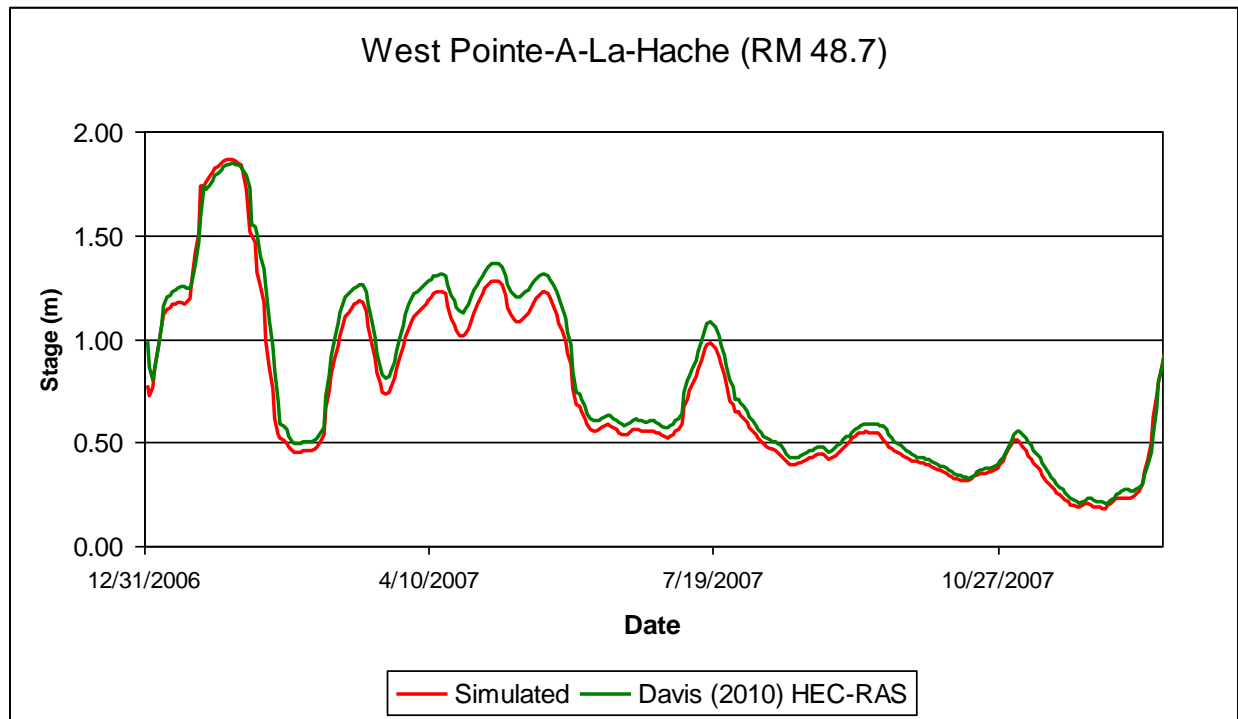


Figure 6.19 – Stage at West Pointe-Á-La-Hache for the 1-D Hydrodynamics Validation – 2007

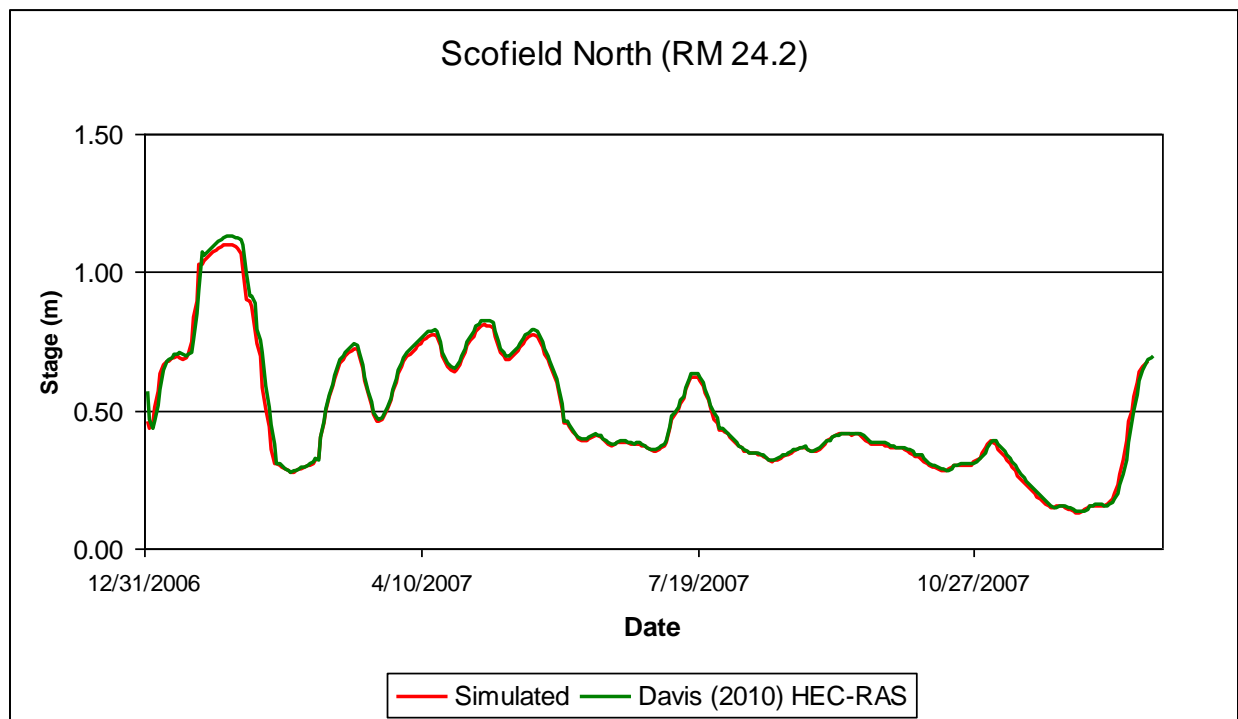


Figure 6.20 – Stage at Scofield North for the 1-D Hydrodynamics Validation – 2007

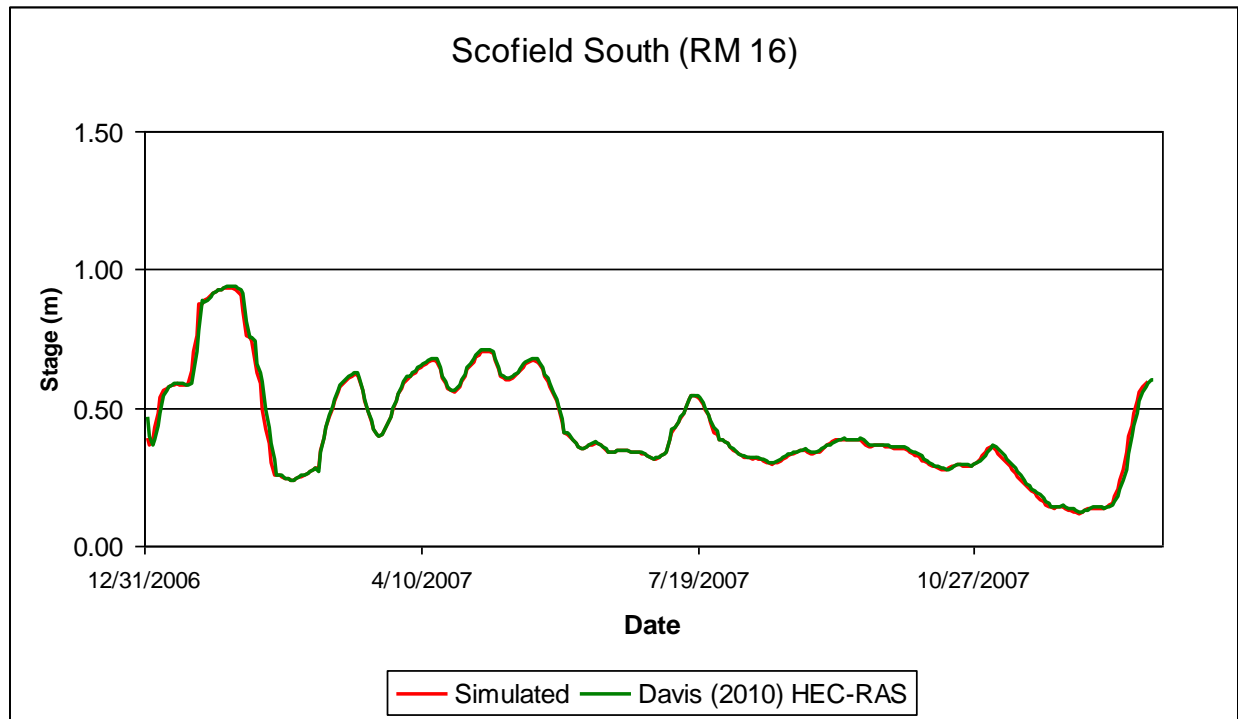


Figure 6.21 – Stage at Scofield South for the 1-D Hydrodynamics Validation – 2007

Table 6-14 – RMSE and Coefficient of Efficiency for the Stage – 2007 Validation

Mississippi River Location	RMSE (m)	RMSE (ft)	Efficiency	Bias (m)	Bias (ft)
Belle Chasse (RM 76)	0.25	0.84	0.859	0.220	0.722
West Pointe-À-La-Hache (RM 49)	0.07	0.24	0.993	0.055	0.181
Scofield North (RM 24)	0.02	0.07	0.991	0.008	0.026
Scofield South (RM 16)	0.02	0.06	0.992	0.003	0.010

The outflows validation results can be seen from Figure 6.22 to Figure 6.32. The RMSE and coefficient of efficiency results are shown in

Table **6-15**. There is a good agreement between the simulation results and the Davis (2010) results for the majority of the outflows. However, there is a significant difference in the cases of Bayou Lamoque South, Bohemia Spillway U/S and Bohemia Spillway D/S. It is important to notice that Bayou Lamoque South and Bohemia D/S are not major flow extractions but Bohemia Spillway U/S is a significant outflow. The overall error is still small.

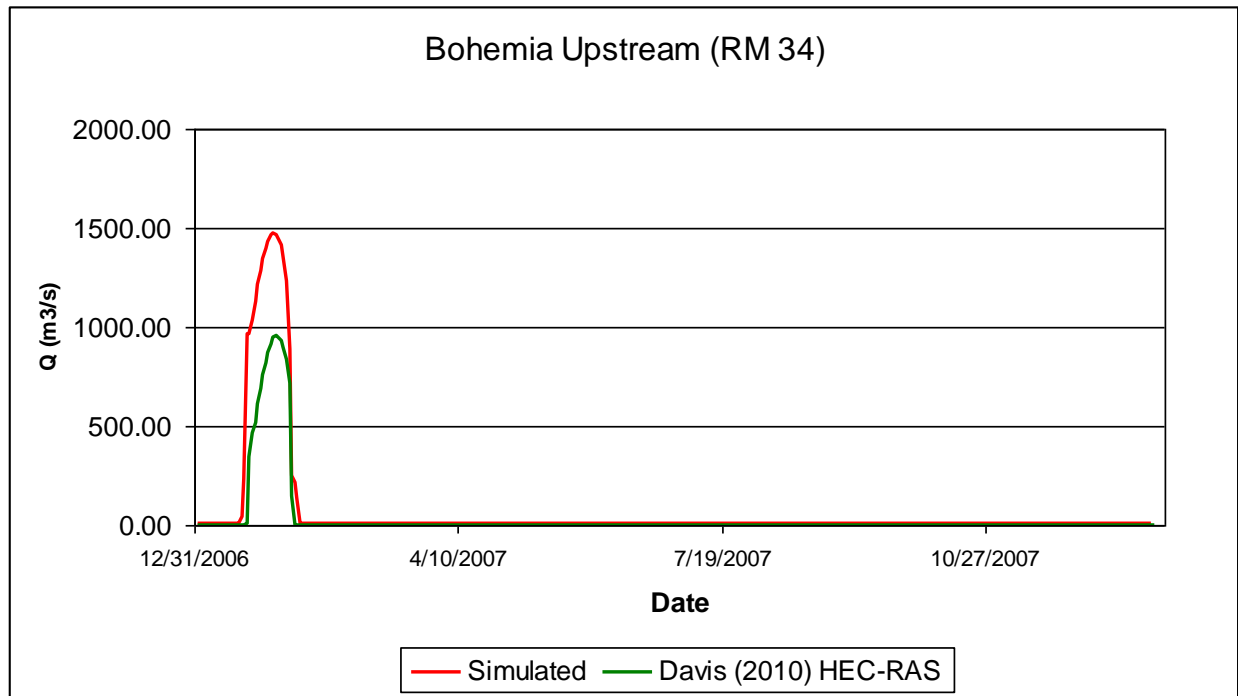


Figure 6.22 – Outflow at Bohemia Spillway Upstream for the 1-D Hydrodynamics Validation – 2007

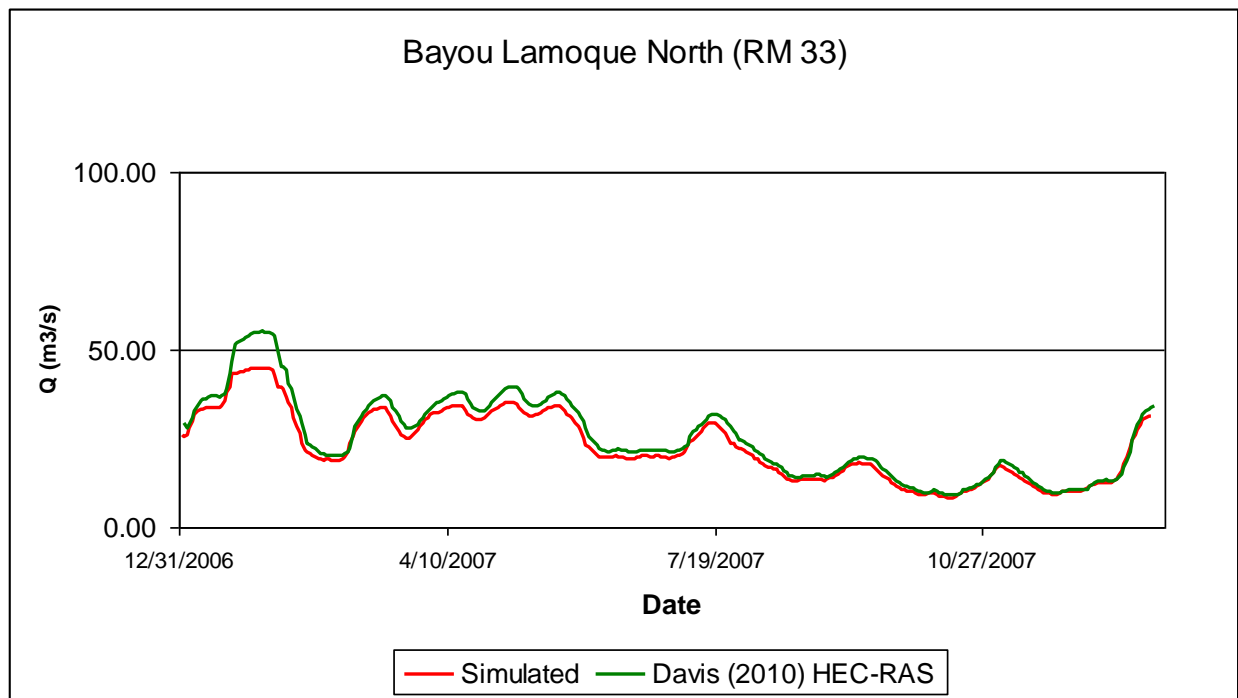


Figure 6.23 – Outflow at Bayou Lamoque North for the 1-D Hydrodynamics Validation – 2007

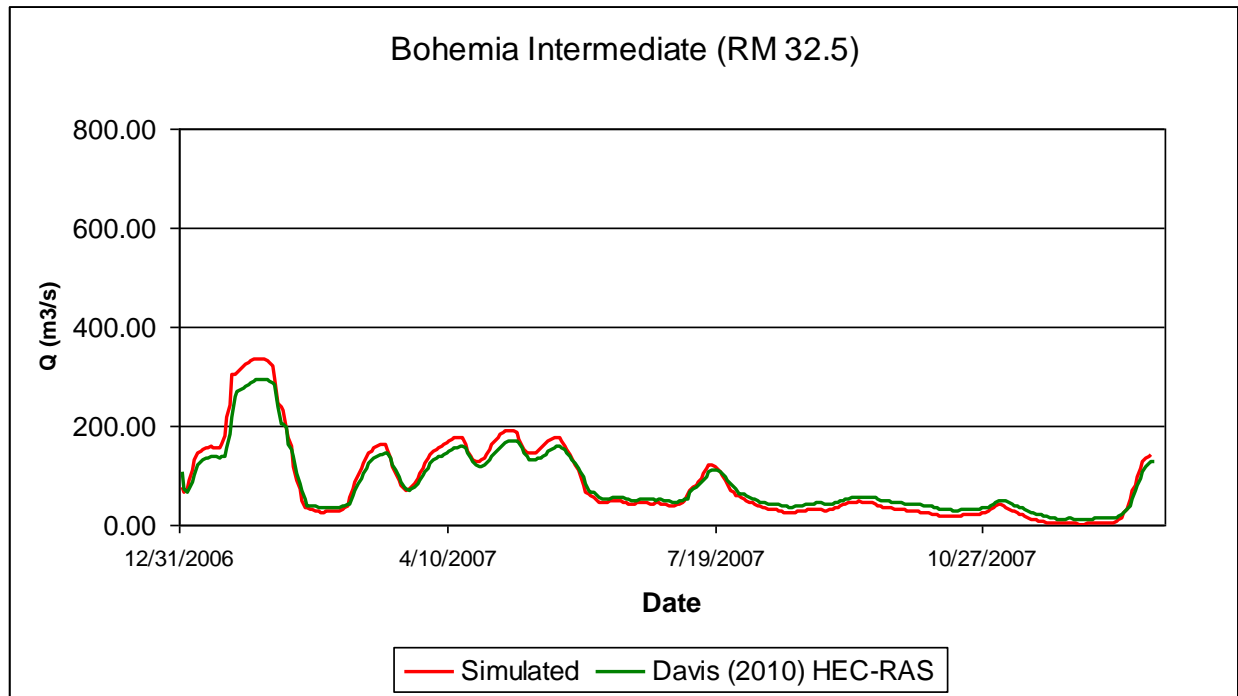


Figure 6.24 – Outflow at Bohemia Intermediate for the 1-D Hydrodynamics Validation – 2007

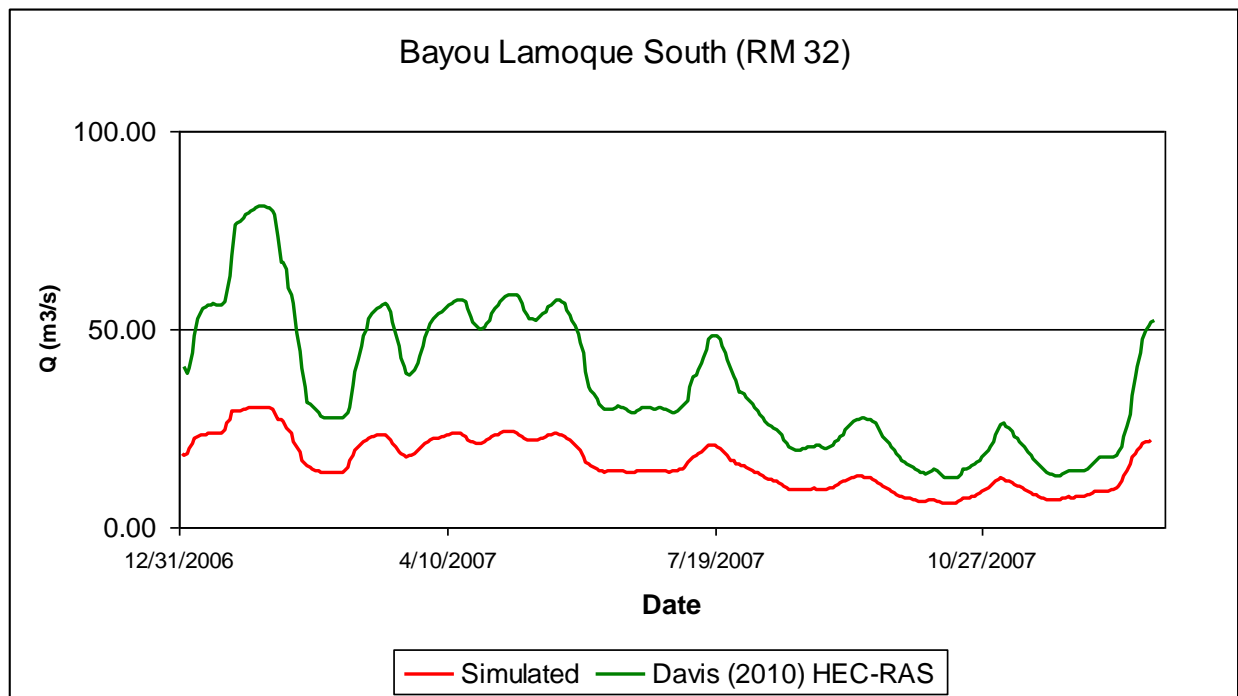


Figure 6.25 – Outflow at Bayou Lamoque South for the 1-D Hydrodynamics Validation – 2007

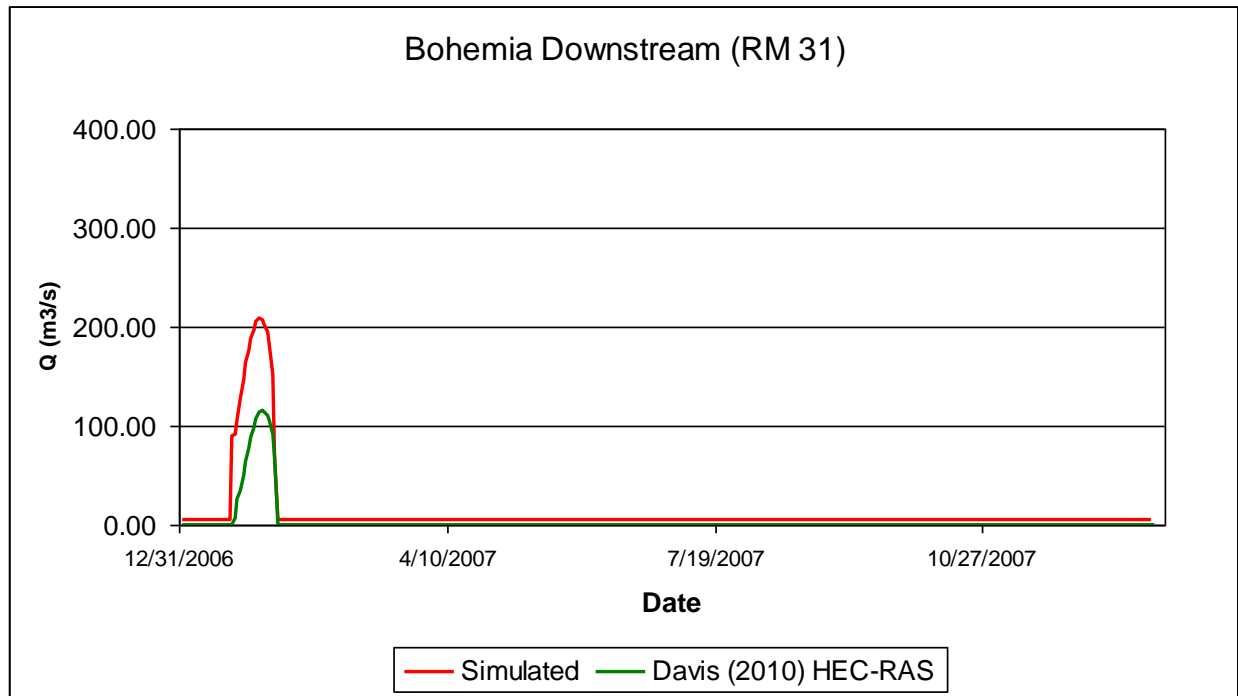


Figure 6.26 – Outflow at Bohemia Downstream for the 1-D Hydrodynamics Validation – 2007

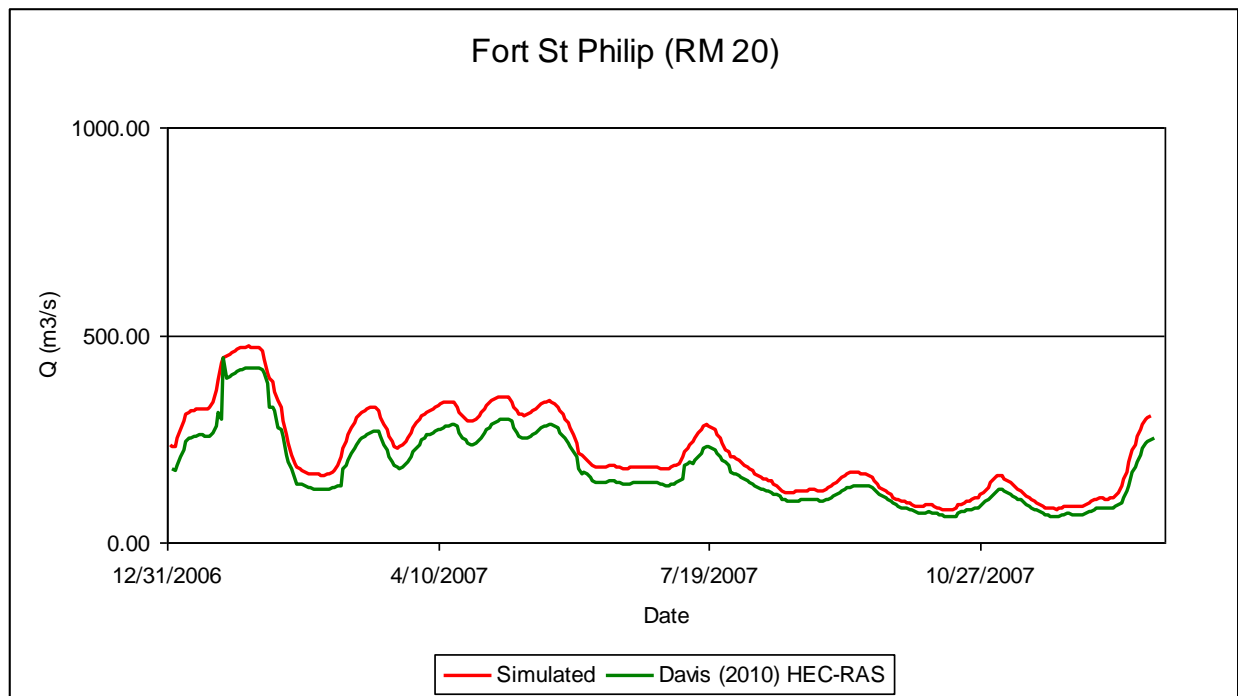


Figure 6.27 – Outflow at Fort St. Philip for the 1-D Hydrodynamics Validation – 2007

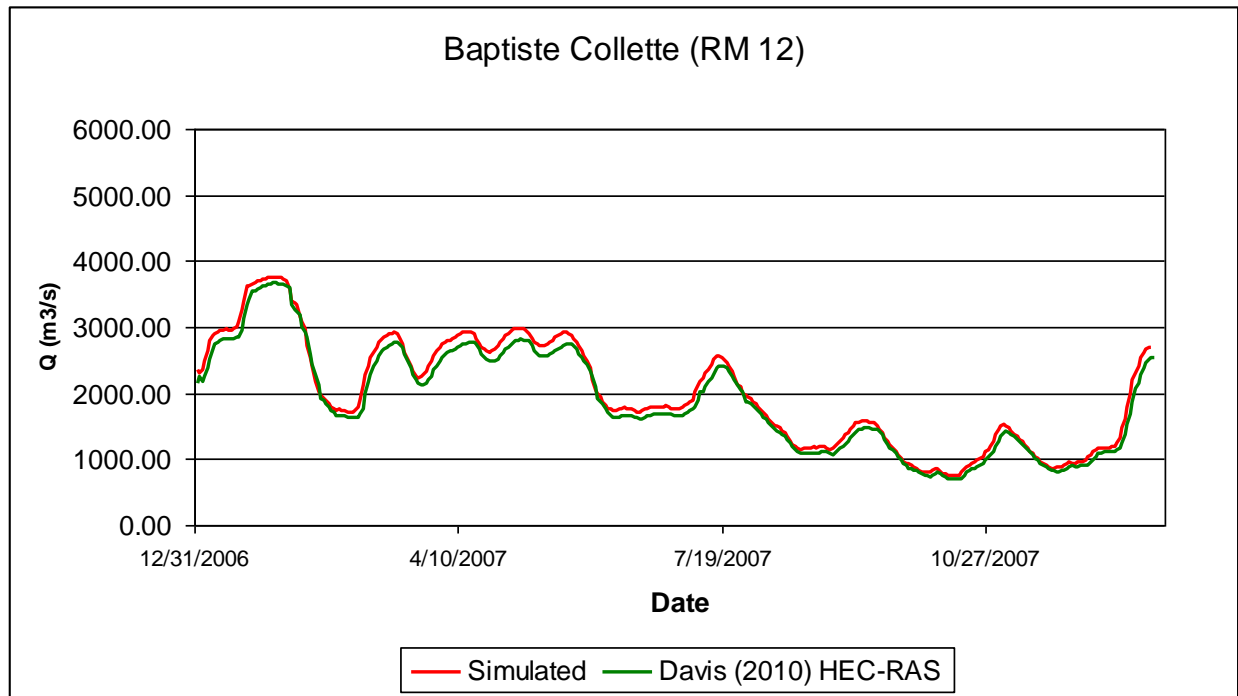


Figure 6.28 – Outflow at Baptiste Collette for the 1-D Hydrodynamics Validation – 2007

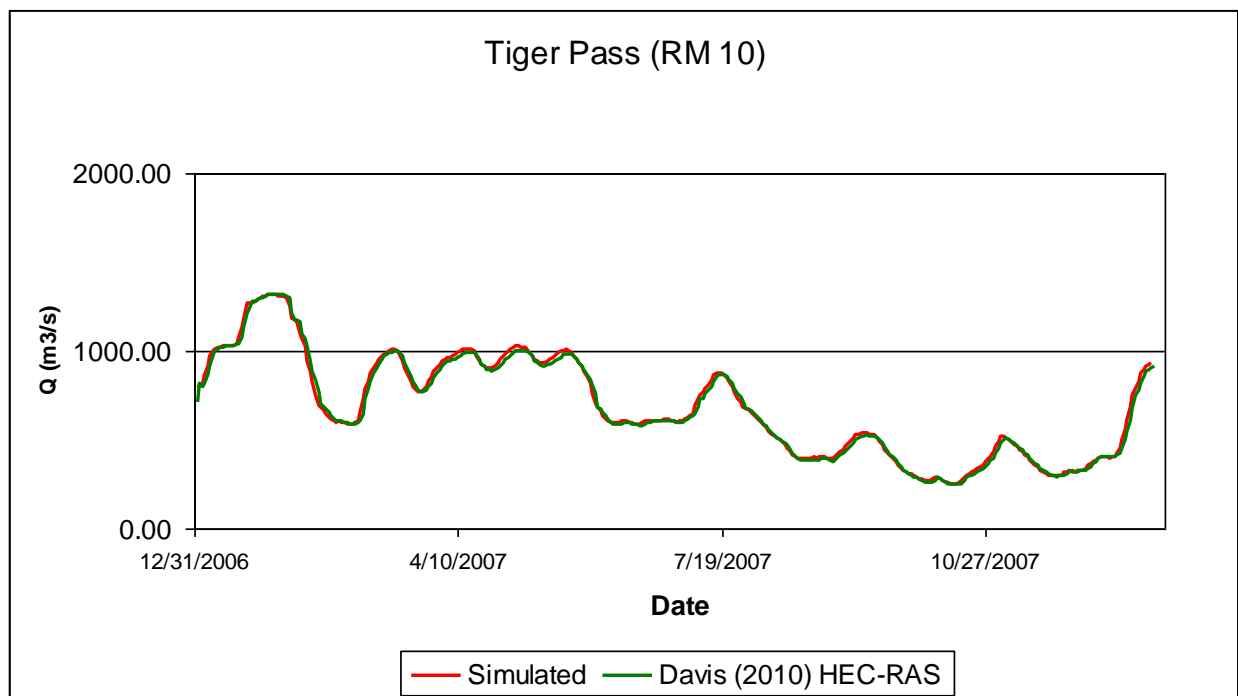


Figure 6.29 – Outflow at Tiger Pass for the 1-D Hydrodynamics Validation – 2007

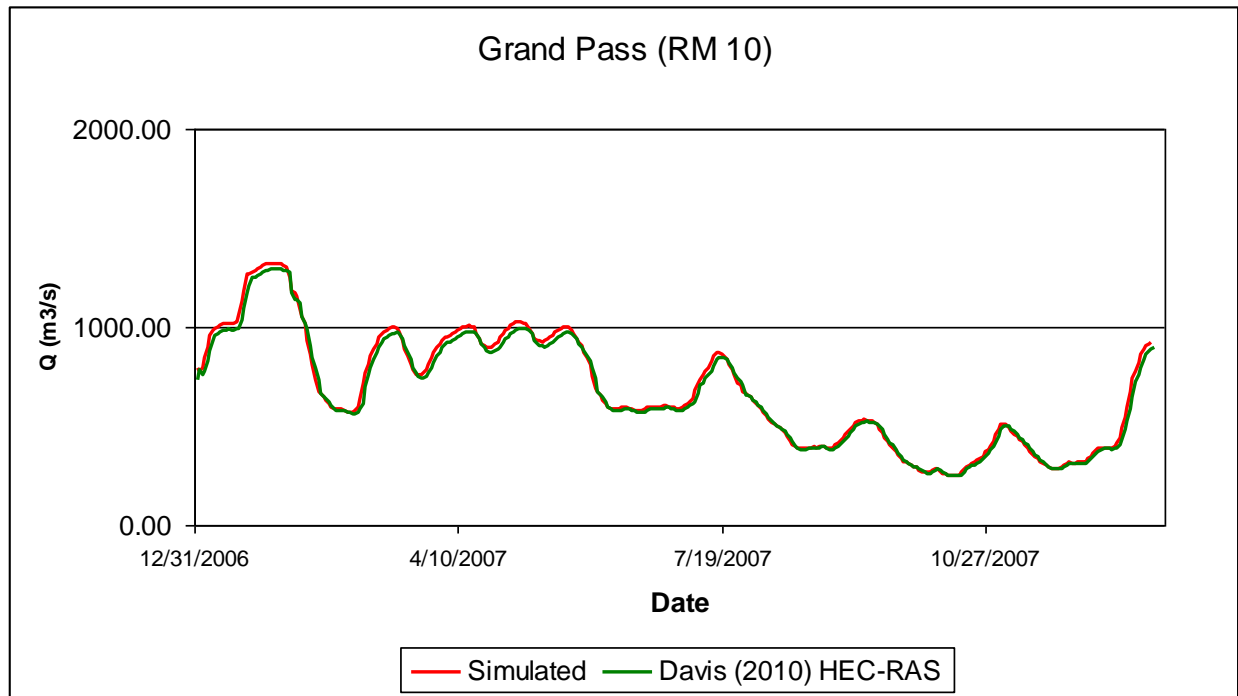


Figure 6.30 – Outflow at Grand Pass for the 1-D Hydrodynamics Validation – 2007

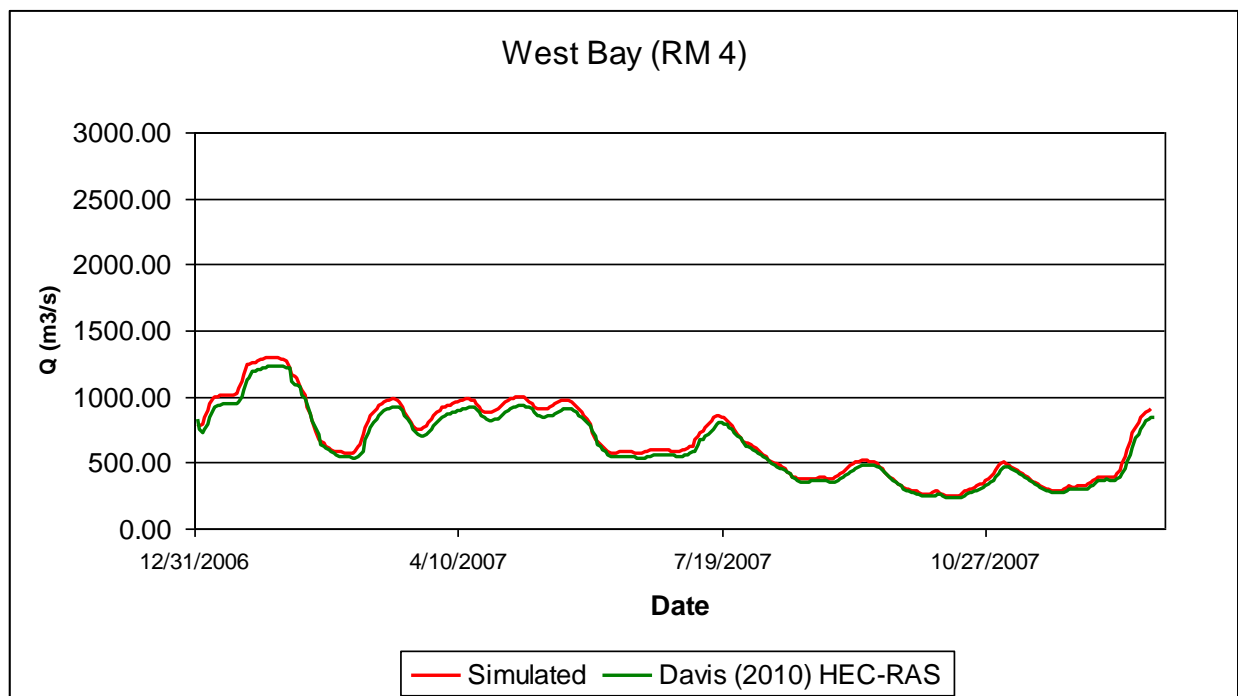


Figure 6.31 – Outflow at West Bay for the 1-D Hydrodynamics Validation – 2007

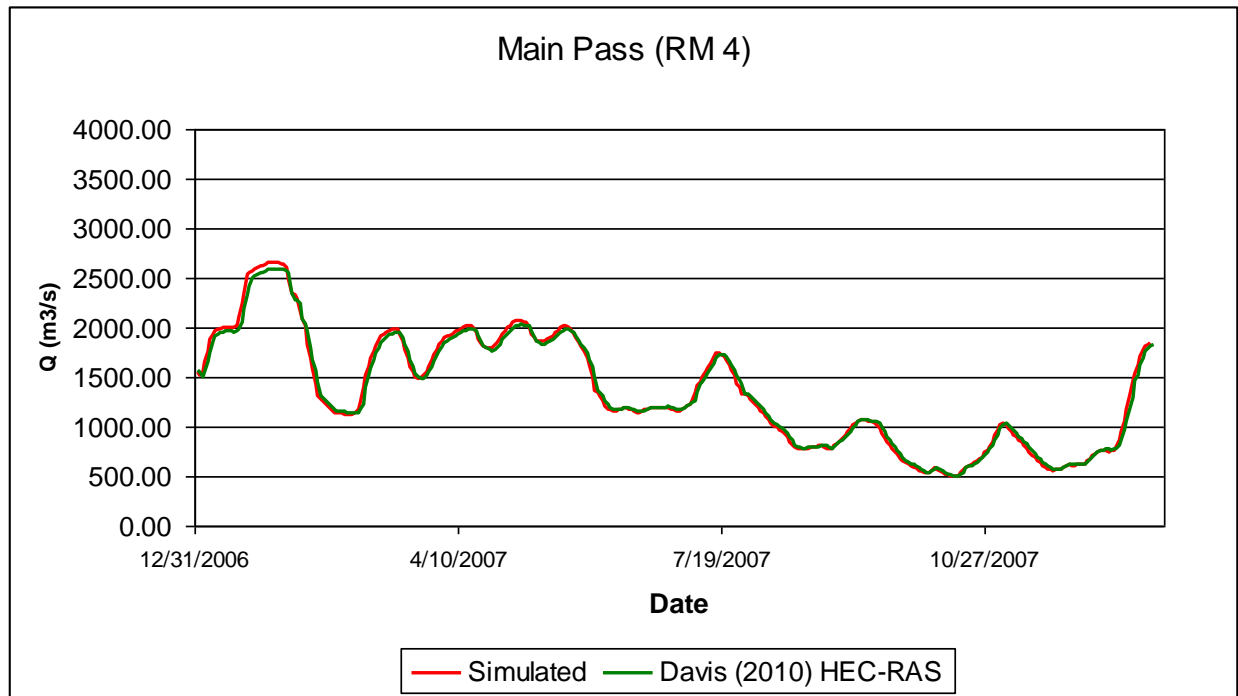


Figure 6.32 – Outflow at Main Pass for the 1-D Hydrodynamics Validation – 2007

Table 6-15 – RMSE and Coefficient of Efficiency for the Outflows – 2007 Validation

Site	RMSE (m ³ /s)	RMSE (cfs)	Efficiency	Bias Error (m)	Bias Error (cfs)
Bohemia U/S (RM 34)	0.58	21	0.412	0	0
Bayou Lamoque North (RM 33)	0.09	3	0.924	2	82
Bohemia Spillway Interm (RM 32.5)	0.44	15	0.932	-1	-52
Bayou Lamoque South (RM 32)	0.80	28	-0.712	20	715
Bohemia Spillway D/S (RM 31)	0.26	9	-0.214	-9	-305
Fort St. Philip (RM 20)	1.97	69	0.764	-39	-1391
Baptiste Collette (RM 12)	5.51	195	0.972	-109	-3865
Tiger Pass (RM 10)	0.38	13	0.993	-8	-272
Grand Pass (RM 10)	0.50	17	0.989	-15	-530
West Bay (RM 4)	1.88	66	0.965	-41	-1445
Main Pass (RM 4)	0.43	15	0.992	-8	-286

Once the model was calibrated and validated for hydrodynamics it was time to calibrate it for the suspended sand transport. Some adjustments to the roughness coefficients and to the hydraulic structures geometry were necessary. The stage calibration with mobile-bed is shown in Figure 6.33 to Figure 6.36.

The outflows calibration with mobile-bed is shown from Figure 6.33 to Figure 6.47.

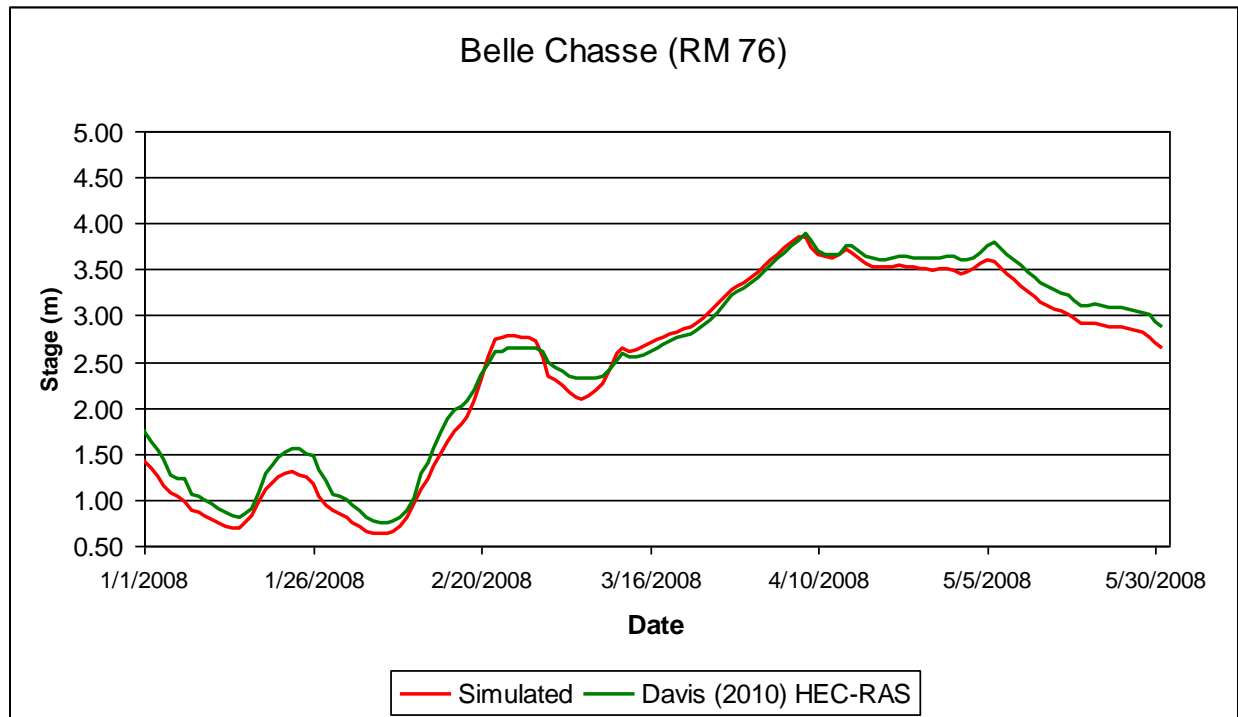


Figure 6.33 – Stage at Belle Chasse for the 1-D Mobile-Bed Calibration – 2008

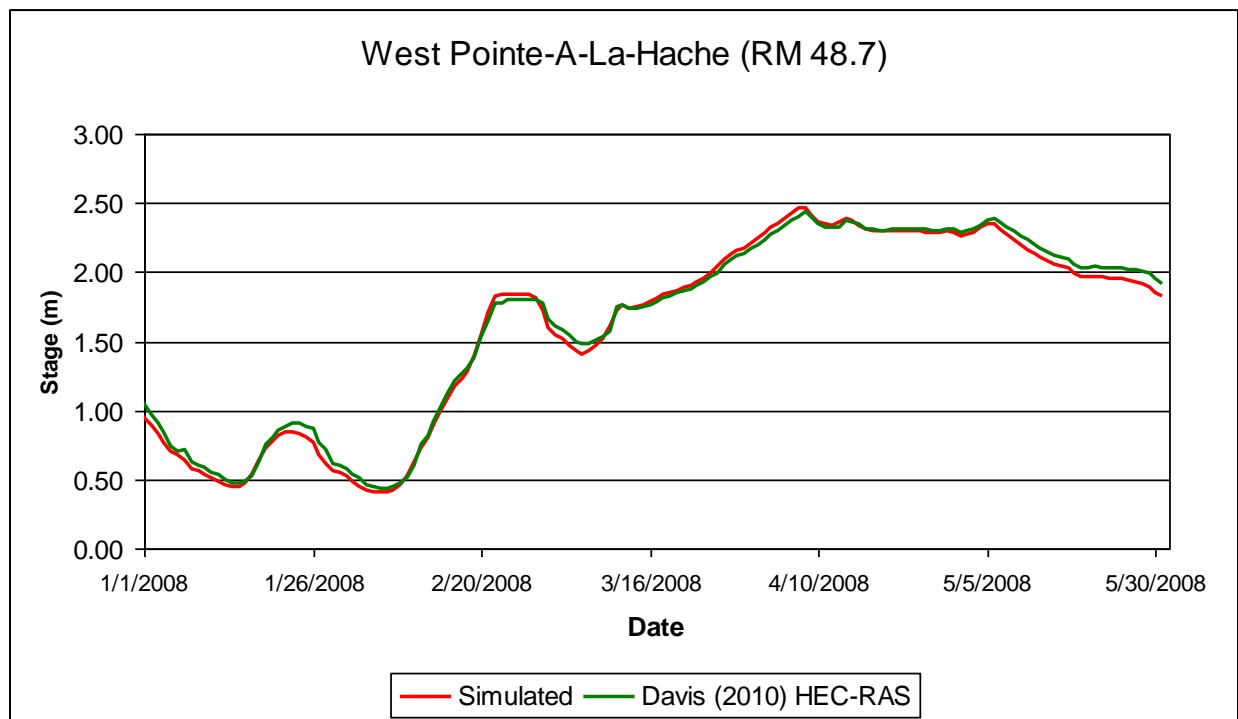


Figure 6.34 – Stage at West Pointe-À-La-Hache for the 1-D Mobile-Bed Calibration – 2008

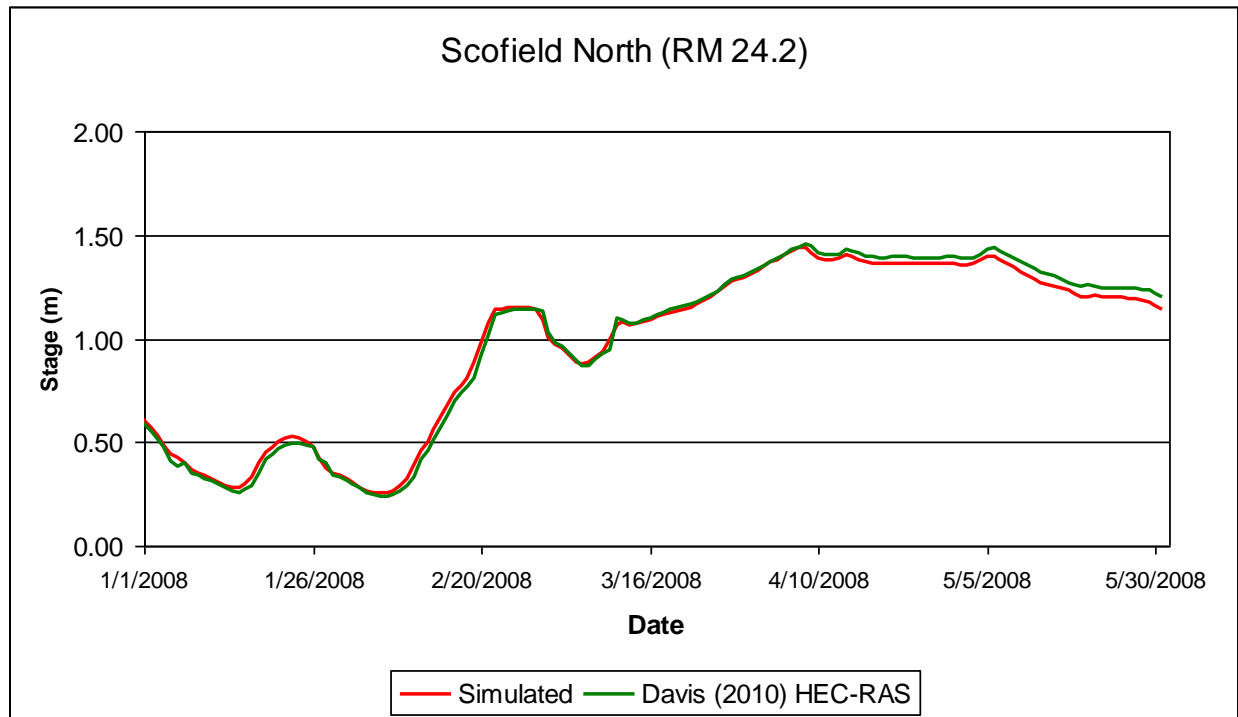


Figure 6.35 – Stage at Scofield North for the 1-D Mobile-Bed Calibration – 2008

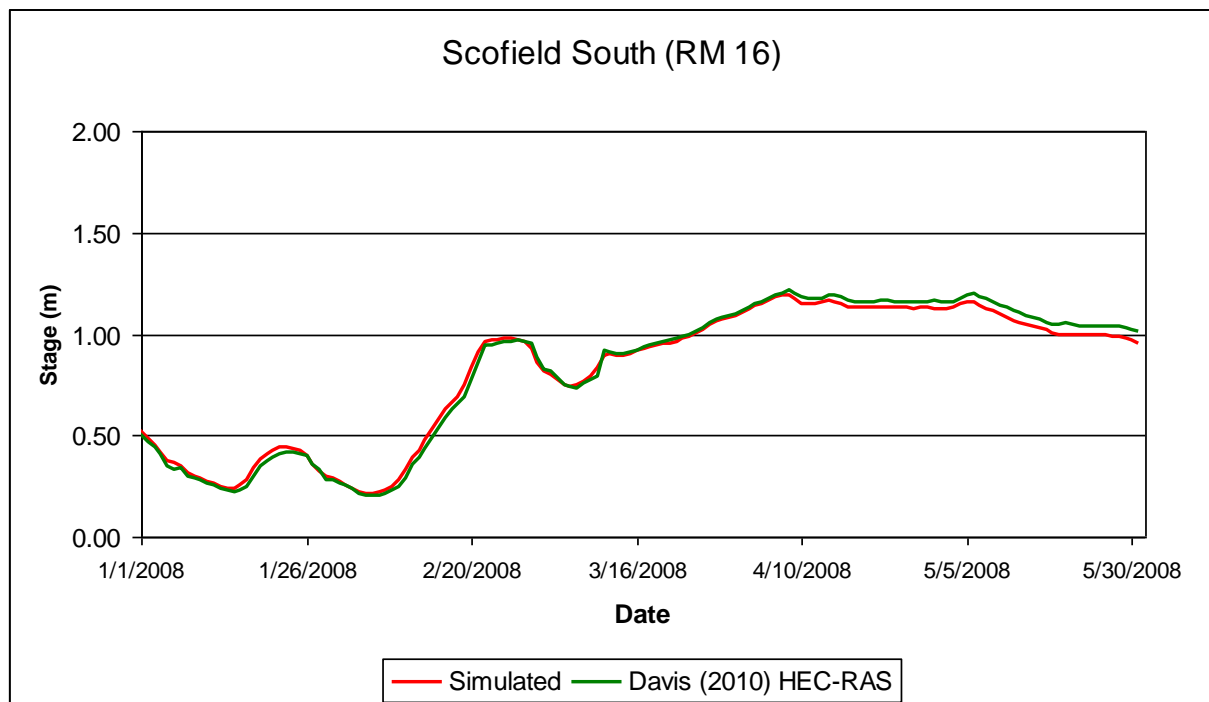


Figure 6.36 – Stage at Scofield South for the 1-D Mobile-Bed Calibration – 2008

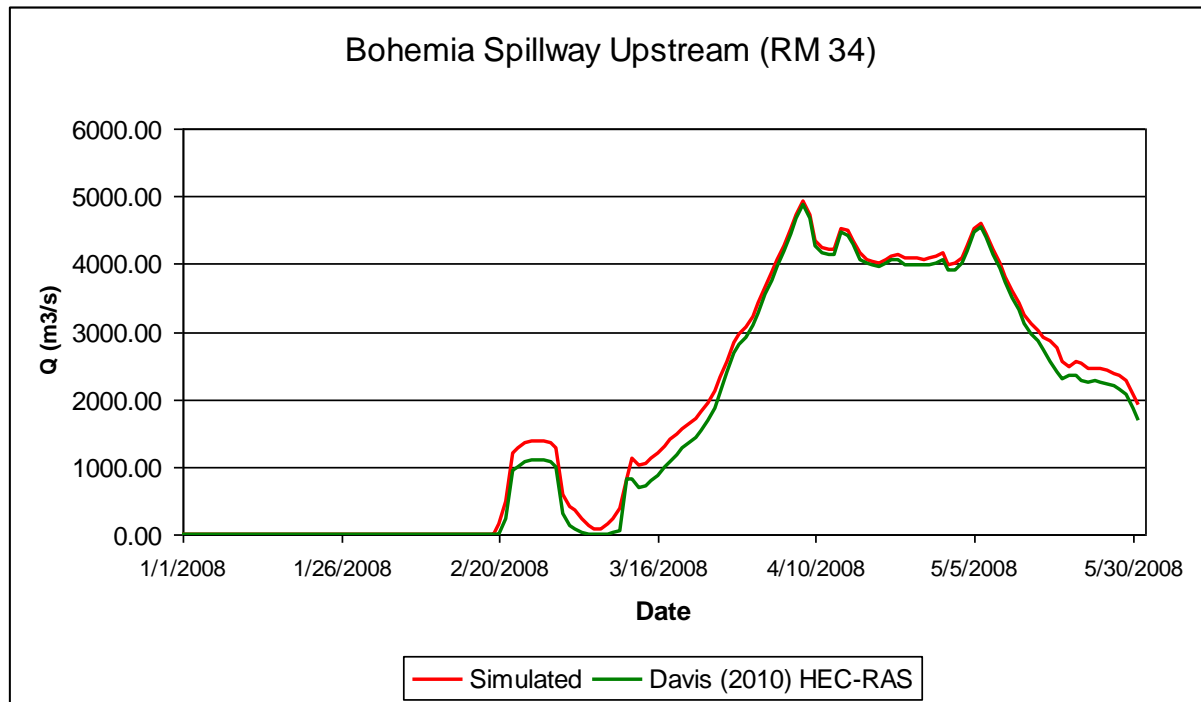


Figure 6.37 – Outflow at Bohemia Spillway Upstream for the 1-D Mobile-Bed Calibration – 2008

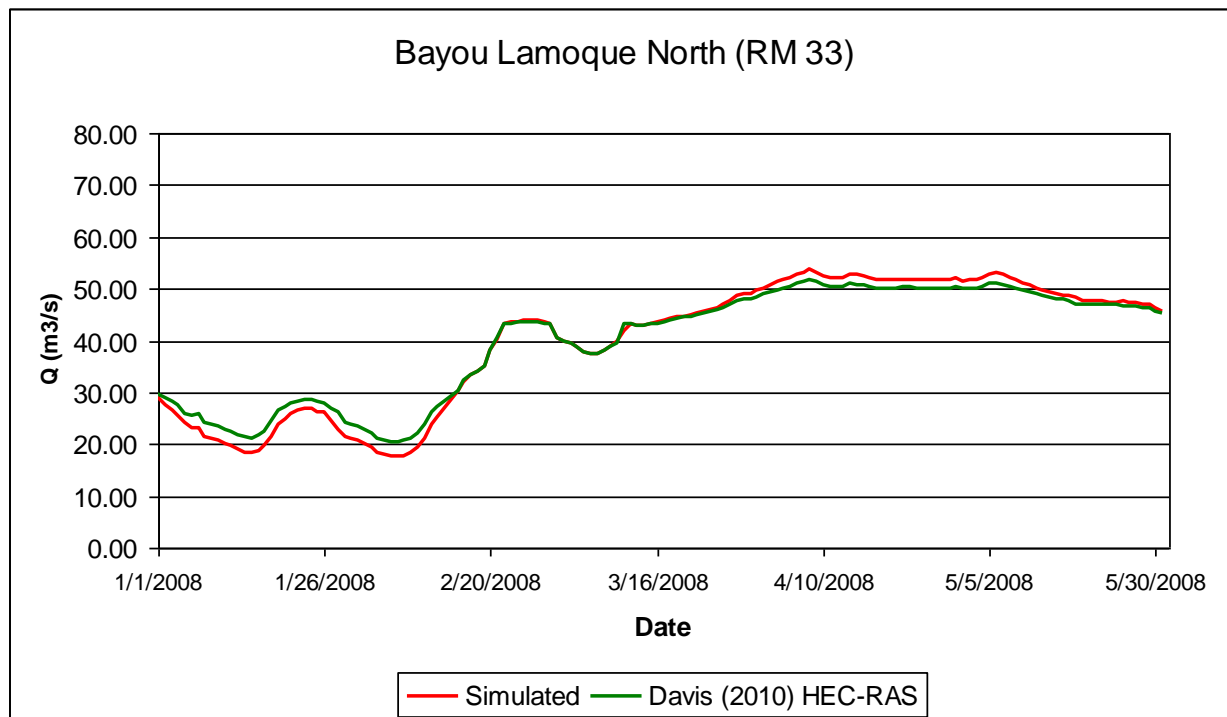


Figure 6.38 – Outflow at Bayou Lamoque North for the 1-D Mobile-Bed Calibration – 2008

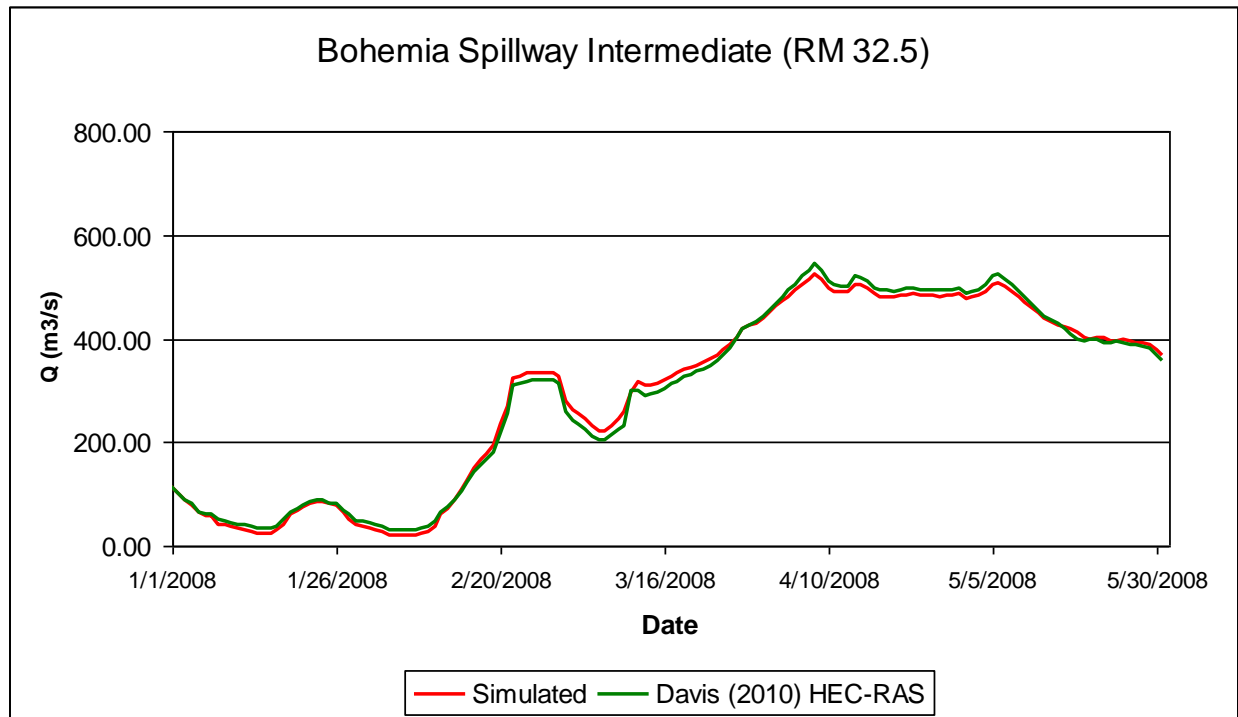


Figure 6.39 – Outflow at Bohemia Intermediate for the 1-D Mobile-Bed Calibration – 2008

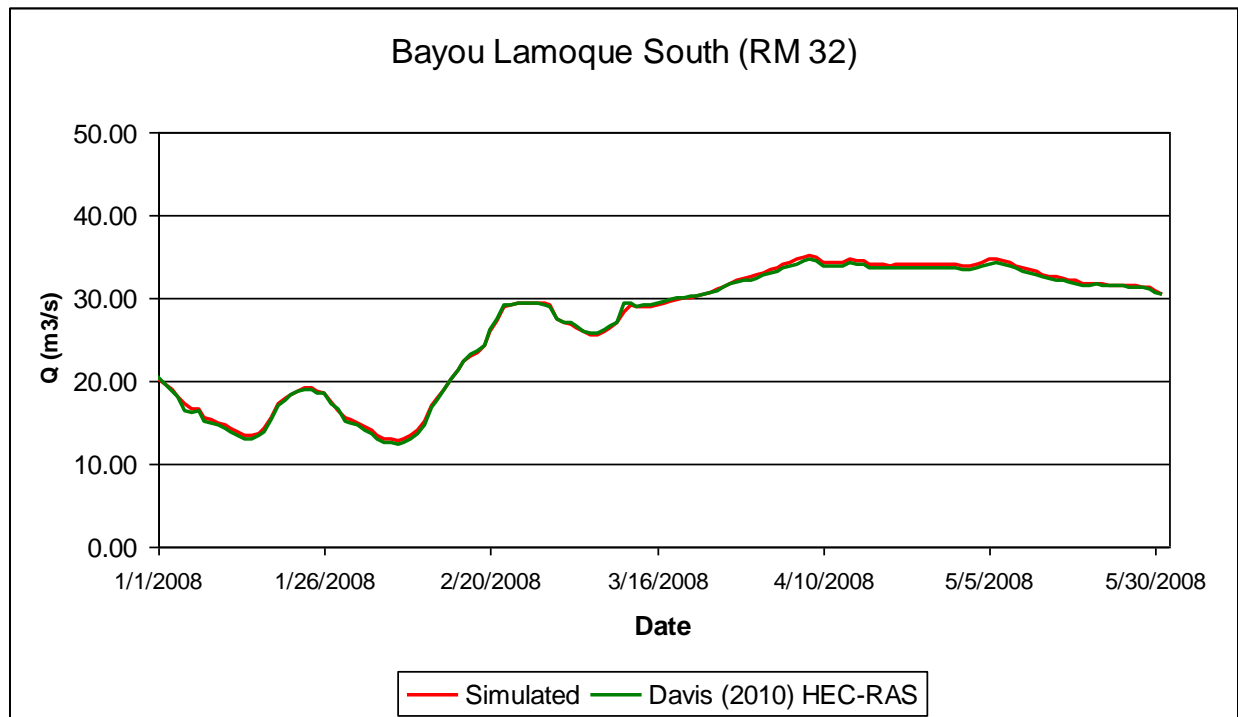


Figure 6.40 – Outflow at Bayou Lamoque South for the 1-D Mobile-Bed Calibration – 2008

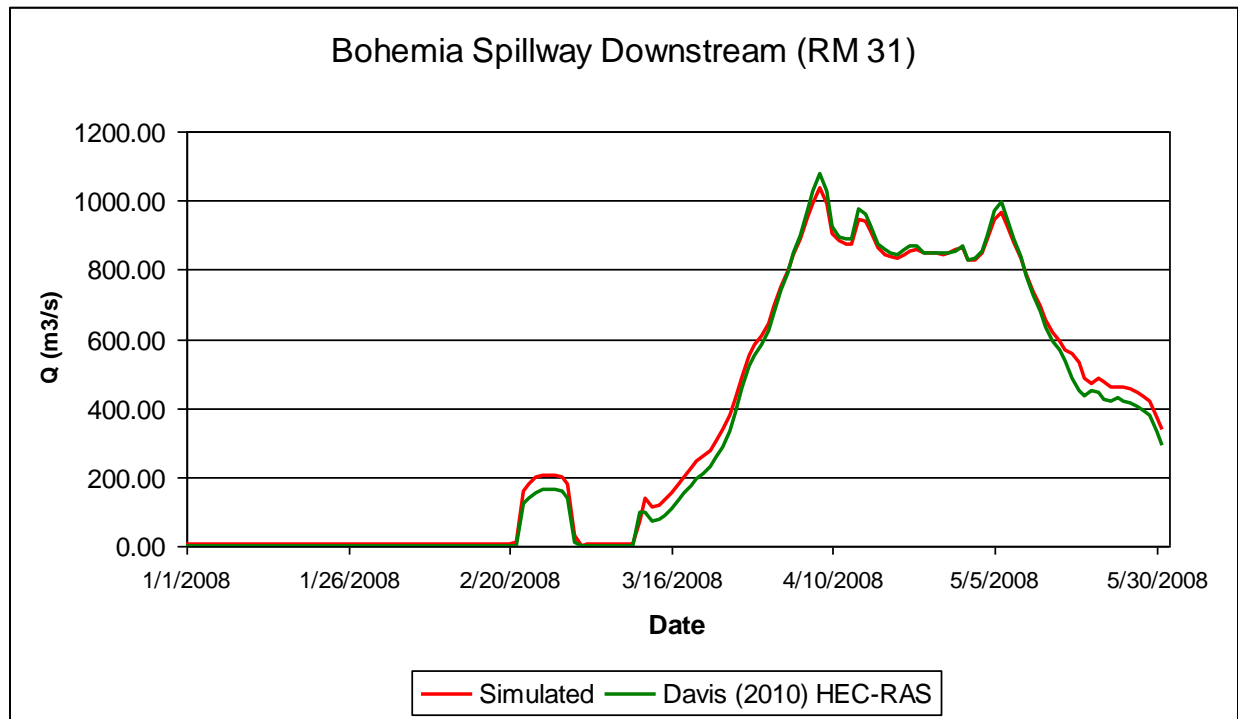


Figure 6.41 – Outflow at Bohemia Spillway Downstream for the 1-D Mobile-Bed Calibration – 2008

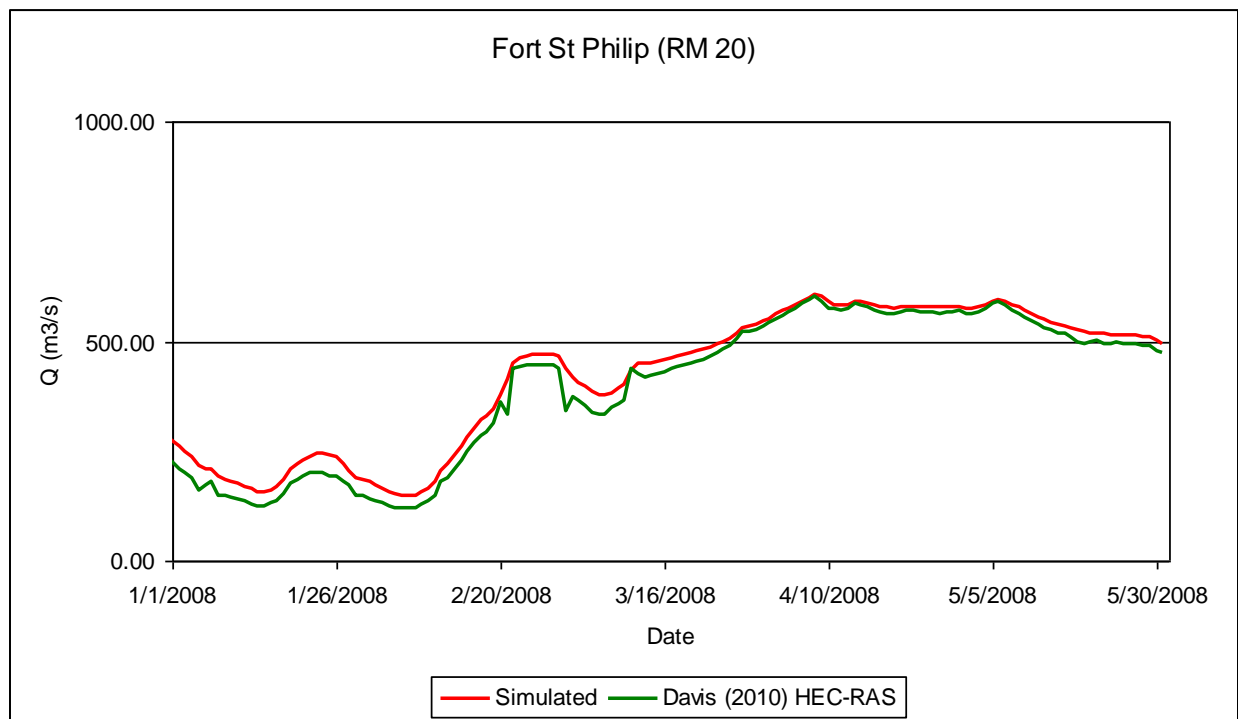


Figure 6.42 – Outflow at Fort St. Philip for the 1-D Mobile-Bed Calibration – 2008

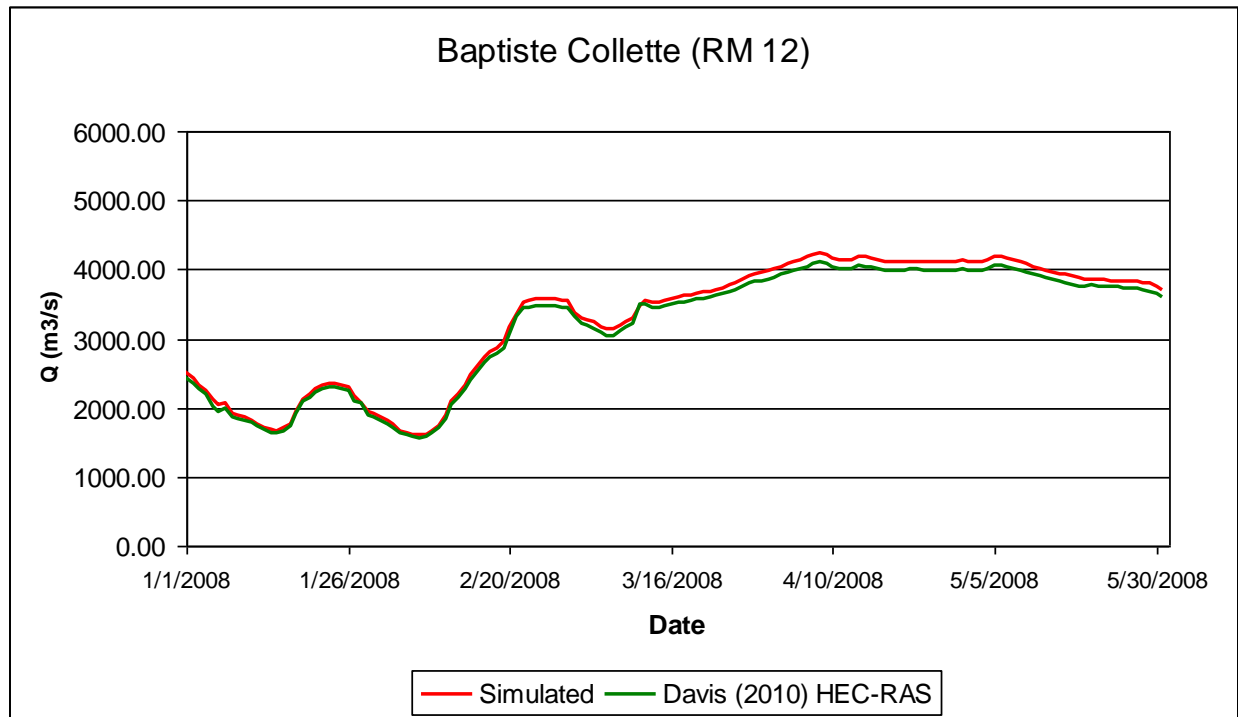


Figure 6.43 – Outflow at Baptiste Collette for the 1-D Mobile-Bed Calibration – 2008

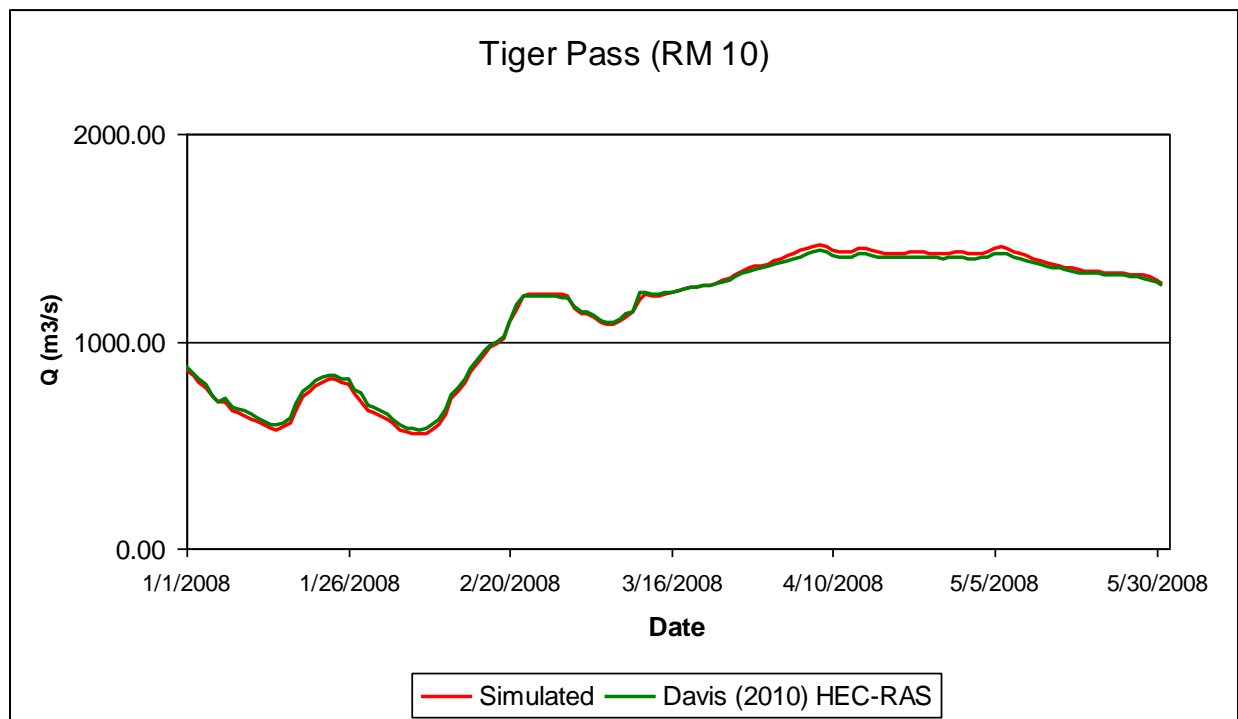


Figure 6.44 – Outflow at Tiger Pass for the 1-D Mobile-Bed Calibration – 2008

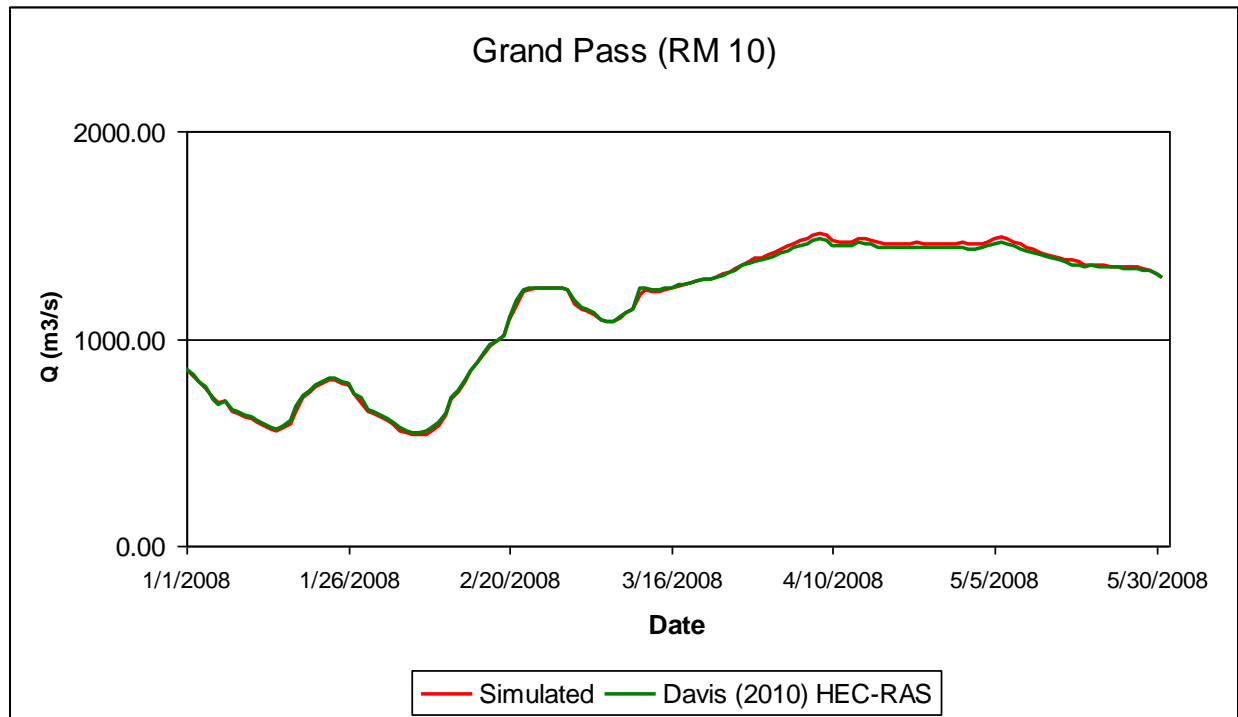


Figure 6.45 – Outflow at Grand Pass for the 1-D Mobile-Bed Calibration – 2008

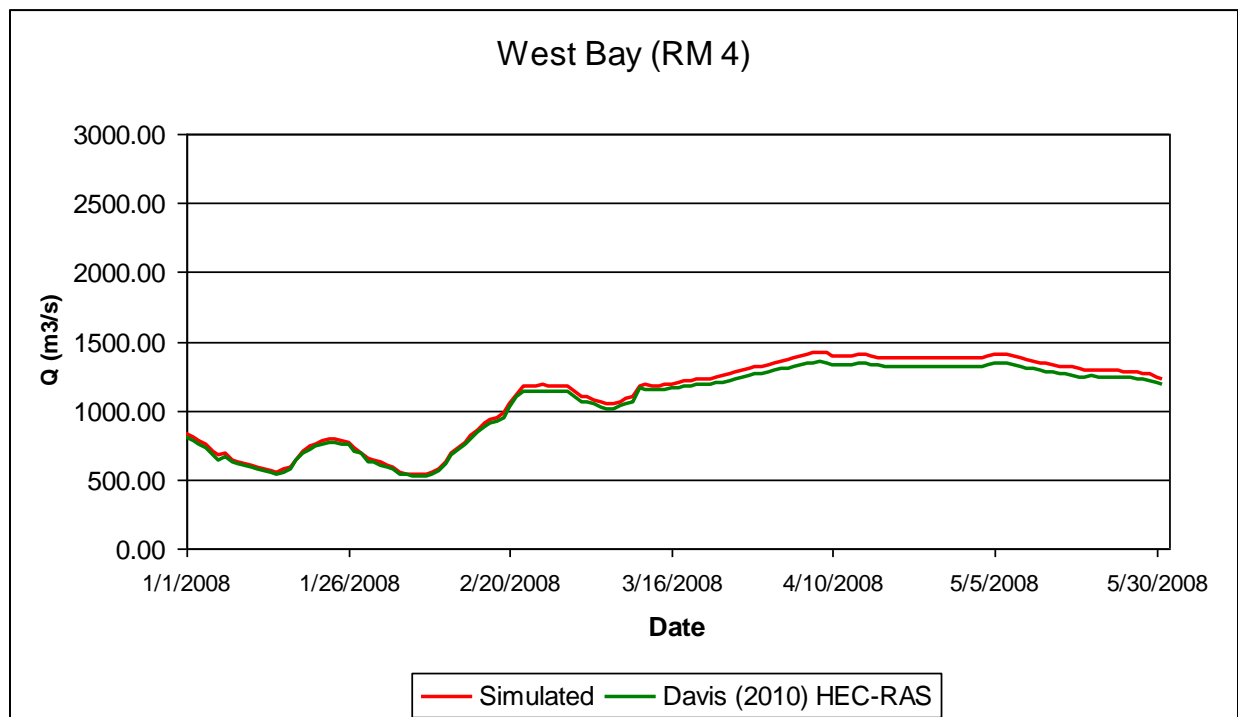


Figure 6.46 – Outflow at West Bay for the 1-D Mobile-Bed Calibration – 2008

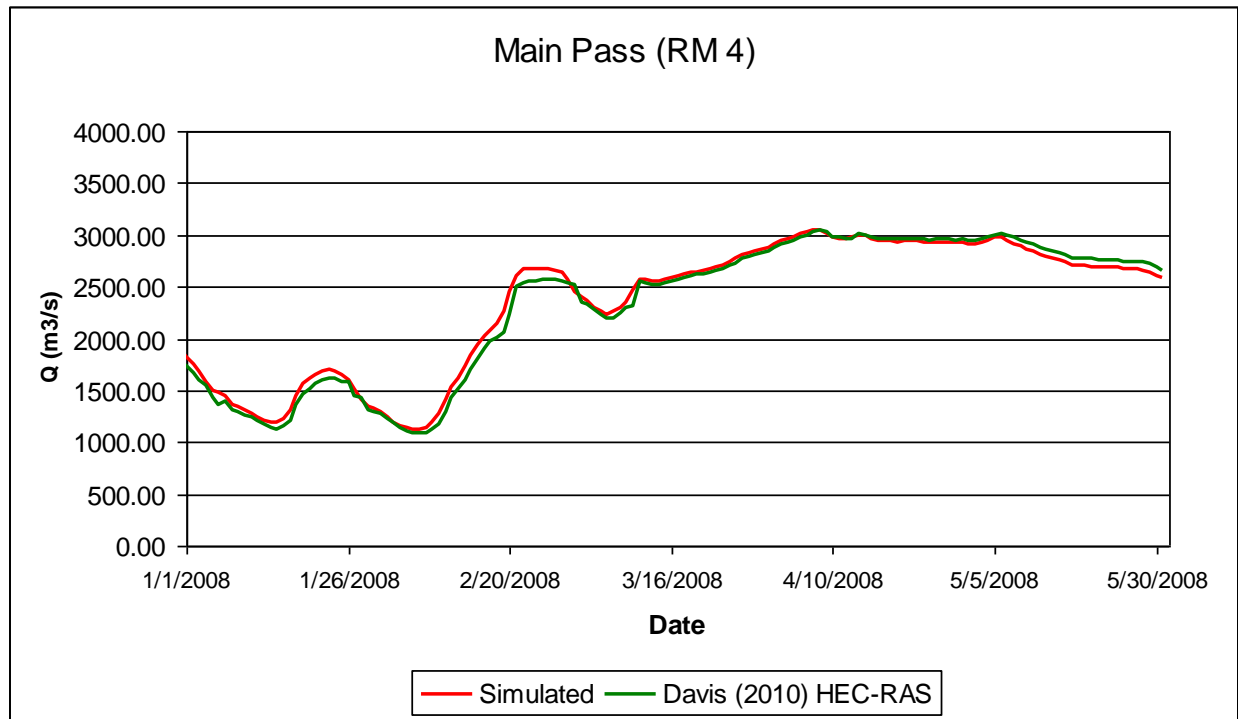


Figure 6.47 – Outflow at Main Pass for the 1-D Mobile-Bed Calibration – 2008

The model's predictions of sand load at Scofield (RM 24, RK 39 to RM 16, RK 26) and at Myrtle Grove (RM 59) were calibrated against field measurements available for the years of 2008 and 2009 obtained from Nittrouer *et al.* (2008) and Allison (2010). Three days of measurements were used: one obtained during low flow conditions (January 2008), one obtained during high flow conditions (April 2008) and one obtained during mean flow conditions (March 2009). The TLTM (Karim 1985), Engelund-Hansen, and Ackers-White entrainment formulas were tested. The results are presented in Table 6-16. The Ackers-White formula produced the most accurate results. It is noted that the predictions are in better agreement with observations during high flow conditions when compared with those obtained during low flow. Since most of the sand mass is transported at high flows, the results can be considered encouraging.

Table 6-16 – Observed versus Modeled – 1-D Mobile-bed Simulations

Date/Station	Suspended Sand Concentration (mg/L)			
	Myrtle Grove (RM 59)		Scofield (RM 16-24)	
	<i>Observed</i> ⁺ *	<i>Simulated</i>	<i>Observed</i> ⁺	<i>Simulated</i>
1/10/08	-	-	4.1	1.1**
3/10/08	57.0*	51.6	-	-
4/15/08	-	-	71.0	66.7**

+Data Collected by Allison (2010) *Value measured in April 2009 for a similar water discharge

** Arithmetic average of RM 24, RM 20 and RM 16 results

The results in Table 6-16 are presented in graphical form in Figure 6.48 to Figure 6.50 for an easier visualization.

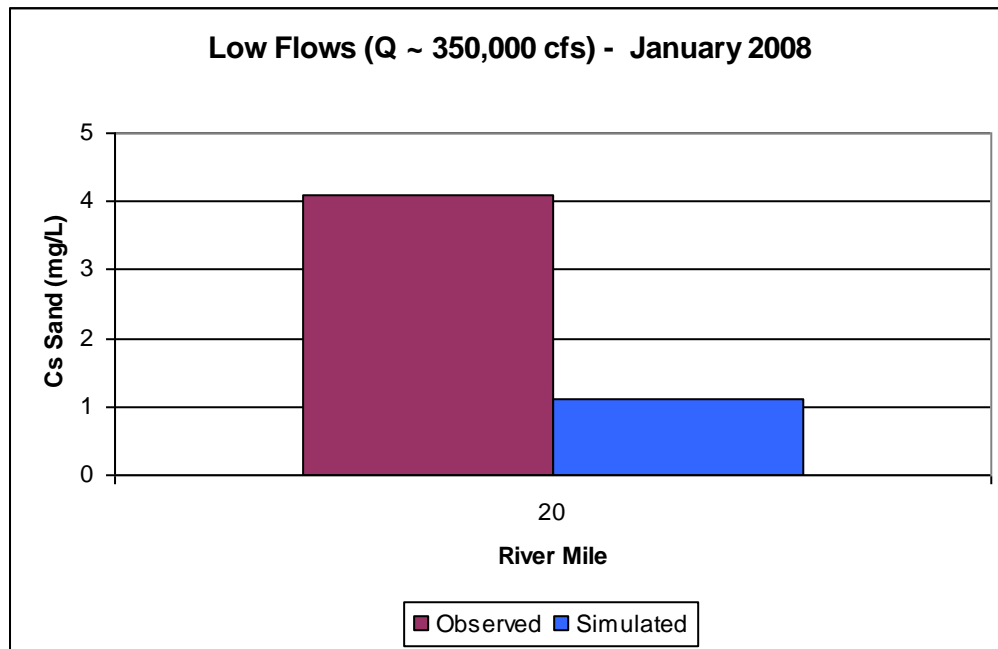


Figure 6.48 – 1-D Existing Outflows – Suspended Sand Concentration at Low Flows – Calibration

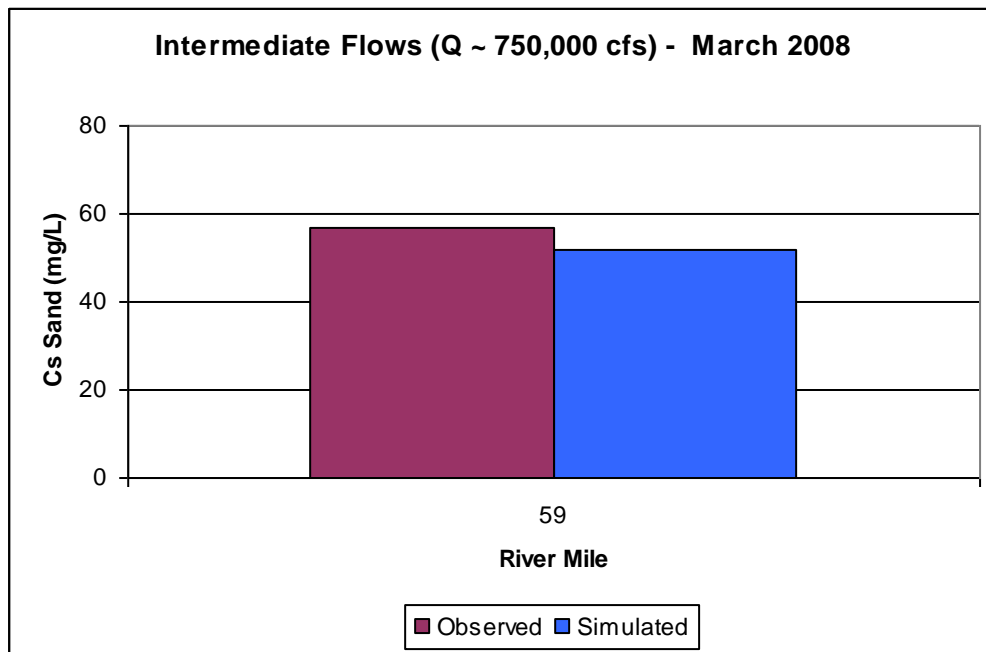


Figure 6.49 – 1-D Existing Outflows – Suspended Sand Concentration at Intermediate Flows – Calibration

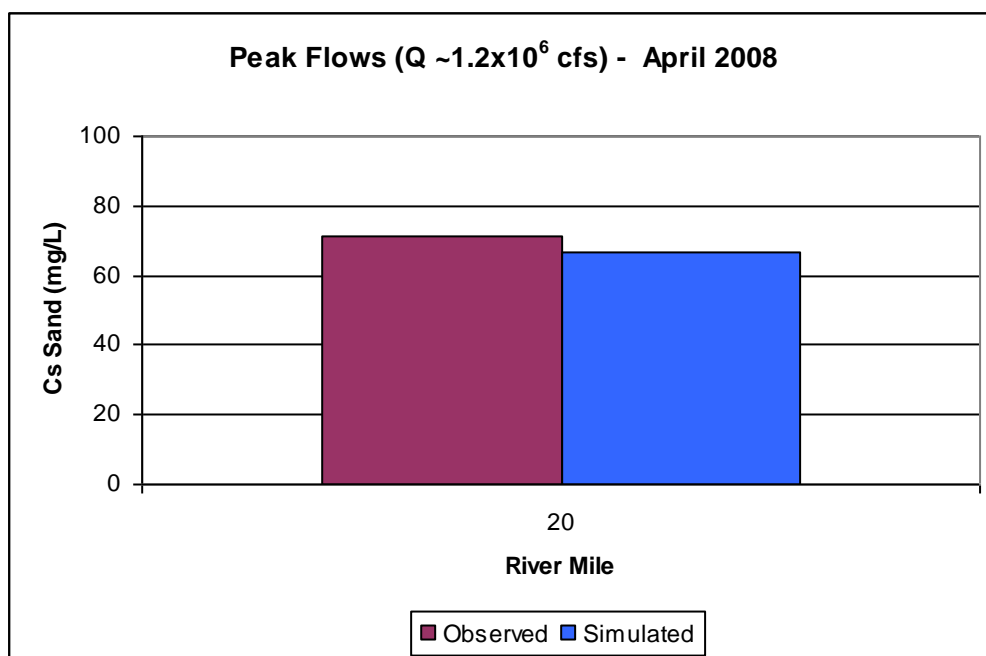


Figure 6.50 – 1-D Existing Outflows – Suspended Sand Concentration at Peak Flows – Calibration

The sand concentration results obtained during the mobile-bed calibration at some stations in the main channel are shown from Figure 6.51 to Figure 6.55. These plots show a reduction in sand concentration while traveling downstream. Once again it can be seen that at low flows there is almost no coarse sediment transport. Possibly the main reason for the lower sand concentrations closer to the downstream end of the domain is the reduction in the amount of flow in the main channel, which is also more pronounced at peak flows. Another reason for the reduction of sand transport is the reduction in the flow energy, which happens in two different ways: 1) the reduction of flow leads to a reduction of the velocity and, consequently, of the kinetic term; 2) the water stage is reduced due to the reduction of flow and so the potential term is reduced.

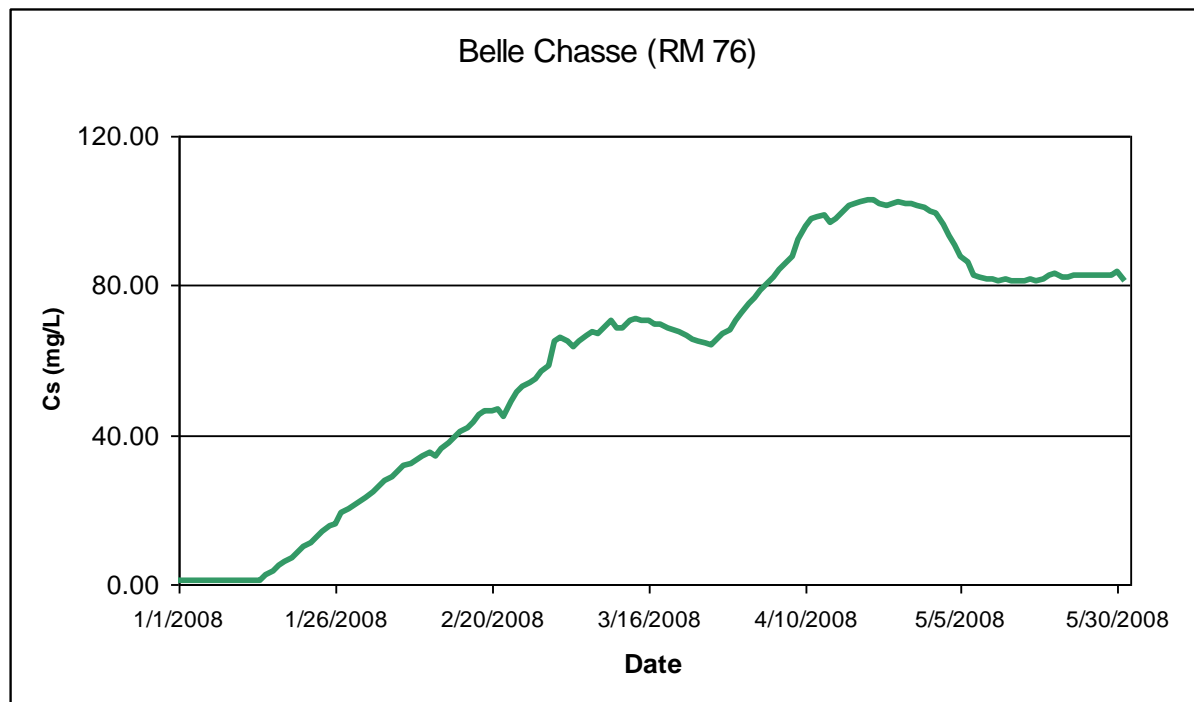


Figure 6.51 – Suspended Sand Concentration at Belle Chasse for the 1-D Mobile-Bed Calibration – 2008

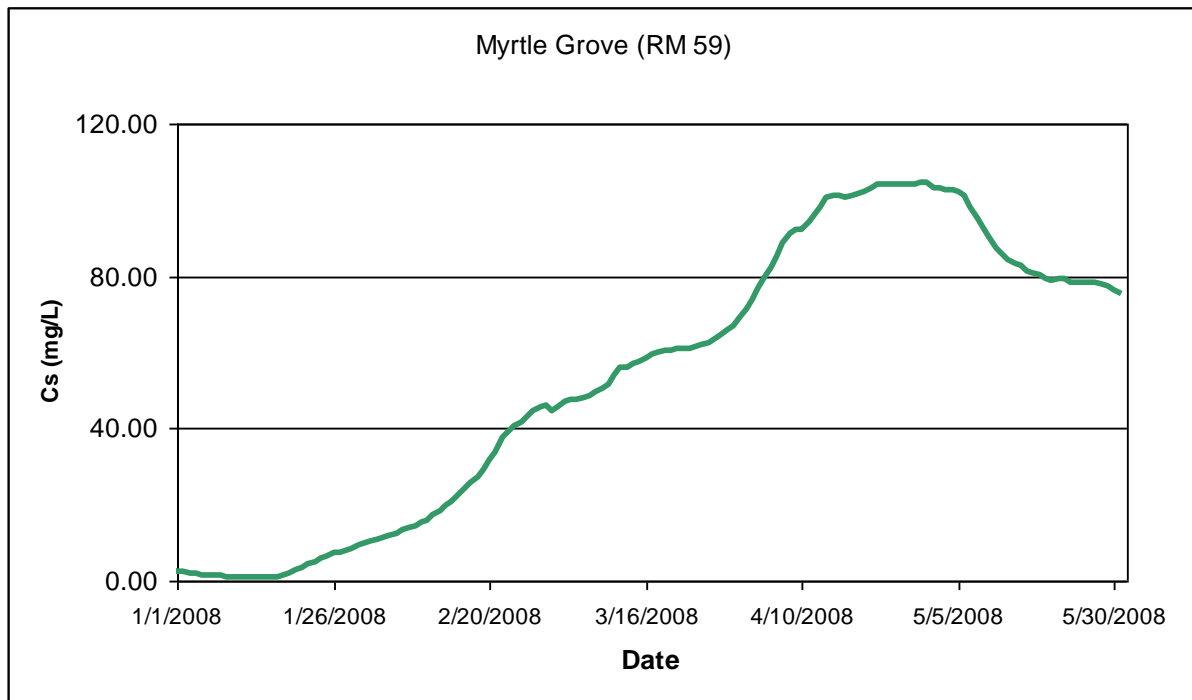


Figure 6.52 – Suspended Sand Concentration at Myrtle Grove for the 1-D Mobile-Bed Calibration – 2008

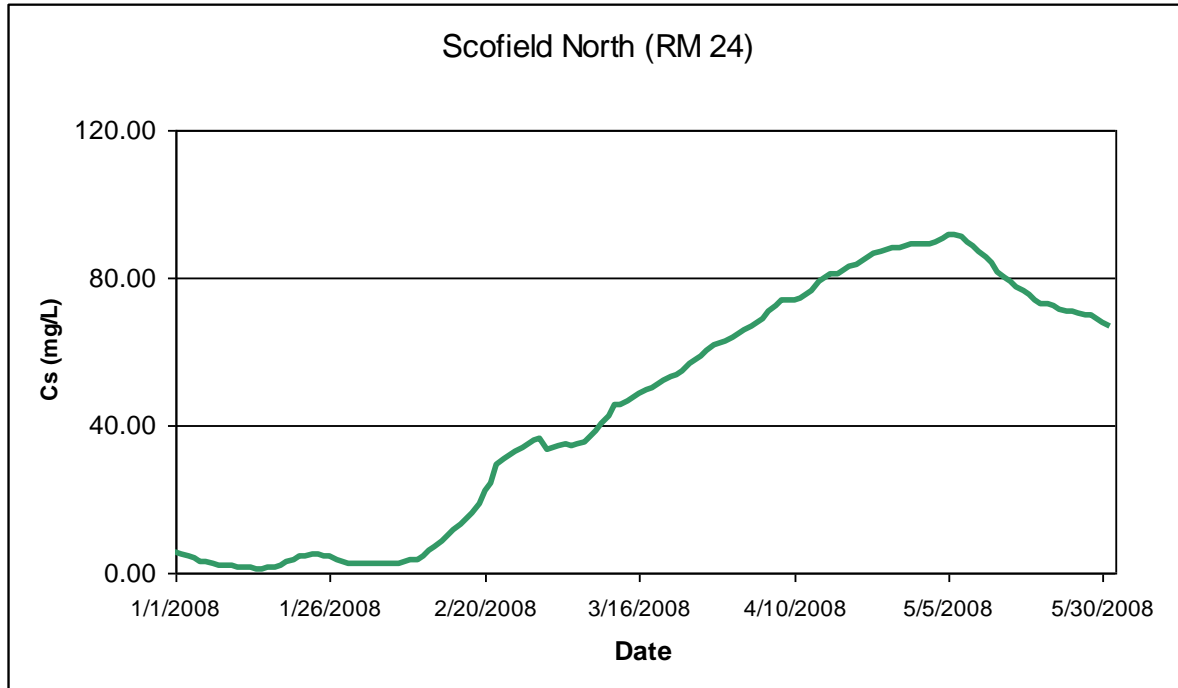


Figure 6.53 – Suspended Sand Concentration at Scofield North for the 1-D Mobile-Bed Calibration – 2008

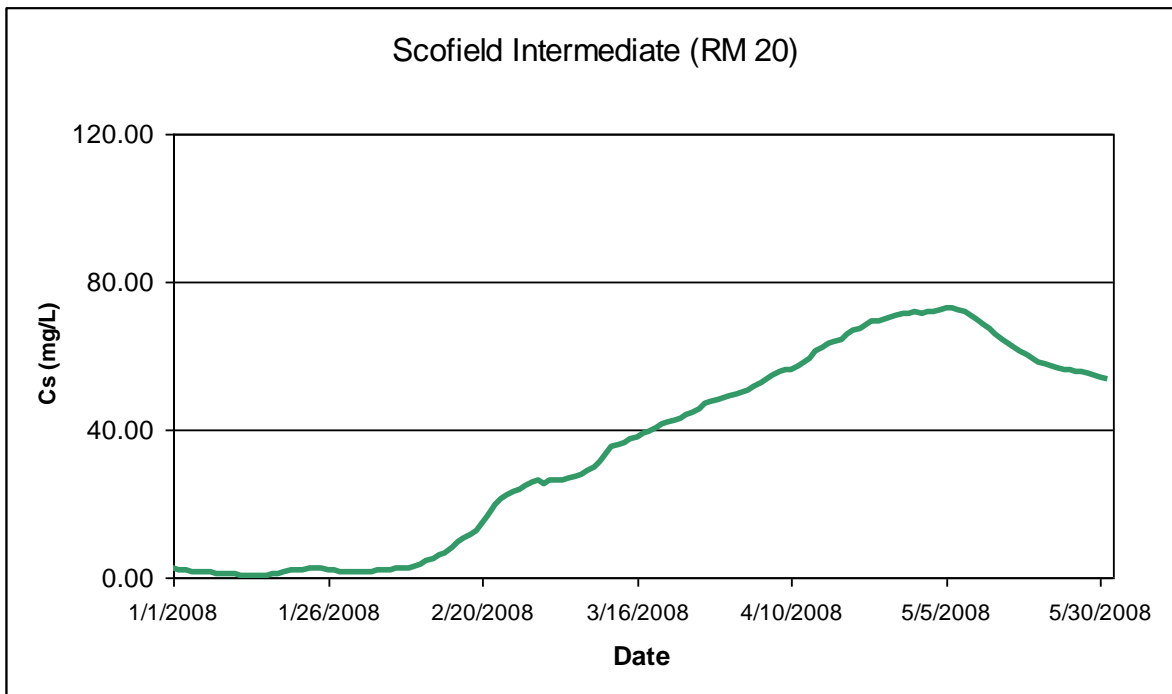


Figure 6.54 – Suspended Sand Concentration at Scofield Intermediate for the 1-D Mobile-Bed Calibration – 2008

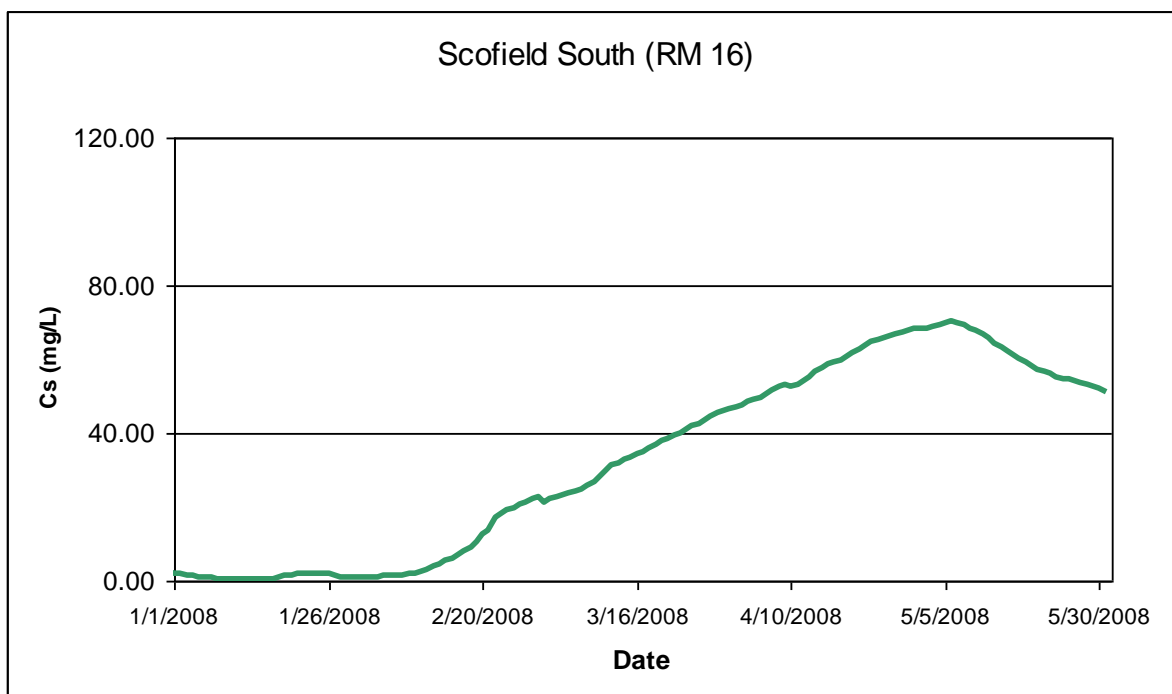


Figure 6.55 – Suspended Sand Concentration at Scofield South for the 1-D Mobile-Bed Calibration – 2008

The sand load results obtained during the mobile-bed calibration at some stations in the main channel are shown from Figure 6.61 to Figure 6.60. The pattern is similar to the one seen for the sand concentration. It is visible a pronounced reduction in sand load while traveling downstream. At low flows there is almost no coarse sediment transport and the peak sand load at Belle Chasse is about the double of that at Scofield South.

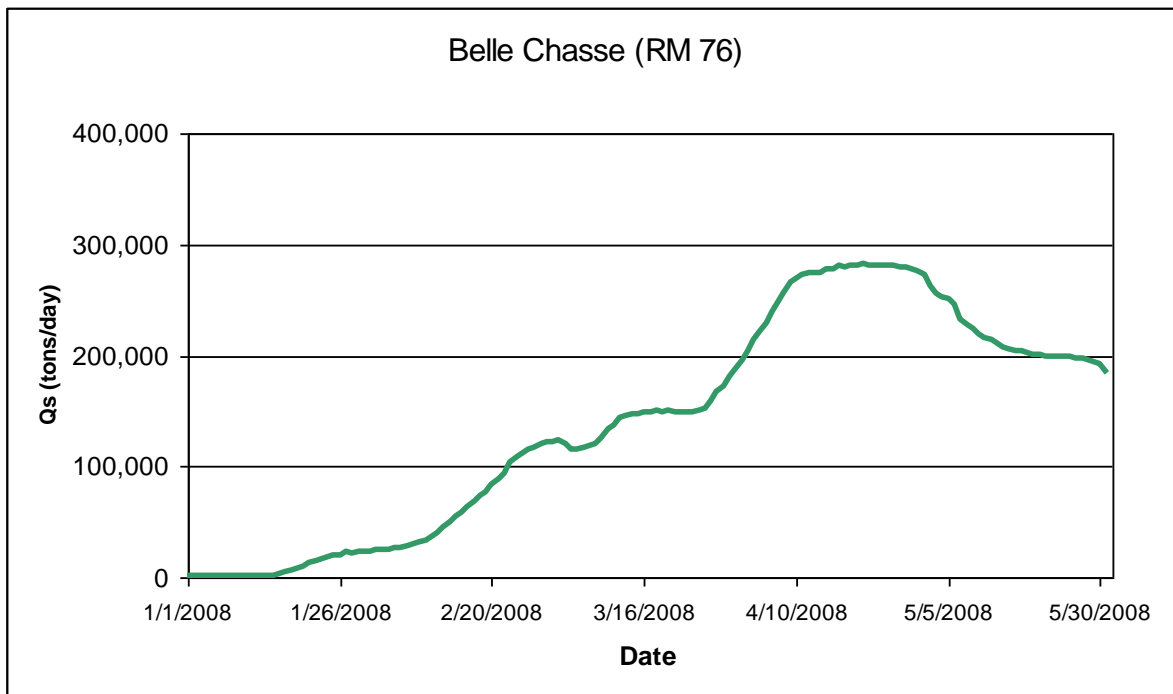


Figure 6.56 – Suspended Sand Load at Belle Chasse for the 1-D Mobile-Bed Calibration – 2008

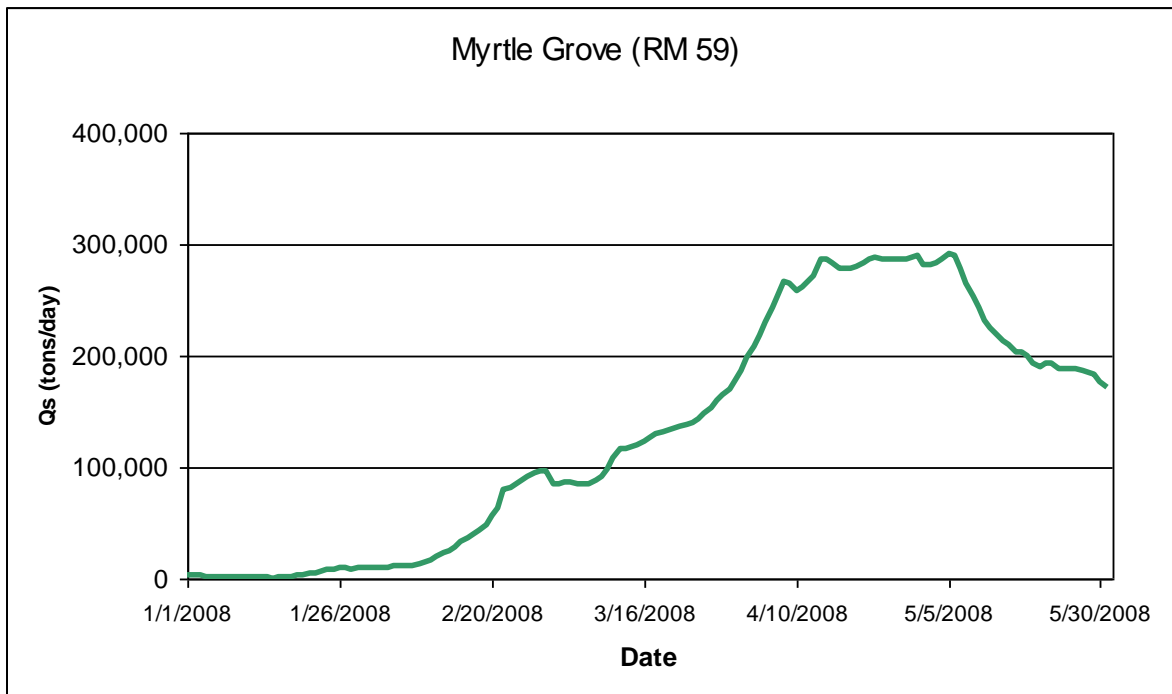


Figure 6.57 – Suspended Sand Load at Myrtle Grove for the 1-D Mobile-Bed Calibration – 2008

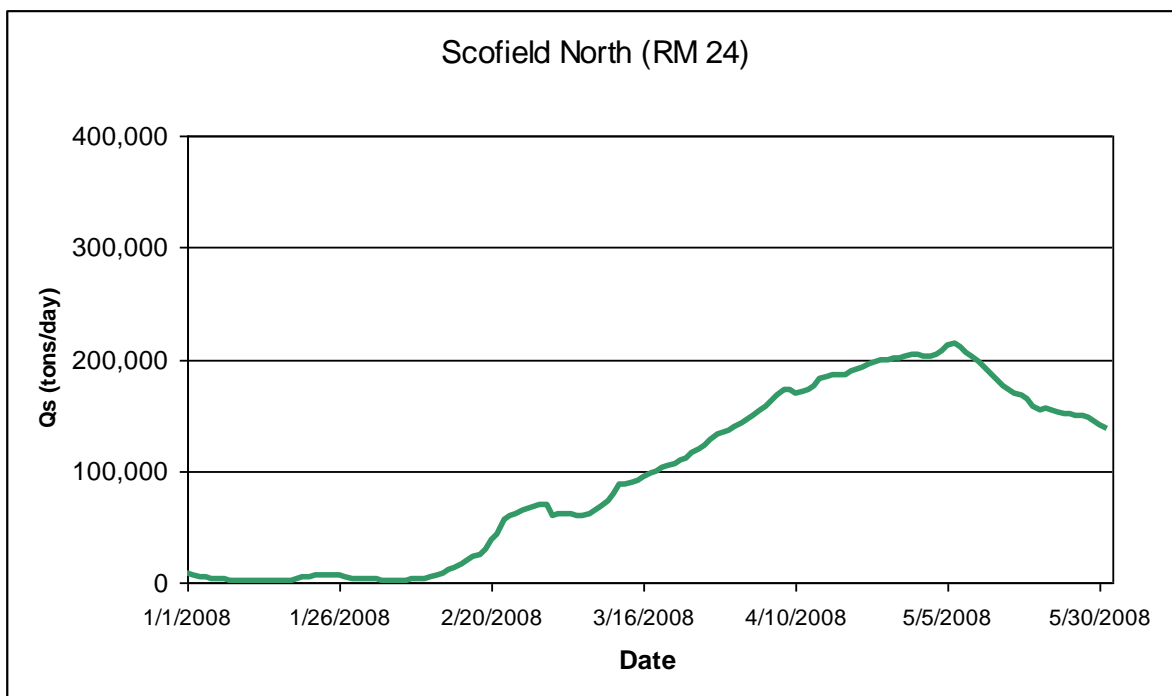


Figure 6.58 – Suspended Sand Load at Scofield North for the 1-D Mobile-Bed Calibration – 2008

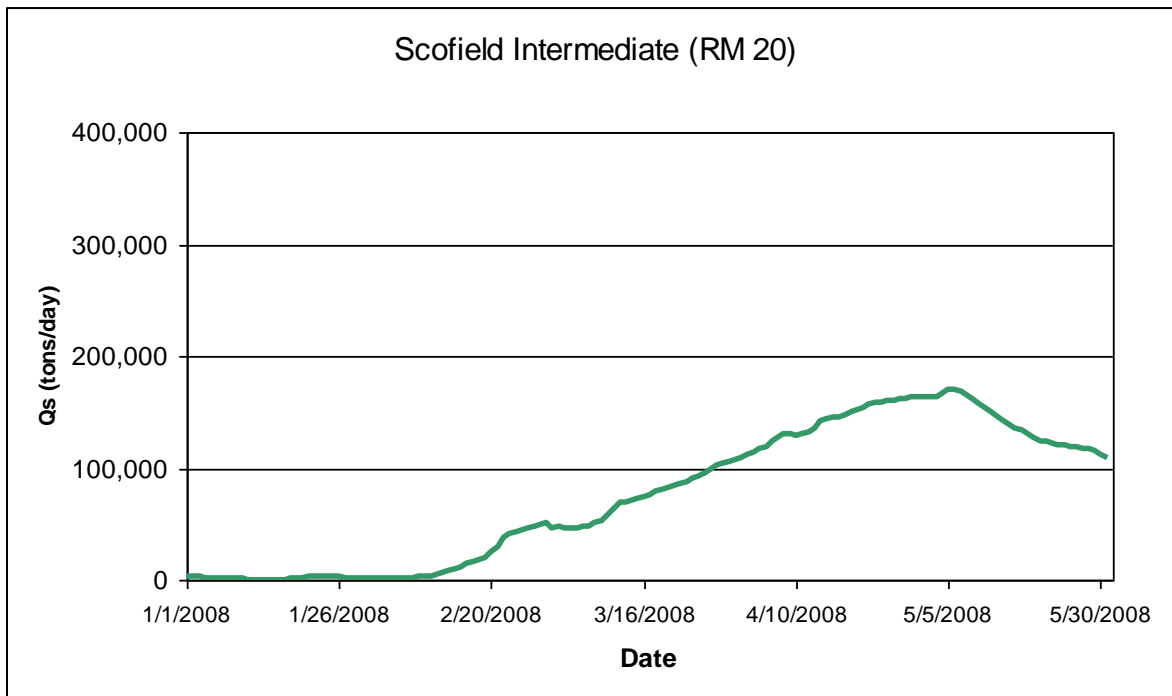


Figure 6.59 – Suspended Sand Load at Scofield Intermediate for the 1-D Mobile-Bed Calibration – 2008

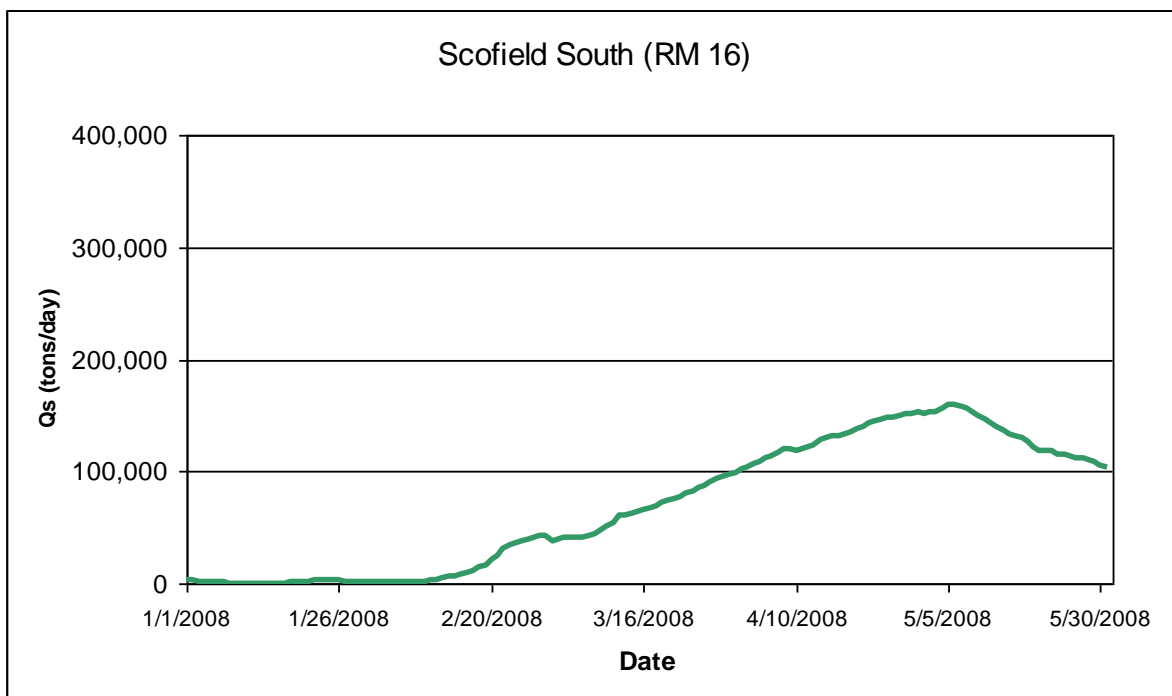


Figure 6.60 – Suspended Sand Load at Scofield South for the 1-D Mobile-Bed Calibration – 2008

Since the focus of this study is to determine the effect of river diversions, it is important to determine not only how much sand is transported in the main channel but also how much sand is transported in the outflow channels. Almost no coarse sediment is transported at low flow conditions so we will concentrate on peak flow results ($Q \sim 35,000 \text{ m}^3/\text{s}$ or $1.2 \times 10^6 \text{ cfs}$) and intermediate flow results ($Q \sim 22,000 \text{ m}^3/\text{s}$ or $750,000 \text{ cfs}$). Figure 6.61 and Figure 6.62 show, respectively, the sand concentration results obtained at peak flow and at intermediate flow conditions. These results show that the concentrations at peak flow are more than double of the ones at intermediate flows. It is important to state that the sand load is not directly proportional to the water discharge, e.g. in this case, an increase of less than 40% in the water discharge leads to an increase of more than 50% in the sand concentration. Increasing the water discharge increases the sand concentration and, thus the sediment load, which is a product of the concentration by the water discharge, will be approximately three times higher for peak flows than for intermediate flows.

It is evident from Figure 6.61 and Figure 6.62 that most of values are in the range between 20 and 80 mg/L at peak flows. The exception is Tiger Pass, which shows a concentration that is higher than the one obtained at Grand Pass. At intermediate flows the concentrations are about half of the ones obtained with peak flows. Tiger Pass remains as the diversion with the highest sand concentration value. The concentrations obtained are of the same order of magnitude of the ones in the main channel but slightly lower.

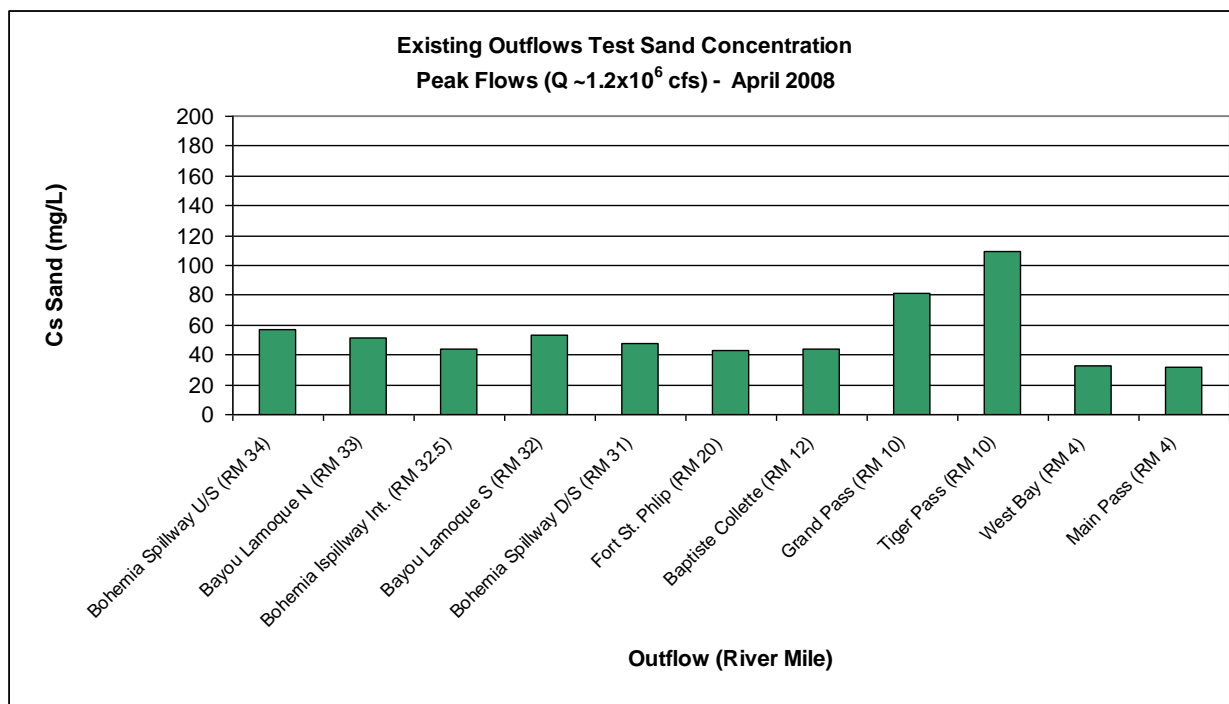


Figure 6.61 – 1-D Simulations - Existing Outflows – Outflows Suspended Sand Concentration at Peak Flows

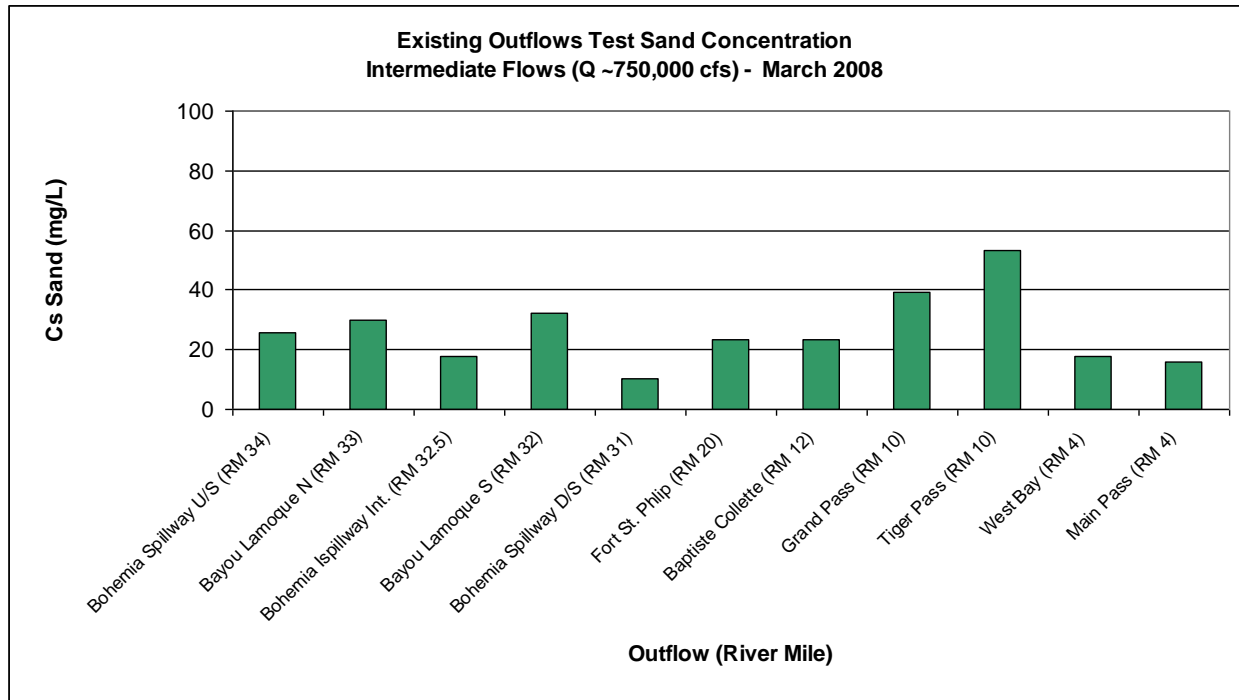


Figure 6.62 – 1-D Simulations - Existing Outflows – Outflows Suspended Sand Concentration at Intermediate Flows

6.2 Myrtle Grove + Existing Outflows

To study the effect of proposed diversions in the system two cases were tested. The first one consisted on the introduction of a diversion on the West Bank at Myrtle Grove (RM 59). This diversion was included in the model by adding the Wilkinson Canal, using the same geometry that was used by Davis (2010), and a gated structure to the previously presented existing outflows model. The new model was calibrated for a diverted Myrtle Grove peak flow of 850 m³/s (or 30,000 cfs).

The Myrtle Grove case includes 14 outflows: Myrtle Grove and the existing outflows at White Ditch & Naomi, West Pointe-À-La-Hache, Bohemia Spillway U/S, Bohemia Spillway Intermediate, Bohemia Spillway D/S, Bayou Lamoque N, Bayou Lamoque S, Fort St. Philip, Baptiste Collette, Tiger Pass, Grand Pass, West Bay and Main Pass. Figure 6.63 shows the topology of the fluvial network for this case.

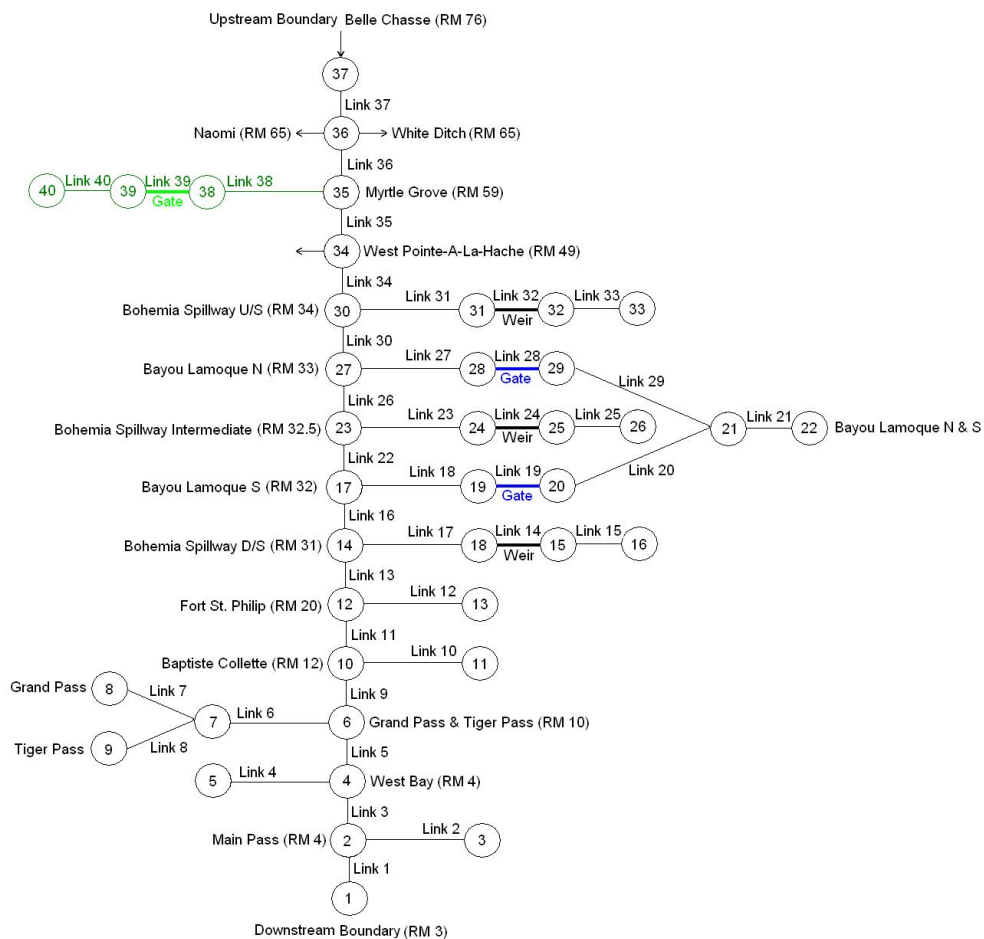


Figure 6.63 – Schematic diagram of the Myrtle Grove Case Topology

6.2.1 Boundary Conditions

Hydrographs of daily averaged values were used for upstream (flow and sediment load), downstream boundaries. The 01/01/2008 to 06/05/2008 period was simulated for both hydrodynamics and sediment transport. The boundary conditions used in this case were basically the same used for the existing outflows calibration simulations given in Table 6-1, Table 6-2, Table 6-3 and in Appendix A. A new stage boundary condition, equal to the downstream boundary condition, was added for the downstream end of the Wilkinson Canal for the Myrtle Grove diversion. The maximum, minimum and average values can be seen in Table 6-17.

Table 6-17 – Stage Boundary Condition – Myrtle Grove Case – 1-D Calibration - 2008

Site	Stage maximum (m, ft)		Stage minimum (m, ft)		Stage average (m, ft)	
Wilkinson Canal (RM 59)	0.01	0.03	-0.04	-0.12	-0.01	-0.03

The model including the Myrtle Grove diversion was ran first in fixed-bed mode. The Wilkinson Canal Manning-Strickler coefficient (K_s) values and the gated structure parameters were calibrated to allow the extraction of the desired 850 m³/s (30,000) under peak flow conditions, meaning a Belle Chasse inflow of around 34,000 m³/s (1.2x10⁶ cfs). All the remaining structure parameters and K_s values used remained equal to the ones obtained during the existing outflows hydrodynamics calibration.

For hydrodynamics calibration, K_s values of 65.00 were used for the Wilkinson Canal. The parameters used in the hydrodynamics simulations for the gate structure are presented in Table 6-18.

Table 6-18 – Gates Parameters – Myrtle Grove Case – 1-D Hydrodynamics Calibration - 2008

Site	Gate Sill Width (m, ft)		Gate Sill Elevation (m, ft)		Discharge Coefficients (submerged, free flow)	
Wilkinson Canal (Link 39)	6.70	22.00	-7.62	-25.00	2.3	1.0

After the calibration with fixed-bed for hydrodynamics, the model ran in mobile-bed mode for the sand transport. The starting point for this calibration was the calibration for the existing outflows mobile-bed model. Once again, the Wilkinson Canal Manning-Strickler coefficient (K_s) values and the gated structure parameters were calibrated to allow the extraction of the desired 850 m³/s (30,000) under peak flow conditions.

For mobile-bed calibration, it was found that there was no need to adjust the K_s value of 65.00 used for Wilkinson Canal. The values used in the mobile-bed simulations for the gates parameters used in the same simulations are presented in Table 6-19.

Table 6-19 – Gates Parameters – Myrtle Grove Case – 1-D Mobile-Bed Calibration - 2008

Site	Gate Sill Width (m, ft)		Gate Sill Elevation (m, ft)		Discharge Coefficients (submerged, free flow)	
Wilkinson Canal (Link 39)	6.70	22.00	-6.10	-20.00	2.6	1.0

For the main channel and existing outflows the bed material sediment sizes were equal to those used in the existing outflows simulations which were presented in Table 6-8. A constant sediment size of 0.200 mm and a 30 m sediment control depth were used for the Wilkinson Canal bed, which matches the values used in the remaining outflow channels.

6.2.2 Results

The Myrtle Grove diversion outflow obtained in fixed-bed mode for hydrodynamics calibration is presented in Figure 6.64. It can be noticed that the result obtained is not very different from the one presented by Davis (2010), although the model was exclusively calibrated for the maximum outflow value and there was no attempt to adjust the whole hydrograph to the HEC-RAS results.

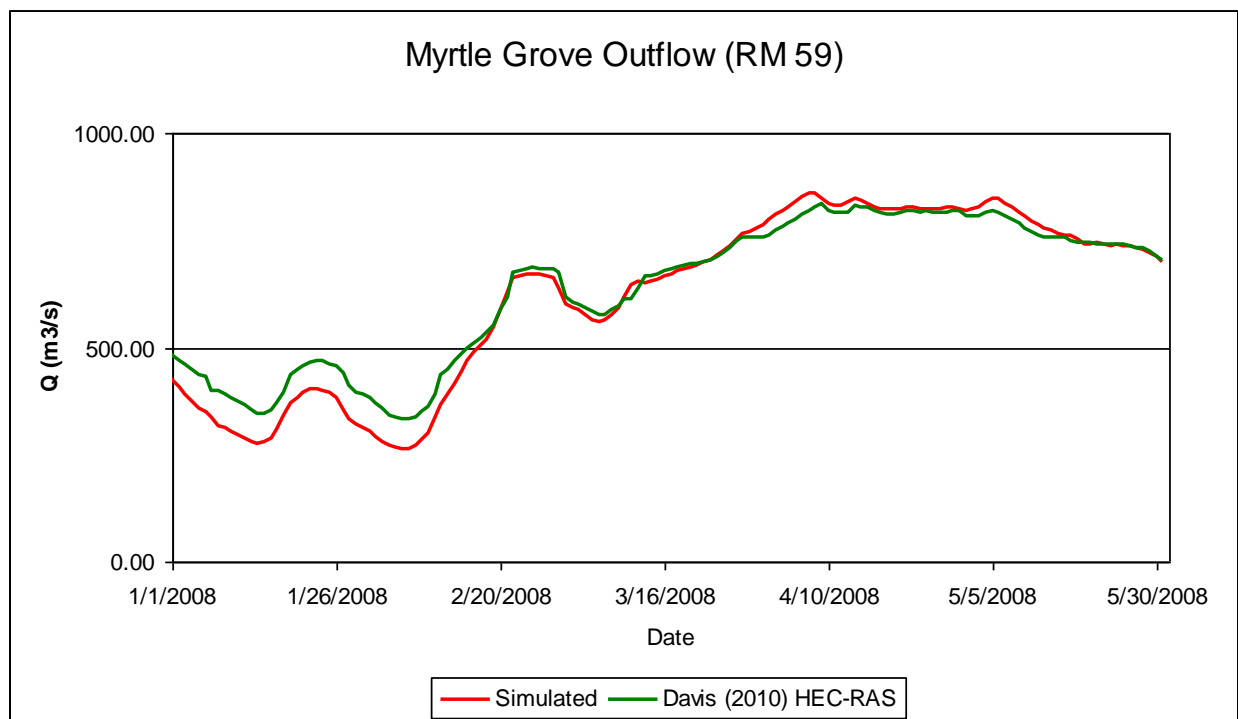


Figure 6.64 –Myrtle Grove Outflow – Myrtle Grove Case - 1-D Hydrodynamics Calibration – 2008

The model results are compared with those obtained with existing outflows. The hydrodynamics stage calibration results are shown from Figure 6.65 to Figure 6.68 . The results show that the introduction of the Myrtle Grove diversion doesn't impact significantly the hydrodynamics in the main channel. This outcome was expected because we are introducing a relatively small diversion in the system.

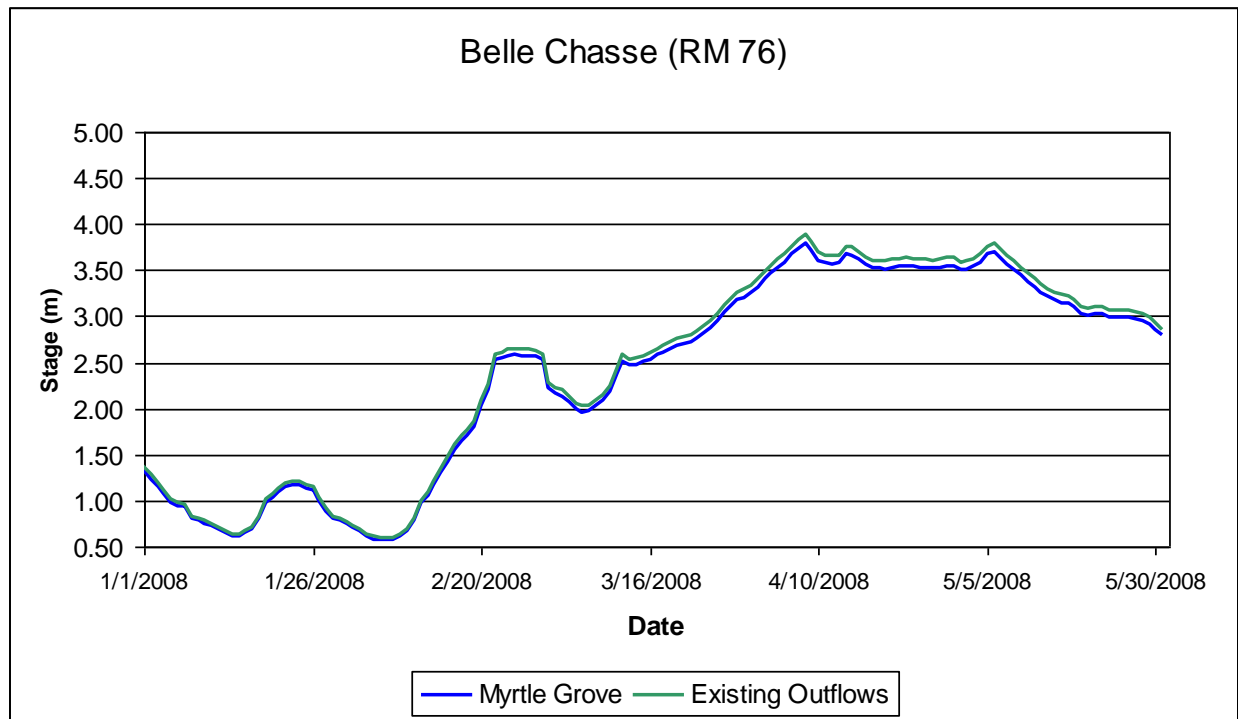


Figure 6.65 – Stage at Belle Chasse – Myrtle Grove - 1-D Hydrodynamics Calibration – 2008

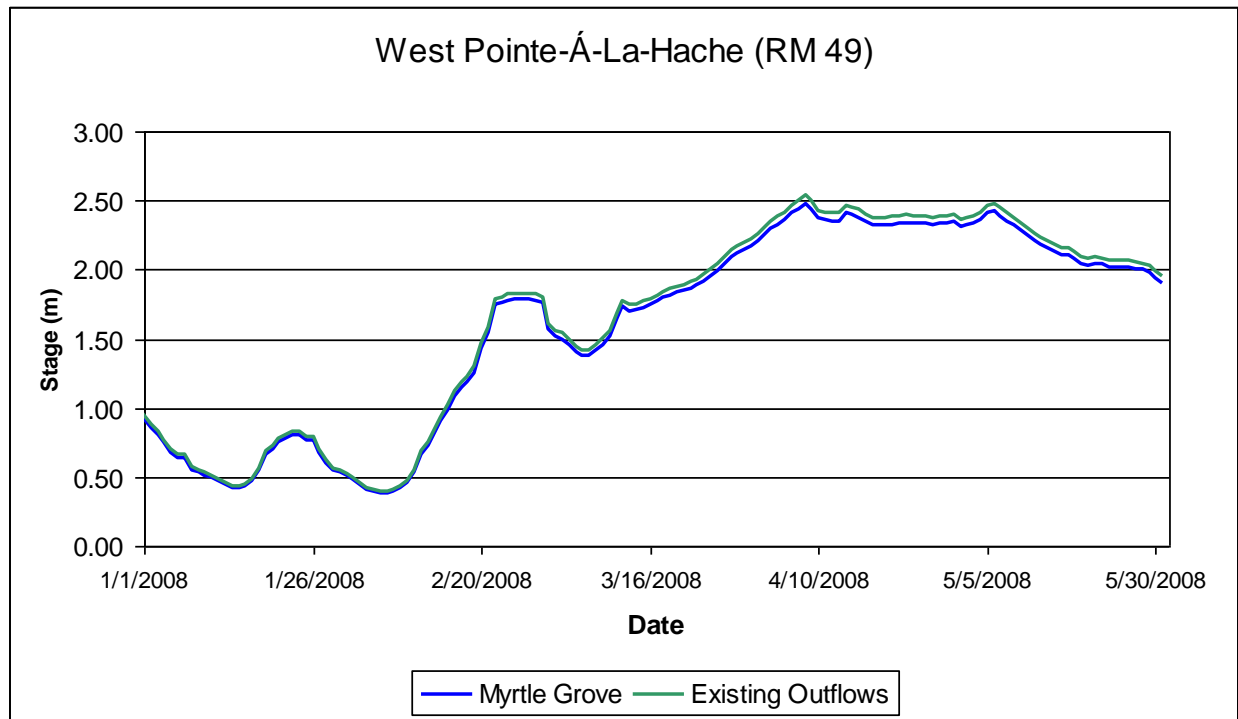


Figure 6.66 – Stage at West Pointe-À-La-Hache - Myrtle Grove - 1-D Hydrodynamics Calibration – 2008

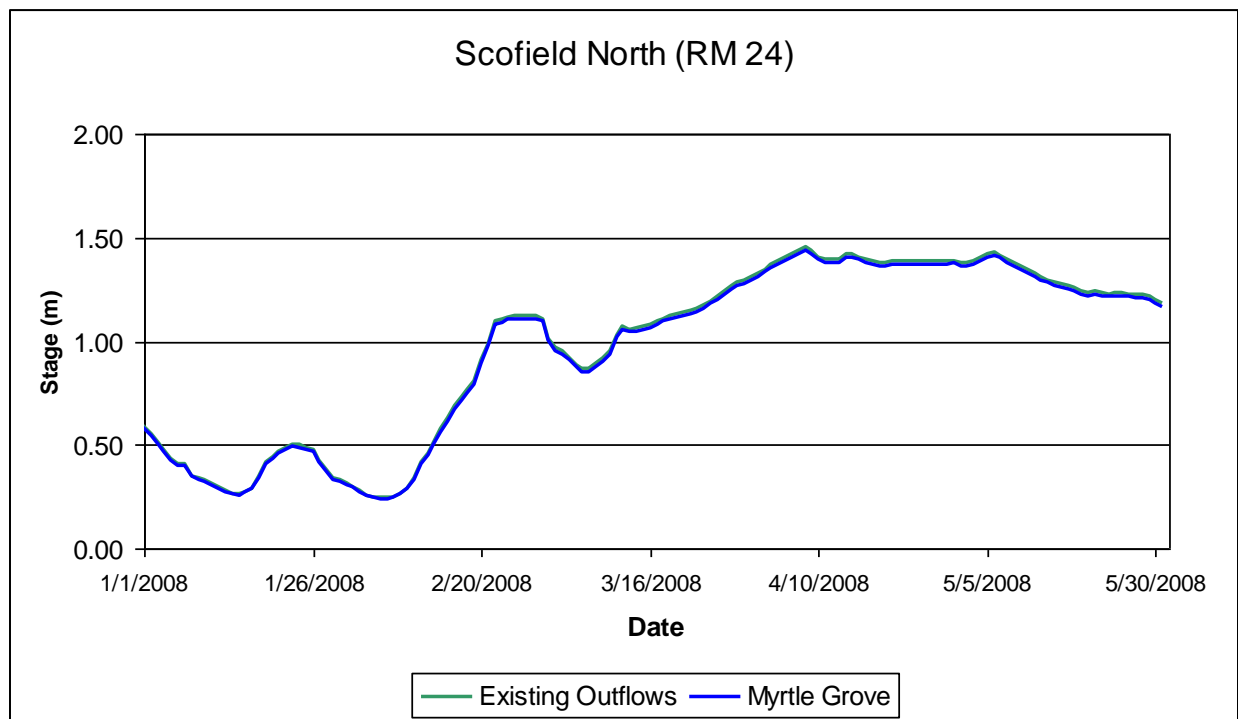


Figure 6.67 – Stage at Scofield North – Myrtle Grove – 1-D Hydrodynamics Calibration 2008

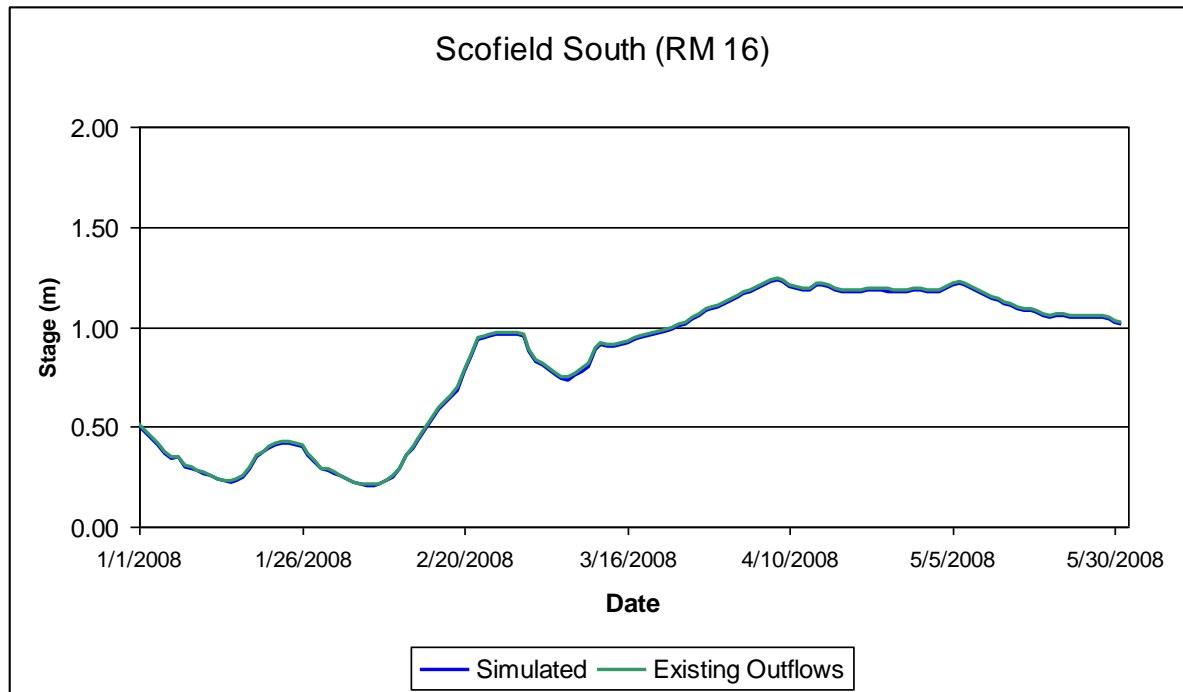


Figure 6.68 – Stage at Scofield South – Myrtle Grove 1-D Hydrodynamics Calibration – 2008

The introduction of the Myrtle Grove diversion reduces only slightly the flow being extracted at other outflows. A summary of the inflows and outflows maximum, minimum and average values for the Myrtle Grove fixed-bed results is shown in Table 6-20.

Table 6-20 – Inflows and Outflows for the Myrtle Grove Case – 1-D Calibration - 2008

Site	Q maximum (m ³ /s, cfs)		Q minimum (m ³ /s, cfs)		Q average (m ³ /s, cfs)	
Belle Chasse* (RM 76)	33,830	1.18x10 ⁶	10,331	364,850	22,556	796,549
White Ditch and Naomi (RM 65)	-42	-1500	-42	-1500	-42	-1500
Myrtle Grove (RM 59)	-862	-30,446	-263	-9,300	-616	-21,769
West-Pointe-À-La-Hache (RM 49)	-14	-500	-14	-500	-14	-500
Bohemia Spillway U/S (RM 34)	-4,615	-162,981	-11	-389	-1,530	-58,958
Bohemia Spillway Int. (RM 32.5)	-510	-18,027	-18	-625	-283	-9,993
Bohemia Spillway D/S (RM 31)	-976	-34,454	-1	-21	-325	-11,473
Bayou Lamoque North (RM 33)	-53	-1,874	-17	-612	-39	-1,382
Bayou Lamoque South (RM 32)	-35	-1,227	-13	-446	-26	-933
Fort St. Philip** (RM 20)	-600	-21,194	-147	-5,194	-413	-14,593
Baptiste Collette** (RM 12)	-4,222	-1,593	-1,593	-59,245	-3,243	-114,514
Grand Pass** (RM 10)	-1,500	-52,984	-531	-18,759	-1,130	-39,902
Tiger Pass** (RM 10)	-1,463	-51,660	-548	-19,339	-1,120	-39,538
West Bay (RM 4)	-1,420	-50,132	-529	-18,697	-1,086	-38,337
Main Pass** (RM 4)	-3,092	-109,193	-1,031	-36,420	-2,294	-80,997
Downstream of Main Pass*** (RM 3)	14,426	639,235	5,573	193,803	10,395	363,542

*Upstream Boundary

**Natural Outflows (Distributaries)

***Downstream Boundary

Table 6-20 shows that the amounts of flow being diverted in other diversions were not greatly affected by the introduction of the Myrtle Grove diversion. On Table 6-21 it is presented a comparison between the average outflows obtained with the introduction of the Myrtle Grove in the system and with the existing conditions. The flow change in percent is obtained by the formula:

$$Q_{average\ change}(\%) = 100 \left[\frac{(Q_{average\ Myrtle} - Q_{average\ Existing})}{Q_{average\ Existing}} \right] \quad (6.4)$$

The maximum change is registered at the Bohemia Spillway U/S structure, with a 15.8% decrease in the outflow. A reduction of more than 8% is registered for the Bohemia Spillway D/S structure. For the remaining cases the flow reduction is under 4%. The downstream boundary outflow is reduced in only 2.35%.

Table 6-21 – Change in the average flow with the introduction of the Myrtle Grove Diversions – 1-D Calibration - 2008

Site	Q average Myrtle (m ³ /s)	Q average Existing (m ³ /s)	Q average Change (%)
Bohemia Spillway U/S (RM 34)	-1,530	-1,817	-15.80%
Bohemia Spillway Int. (RM 32.5)	-283	-292	-3.08%
Bohemia Spillway D/S (RM 31)	-325	-355	-8.45%
Bayou Lamoque North (RM 33)	-39	-40	-2.50%
Bayou Lamoque South (RM 32)	-26	-27	-3.70%
Fort St. Philip** (RM 20)	-413	-417	-0.96%
Baptiste Collette** (RM 12)	-3,243	-3,258	-0.46%
Grand Pass** (RM 10)	-1,130	-1,136	-0.53%
Tiger Pass** (RM 10)	-1,120	-1,125	-0.44%
West Bay (RM 4)	-1,086	-1,088	-0.18%
Main Pass** (RM 4)	-2,294	-2,300	-0.26%
Downstream of Main Pass*** (RM 3)	10,395	10,645	-2.35%

*Upstream Boundary

**Natural Outflows (Distributaries)

***Downstream Boundary

After the hydrodynamics calibration the Myrtle Grove model was calibrated for sediment transport. The stage calibration results with mobile-bed are shown in Figure 6.69 to Figure 6.72. Once again it can be seen that the Myrtle Grove diversion has a small impact in the hydrodynamics of the main channel.

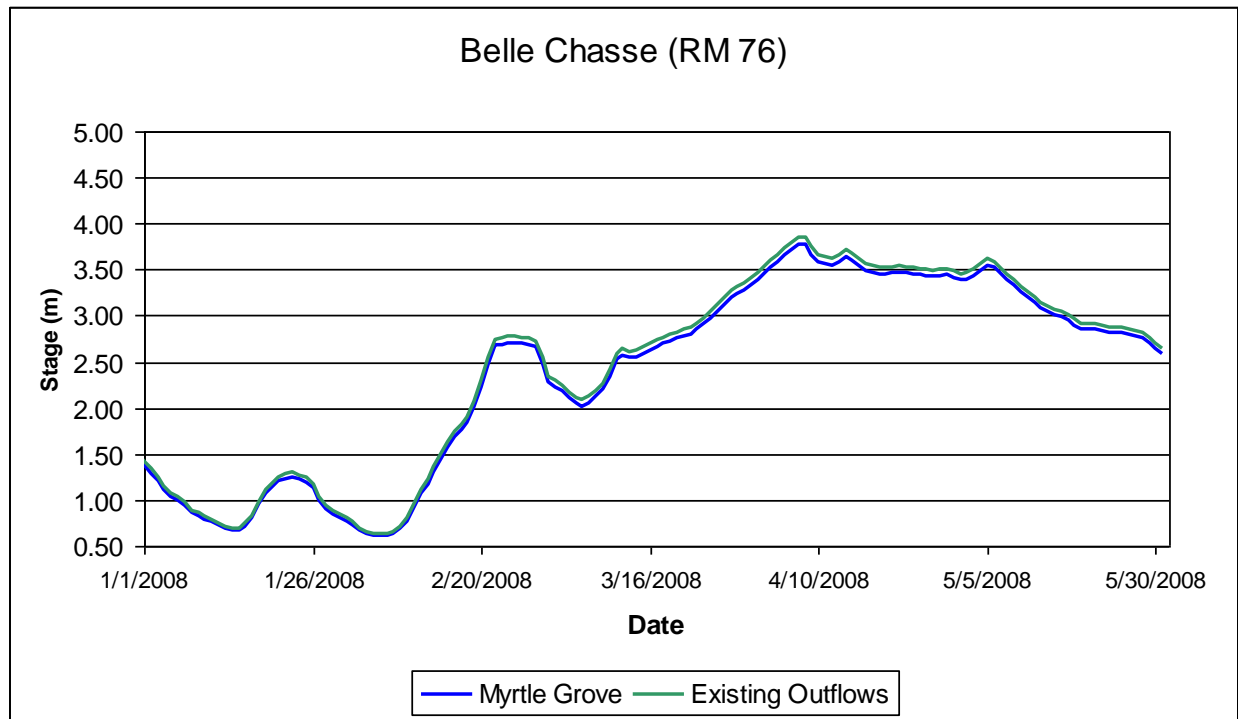


Figure 6.69 – Stage at Belle Chasse – Myrtle Grove 1-D Mobile-Bed Calibration – 2008

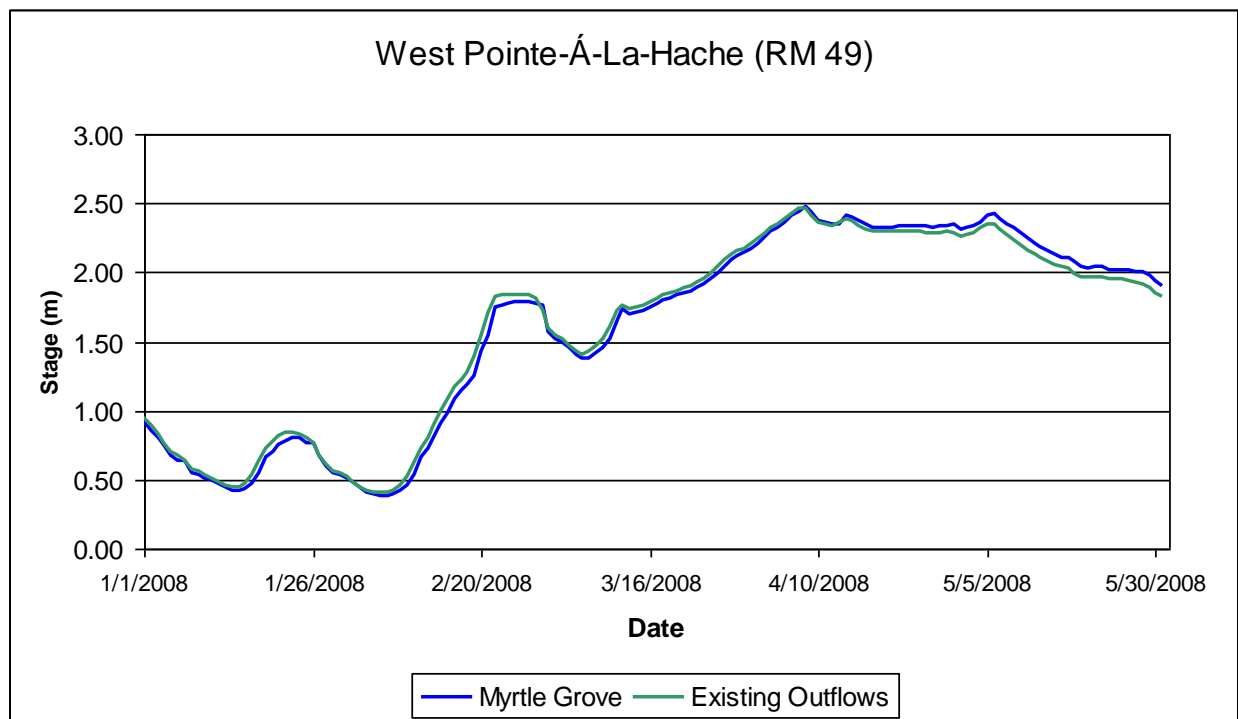


Figure 6.70 – Stage at West Pointe-À-La-Hache - Myrtle Grove 1-D Mobile-Bed Calibration – 2008

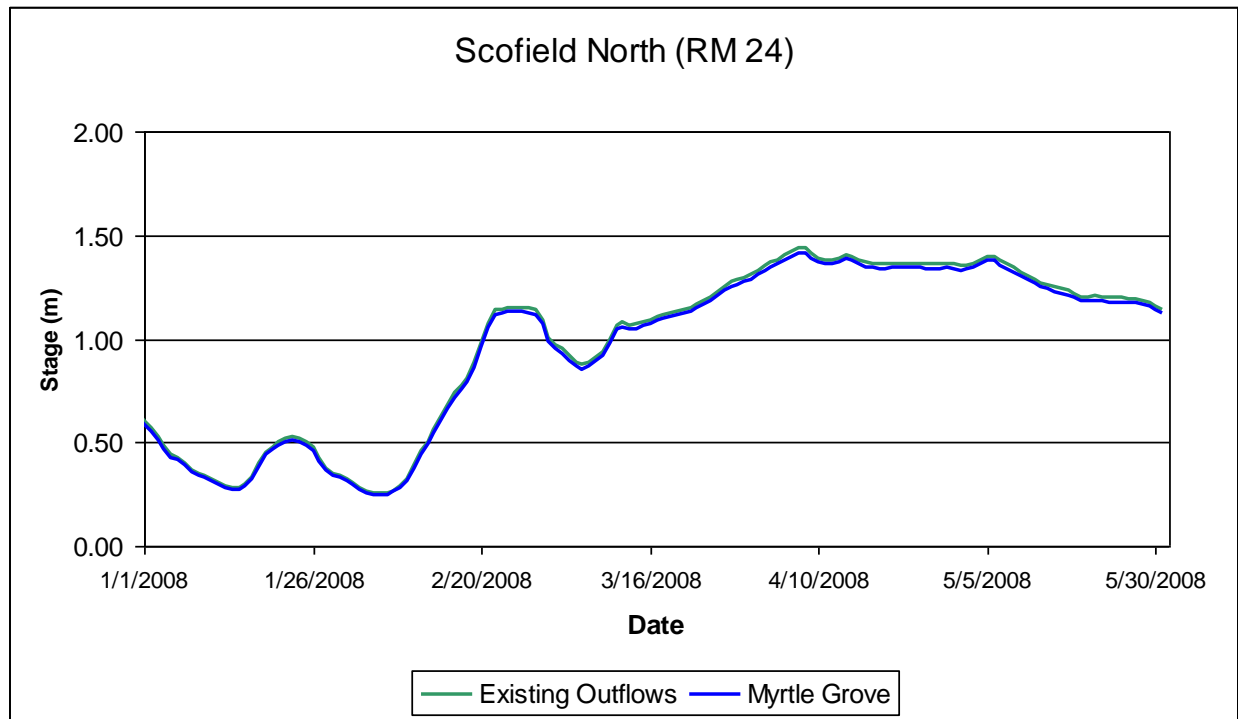


Figure 6.71 – Stage at Scofield North – Myrtle Grove 1-D Mobile-Bed Calibration – 2008

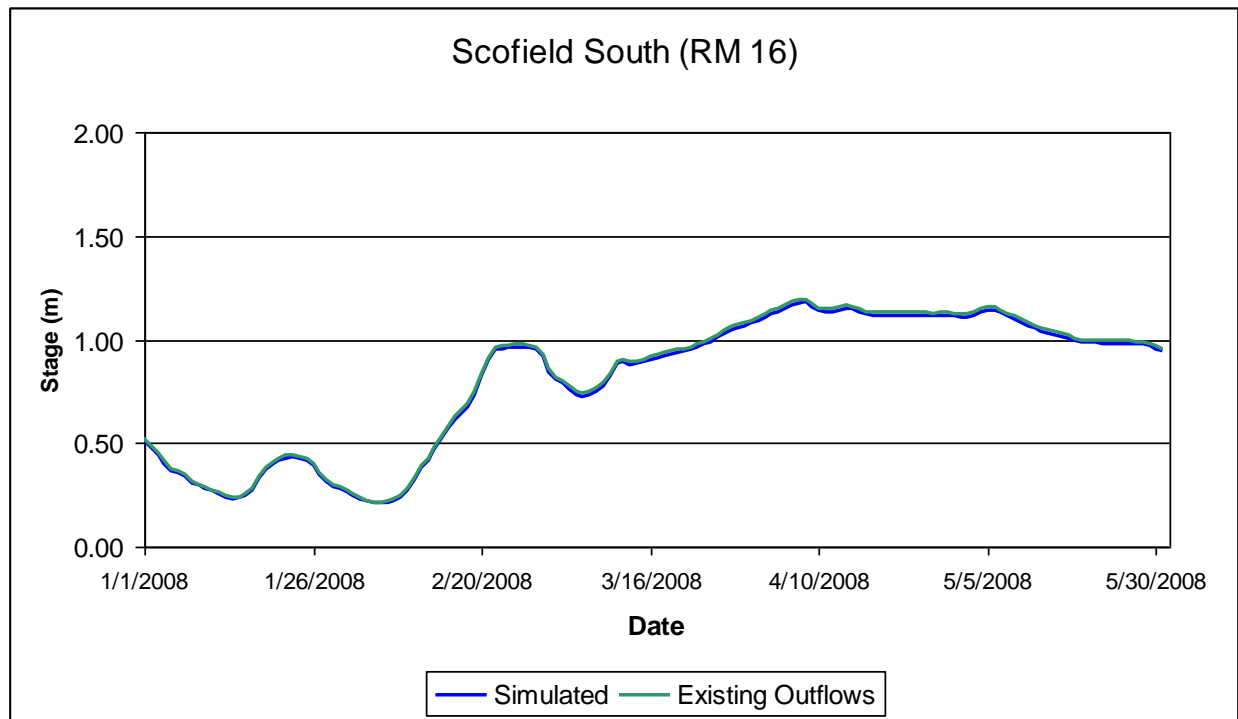


Figure 6.72 – Stage at Scofield South – Myrtle Grove 1-D Mobile-Bed Calibration – 2008

The suspended sand concentration results obtained during the mobile-bed calibration at selected stations in the main channel are shown from Figure 6.73 to Figure 6.76. The results are very close to the ones obtained for the existing outflows test.

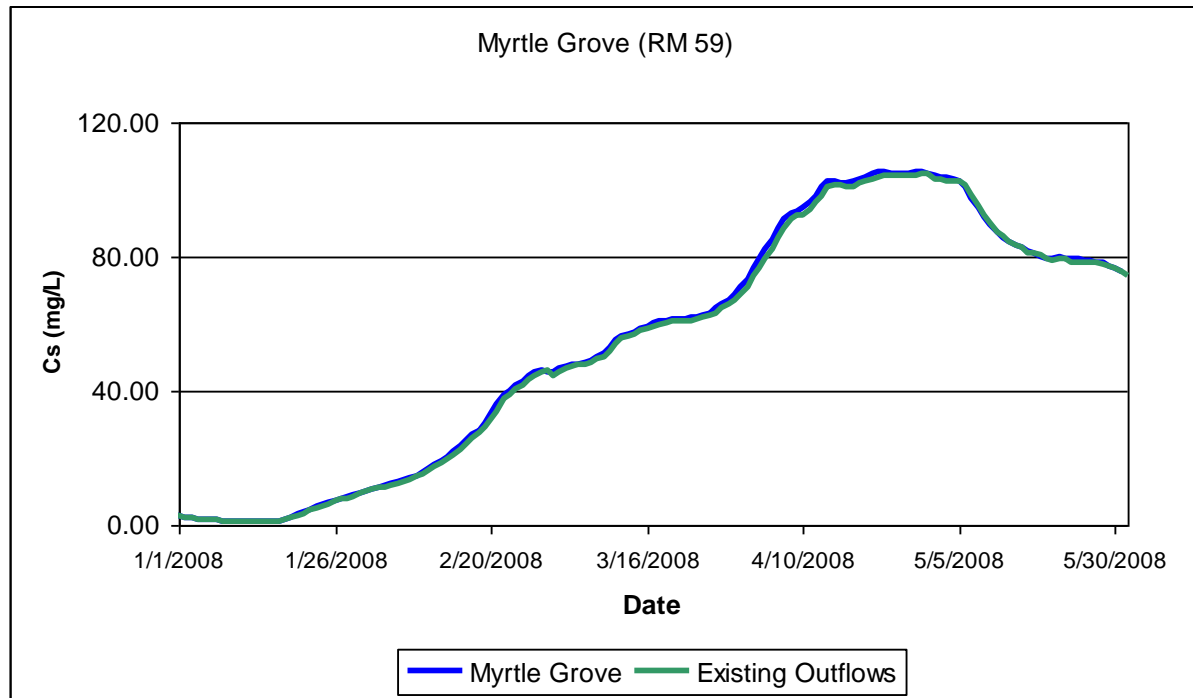


Figure 6.73 – Suspended Sand Concentration at Myrtle Grove for the 1-D Mobile-Bed Calibration – 2008

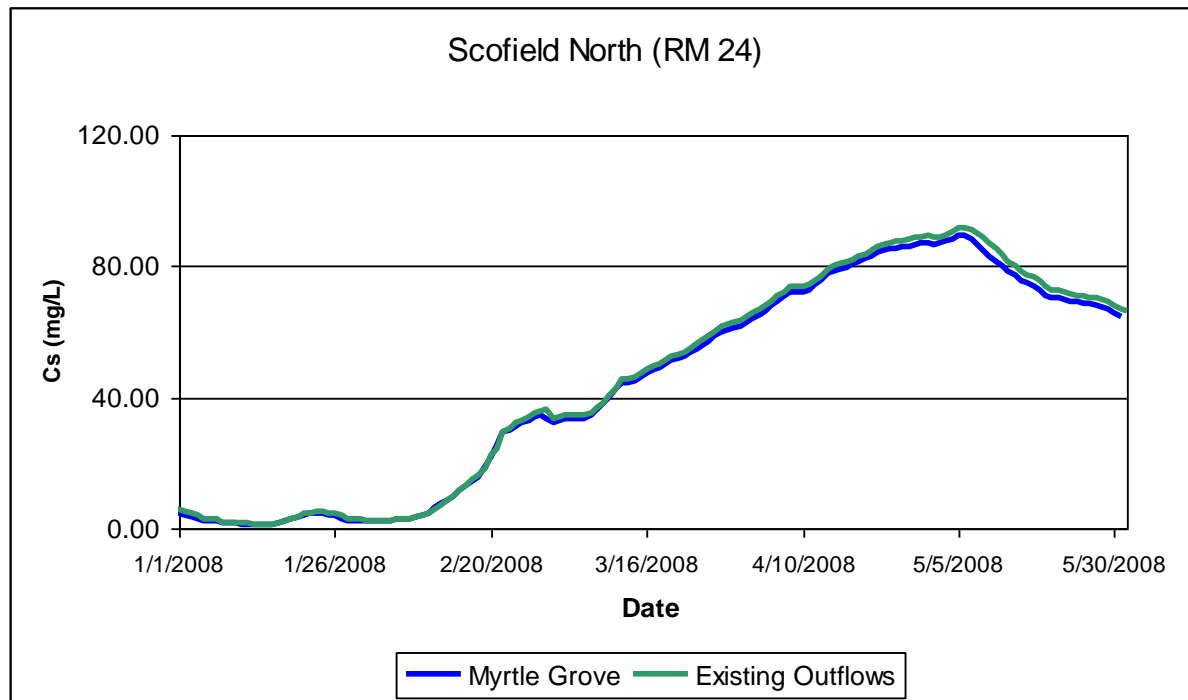


Figure 6.74 – Suspended Sand Concentration at Scofield North for the 1-D Mobile-Bed Calibration – 2007/08

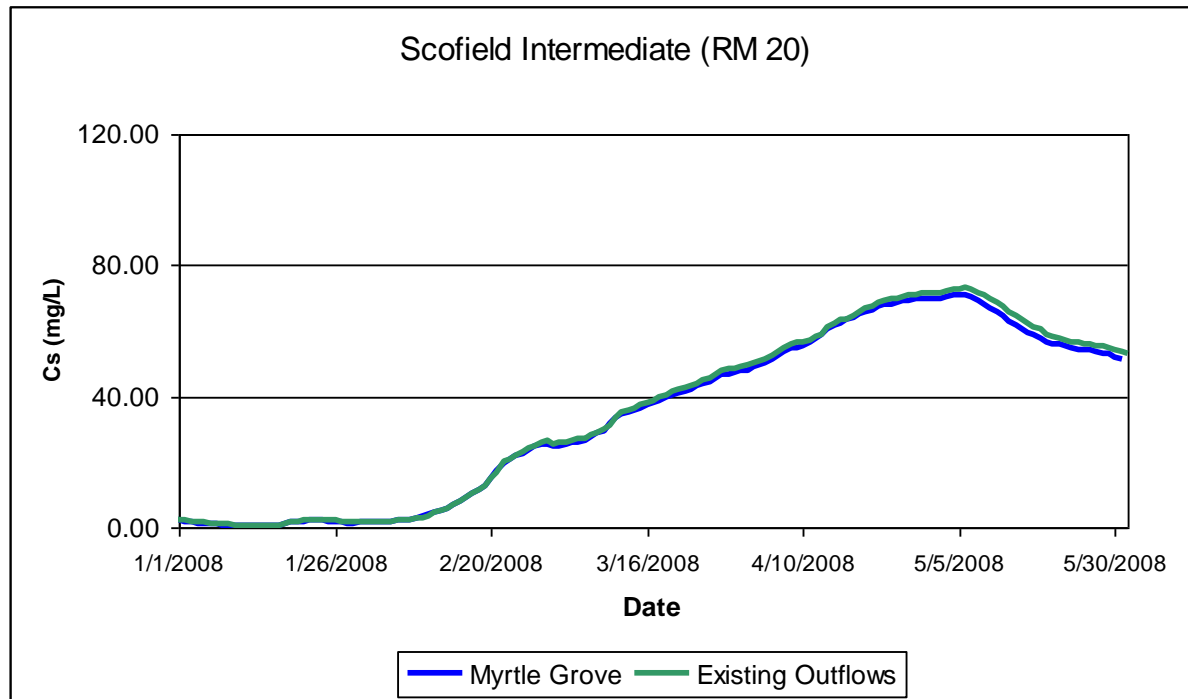


Figure 6.75 – Suspended Sand Concentration at Scofield Intermediate for the 1-D Mobile-Bed Calibration – 2007/08

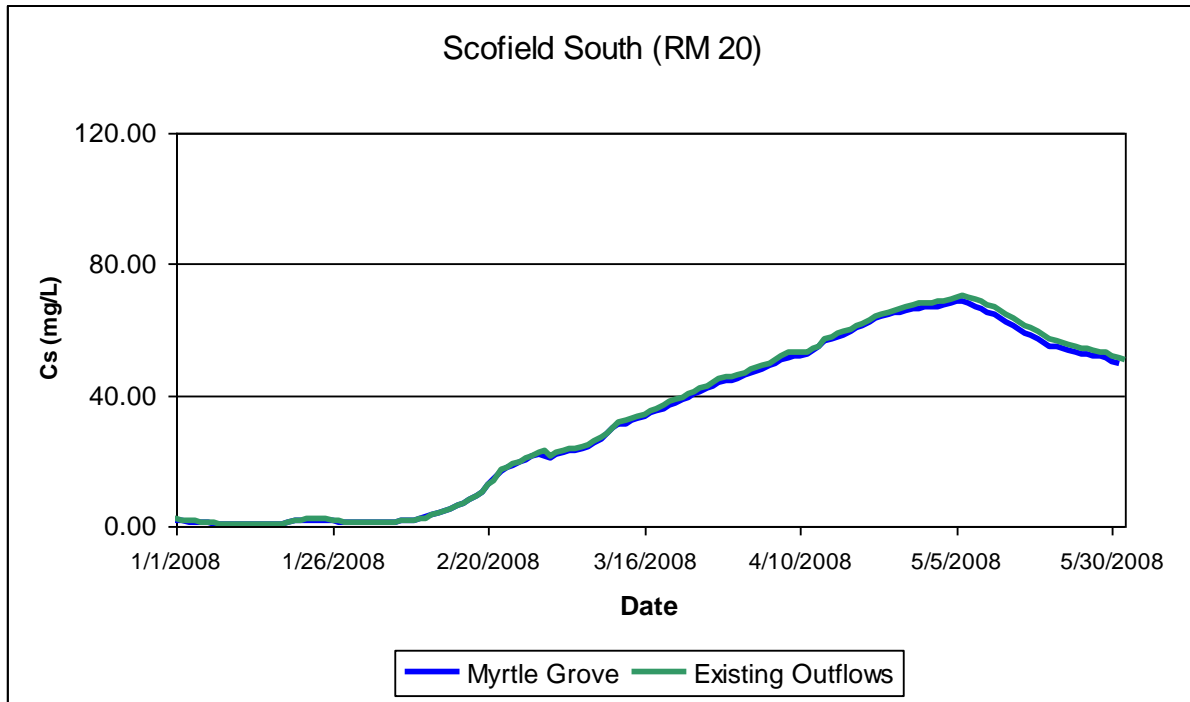


Figure 6.76 – Suspended Sand Concentration at Scofield South for the 1-D Mobile-Bed Calibration – 2007/08

Figure 6.77 and Figure 6.78 show respectively the peak flow and the intermediate flow sand concentration at each outflow in graphical form for both the existing and the Myrtle Grove tests. The results with the introduction of the diversion are not very different from the ones with the existing outflows only.

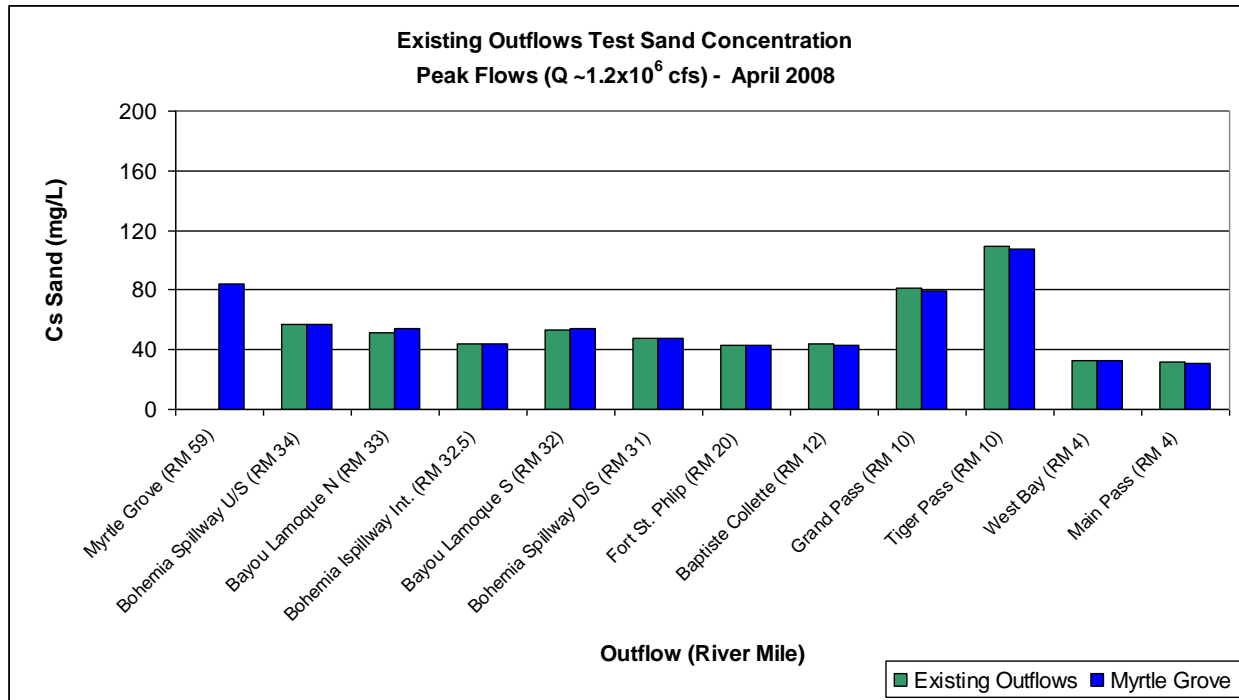


Figure 6.77 – 1-D Simulations – Myrtle Grove – Outflows Suspended Sand Concentration at Peak Flows

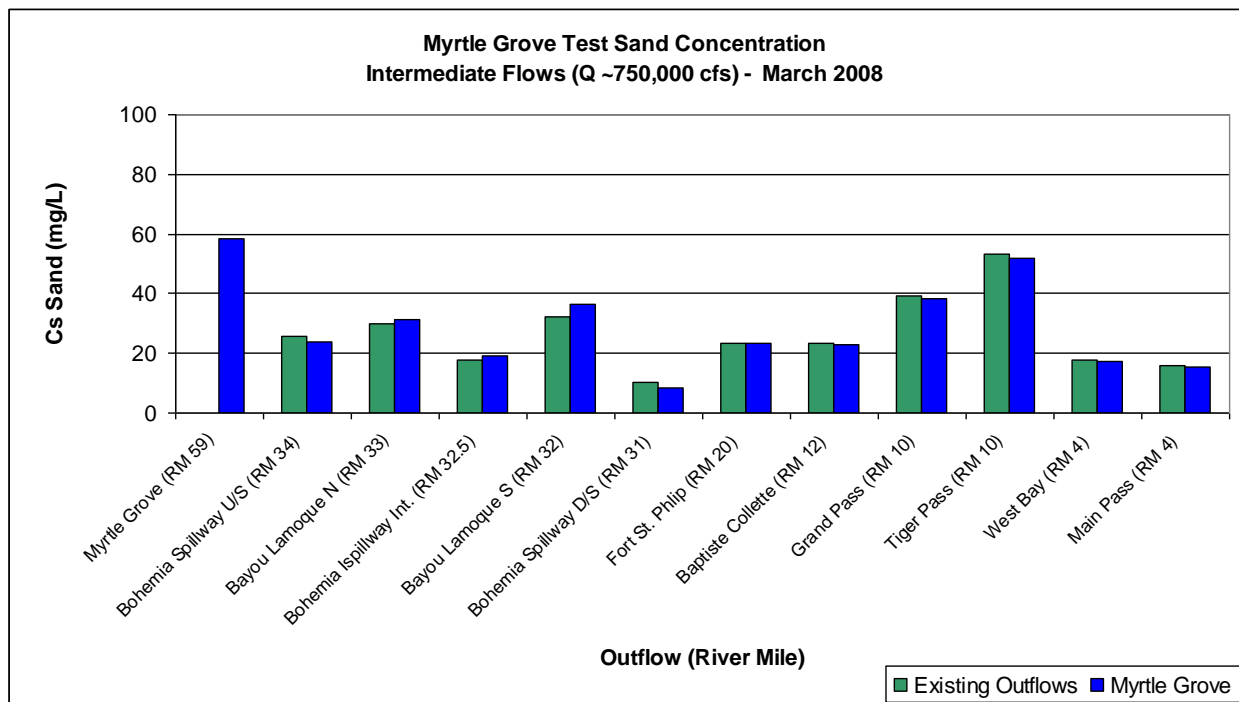


Figure 6.78 – 1-D Simulations – Myrtle Grove – Outflows Suspended Sand Concentration at Intermediate Flows

6.3 Belair + Existing Outflows

The second test with the introduction of a new diversion consists on the introduction of a structure on the East Bank at Belair (RM 65). The diversion was included in the model by adding a gate structure lateral to the main channel. In order to include this structure two short links (1 mile long) were included upstream and downstream of it. The new model was calibrated for a diverted Belair peak flow equal to 5,700 m³/s (200,000 cfs). The Belair case includes 13 outflows: a new outflow at Belair, West Pointe-À-La-Hache, Bohemia Spillway U/S, Bohemia Spillway Intermediate, Bohemia Spillway D/S, Bayou Lamoque N, Bayou Lamoque S, Fort St. Philip, Baptiste Collette, Tiger Pass, Grand Pass, West Bay and Main Pass. It was decided to not include White Ditch and Naomi diversions while running the Belair case since the three outflows are located around the same River Mile and both White Ditch and Naomi are very small outflows, particularly when compared to the Belair diversion. Figure 6.79 shows the topology of the fluvial network for this case.

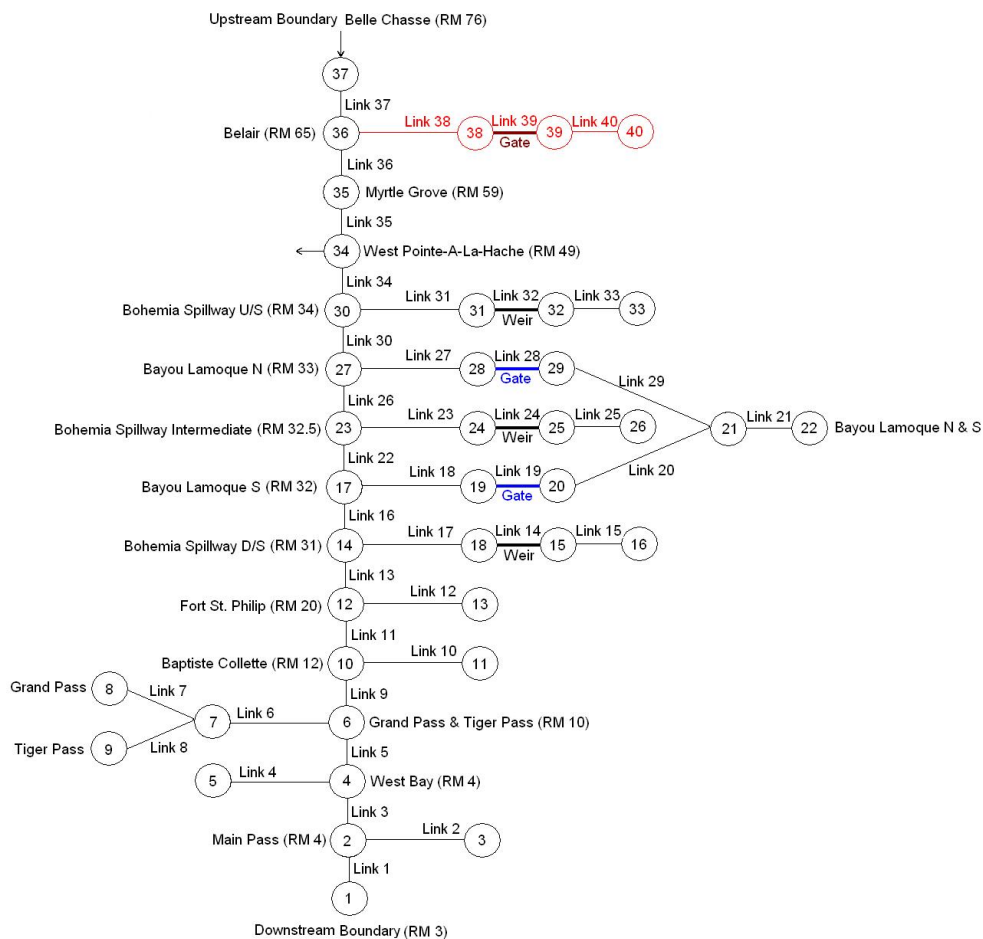


Figure 6.79 – Schematic diagram of the Belair Case Topology

6.3.1 Boundary Conditions

Once again the 01/01/2008 to 06/05/2008 period was simulated for both hydrodynamics and sediment transport. The boundary conditions used in this case were basically the same used for the existing outflows calibration simulations given in Table 6-1, Table 6-2, Table 6-3, and in Appendix A. However, the White Ditch and Naomi outflows were considered to be equal to zero and a new stage boundary condition, equal to the remaining distributaries boundary condition, was added for the downstream end of the reach used for the Belair structure. The maximum, minimum and average values of stage can be seen in Table 6-22.

Table 6-22 – Stage Boundary Condition – Belair Case – 1-D Calibration - 2008

Site	Stage maximum (m, ft)		Stage minimum (m, ft)		Stage average (m, ft)	
Belair (RM 65)	0.01	0.03	-0.04	-0.12	-0.01	-0.03

The Belair model was ran first in fixed-bed mode. The Belair Manning-Strickler coefficient (K_s) values and the gate structure parameters were calibrated to allow the extraction of the desired 5,700 m³/s (200,000 cfs) under peak flow conditions. All the remaining structure parameters and K_s values used are the ones obtained during the existing outflows calibration.

For both the hydrodynamics and the mobile-bed calibration, K_s values of 65.00 were used for the Belair diversion. The parameters used in the hydrodynamics and the mobile-bed simulations for the gate structure were also the same and are presented in Table 6-23.

Table 6-23 – Gate Parameters – Belair Case – 1-D Hydrodynamics and Mobile-Bed Calibrations - 2008

Site	Gate Sill Width (m, ft)		Gate Sill Elevation (m, ft)		Discharge Coefficients (submerged, free flow)	
Belair (Link 39)	701	2,300	0.61	2.00	3.0	3.0

For the main channel and existing outflows the bed material sediment sizes were equal to the ones used in the existing outflows simulations which were presented in Table 6-8. A constant sediment size of 0.200 mm material and a 30 m sediment control depth were used for the Belair diversion bed, which match the values used in the remaining outflow channels.

6.3.2 Results

The Belair diversion outflow obtained in fixed-bed mode for hydrodynamics calibration is presented in Figure 6.80. It can be noticed that the result obtained is not very different from the one obtained by Davis (2010) with HEC-RAS.

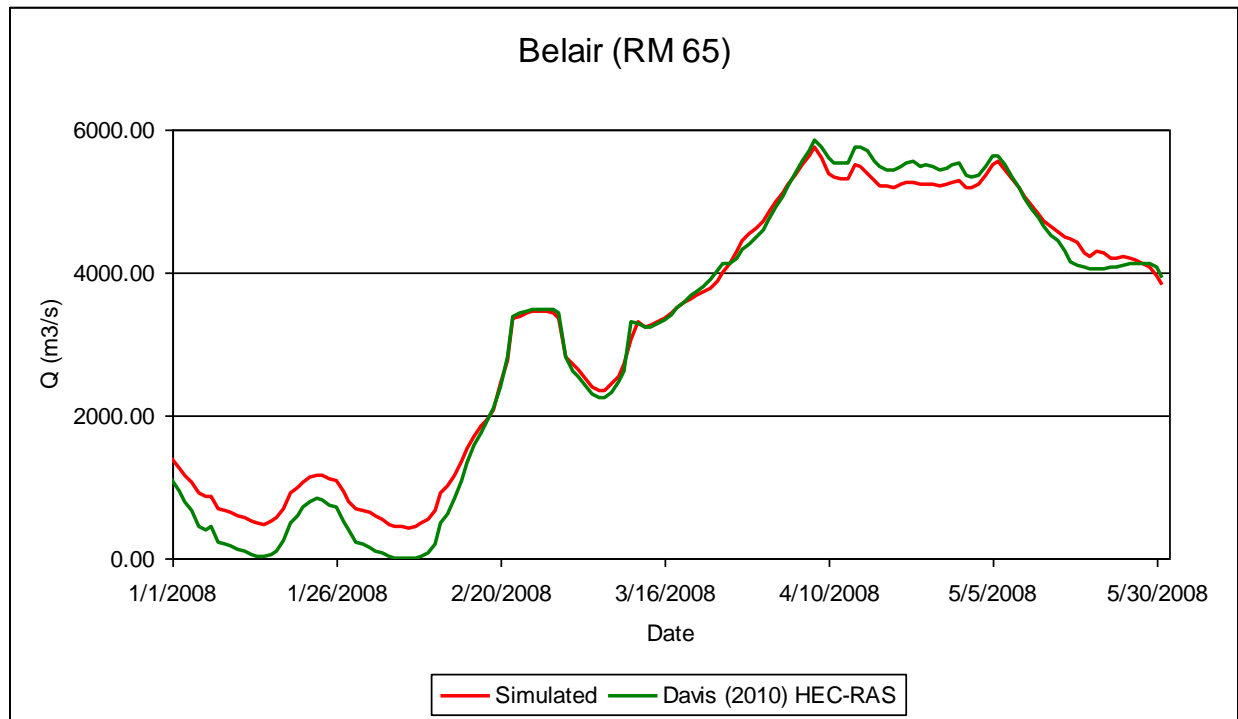


Figure 6.80 – Belair Outflow – Belair Case - 1-D Hydrodynamics Calibration – 2008

The model results are compared with the ones obtained with existing outflows. The hydrodynamics stage calibration results are shown from Figure 6.81 to Figure 6.84. The results show that the introduction of this large diversion impacts significantly the hydrodynamics in the main channel, contrarily to what happens with the smaller Myrtle Grove diversion.

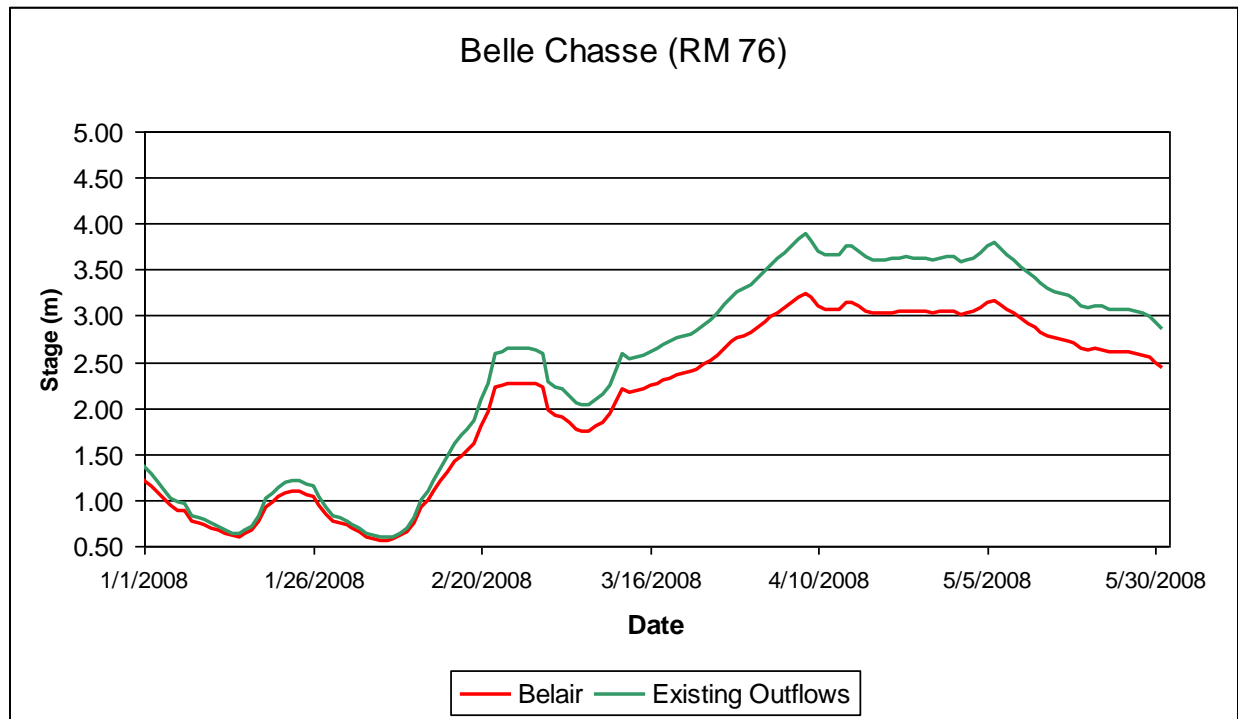


Figure 6.81 – Stage at Belle Chasse – Belair - 1-D Hydrodynamics Calibration – 2008

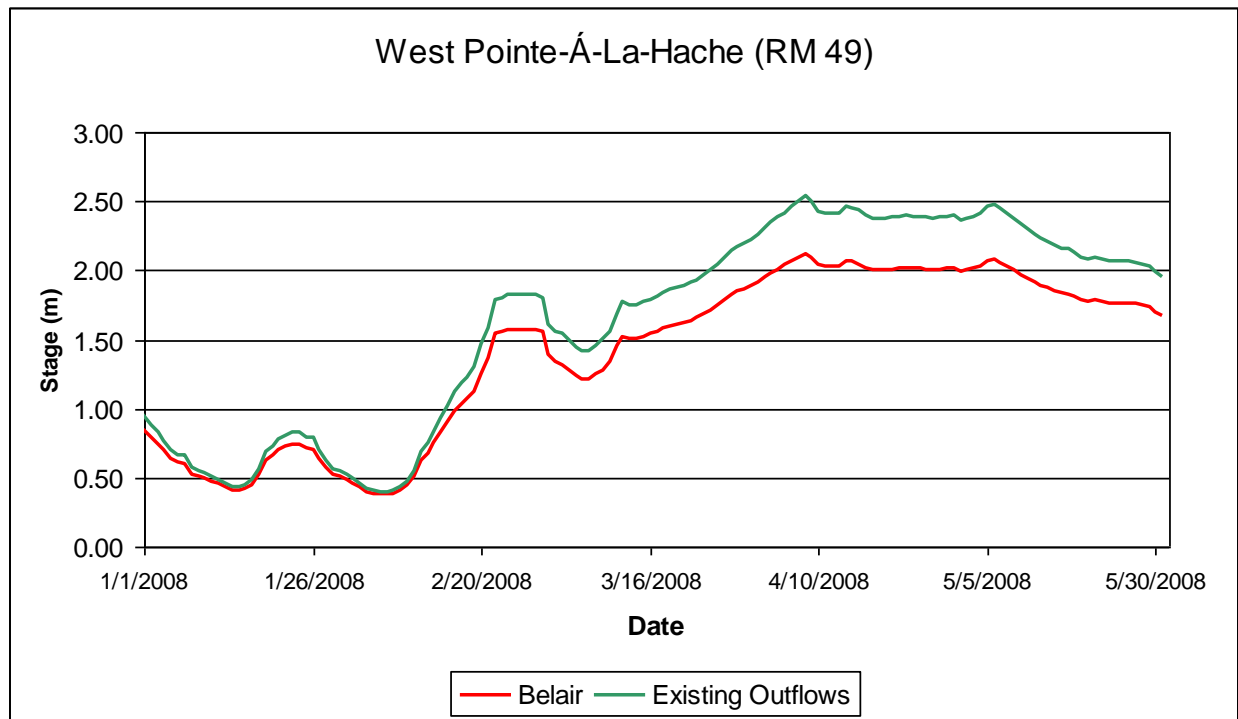


Figure 6.82 – Stage at West Pointe-À-La-Hache - Belair - 1-D Hydrodynamics Calibration – 2008

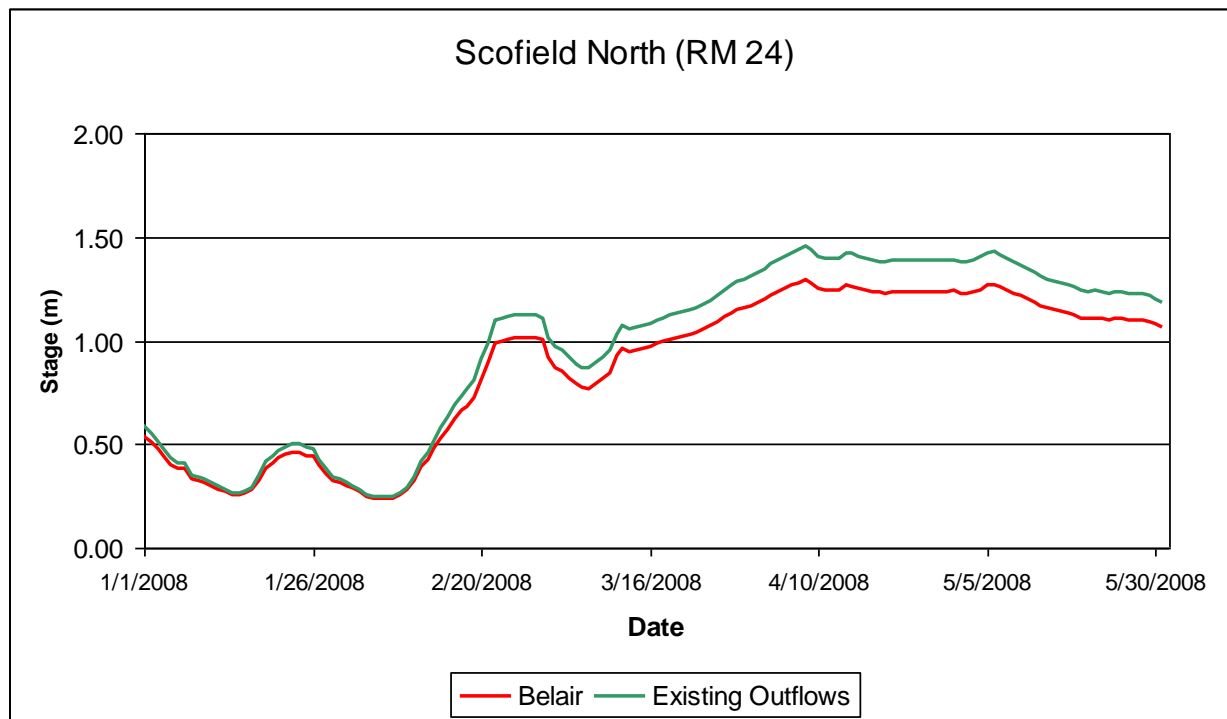


Figure 6.83 – Stage at Scofield North – Belair – 1-D Hydrodynamics Calibration 2008

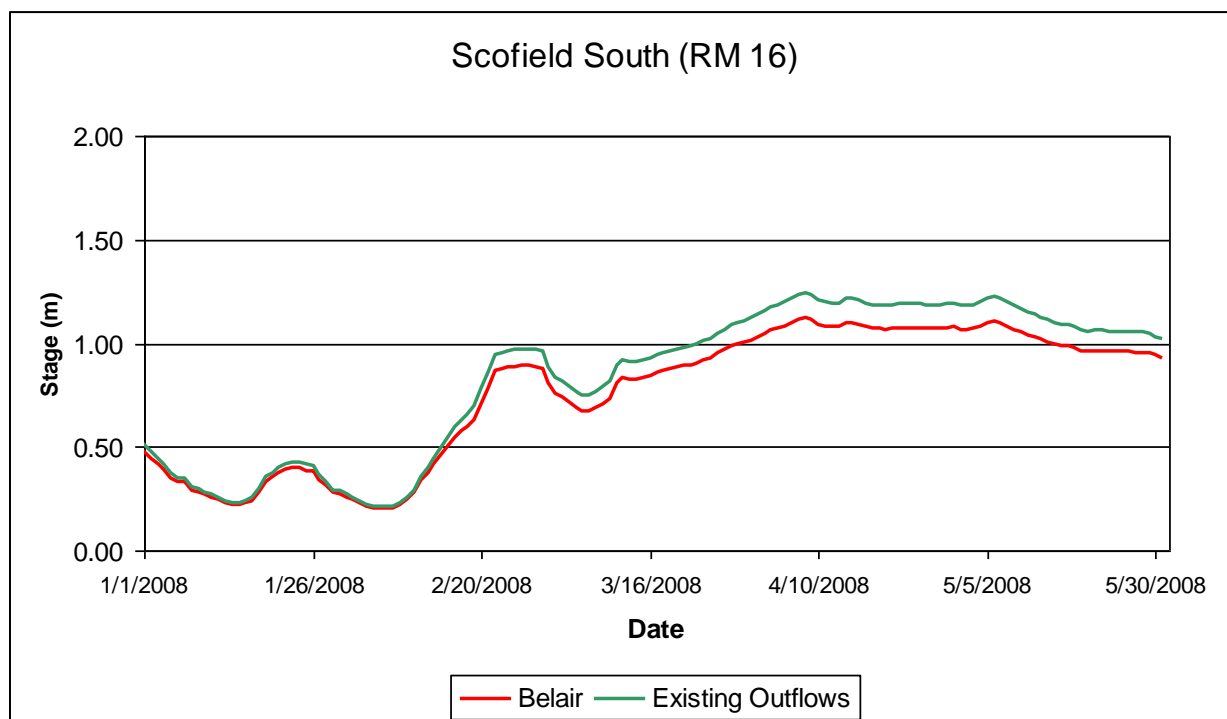


Figure 6.84 – Stage at Scofield South – Belair - 1-D Hydrodynamics Calibration – 2008

The introduction of the Belair diversion reduces considerably the amount of flow leaving the main channel at other outflows. A summary of the inflows and outflows maximum, minimum and average values for the fixed-bed results is shown in Table 6-24.

Table 6-24 – Inflows and Outflows for the Belair Case – 1-D Calibration - 2008

Site	Q maximum (m ³ /s, cfs)		Q minimum (m ³ /s, cfs)		Q average (m ³ /s, cfs)	
Belle Chasse* (RM 76)	33,830	1.18x10 ⁶	10,331	364,850	22,556	796,549
Belair (RM 65)	-5,746	-202,928	-432	-15,256	-3,194	-112,808
West-Pointe-À-La-Hache (RM 49)	-14	-500	-14	-500	-14	-500
Bohemia Spillway U/S (RM 34)	-2,762	-97,550	-11	-387	-910	-32,151
Bohemia Spillway Int. (RM 32.5)	-418	-14,757	-17	-593	-235	-8,306
Bohemia Spillway D/S (RM 31)	-557	-19,685	-2	-76	-156	-5,495
Bayou Lamoque North (RM 33)	-49	-1,714	-17	-604	-36	-1,286
Bayou Lamoque South (RM 32)	-32	-1,137	-12	-441	-25	-877
Fort St. Philip** (RM 20)	-544	-19,216	-145	-5,137	-382	-13,484
Baptiste Collette** (RM 12)	-3,994	-141,034	-1,579	-55,764	-3,099	-109,441
Grand Pass** (RM 10)	-1,410	-49,780	-527	-18,595	-1,075	-37,953
Tiger Pass** (RM 10)	-1,382	-48,799	-543	-19,173	-1,069	-37,754
West Bay (RM 4)	-1,348	-47,596	-525	-18,551	-1,041	-36,763
Main Pass** (RM 4)	-2,910	-102,753	-1,023	-36,126	-2,185	-77,168
Downstream of Main Pass*** (RM 3)	12,664	429,551	5,484	193,647	9,135	322,563

*Upstream Boundary

**Natural Outflows (Distributaries)

***Downstream Boundary

Table 6-24 shows that the introduction of the Belair diversion provokes a significant reduction in the other outflows.

Table 6-25 shows a comparison between the average outflows obtained with the introduction of the Belair diversion in the system and with the existing conditions. The flow change in percent is obtained by the formula:

$$Q_{average\ change(\%)} = 100 \left[\frac{(Q_{average\ Belair} - Q_{average\ Existing})}{Q_{average\ Existing}} \right] \quad (6.5)$$

The results obtained with the introduction of the larger Belair diversion are considerably different from the ones obtained with the introduction of the Myrtle Grove structure. The maximum change is now registered at the Bohemia Spillway D/S structure, with a 56% decrease in the outflow while there is a 50% decrease in the outflow at the Bohemia Spillway U/S structure. For the remaining cases the flow reduction ranges between 4% and 20%. The downstream boundary outflow is reduced in more than 14%.

Table 6-25– Change in the average flow with the introduction of the Belair Diversion – 1-D Calibration - 2008

Site	Q average Belair (m ³ /s)	Q average Existing (m ³ /s)	Q average Change (%)
Bohemia Spillway U/S (RM 34)	-910	-1,817	-49.92%
Bohemia Spillway Int. (RM 32.5)	-235	-292	-19.52%
Bohemia Spillway D/S (RM 31)	-156	-355	-56.06%
Bayou Lamoque North (RM 33)	-36	-40	-10.00%
Bayou Lamoque South (RM 32)	-25	-27	-7.41%
Fort St. Philip** (RM 20)	-382	-417	-8.39%
Baptiste Collette** (RM 12)	-3,099	-3,258	-4.88%
Grand Pass** (RM 10)	-1,075	-1,136	-5.37%
Tiger Pass** (RM 10)	-1,069	-1,125	-4.98%
West Bay (RM 4)	-1,041	-1,088	-4.32%
Main Pass** (RM 4)	-2,185	-2,300	-5.00%
Downstream of Main Pass*** (RM 3)	9,135	10,645	-14.19%

*Upstream Boundary

**Natural Outflows (Distributaries)

***Downstream Boundary

After the hydrodynamics calibration the Belair model was calibrated for sediment transport. The stage calibration results with mobile-bed are shown in Figure 6.85 to Figure 6.88. It is visible the significant impact of the Belair diversion in the main channel hydrodynamics.

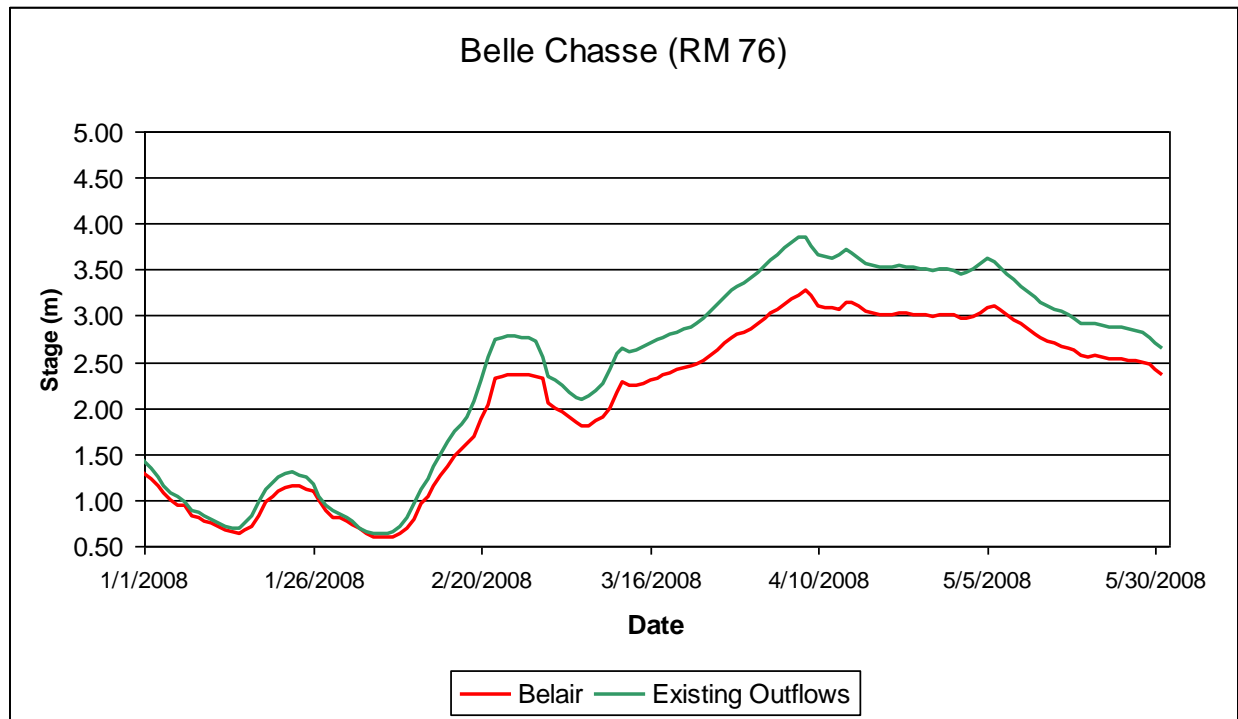


Figure 6.85 – Stage at Belle Chasse – Belair 1-D Mobile-Bed Calibration – 2008

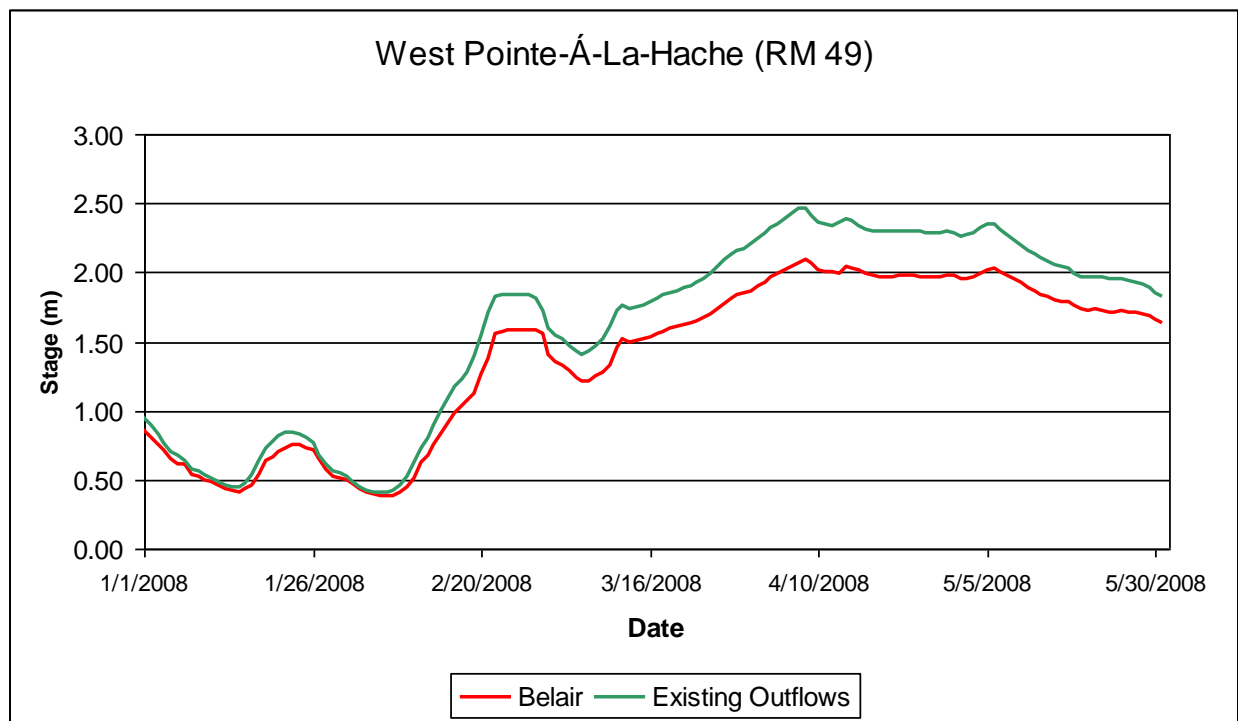


Figure 6.86 – Stage at West Pointe-À-La-Hache - Belair 1-D Mobile-Bed Calibration – 2008

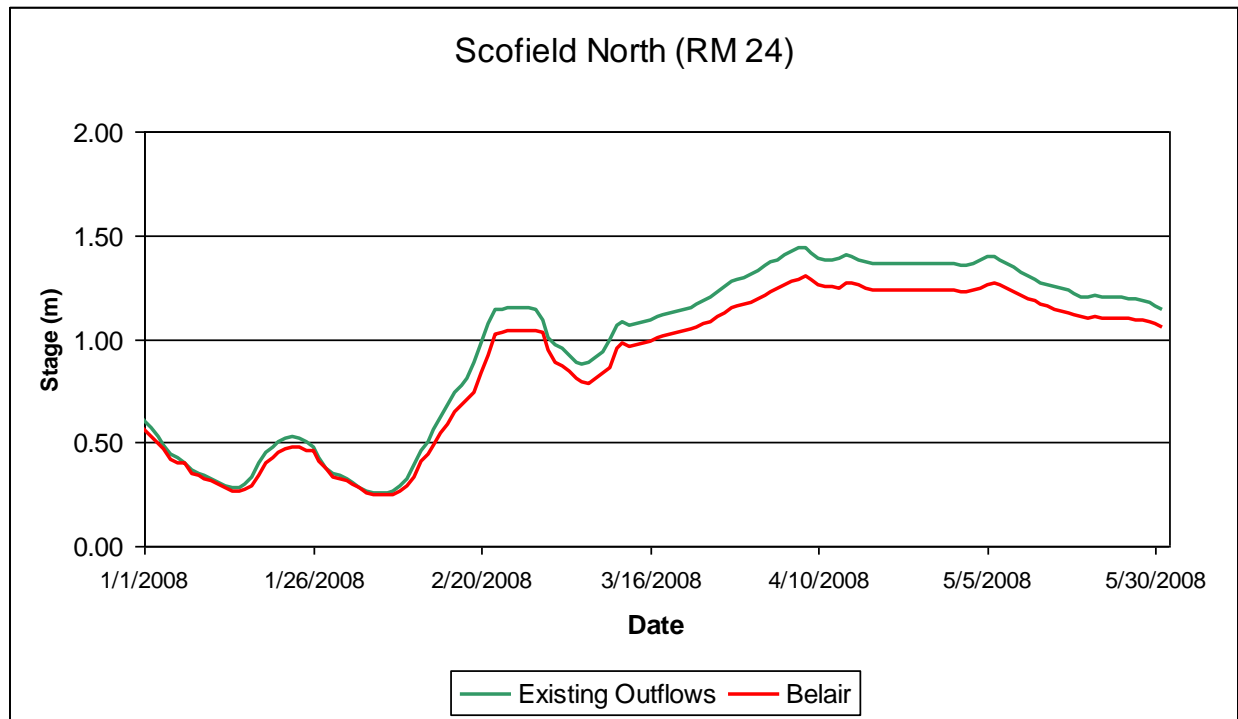


Figure 6.87 – Stage at Scofield North – Belair 1-D Mobile-Bed Calibration – 2008

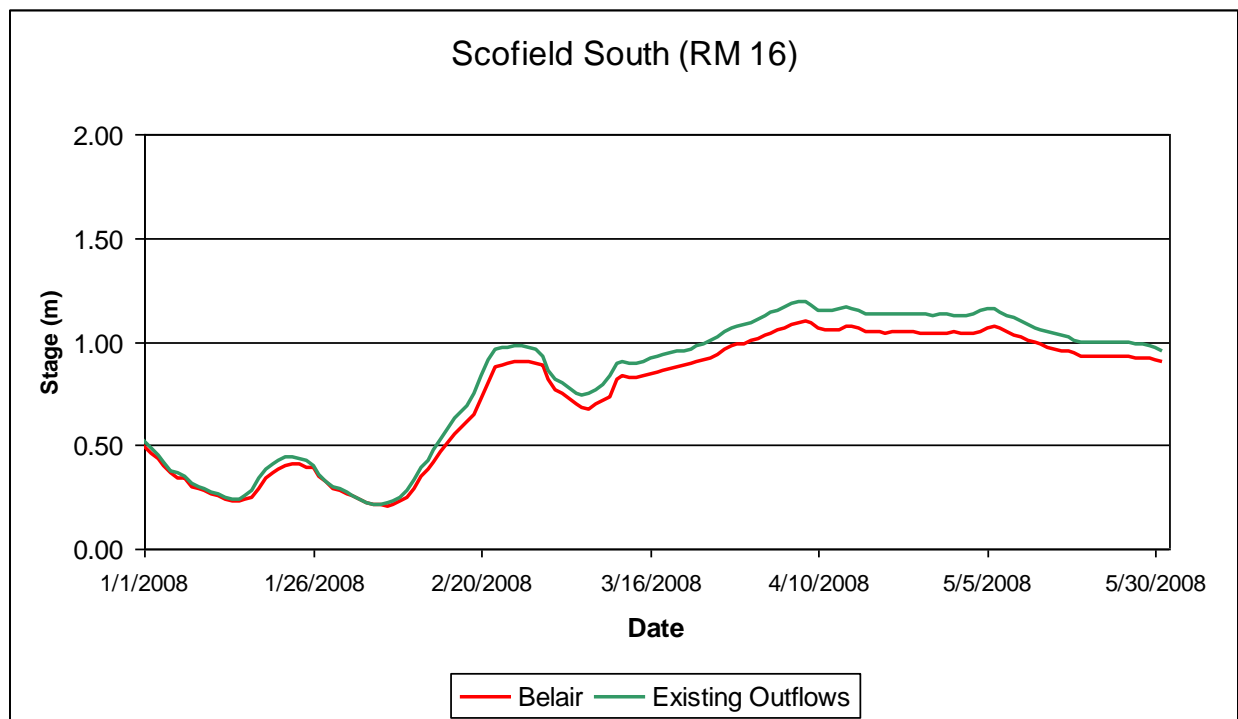


Figure 6.88 – Stage at Scofield South – Belair 1-D Mobile-Bed Calibration – 2008

The suspended sand concentration results obtained during the mobile-bed calibration at some stations in the main channel are shown from Figure 6.89 to Figure 6.92.

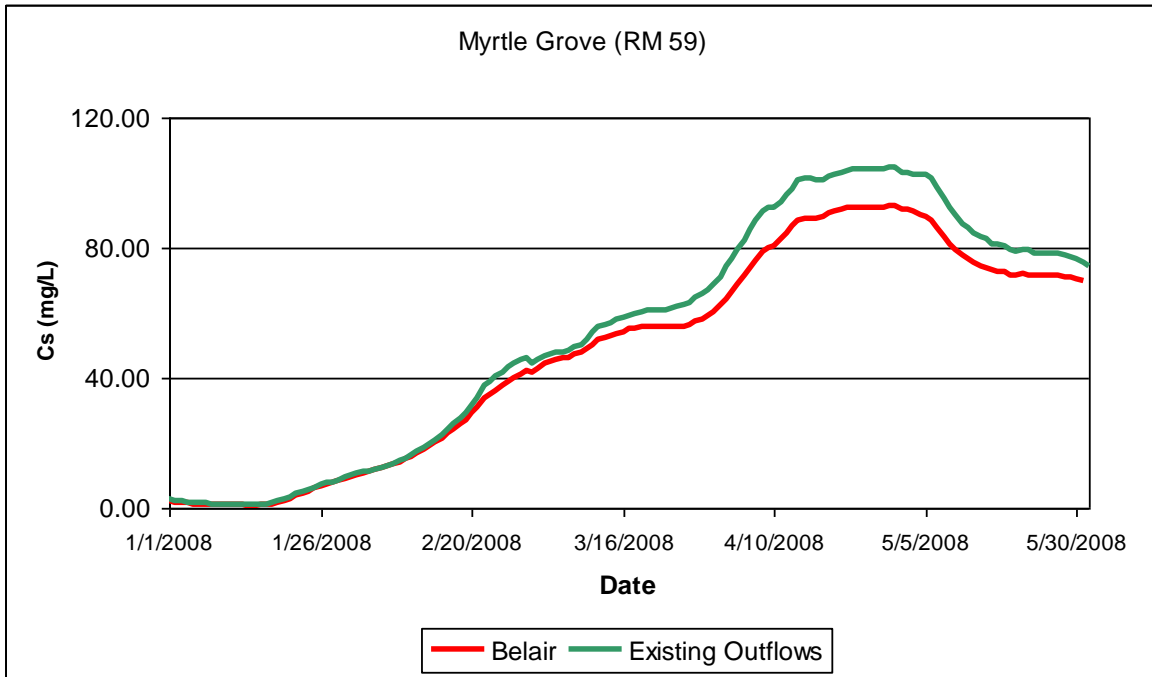


Figure 6.89 – Suspended Sand Concentration at Myrtle Grove for the Belair 1-D Mobile-Bed Calibration – 2008

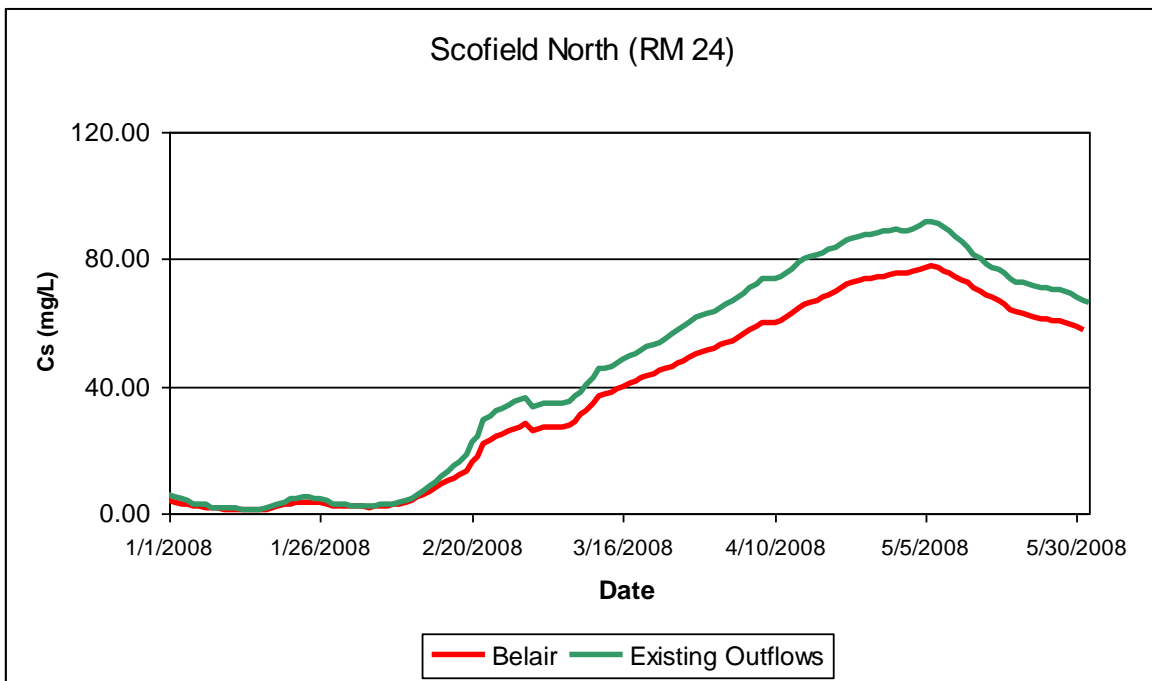


Figure 6.90 – Suspended Sand Concentration at Scofield North for the Belair 1-D Mobile-Bed Calibration – 2008

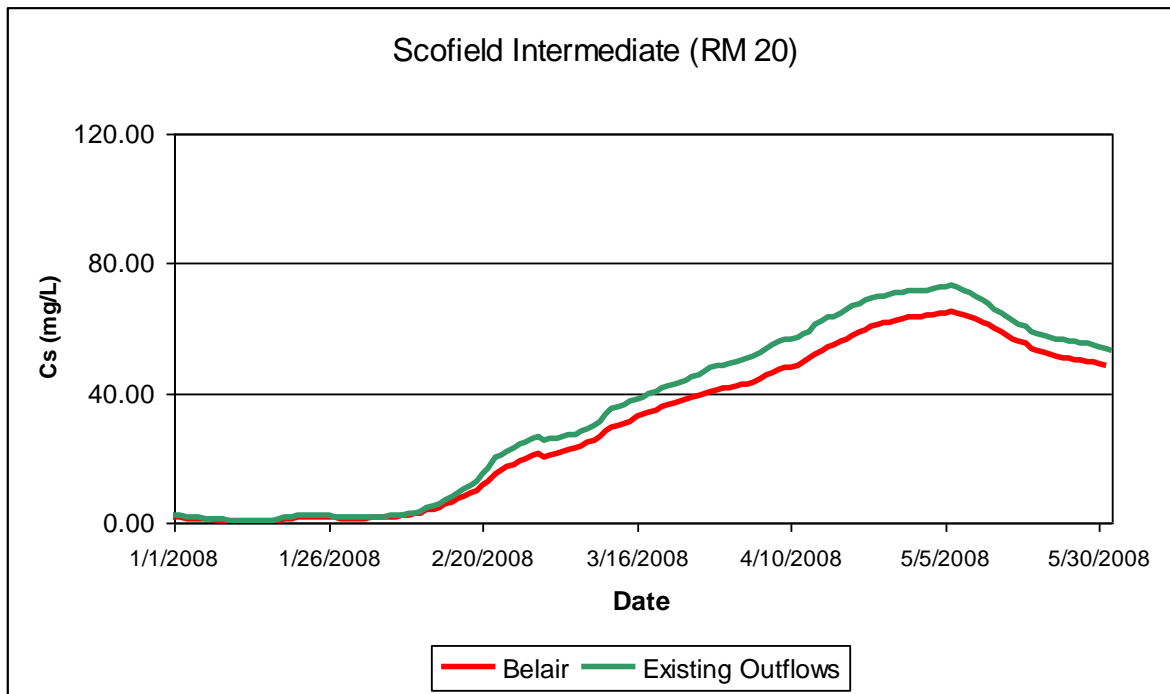


Figure 6.91 – Suspended Sand Concentration at Scofield Intermediate for the Belair 1-D Mobile-Bed Calibration – 2008

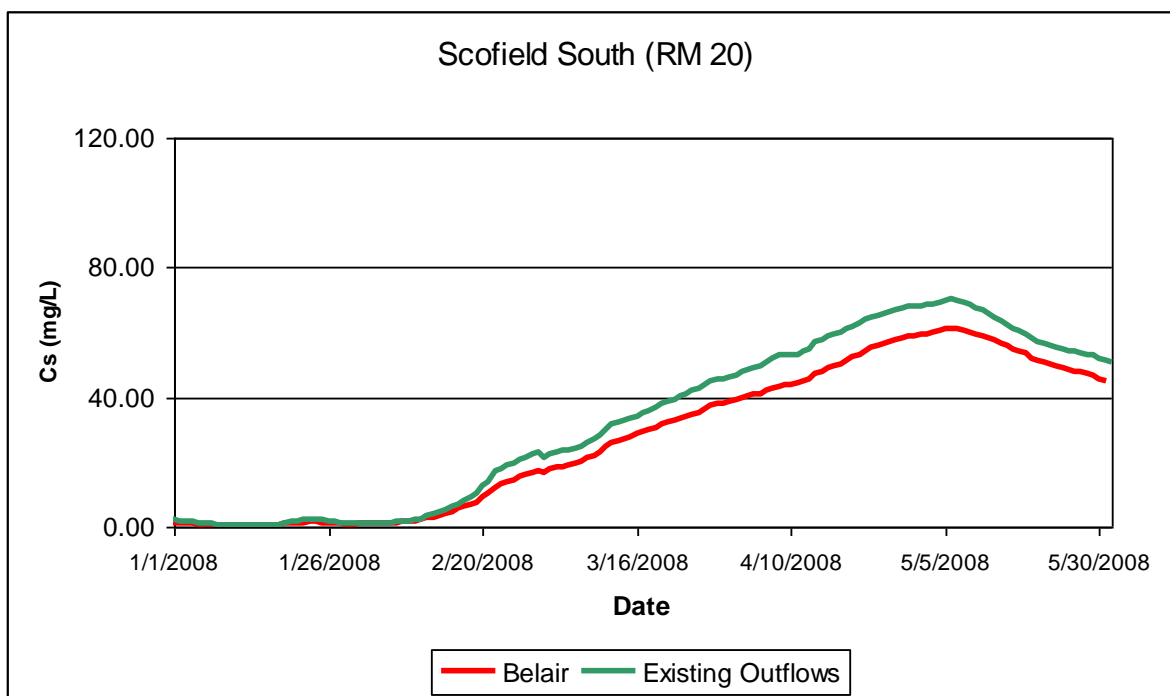


Figure 6.92 – Suspended Sand Concentration at Scofield South for the Belair 1-D Mobile-Bed Calibration – 2008

Figure 6.93 and Figure 6.94 show respectively the peak flow and the intermediate flow sand concentration at each outflow in graphical mode for both the existing and the Belair tests. The results with the introduction of the diversion are considerably lower than the ones with the existing outflows only.

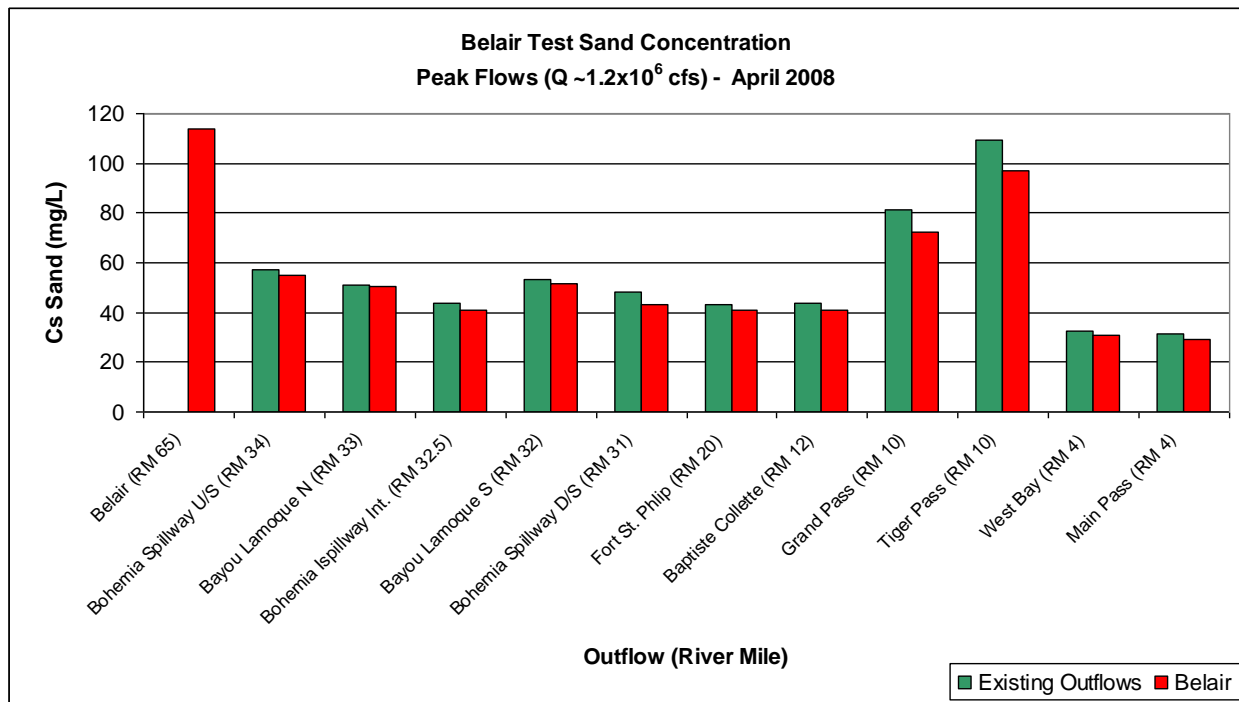


Figure 6.93 – 1-D Simulations – Belair – Outflows Suspended Sand Concentration at Peak Flows

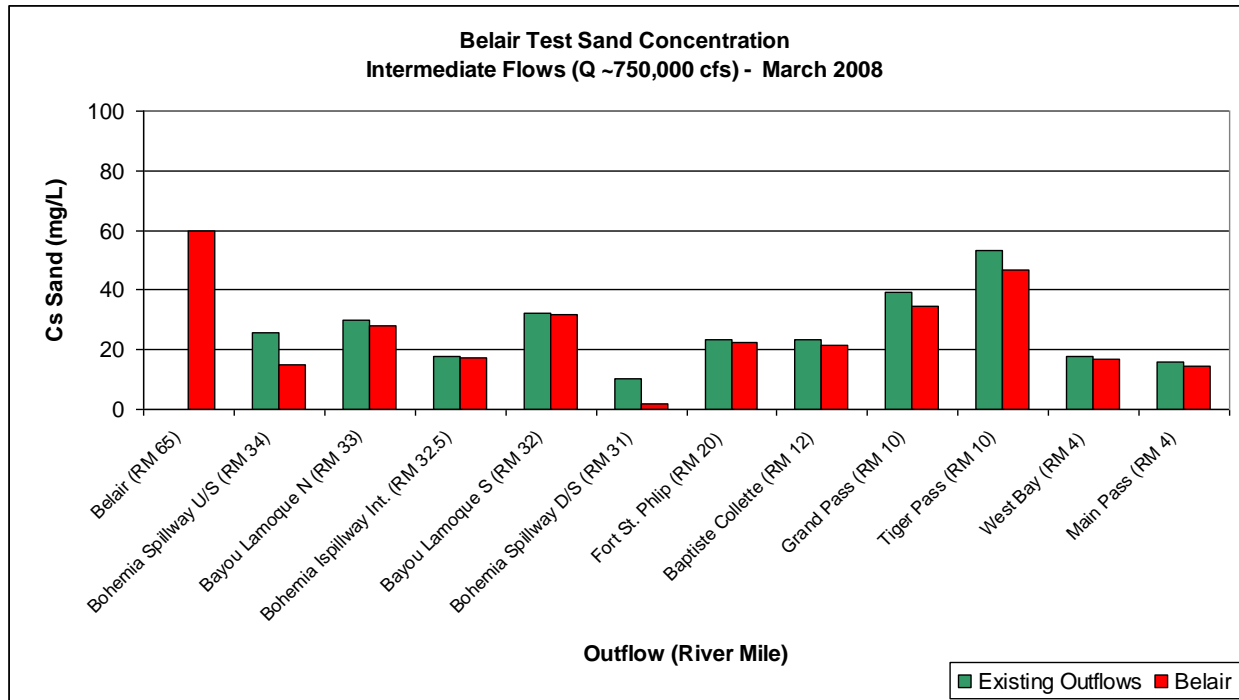


Figure 6.94 – 1-D Simulations – Belair – Outflows Suspended Sand Concentration at Intermediate Flows

7) THREE-DIMENSIONAL ECOMSED MODELING

7.1 Computational Grid Domain

The model was applied to the Lower Mississippi River Reach from Belle Chasse (RM 76, RK 121) to downstream of Main Pass (RM3, RK 5). The computational domain consists of 51,250 cells organized in a structured orthogonal curvilinear grid with a resolution of 100 m by 50 m. Figure 7.1 shows (a) a plan view of the bathymetry and (b) the structured mesh cells at the Myrtle Grove area (RM 59, RK 95). There are 11 uniformly spaced sigma levels. The upstream river boundary includes 12 nodes and the downstream open boundary is composed of 26 nodes

The number of open boundary conditions used depends on the case simulated. Four different cases are presented herein: i) Existing outflows, ii) Myrtle Grove Diversion + Existing outflows, iii) Belair Diversion + Existing outflows, and iv) Proposed Diversions + Existing outflows. The existing case includes 7 outflows divided into 4 distributaries and 3 man-made diversions, with each outflow corresponding to an open boundary condition. The Myrtle Grove and Belair cases include 8 outflows (existing plus the diversion being tested). The Proposed Diversions + Existing outflows case includes a total of 12 outflows (7 existing and 5 proposed).

In the CHARIMA modeling presented in Chapter 6, White Ditch and Naomi siphons were included as point flow extractions ($14 \text{ m}^3/\text{s}$ and $28 \text{ m}^3/\text{s}$, respectively). Initial 3-D modeling tests showed that it would be problematic to include such small outflows in the reach near (RM 65) where there is high sand transport; the model tended to generate unrealistic sand concentrations in the diversions as well as local disturbances in the stages and velocities. Taking into account that the total amount of flow being extracted by these two siphons corresponds to only 0.12% of the main channel upstream inflow it was decided not to include the existing Naomi or White Ditch flows in the final 3-D simulations.

The West Bay diversion was included in the CHARIMA simulations. However, this diversion is scheduled to close. Thus, it was decided to not include it in the 3-D Modeling study.

7.2 Existing Outflows

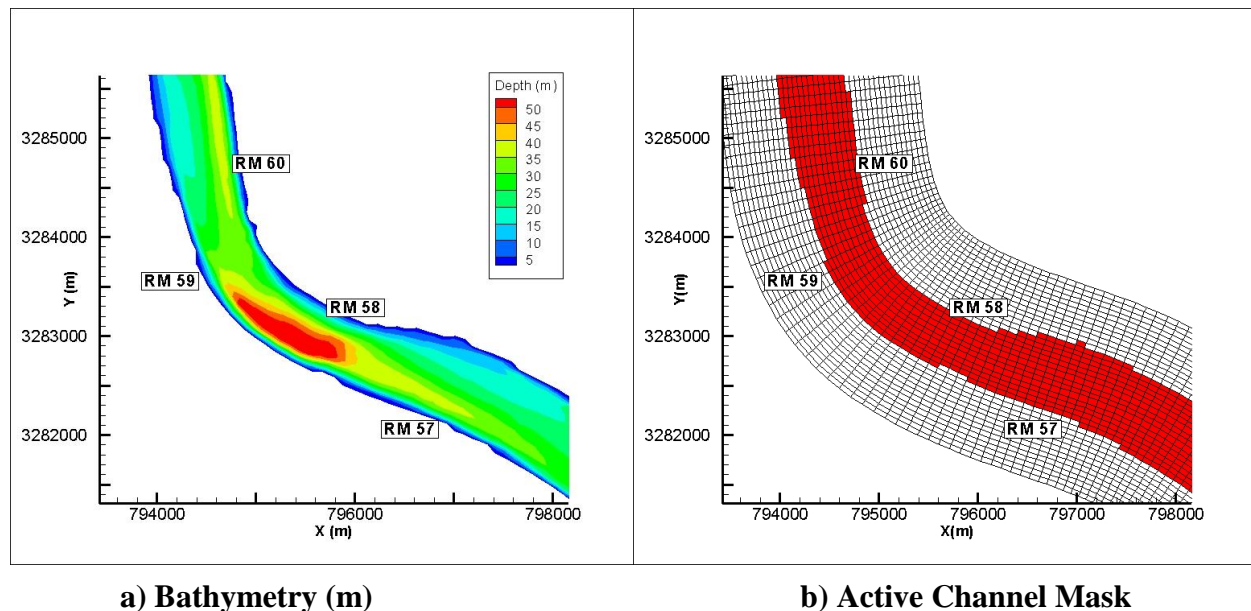
The first step consisted of calibrating and validating a model that included only the existing diversions and distributaries within the domain. The year 2008 was selected for calibration since it had a wide range of river flow; the year 2007 was used for validation. A total of seven (7) outflows were introduced in the reach as shown on Table 7-1 (negative discharge values). The model was stable with an external time-step of 0.4 s and a split between internal and external mode equal to 3.

Table 7-1 – Inflows and Outflows for the Existing Outflows Modeling

Site	Q peak (m ³ /s, cfs)		Q med (m ³ /s, cfs)		Q low (m ³ /s, cfs)	
Belle Chasse*	+32,396	+1,140,000	+21,323	+753,000	+12,408	+438,192
West-Pointe-À-La-Hache	-28	-1000	-28	-1000	-28	-1000
Bohemia Spillway	-5,658	-200,000	-372	-13,121	-51	-1,809
Bayou Lamoque	-84	-2,980	-66	-2,330	-39	-1,383
Fort St. Philip**	-576	-20,000	-359	-12,664	-152	-5,366
Baptiste Collette**	-4,022	-142,000	-3,183	-112,405	-1,866	-65,898
Grand Pass + Tiger Pass**	-4,271	-151,000	-3,395	-119,987	-2,006	-70,835
Main Pass**	-2,992	-106,000	-2,311	-81,610	-1,305	-46,085

*Upstream Boundary

**Natural Outflows (Distributaries)

**a) Bathymetry (m)****b) Active Channel Mask****Figure 7.1 – Sample of Existing ECOMSED Mesh, Bathymetry and Mask at Myrtle Grove (RM 59, RK 94)**

7.2.1 Boundary Conditions

Daily variable hydrographs were used for both upstream (flow) and downstream (water level) hydrodynamic boundary conditions. Ten-day periods from January, March and April 2008 were simulated. The Belle Chasse inflow and the outflow water discharges were obtained from the results obtained with HEC-RAS modeling by Davis (2010) that extends from Tarbert Landing (RM 306, RK 492) to the Gulf of Mexico. The downstream water stage was also obtained from the same model. The total outflow for the modeled reach matches a quadratic function based on field measurements (ADCP) previously shown in Figure 6.17.

The Belle Chasse inflow suspended sand concentrations for April 2008, March 2008 and January 2008 were defined as 90 mg/L, 70 mg/L and 1 mg/L, respectively. These values were based on field data obtained by Nittrouer *et al.* (2008). The suspended sand concentrations in the receiving waters of the outflows were assigned concentrations of 40 mg/L for April 2008, 30 mg/L for March 2008 and 0 (zero) mg/L for January 2008. The model is not very sensitive to the outflow concentrations except where there is tidal reversal of the flow.

The ECOMSED code was modified to allow the use of the Manning's formulation and user defined spatially variable roughness coefficients, given as an input file. The latter feature was necessary for calibration of the January and March 2008 river hydrodynamics, where a constant roughness for the entire reach did not allow an accurate reproduction of the 1-D model results. A reference Manning's n value of 0.0316 was used for all simulations but different multipliers were used for each River flow. To accurately reproduce and maintain the observed flow and transport trends near the deep holes throughout the domain, different roughness coefficients were applied for depths equal to or higher than 30 m. The roughness coefficients used in the simulations are show in Table 7-2. This was thought to be necessary to account for the additional energy due to the bend and the flow expansion.

Table 7-2 – Roughness Coefficients used in the ECOMSED Model

Period Simulated	Roughness Coefficients*				
	Depth $\geq 30\text{m}$	River Mile			
		76-50	50-25	25-13	13-3
April 2008	1.2(Depth/30)	0.95	0.83	1.00	0.92
March 2008	1.05(Depth/30)	1.25	1.10	1.00	1.00
January 2008	1.05(Depth/30)	1.70	1.20	1.00	1.00

* Values multiplied by the reference $n=0.0316$ to obtain the used value of n

El Kheishy (2007) showed the bed shear stress increases in the upstream direction, for example it is lower in the reach from RM 0 to RM 50 compared to RM 50 to RM 100 (Figure 7.2). In general, the upper portion of the reach has higher effective roughness which may be due to the tendency for bed forms to increase in size in the upstream direction (El Kheishy 2007). This is shown in Figure 7.2 and Figure 7.3.

A sediment control depth of 30 m, and uniform suspended and bed sediments with a $D_m=0.20$ mm were used. This diameter represents a good estimate of the material available in the Lower Mississippi River based on measurements (Nittrouer *et al.* 2008; Allison 2010). However, it was necessary to calibrate the sediment sizes in order to reproduce the measured sediment loads. The armoring coefficient, defined from 1.0 to 0.0, that accounts for the availability of sediment to be picked up from the bed, was set equal to 1.0. This allows for 100% of the bed material to be available for transport.

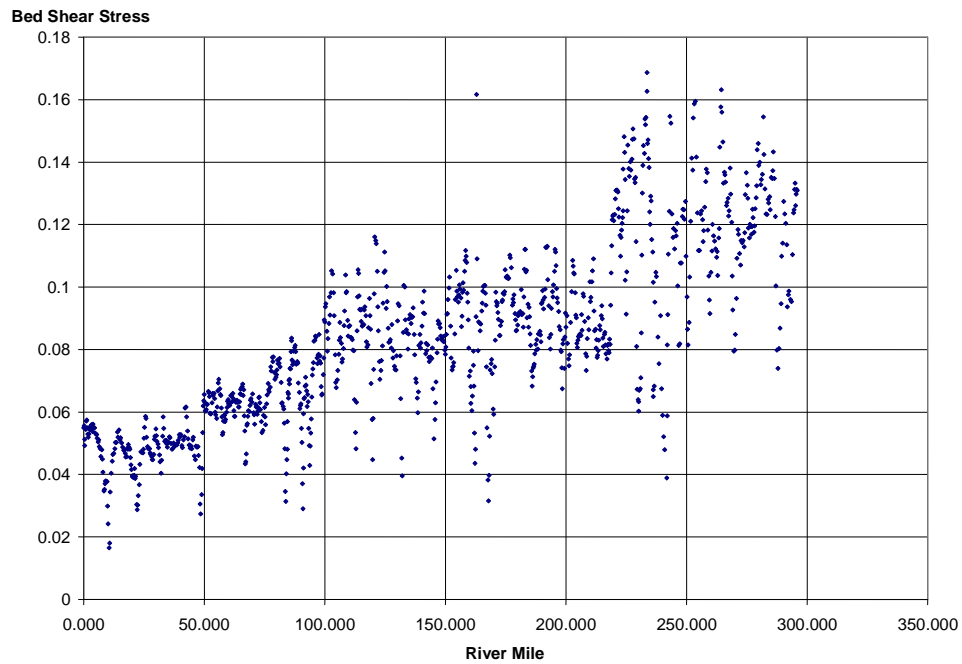


Figure 7.2 – Variation of Bed Shear Stress for the Lower Mississippi River Miles 0 to 300
(Source: El Kheiashy 2007)

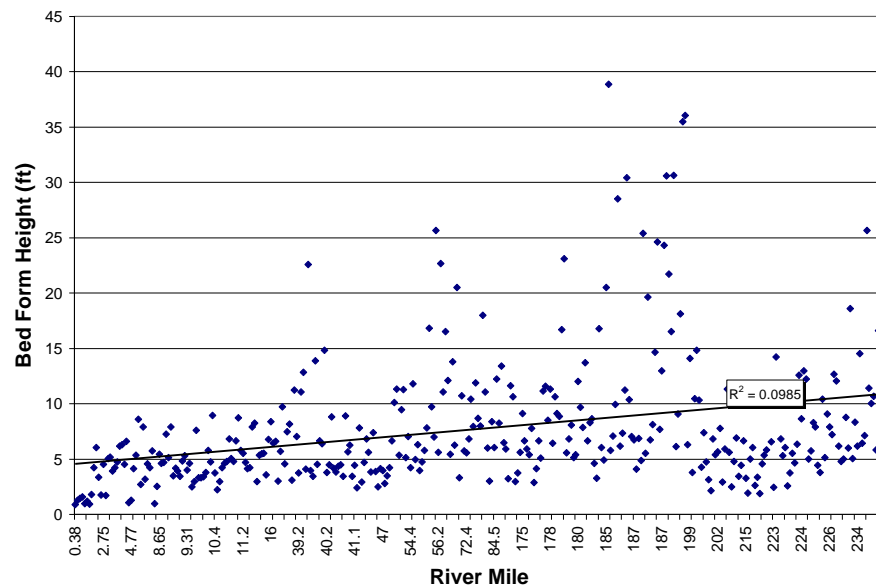


Figure 7.3 – Variation of Bed Form Height for the Lower Mississippi River Miles 0 to 300
(Source: El Kheiashy 2007)

In order to control initial instabilities originated by the existence of very low active-layer depths/volumes, the code was modified to guarantee a minimum active layer volume of $1.0 \times 10^{-5} \text{ m}^3$ and a maximum of 1% change on bed-thickness in one time-step. The original formulation was also changed to set the reference height equal to 3% of the flow depth instead of the original 1%. This change is justified by the dimensions of the Lower Mississippi River bedforms as described by El Kheishy (2007) and shown in Figure 7.3. The bottom layer sediment concentration was limited to a maximum of 500 mg/L to prevent an uncontrolled feedback that resulted in unrealistic bed elevation changes.

7.2.2 Results

The hydrodynamics calibration results for River stage are shown from Figure 7.4 through Figure. The model was calibrated for flows that range from 350,000 cfs to 1.2×10^6 cfs. At some stations there were no reliable stage records, so the Davis (2010) HEC-RAS time series was used for comparison purposes. It is also noted that there may be datum errors in the West Pointe-À-La-Hache record which may be due to the high subsidence rate in this reach. The results indicate that the model is well calibrated for water level.

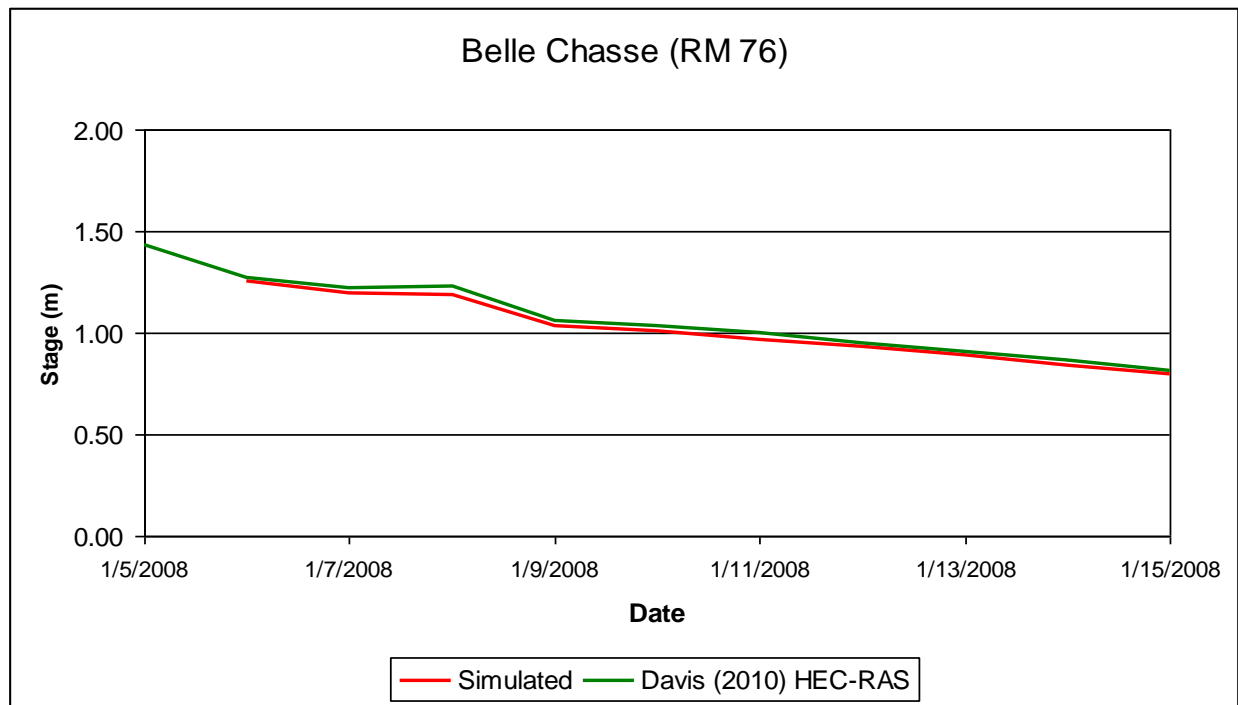


Figure 7.4 – Stage at Belle Chasse for the ECOMSED Hydrodynamics Calibration at High Flows (2008)

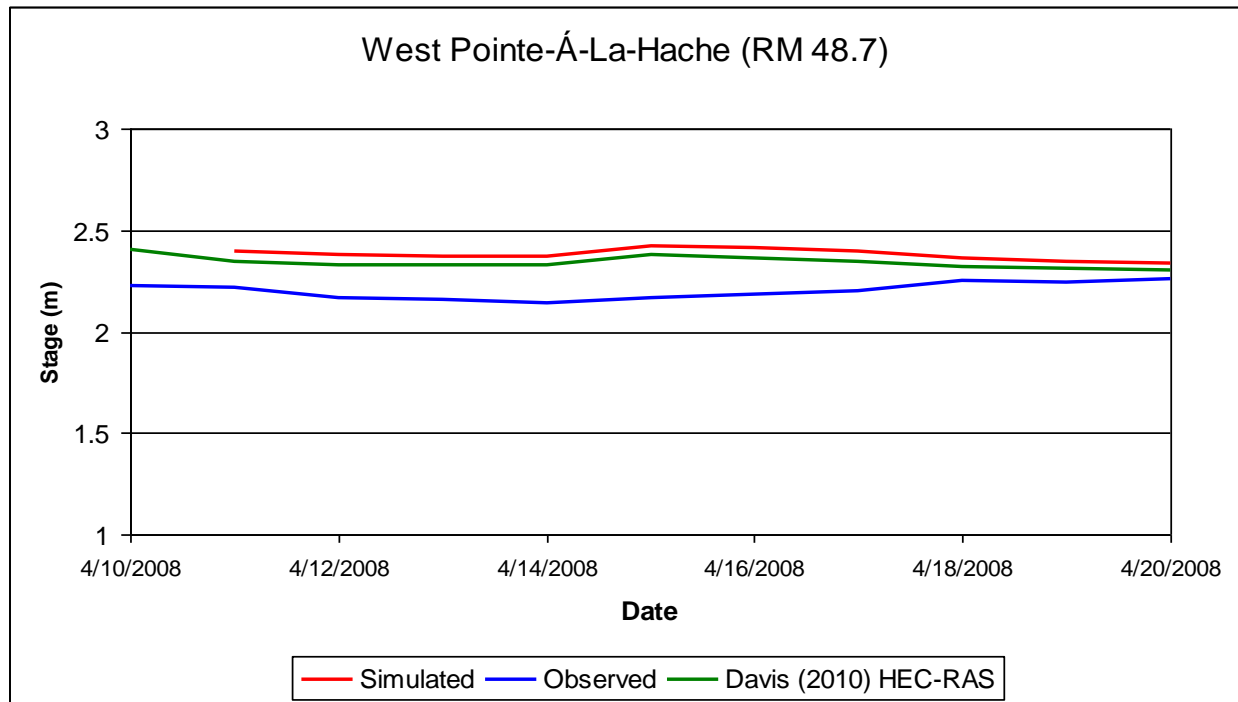


Figure 7.5 – Stage at West Pointe-À-La-Hache for the ECOMSED Hydrodynamics Calibration at Low Flows (2008)

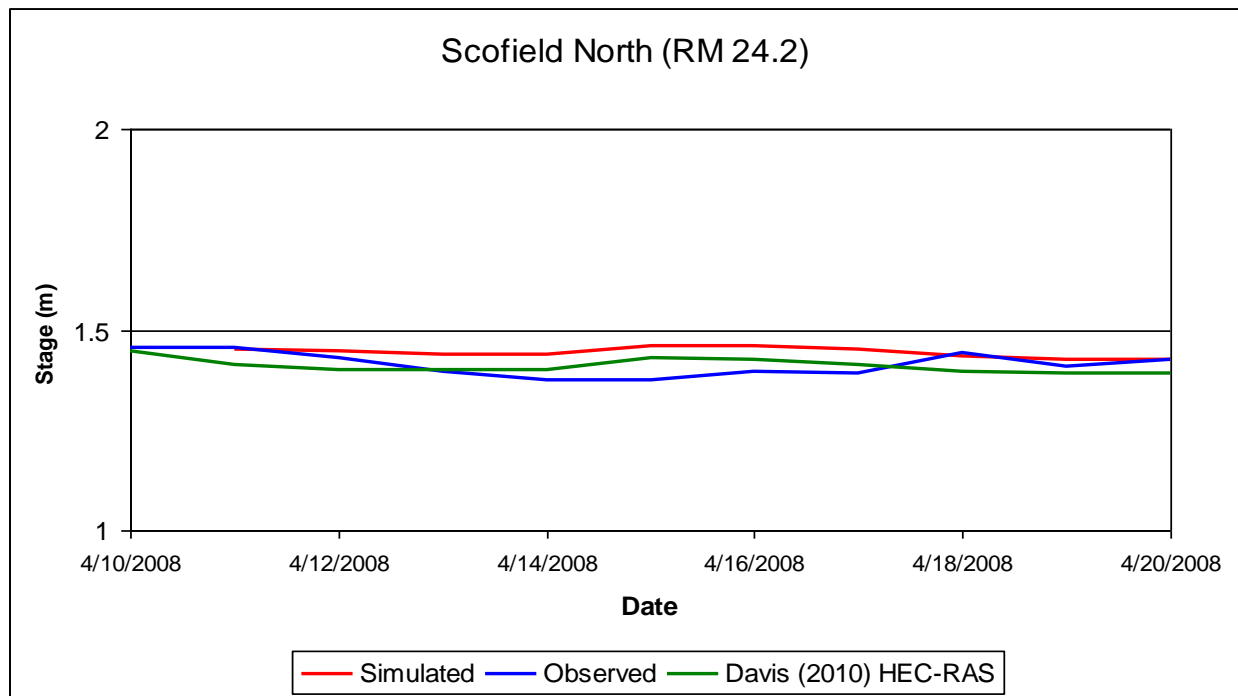


Figure 7.6 – Stage at Scofield North for the ECOMSED Hydrodynamics Calibration at High Flows (2008)

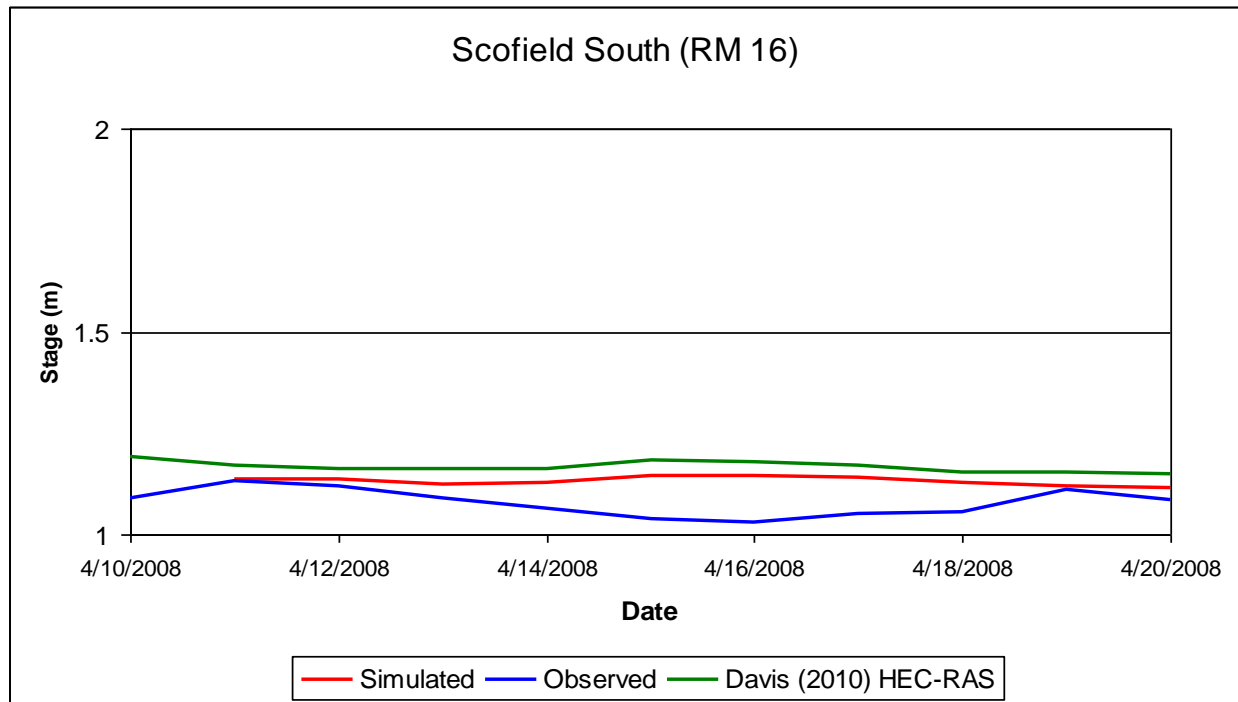


Figure 7.7 – Stage at Scofield South for the ECOMSED Hydrodynamics Calibration at High Flows (2008)

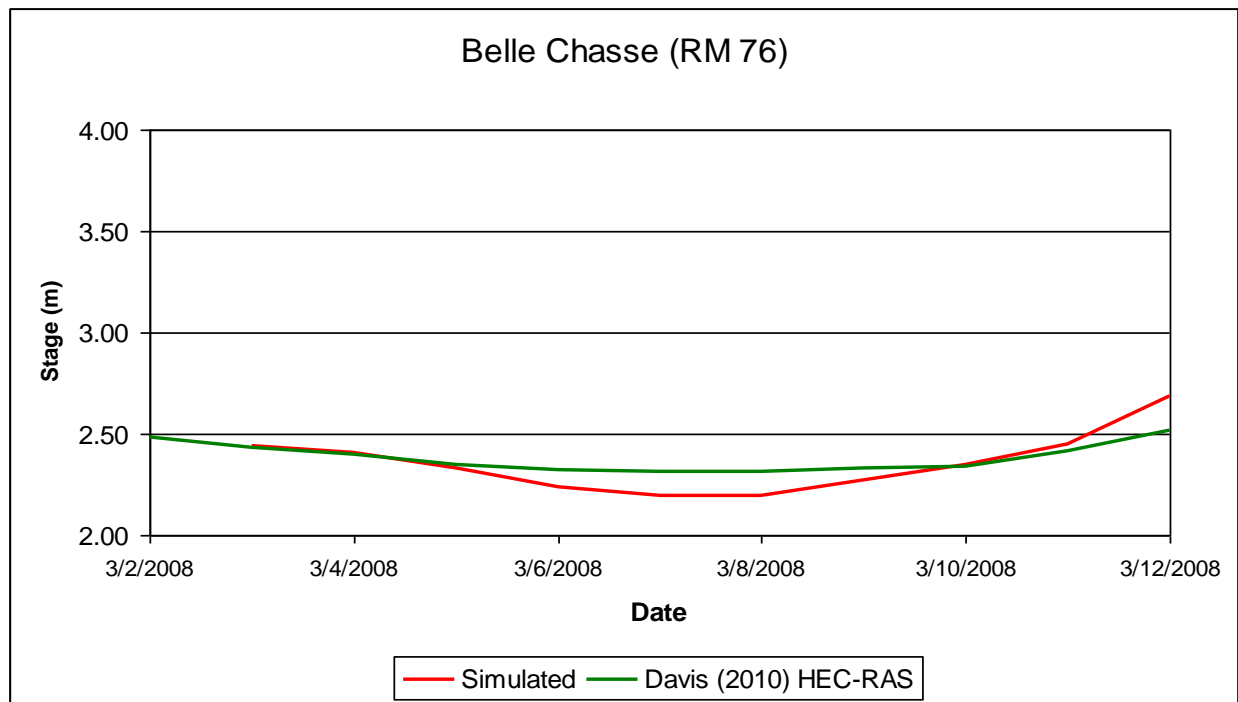


Figure 7.8 – Stage at Belle Chasse for the ECOMSED Hydrodynamics Calibration at Intermediate Flows (2008)

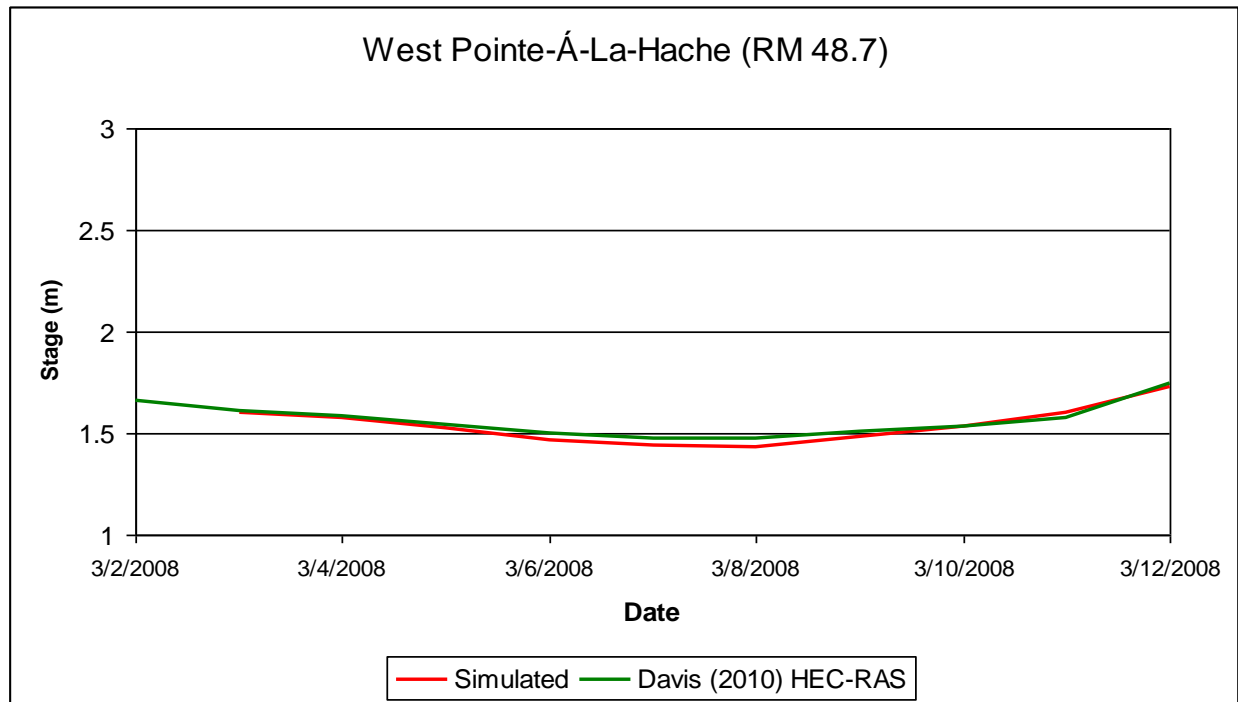


Figure 7.9 – Stage at West Pointe-À-La-Hache for the ECOMSED Hydrodynamics Calibration at Intermediate Flows (2008)

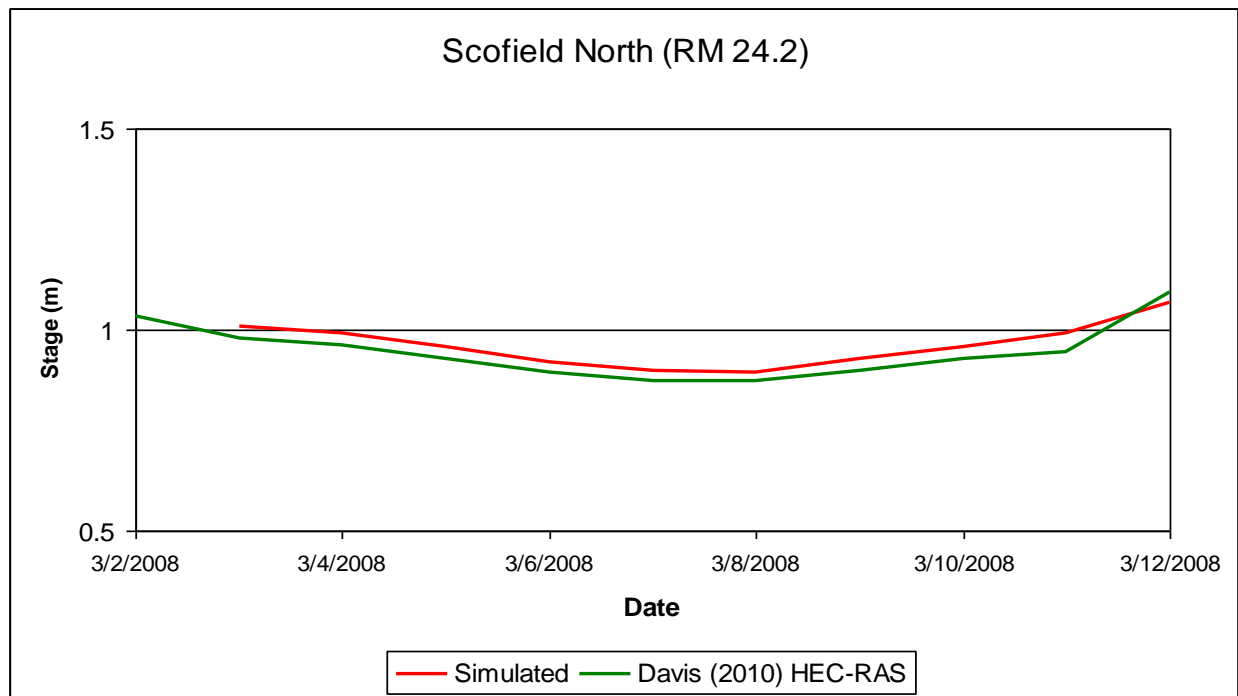


Figure 7.10 – Stage at Scofield North for the ECOMSED Hydrodynamics Calibration at Intermediate Flows (2008)

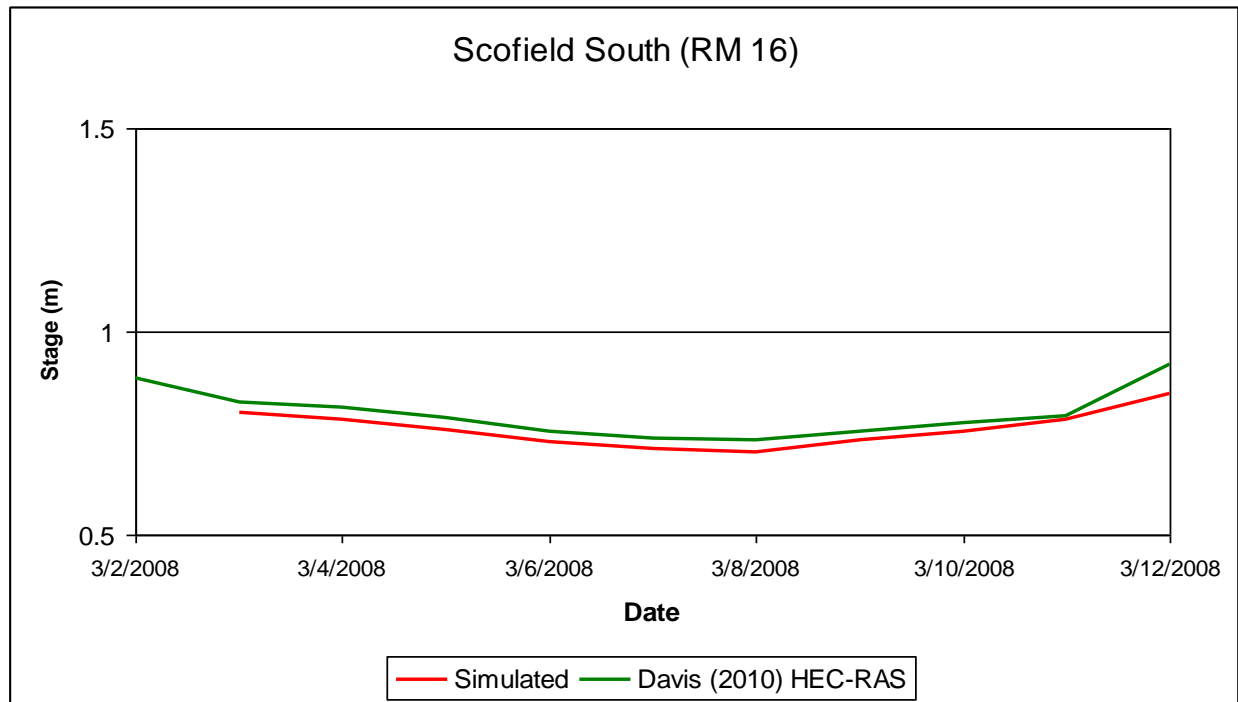


Figure 7.11 – Stage at Scofield South for the ECOMSED Hydrodynamics Calibration at Intermediate Flows (2008)

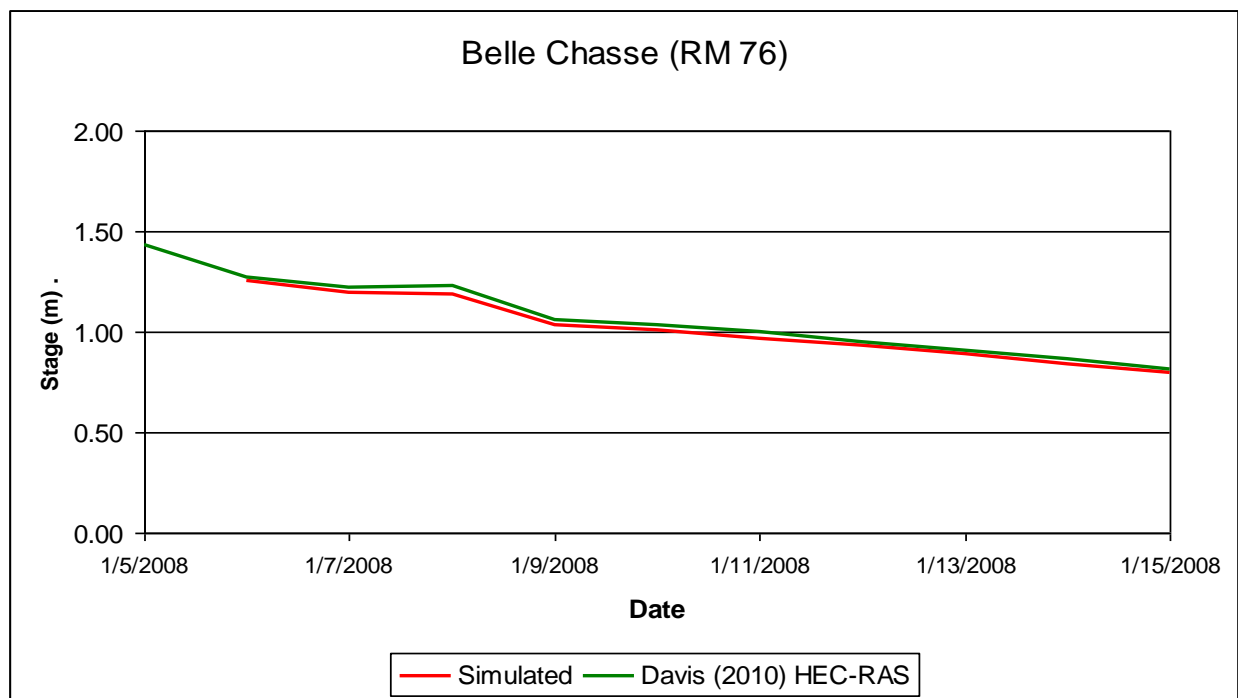


Figure 7.12 – Stage at Belle Chasse for the ECOMSED Hydrodynamics Calibration at Low Flows (2008)

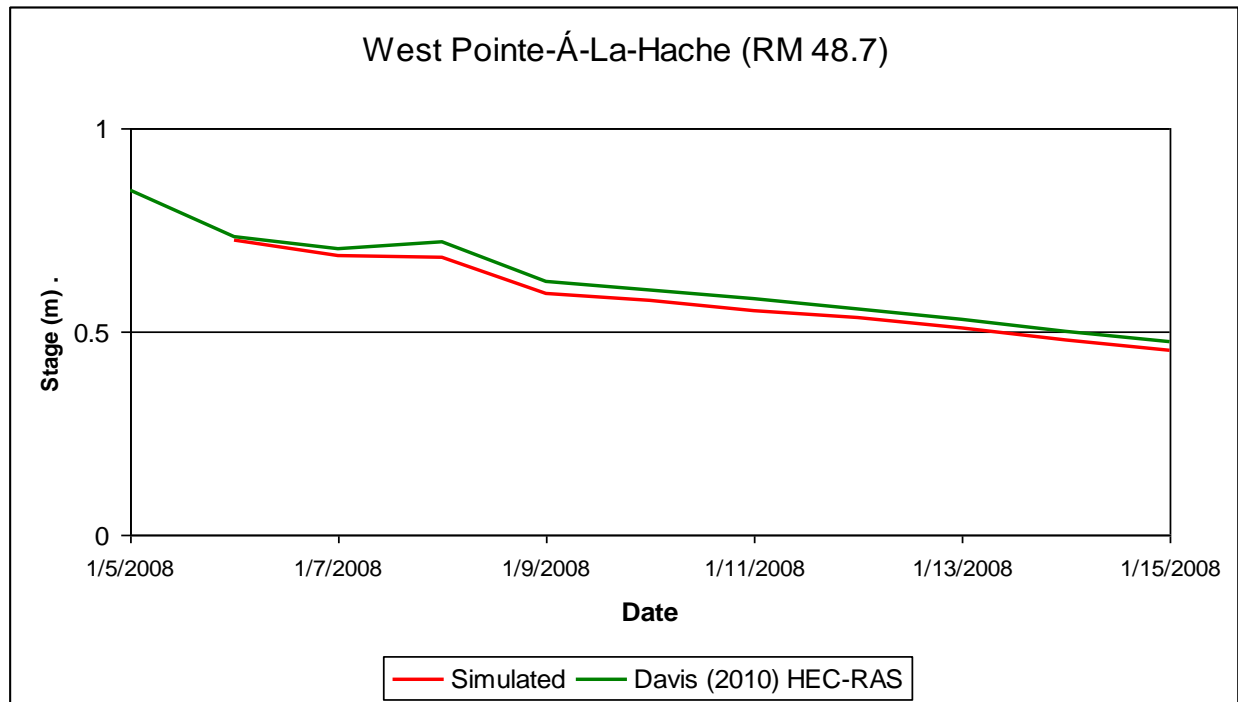


Figure 7.13 – Stage at West Pointe-À-La-Hache for the ECOMSED Hydrodynamics Calibration at Low Flows (2008)

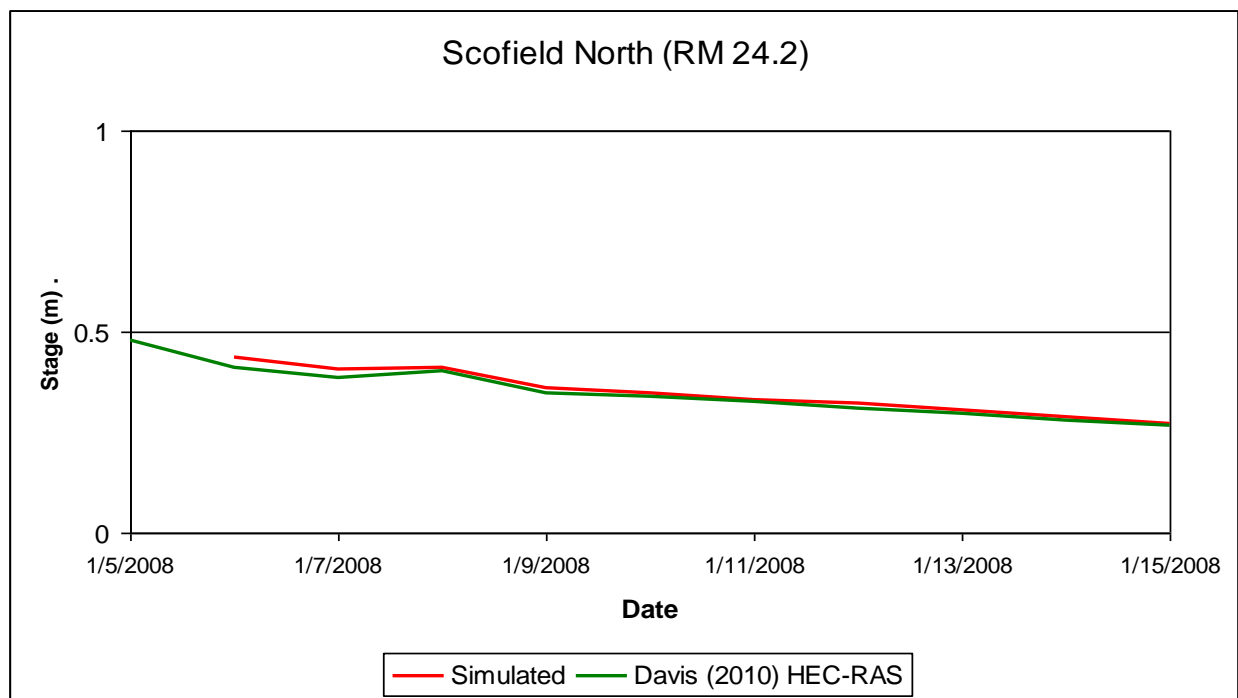


Figure 7.14 – Stage at Scofield North for the ECOMSED Hydrodynamics Calibration at Low Flows (2008)

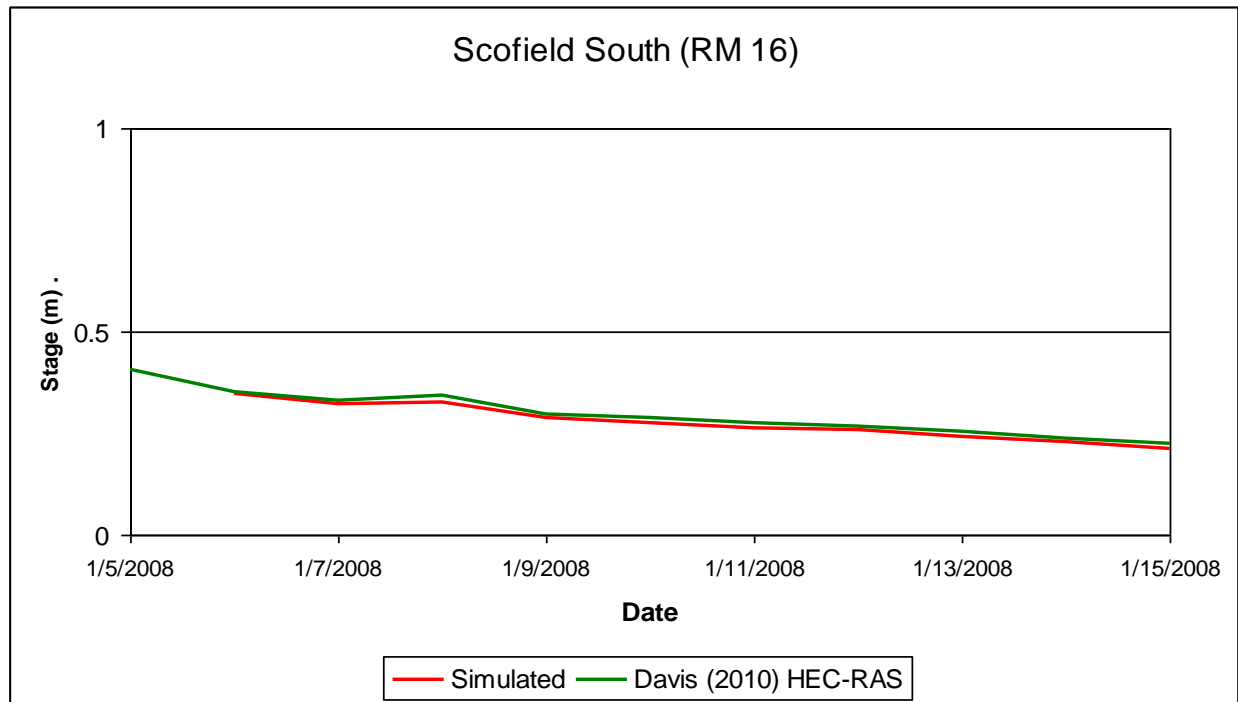
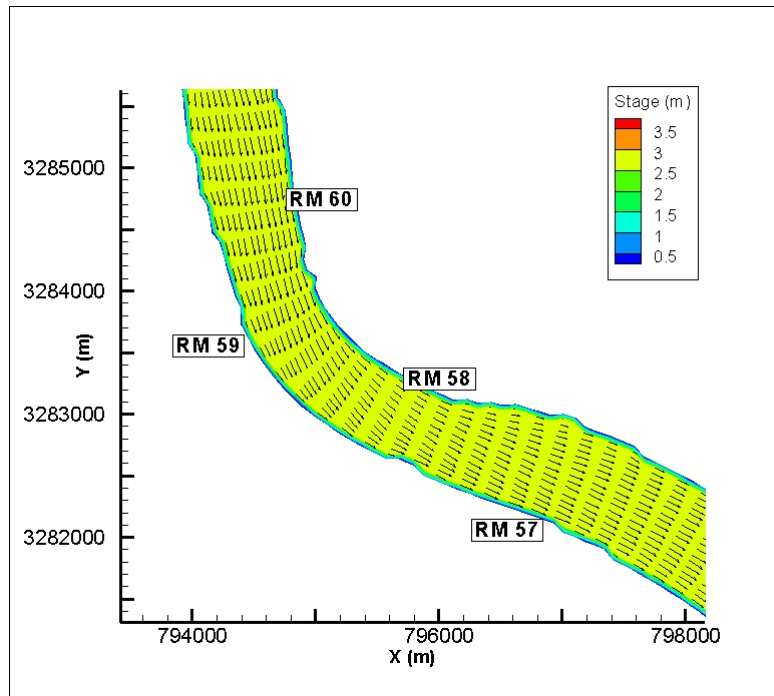
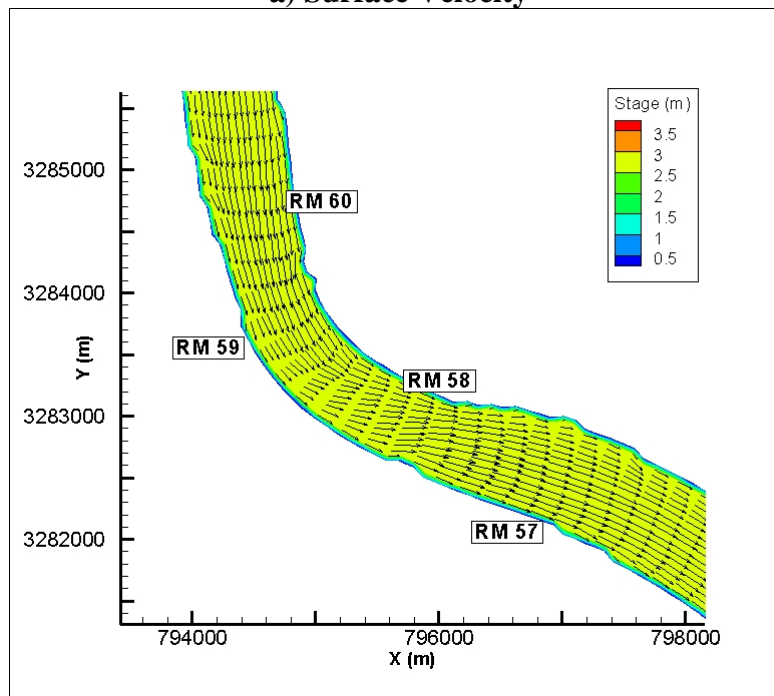


Figure 7.15 – Stage at Scofield South for the ECOMSED Hydrodynamics Calibration at Low Flows (2008)

Plots of the surface and bottom velocity vectors for the Myrtle Grove (RM 59, RK 94) area at peak flow conditions can be seen in Figure 7.16. The low velocity values on the outer bend can be explained by the presence of a deep hole, of approximately 40 m, that can be seen in Figure 7.1a. The velocity directions for both surface and bottom show the expected secondary currents (Figure 7.16b). The bottom shear-stress distributions for high and intermediate flows at Myrtle Grove are shown in Figure 7.17.

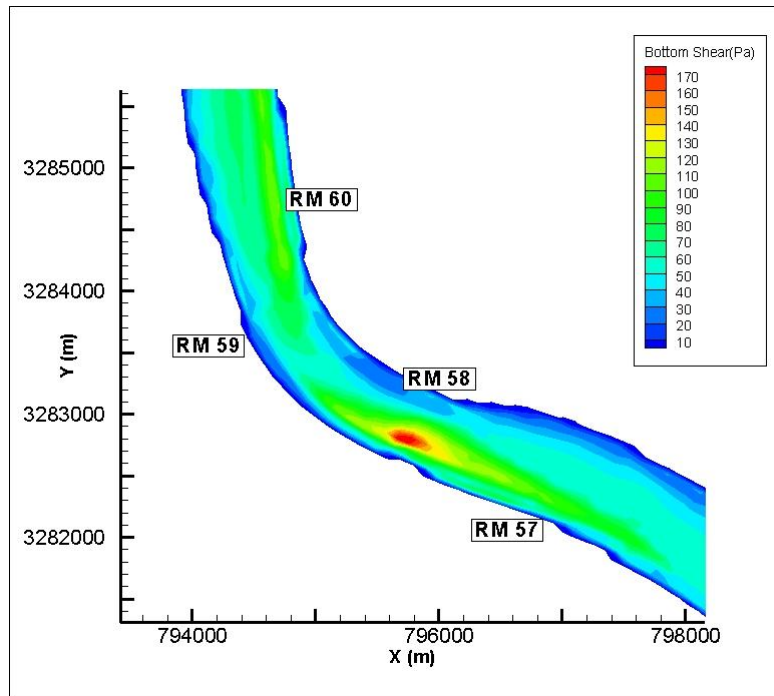


a) Surface Velocity

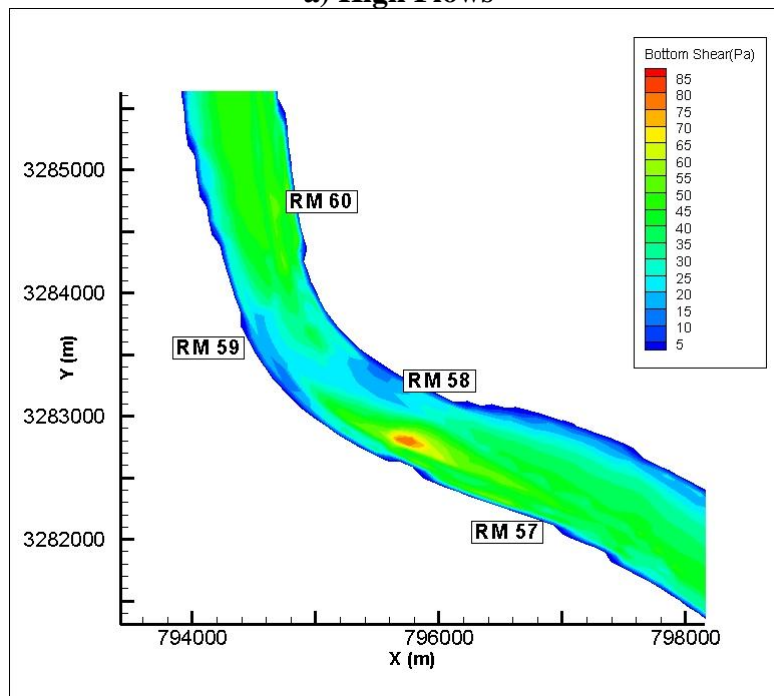


b) Bottom Velocity

Figure 7.16 –Velocity Vectors at Myrtle Grove (RM 59, RK 94)



a) High Flows



b) Intermediate Flows

Figure 7.17 – Bottom Shear Stress at Myrtle Grove (RM 59, RK 92) for Peak Flows

To aid in the analysis of the model results, several changes had to be made to the code. It was necessary to modify the output to include the calculation of water discharge (Q), sediment load (Q_s), depth averaged sediment concentration (C_s), stage (h), total energy (E) and kinetic energy of the flow (ke), for both the main channel cross-sections and the River diversions. The energy quantities are defined as follows:

$$ke = \frac{v^2}{2g} \quad (6.1)$$

$$E = h + ke = h + \frac{v^2}{2g} \quad (6.2)$$

where v = the cross-sectional depth-averaged velocity, g = acceleration of gravity which is constant assumed constant and equal to 9.81 m/s^2 , and h = water surface elevation.

A total of twenty-four main channel cross-sections, including the one immediately upstream and downstream of each river diversion, in the vicinity of both upstream and downstream boundaries, and at areas of interest [Myrtle Grove (RM 59) and Scofield (RM 16 to 24)], and seven diversion cross-sections, were used; and Q , Q_s , C_s , h , E and ke time-series were extracted from each of these locations. These outputs were used for calibration of the sand transport, checking continuity, determining the effect of diversions on the main channel flow and sediment transport, and estimating the amount of sediment available for diversion.

Figure 7.18 to Figure 7.20 show the Q , h , E and ke obtained for the main channel under peak flow conditions. The continuity is verified, although there are some small oscillations on the water discharge values (Figure 7.18). These oscillations are localized and usually occur near the River diversions where some disturbance is introduced in the system, as is confirmed by the stage results shown in Figure 7.19. The water discharge results have been smoothed by using a 5-point filter.

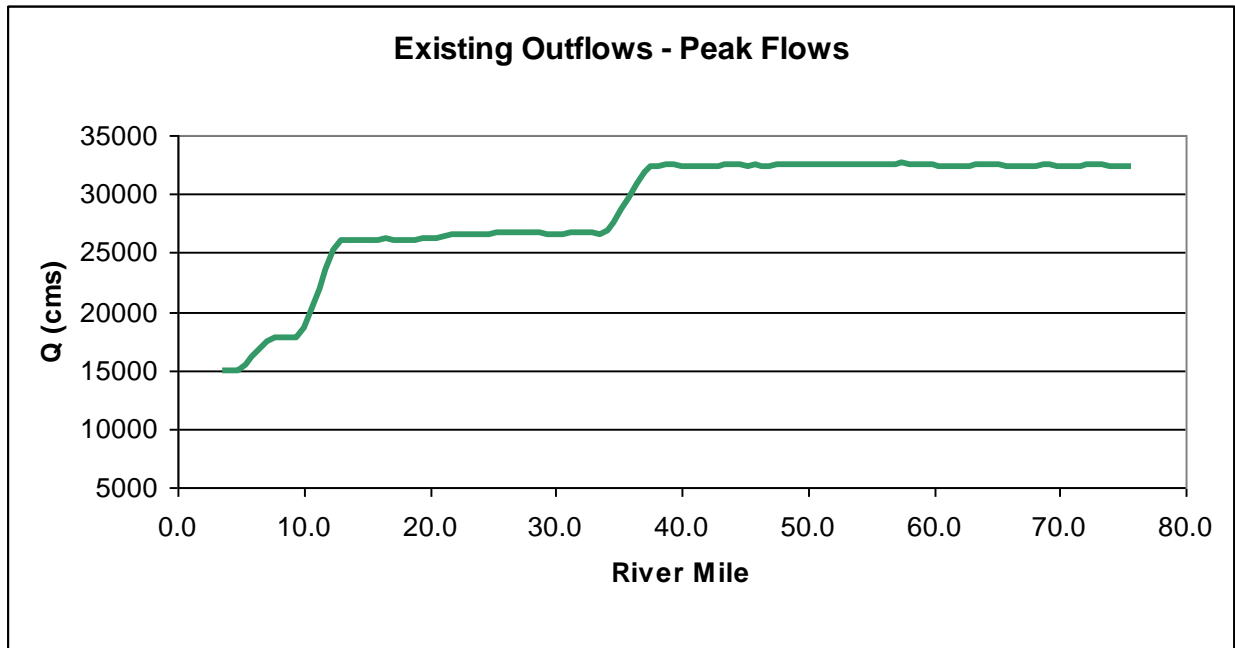


Figure 7.18 – Main Channel Water Discharge at Peak Flows for the Existing Outflows Case

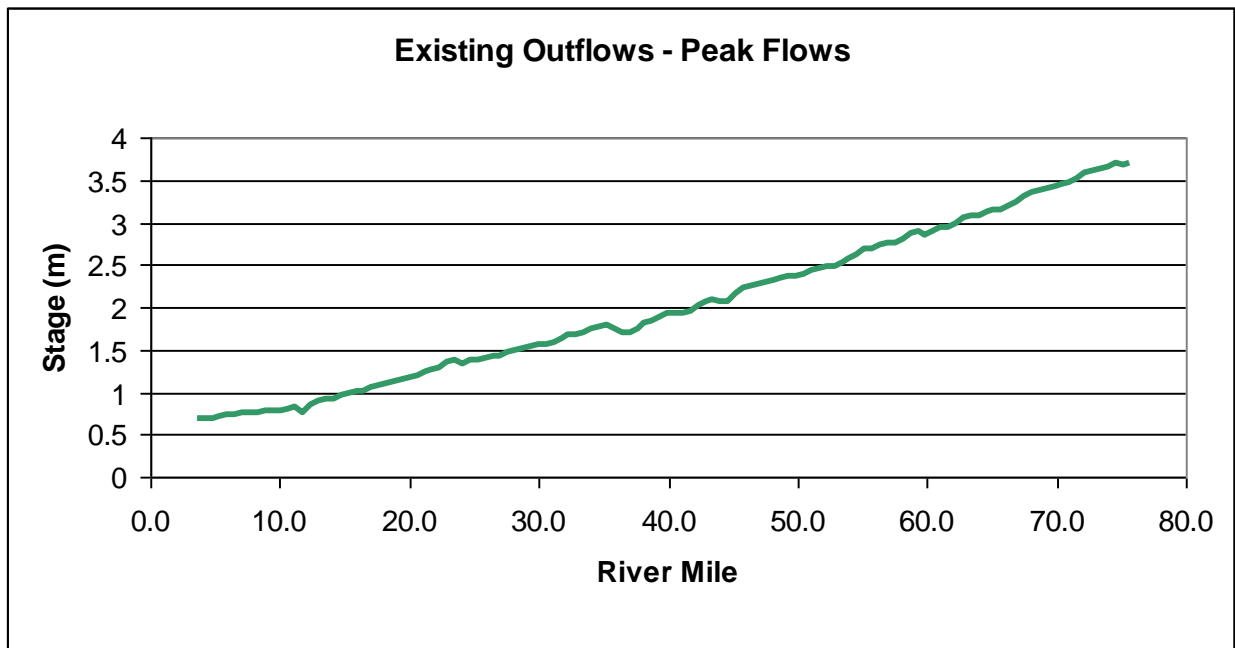


Figure 7.19 – Main Channel Stage at Peak Flows for the Existing Outflows Case

The total energy of the flow (Figure 7.20) ranges from 4.0 m at the upstream boundary to 0.7 m at the downstream boundary. The kinetic energy of the flow (Figure 7.21) varies between 0.28 m and 0.04 m with the peak corresponding to a current of approximately 2.3 m/s.

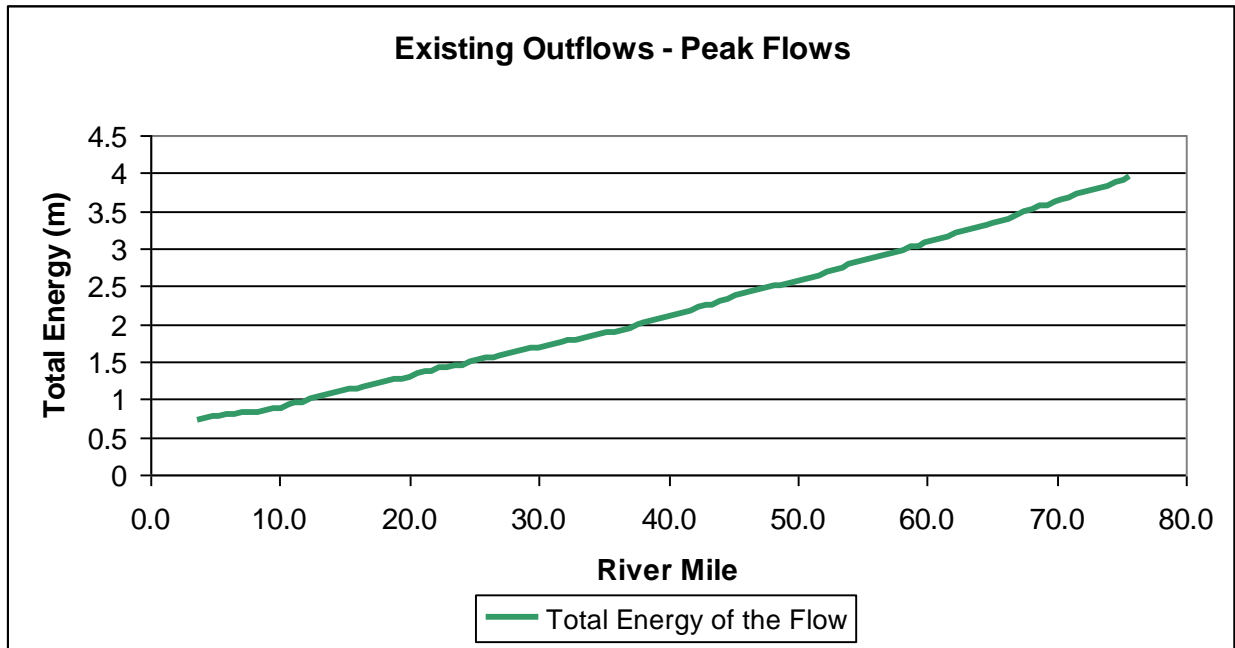


Figure 7.20 – Main Channel Total Energy of the Flow at Peak Flows for the Existing Outflows Case

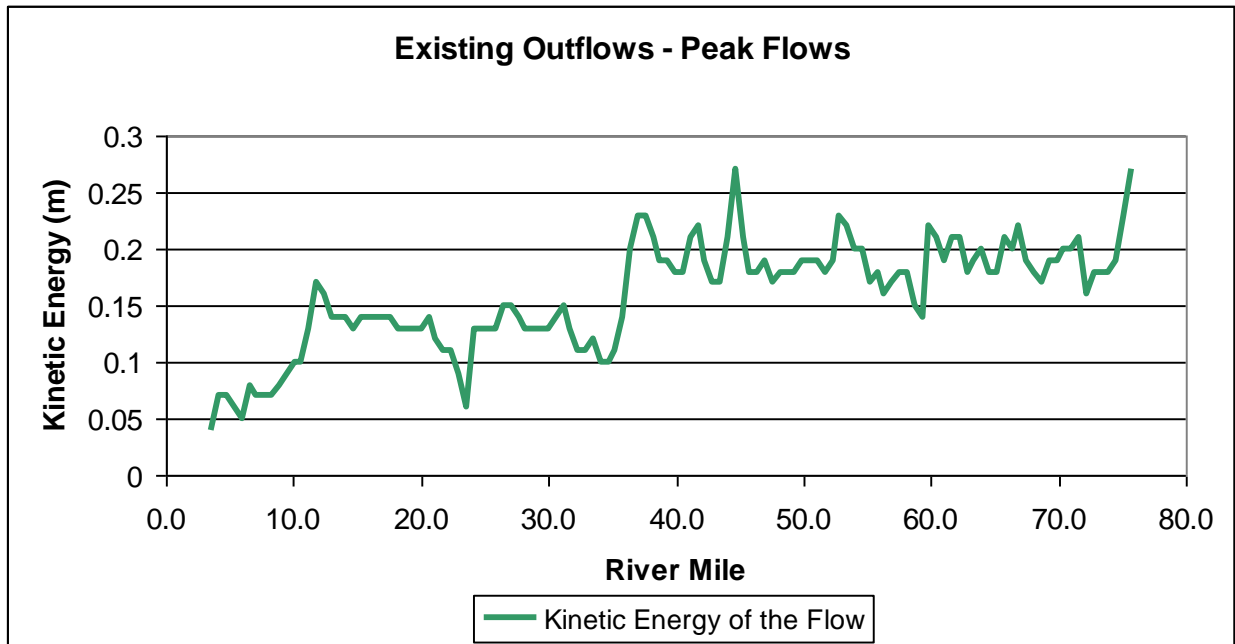


Figure 7.21 – Main Channel Kinetic Energy of the Flow at Peak Flows for the Existing Outflows Case

To have a more precise idea of the energy variations along the main channel, it was decided to calculate the kinetic, potential and total power (energy per unit of time) with base on the energy head results. The following equations are used:

$$P_E = Q\gamma E \quad (6.3)$$

$$P_{ke} = Q\gamma k_e \quad (6.4)$$

where P_E is the Total Energy Power in J/s (Watt); P_{ke} is the Kinetic Energy Power in Watt ; E is the total energy head in m; k_e is the kinetic energy head in m; and Q is the water discharge in m^3/s .

Figure 7.22, Figure 7.23 and Figure 7.24 show respectively, the main channel total, potential and kinetic energy fluxes under peak flow conditions.

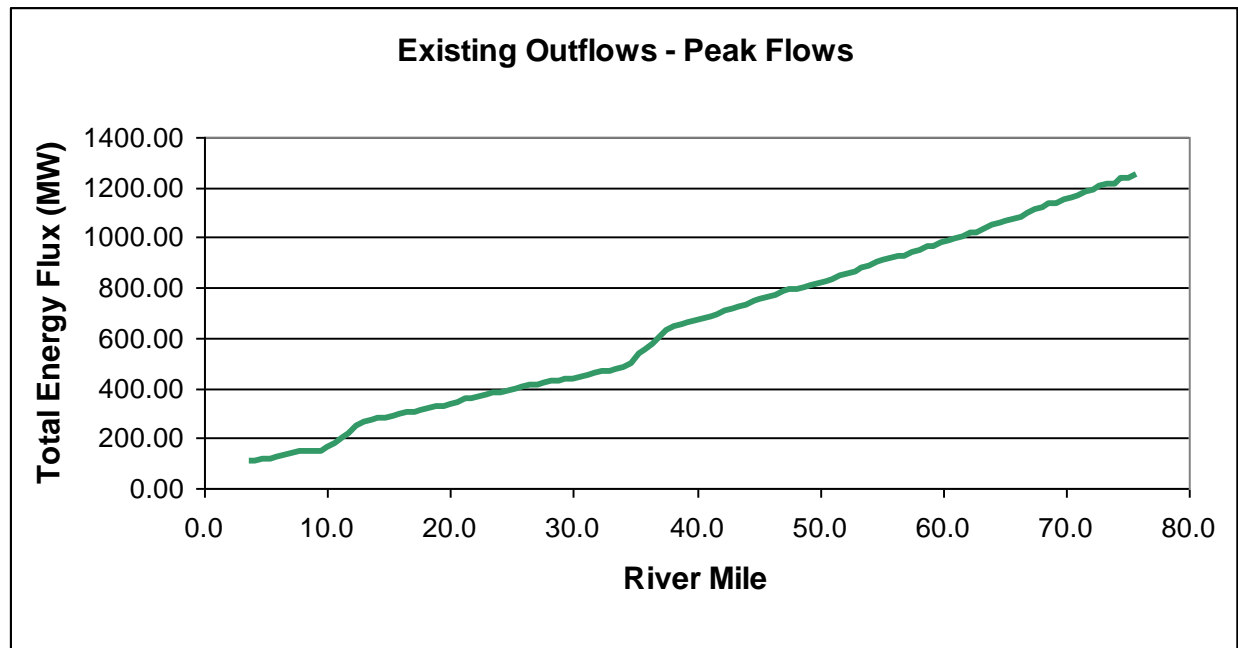


Figure 7.22 – Main Channel Total Energy Flux of the Flow at Peak Flows for the Existing Outflows Case

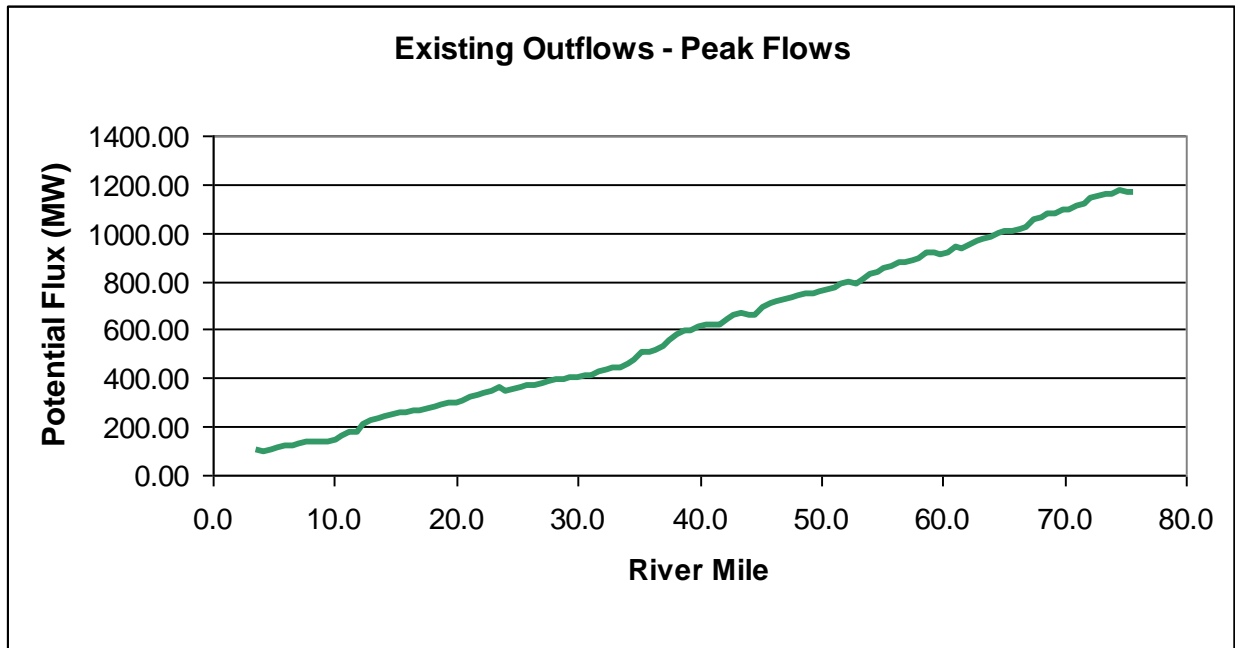


Figure 7.23 – Main Channel Potential Energy Flux of the Flow at Peak Flows for the Existing Outflows Case

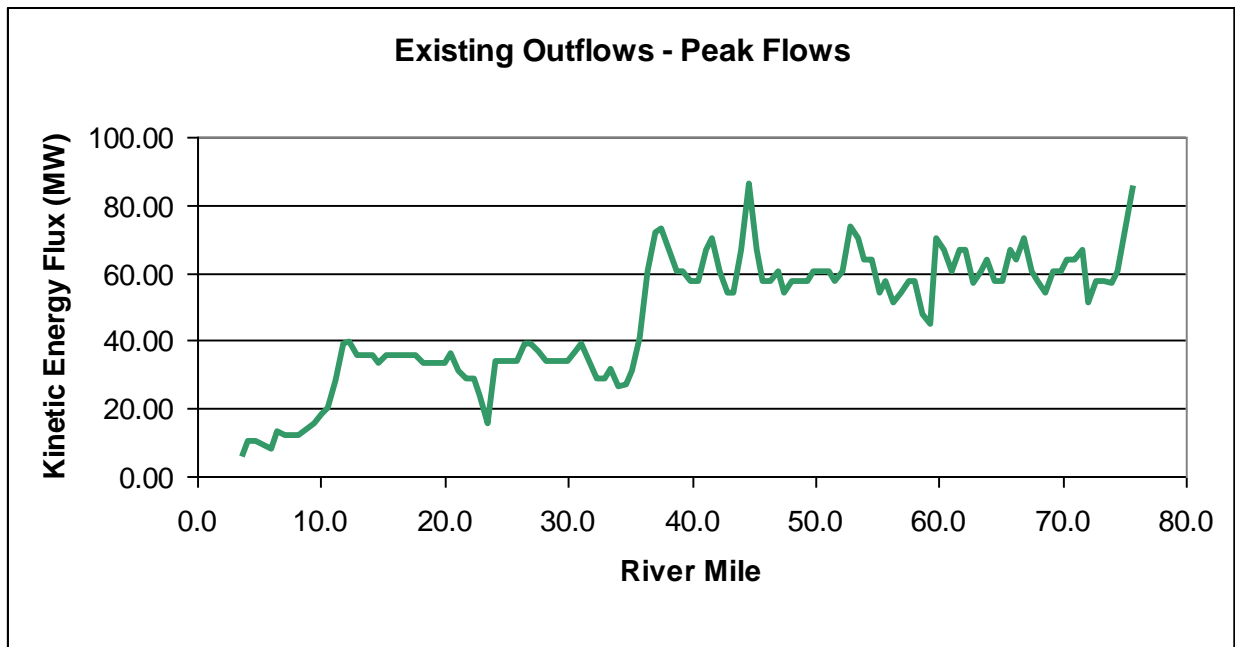


Figure 7.24 – Main Channel Kinetic Energy Flux of the Flow at Peak Flows for the Existing Outflows Case

Figure 7.25 to Figure 7.28 show the Q, h, E and ke obtained for the main channel under intermediate flow conditions. As before, the continuity is verified and there are some small oscillations on the water discharge values. These oscillations are localized and occur near the River diversions where some disturbance is introduced in the system, as is confirmed by the stage results shown in Figure 7.26. Once again, the water discharge results have been smoothed by using a 5-point filter.

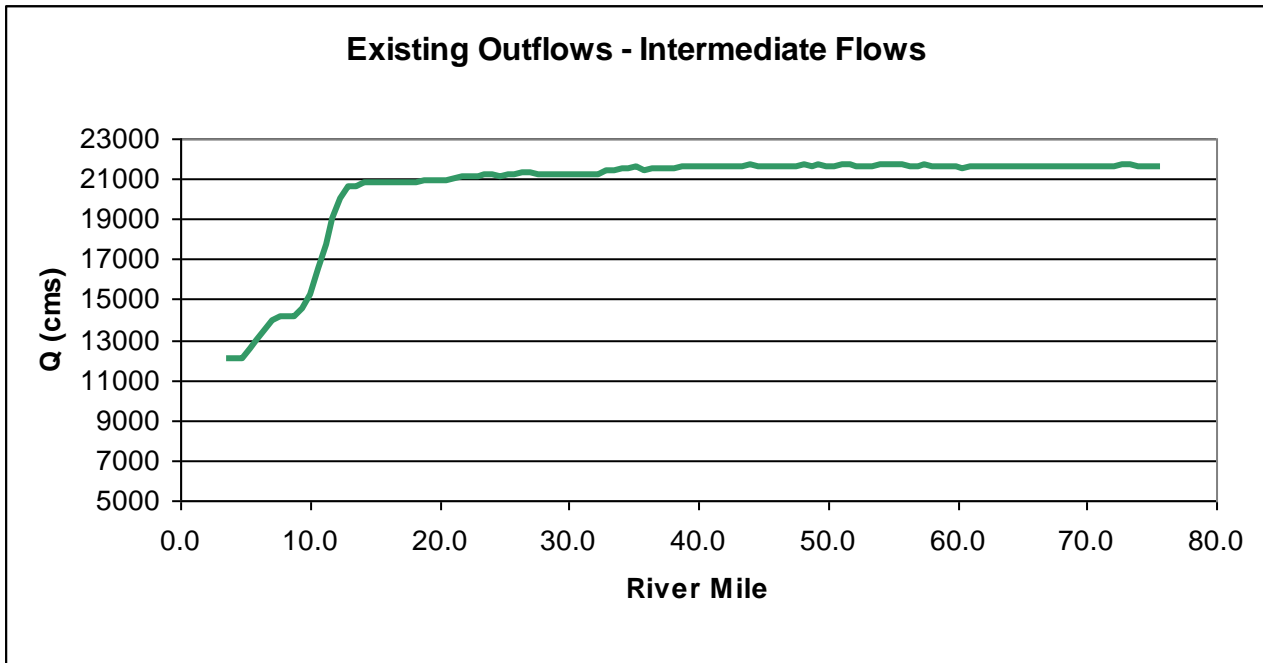


Figure 7.25 – Main Channel Water Discharge at Intermediate Flows for the Existing Outflows Case

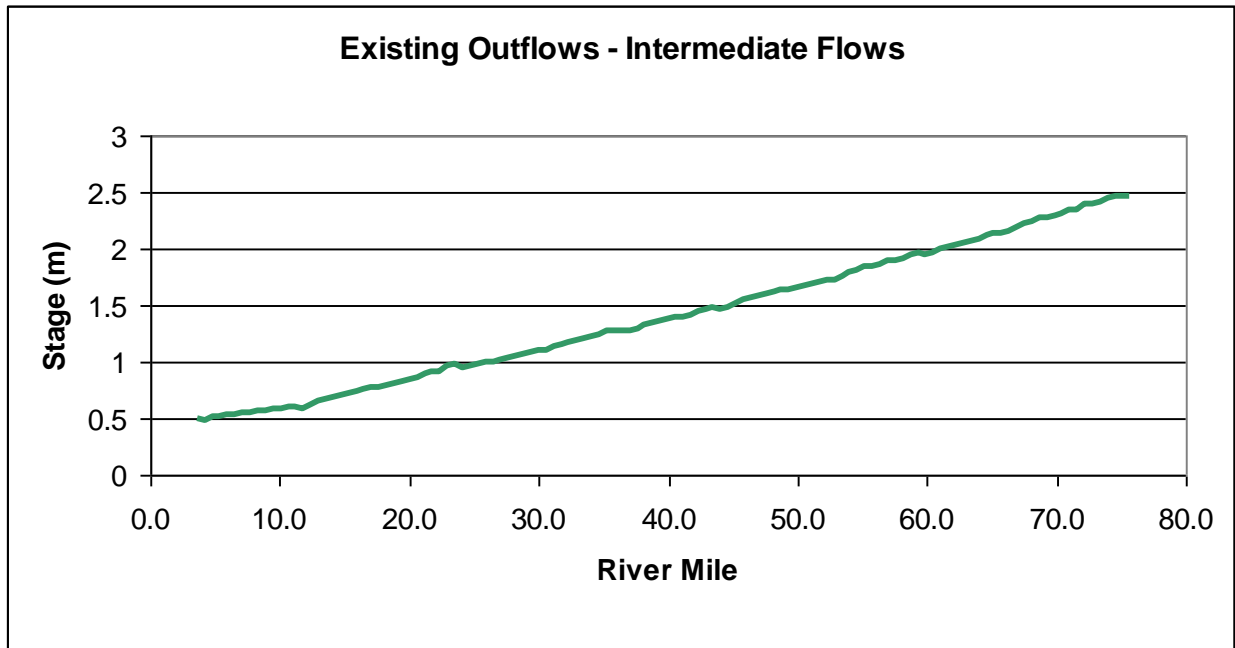


Figure 7.26 – Main Channel Total Stage at Intermediate Flows for the Existing Outflows Case

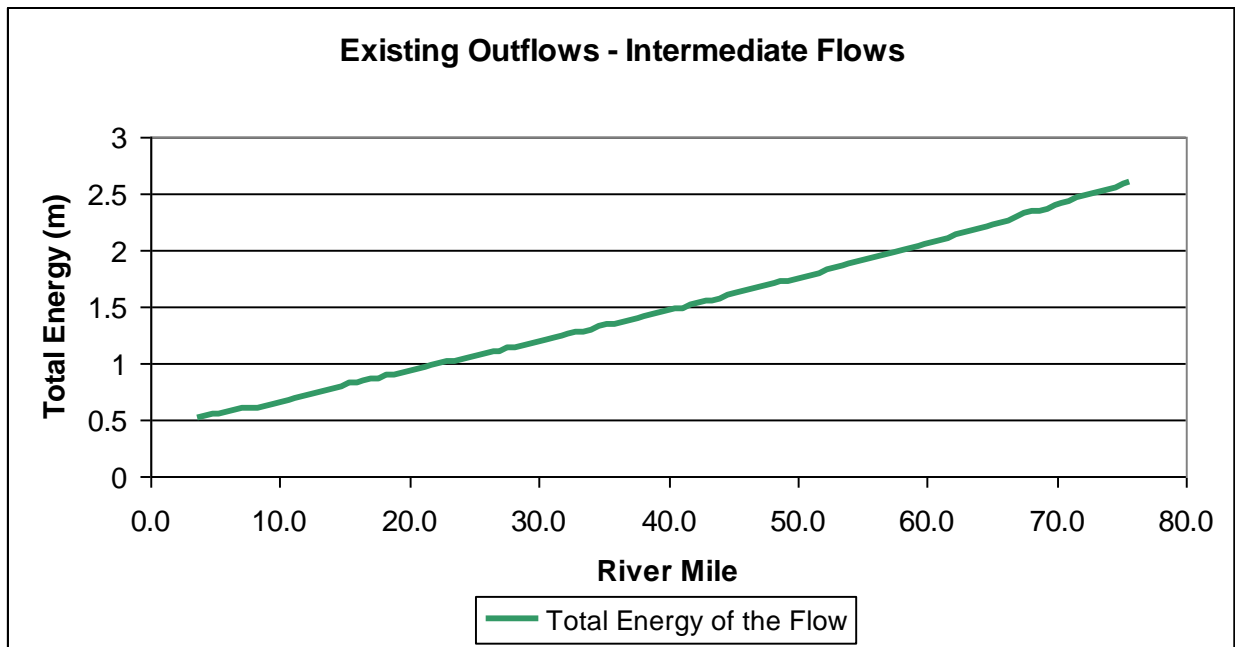


Figure 7.27 – Main Channel Total Energy of the Flow at Intermediate Flows for the Existing Outflows Case

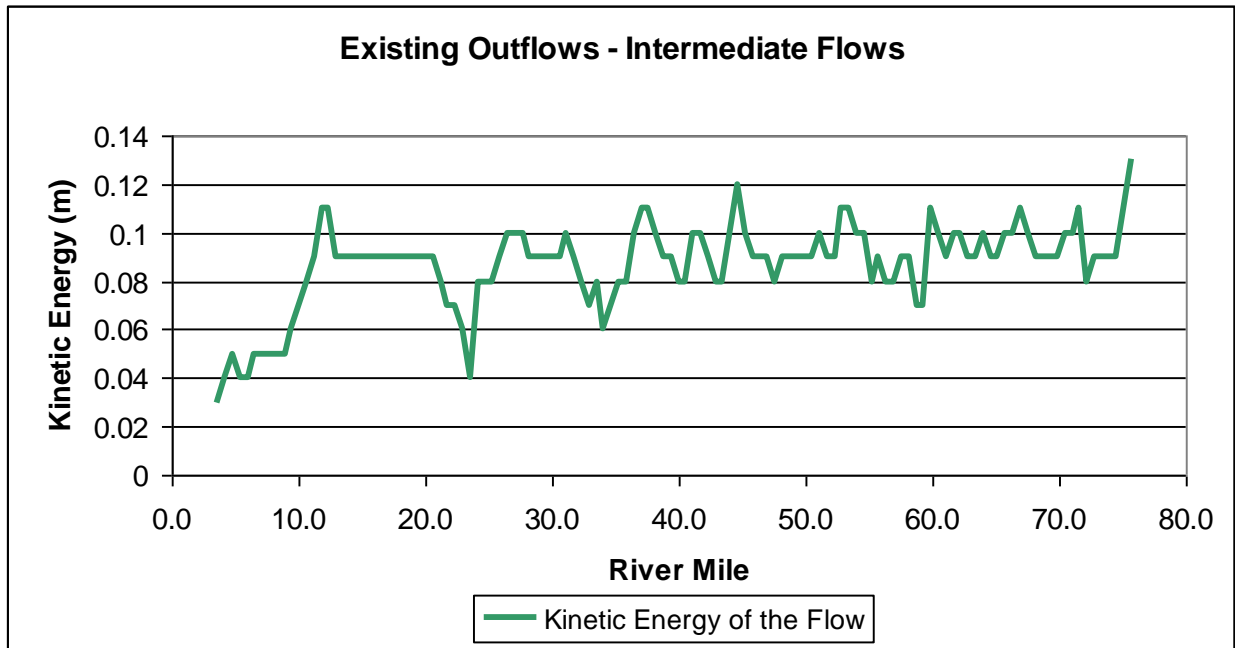


Figure 7.28 – Main Channel Kinetic Energy of the Flow at Intermediate Flows for the Existing Outflows Case

Figure 7.29, Figure 7.30 and Figure 7.31 show respectively, the main channel total, potential and kinetic energy fluxes under intermediate flow conditions.

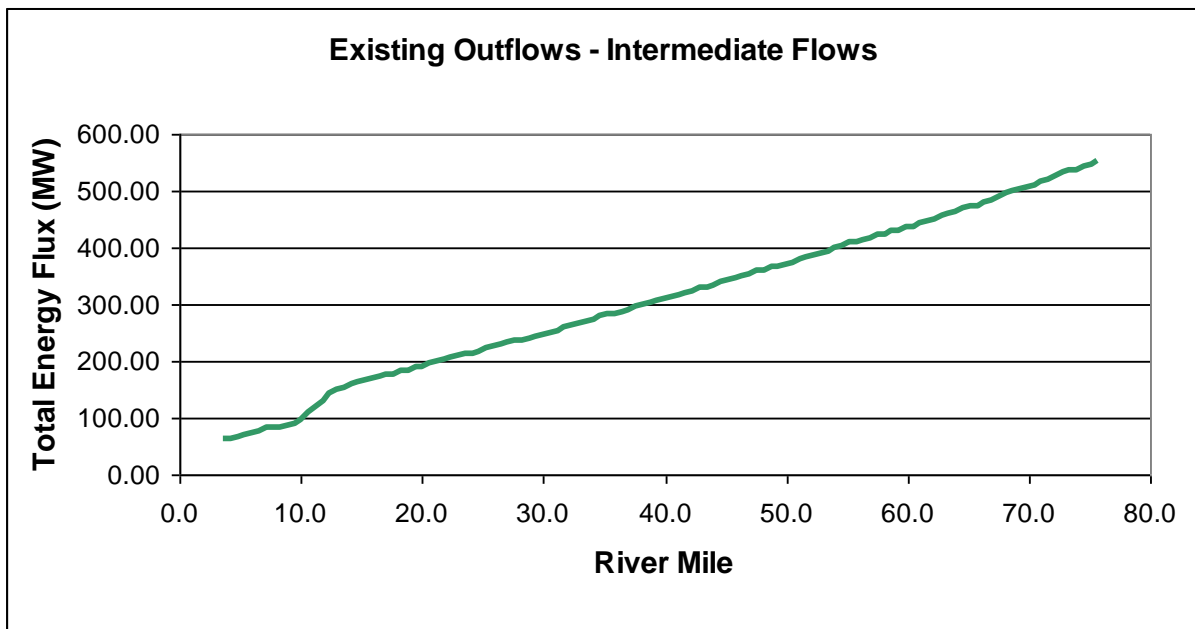


Figure 7.29 – Main Channel Total Energy Flux of the Flow at Intermediate Flows for the Existing Outflows Case

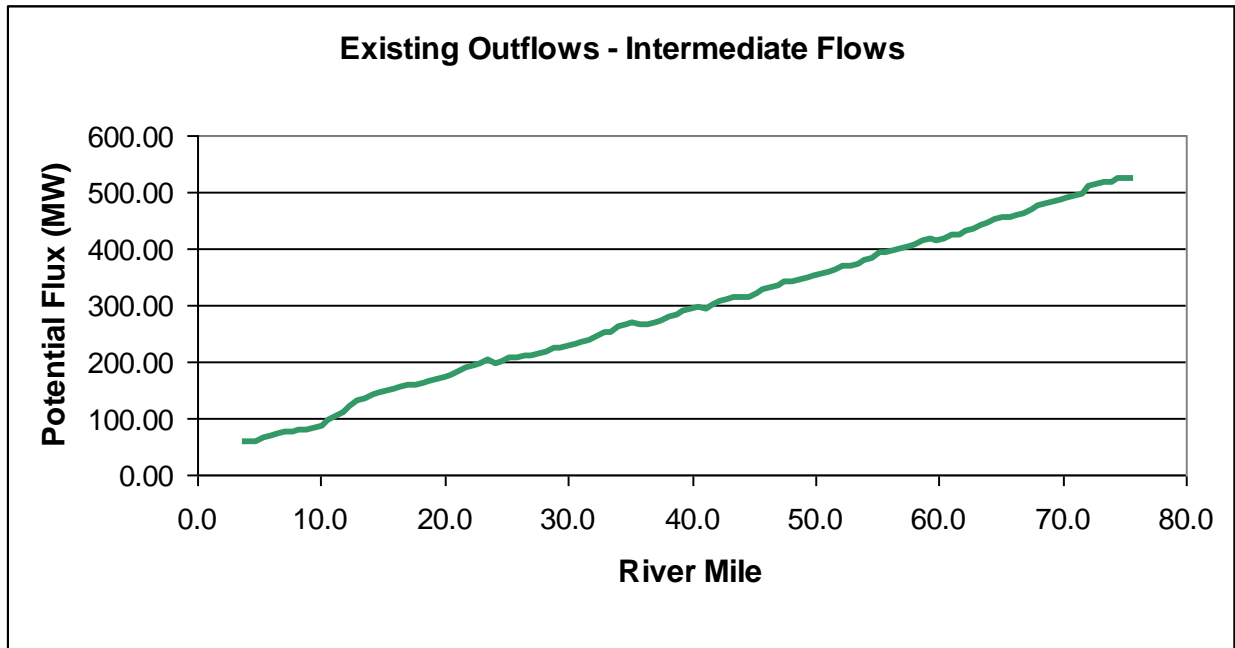


Figure 7.30 – Main Channel Potential Energy Flux of the Flow at Intermediate Flows for the Existing Outflows Case

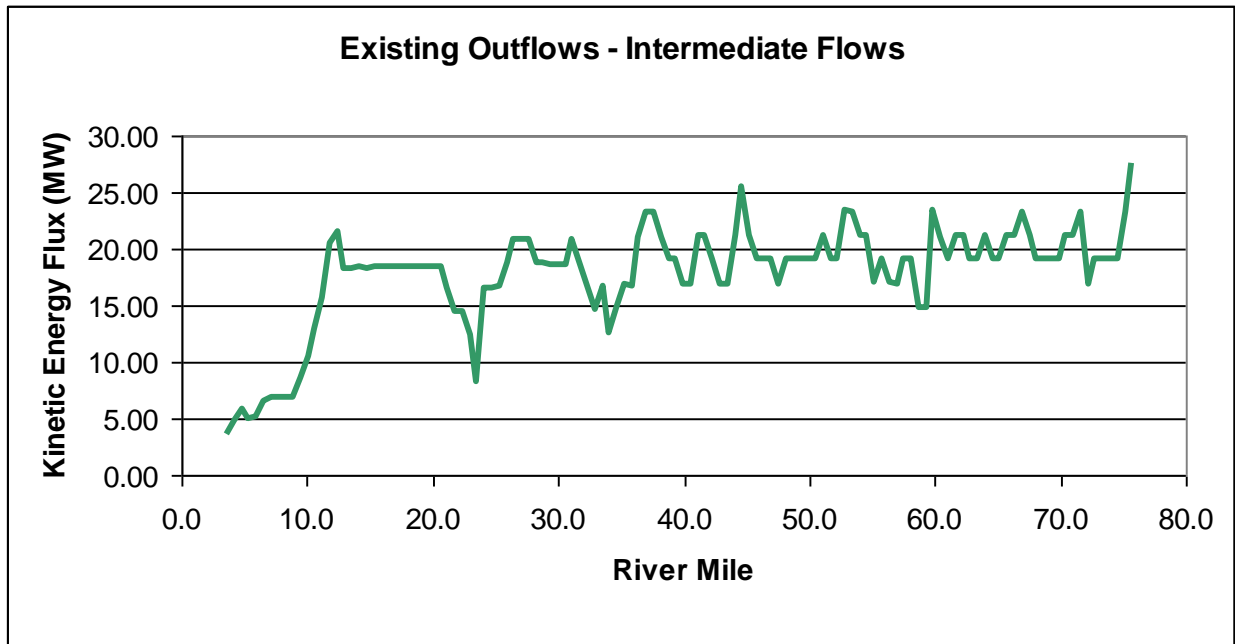


Figure 7.31 – Main Channel Kinetic Energy Flux of the Flow at Intermediate Flows for the Existing Outflows Case

Using the same 2008 period, tests were performed to calibrate and validate the sand concentration for some available episodic measurements performed by Allison (2010). Three days of measurements were used, one with low flow conditions, one with intermediate flow conditions and another one with high flow conditions. The van Rijn (1984) entrainment formula was used within ECOMSED. The results are summarized in Table 7-3. April 2008 was used for calibration while January and March 2008 were used for validation. It can be seen that the model is validated as the results obtained for different stations and under different flow conditions are very close to the measurements of Nittrouer *et al.* (2008) and Allison (2010), particularly for higher flows when most of the coarser sediment is transported.

Table 7-3 – Observed versus Modeled – 3-D Mobile-bed Simulations

Date/Station	Suspended Sand Concentration (mg/L)					
	Belle Chasse (RM 76)		Myrtle Grove (RM 57)		Scofield (RM 16-24)	
	<i>Observed</i> ⁺	<i>Simulated</i>	<i>Observed</i> ⁺ *	<i>Simulated</i>	<i>Observed</i> ⁺	<i>Simulated</i>
1/10/08 (Validation)	1.0	3.0	-	-	4.1	3.5
3/3/08 (Validation)	70.0	68.0	57.0*	52.0	-	-
4/15/08 (Calibration)	90.0	92.0	-	-	71.0	69.8

+Data from Allison (2010)

*Value measured in April 2009 for a similar water discharge

The same results shown in Table 7-3 are presented in Graphical form in Figure 7.32 to Figure 7.34 for an easier visualization.

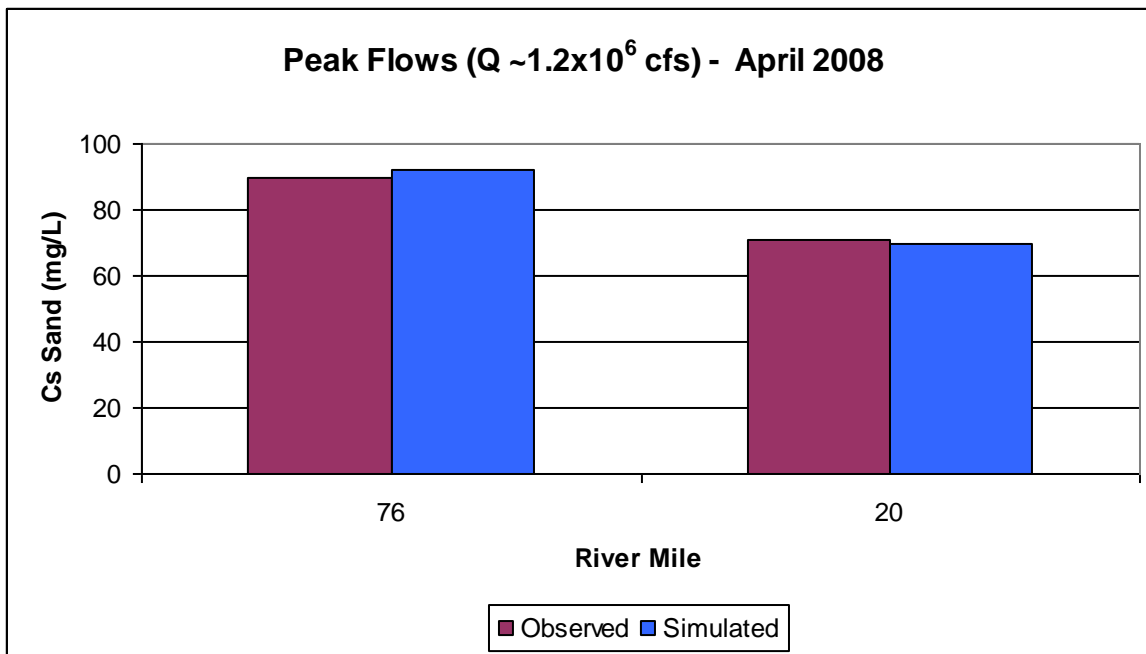


Figure 7.32 – Suspended Sand Concentration at Peak Flows – Calibration

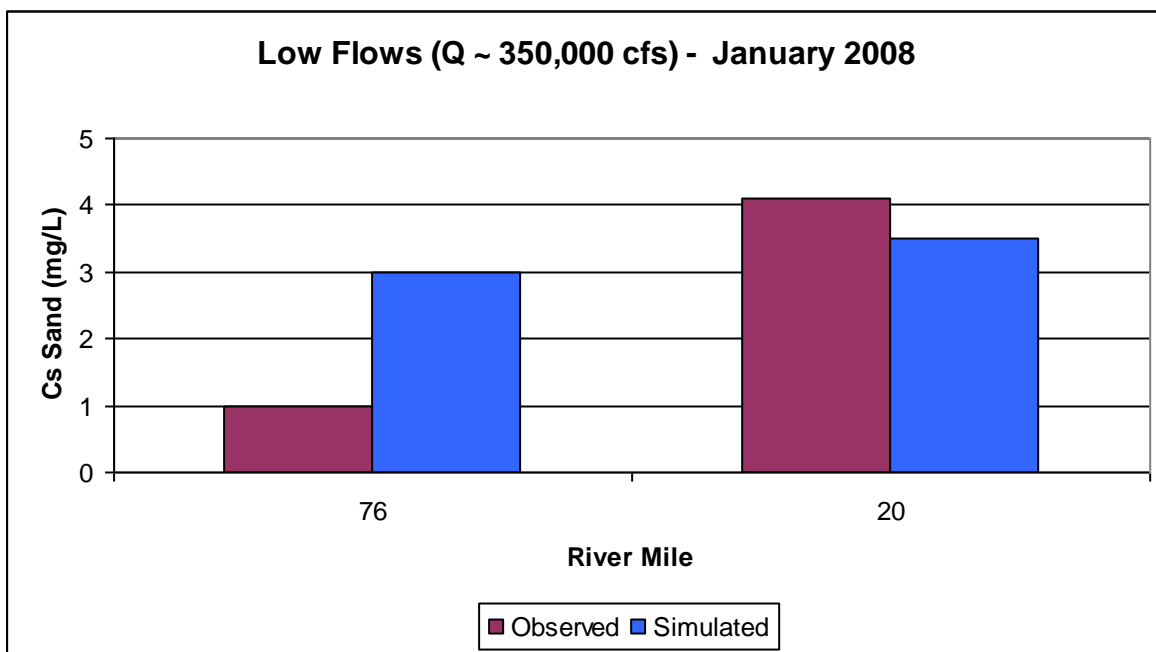


Figure 7.33 – Suspended Sand Concentration at Low Flows – Validation

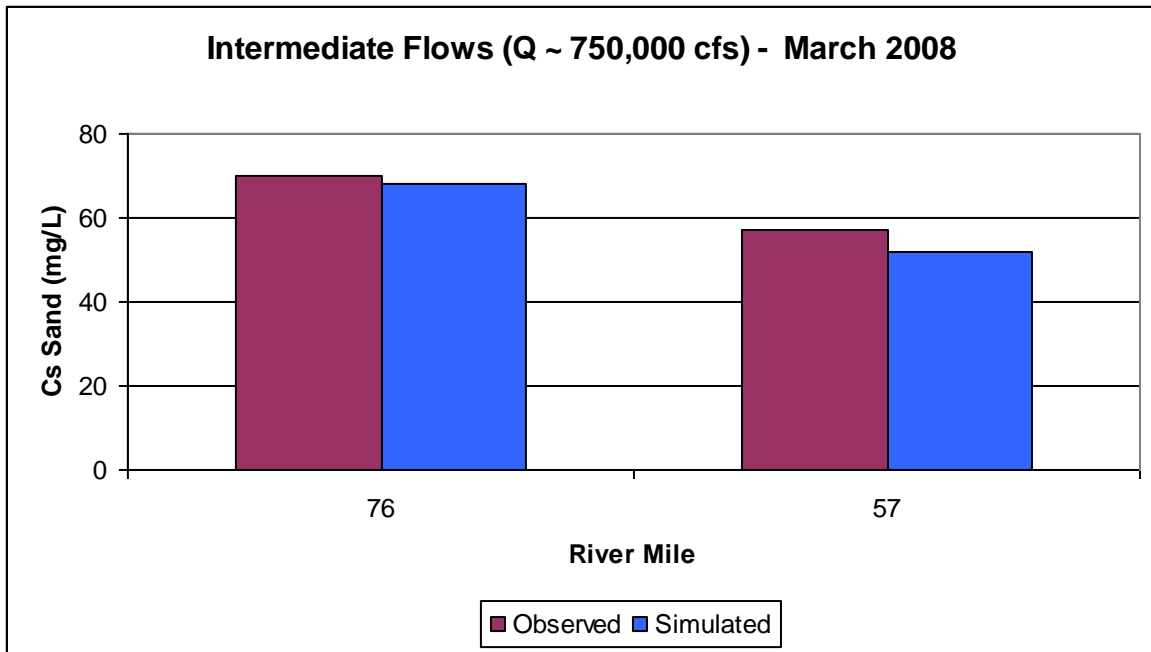


Figure 7.34 – Suspended Sand Concentration at Intermediate Flows – Validation

Figure 7.35 shows the sand concentration vertical profile in the center of the main channel at Scofield North (RM 24) for peak flow conditions. The profile follows an exponential function, as expected.

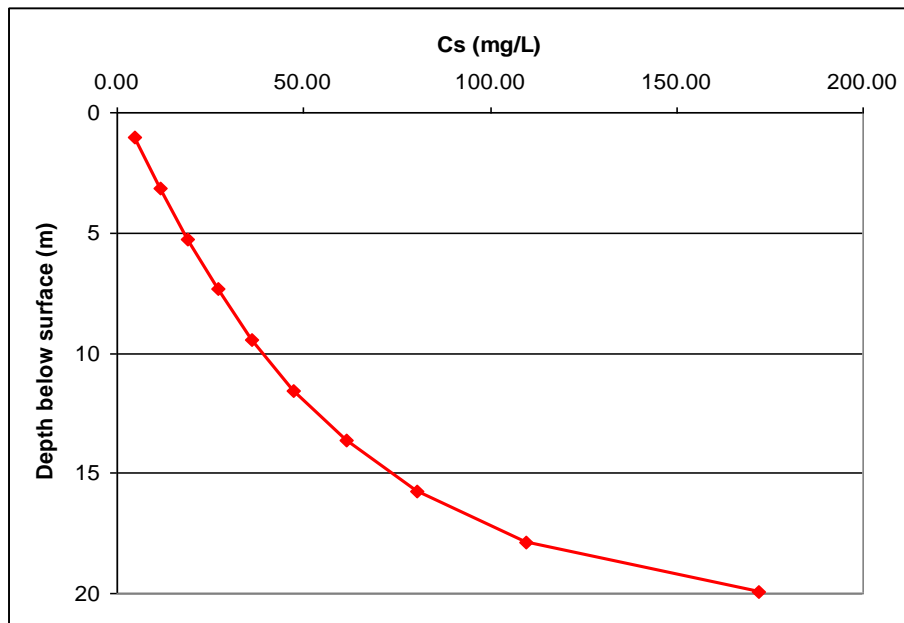


Figure 7.35 – Scofield North (RM 24) Sand Concentration Vertical Profile in the Center of the Channel at Peak Flows

A comparison between the modeling results and measurements by Allison (2010) for the vertical sand concentration profile can be seen in Figure 7.36 where y is the depth below the surface and d is the local depth. There is a good match between three of the four vertical profiles shown and the modeling results.

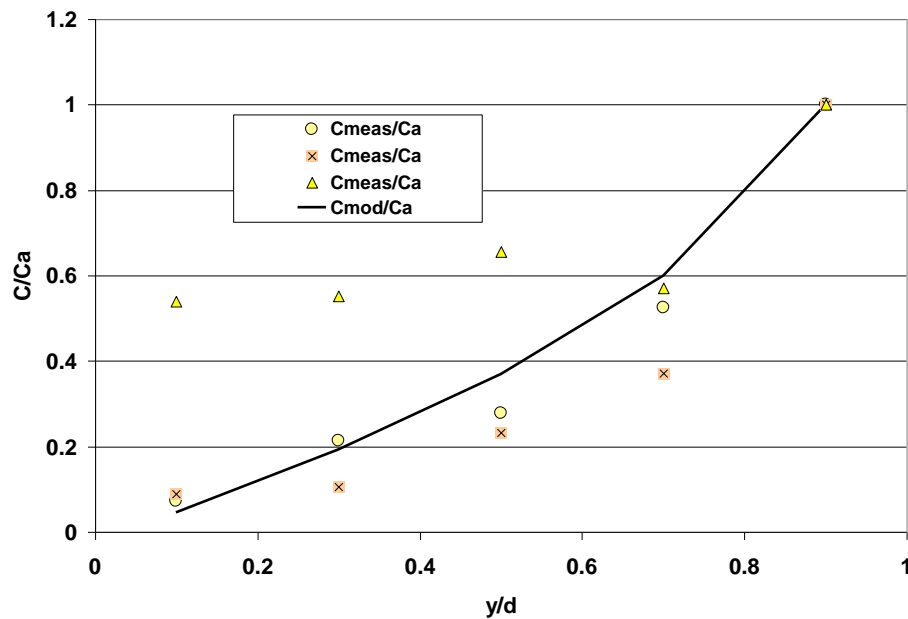


Figure 7.36 – Modeling versus Field Data (Source: Allison 2010)

The depth averaged sand concentrations in the model domain are shown in Figure 7.37 and Figure 7.38, while Figure 7.39, Figure 7.40, Figure 7.41 and Figure 7.42 show the sand concentration and sand load cross-sectional averaged values along the main channel for both peak and intermediate flows. Globally the sand concentration tends to decrease from upstream to downstream, with much higher values closer to the upstream limit of the model. This pattern agrees with the available field data. The extraction of flow and sediment, and the reduction of available energy contribute to a clear reduction of the sediment transport in the downstream area of the reach.

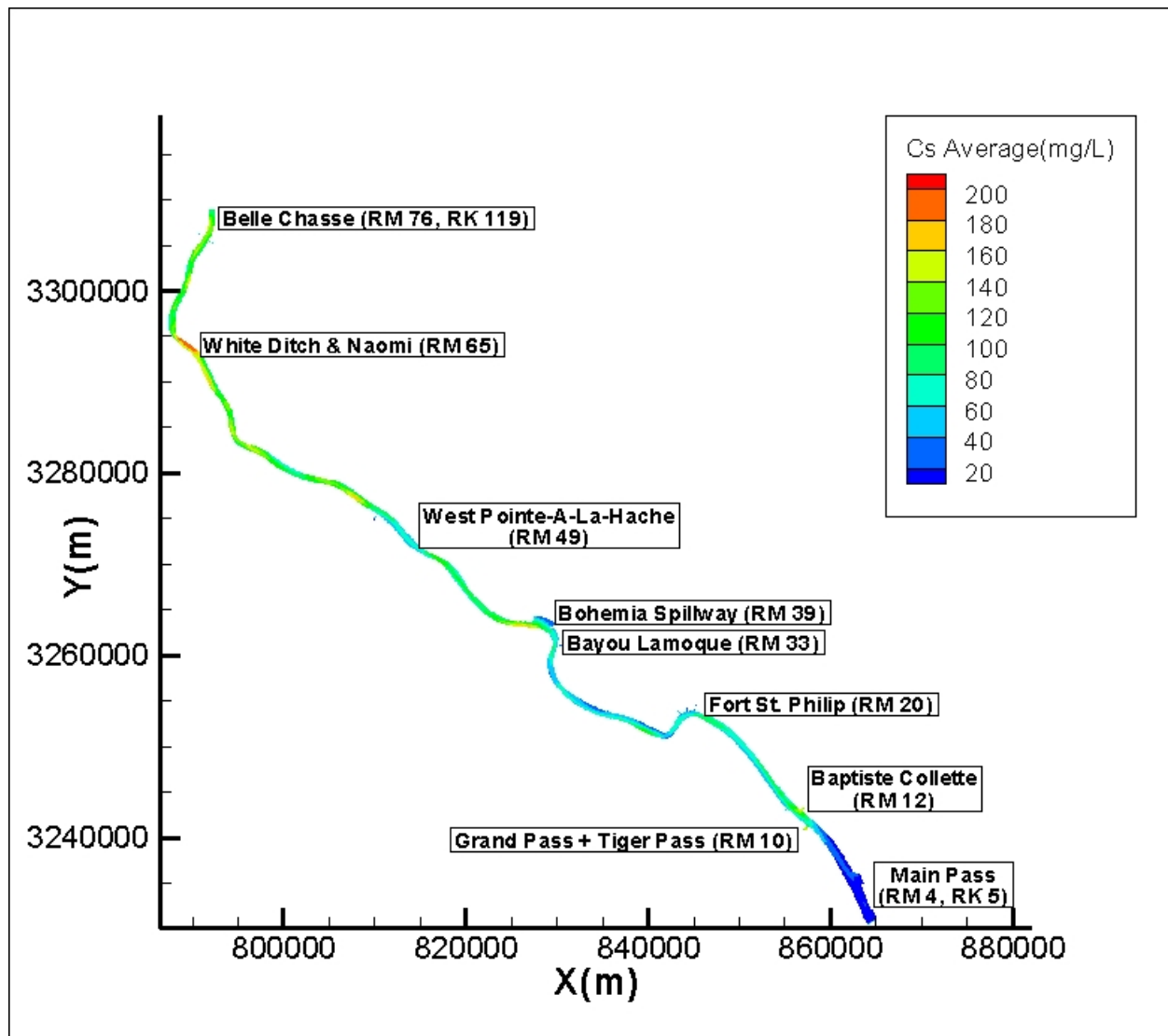


Figure 7.37 – Depth Average Suspended Sand Concentration for ECOMSED Mobile-Bed Calibration at Peak Flows (2008)

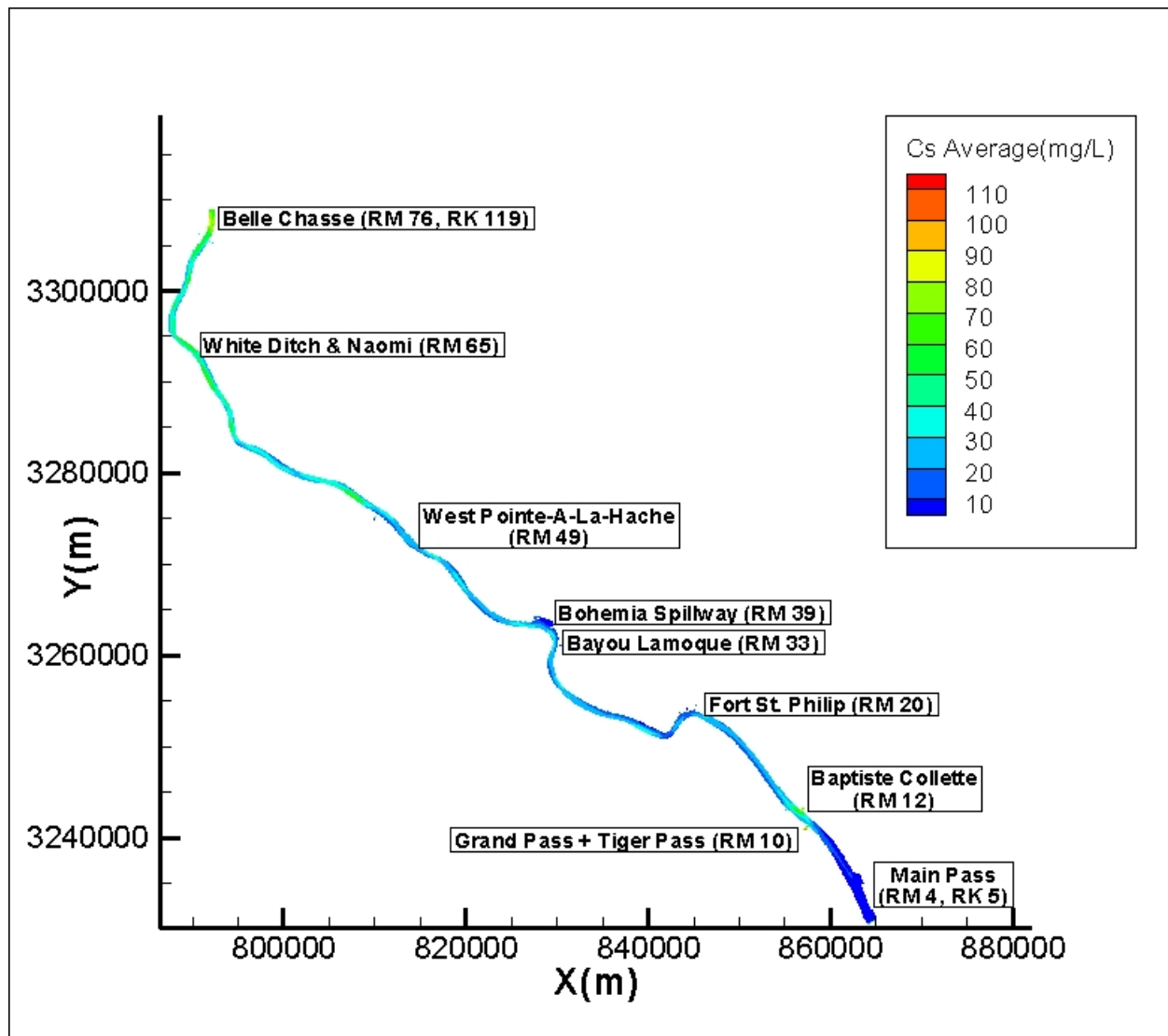


Figure 7.38 – Depth Average Suspended Sand Concentration for ECOMSED Mobile-Bed Calibration at Intermediate Flows (2008)

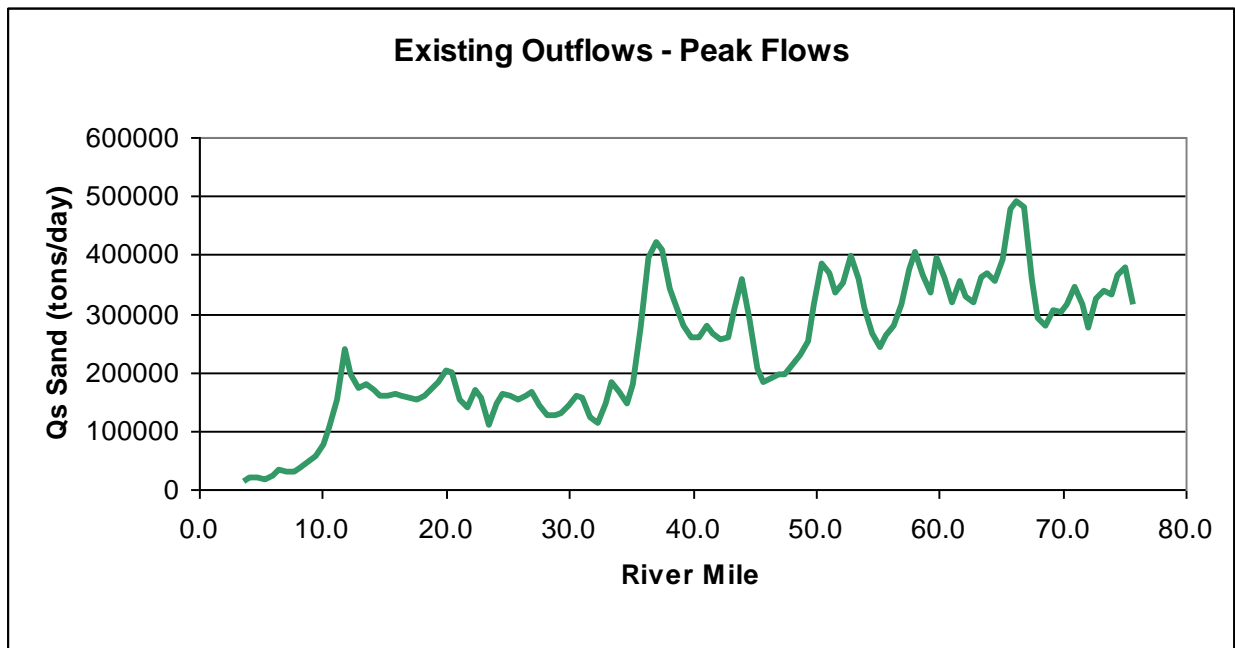


Figure 7.39 – Main Channel Suspended Sand Load at Peak Flows for the Existing Outflows Case

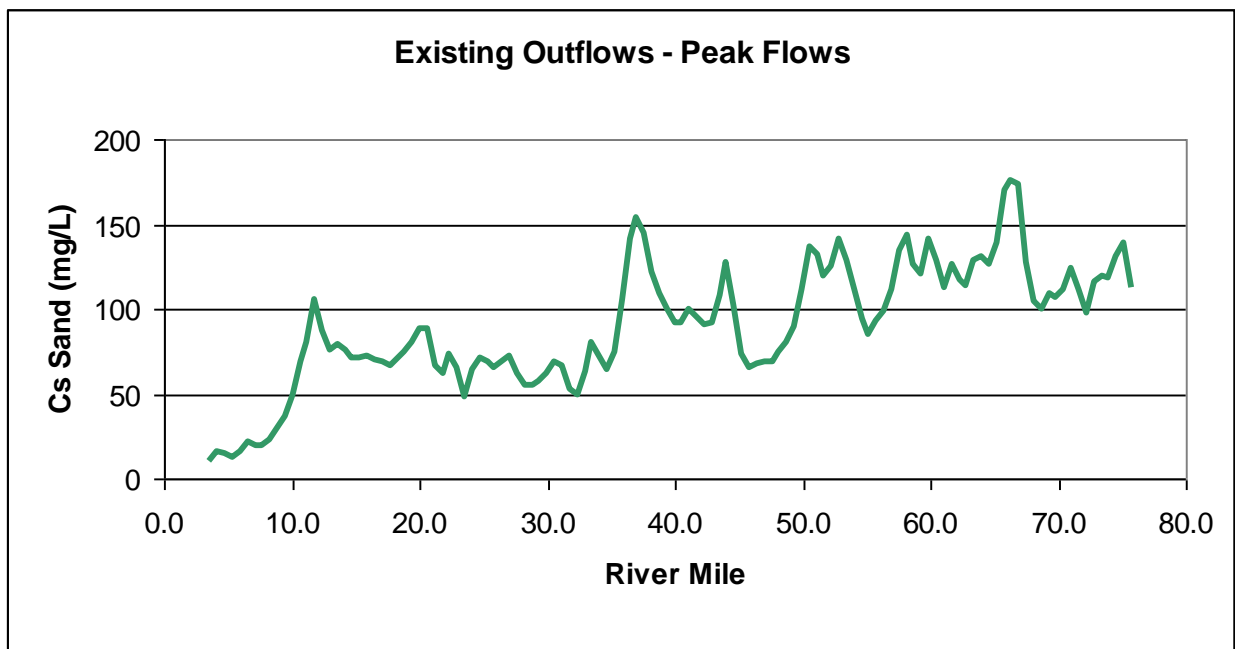


Figure 7.40 – Main Channel Suspended Sand Concentration at Peak Flows for the Existing Outflows Case

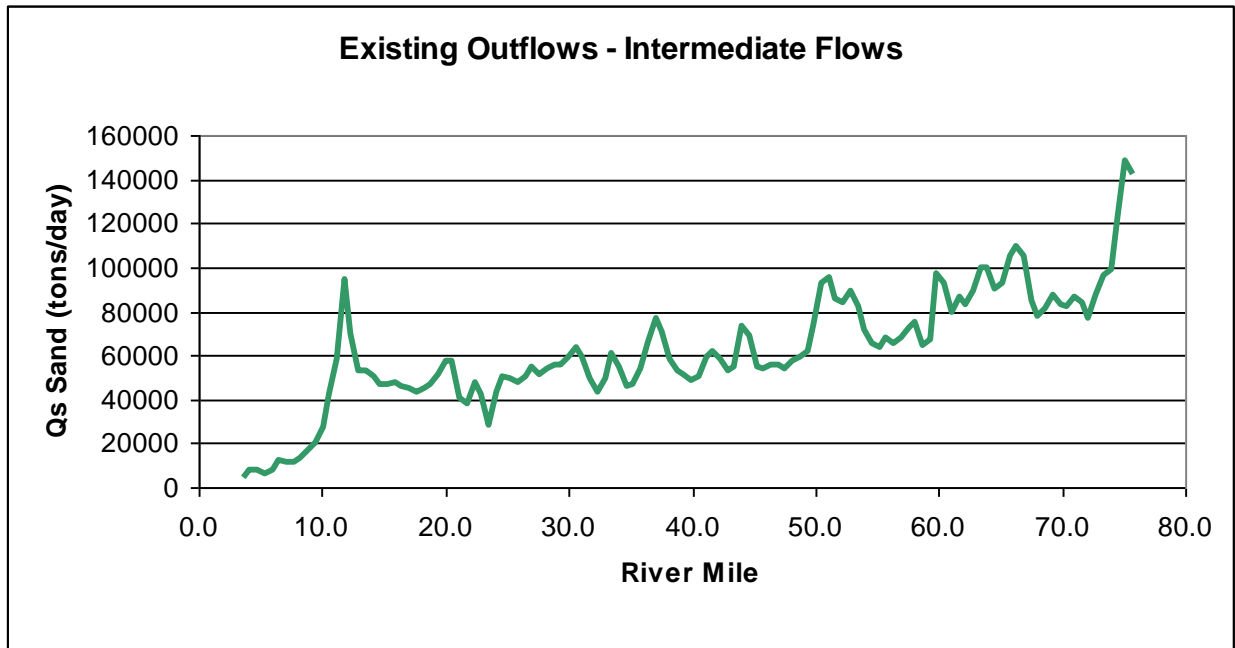


Figure 7.41 – Main Channel Suspended Sand Load at Intermediate Flows for the Existing Outflows Case

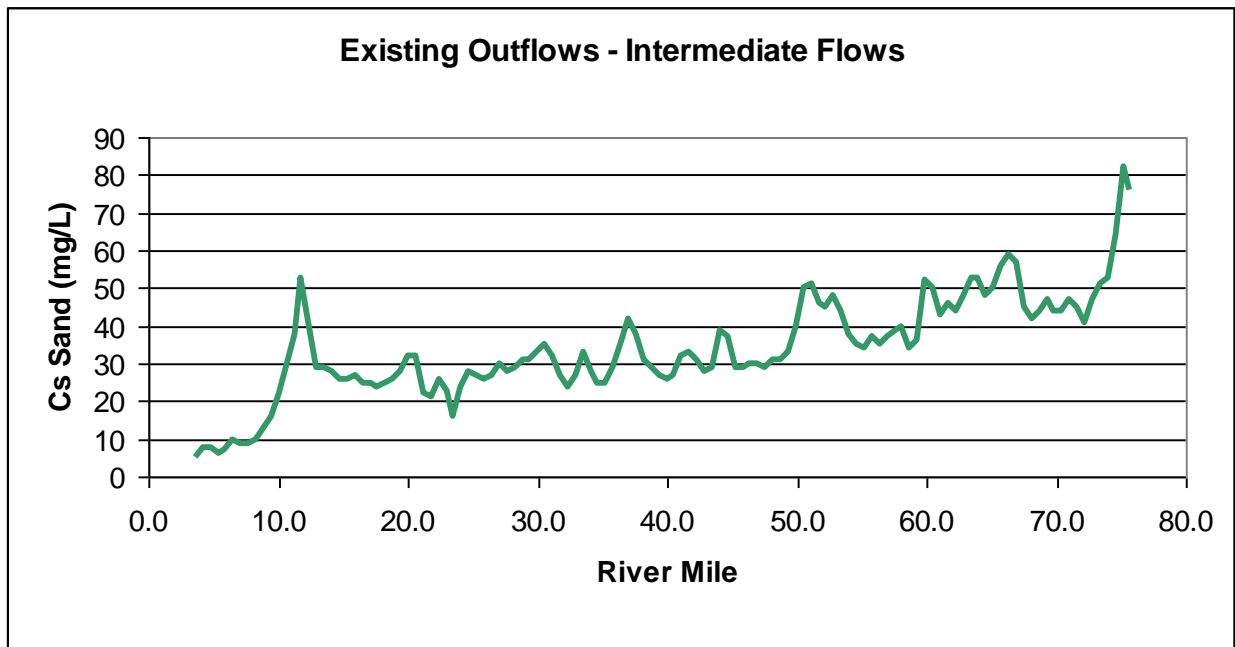


Figure 7.42 – Main Channel Suspended Sand Concentration at Intermediate Flows for the Existing Outflows Case

The sediment concentration, the sediment load, and the erosion and deposition patterns occurring in the river are the most relevant outputs of the sediment simulations. Figure 7.43 shows the model domain bed thickness change registered after 1 day of simulation at peak flows. It can be seen that there are not very pronounced erosion or deposition areas, with the maximum deposition being of the order of 0.15 m and a maximum erosion of nearly 0.4 m. There is less change closer to the downstream boundary of the domain. Figure 7.44 shows the change registered after 10 days. The patterns are similar to the ones registered after one day. A maximum cumulative erosion of more than 5 meters may happen but only in localized areas such as the boundary points of flow extraction. These exaggerated erosion values close to a boundary are unrealistic but don't have any global significant effect in the results. A maximum deposition of around 1.5 m is shown.

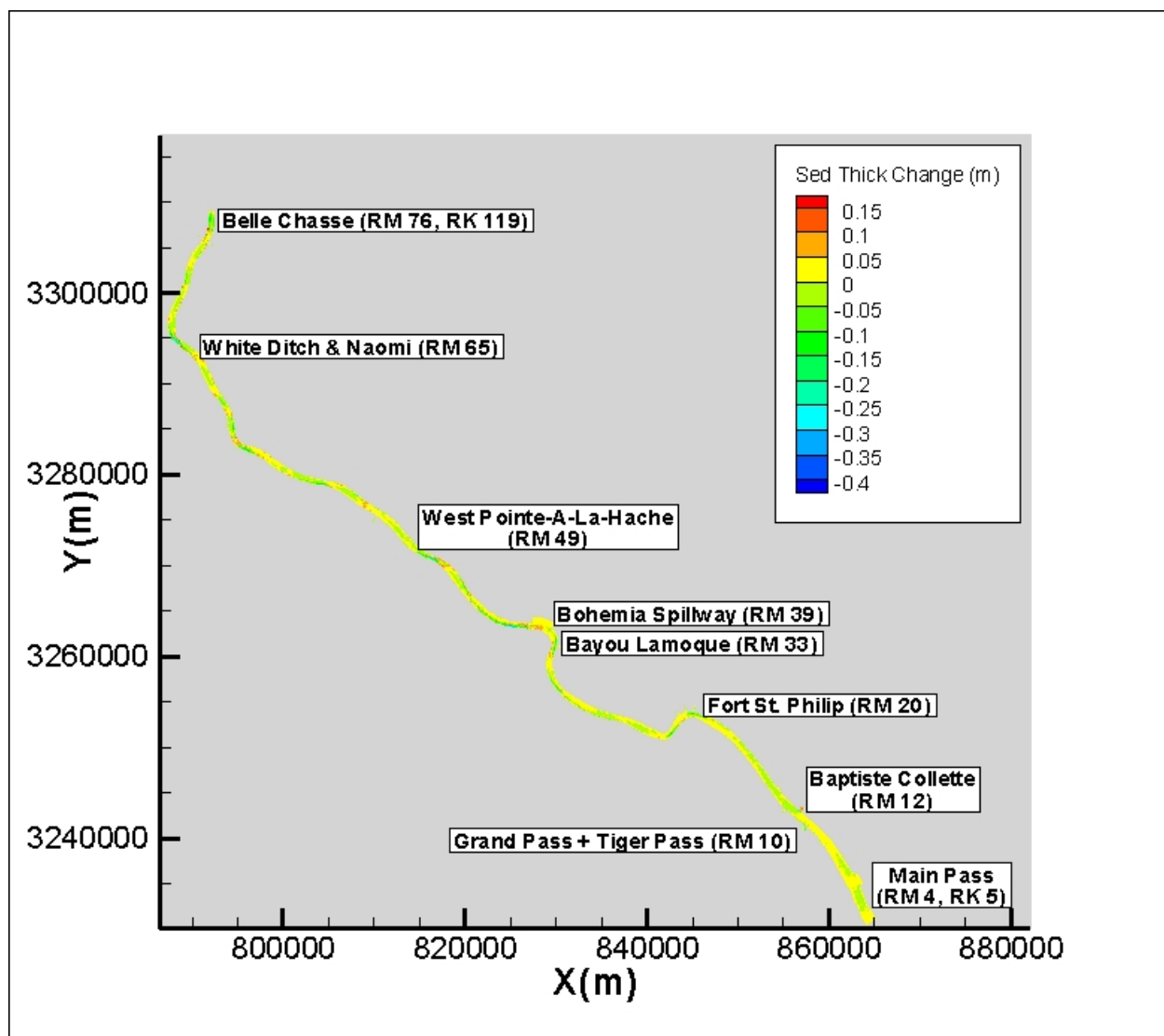


Figure 7.43 – Existing Outflows – Model Domain - Bed Sediment Thickness Change after 1 day at Peak Flows. Positive values indicate deposition and negative values indicate erosion

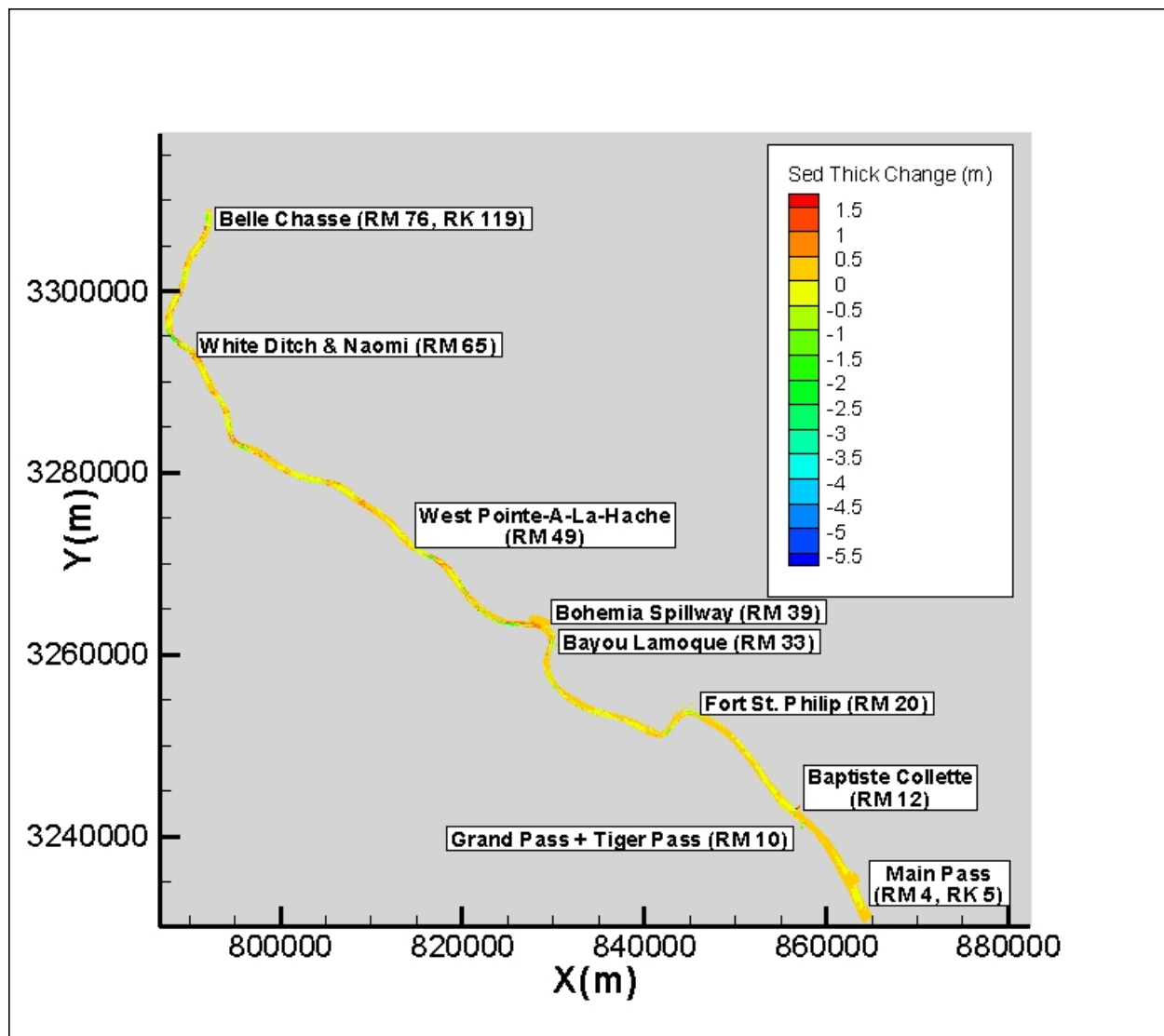


Figure 7.44 – Existing Outflows – Model Domain - Bed Sediment Thickness Change after 10 days at Peak Flows. Positive values indicate deposition and negative values indicate erosion

A closer look at bed thickness variation after 1 day near Myrtle Grove (RM 59) and Belair (RM 65) are shown in Figure 7.45 and Figure 7.46. These are the locations where the introduction of new diversions was tested. The deep hole areas show significant erosion as expected and are consistent with the bed shear stress pattern shown in Figure 7.46. The formation of sand bars and the existence of deposition immediately downstream of erosional areas once the channel straightens are consistent with theory and occur as expected. The change registered after 10 days is shown in Figure 7.47 and Figure 7.48. The erosion and deposition patterns are consistent with the ones shown after 1 day.

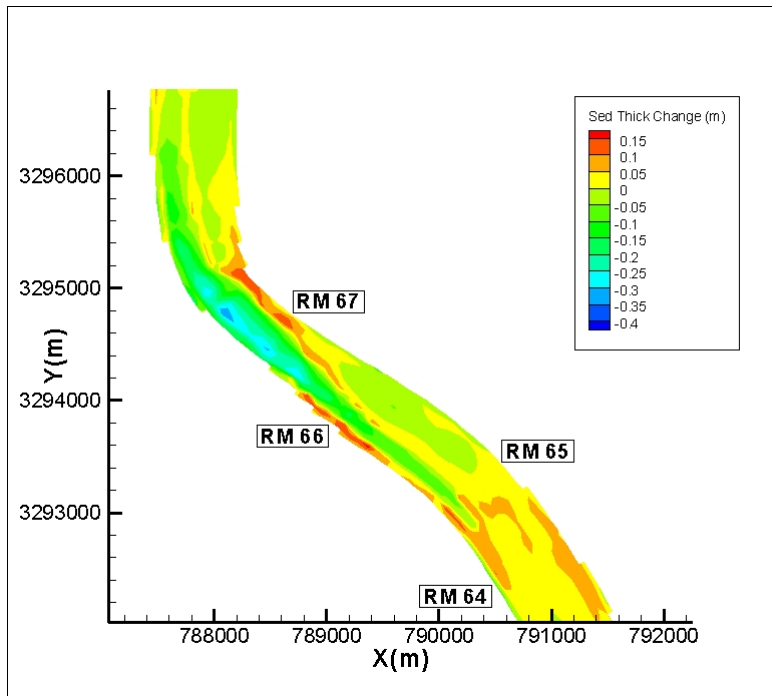


Figure 7.45 – Existing Outflows – Belair Area (RM 65) - Bed Sediment Thickness Change after 1 day at Peak Flows. Positive values indicate deposition and negative values indicate erosion

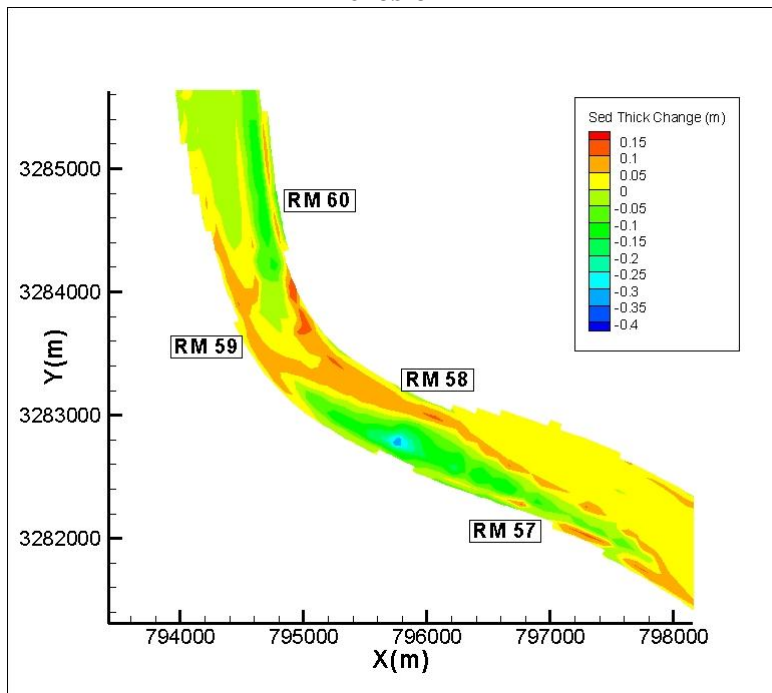


Figure 7.46 – Existing Outflows – Myrtle Grove Area (RM 59) - Bed Sediment Thickness Change after 1 day at Peak Flows. Positive values indicate deposition and negative values indicate erosion

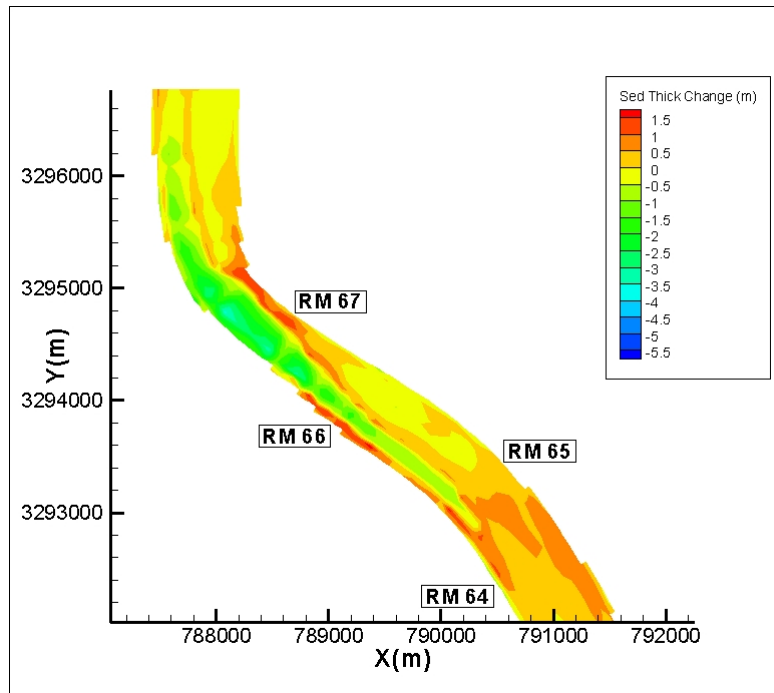


Figure 7.47 – Existing Outflows – Belair Area (RM 65) - Bed Sediment Thickness Change after 10 days at Peak Flows. Positive values indicate deposition and negative values indicate erosion

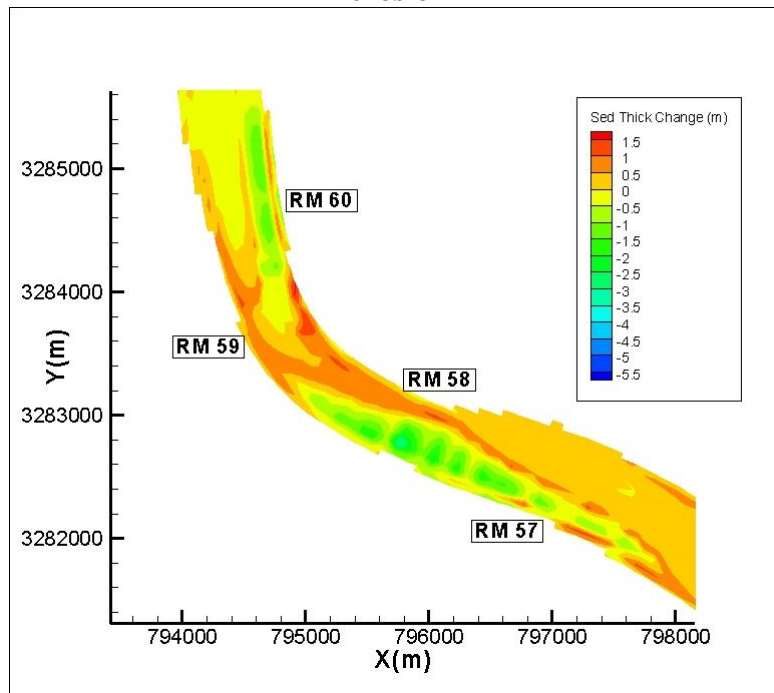


Figure 7.48 – Existing Outflows – Myrtle Grove Area (RM 59) - Bed Sediment Thickness Change after 10 days at Peak Flows. Positive values indicate deposition and negative values indicate erosion

Figure 7.49 shows the model domain bed thickness change registered after 1 day of simulation and Figure 7.50 shows the change registered after 10 days at intermediate flows. The maximum deposition is of the order of 0.05 m for 1 day and 0.5 m for 10 days. The maximum erosion is of nearly -0.05 m for 1 day and -0.5 m for 10 days. These values are lower than those obtained for peak flows, as expected. Closer to the downstream end there is almost no change after 1 day but some deposition is evident.

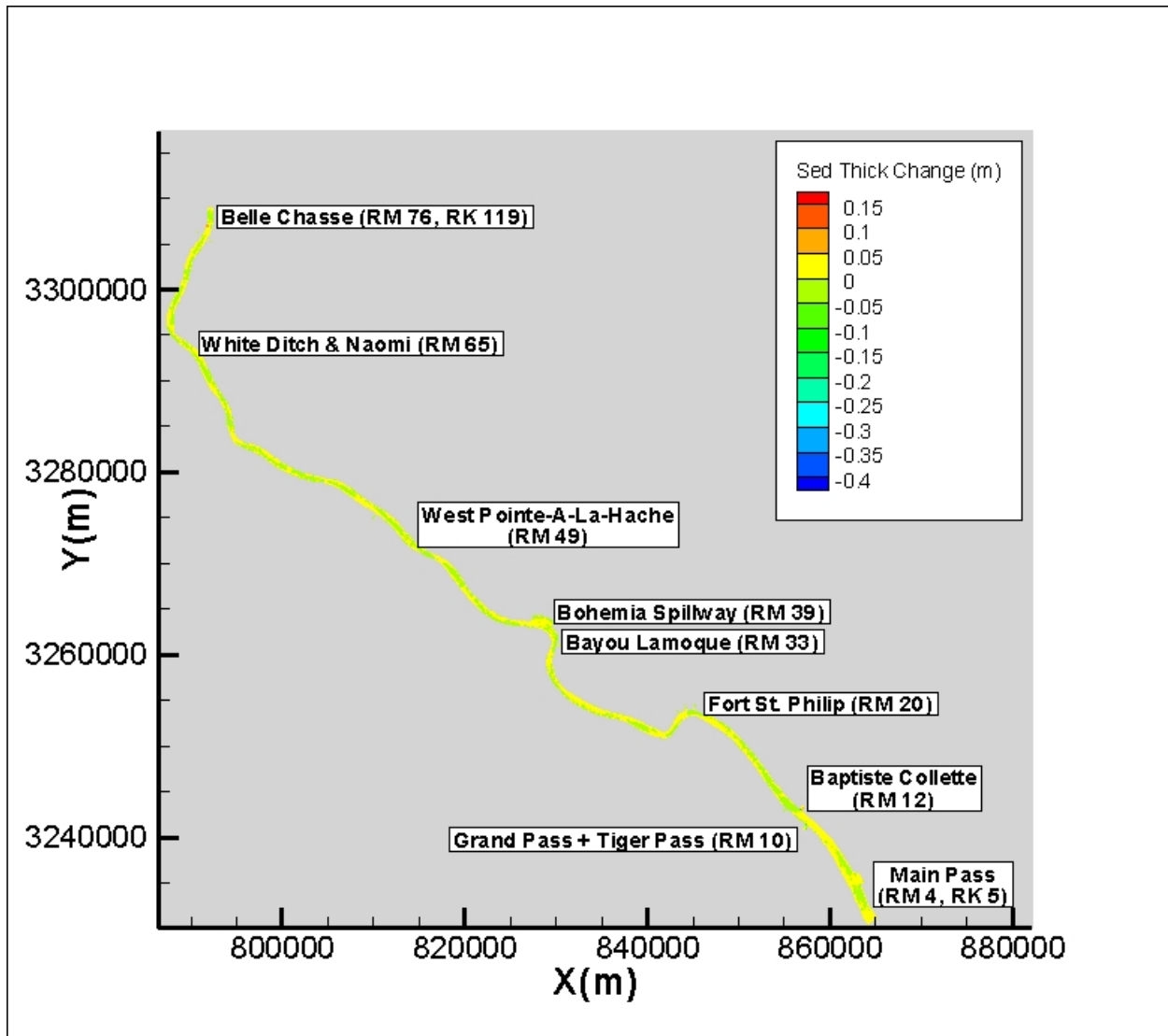


Figure 7.49 – Existing Outflows – Model Domain - Bed Sediment Thickness Change after 1 day at Intermediate Flows. Positive values indicate deposition and negative values indicate erosion

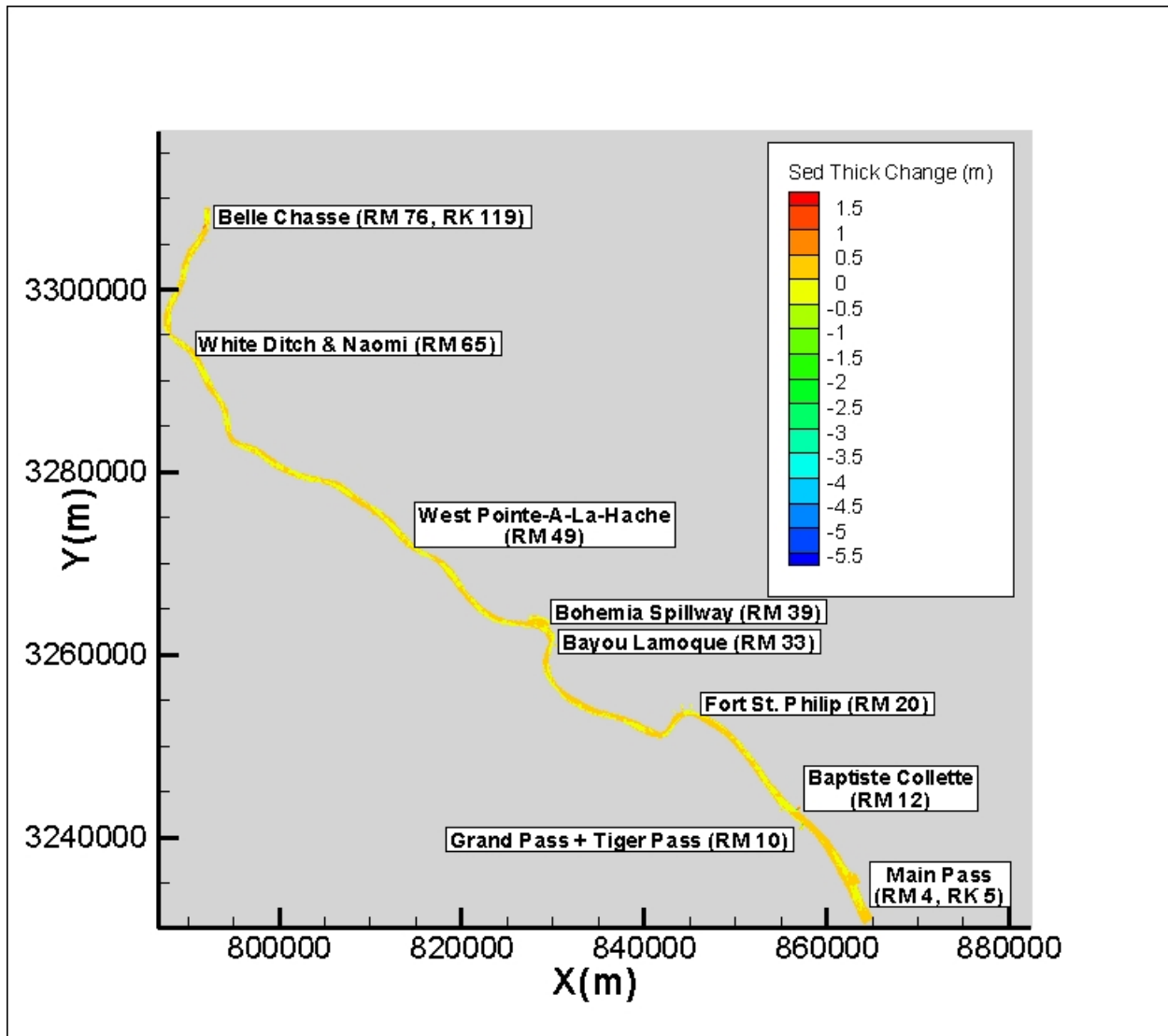


Figure 7.50 – Existing Outflows – Model Domain - Bed Sediment Thickness Change after 10 days at Intermediate Flows. Positive values indicate deposition and negative values indicate erosion

A closer look at bed thickness variation near Myrtle Grove (RM 59) and Belair (RM 65) after 1 day and 10 days of simulation for intermediate flows is shown in Figure 7.51, Figure 7.52, Figure 7.53 and Figure 7.54. Once again, the deep hole areas show significant erosion as expected. Similarly to the peak flow results, the formation of sand bars and the existence of deposition immediately downstream of erosional areas once the channel straightens are consistent with theory and occur as expected.

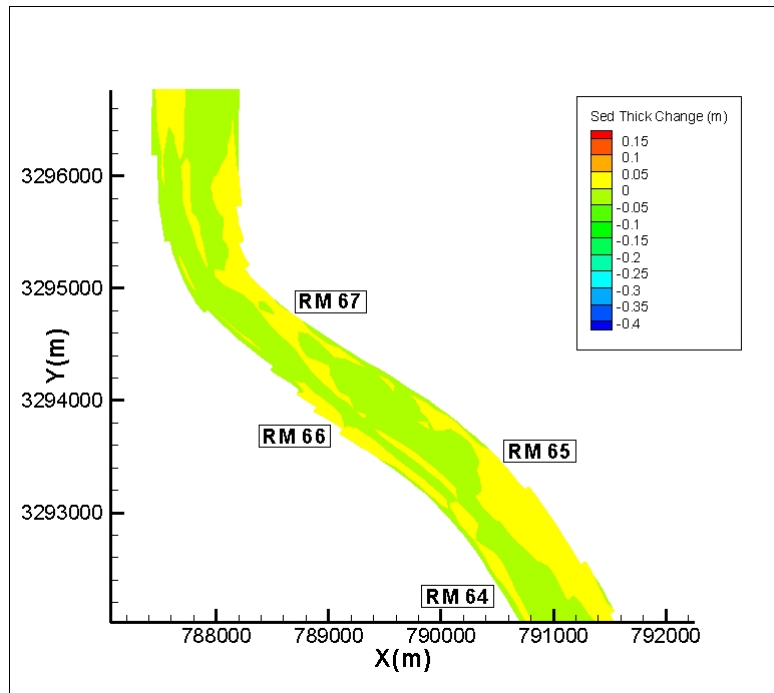


Figure 7.51 – Existing Outflows – Belair Area (RM 65) - Bed Sediment Thickness Change after 1 day at Intermediate Flows. Positive values indicate deposition and negative values indicate erosion

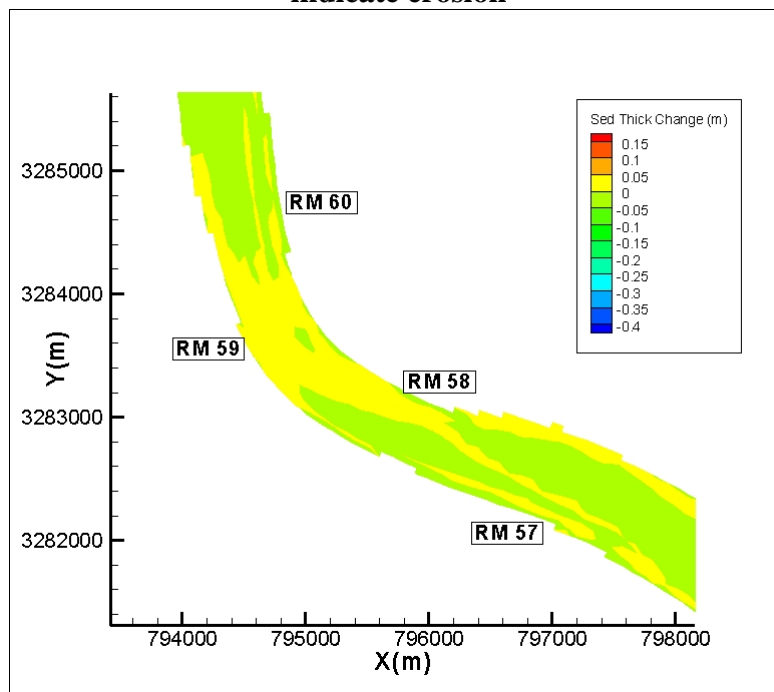


Figure 7.52 – Existing Outflows – Myrtle Grove Area (RM 59) - Bed Sediment Thickness Change after 1 day at Intermediate Flows. Positive values indicate deposition and negative values indicate erosion

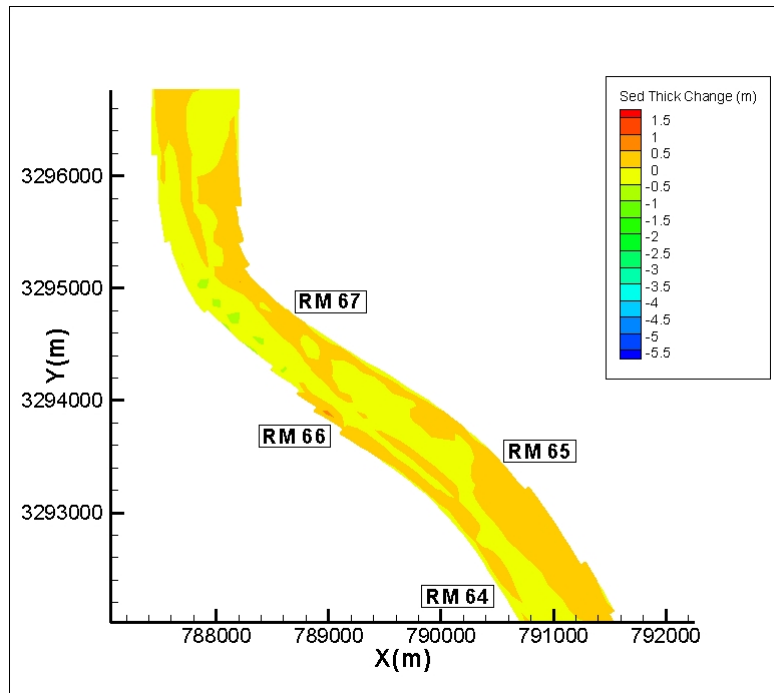


Figure 7.53 – Existing Outflows – Belair Area (RM 65) - Bed Sediment Thickness Change after 10 days at Intermediate Flows. Positive values indicate deposition and negative values indicate erosion

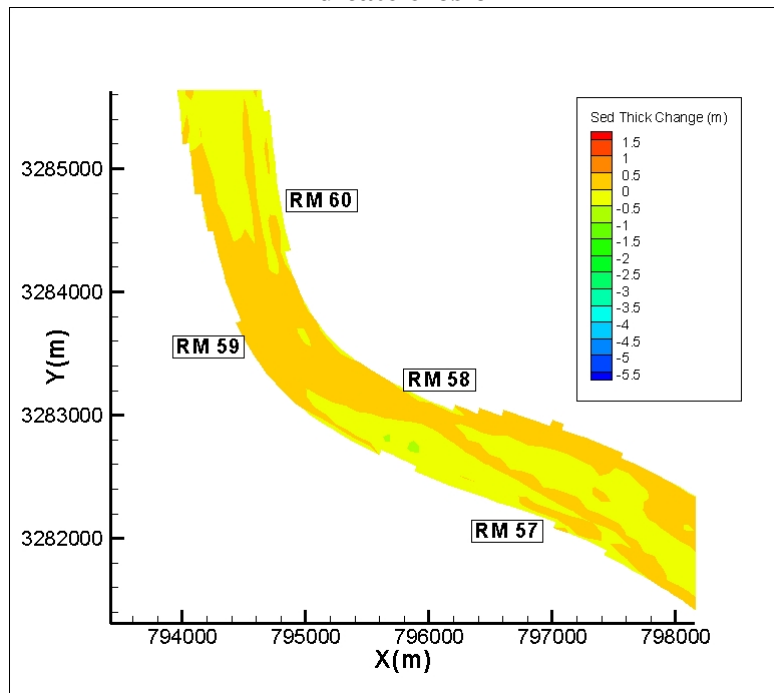


Figure 7.54 – Existing Outflows – Myrtle Grove Area (RM 59) - Bed Sediment Thickness Change after 10 days at Intermediate Flows. Positive values indicate deposition and negative values indicate erosion

The estimated amount of sediment being extracted at each outflow for both peak and intermediate flows is shown in Table 7-4. It is evident that, at peak flows, the 3 largest outflows (Bohemia, Baptiste Collette, Grand Pass + Tiger Pass) divert disproportionately the largest amount of sand. At intermediate flows, Baptiste Collette and Grand Pass + Tiger Pass divert more sand; Bohemia flows are reduced to around 6% of the peak flow values and the sediment load drops to 1% of the peak flow value. For peak and for intermediate flows, the amount of bed material extracted at Main Pass, also a large diversion, is very low. This is probably due to the low energy gradient to the downstream boundary.

Table 7-4 – Water Discharge, Suspended Sand Concentration and Suspended Sand Load at Outflows – Existing Outflows Case Study – Peak Flows

Site	Peak Flows			Intermediate Flows		
	Q (m ³ /s)	Cs (mg/L)	Qs (metric tons/day)	Q (m ³ /s)	Cs (mg/L)	Qs (metric tons/day)
West Pointe-À-La-Hache	27	70	166	19	21	35
Bohemia Spillway	6,072	62	32,528	370	13	427
Bayou Lamoque	84	30	216	66	9	52
Fort St. Philip	593	29	1,492	389	9	288
Baptiste Collette	4,032	127	43,346	3,240	67	18,777
Grand Pass + Tiger Pass	4,231	101	36,905	3,350	54	15,708
Main Pass	2,955	13	3,256	2,266	5	1,075

Figure 7.55 and Figure 7.56 show graphically the peak flow sand concentration at each outflow. It can be seen that globally the concentrations tend to be reduced from upstream to downstream for similar River flows, e.g., Grand Pass + Tiger Pass has lower concentrations than Baptiste Collette.

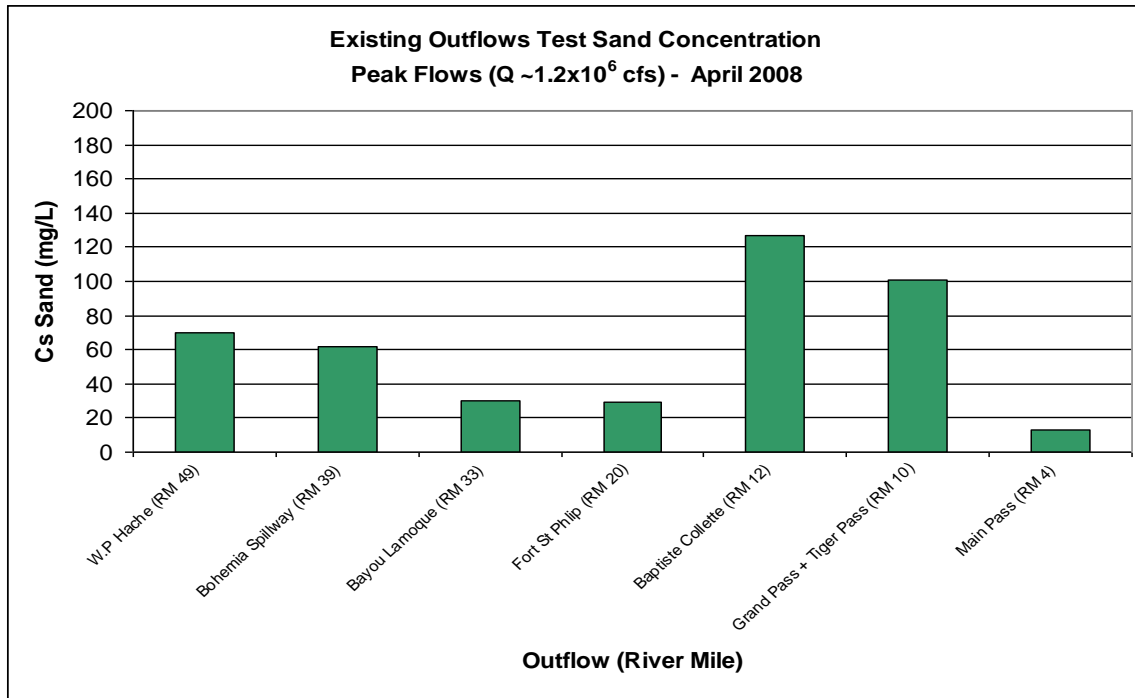


Figure 7.55 – Existing Outflows – Outflows Suspended Sand Concentration at Peak Flows

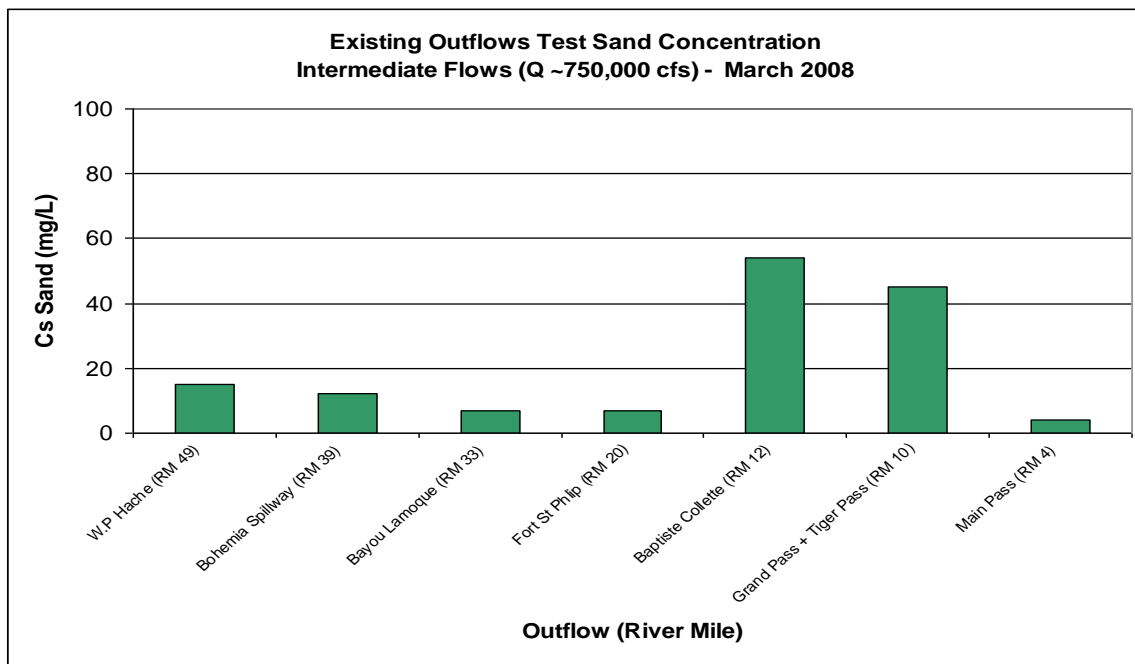


Figure 7.56 – Existing Outflows – Outflows Suspended Sand Concentration at Intermediate Flows

7.3 Myrtle Grove + Existing Outflows

To study the effect of proposed diversions on the system, several cases were tested. The first one consisted of the introduction of a diversion on the West Bank at Myrtle Grove (RM 59). The diversion is located upstream of the meander as shown in Figure 7.57. The diversion was included in the model by activating a row of cells, corresponding to a width of around 100 m, as proposed. A uniform depth of 10 m (30 ft) was defined for the diversion.

Simulations were performed for Peak Flow conditions with an extracted water flow of approximately 30,000 cfs (850 cms), which matches the values used in the CHARIMA simulations. A sand concentration of 40 mg/L was given as the proposed diversion boundary condition.

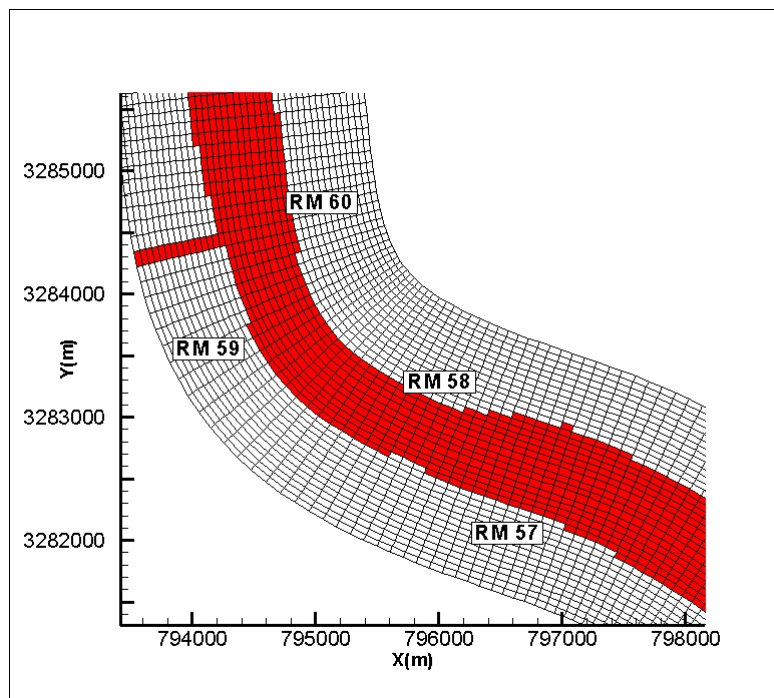


Figure 7.57 – Existing Outflows + Myrtle Grove ECOMSED Mesh and Mask at Myrtle Grove (RM 59, RK 94)

Figure 7.58 and Figure 7.59 show the total and the kinetic energy profiles for the main channel at peak flows with and without the introduction of the Myrtle Grove diversion. The introduction of this diversion does not greatly change either the kinetic energy or the total energy lines.

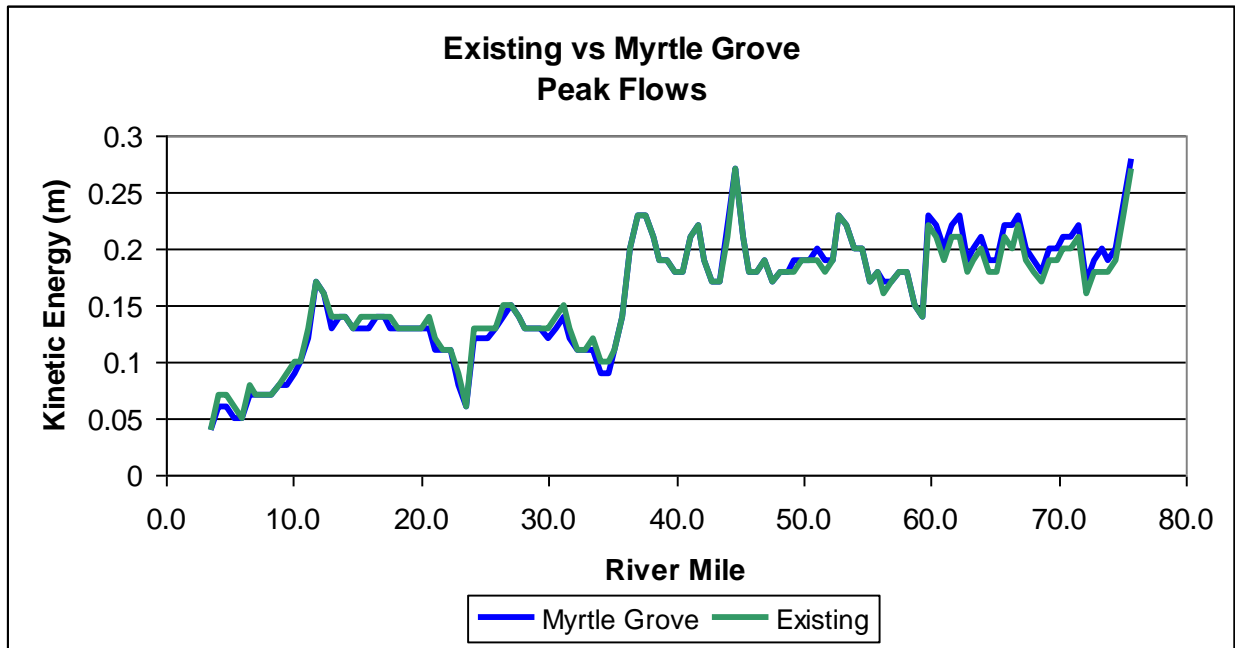


Figure 7.58 – Existing Outflows + Myrtle Grove (RM 59, RK 94) – Main Channel Kinetic Energy of the Flow at Peak Flows

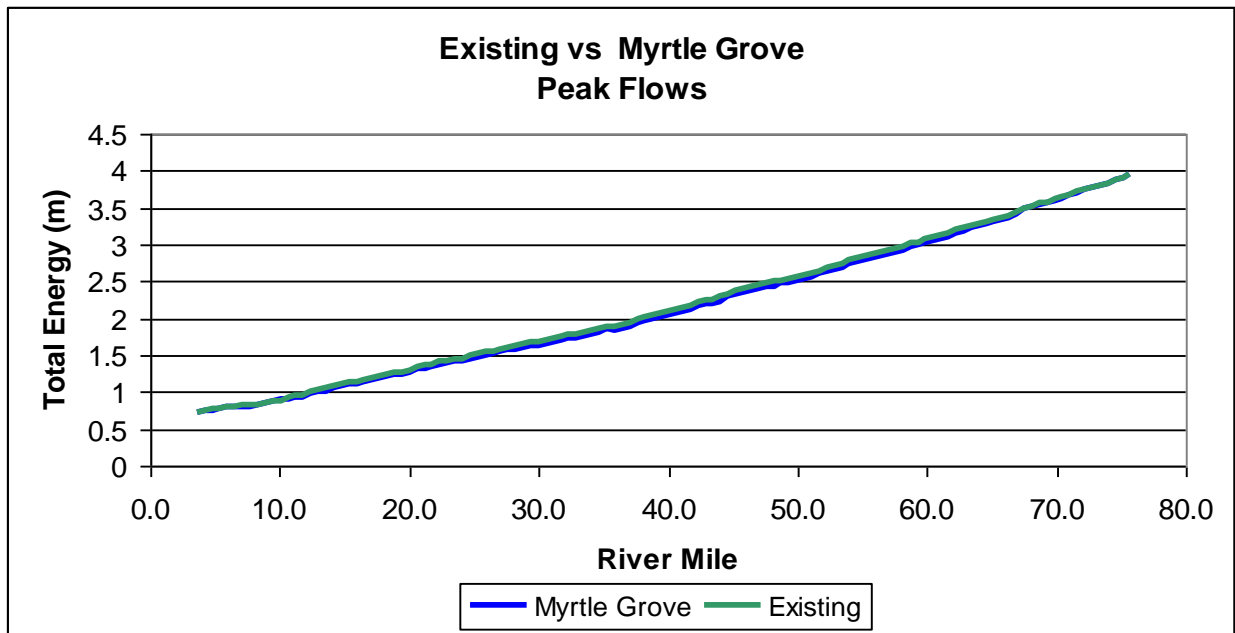


Figure 7.59 – Existing Outflows + Myrtle Grove (RM 59, RK 94) – Main Channel Total Energy of the Flow at Peak Flows

Figure 7.60, Figure 7.61 and Figure 7.62 show respectively, the main channel total, potential and kinetic energy fluxes under peak flow conditions for the Myrtle Grove test.

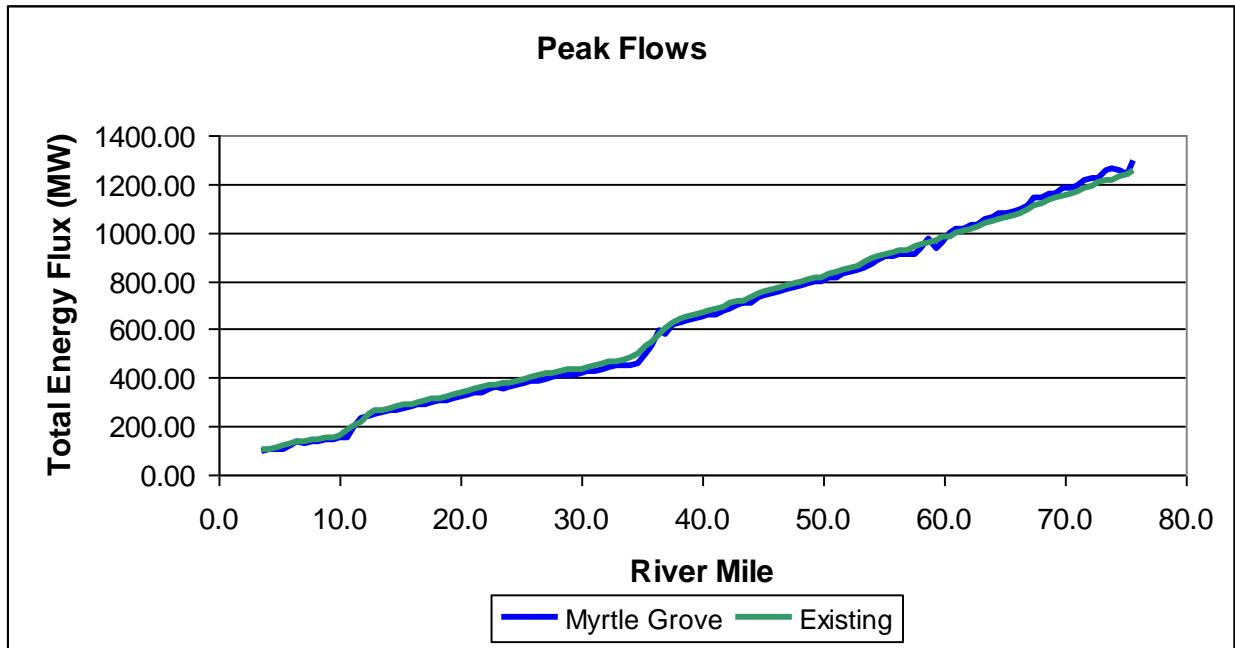


Figure 7.60 – Existing Outflows + Myrtle Grove (RM 59, RK 94) – Main Channel Total Energy Flux of the Flow at Peak Flows

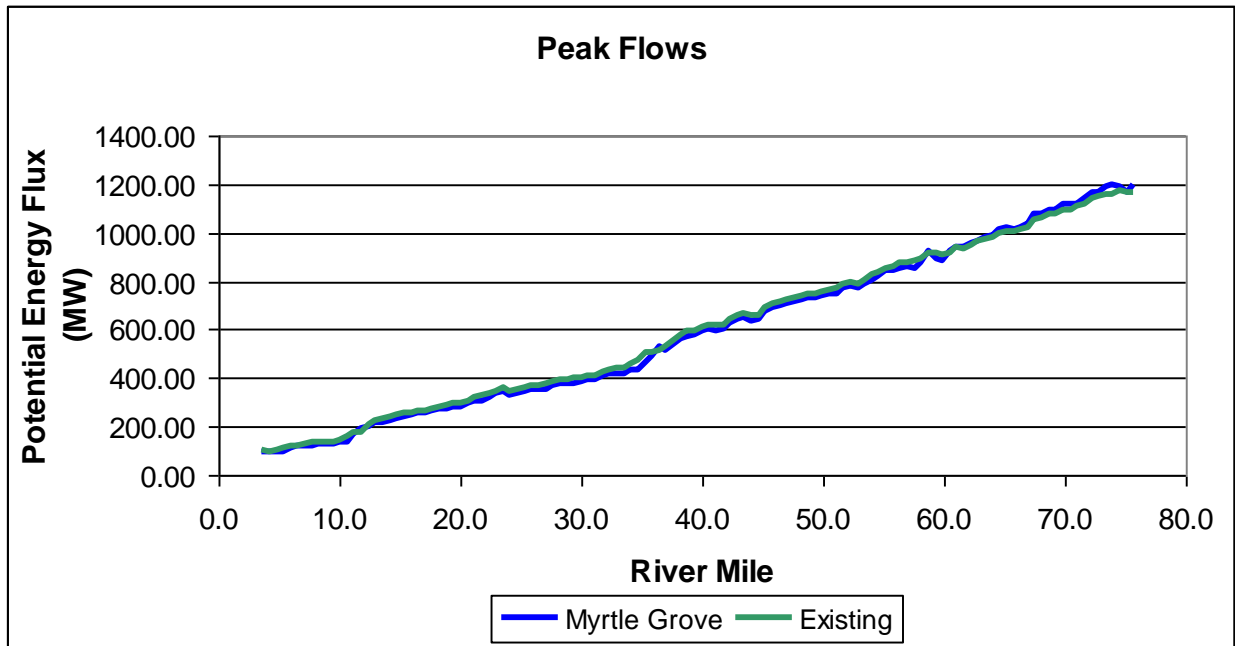


Figure 7.61 – Existing Outflows + Myrtle Grove (RM 59, RK 94) – Main Channel Potential Energy Flux of the Flow at Peak Flows

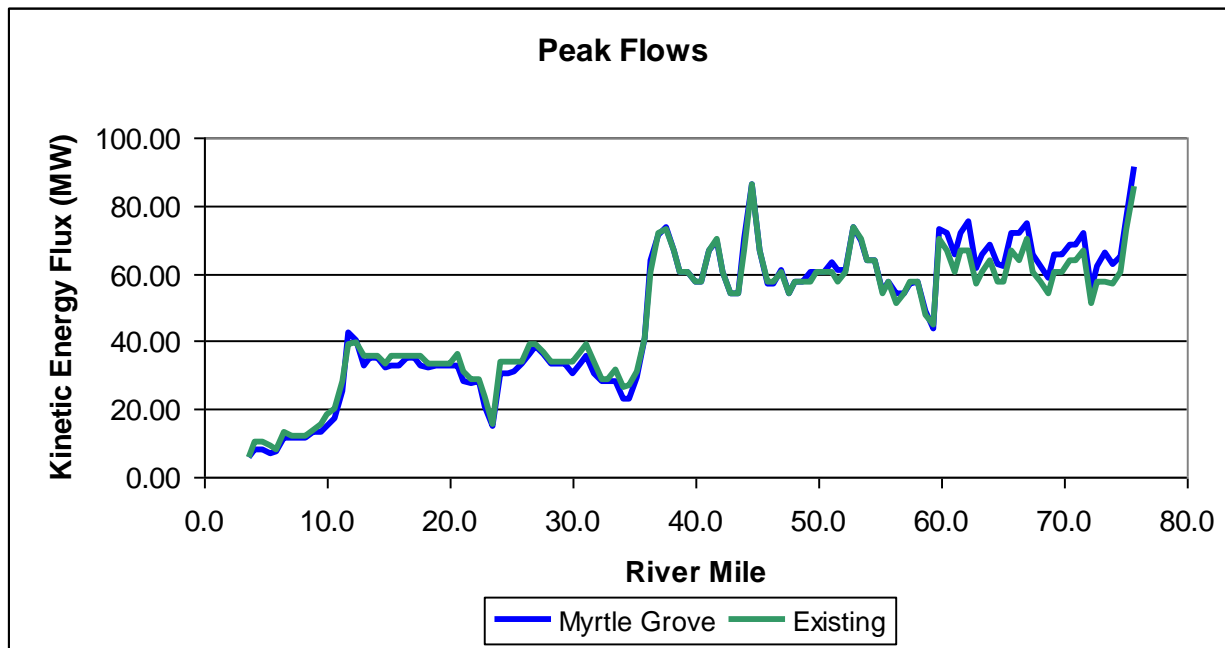


Figure 7.62 – Existing Outflows + Myrtle Grove (RM 59, RK 94) – Main Channel Kinetic Energy Flux of the Flow at Peak Flows

Figure 7.63 and Figure 7.64 show the sand load and the sand concentration profiles at peak flows. In this case, the effect of the new diversion is more evident. Basically, the introduction of the diversion leads to an increase of the sediment transport upstream of the diversion and a reduction of the transport in the lower 35 miles of the domain. The upstream increase is due to the increase in the total energy gradient and a small increase in the currents. The downstream reduction may be the result of a lower flow, reduced energy gradient and reduced shear stress.

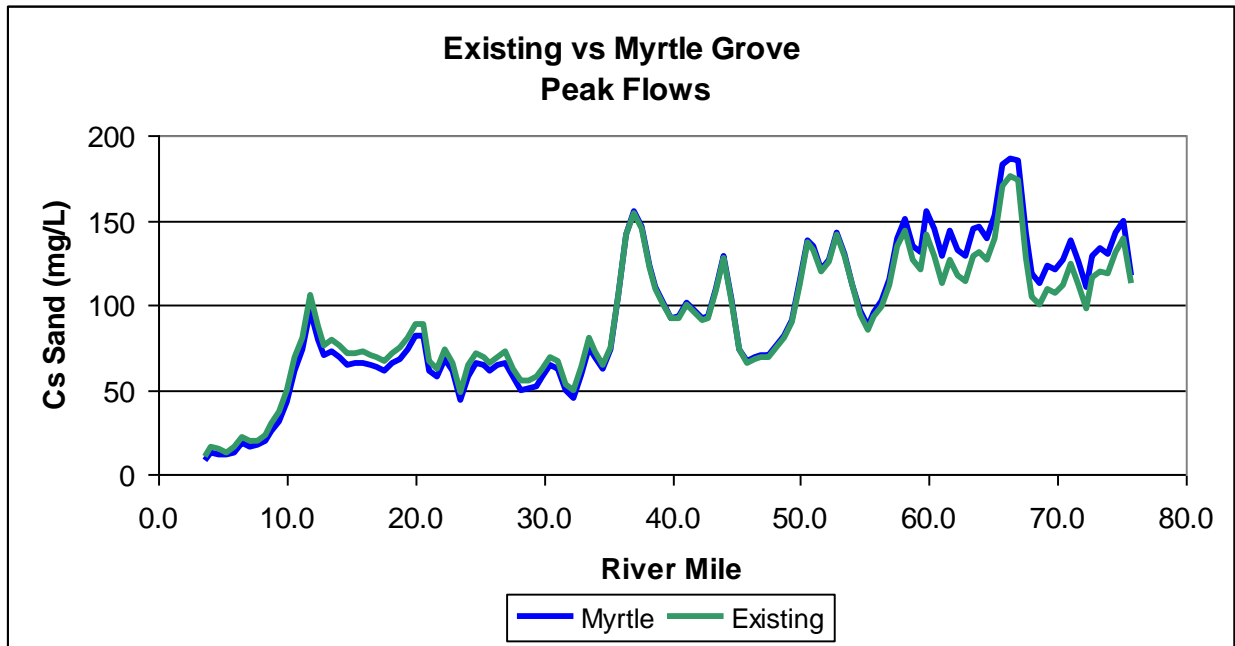


Figure 7.63 – Existing Outflows + Myrtle Grove (RM 59, RK 94) – Main Channel Suspended Sand Concentration at Peak Flows

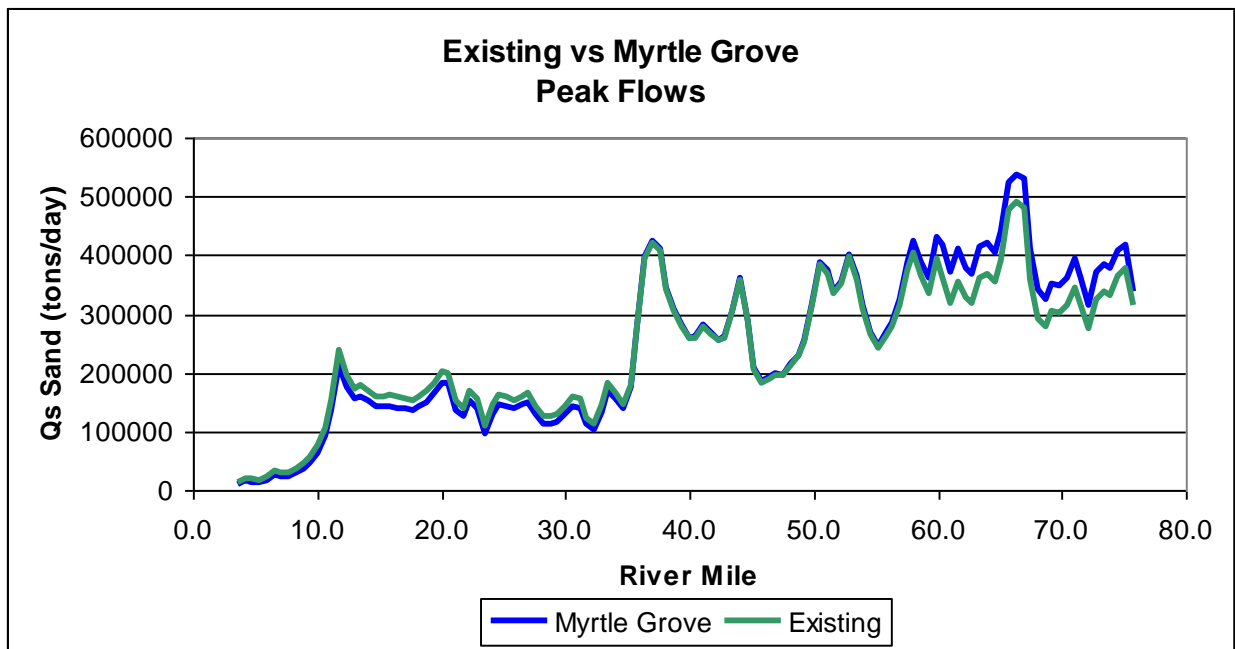


Figure 7.64 – Existing Outflows + Myrtle Grove (RM 59, RK 94) – Main Channel Suspended Sand Load at Peak Flows

Figure 7.65 and Figure 7.66 show the total and the kinetic energy profiles for the main channel at intermediate flows with and without the introduction of the Myrtle Grove diversion. As seen for peak flows, the introduction of this diversion does not greatly change either the kinetic energy or the total energy lines.

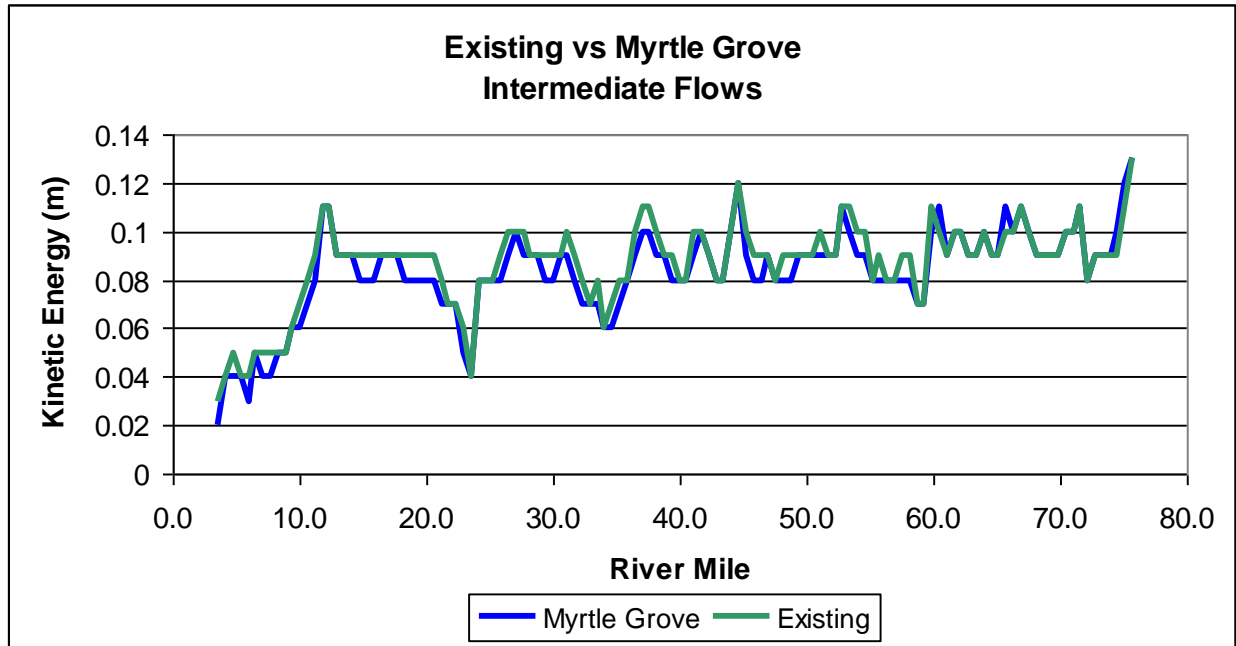


Figure 7.65 – Existing Outflows + Myrtle Grove (RM 59, RK 94) – Main Channel Kinetic Energy of the Flow at Intermediate Flows

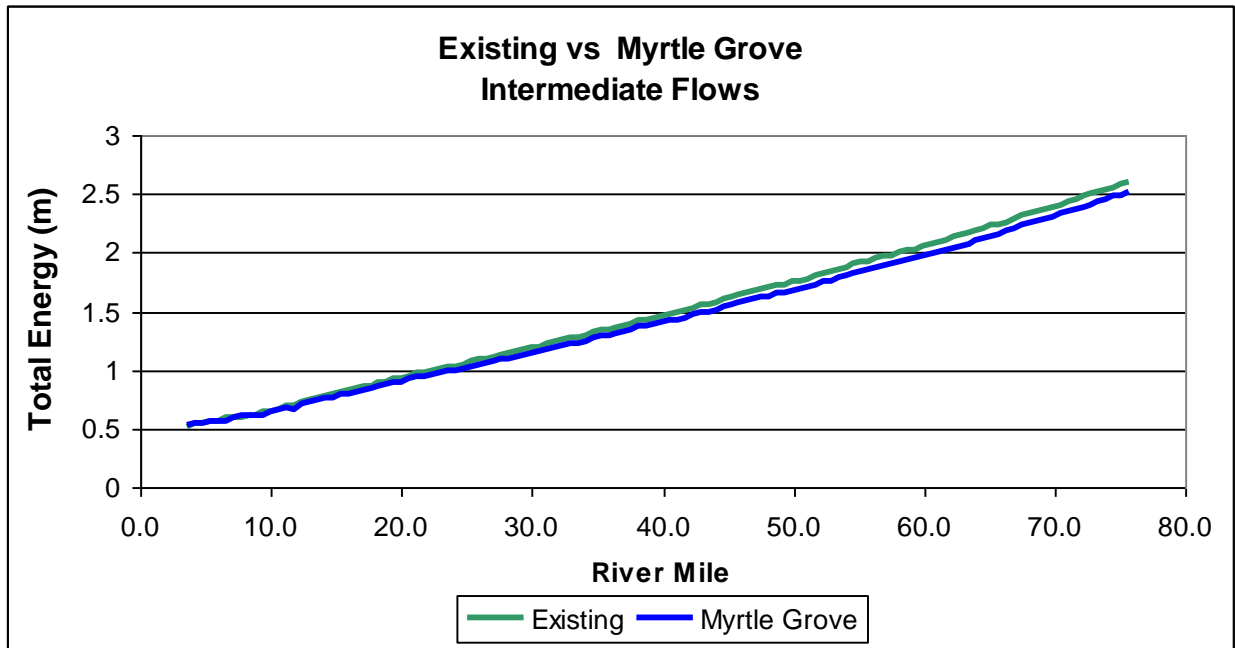


Figure 7.66 – Existing Outflows + Myrtle Grove (RM 59, RK 94) – Main Channel Total Energy of the Flow at Intermediate Flows

Figure 7.67, Figure 7.68 and Figure 7.69 show respectively, the main channel total, potential and kinetic energy fluxes under intermediate flow conditions for the Myrtle Grove test.

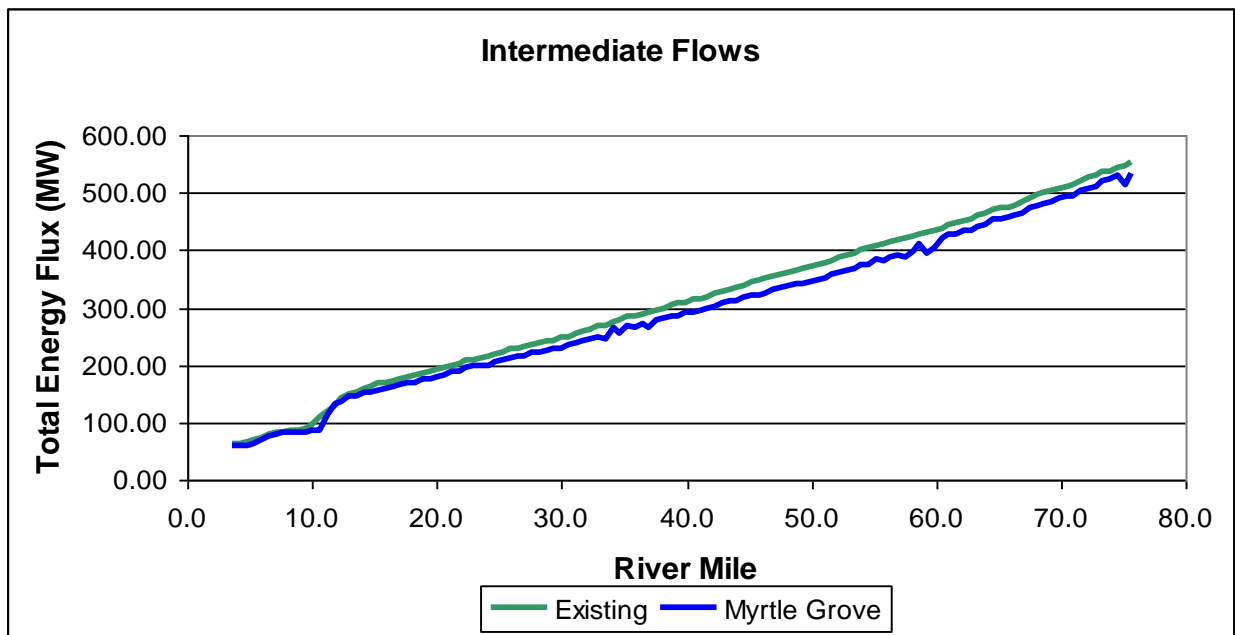


Figure 7.67 – Existing Outflows + Myrtle Grove (RM 59, RK 94) – Main Channel Total Energy Flux of the Flow at Intermediate Flows

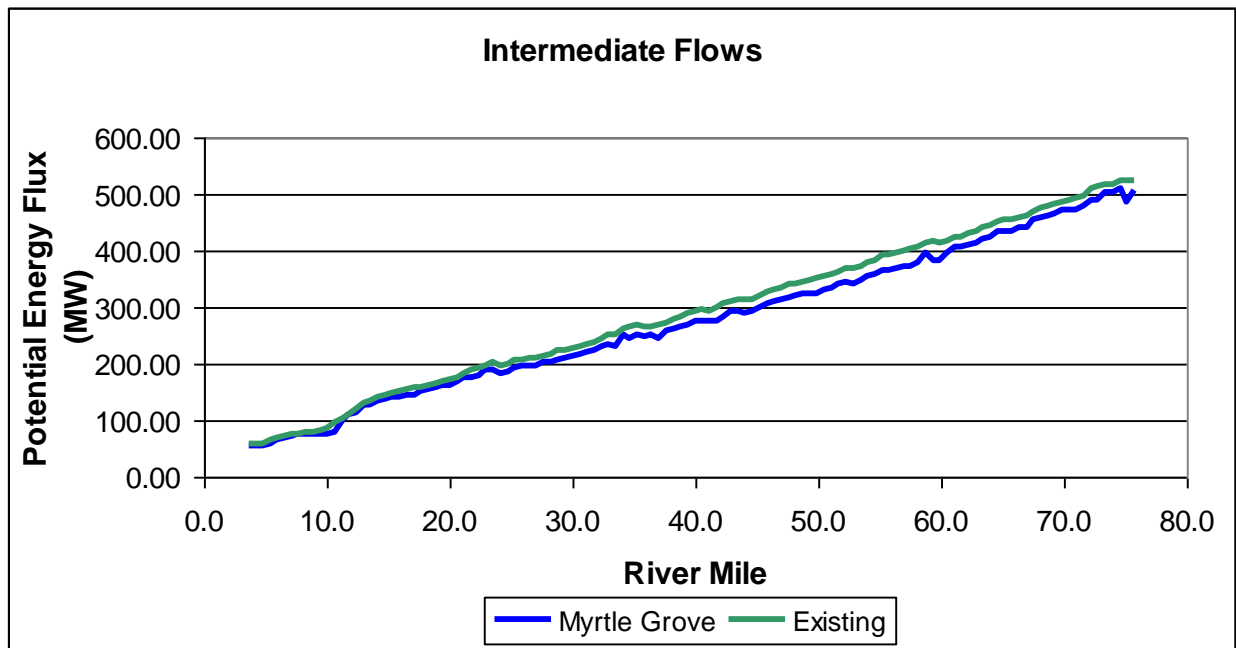


Figure 7.68 – Existing Outflows + Myrtle Grove (RM 59, RK 94) – Main Channel Potential Energy Flux of the Flow at Intermediate Flows

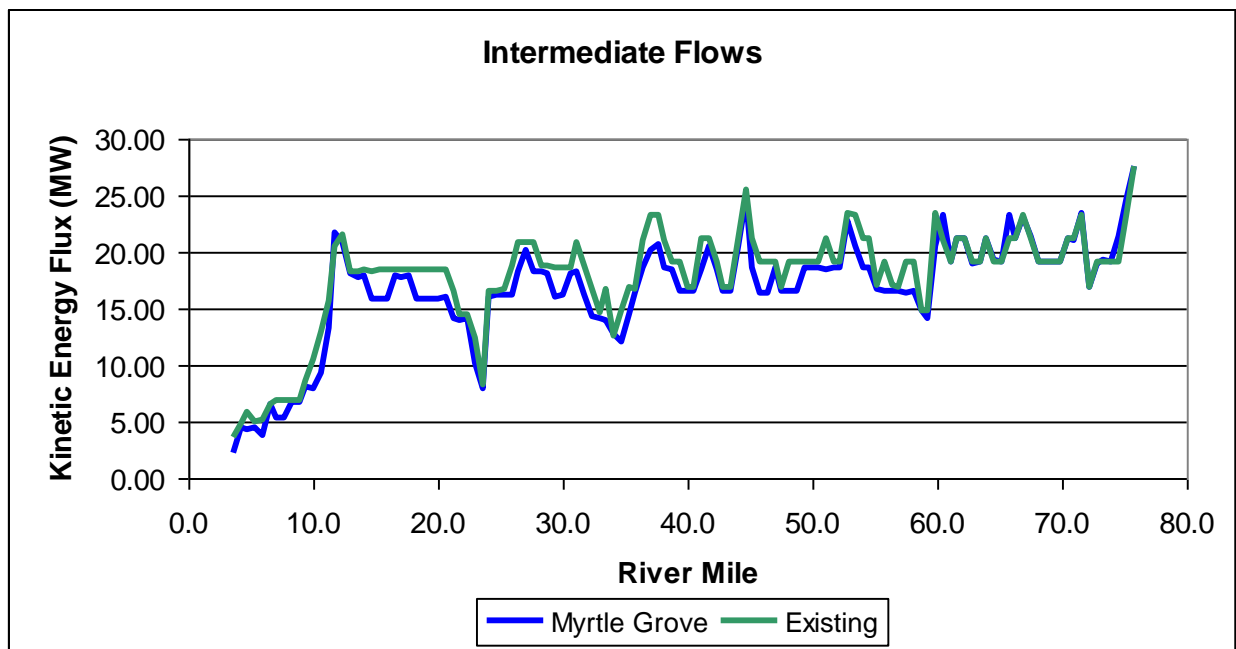


Figure 7.69 – Existing Outflows + Myrtle Grove (RM 59, RK 94) – Main Channel Kinetic Energy Flux of the Flow at Intermediate Flows

Figure 7.70 and Figure 7.71 show the sand load and the sand concentration profiles at intermediate flows. The introduction of the diversion leads to a slight increase of the sediment transport upstream of the diversion and a slight reduction of the transport in the lower 35 miles of the domain. As stated before, the upstream increase is due to the increase in the total energy gradient and a small increase in the currents. The downstream reduction may be the result of a lower flow and reduced shear stress.

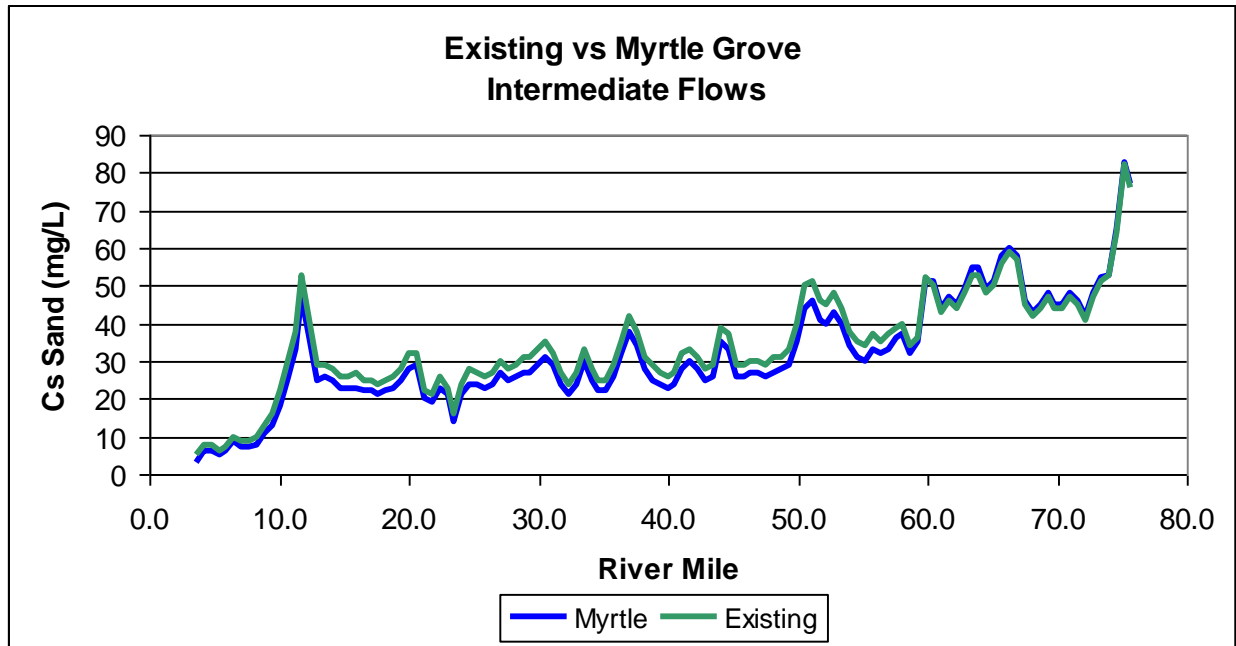


Figure 7.70 – Existing Outflows + Myrtle Grove (RM 59, RK 94) – Main Channel Suspended Sand Concentration at Intermediate Flows

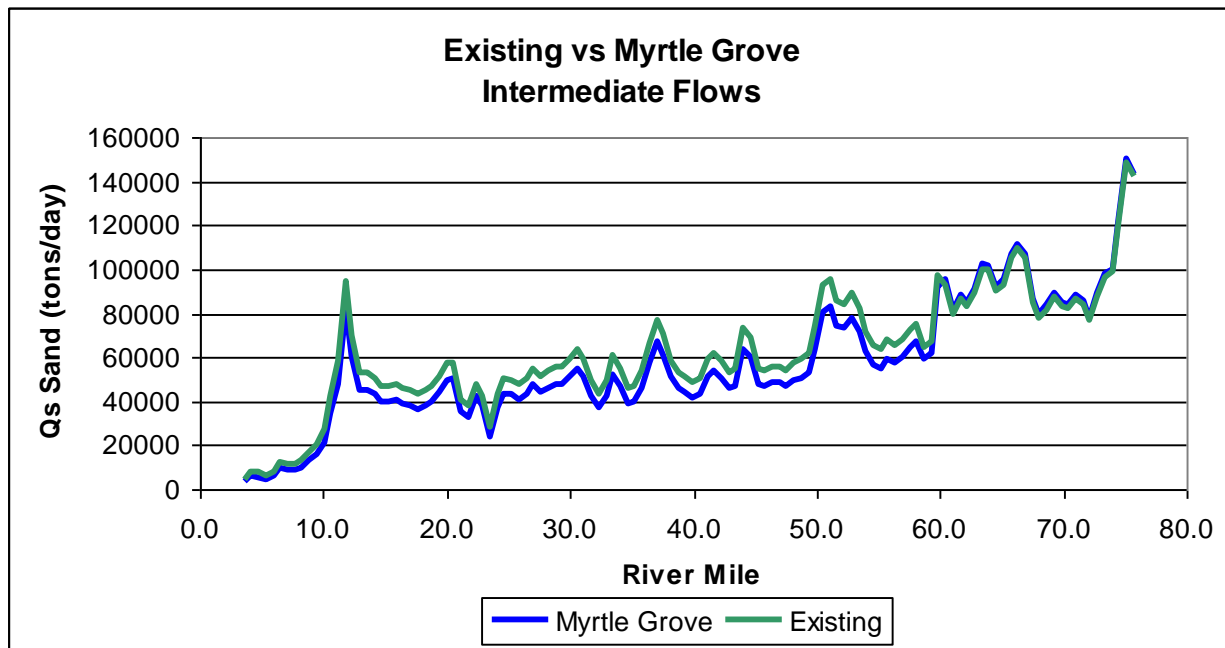
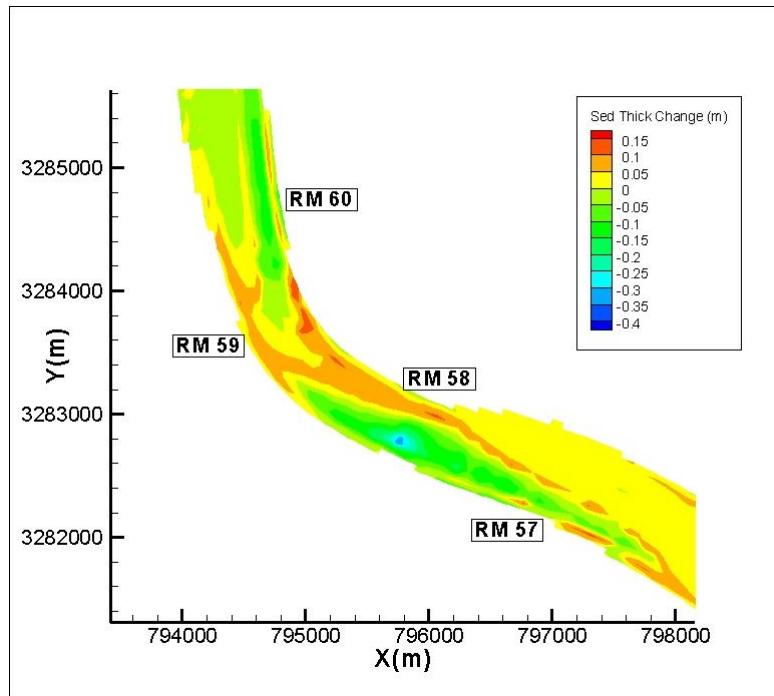
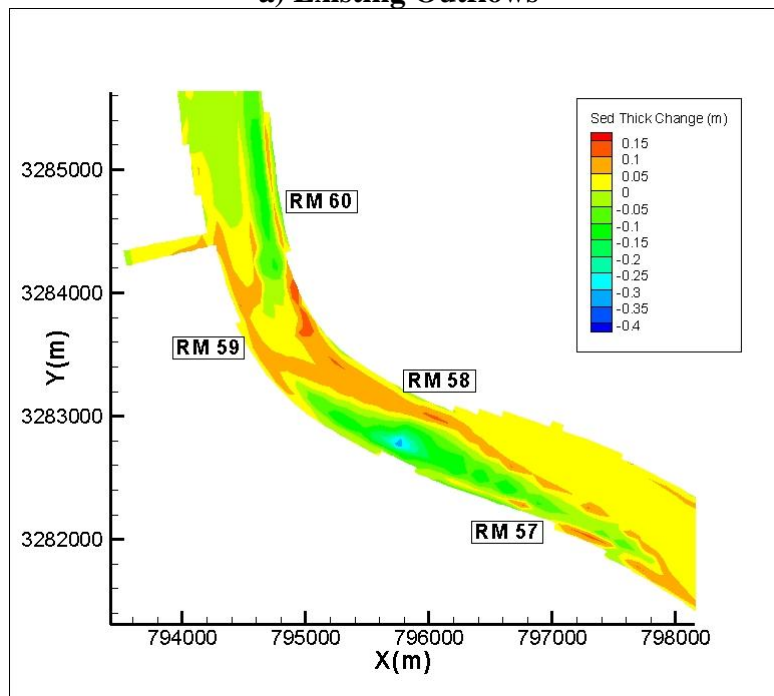


Figure 7.71 – Existing Outflows + Myrtle Grove (RM 59, RK 94) – Main Channel Sand Load at Intermediate Flows

The bed sediment thickness change after 1 day of simulation and 10 days of simulation for the existing diversions and the Myrtle Grove diversion cases at peak flows are presented in Figure 7.72 and Figure 7.73. Once again, the introduction of the 30,000 cfs diversion does not greatly change the erosion/deposition pattern. It is evident however, that there is deposition in the diversion. The diversion channel could be designed to minimize this deposition. The model domain bed sediment change at peak flows is shown in Figure 7.74 and in Figure 7.75 and it can be seen that the results with (b) and without (a) diversions are very similar.

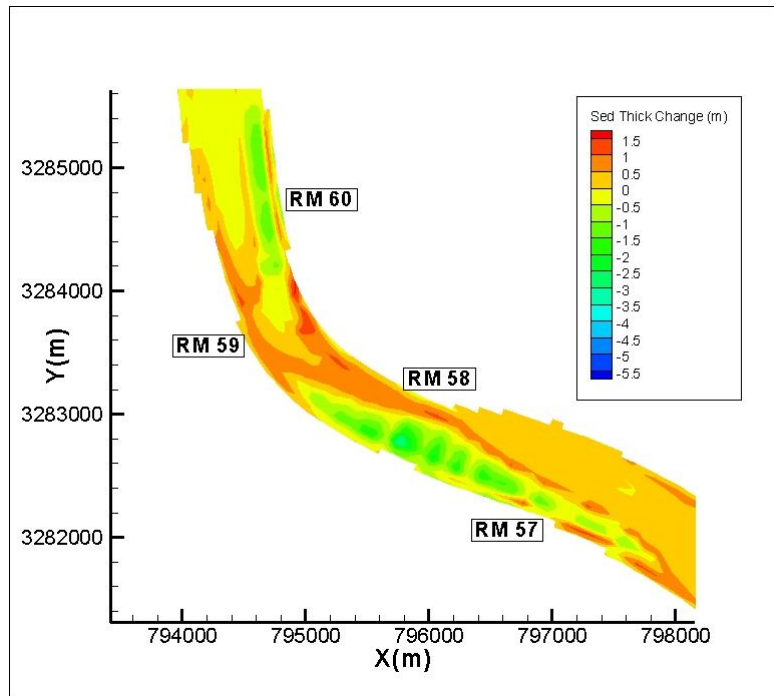


a) Existing Outflows

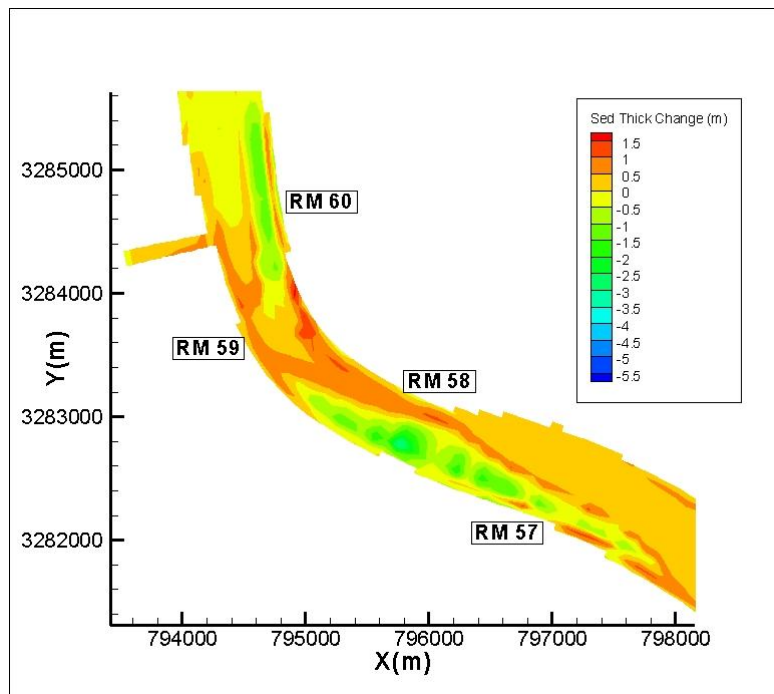


b) Myrtle Grove (RM 59, RK 94) + Existing Outflows

Figure 7.72 – Myrtle Grove Area (RM 59) - Bed Sediment Thickness Change after 1 day at Peak Flows. Positive values indicate deposition and negative values indicate erosion

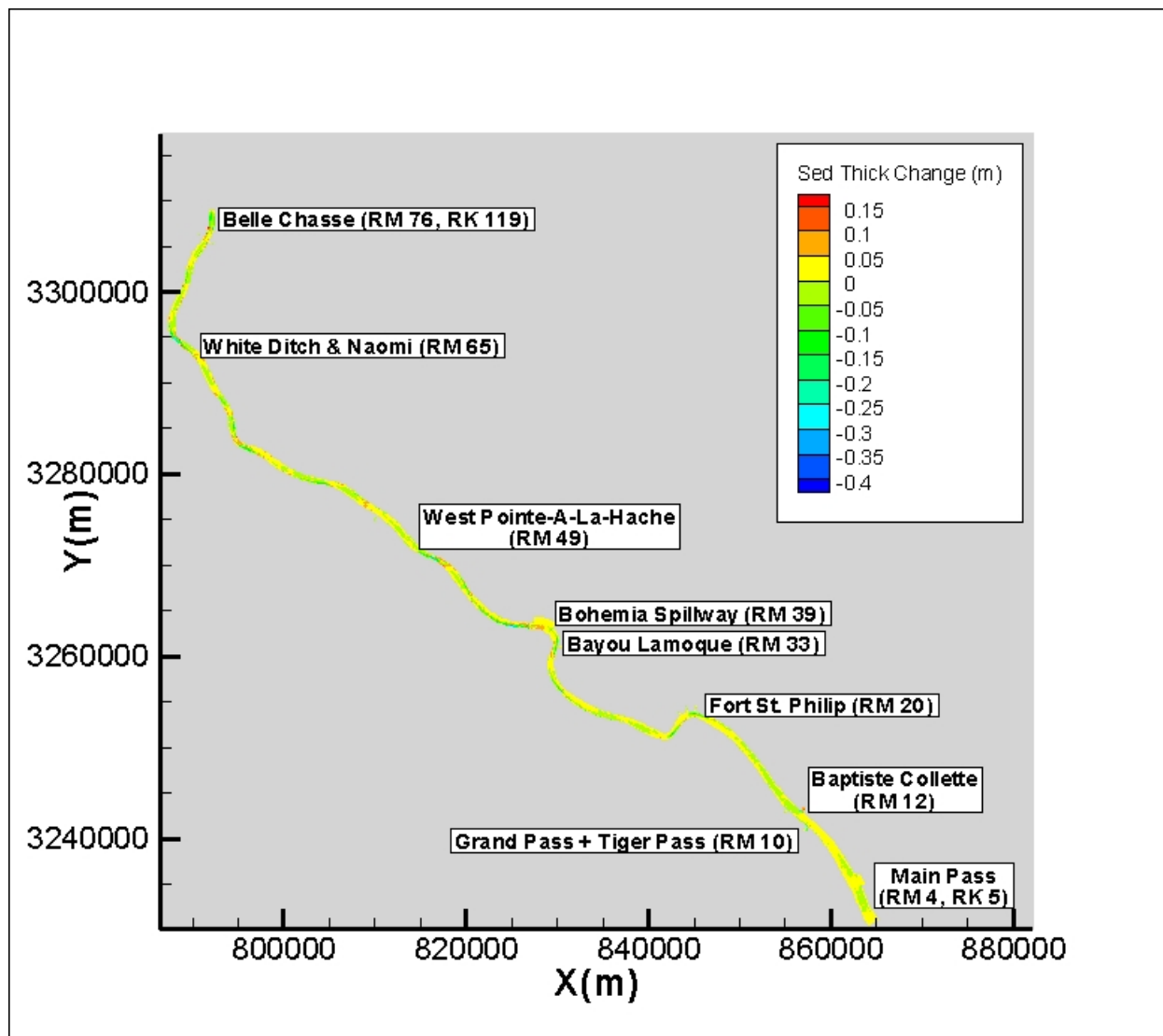


a) Existing Outflows

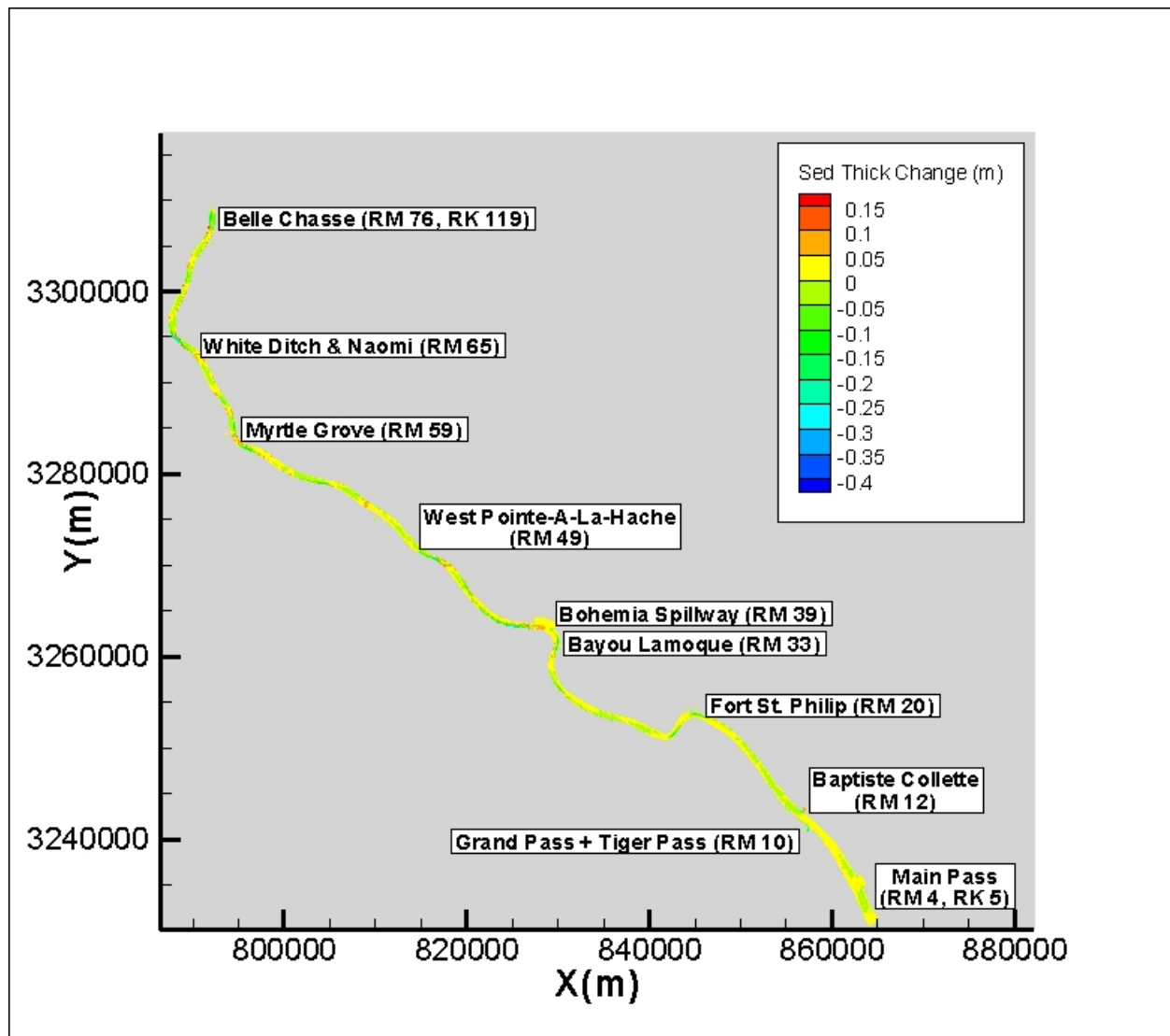


b) Myrtle Grove Myrtle Grove (RM 59, RK 94) + Existing Outflows

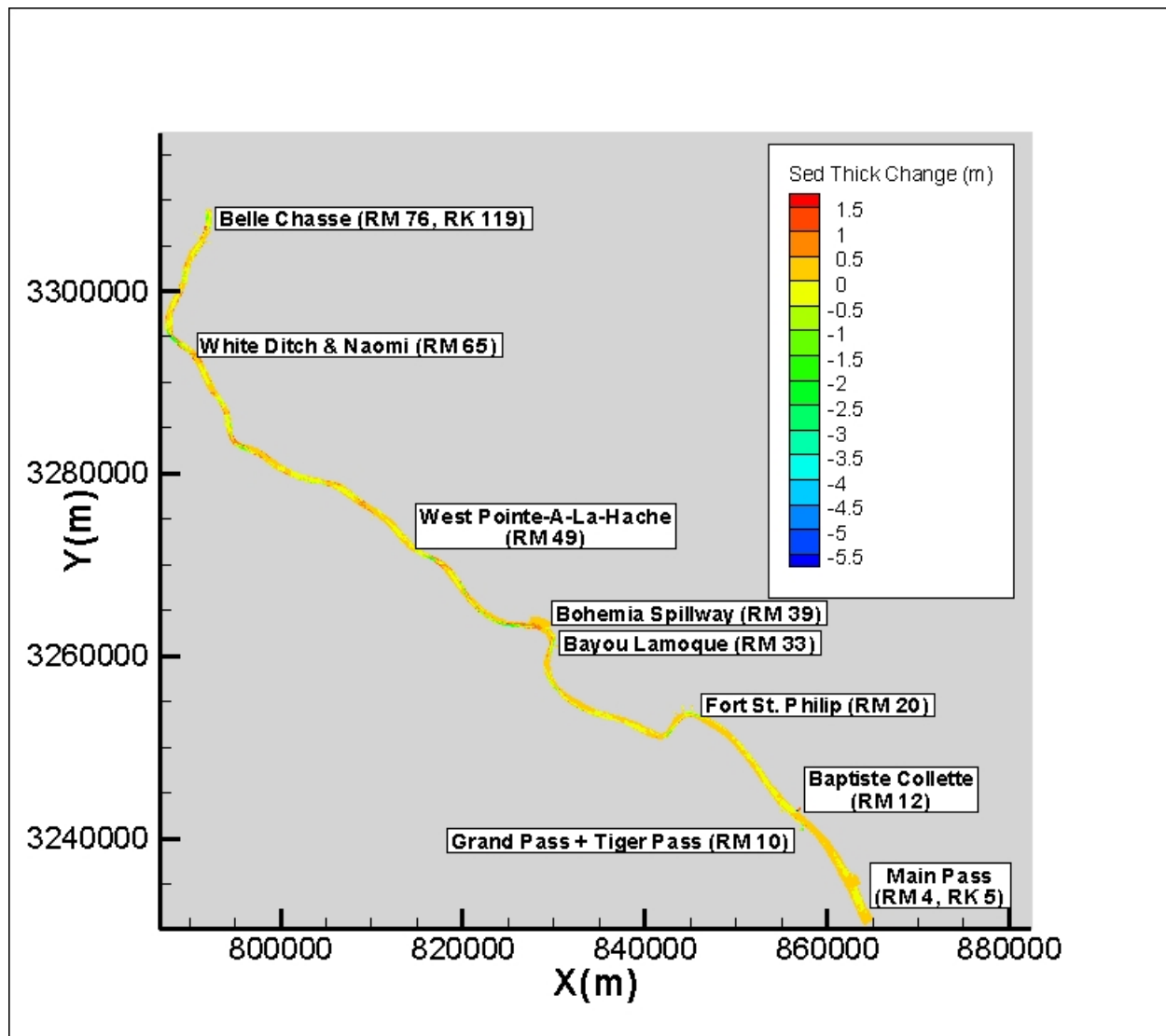
Figure 7.73 – Myrtle Grove Area (RM 59, RK 94) - Bed Sediment Thickness Change after 10 days at Peak Flows. Positive values indicate deposition and negative values indicate erosion



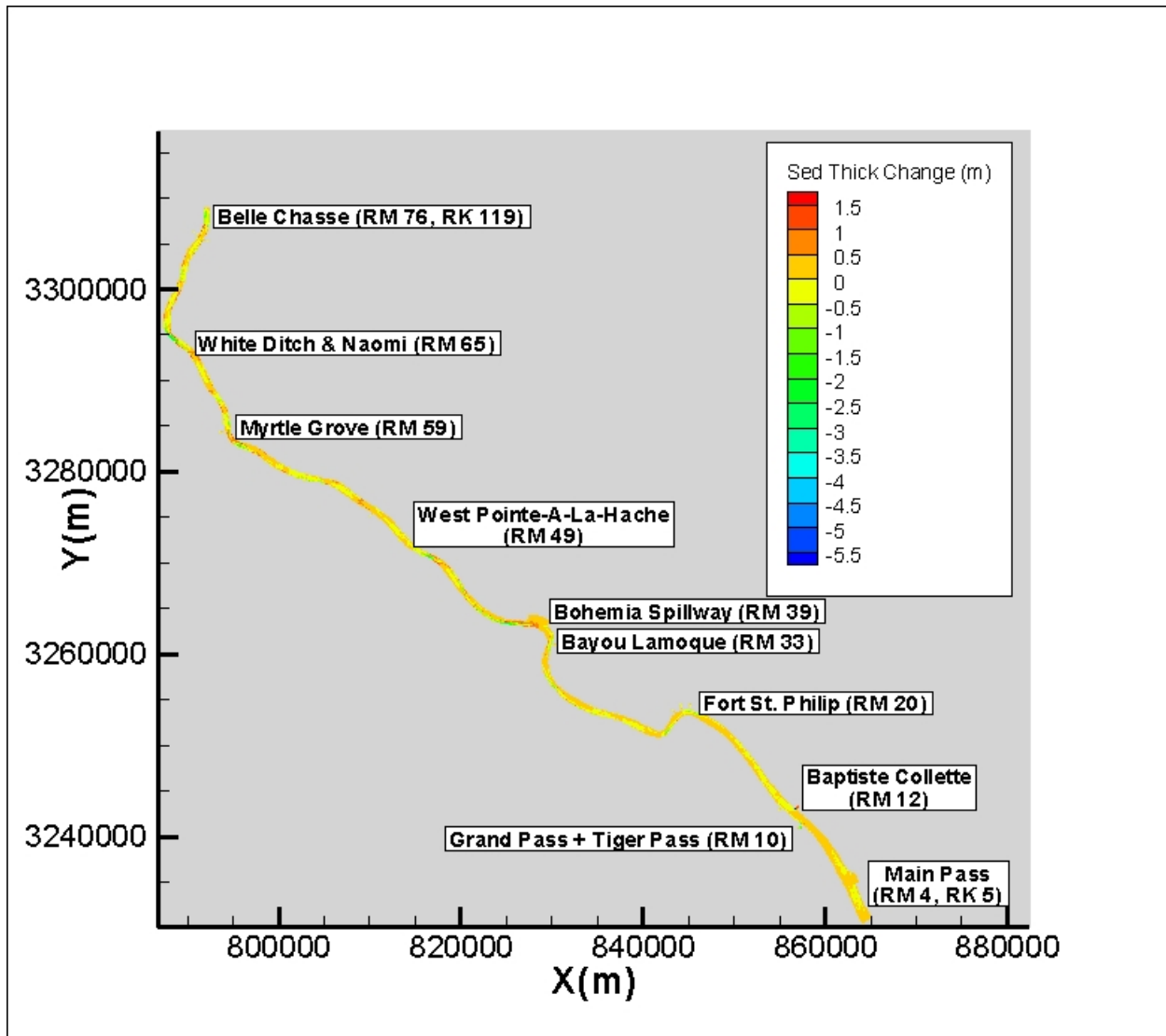
a) Existing Outflows



b) Myrtle Grove Myrtle Grove (RM 59, RK 94) + Existing Outflows
 Figure 7.74 – Model Domain - Bed Sediment Thickness Change after 1 day at Peak Flows.
 Positive values indicate deposition and negative values indicate erosion



a) Existing Outflows



b) Myrtle Grove Myrtle Grove (RM 59, RK 94) + Existing Outflows
Figure 7.75 – Model Domain - Bed Sediment Thickness Change after 10 days at Peak Flows. Positive values indicate deposition and negative values indicate erosion

Figure 7.76 summarizes the difference between the results obtained with the Existing Outflows and with the Myrtle Grove Diversion Scenario. There is not a very significant difference between the two results and there are no visible areas of significant difference in erosion.

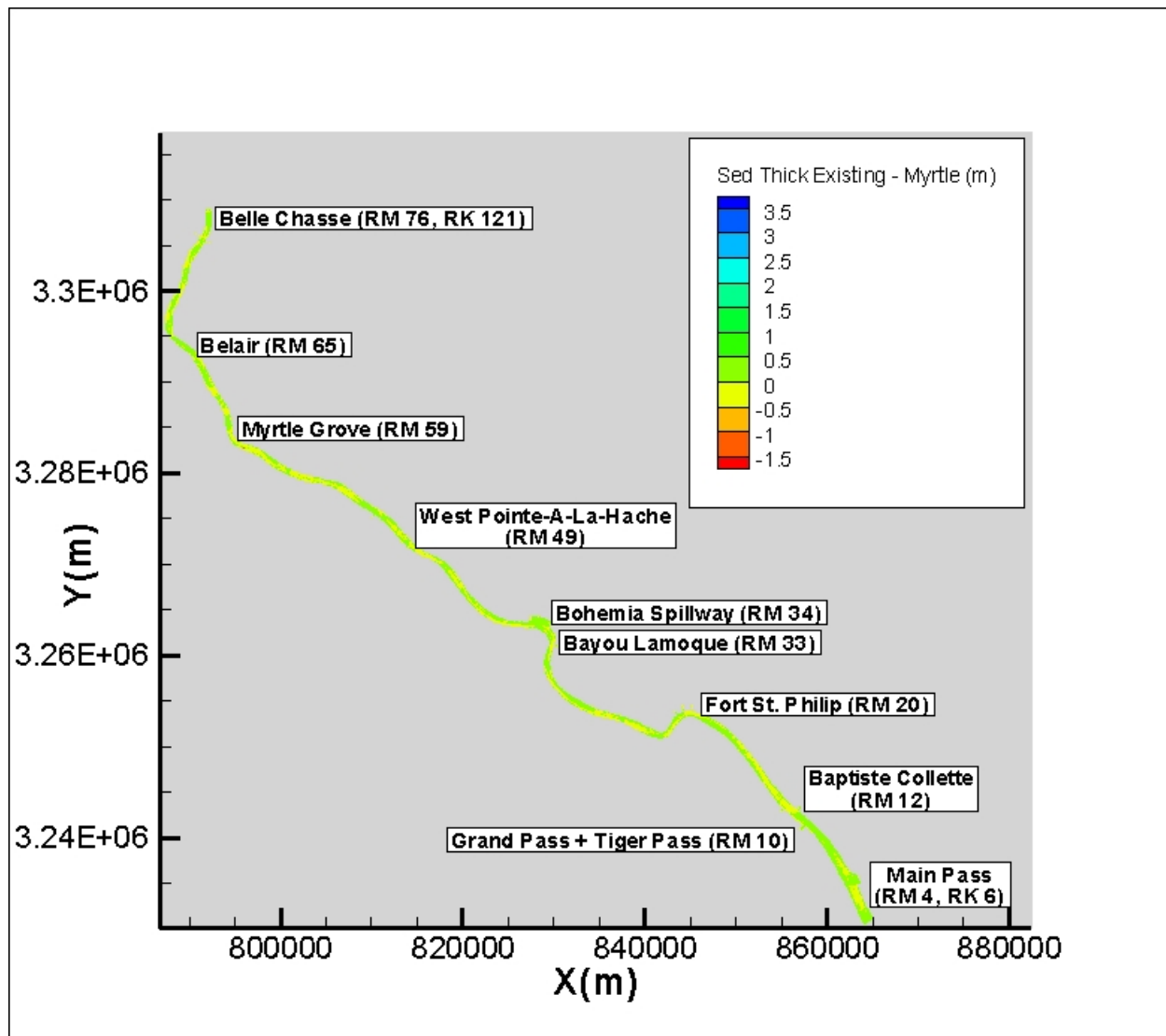
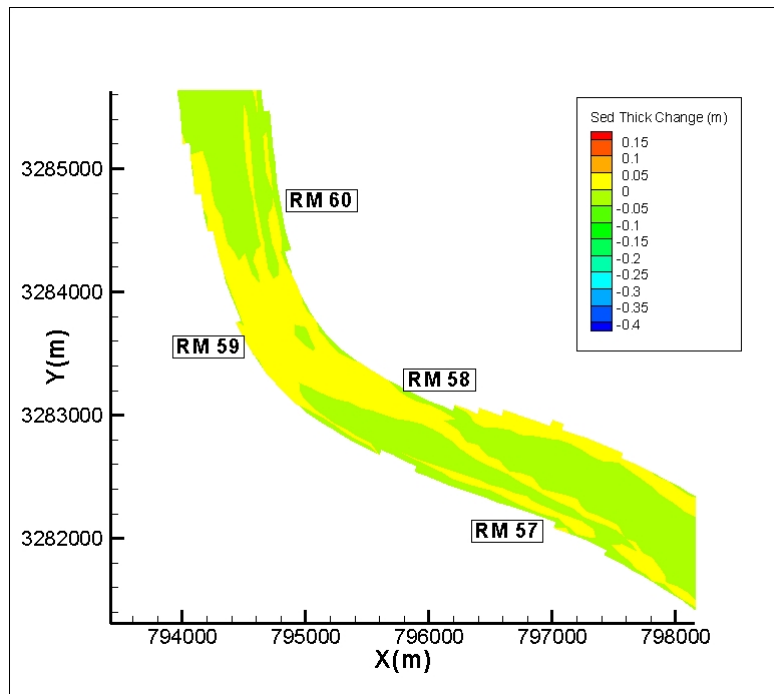
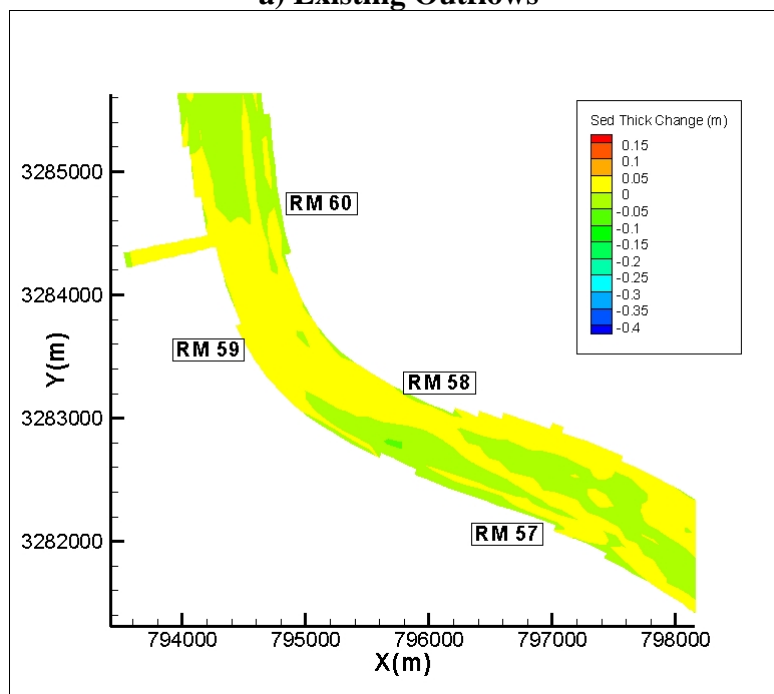


Figure 7.76 – Model Domain – Difference between Existing and Myrtle Grove Test Bed Sediment Thickness Change after 10 days at Peak Flows. Positive values indicate that the addition of the Myrtle Grove Diversion increased deposition. Negative values indicate that the addition of the Myrtle Grove Diversion Myrtle Grove (RM 59, RK 94) increased erosion

The bed sediment thickness change after 1 day and after 10 days of simulation for the existing diversions and the Myrtle Grove diversion cases at intermediate flows are presented respectively in Figure 7.77 and Figure 7.78. Once again, the introduction of the diversion does not greatly change the erosion/deposition pattern. It is evident however, that there is some deposition in the diversion and downstream of it. The model domain bed sediment change at intermediate flows is shown in Figure 7.79 and Figure 7.80. It can be seen that the results with (b) and without (a) diversions are very similar.

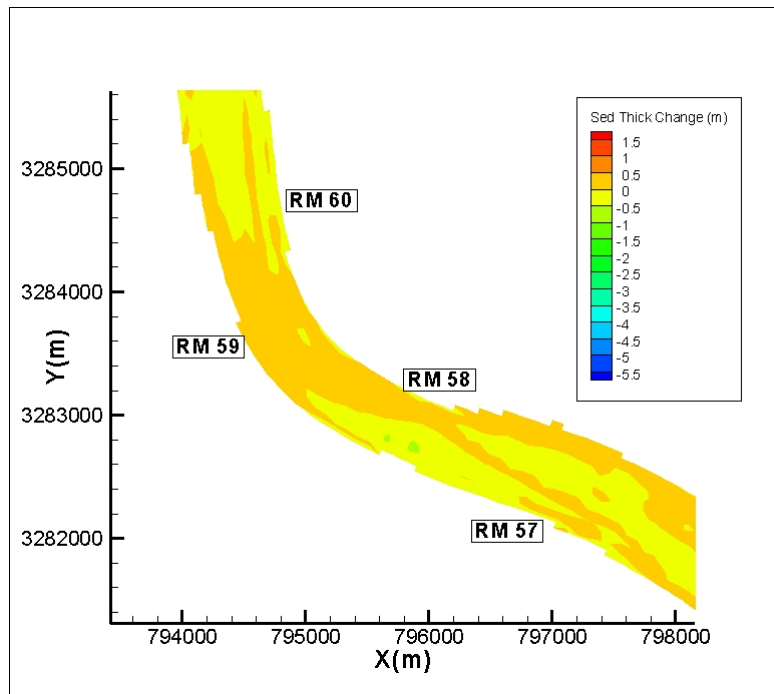


a) Existing Outflows

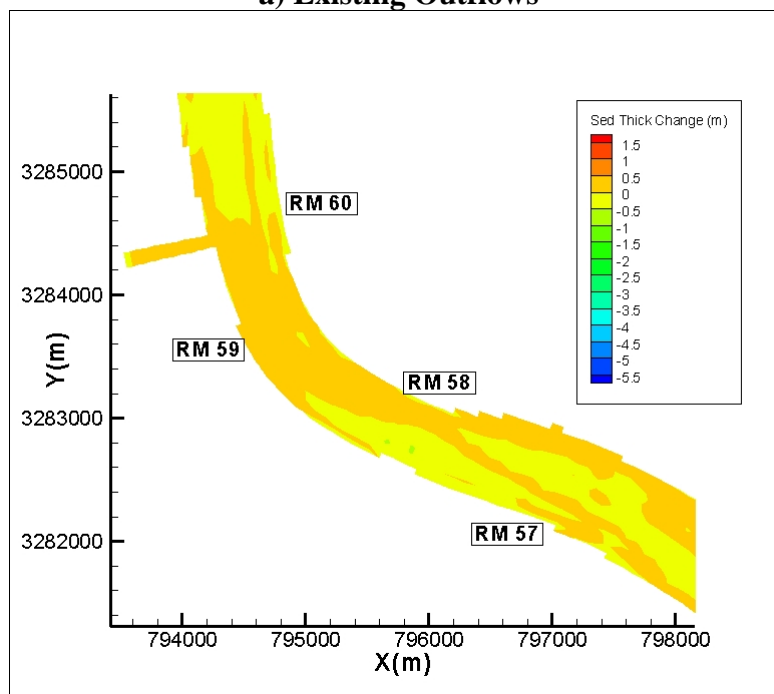


b) Myrtle Grove (RM 59, RK 94) + Existing Outflows

Figure 7.77 – Myrtle Grove Area (RM 59, RK 94) - Bed Sediment Thickness Change after 1 day at Intermediate Flows. Positive values indicate deposition and negative values indicate erosion



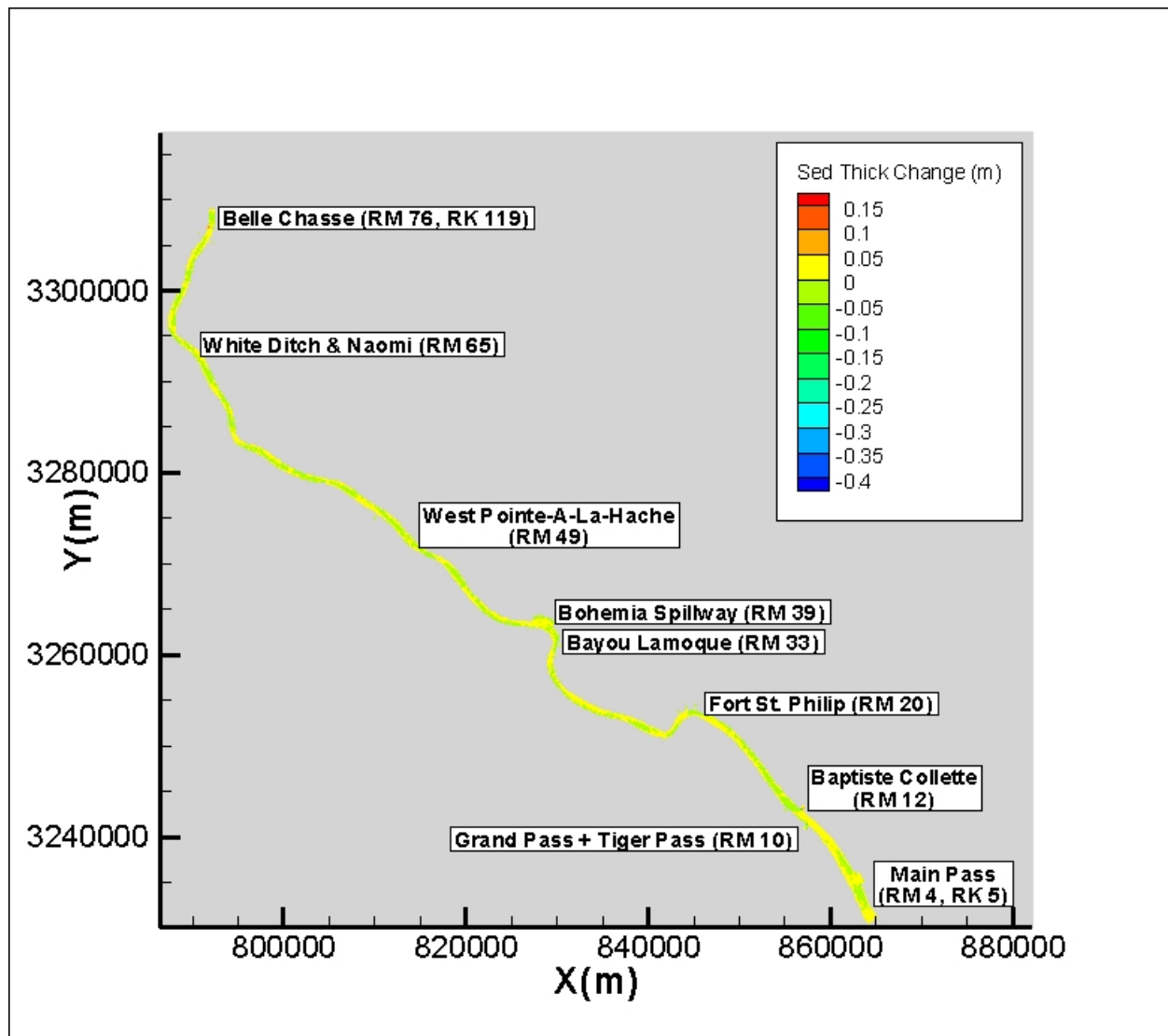
a) Existing Outflows



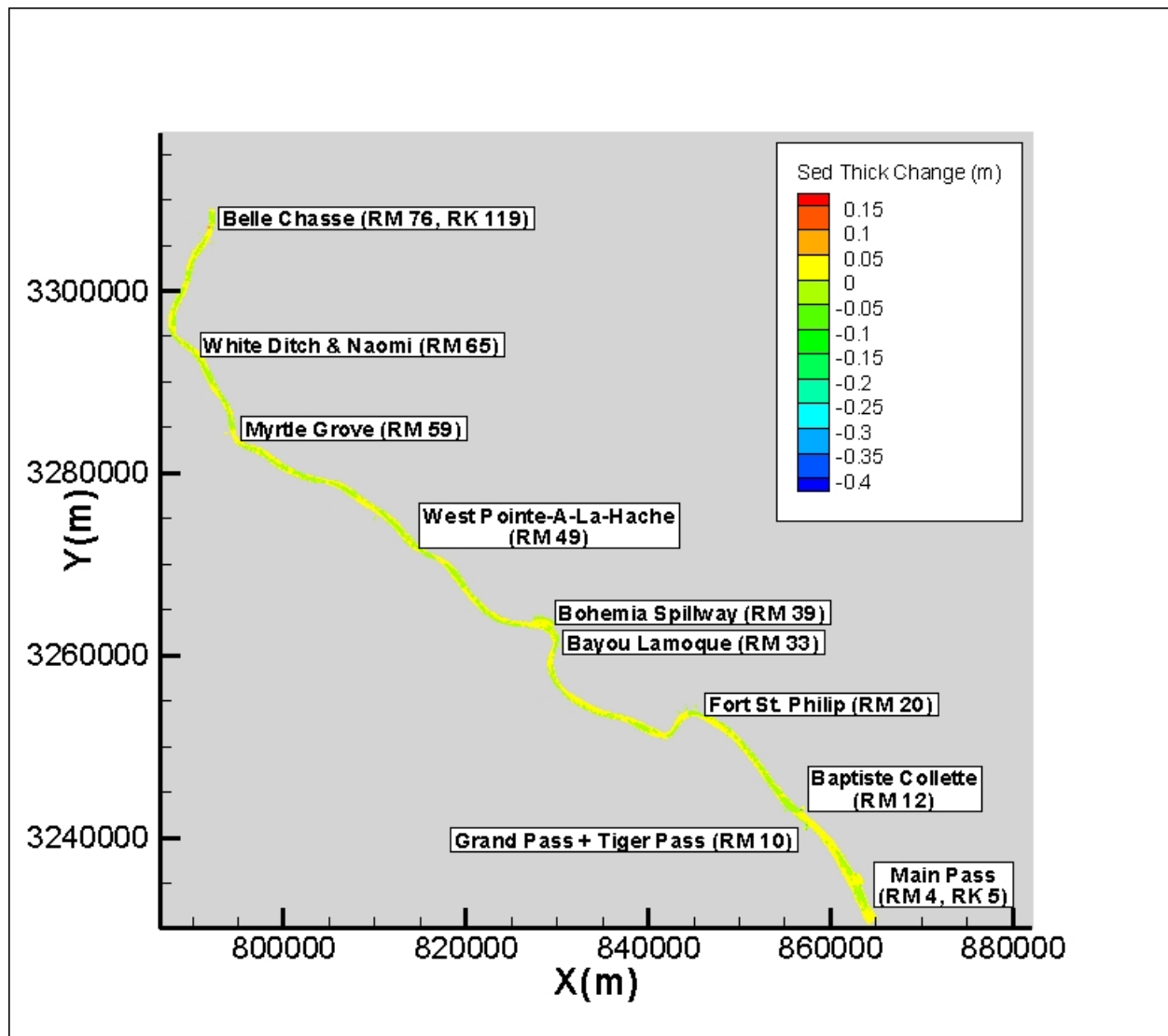
b) Myrtle Grove (RM 59, RK 94) + Existing Outflows

Figure 7.78 – Myrtle Grove Area (RM 59, RK 94) - Bed Sediment Thickness Change after 10 days at Intermediate Flows. Positive values indicate deposition and negative values indicate erosion

The estimated amount of sediment being extracted at each outflow for the Myrtle Grove Test is shown in Table 7-5. Once again, the 3 largest outflows (Bohemia, Baptiste Collette, Grand Pass+Tiger Pass) are the ones that divert the largest amount of sand at peak flows. Similar to the Existing Outflows result, the amount of bed material extracted at Main Pass is very low. This is possibly due to the low energy gradient near the downstream boundary.

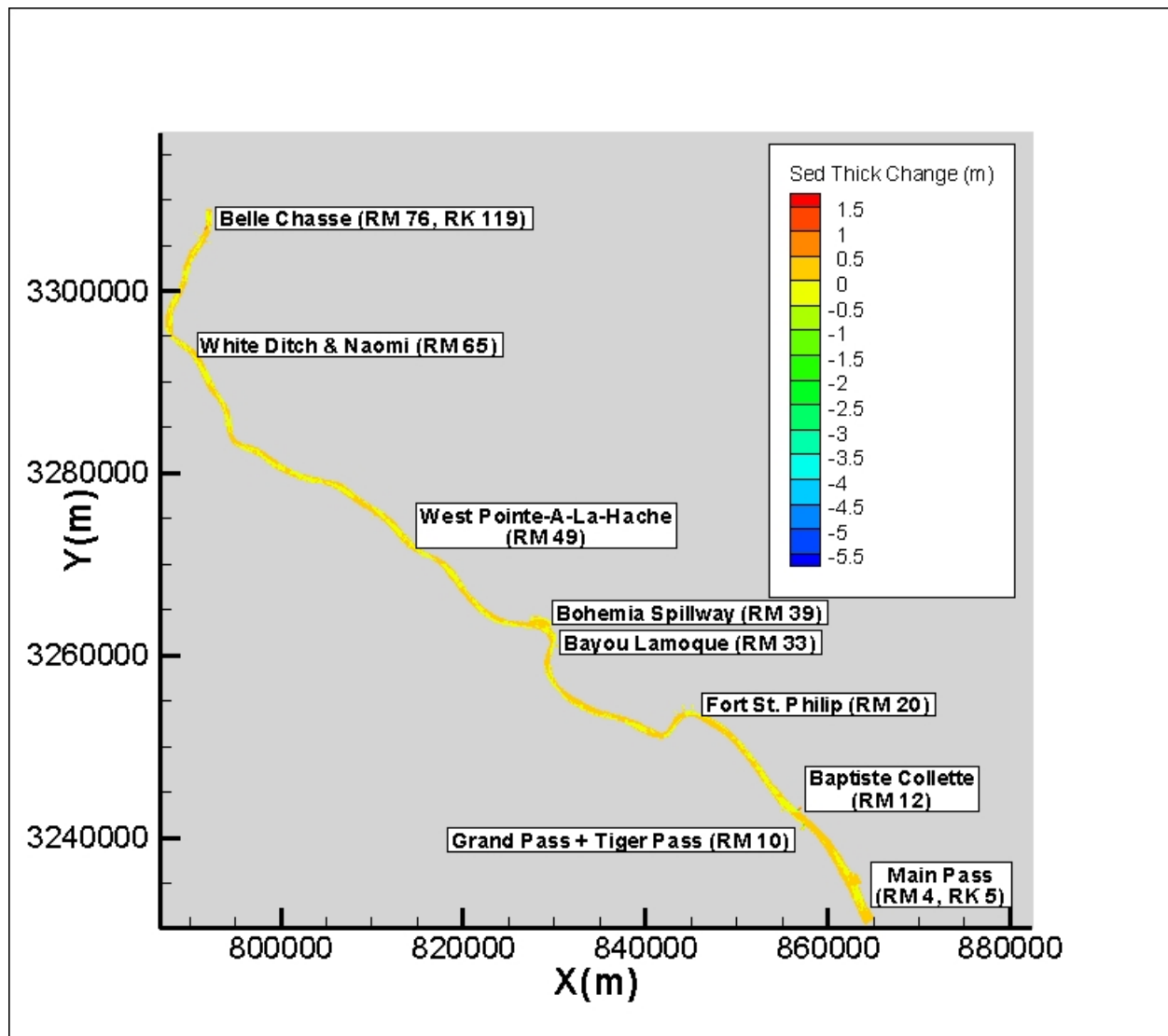


a) Existing Outflows

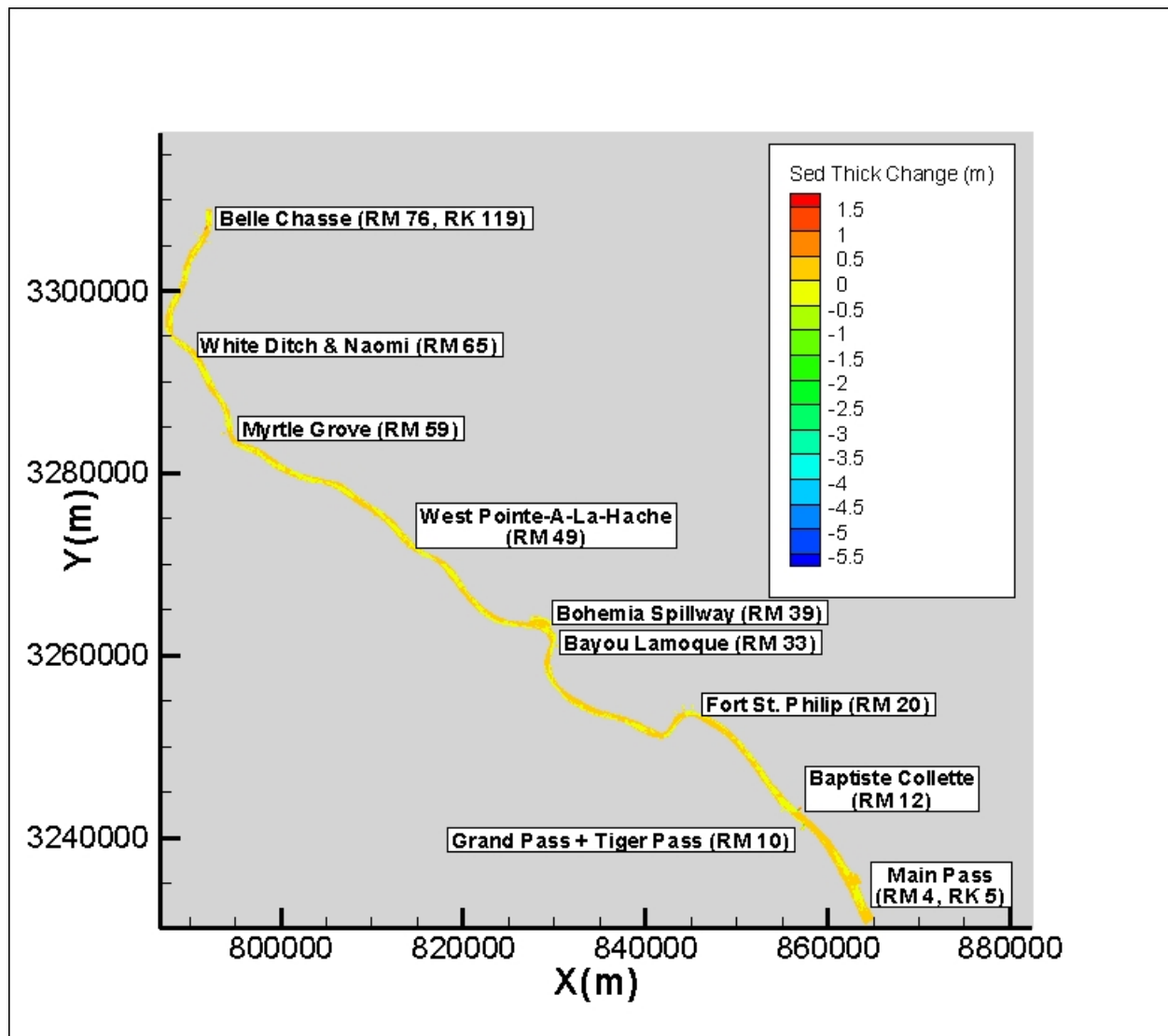


b) Myrtle Grove (RM 59, RK 94) + Existing Outflows

Figure 7.79 – Model Domain - Bed Sediment Thickness Change after 1 day at Intermediate Flows. Positive values indicate deposition and negative values indicate erosion



a) Existing Outflows



b) Myrtle Grove (RM 59, RK 94) + Existing Outflows

Figure 7.80 – Model Domain - Bed Sediment Thickness Change after 10 days at Intermediate Flows. Positive values indicate deposition and negative values indicate erosion

Table 7-5 – Water Discharge, Suspended Sand Concentration and Suspended Sand Load at Outflows – Myrtle Grove Myrtle Grove (RM 59, RK 94) Case Study

Site	Peak Flows			Intermediate Flows		
	Q (m ³ /s)	Cs (mg/L)	Qs (metric tons/day)	Q (m ³ /s)	Cs (mg/L)	Qs (metric tons/day)
Myrtle Grove	841	117	8,533	599	40	2,085
West Pointe-À-La-Hache	27	68	162	19	18	30
Bohemia Spillway	6,424	61	33,884	370	11	364
Bayou Lamoque	85	28	203	66	8	46
Fort St. Philip	613	26	1,375	381	8	248
Baptiste Collette	4,126	120	45,722	3,188	61	16,854
Grand Pass + Tiger Pass	4,262	95	35,004	3,412	50	14,814
Main Pass	3,113	11	2,887	2,337	5	916

Figure 7.81 and Figure 7.82 show respectively the peak flow and the intermediate flow sand concentration at each outflow in graphical form for both the existing and the Myrtle Grove tests. The results with the introduction of the diversion are not very different from the ones with the existing outflows only. There is a slight decrease in the sand concentration downstream of the diversion.

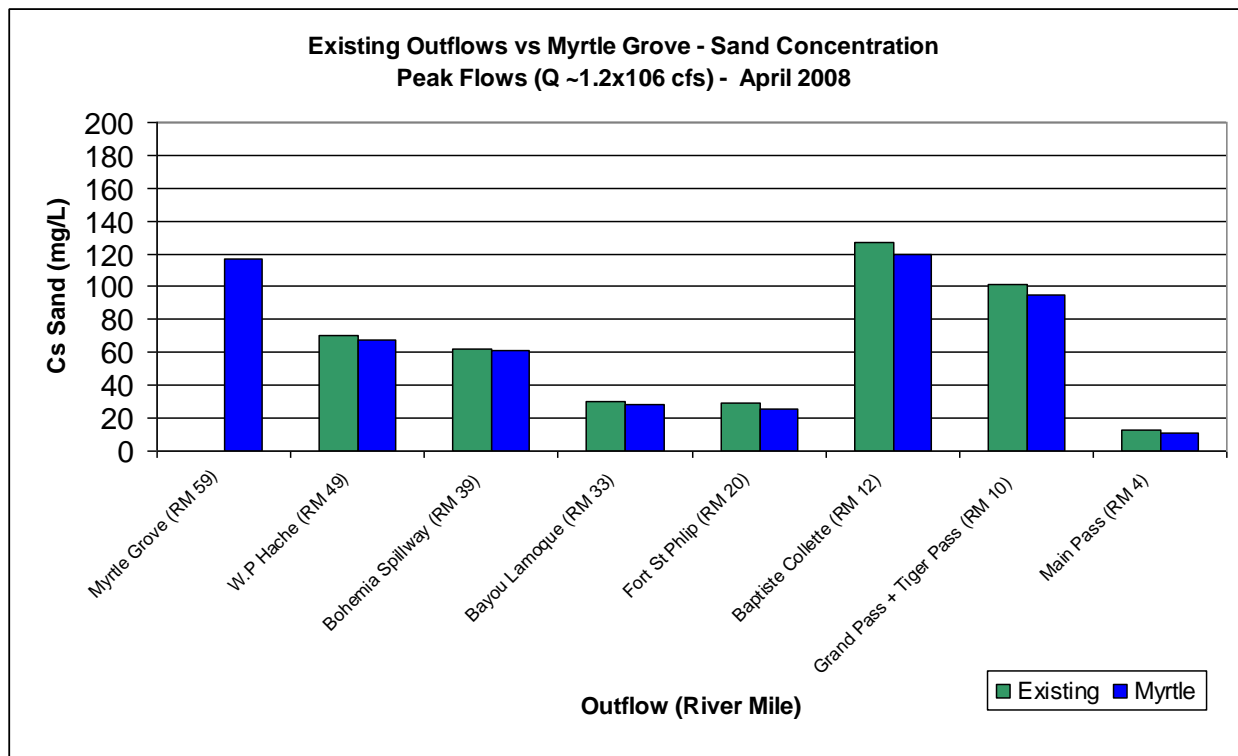


Figure 7.81 – Existing Outflows + Myrtle Grove (RM 59, RK 94) – Outflow Suspended Sand Concentrations at Peak Flows

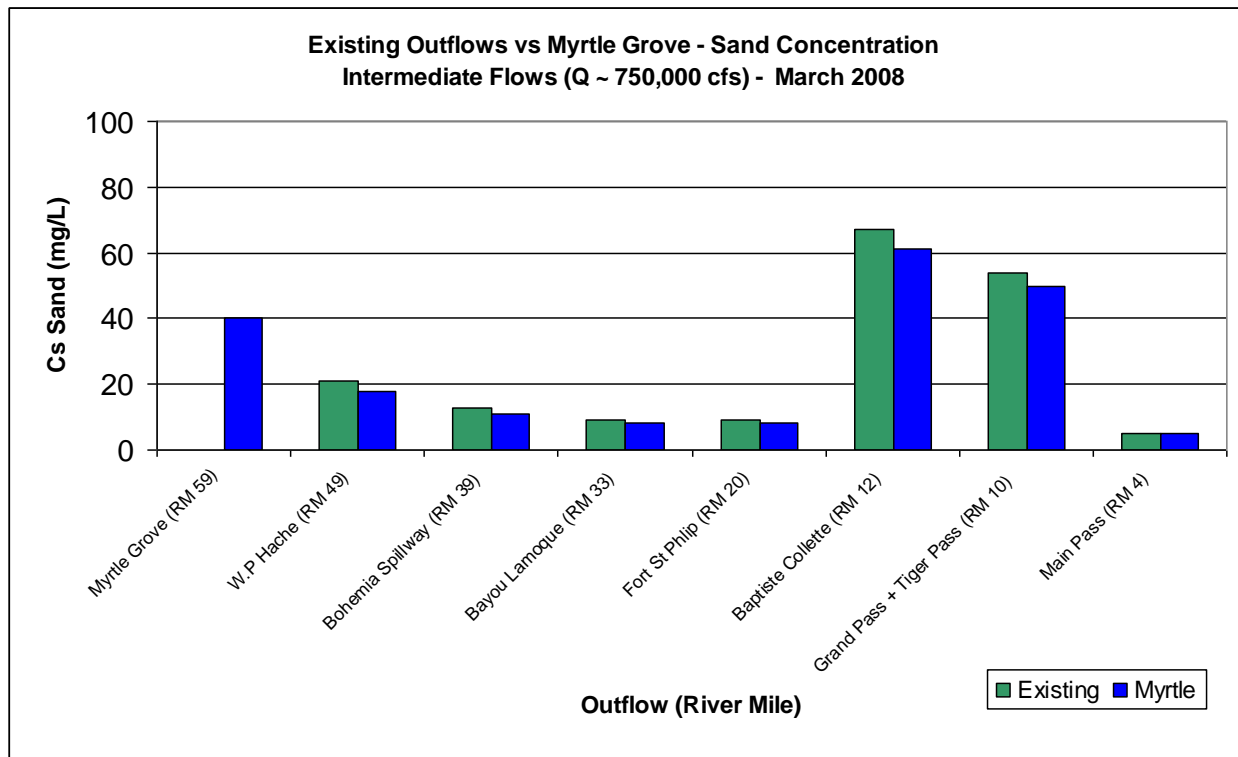


Figure 7.82 – Existing Outflows + Myrtle Grove (RM 59, RK 94) – Outflow Suspended Sand Concentrations at Intermediate Flows

7.4 Belair + Existing Outflows

The second proposed diversion test consisted of the introduction of an East Bank diversion at Belair (RM 65). In this case, the diversion is located downstream of a meander as shown in Figure 7.83. The diversion was included in the model by activating 13 rows of cells, corresponding to a width of around 1.3 km. The depth of the implemented diversion varies linearly from 10 m at the main channel entrance to 2 m at the external boundary.

Simulations were performed for Peak Flow conditions with an extracted water flow of about 200,000 cfs (5,700 m³/s) and for Intermediate Flow conditions with an outflow of about 80,000 cfs (2,300 m³/s), corresponding to the outflows obtained with CHARIMA and the target flow proposed for the diversion in the MLODS (Lopez and LPBF, 2008). Suspended sand concentrations of 40 mg/L and of 30 mg/L were given as boundary condition respectively for Peak and Intermediate Flow conditions.

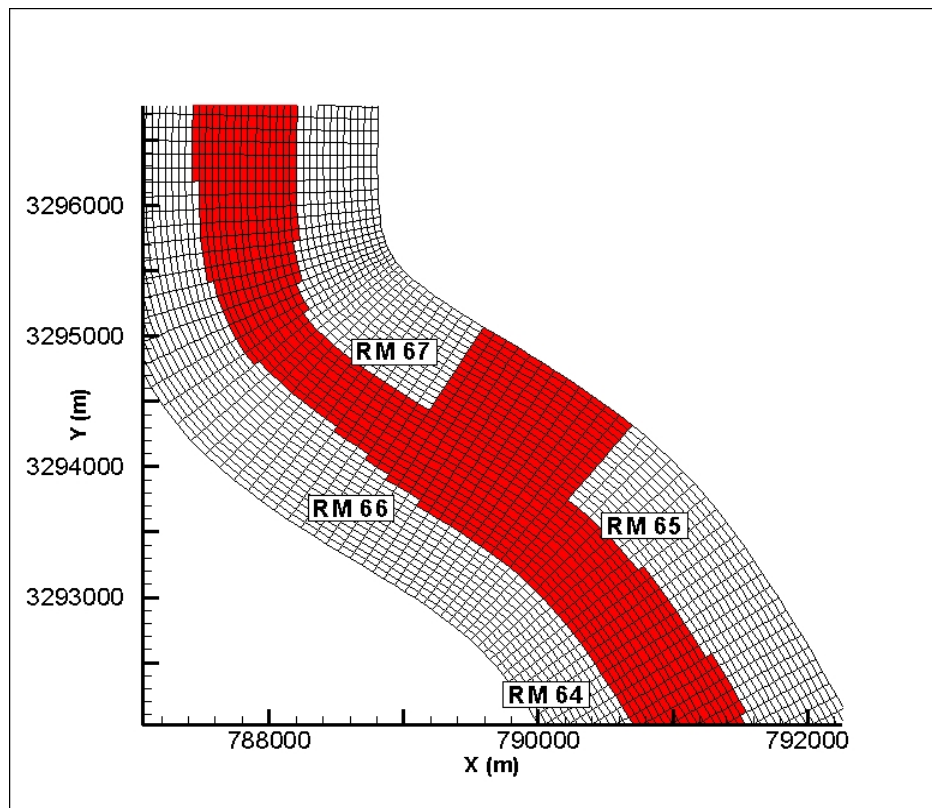


Figure 7.83 – Existing Diversions + Belair ECOMSED Mesh and Mask at Belair (RM 65, RK 105)

Similar to the Myrtle Grove test, the total energy, kinetic energy, sand concentration and sand load longitudinal profiles obtained for the main channel with the Belair diversion were plotted

against the ones obtained with the existing diversions only. Figure 7.84 to Figure 7.90 show these plots for peak flows.

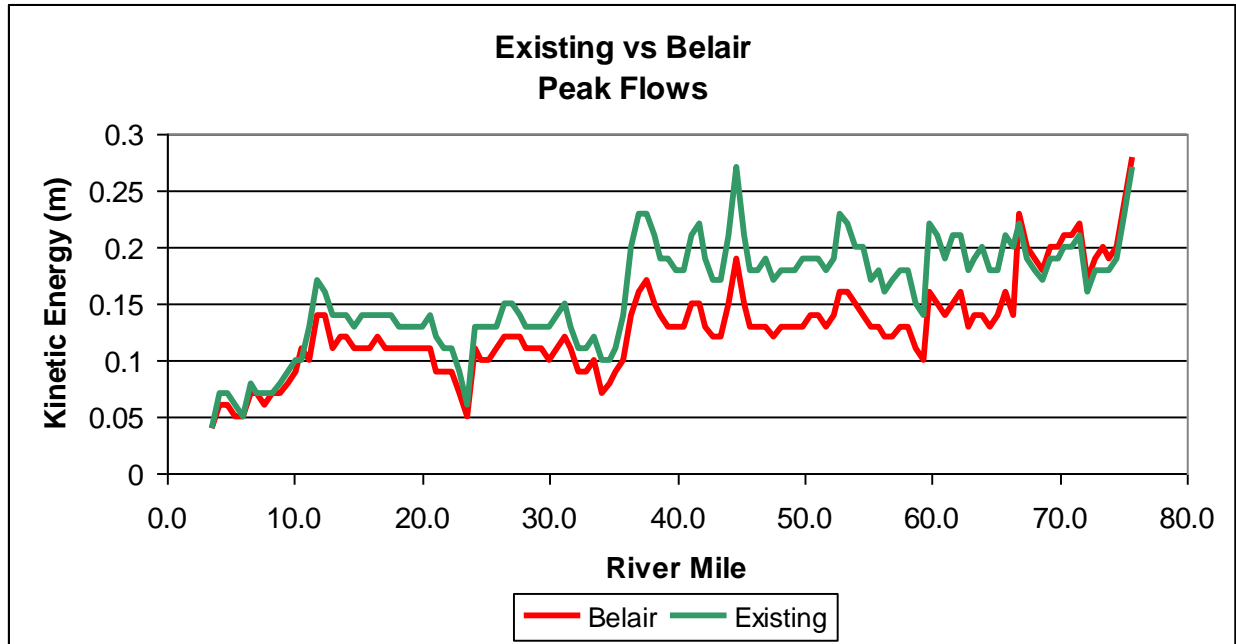


Figure 7.84 – Existing Diversions + Belair (RM 65, RK 105)– Main Channel Kinetic Energy of the Flow at Peak Flows

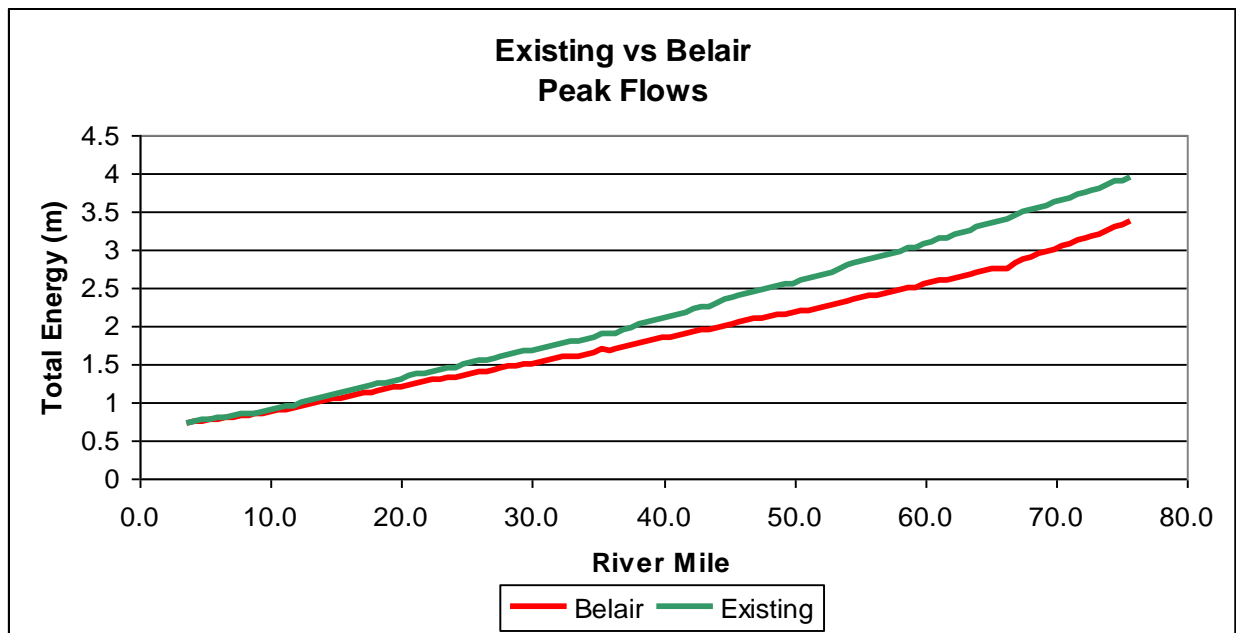


Figure 7.85 – Existing Diversions + Belair (RM 65, RK 105)– Main Channel Total Energy of the Flow at Peak Flows

Figure 7.86, Figure 7.87 and Figure 7.88 show respectively, the main channel total, potential and kinetic energy fluxes under peak flow conditions for the Belair test.

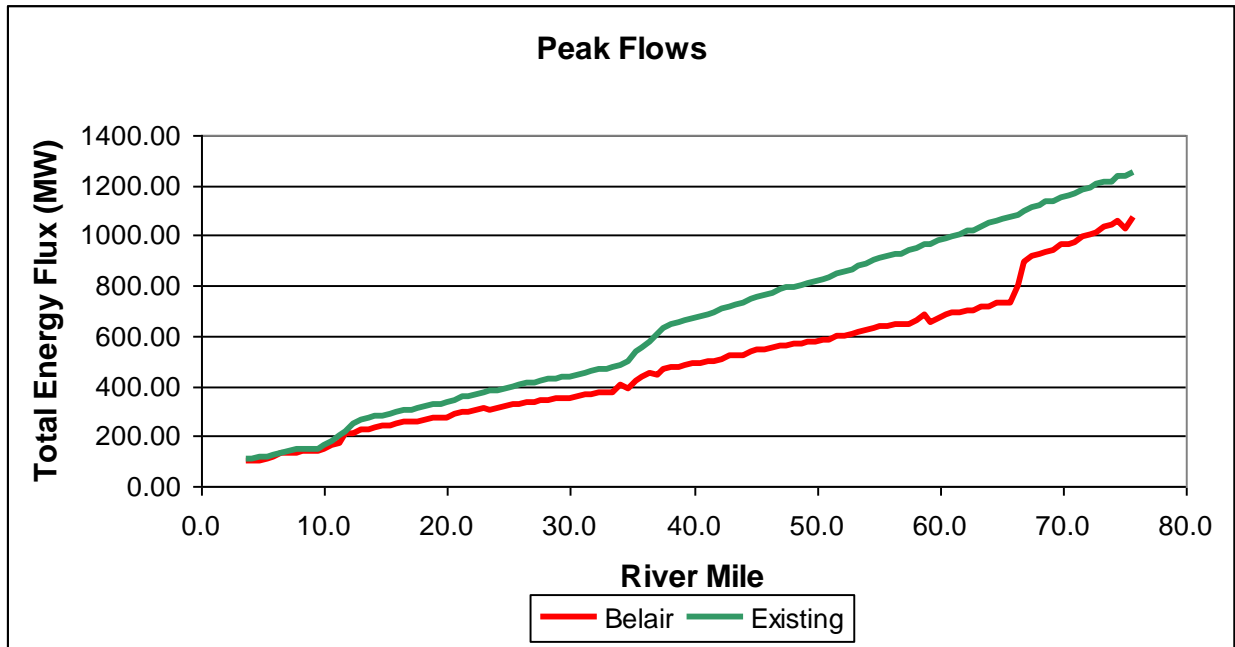


Figure 7.86 – Existing Diversions + Belair (RM 65, RK 105)– Main Channel Total Energy Flux of the Flow at Peak Flows

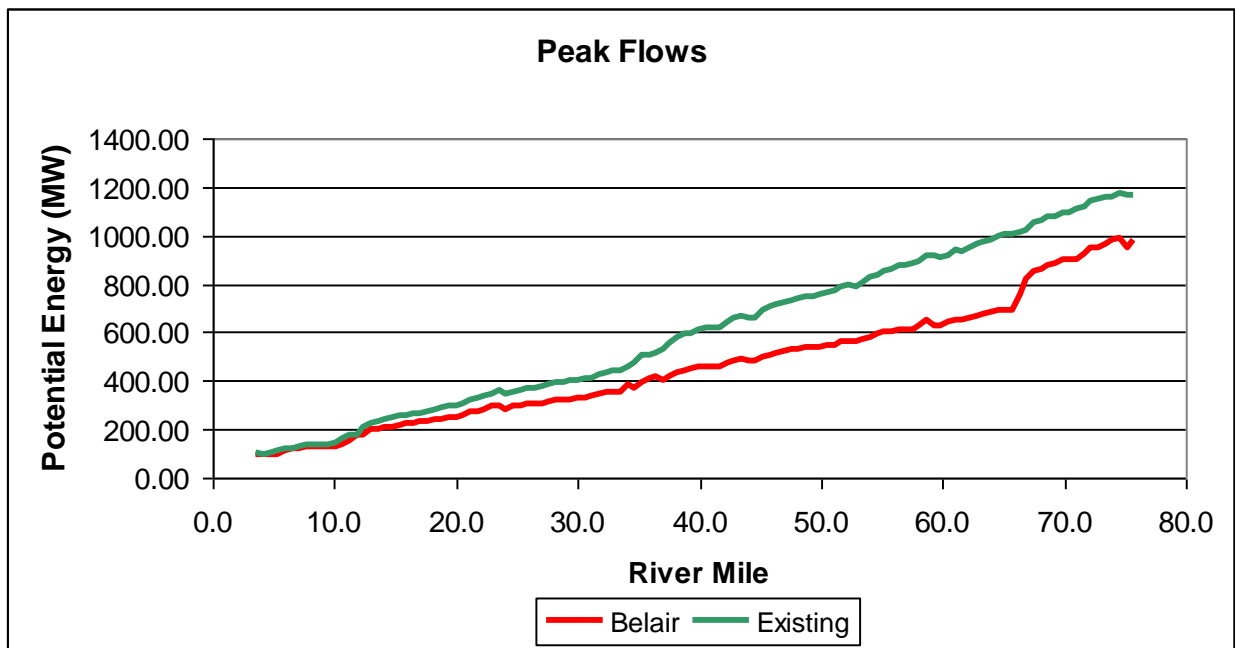


Figure 7.87 – Existing Diversions + Belair (RM 65, RK 105)– Main Channel Potential Energy Flux of the Flow at Peak Flows

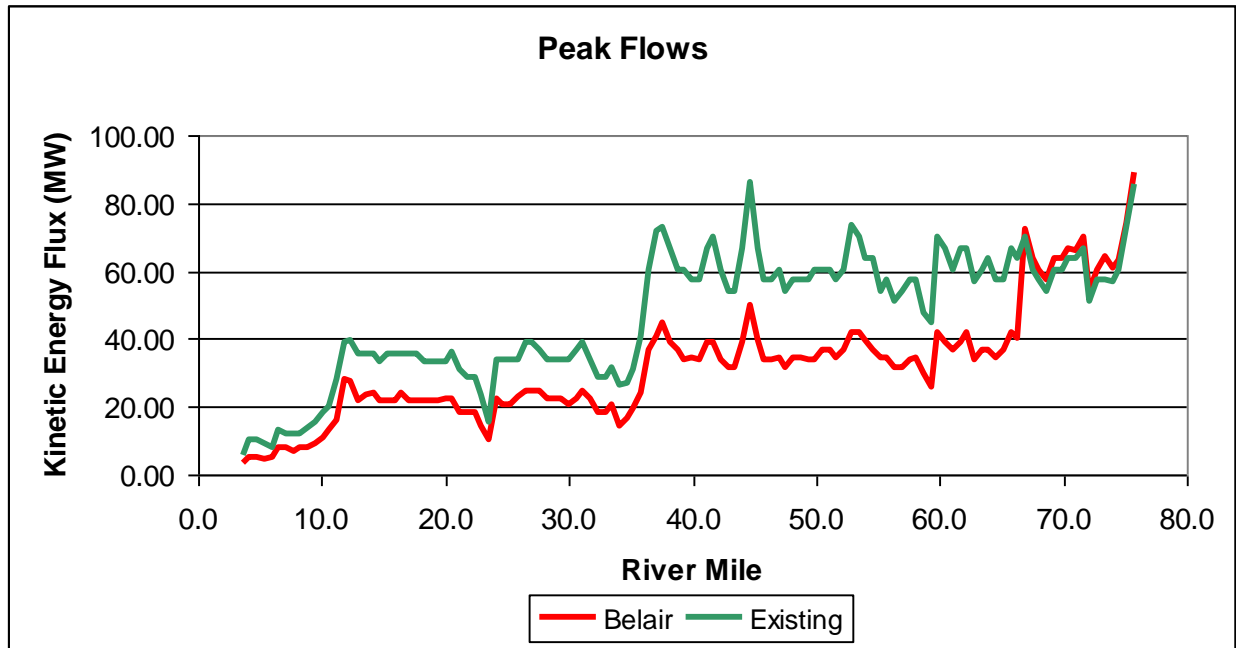


Figure 7.88 – Existing Diversions + Belair (RM 65, RK 105)– Main Channel Kinetic Energy Flux of the Flow at Peak Flows

Figure 7.84 and Figure 7.85 show a significant impact in the amount of energy available in the River due to the Belair diversion. At the upstream boundary of the model, the total energy is reduced by around 0.5 m with the introduction of the diversion, which corresponds to a 12% reduction. The kinetic energy downstream of the Belair diversion is reduced by values on the order of 0.03 m. These results are very different from the ones obtained with the Myrtle Grove diversion, which can be explained primarily by the difference in the amount of flow being extracted: 30,000 cfs at Myrtle Grove versus 200,000 cfs at Belair (almost seven times more).

Figure 7.89 and Figure 7.90 confirm the significant impact of the Belair diversion on the sediment transport. A reduction of the energy leads to a reduction of the transported sand. The presence of the diversion contributes to an increase in the transport of bed material upstream (erosion) and an extraction of sediment at the diversion, which leaves the downstream area more starved of both material to be transported and of flow to transport the available material.

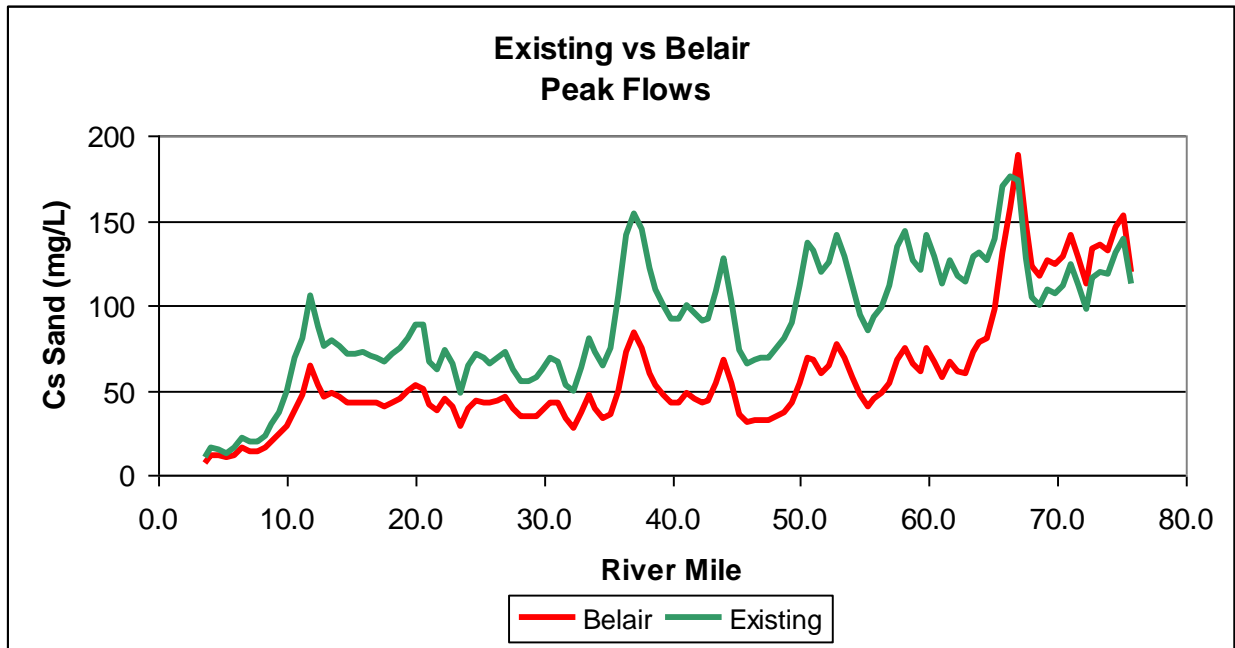


Figure 7.89 – Existing Diversions + Belair (RM 65, RK 105) – Main Channel Sand Concentration at Peak Flows

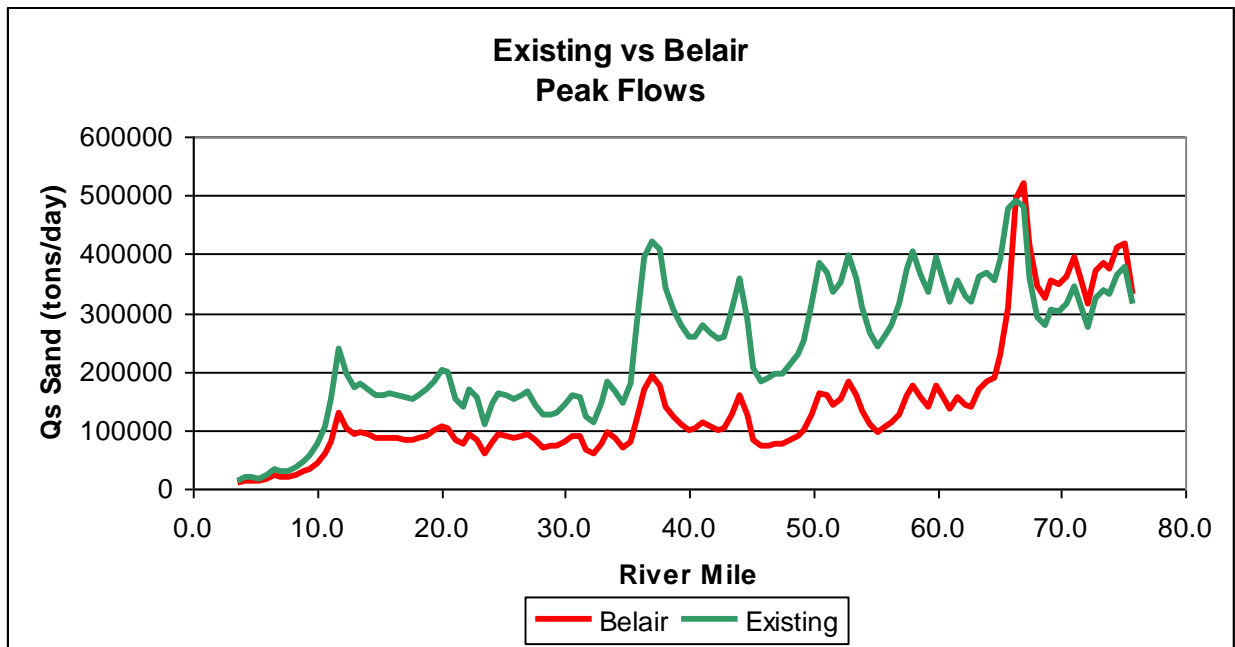


Figure 7.90 – Existing Diversions + Belair (RM 65, RK 105) – Main Channel Sand Load at Peak Flows

The total energy, kinetic energy, sand concentration and sand load longitudinal profiles obtained for the main channel with the Belair diversion were plotted against the ones obtained with the existing diversions only. Figure 7.91 to Figure 7.97 present these plots for intermediate flows.

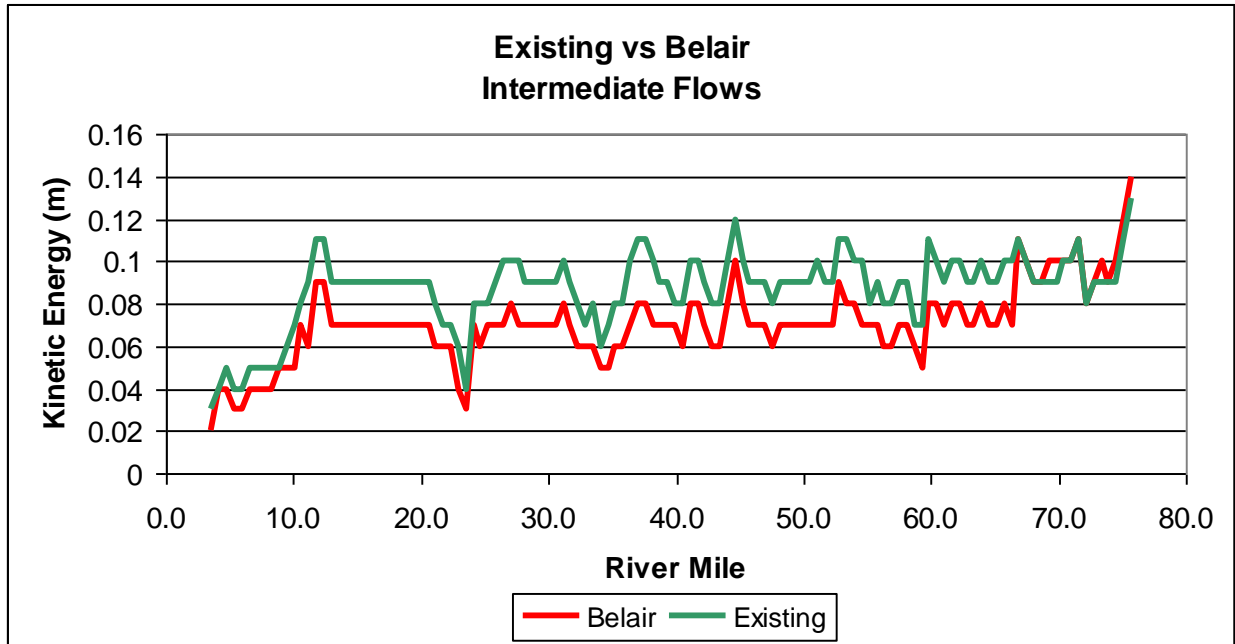


Figure 7.91 – Existing Diversions + Belair (RM 65, RK 105)– Main Channel Kinetic Energy of the Flow at Intermediate Flows

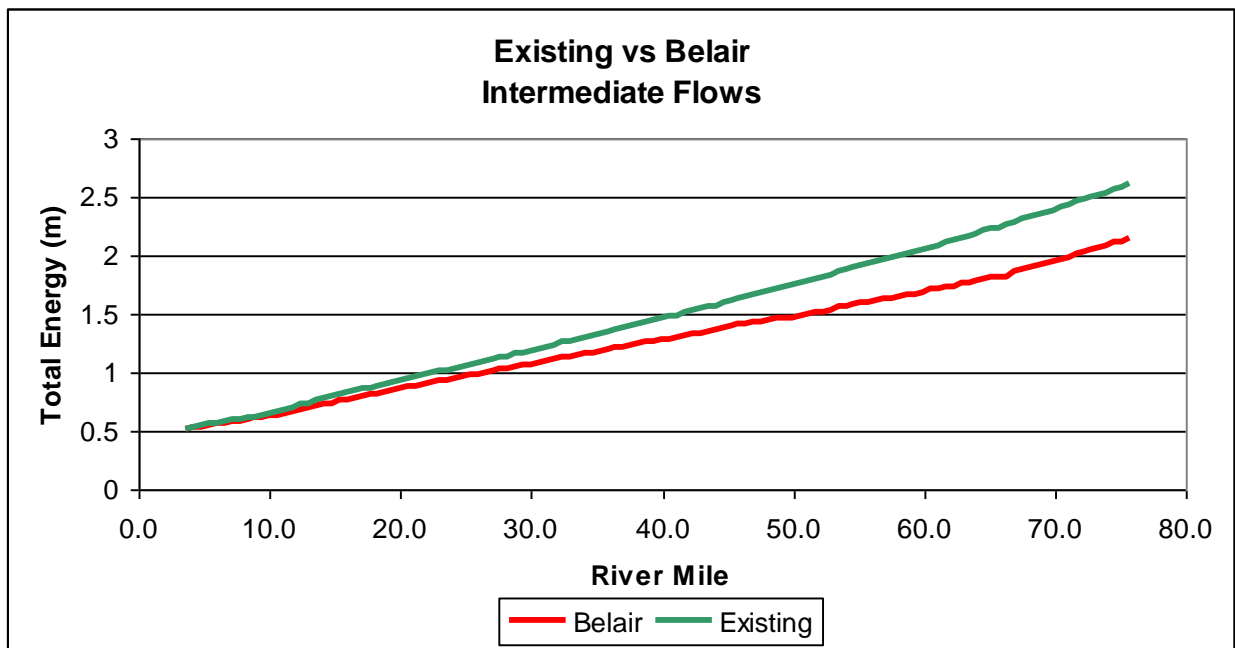


Figure 7.92 – Existing Diversions + Belair (RM 65, RK 105)– Main Channel Total Energy of the Flow at Intermediate Flows

Figure 7.93, Figure 7.94 and Figure 7.95 show respectively, the main channel total, potential and kinetic energy fluxes under intermediate flow conditions for the Belair test.

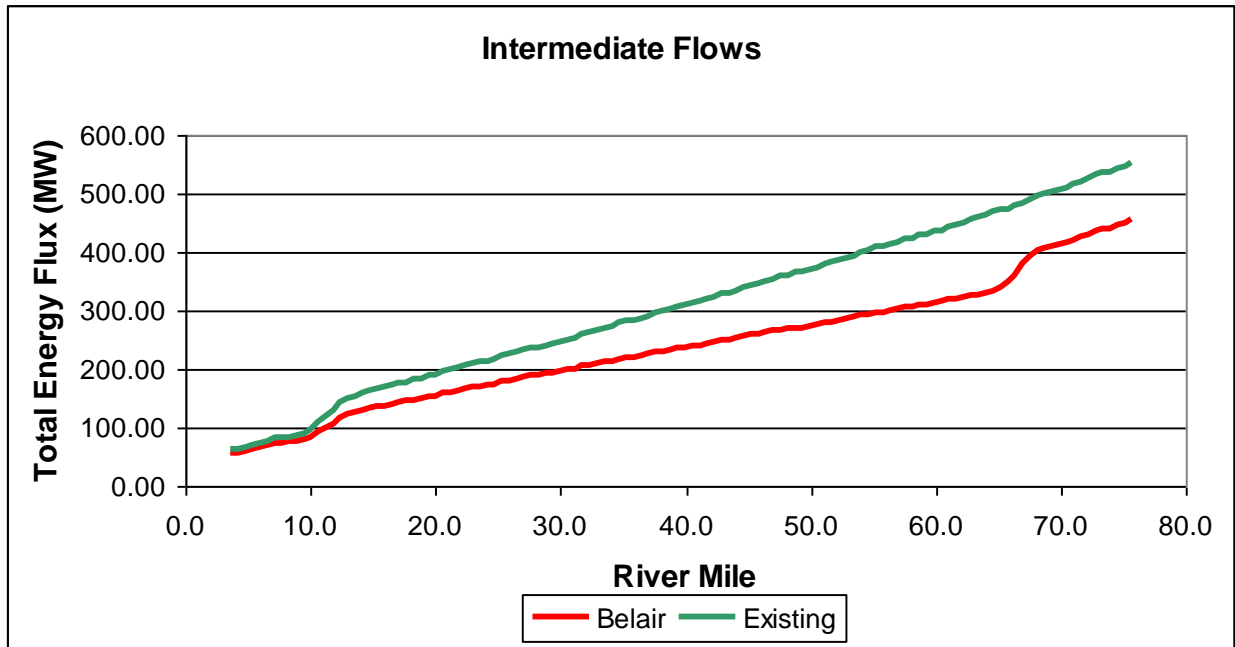


Figure 7.93 – Existing Diversions + Belair (RM 65, RK 105)– Main Channel Total Energy Flux of the Flow at Intermediate Flows

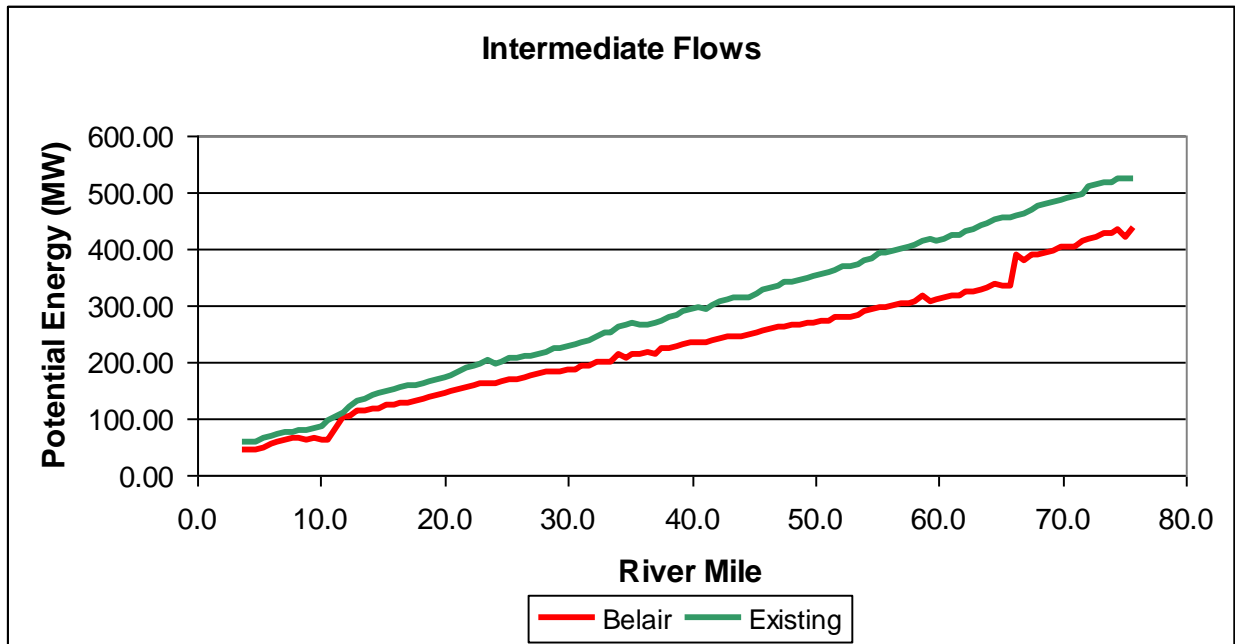


Figure 7.94 – Existing Diversions + Belair (RM 65, RK 105) – Main Channel Potential Energy Flux of the Flow at Intermediate Flows

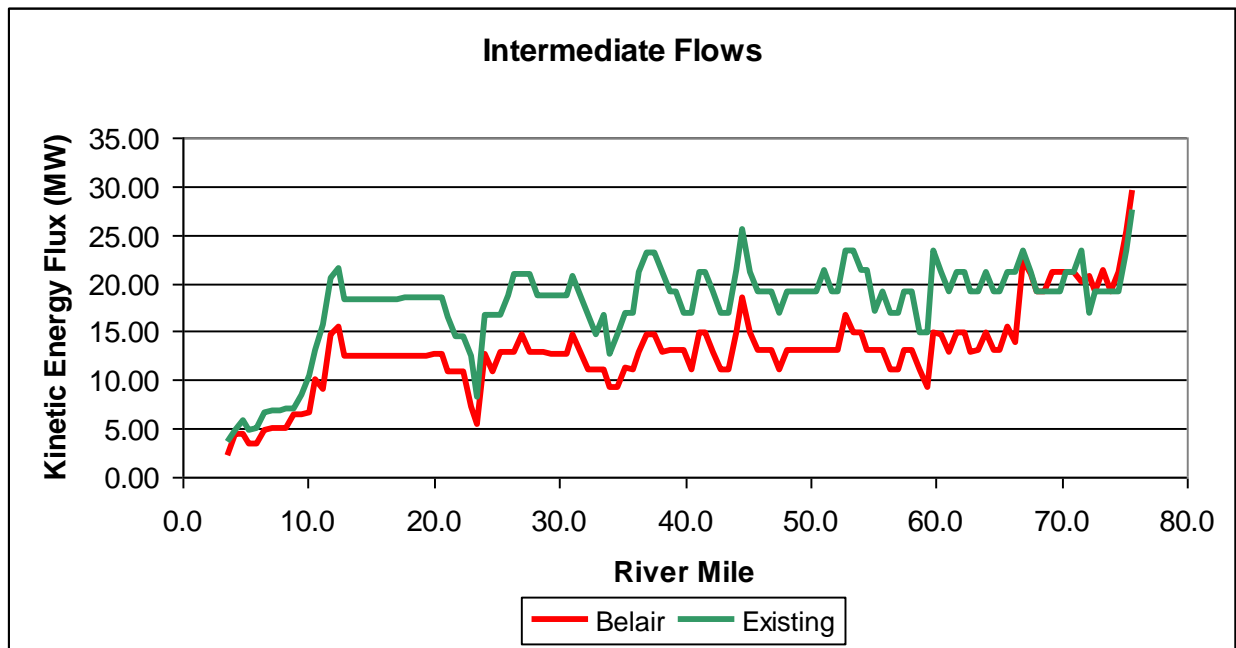


Figure 7.95 – Existing Diversions + Belair (RM 65, RK 105)– Main Channel Kinetic Energy Flux of the Flow at Intermediate Flows

Figure 7.91 and Figure 7.92 show a significant impact in the amount of energy available in the River due to the Belair diversion. At the upstream boundary of the model, the total energy is reduced by around 0.5 m with the introduction of the diversion. The kinetic energy downstream of the Belair diversion is reduced by values on the order of 0.01 m. Once again, the results are very different from the ones obtained with the Myrtle Grove diversion, which can be explained primarily by the difference in the amount of flow being extracted.

Figure 7.96 and Figure 7.97 confirm the significant impact of the Belair diversion on the sediment transport. As stated before, the reduction of the energy leads to a reduction of the transported sand. The presence of the diversion contributes to an increase in the transport of bed material upstream (erosion) and an extraction of sediment at the diversion, which leaves the downstream area more starved of both material to be transported and of flow to transport the available material.

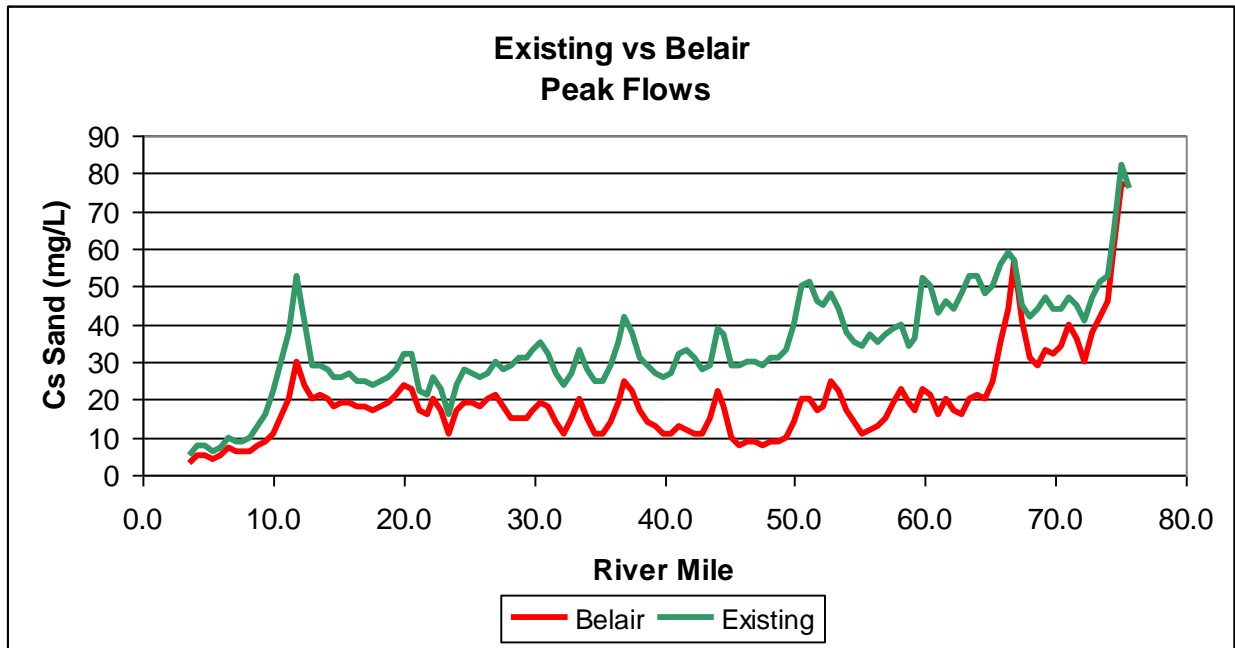


Figure 7.96 – Existing Diversions + Belair (RM 65, RK 105)– Main Channel Suspended Sand Concentration at Intermediate Flows

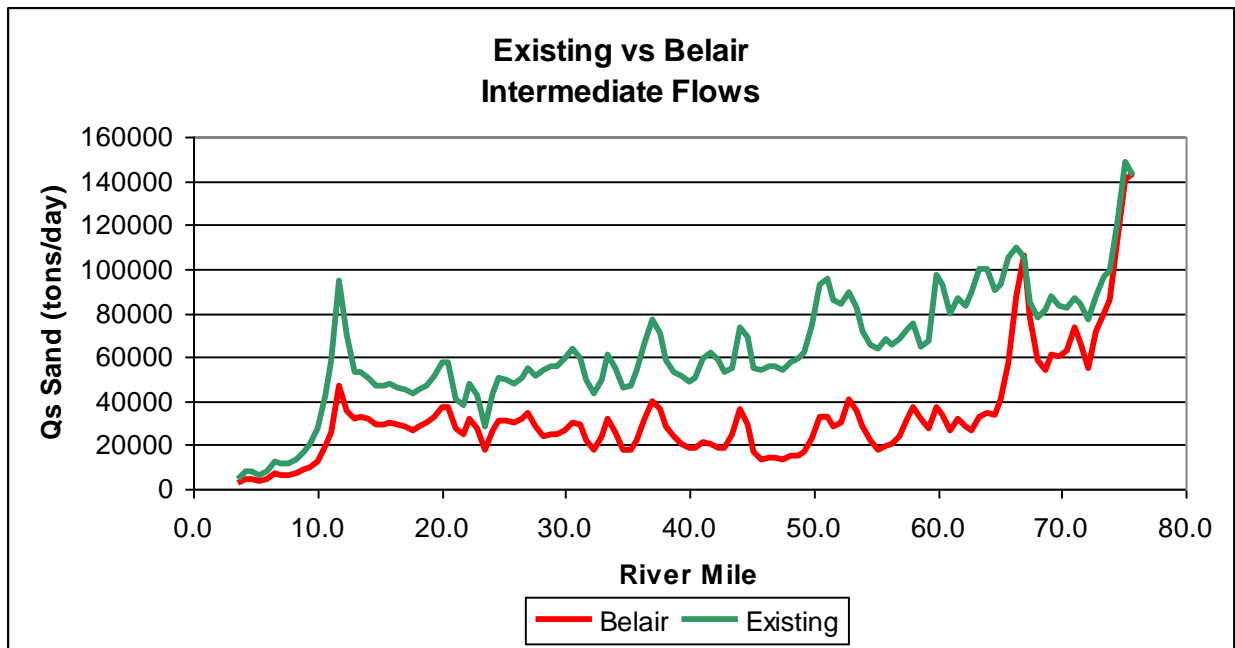
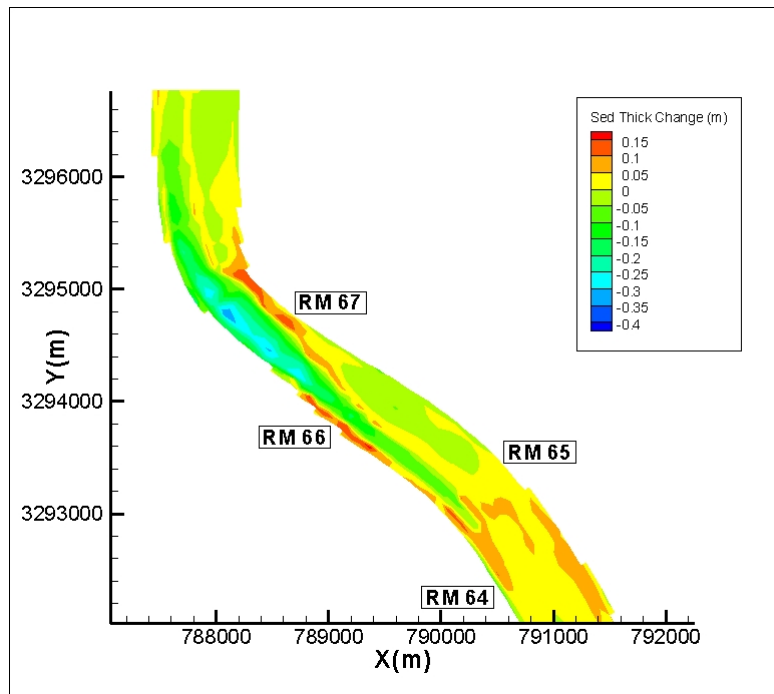
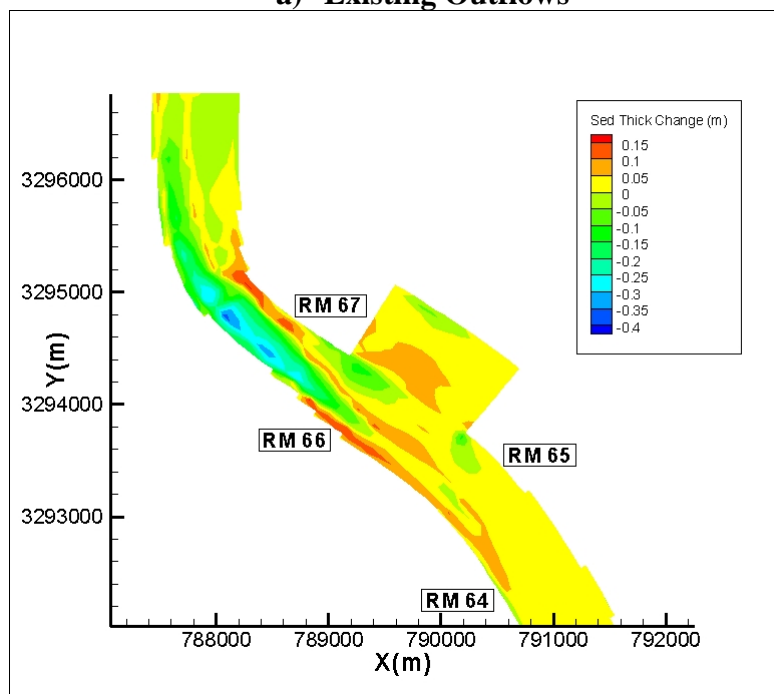


Figure 7.97 – Existing Diversions + Belair (RM 65, RK 105) – Main Channel Suspended Sand Load at Intermediate Flows

The bed sediment thickness change after 1 day and after 10 days of simulation for peak flows and for the existing diversions and the Belair diversion cases are presented in Figure 7.98 and Figure 7.99. In this case, the effect of the introduction of the diversion changes the erosion/deposition pattern significantly. It is evident that there is more deposition downstream of the diversion than without a diversion. The presence of more deposition areas and the almost non-existence of erosion downstream of the implemented diversion can be seen in the comparison shown in Figure 7.100 and in Figure 7.101 for the whole model domain results.

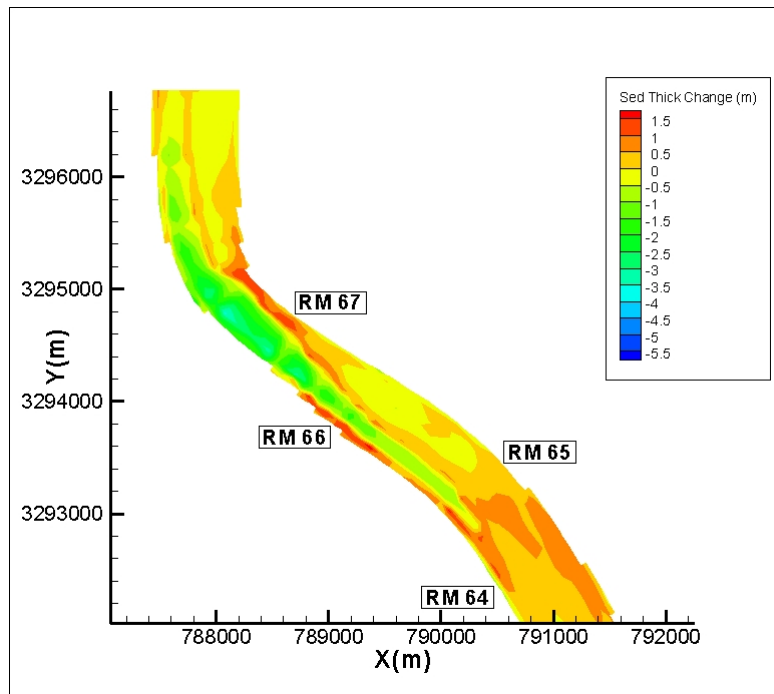


a) Existing Outflows

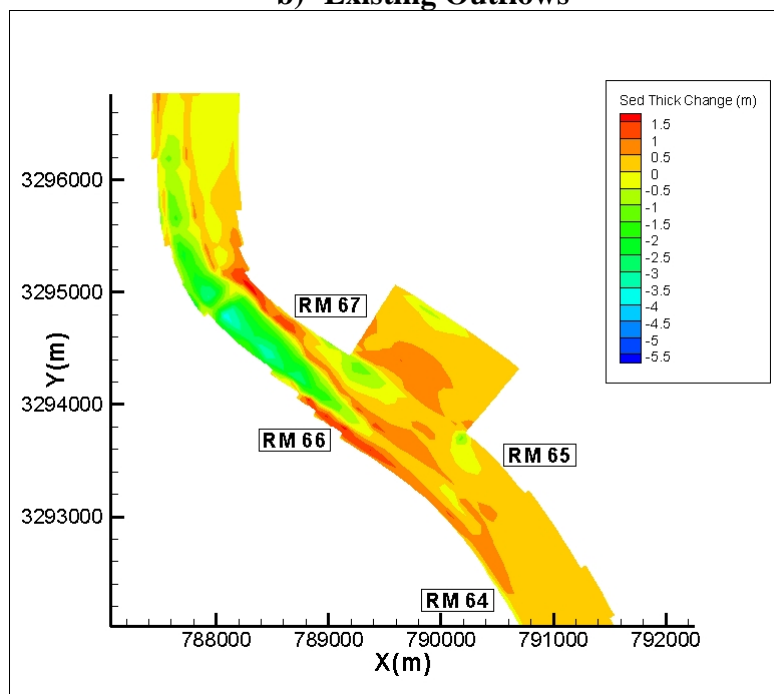


b) Belair (RM 65, RK 105) + Existing Outflows

Figure 7.98 – Existing Diversions + Belair (RM 65, RK 105)- Bed Sediment Thickness Change after 1 day at Peak Flows. Positive values indicate deposition and negative values indicate erosion

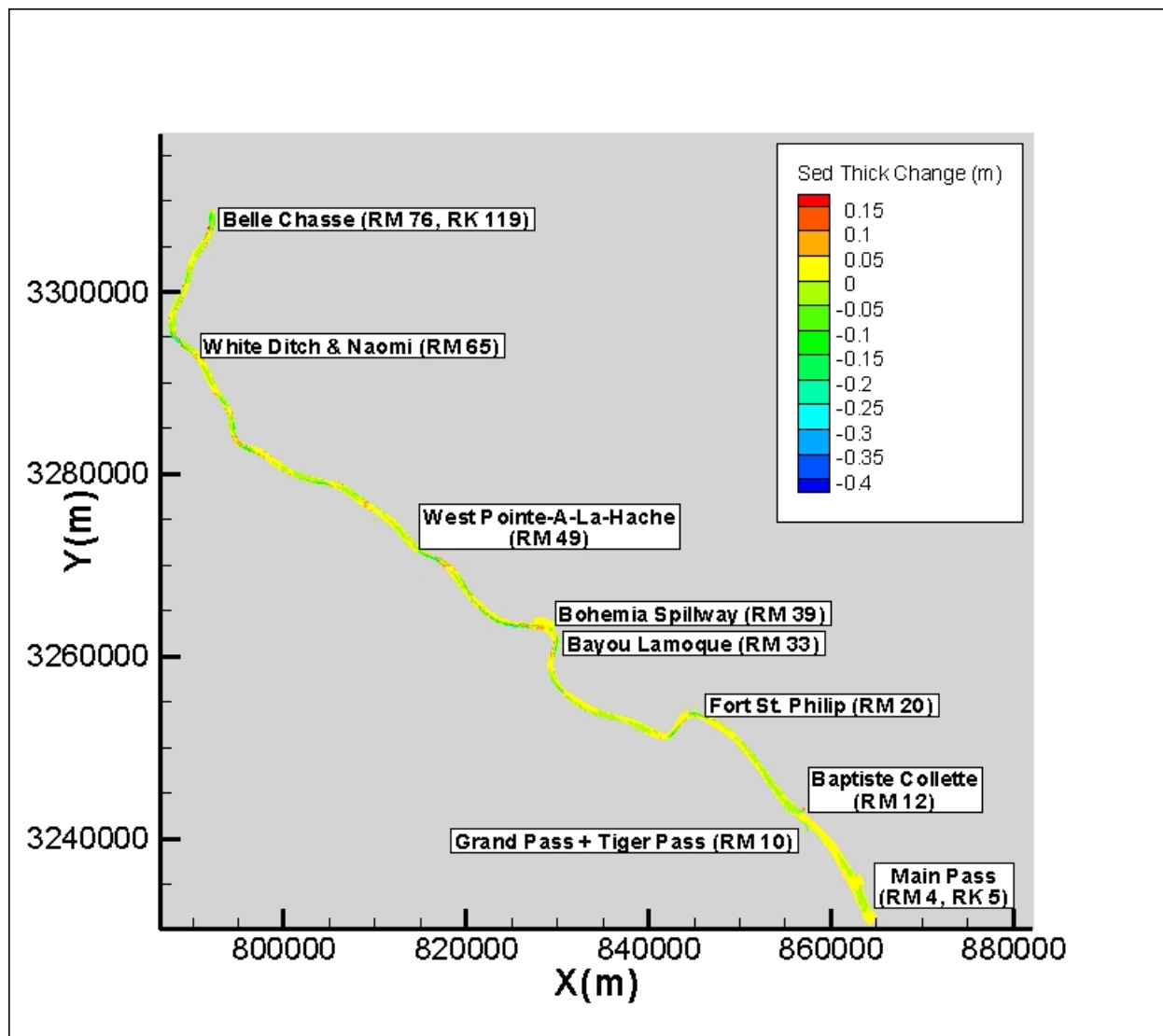


b) Existing Outflows

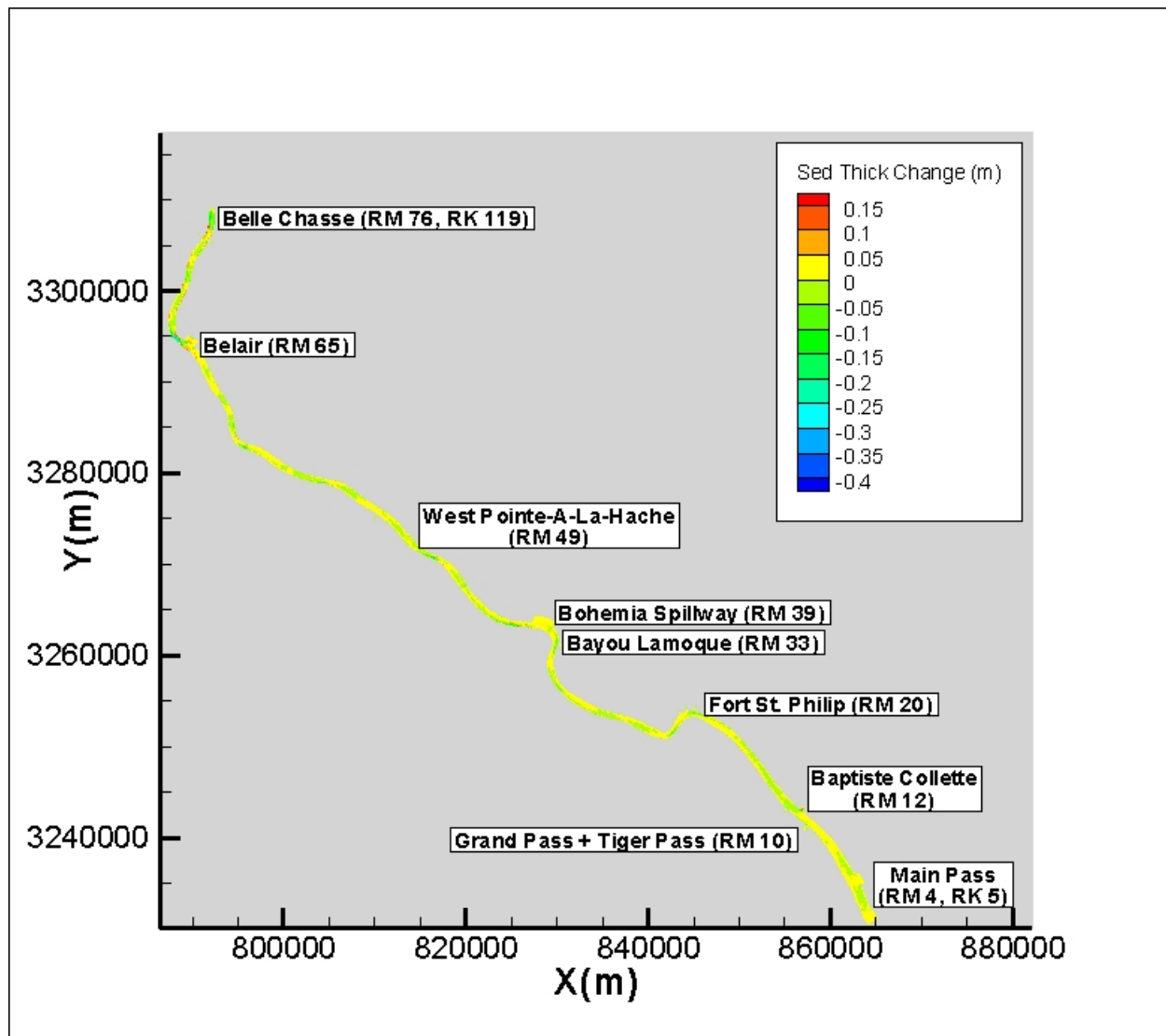


c) Belair (RM 65, RK 105) + Existing Outflows

Figure 7.99 – Existing Diversions + Belair (RM 65, RK 105) - Bed Sediment Thickness Change after 10 days at Peak Flows. Positive values indicate deposition and negative values indicate erosion

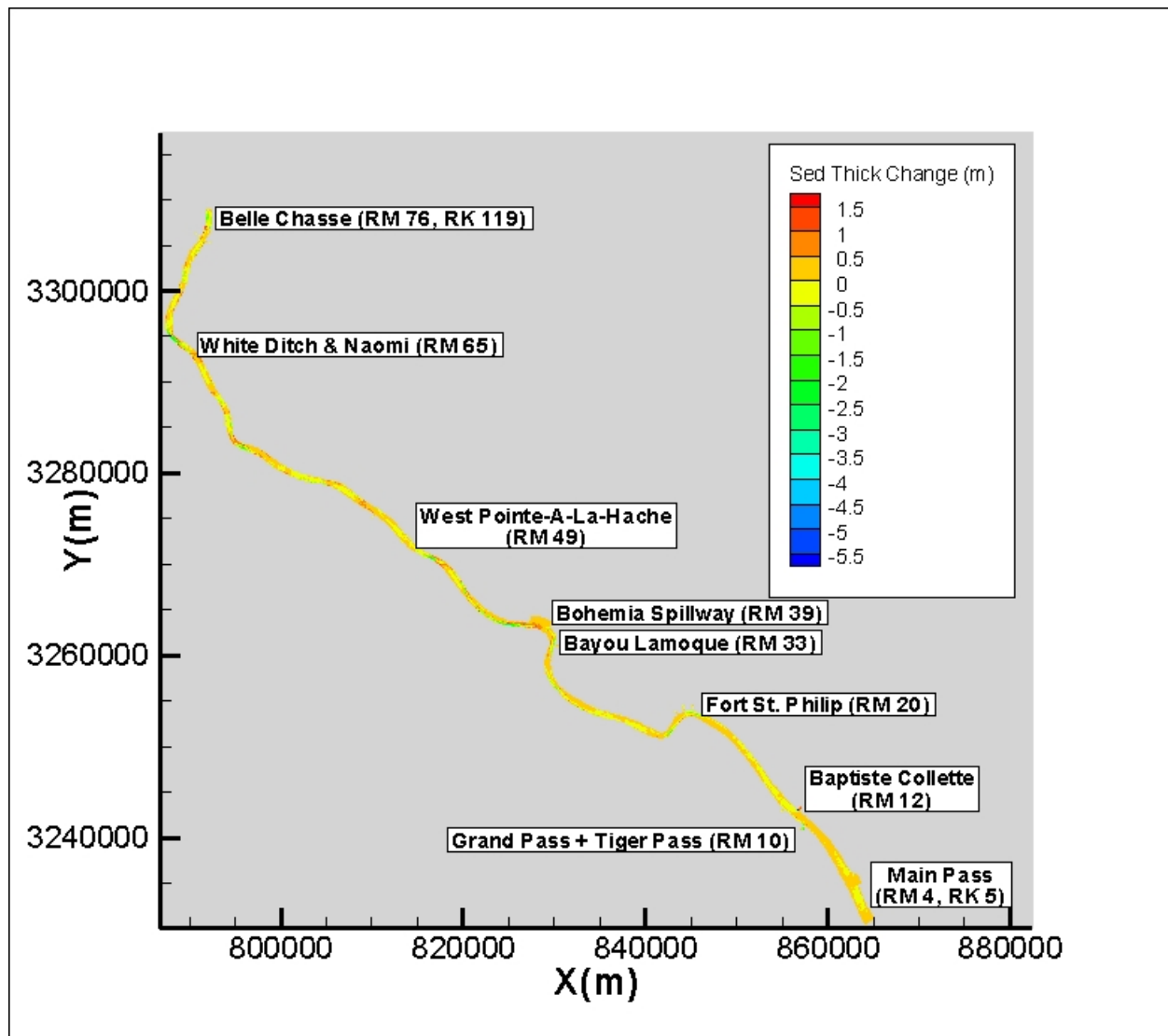


a) Existing Outflows

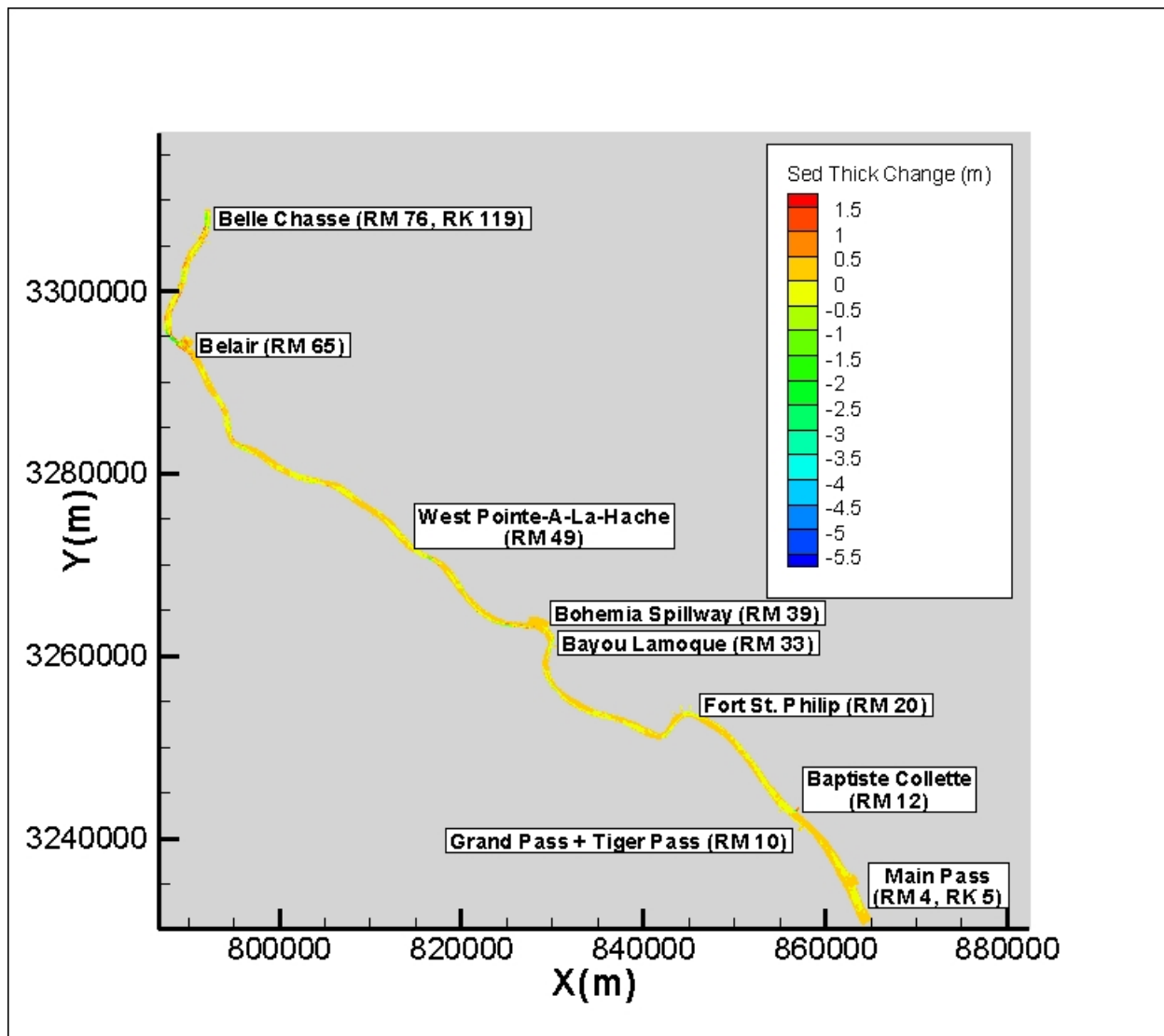


b) Belair (RM 65, RK 105)+ Existing Outflows

Figure 7.100 – Model Domain - Bed Sediment Thickness Change after 1 day at Peak Flows.
Positive values indicate deposition and negative values indicate erosion



a) Existing Outflows



b) Belair (RM 65, RK 105) + Existing Outflows

Figure 7.101 – Model Domain - Bed Sediment Thickness Change after 10 days at Peak Flows. Positive values indicate deposition and negative values indicate erosion

Figure 7.102 summarizes the difference between the results obtained with the Existing Outflows and with the Belair Diversion Scenario. The downstream reach is dominated by increased deposition (green) with a few localized areas in red where the erosion is increased for the Belair Case compared to the existing conditions. These localized areas where erosion increases may be caused by a response of the system to a discontinuity in the sediment available for transport, i.e. the incoming sediment is less than the local sediment pickup rate. Nonetheless, this sediment is probably picked up and deposited a short distance downstream, as the water flow is reduced and so the capacity for transporting sediment is also reduced. This is a localized phenomenon. Once again, the Belair diversion seems to have more impact in the system than the Myrtle Grove diversion.

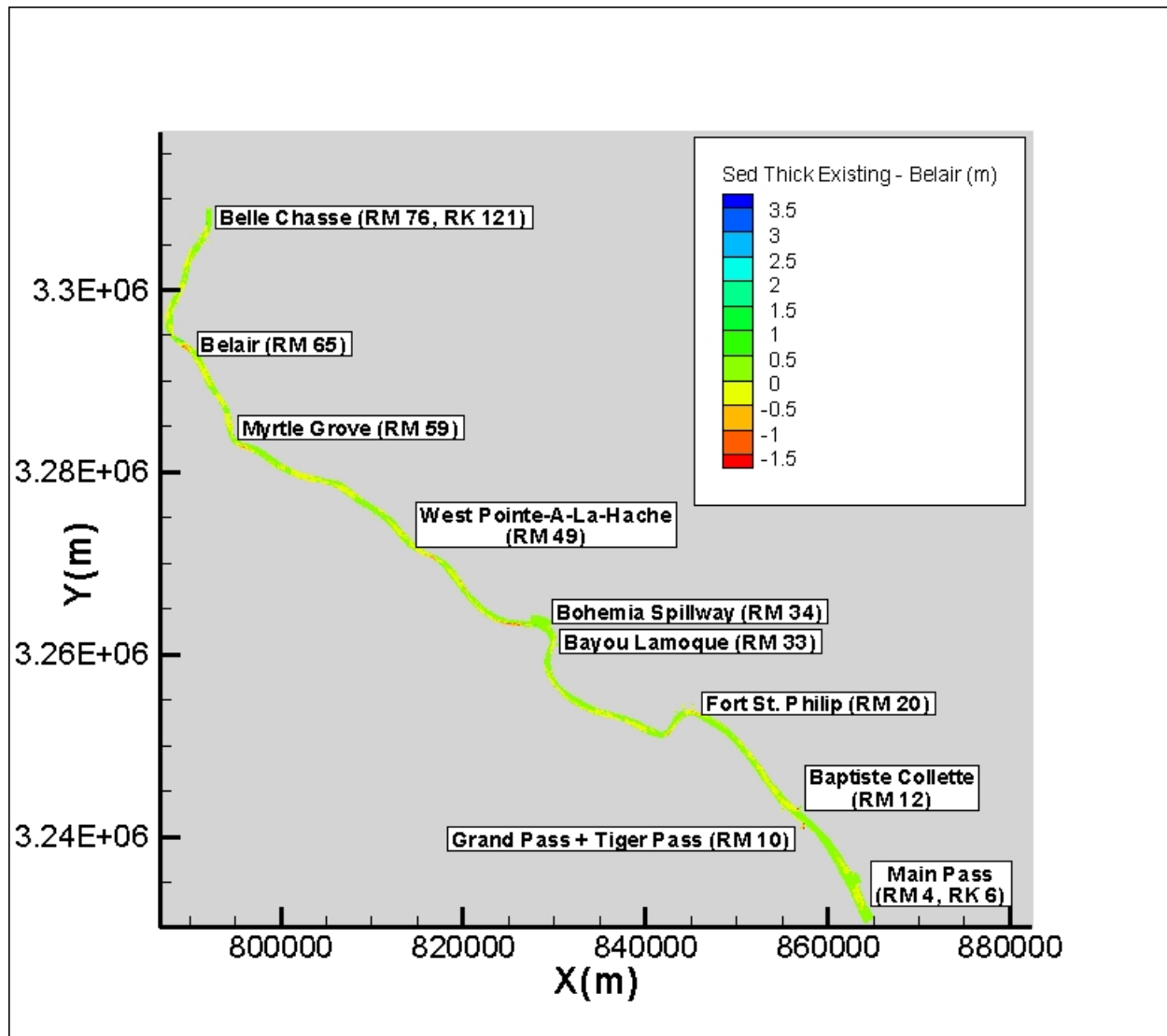
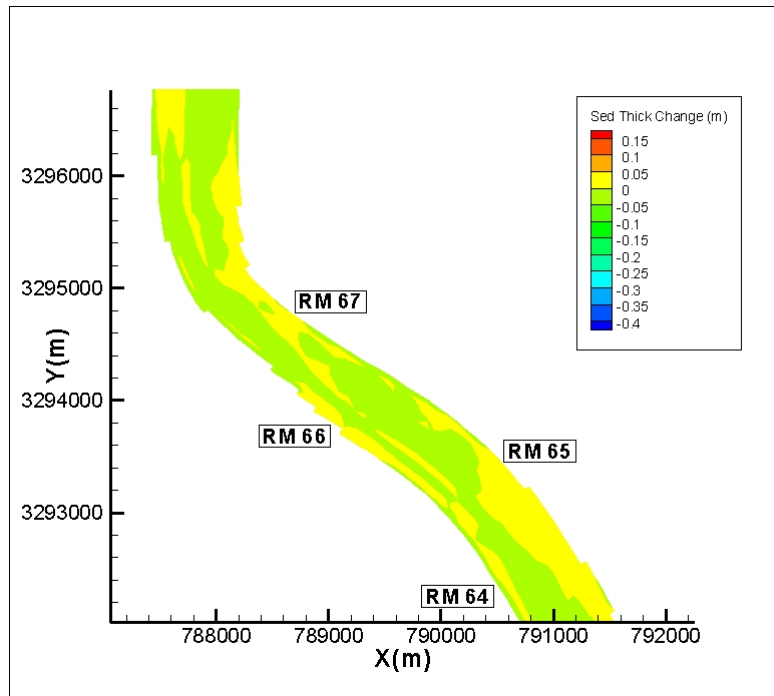
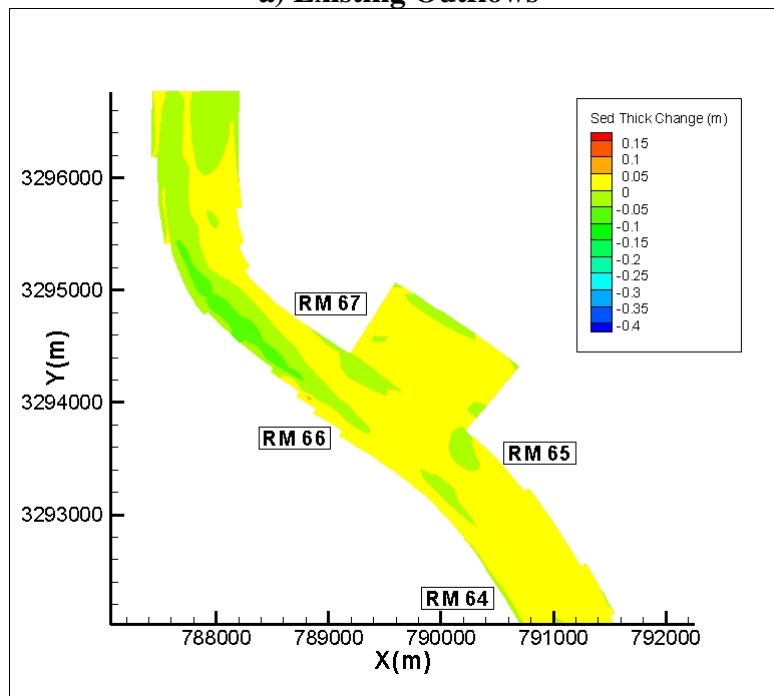


Figure 7.102 – Model Domain – Difference between Existing and Belair Test Bed Sediment Thickness Change after 10 days at Peak Flows. Positive values indicate that the addition of the Belair Diversion increased deposition. Negative values indicate that the addition of the Belair (RM 65, RK 105) Diversion increased erosion

The bed sediment thickness changes after 1 day and after 10 days of simulation for intermediate flows and for the existing diversions and the Belair diversion cases are presented in Figure 7.103 and Figure 7.104. It is evident that there is more deposition downstream of the diversion than without a diversion. The presence of more deposition areas and the almost non-existence of erosion downstream of the implemented diversion can be seen in the comparisons shown in Figure 7.105 and Figure 7.106 for the whole model domain.

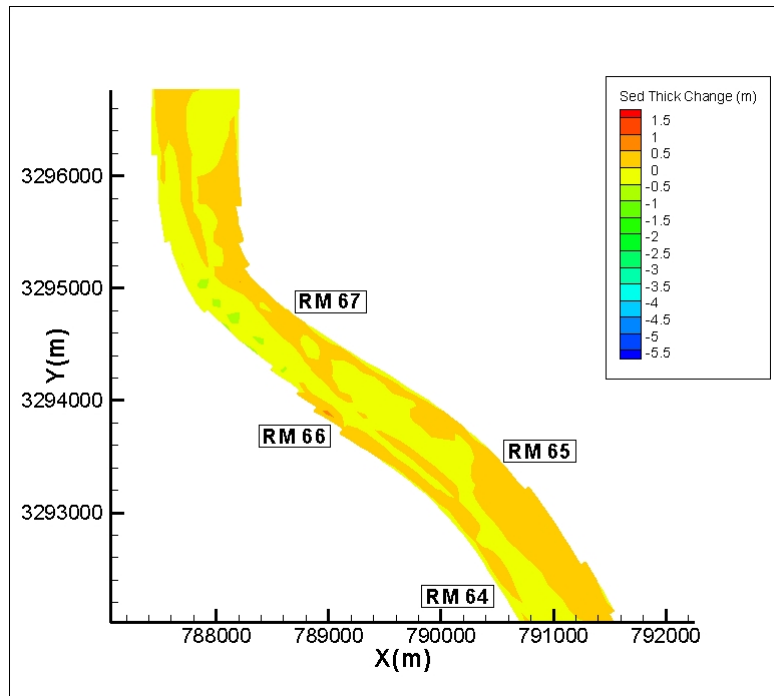


a) Existing Outflows

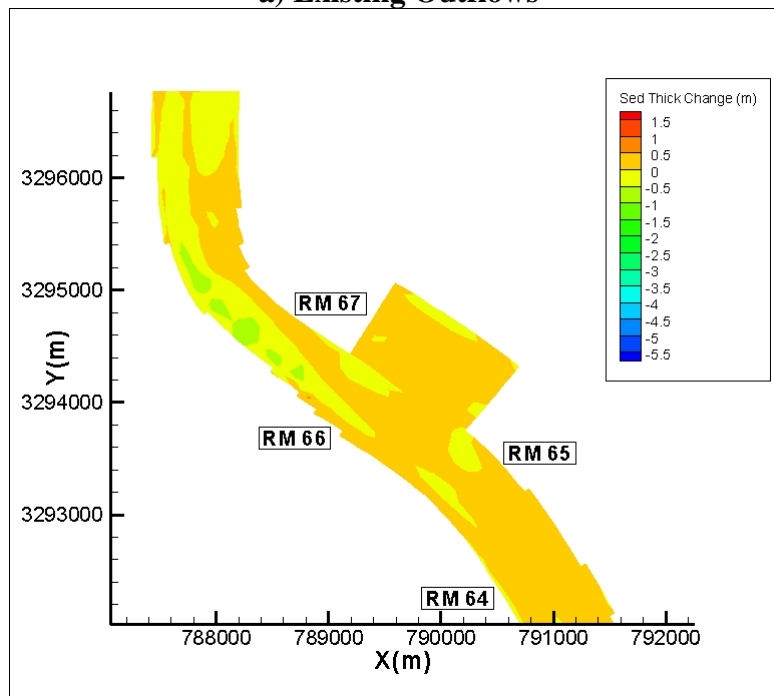


b) Belair (RM 65, RK 105) + Existing Outflows

Figure 7.103 – Belair Area (RM 65, RK 105) - Bed Sediment Thickness Change after 1 day at Intermediate Flows. Positive values indicate deposition and negative values indicate erosion

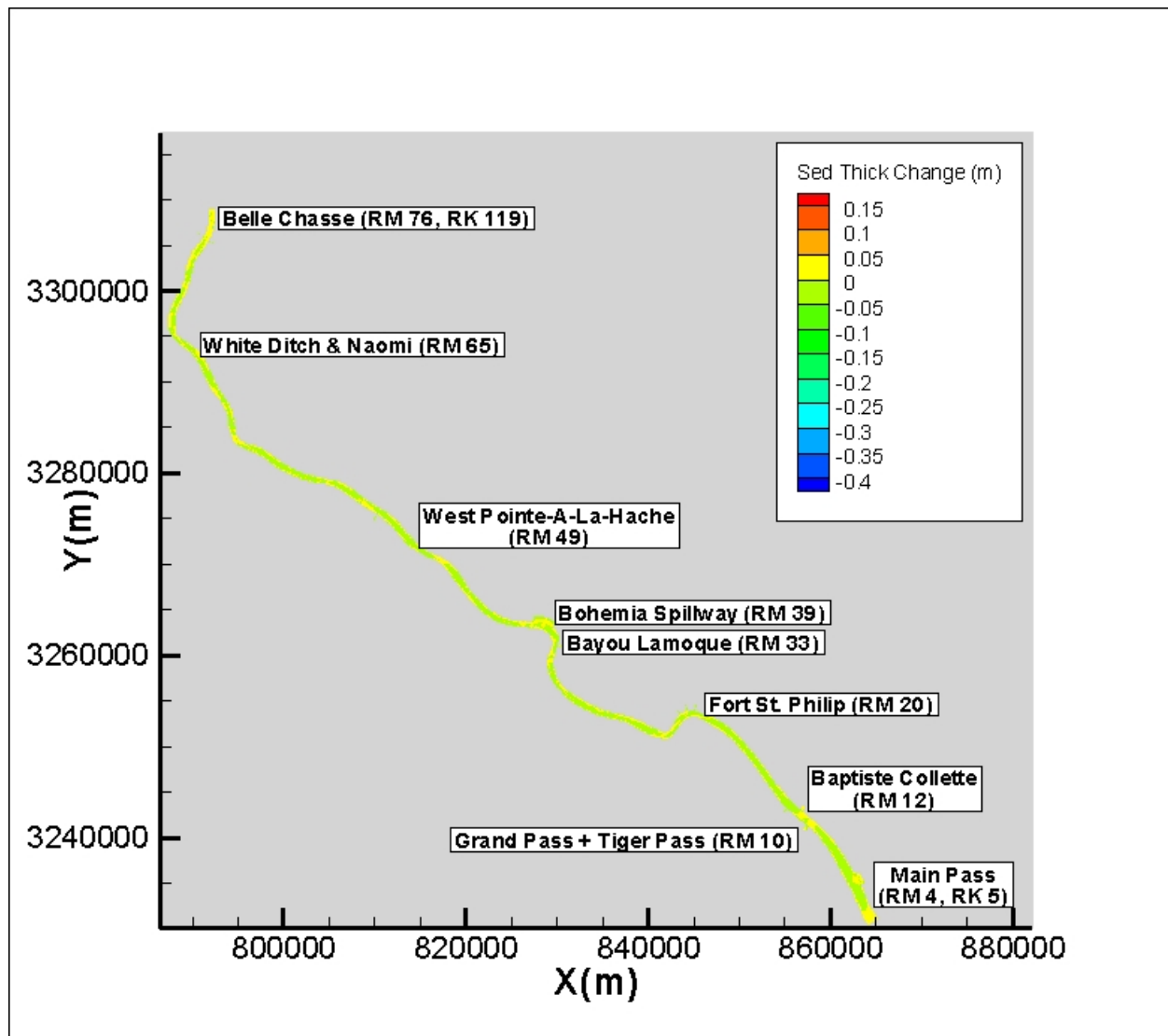


a) Existing Outflows

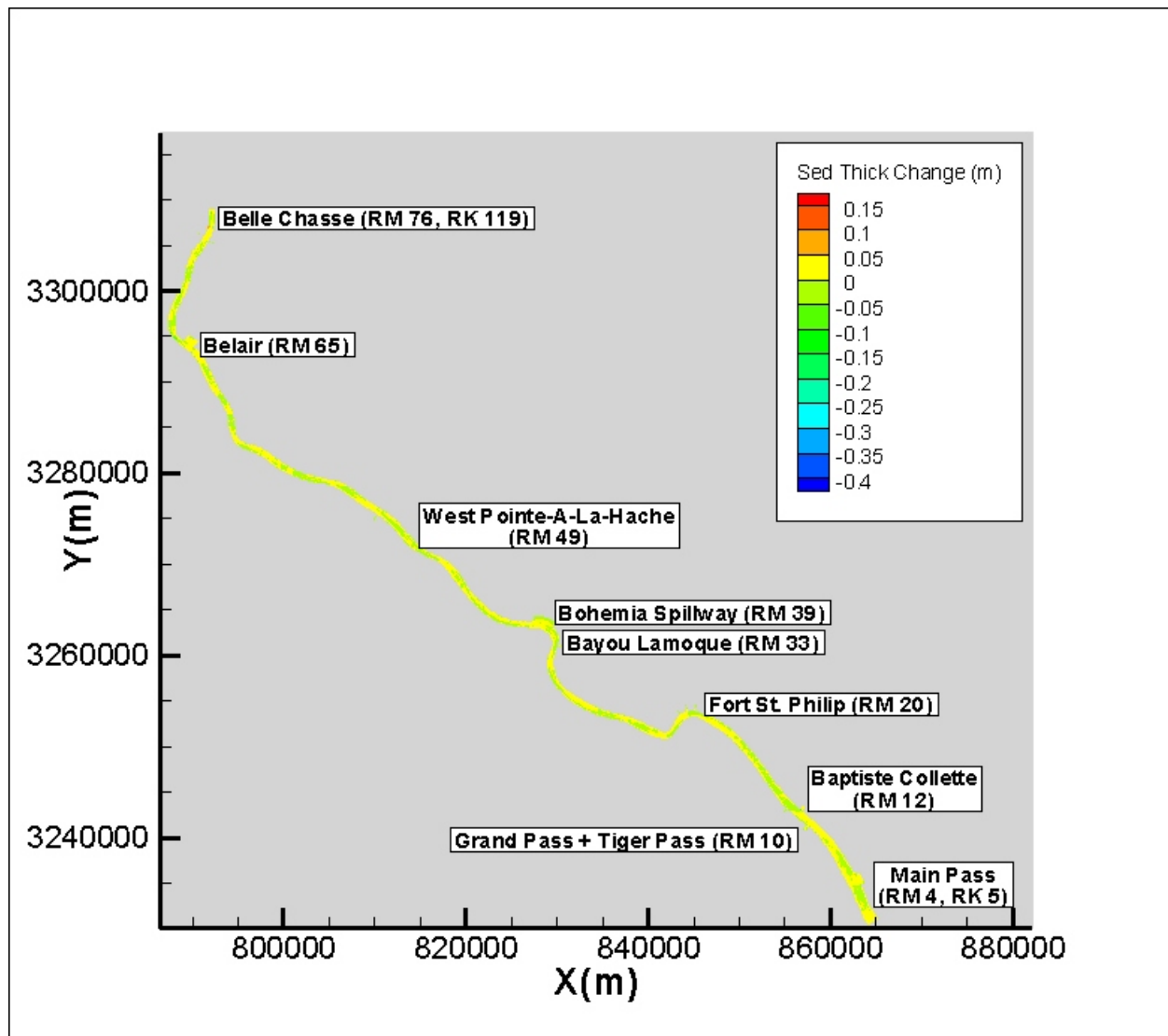


b) Belair (RM 65, RK 105) + Existing Outflows

Figure 7.104 – Belair (RM 65, RK 105)- Bed Sediment Thickness Change after 10 days at Intermediate Flows. Positive values indicate deposition and negative values indicate erosion

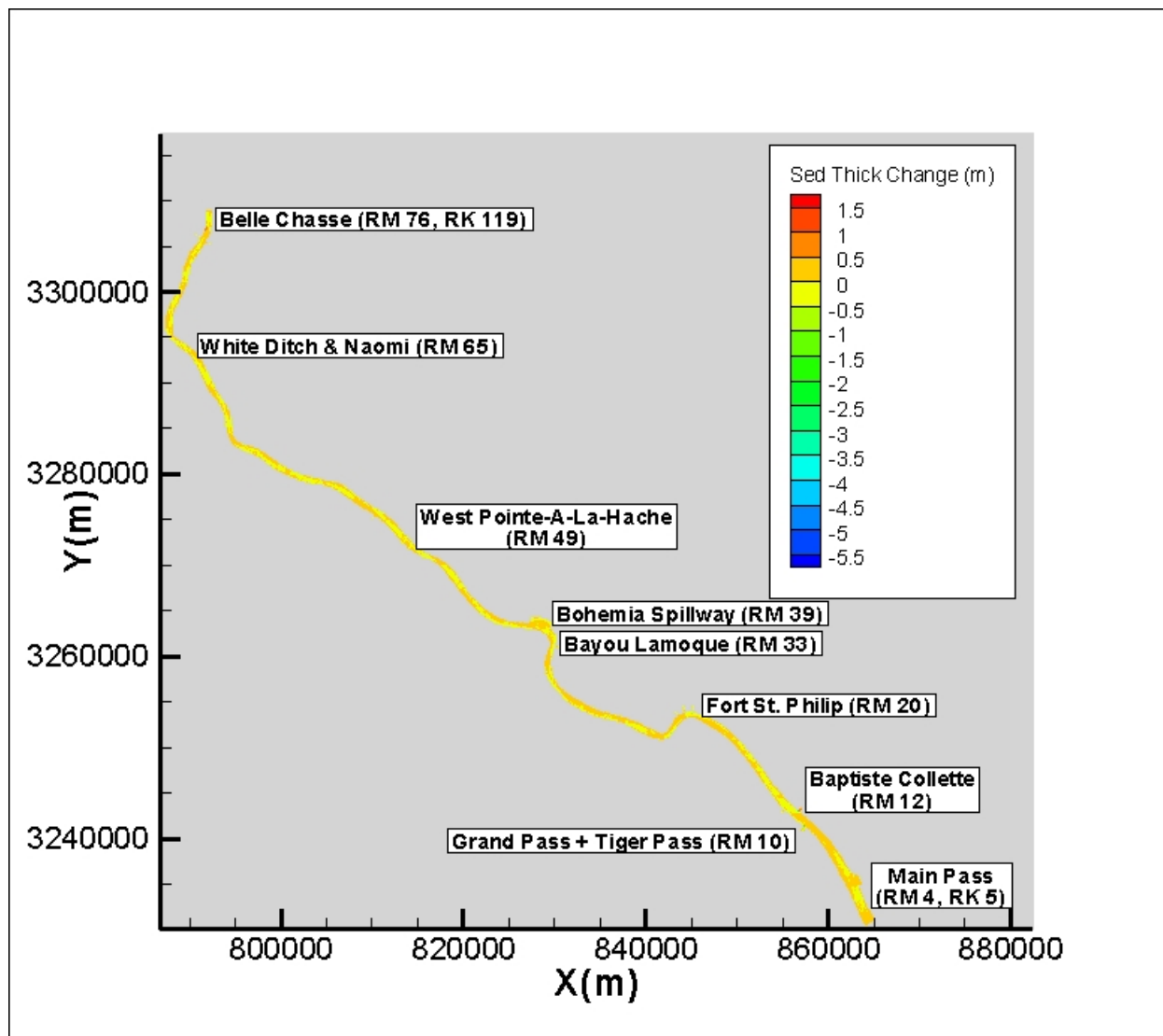


a) Existing Outflows

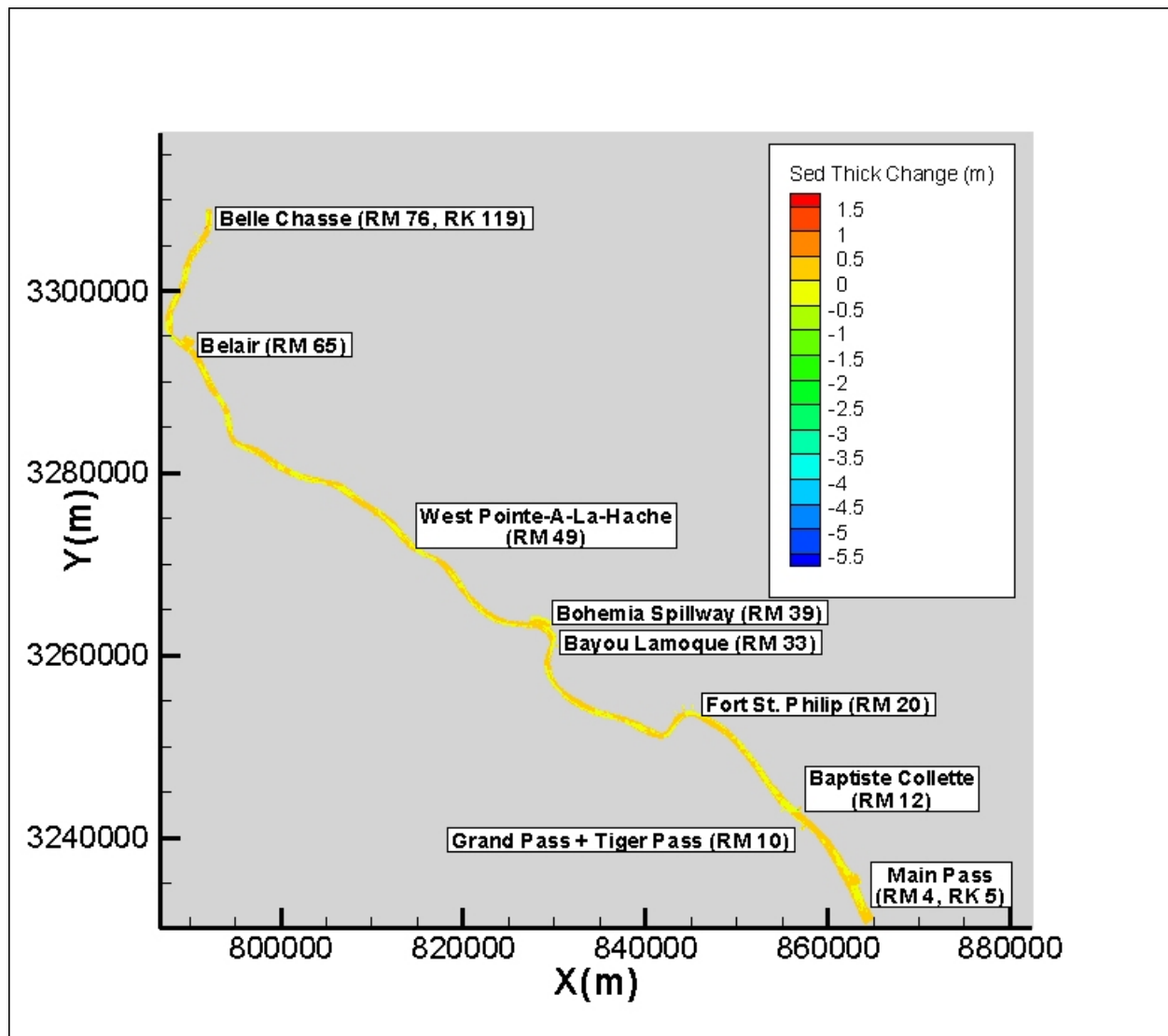


b) Belair (RM 65, RK 105) + Existing Outflows

Figure 7.105 – Belair (RM 65, RK 105) - Bed Sediment Thickness Change after 1 day at Intermediate Flows. Positive values indicate deposition and negative values indicate erosion



a) Existing Outflows



b) Belair (RM 65, RK 105) + Existing Outflows

Figure 7.106 – Model Domain - Bed Sediment Thickness Change after 10 days at Intermediate Flows. Positive values indicate deposition and negative values indicate erosion

The estimated amount of sediment being extracted at each outflow for the Belair Test is shown in Table 7-6. In this case, it is clear that at peak flows, a disproportionate amount of the sand is extracted through the Belair diversion.

Table 7-6 – Water Discharge, Suspended Sand Concentration and Suspended Sand Load at Outflows – Belair (RM 65, RK 105) Case Study – Peak Flows

Site	Peak Flows			Intermediate Flows		
	Q (m ³ /s)	Cs (mg/L)	Qs (metric tons/day)	Q (m ³ /s)	Cs (mg/L)	Qs (metric tons/day)
Belair	5,454	151	71,288	2,779	35	8,489
West Pointe-À-La-Hache	27	27	63	14	7	8
Bohemia Spillway	3,244	22	6,220	235	5	91
Bayou Lamoque	78	15	99	61	4	22
Fort St. Philip	538	16	752	392	6	203
Baptiste Collette	3,913	83	28,039	3,129	38	10,139
Grand Pass + Tiger Pass	2,689	35	8,241	2,121	15	2,742
Main Pass	2,831	9	2,205	2,191	3	645

Figure 7.107 and Figure 7.108 show the peak flow sand concentration at each outflow in graphical form for both the existing and the Belair tests. The results with the introduction of the large diversion are very different from the ones with the existing outflows only. At peak flows, the concentration of sand downstream of the introduced diversion dropped in some of the cases by more than 50%. The extraction of such a large outflow at Belair seems to reduce the capacity of the downstream channel use for other large diversions.

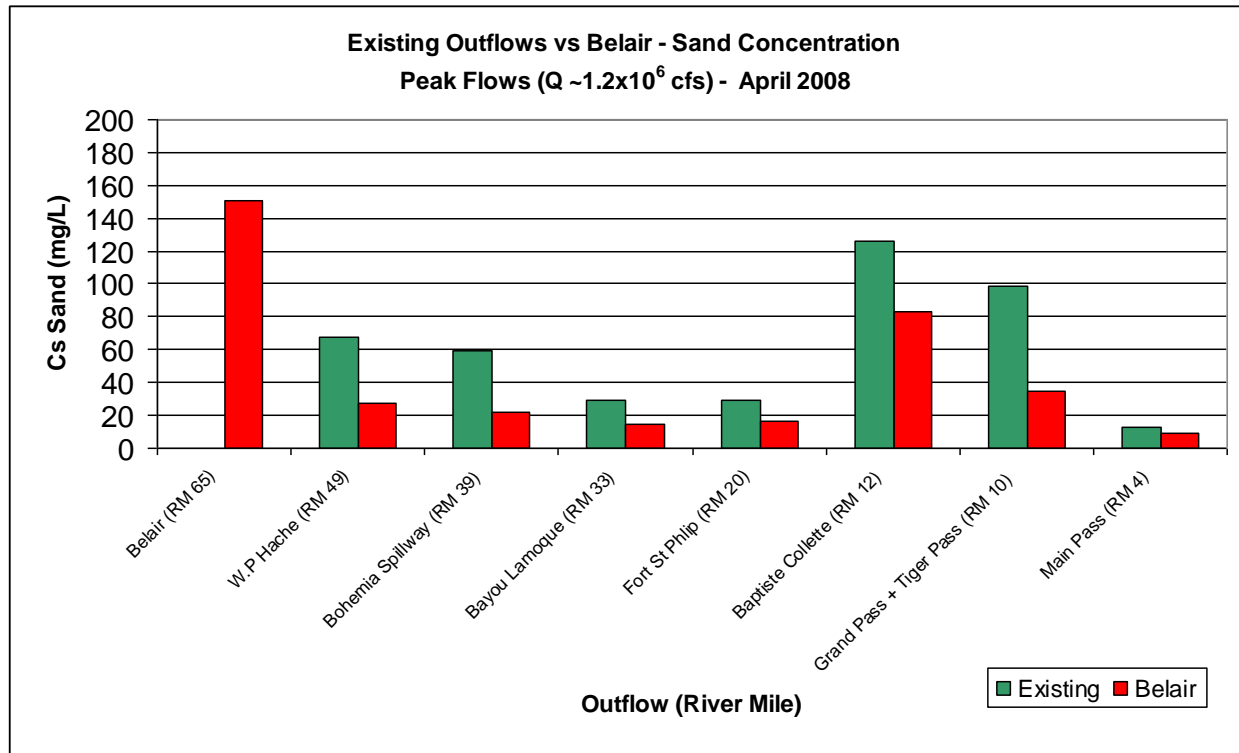


**Figure 7.107 – Existing Outflows + Belair (RM 65, RK 105) Diversion – Outflows
 Suspended Sand Concentration at Peak Flows**

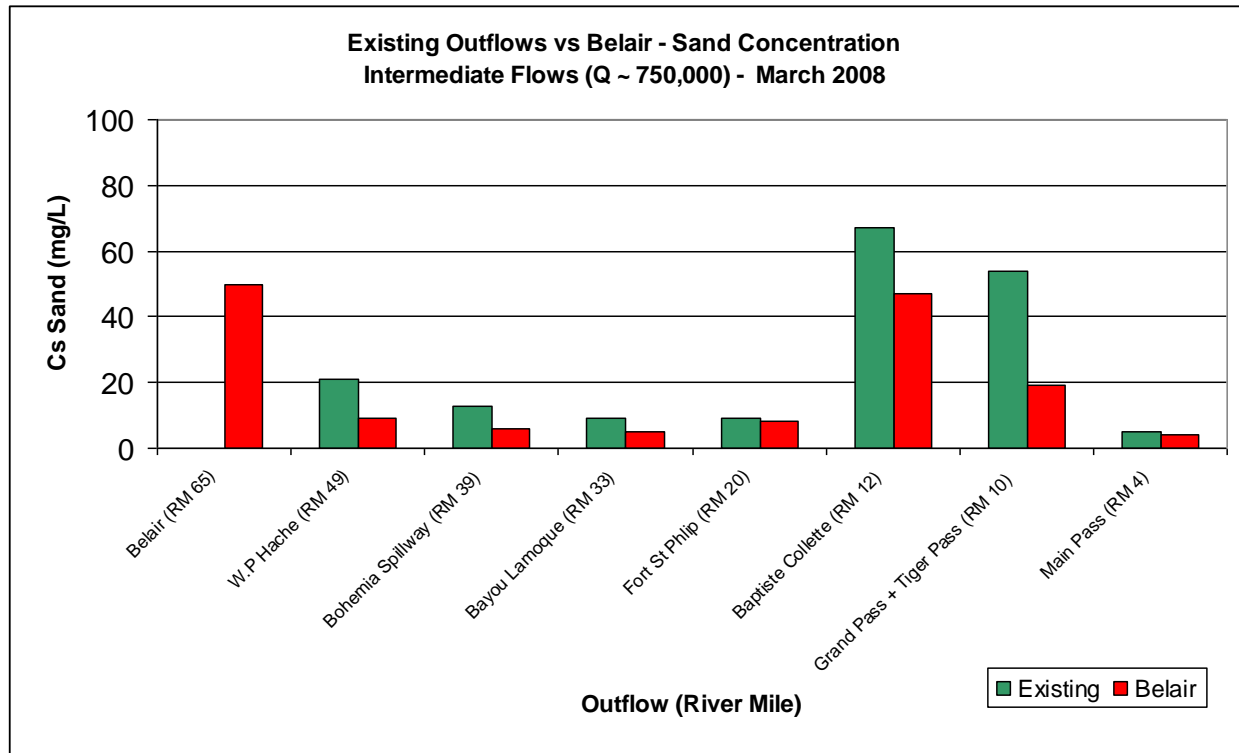


Figure 7.108 – Existing Outflows + Belair (RM 65, RK 105) – Outflows Suspended Sand Concentration at Intermediate Flows

7.5 Proposed MLODS Diversions + Existing Outflows

The third case set up consisted of the introduction of 5 proposed diversions, namely Jesuit Bend, Belair, Myrtle Grove, Deer Range and Buras with closure of the South and Southwest Passes and dredging of Pass a Loutr  as described in the MLODS (Lopez and LPBF, 2008), in addition to the existing outflows. The boundary conditions for this case were obtained from the Davis (2010) HEC-RAS model. Table 7-7 lists the proposed diversions added to the model, their locations and the water flows extracted.

Table 7-7 – Outflows for the Proposed Diversions Modeling

Site	Q peak (m ³ , cfs)		Q med (m ³ /s, cfs)	
Upstream Boundary				
Belle Chasse (RM 76)	32,356	1.14x10 ⁶	20,704	731,156
Proposed Diversions				
Jesuit Bend (RM 68)	-199	-7,030	-192	-6,796
Belair (RM 65)	-4,906	-173,270	-4,218	-148,966
Myrtle Grove (RM 59)	-820	-28,970	-785	-27,731
Deer Range (RM 54)	-423	-14,940	-407	-14,360
Buras (RM 25)	-4,006	-141,164	-3,891	-137,412
Existing Outflows inside the Model Domain				
West Pointe-�-La-Hache (RM 49)	-28	-1,000	-28	-1,000
Bohemia Spillway (RM 39)	-5,107	-180,346	-294	-10,379
Bayou Lamoque (RM 33)	-74	-2,607	-72	-2,537
Fort St. Philip (RM 20)	-497	-17,542	-470	-16,594
Baptiste Collette (RM 12)	-4,102	-144,846	-3,992	-140,978
Grand Pass + Tiger Pass (RM 10)	-2,942	-103,896	-2,863	-101,120
Main Pass (RM 4)	-3,675	-129,785	-3,566	-125,929
Existing Outflows located downstream of the Model Domain (Davis (2010) HEC-RAS Results)				
Southwest Pass (Gulf of Mexico)	0	0	0	0
South Pass (Gulf of Mexico)	0	0	0	0
Pass a Loutr� (RM 0)	-3,799	-134,173	-3,433	-121,228

The introduction of new diversions in the system limits the flows available to be extracted at the existing outflows. Thus, some of the outflow values given as River boundary conditions used in this case differ from the ones used for the case with only existing outflows. The Belle Chasse inflow values were changed slightly to reflect the implementation of proposed diversions upstream of the model domain. The open boundary condition at RM 3 was also changed. The downstream stage was raised by approximately 0.25 m at peak flow conditions, based on the assumption that 2 of the passes will be closed, i.e. South and Southwest Pass, and Pass a Loutr  will be dredged for navigation purposes.

Figure 7.109 shows the longitudinal profile of water discharge in the main channel at peak flows for both proposed diversions and existing outflows tests. It can be seen that an extra 9,000 m³/s of flow was extracted with the implementation of the proposed diversions.

Figure 7.110 and Figure 7.111 show the main channel total and kinetic energy with the introduction of the proposed diversions. There is a clear the drop in both kinetic and total energy as a result of the extraction of so much flow. The effect of the Belair diversion (RM 65) is very clear with a significant reduction in the values downstream of it.

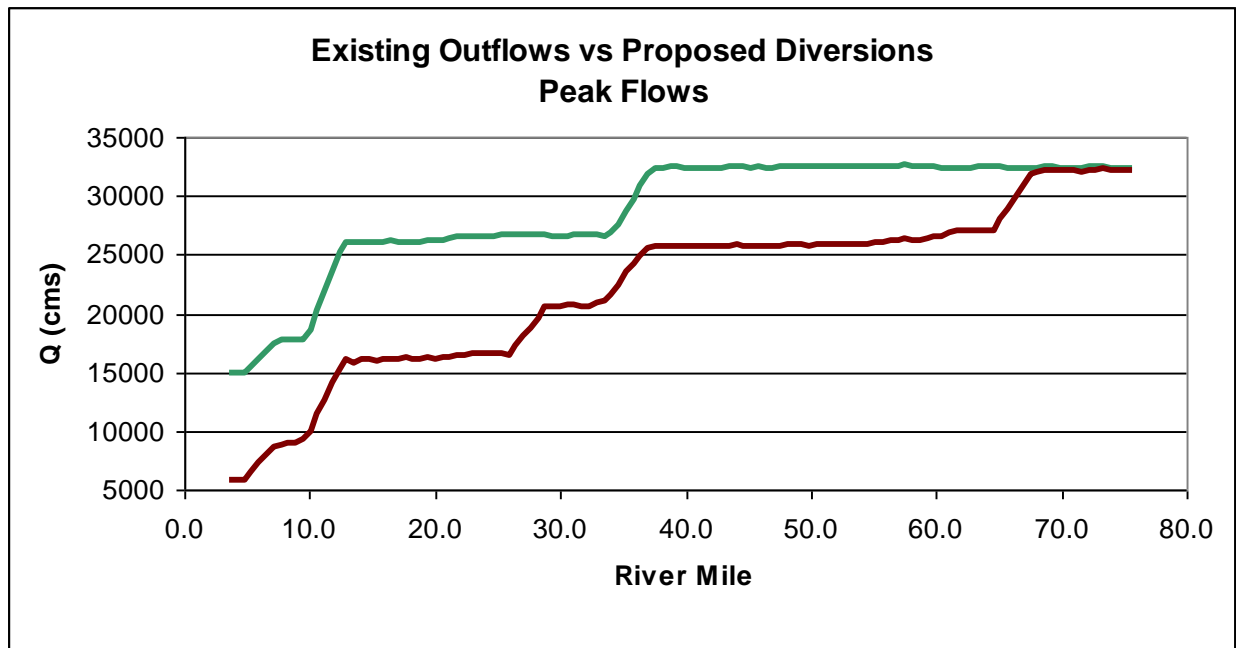


Figure 7.109 – Existing Outflows + Proposed Diversions – Main Channel Water Discharge at Peak Flows. *Proposed Diversions: Jesuit Bend (RM 68, RK 109), Belair (RM 65, RK 105), Myrtle Grove (RM 59, RK 94), Deer Range (RM 54, RK 87) and Buras (RM 25, RK 40).*

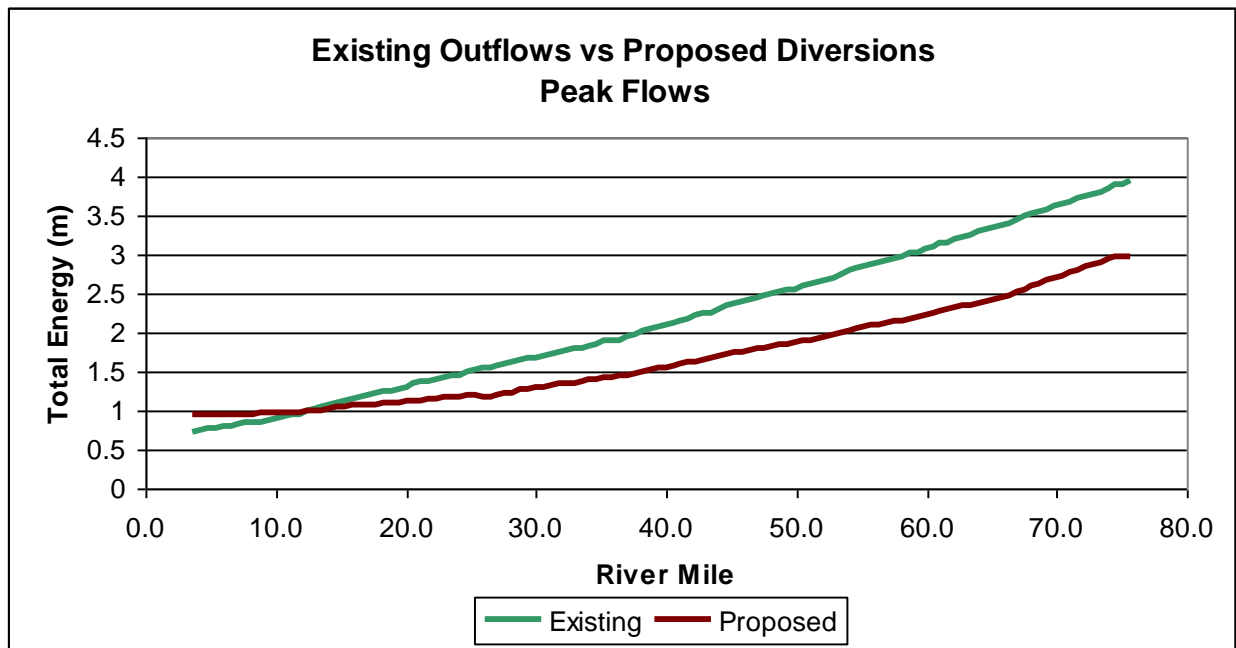


Figure 7.110 – Existing Outflows + Proposed Diversions – Main Channel Total Energy of the Flow at Peak Flows. *Proposed Diversions: Jesuit Bend (RM 68, RK 109), Belair (RM 65, RK 105), Myrtle Grove (RM 59, RK 94), Deer Range (RM 54, RK 87) and Buras (RM 25, RK 40).*

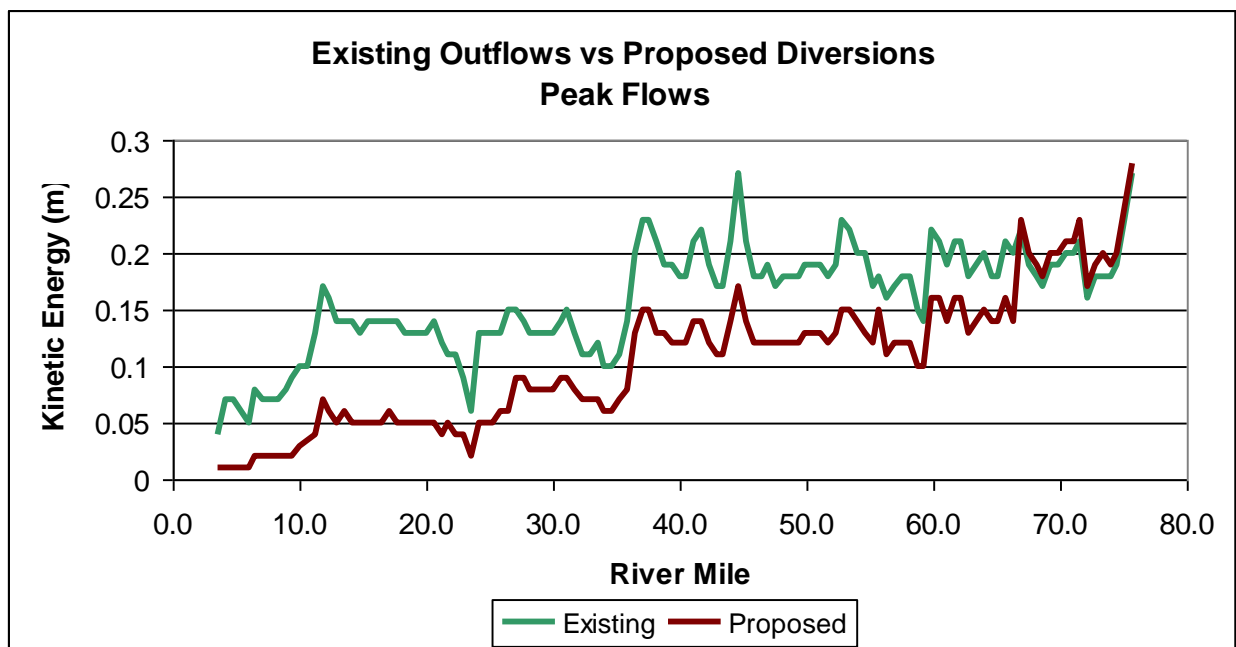


Figure 7.111 – Existing Outflows + Proposed Diversions – Main Channel Kinetic Energy of the Flow at Peak Flows. *Proposed Diversions: Jesuit Bend (RM 68, RK 109), Belair (RM 65, RK 105), Myrtle Grove (RM 59, RK 94), Deer Range (RM 54, RK 87) and Buras (RM 25, RK 40).*

Figure 7.112, Figure 7.113 and Figure 7.114 show respectively, the main channel total, potential and kinetic energy fluxes under peak flow conditions for the Proposed MLODS Diversions test.

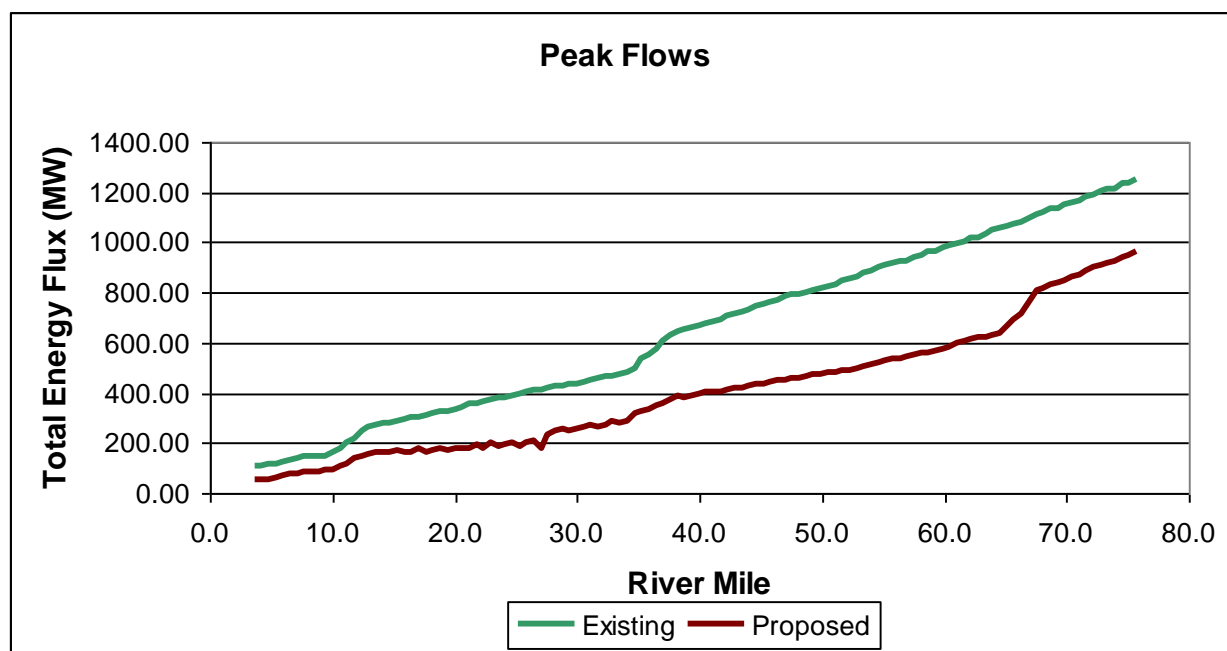


Figure 7.112 – Existing Outflows + Proposed Diversions – Main Channel Total Energy Flux of the Flow at Peak Flows. *Proposed Diversions: Jesuit Bend (RM 68, RK 109), Belair (RM 65, RK 105), Myrtle Grove (RM 59, RK 94), Deer Range (RM 54, RK 87) and Buras (RM 25, RK 40)*

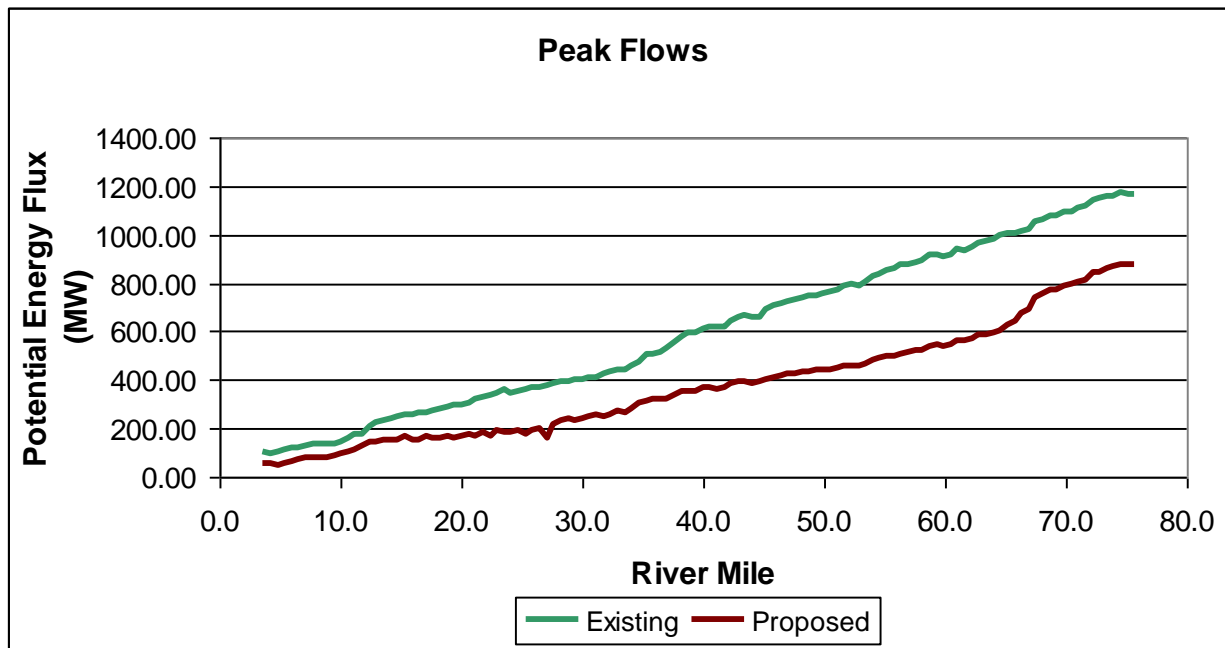


Figure 7.113 – Existing Outflows + Proposed Diversions – Main Channel Potential Energy Flux of the Flow at Peak Flows. *Proposed Diversions: Jesuit Bend (RM 68, RK 109), Belair (RM 65, RK 105), Myrtle Grove (RM 59, RK 94), Deer Range (RM 54, RK 87) and Buras (RM 25, RK 40).*

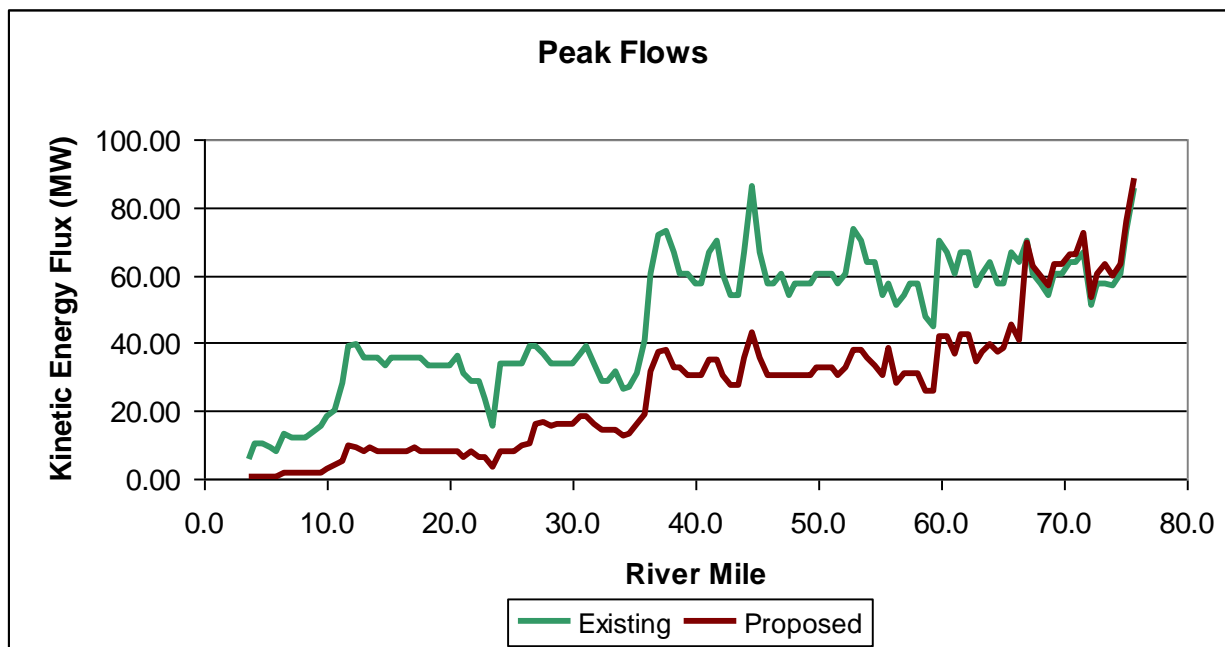


Figure 7.114 – Existing Outflows + Proposed Diversions – Main Channel Kinetic Energy Flux of the Flow at Peak Flows. *Proposed Diversions: Jesuit Bend (RM 68, RK 109), Belair (RM 65, RK 105), Myrtle Grove (RM 59, RK 94), Deer Range (RM 54, RK 87) and Buras (RM 25, RK 40).*

The main channel sand concentration and load changes with the introduction of the proposed MLODS diversions are shown in Figure 7.115 and Figure 7.116. These results confirm the very significant reduction of the transport downstream of the Belair diversion and indicate a sediment starved system in the lower 35 miles of the reach.

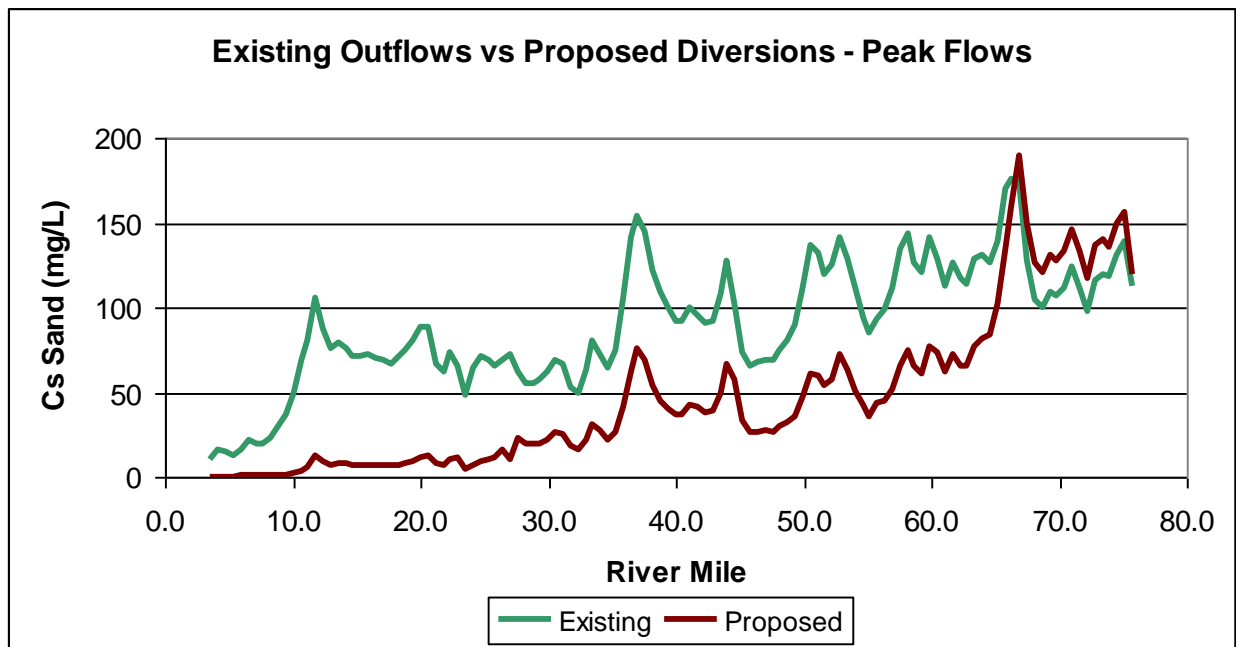


Figure 7.115 – Existing Outflows + Proposed Diversions – Main Channel Suspended Sand Concentration at Peak Flows. *Proposed Diversions: Jesuit Bend (RM 68, RK 109), Belair (RM 65, RK 105), Myrtle Grove (RM 59, RK 94), Deer Range (RM 54, RK 87) and Buras (RM 25, RK 40).*

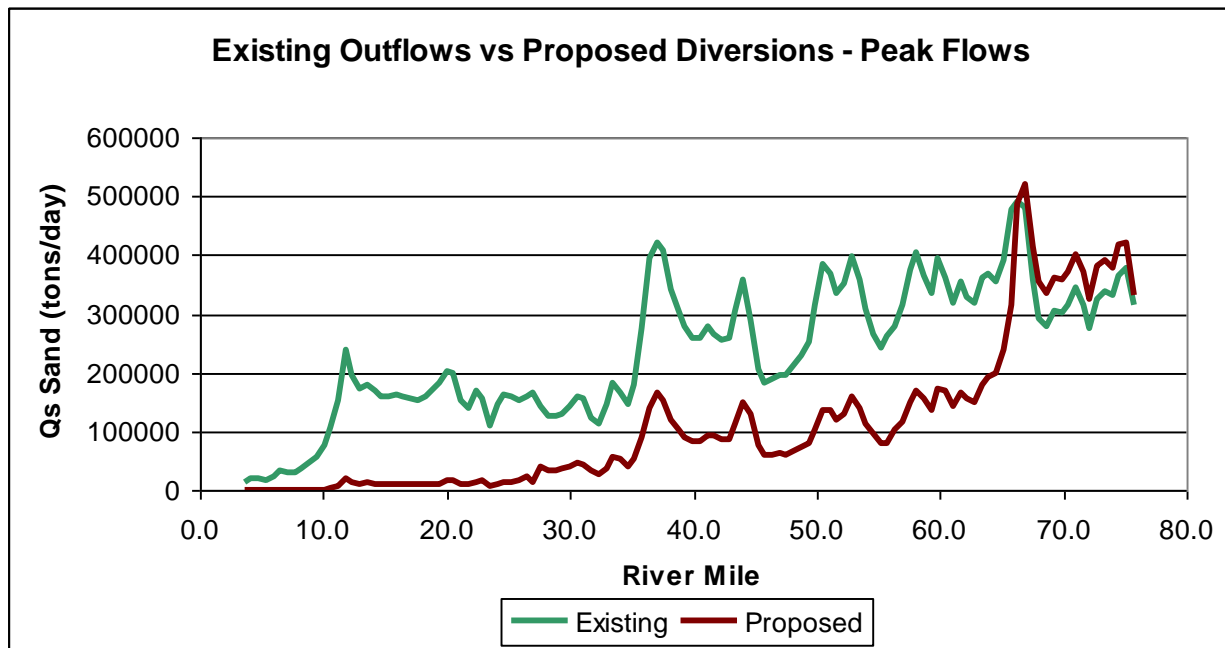


Figure 7.116 – Existing Outflows + Proposed Diversions – Main Channel Sand Load at Peak Flows. *Proposed Diversions: Jesuit Bend (RM 68, RK 109), Belair (RM 65, RK 105), Myrtle Grove (RM 59, RK 94), Deer Range (RM 54, RK 87) and Buras (RM 25, RK 40).*

Figure 7.117 shows the longitudinal profile of water discharge in the main channel at intermediate flows for both proposed diversions and existing outflows scenarios. It can be seen that an extra 11,000 m³/s of flow was extracted with the implementation of the proposed diversions leaving the downstream end of the channel with a flow of approximately 600 m³/s.

Figure 7.118 and Figure 7.119 show the main channel total and kinetic energy change with the introduction of the proposed diversions at intermediate flows. There is pronounced drop in both kinetic and total energy as a result of the extraction of so much flow. Once again, the effect of the Belair diversion (RM 65) is dominant.

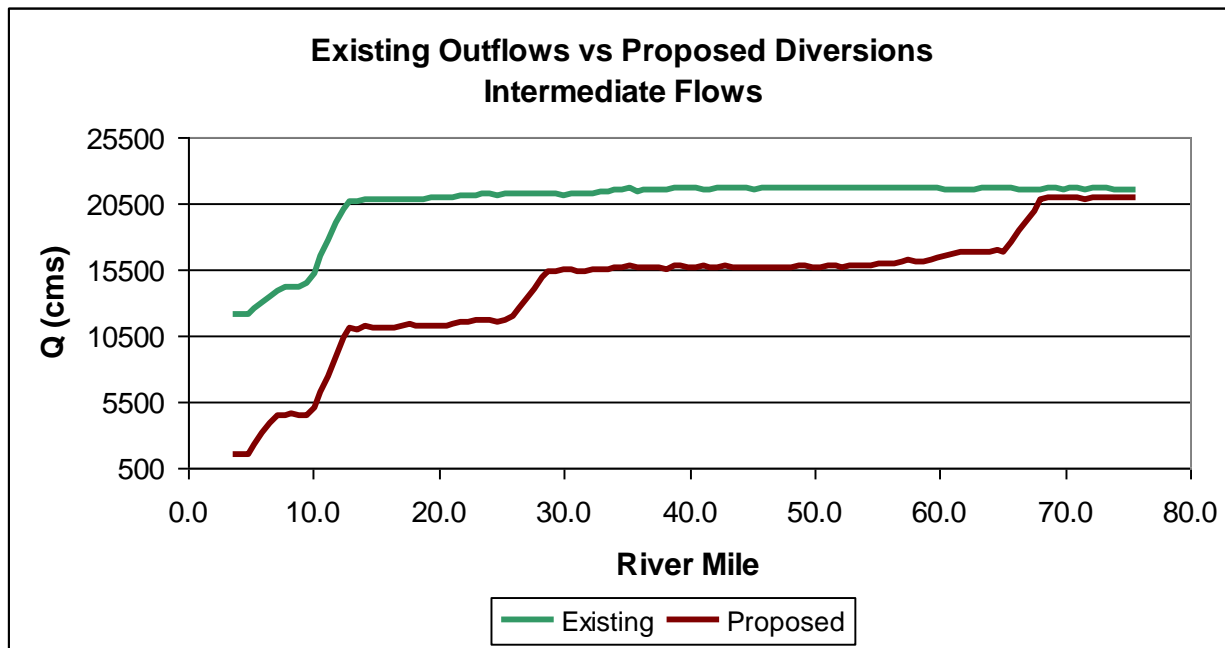


Figure 7.117 – Existing Outflows + Proposed Diversions – Main Channel Water Discharge at Intermediate Flows. *Proposed Diversions: Jesuit Bend (RM 68, RK 109), Belair (RM 65, RK 105), Myrtle Grove (RM 59, RK 94), Deer Range (RM 54, RK 87) and Buras (RM 25, RK 40).*

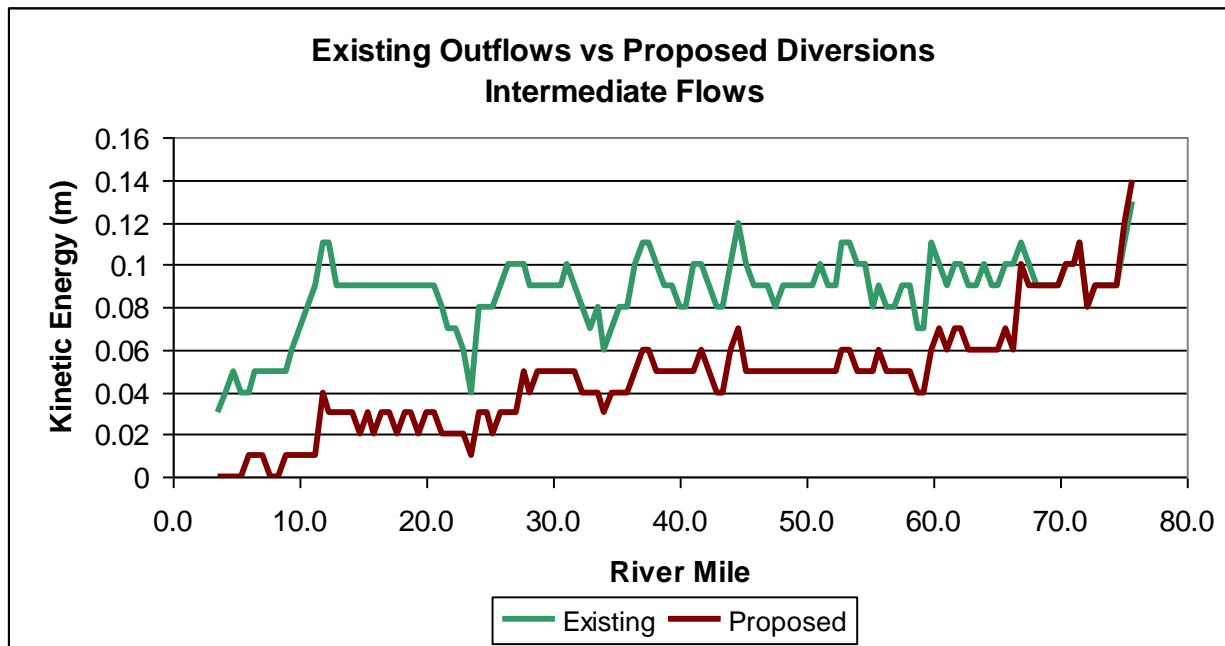


Figure 7.118 – Existing Outflows + Proposed Diversions – Main Channel Kinetic Energy of the Flow at Intermediate Flows. *Proposed Diversions: Jesuit Bend (RM 68, RK 109), Belair (RM 65, RK 105), Myrtle Grove (RM 59, RK 94), Deer Range (RM 54, RK 87) and Buras (RM 25, RK 40).*

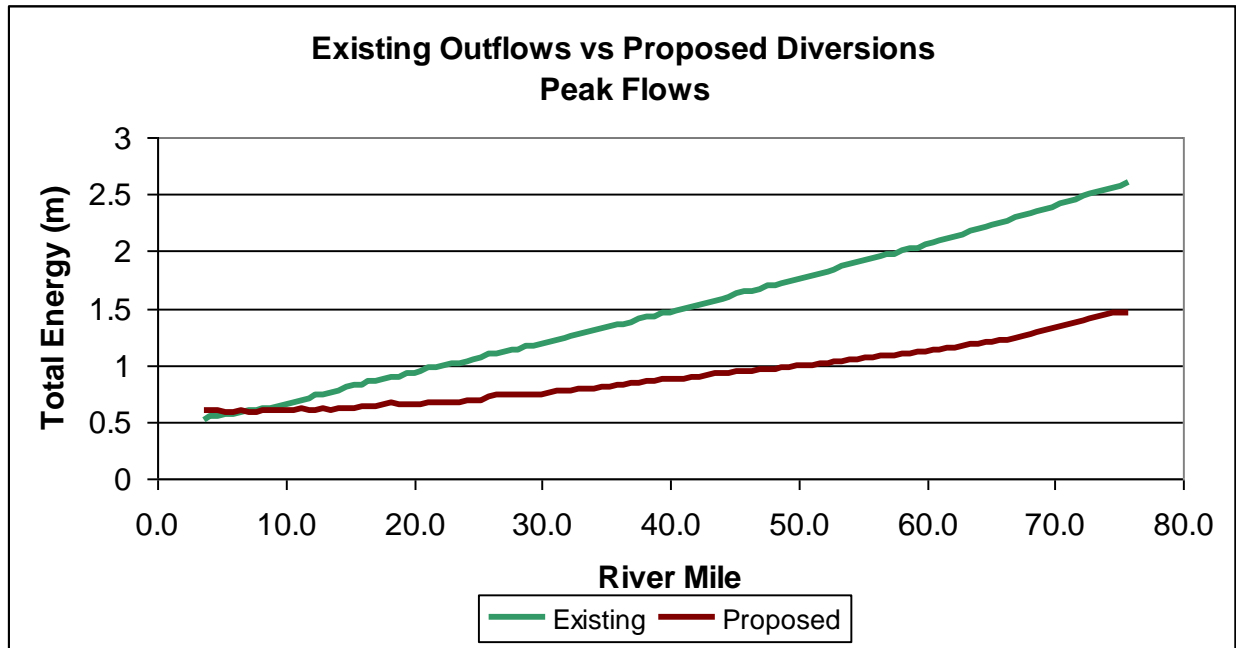


Figure 7.119 – Existing Outflows + Proposed Diversions – Main Channel Total Energy of the Flow at Intermediate Flows. *Proposed Diversions: Jesuit Bend (RM 68, RK 109), Belair (RM 65, RK 105), Myrtle Grove (RM 59, RK 94), Deer Range (RM 54, RK 87) and Buras (RM 25, RK 40).*

Figure 7.112, Figure 7.113 and Figure 7.114 show respectively, the main channel total, potential and kinetic energy fluxes under intermediate flow conditions for the Proposed MLODS Diversions Scenario.

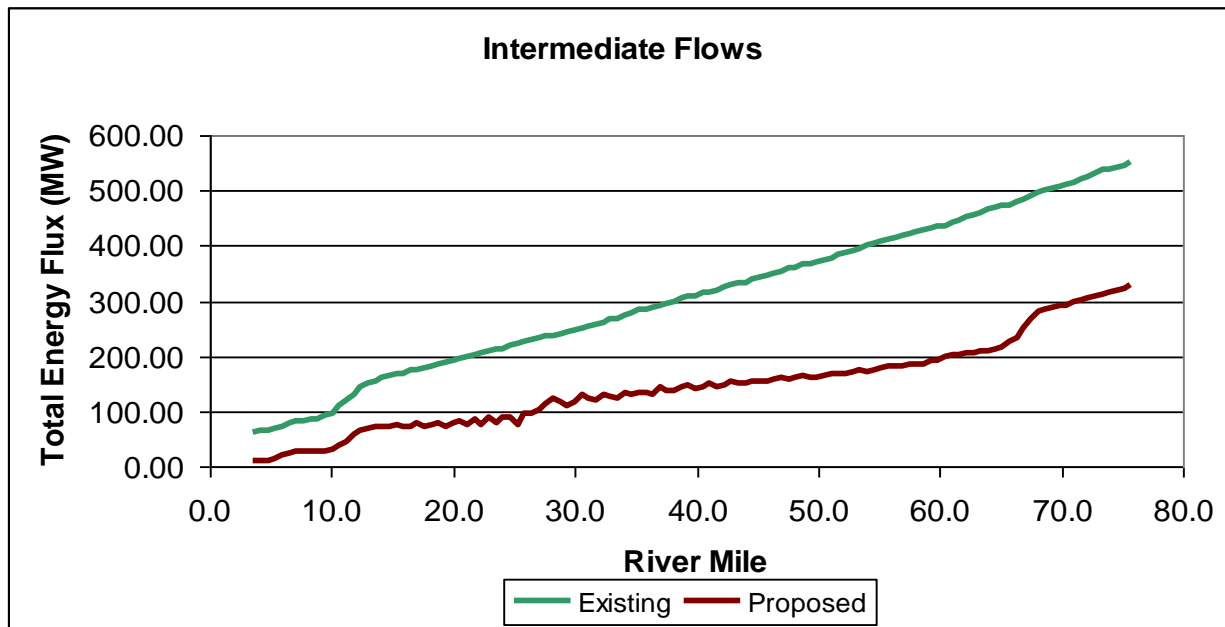


Figure 7.120 – Existing Outflows + Proposed Diversions – Main Channel Total Energy Flux of the Flow at Intermediate Flows. *Proposed Diversions: Jesuit Bend (RM 68, RK 109), Belair (RM 65, RK 105), Myrtle Grove (RM 59, RK 94), Deer Range (RM 54, RK 87) and Buras (RM 25, RK 40).*

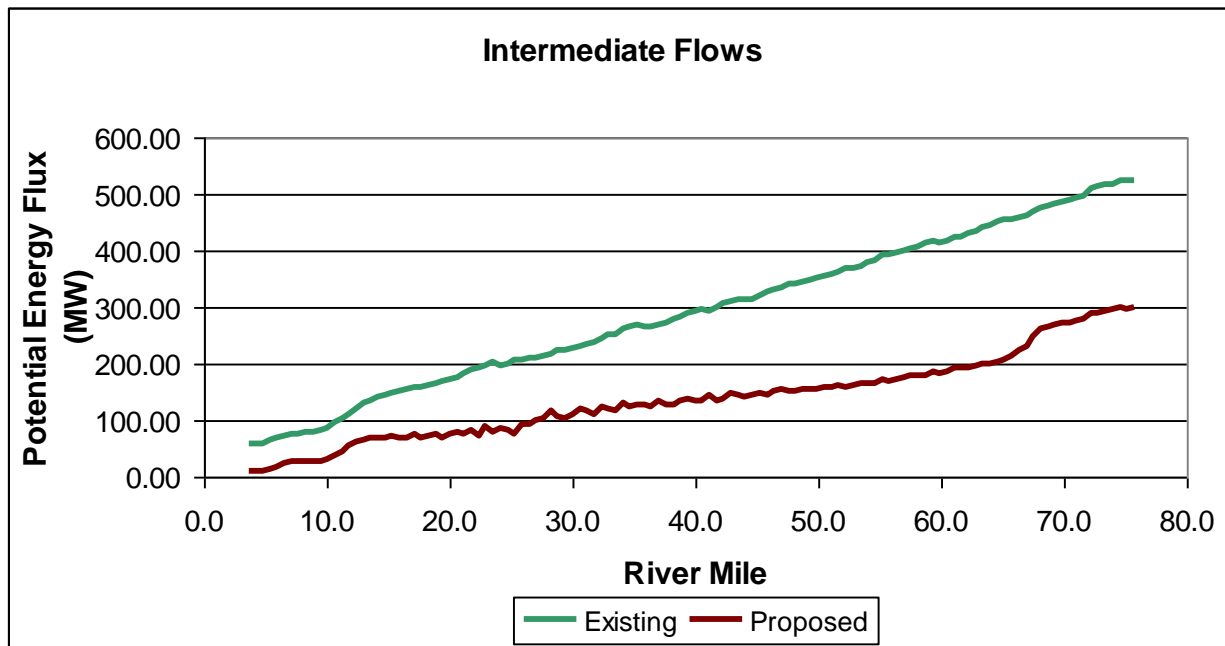


Figure 7.121 – Existing Outflows + Proposed Diversions – Main Channel Potential Energy Flux of the Flow at Intermediate Flows. *Proposed Diversions: Jesuit Bend (RM 68, RK 109), Belair (RM 65, RK 105), Myrtle Grove (RM 59, RK 94), Deer Range (RM 54, RK 87) and Buras (RM 25, RK 40).*

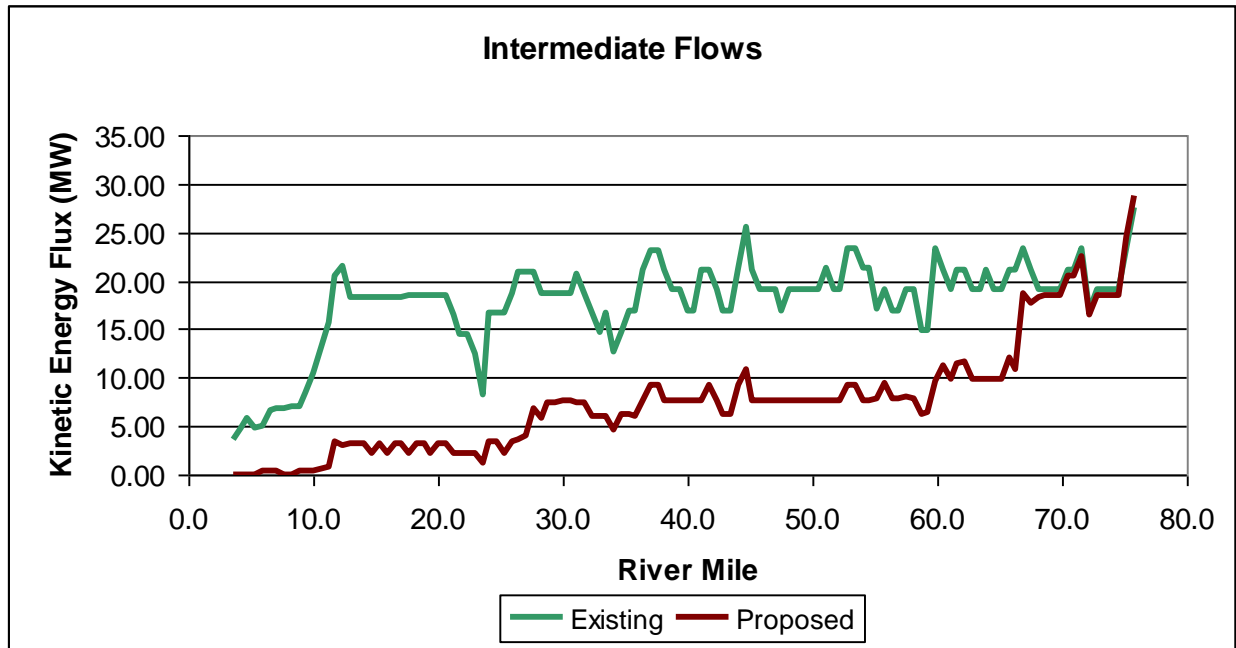


Figure 7.122 – Existing Outflows + Proposed Diversions – Main Channel Kinetic Energy Flux of the Flow at Intermediate Flows. *Proposed Diversions: Jesuit Bend (RM 68, RK 109), Belair (RM 65, RK 105), Myrtle Grove (RM 59, RK 94), Deer Range (RM 54, RK 87) and Buras (RM 25, RK 40).*

The main channel sand concentration and sand load changes due to the proposed suite of diversions at intermediate flows are shown in Figure 7.123 and Figure 7.124. Downstream of the Belair diversion, the sediment concentration drops to extremely low values, particularly in the lower 35 miles of the reach, due to the extraction of most of the flow in the reach.

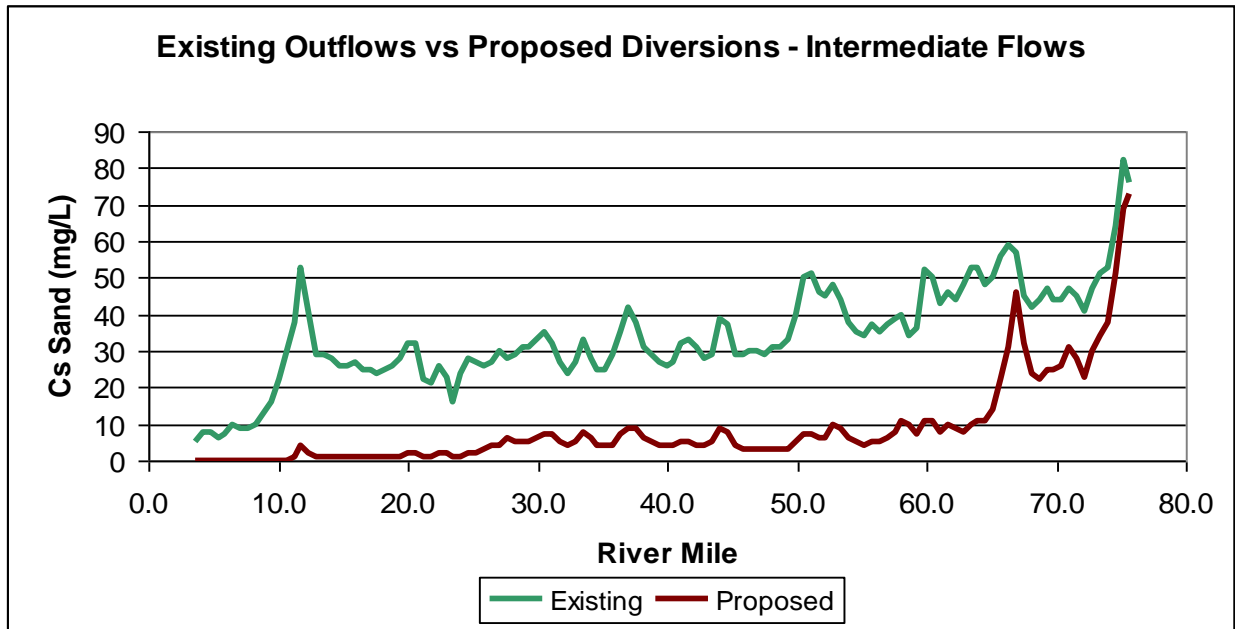


Figure 7.123 – Existing Outflows + Proposed Diversions – Main Channel Suspended Sand Concentration at Intermediate Flows. *Proposed Diversions: Jesuit Bend (RM 68, RK 109), Belair (RM 65, RK 105), Myrtle Grove (RM 59, RK 94), Deer Range (RM 54, RK 87) and Buras (RM 25, RK 40).*

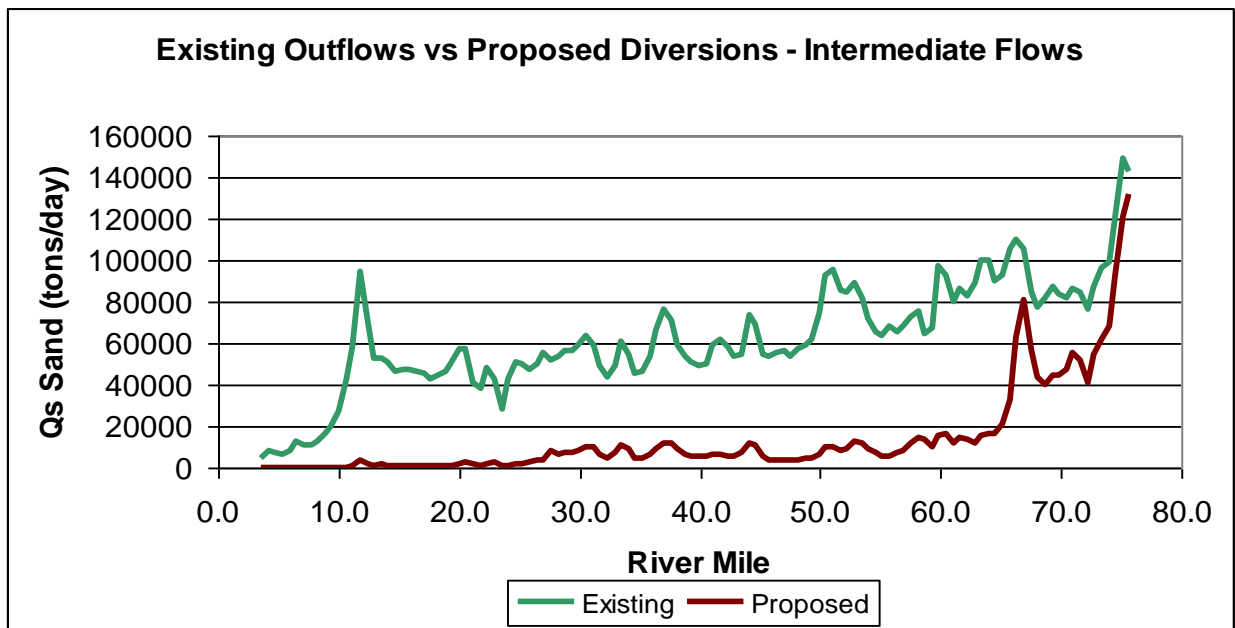
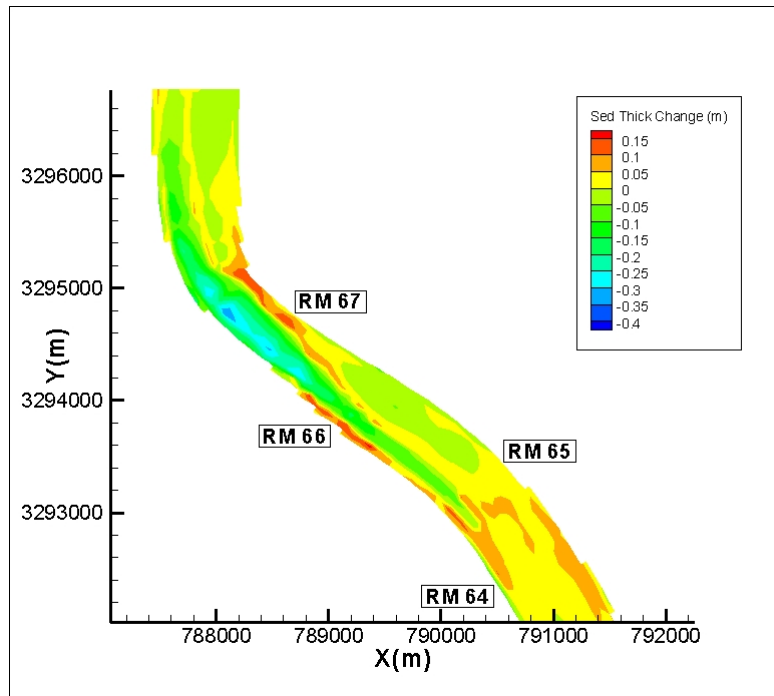
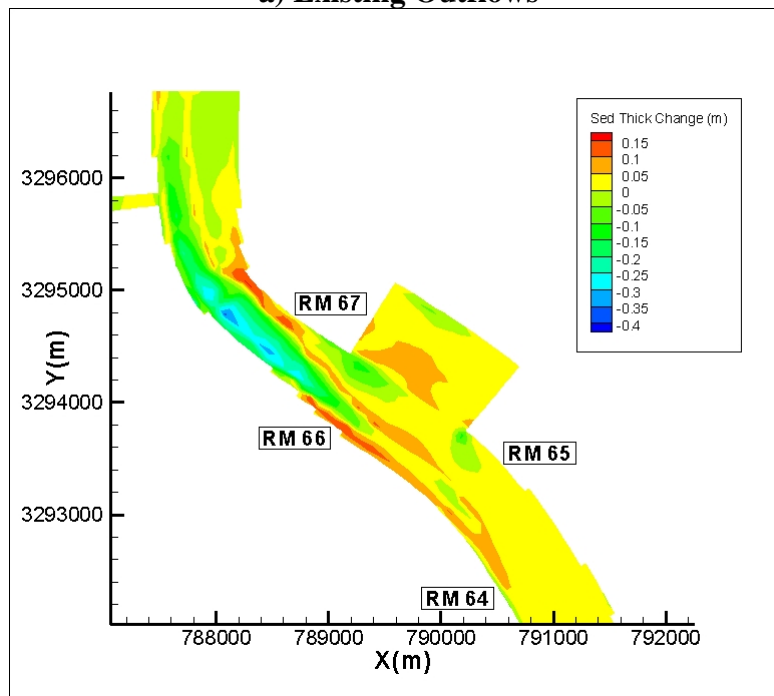


Figure 7.124 – Existing Outflows + Proposed Diversions – Main Channel Suspended Sand Load at Intermediate Flows. *Proposed Diversions: Jesuit Bend (RM 68, RK 109), Belair (RM 65, RK 105), Myrtle Grove (RM 59, RK 94), Deer Range (RM 54, RK 87) and Buras (RM 25, RK 40).*

The bed sediment thickness change under peak flows after 1 day and 10 days of simulation for the existing diversions and the proposed diversions cases is presented in Figure 7.125 and Figure 7.127. The introduction of the diversion changes the erosion/deposition pattern significantly as was found with the Belair test. It is evident that there is more deposition in the locations downstream of the diversions, particularly the large Belair diversion, than without the diversions. The presence of more deposition areas and the almost non-existence of erosion downstream of the Belair diversion can be seen in the comparison shown in Figure 7.126 and Figure 7.128 for the Myrtle Grove area at peak. The Myrtle Grove test showed that the effect of the Myrtle Grove diversion by itself is not very significant. Jesuit Bend (RM 68) does not extract a large amount of flow or sand. Thus, most of the deposition increase shown in Figure 7.126 and in Figure 7.128 can be attributed to the introduction of the Belair diversion.

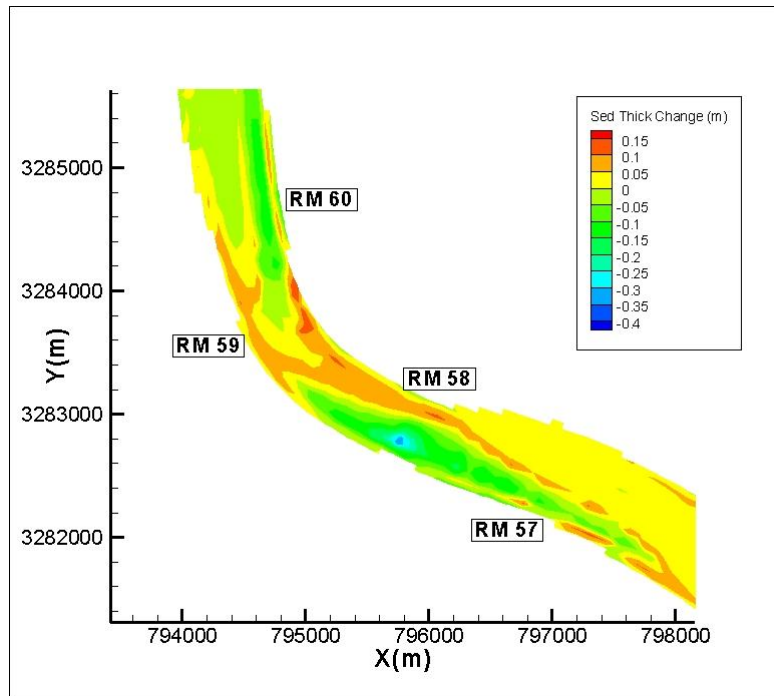


a) Existing Outflows

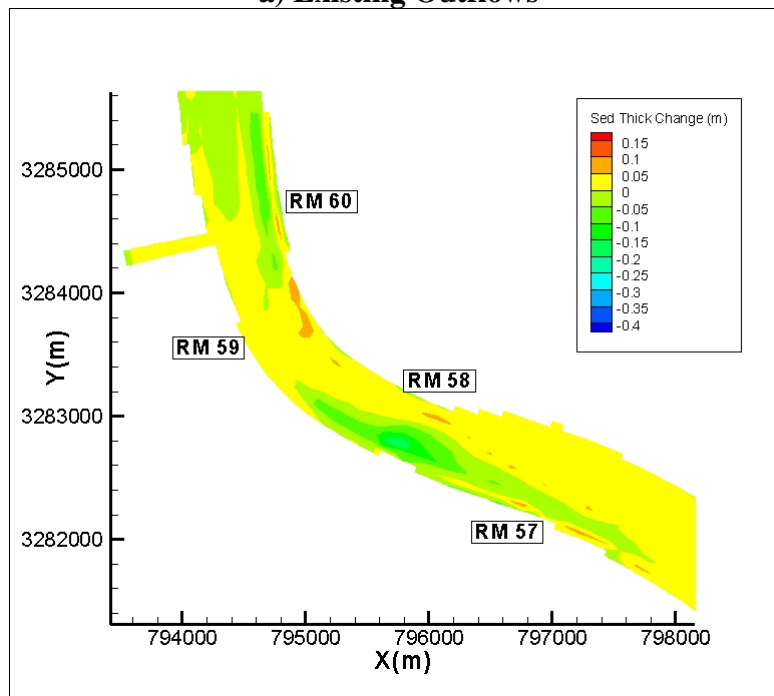


b) Proposed Diversions

Figure 7.125 – Proposed Diversions – Belair Area (RM 65, RK 105) - Bed Sediment Thickness Change after 1 day at Peak Flows. Positive values indicate deposition and negative values indicate erosion

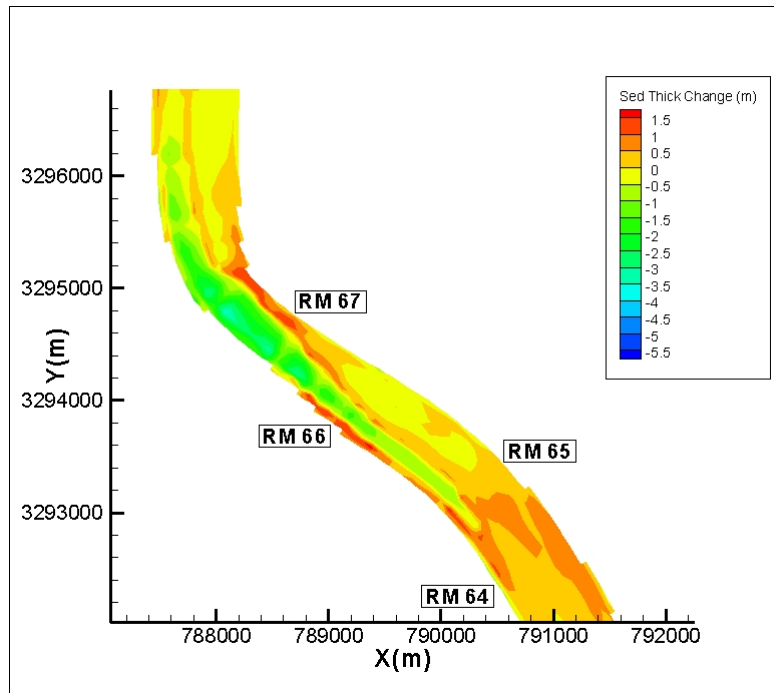


a) Existing Outflows

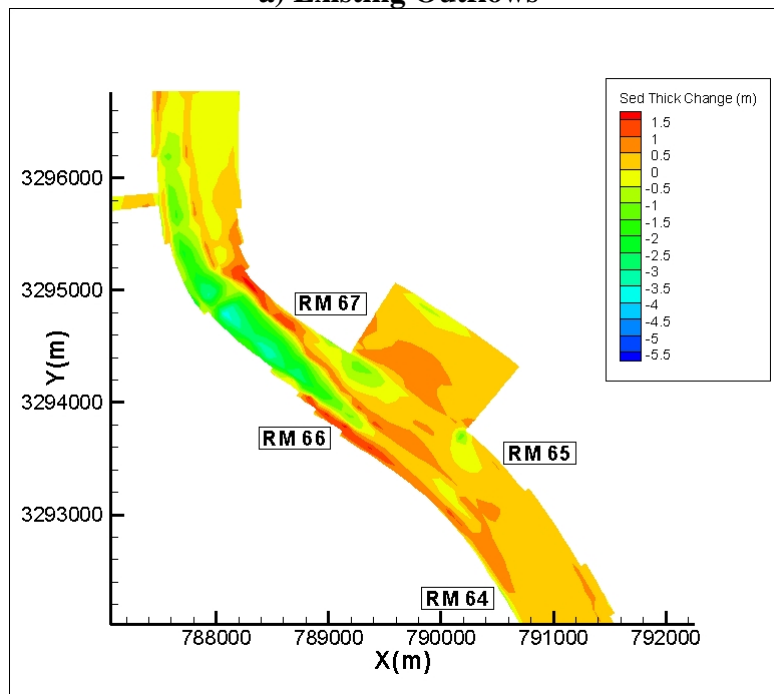


b) Proposed Diversions

Figure 7.126 – Proposed Diversions – Myrtle Grove Area (RM 59, RK 94) - Bed Sediment Thickness Change after 1 day at Peak Flows. Positive values indicate deposition and negative values indicate erosion

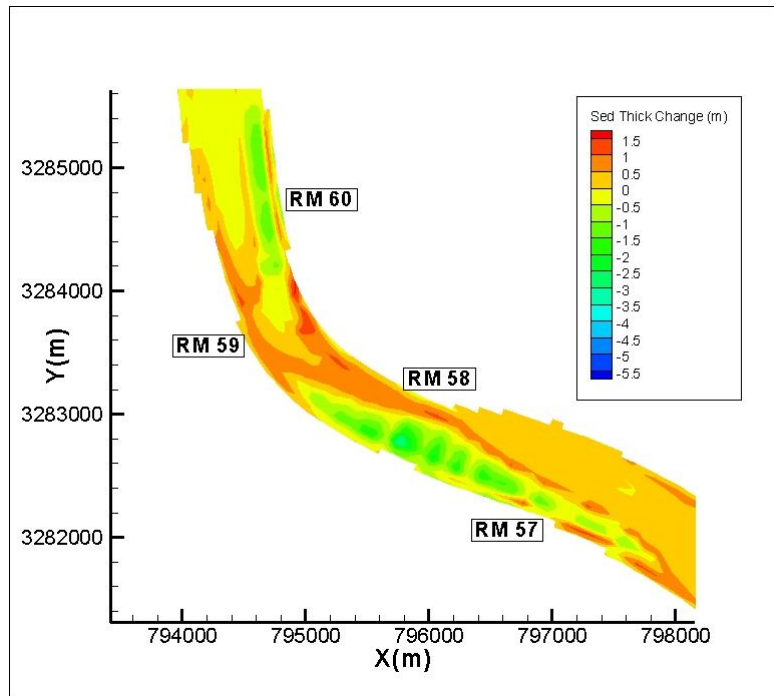


a) Existing Outflows

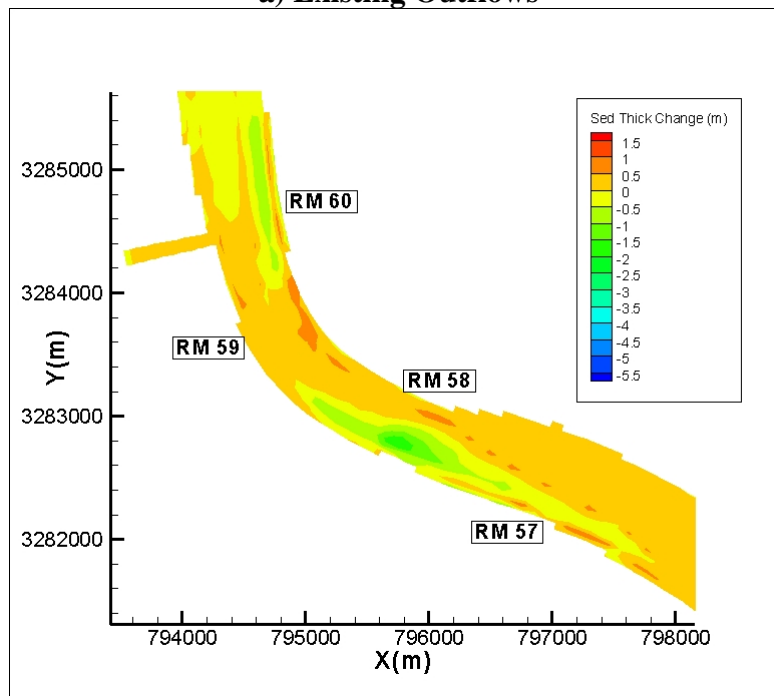


b) Proposed Diversions

Figure 7.127 – Proposed Diversions – Belair Area (RM 65, RK 105) - Bed Sediment Thickness Change after 10 days at Peak Flows. Positive values indicate deposition and negative values indicate erosion



a) Existing Outflows



b) Proposed Diversions

Figure 7.128 – Proposed Diversions – Myrtle Grove Area (RM 59, RK 94) - Bed Sediment Thickness Change after 10 days at Peak Flows. Positive values indicate deposition and negative values indicate erosion

Figure 7.129 summarizes the difference between the results obtained with the Proposed MLODS Diversions Scenario and with the Existing Outflows. The downstream reach is dominated by increased deposition (green or depositional areas) with a few localized areas in red where the erosion is increased for the Proposed Diversions Case compared to the existing conditions. These results are closer to the ones obtained with the introduction of the Belair diversion than those obtained with the introduction of the Myrtle Grove diversion. Among the proposed diversions, the one that causes the most impact in the system sediment transport is clearly the Belair diversion. Both the location of the diversion in an area where there is enough flow, energy and sediment available, and the amount of flow being extracted contribute to its influence in the system. In fact, Belair is so large that it induces upstream erosion. Overall, even when compared with the other large outflows (e.g. Buras) located closer to the downstream end of the modeled reach, the Belair diversion clearly extracts higher sand loads due to its upstream location.

The change in bed sediment thickness under intermediate flows after 1 day and 10 days of simulation for the existing conditions and the proposed MLODS diversions is presented from Figure 7.130 through Figure 7.133. The introduction of the diversions changes the erosion/deposition pattern significantly as was previously shown for the peak flow results. It is evident that there is more deposition at locations downstream of a diversion than without a diversion.

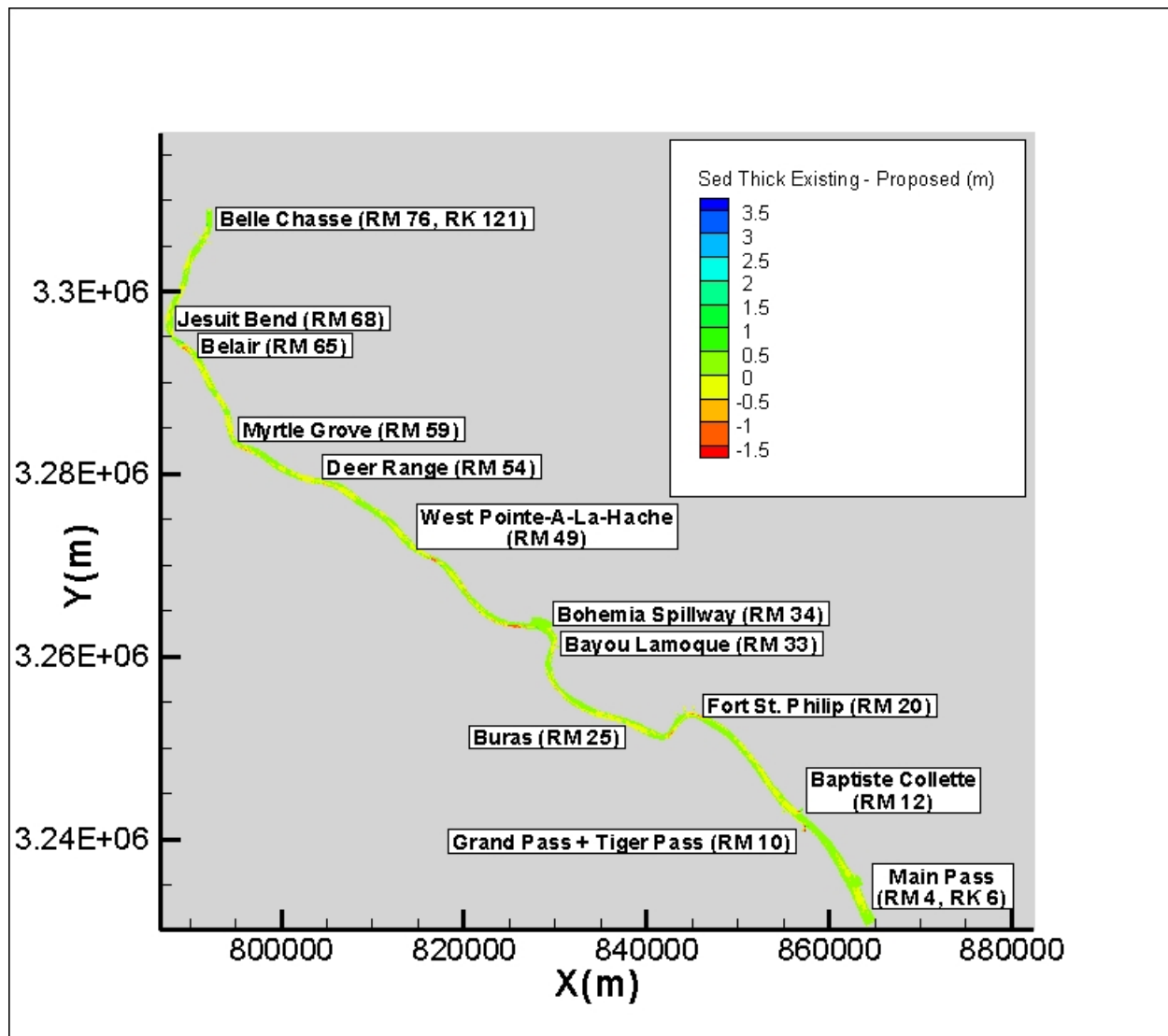
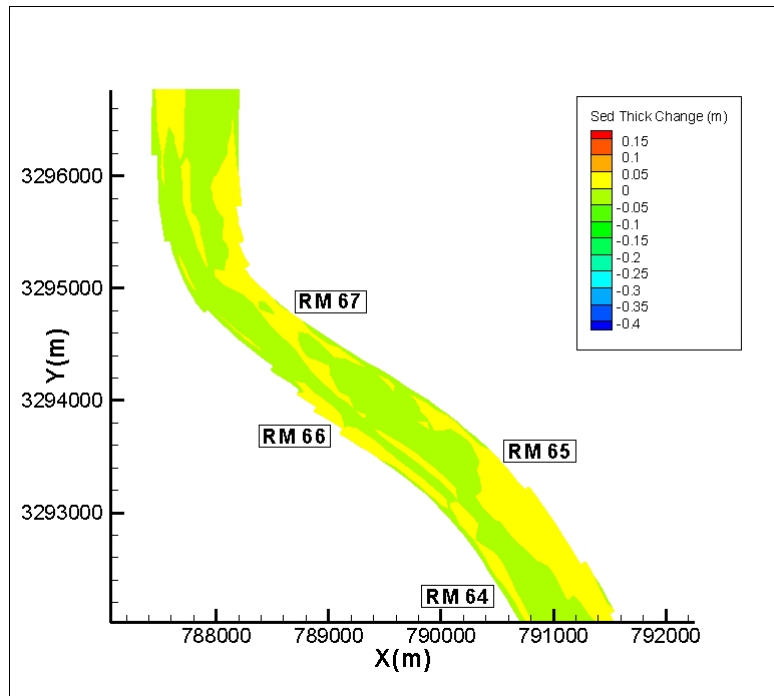
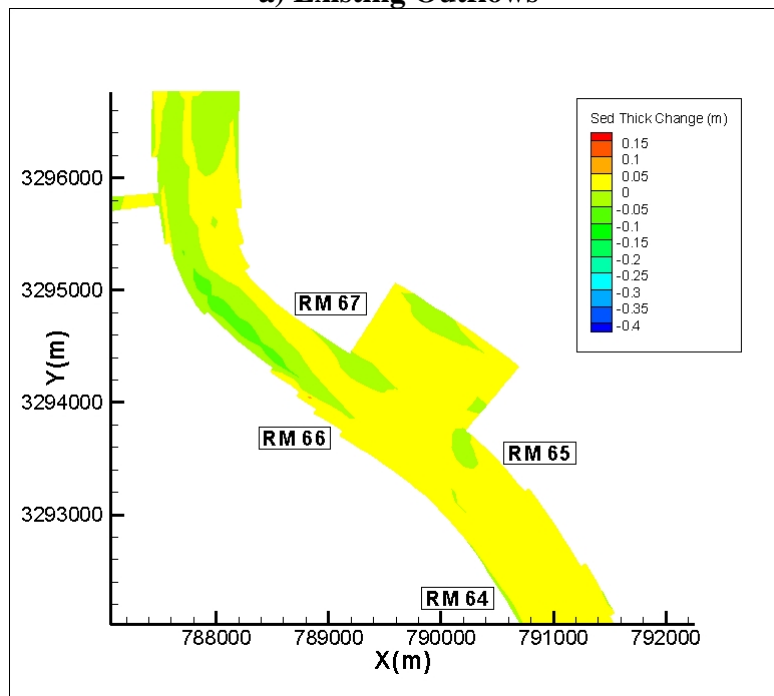


Figure 7.129 – Model Domain – Difference between Existing and Proposed Test Bed Sediment Thickness Change after 10 days at Peak Flows. Positive values indicate that the addition of the Proposed Diversions increased deposition. Negative values indicate that the addition of the Proposed Diversions increased erosion.

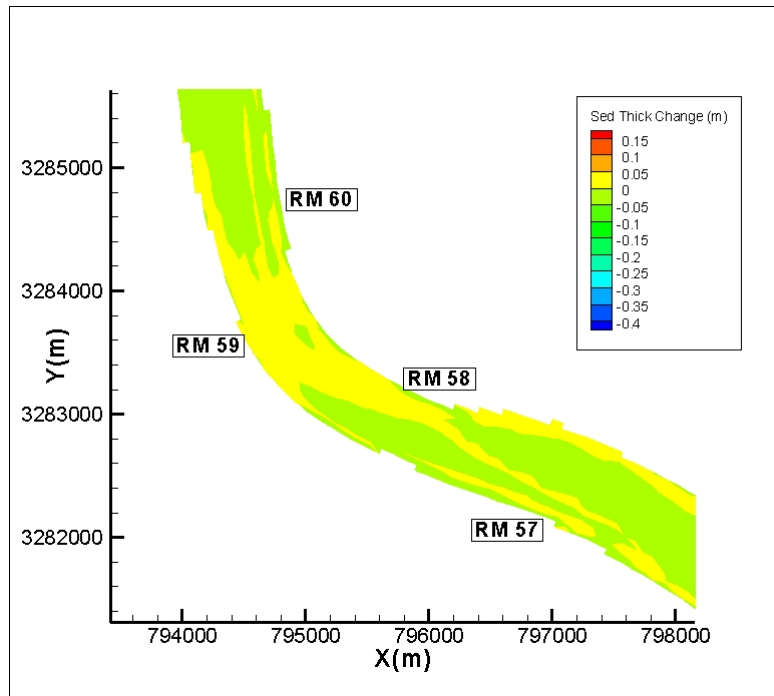


a) Existing Outflows

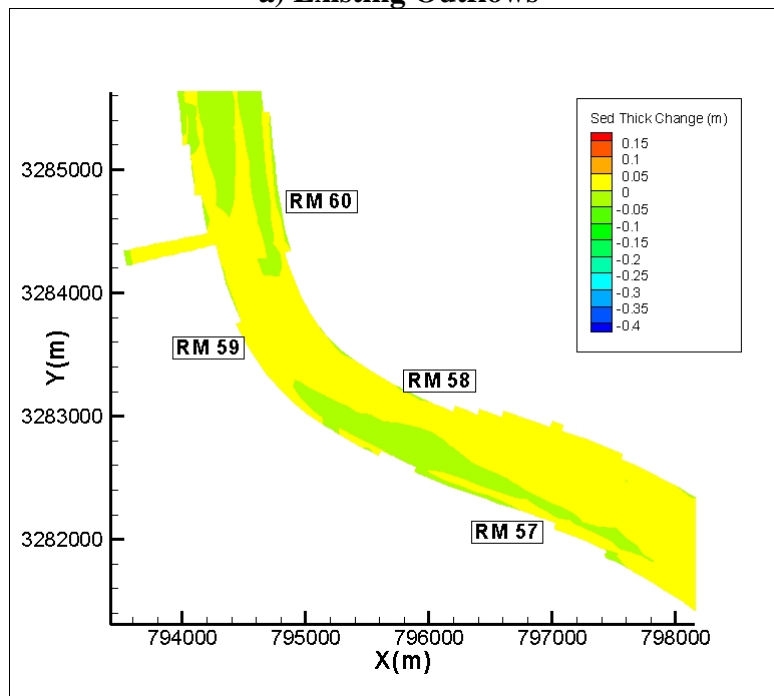


b) Proposed Diversions

Figure 7.130 – Proposed Diversions – Belair Area (RM 65, RK 94) - Bed Sediment Thickness Change after 1 day at Intermediate Flows. Positive values indicate deposition and negative values indicate erosion

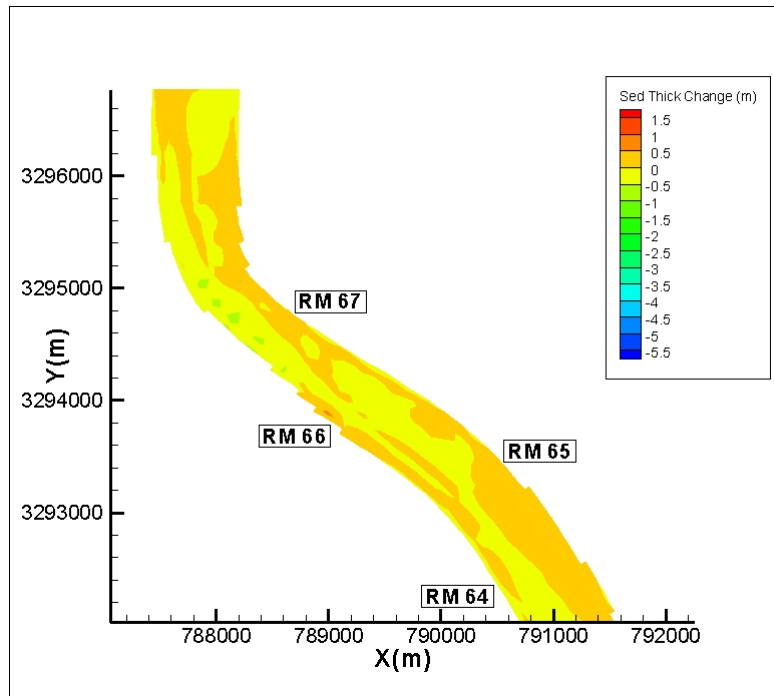


a) Existing Outflows

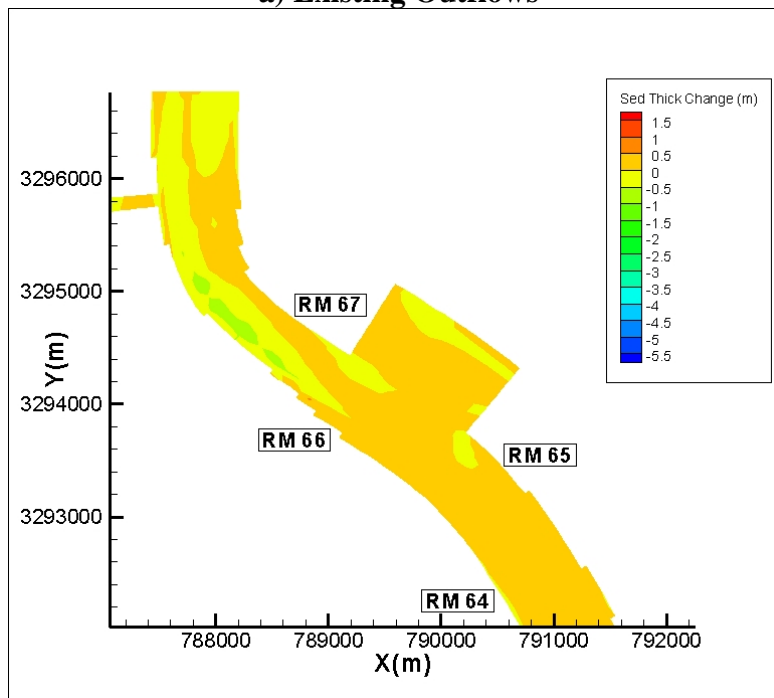


b) Proposed Diversions

Figure 7.131 – Proposed Diversions – Myrtle Grove Area (RM 59, RK 94) - Bed Sediment Thickness Change after 1 day at Intermediate Flows. Positive values indicate deposition and negative values indicate erosion

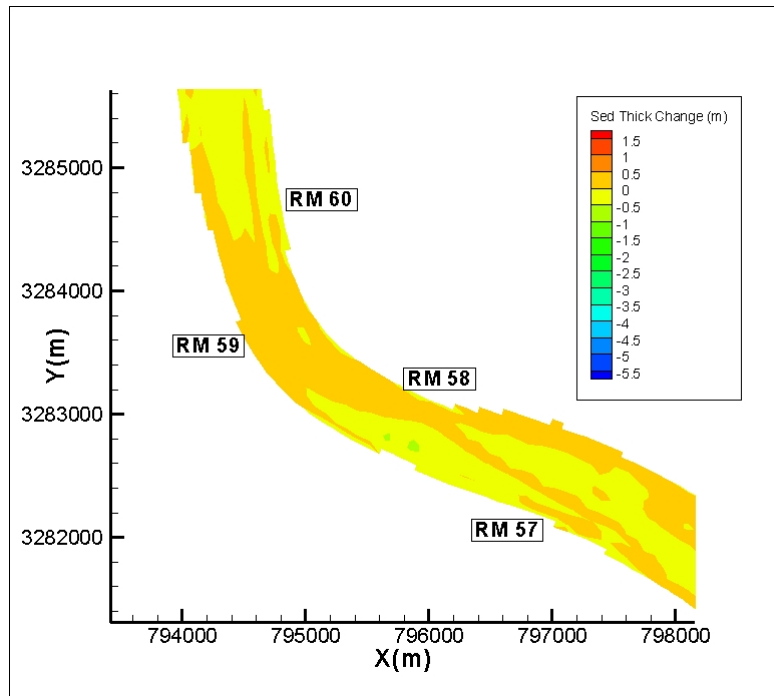


a) Existing Outflows

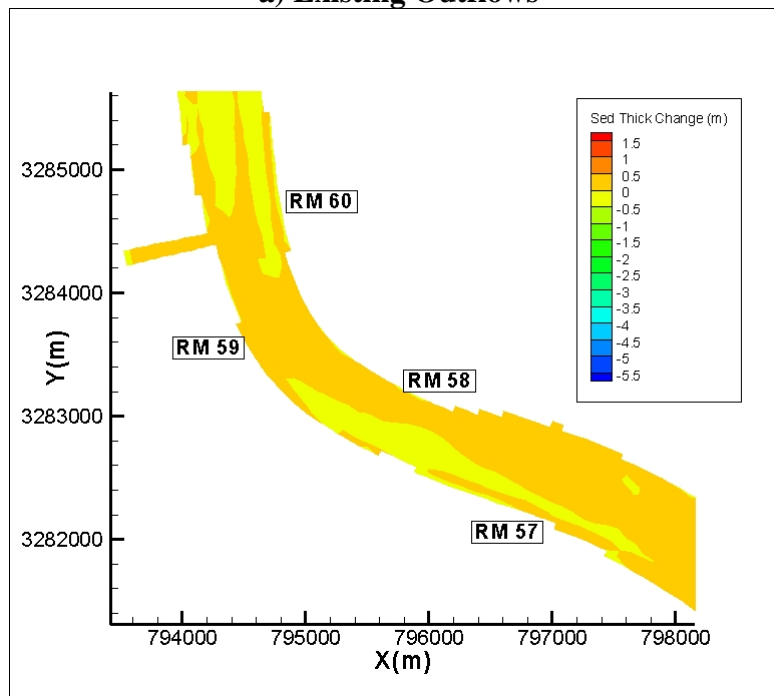


b) Proposed Diversions

Figure 7.132 – Proposed Diversions – Belair Area (RM 65, RK 105) - Bed Sediment Thickness Change after 10 days at Intermediate Flows. Positive values indicate deposition and negative values indicate erosion



a) Existing Outflows



b) Proposed Diversions

Figure 7.133 – Proposed Diversions – Myrtle Grove Area (RM 59, RK 94) - Bed Sediment Thickness Change after 10 days at Intermediate Flows. Positive values indicate deposition and negative values indicate erosion

The estimated amount of sediment being extracted at each outflow for the Proposed Diversions Test is summarized in Table 7-8. It is clear that at peak flows most of the sand extracted leaves the system through the Belair diversion; at intermediate flows Belair is still the diversion with the highest sediment load. Once more, it is obvious the significant impact this diversion has on the system. It can be seen that the sand concentration at the large diversions downstream of Belair is clearly lower than at Belair itself.

Table 7-8 – Water Discharge, Suspended Sand Concentration and Suspended Sand Load at Outflows

Proposed Diversions Study

Site	Peak Flows			Intermediate Flows		
	Q (m ³ /s)	Cs (mg/L)	Qs (metric tons/day)	Q (m ³ /s)	Cs (mg/L)	Qs (metric tons/day)
Jesuit Bend	197	77	1,315	185	13	212
Belair	5,033	151	65,548	3,933	31	10,591
Myrtle Grove	804	54	3,751	750	7	436
Deer Range	412	35	1,239	407	3	121
West Pointe-À-La-Hache	26	22	49	17	2	2
Bohemia Spillway	5,255	21	9,380	266	1	23
Bayou Lamoque	27	13	32	44	2	7
Buras	4,079	32	11,302	3,836	14	4,661
Fort St. Philip	570	3	133	538	0	19
Baptiste Collette	4,068	32	11,374	3,740	16	5,041
Grand Pass + Tiger Pass	2,885	11	2825	2,886	7	1,697
Main Pass	3,600	2	648	3,494	1	331

Figure 7.134 and Figure 7.135 show the peak flow and the intermediate flow sand concentration at each outflow in graphical form for both the existing and the MLODS diversions. The results with the introduction of the proposed diversions are very different from the ones with the existing outflows only. The concentration of sand downstream of Belair dropped sharply, but the concentration of sand at the diversions closer to the downstream boundary is even lower than with the addition of the Belair diversion alone. Baptiste Collette and Grand Pass + Tiger Pass show extremely low sand transport as due to the extraction of around 80% of the flow available at Belle Chasse.

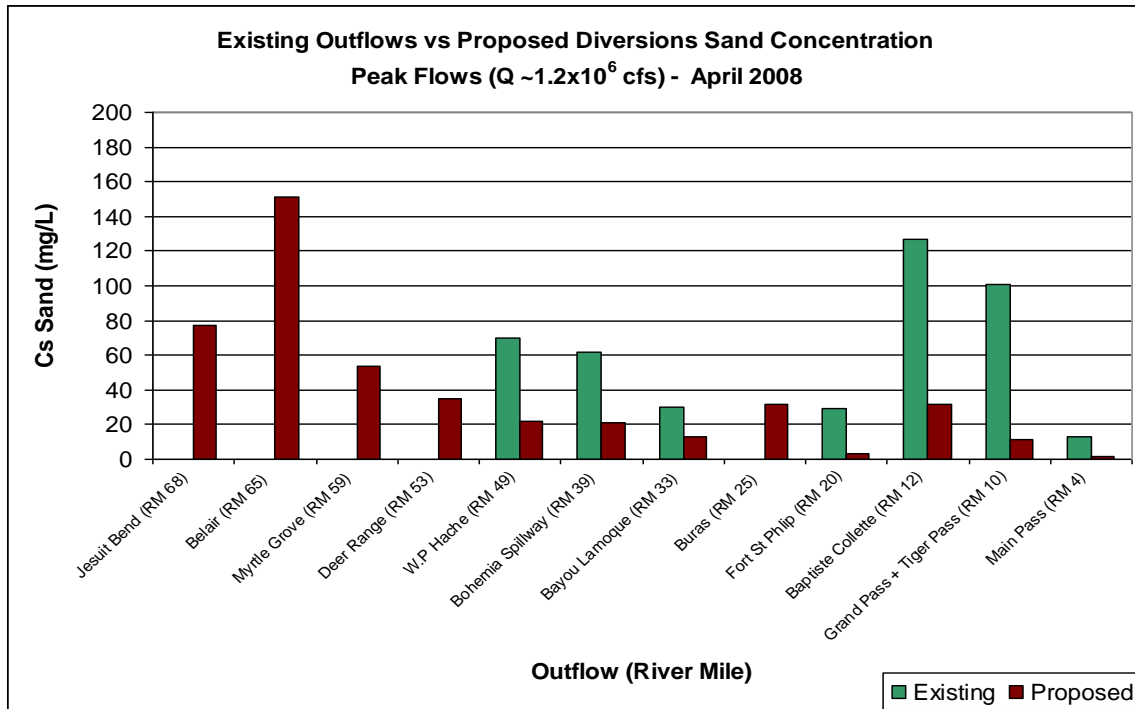


Figure 7.134 – Existing Outflows + Proposed Diversions – Outflows Suspended Sand Concentration at Peak Flows

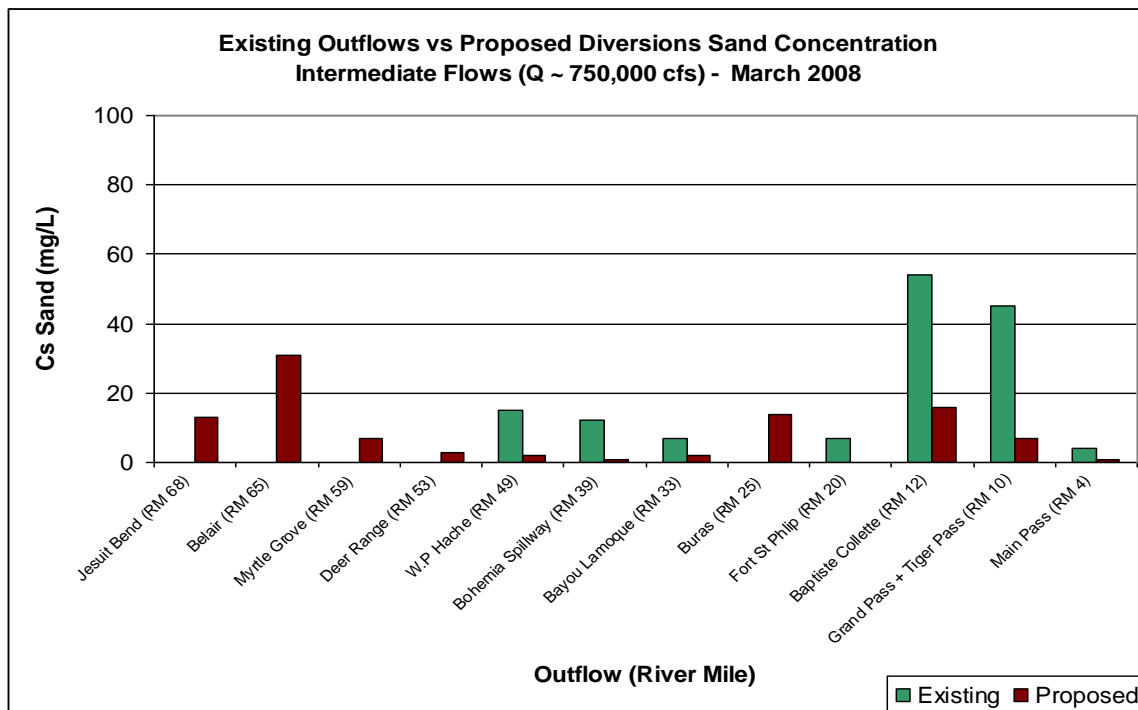


Figure 7.135 – Existing Outflows + Proposed Diversions – Outflows Suspended Sand Concentration at Intermediate Flows

8) DISCUSSION

8.1 One-Dimensional Modeling

CHARIMA was selected over HEC-RAS to be used in the long term 1-D simulation of the bed-material transport of the Lower Mississippi River. CHARIMA was selected because it has the capacity of modeling the split of both flow and sediment at distributaries and is an unsteady-flow model. HEC-RAS has been applied to the Lower River by Pereira *et al.* (2009) to model the sediment transport of the main stem and by Davis (2010) to model the hydrodynamics of river diversions for the reach between Tarbert Landing and the Gulf of Mexico. However, the HEC-RAS sediment module is not coupled with the unsteady flow hydrodynamic module and the model does not automatically simulate the split of sediment at junctions.

The application of CHARIMA to the Lower River was preceded by a series of tests. The model was applied by Pereira (2007) to another alluvial river, the Mondego River in Portugal. During that study, several tests were performed, which cover the use of weir-type links, armoring, sorting and flow extractions. The formulations of Engelund-Hansen and Ackers-White were used. More information about that study can be found in Pereira (2007) and Pereira *et al.* (2007). Thus, these tests were not repeated during this research but other preliminary simulations were necessary.

The first preliminary test involved the use of a rectangular channel with similar geometry to the one used for ECOMSED and FVCOM testing presented in Chapter 5. CHARIMA, HEC-RAS, HEC-6 and Mike 11 Models were tested under steady-state, with a constant Manning's n of 0.026 and a time-step of 1 hour and the results obtained with the four models were compared. Figure 8.1 and Table 8-1 show the results obtained during this test. It is evident that all models gave similar results but it is clear that in HEC-RAS and CHARIMA cases, the profile shows the closest shape to the theoretical H2 curve. This means that in HEC-RAS and CHARIMA, the upstream boundary condition has a more limited effect in the shear stress calculations.

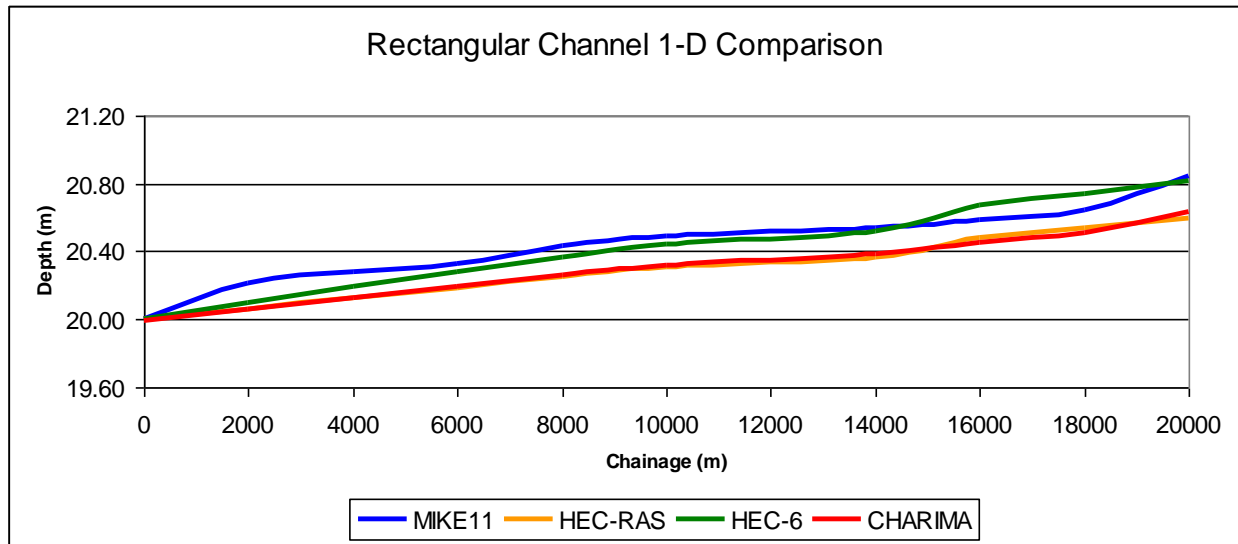


Figure 8.1 – Rectangular Channel Longitudinal Profile with 1-D Models

Table 8-1 – Rectangular Channel Flow Depth Results with 1-D Models

Cross-Section	Chainage (m)	MIKE11		HEC-RAS		HEC-6		CHARIMA	
		flow depth		flow depth		flow depth		flow depth	
		m	ft	m	ft	m	ft	m	ft
1	0	20.00	65.62	20.00	65.62	20.00	65.62	19.99	65.60
2	2,000	20.21	66.32	20.06	65.82	20.09	65.92	20.06	65.82
3	4,000	20.28	66.54	20.13	66.03	20.19	66.25	20.13	66.04
4	6,000	20.33	66.68	20.19	66.23	20.28	66.53	20.19	66.25
5	8,000	20.43	67.03	20.25	66.43	20.36	66.81	20.26	66.46
6	10,000	20.49	67.22	20.31	66.62	20.44	67.07	20.32	66.68
7	14,000	20.54	67.39	20.37	66.82	20.52	67.33	20.39	66.89
8	16,000	20.59	67.55	20.48	67.20	20.67	67.82	20.45	67.09
9	18,000	20.64	67.72	20.54	67.39	20.74	68.06	20.51	67.30
10	20,000	20.85	68.41	20.60	67.58	20.82	68.29	20.64	67.70

CHARIMA was also tested with steady-flow conditions using only the main channel of the Lower River. It was found that the lower the time-step used, the faster the model reached steady-state. Time-steps between 1 minute and 12 hours were used. This test also served the purpose of checking continuity, which was confirmed. The results obtained for a 1.2×10^6 cfs flow, fluctuated by no more than 0.25 cfs around that value, confirming that the model is performing well. Later, some tests were run including distributaries and diversions (Belair Case) and it was verified that the amount of flow at the downstream boundary of the model equaled 99.8% of the expected value which confirms that continuity is also assured in the presence of distributaries.

The hydrodynamic calibration and validation simulations were performed using a time-step of 10 minutes. Nonetheless, a wide range of time-steps was tested (10 minutes to 12 hours) and the model proved to be stable in all cases. The hydrographs obtained with the different time-steps tested are similar, as can be seen in Figure 8.2 and Figure 8.3, but, in theory, the lower the time-step, the more precise will be the result. Thus, the results obtained with the lower time-step are presented.

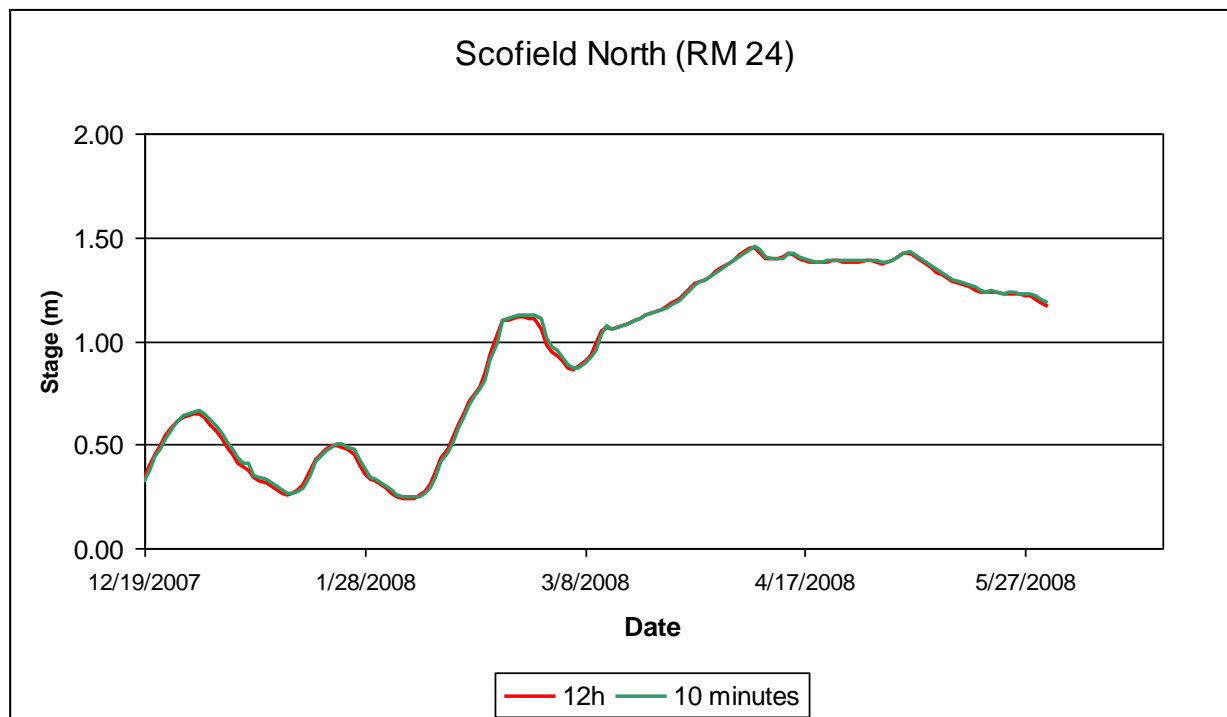


Figure 8.2 – Stage at Scofield North with different time-steps

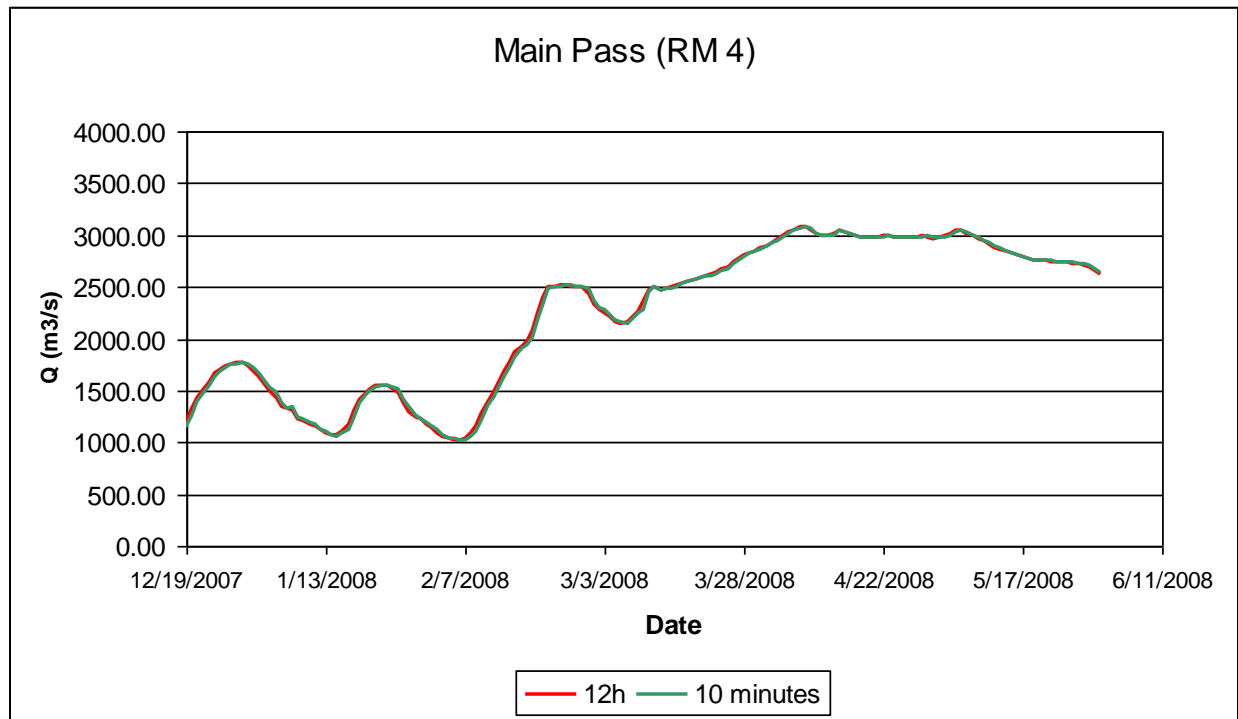


Figure 8.3 – Outflow at the Main Pass with different time-steps

A well calibrated hydrodynamic model is essential for developing a sediment transport model. While testing CHARIMA it was detected that the suspended sediment load results were time-step dependent.

Theoretically, the results obtained with different time-steps should converge but the transport of non-cohesive sediment is a complicated process to describe and simulate. It was noticed that a smaller time-step tends to give a lower suspended-load concentration. Several tests were performed to try to find an explanation for this time-step dependency. A steady-state model with peak flow and with a geometry that included only the main channel and no distributaries was used with time-steps ranging from 1 minute to 12 hours to try to verify if the model would converge to the same bedload and suspended-load concentration values. The bedload concentrations were confirmed to converge to the same values and become independent of the time-step used, as can be seen in Figure 8.4. However, the suspended-load results did not show a consistent convergence, meaning that it is the suspended-load formulation that is not working as expected. This fact is shown in Figure 8.5 where it is evident that the results are erratic.

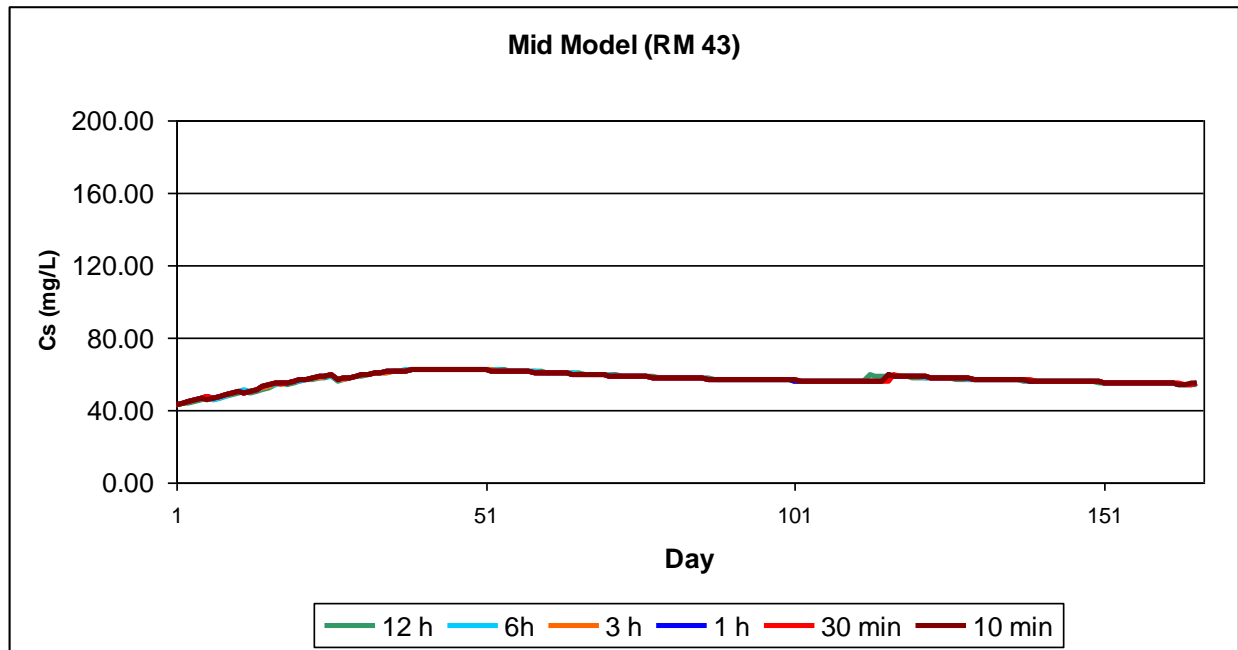


Figure 8.4 – Bed-load concentration for different time-steps (Mobile-Bed)

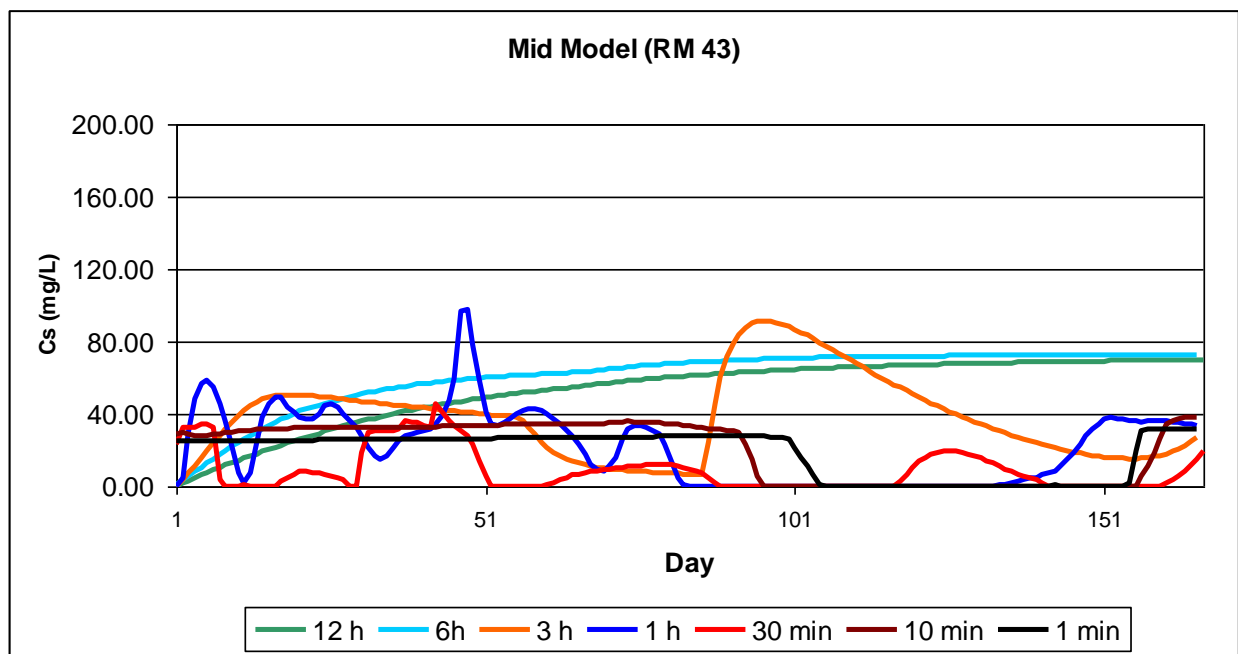


Figure 8.5 – Suspended Load concentration for different time-steps (Mobile-Bed)

Although the model shows an erratic and inconsistent behavior while calculating the suspended-load, Figure 8.5 shows some interesting aspects: 1) results with the larger time-steps (12 h and 6 h) seem consistent with each other and in both cases the model converges monotonically with run time; 2) with the larger time-steps there are no pronounced oscillations as with the smaller time-steps; 3) the 10 minutes and 1 minute results show some consistency; 4) for the time-steps between 30 minutes and 3 hours the results oscillate more than for the lowest or highest time-step values. Possibly, the larger-time step smooths some non-realistic numerical peaks generated by the suspended-load formulation and that is the reason why the results seem more reasonable. Nonetheless, the results contradict the theory.

Once it was verified that the suspended-load results were time-step dependent, it was decided to perform some other tests to see how the suspended-load calculations would affect other sediment transport variables. The cumulative bed degradation and the volume of material leaving a reach in one time-step were also analyzed. These results confirmed that the model was performing well, that the suspended-load calculations are separate from the remaining sediment transport calculations, and that the remaining variables are consistent with theory, as shown in Figure 8.6 and Figure 8.7.

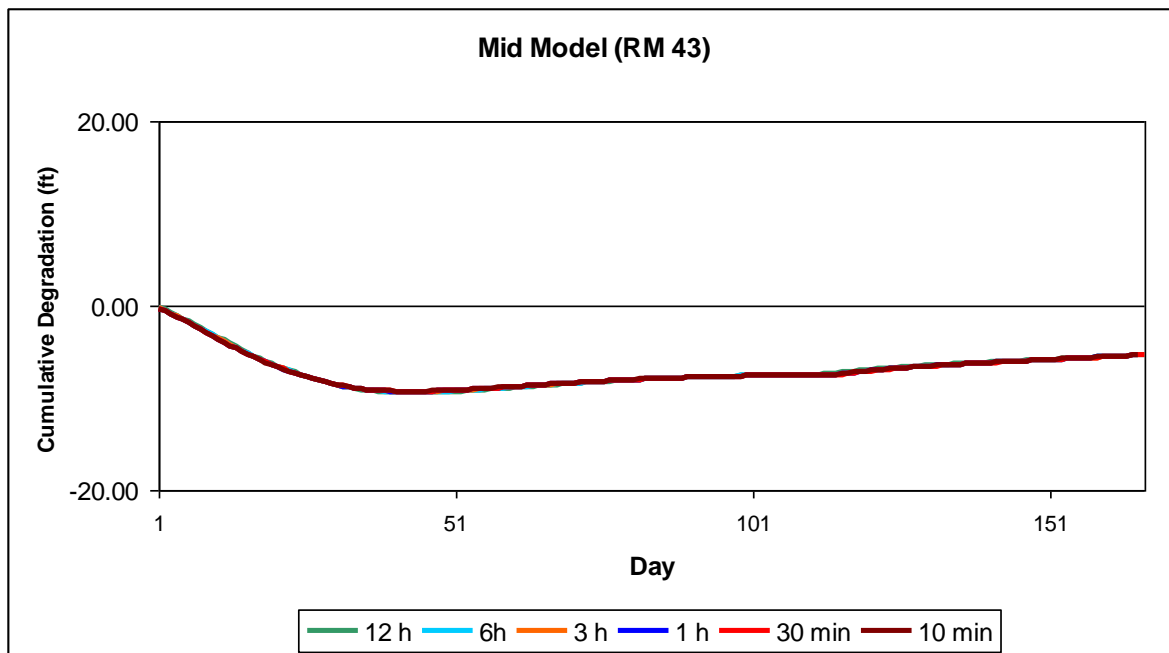


Figure 8.6 – Cumulative Degradation for different time-steps (Mobile-Bed)

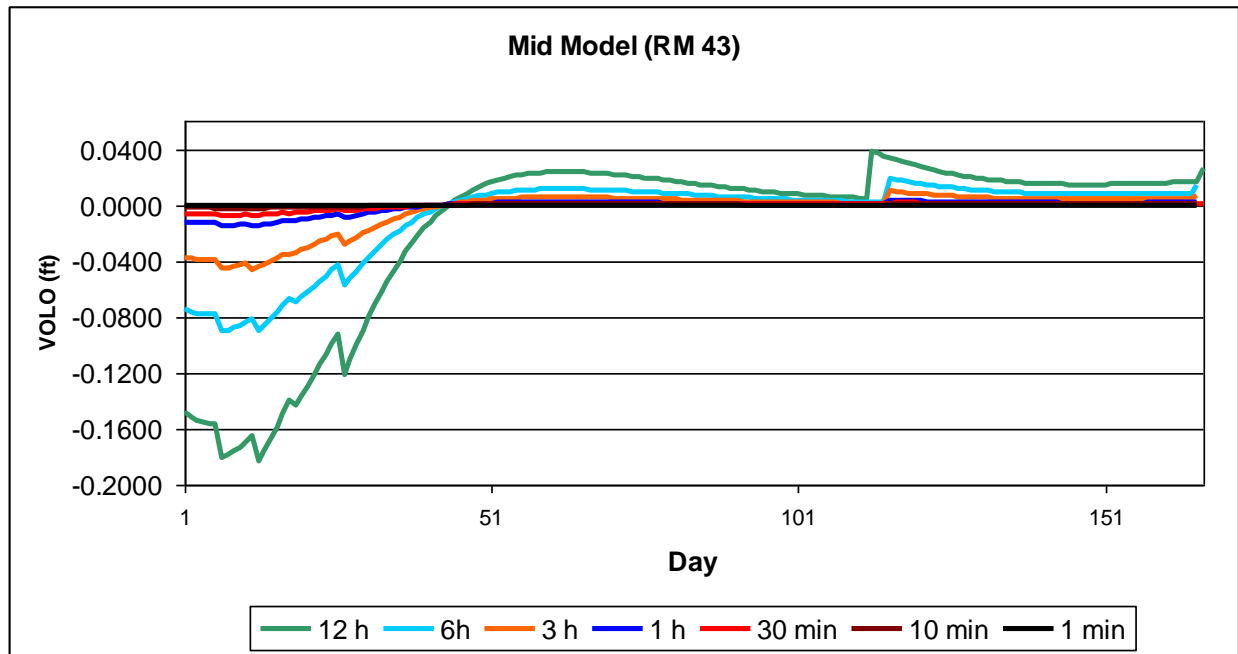


Figure 8.7 – Volume out of a reach in one-time step for different time-steps (Mobile-Bed)

The main channel tests with steady-flow and mobile-bed are a good option to test the sediment module. However, in order to obtain a faster sediment-transport steady-state and try to better analyze the behavior of the suspended-load formulation, new simulations were performed with a fixed-bed but with both bed-load and suspended load active. As the suspended-load is a function of bedload this is the simplest option to study its behavior. In this case, the model reaches a state of equilibrium for all of the time-steps. However, for each time-step, a different suspended-load concentration was obtained. Figure 8.8 shows the results. Figure 8.8 indicates that there is a tendency for higher suspended loads with high time-steps, although there are oscillations in this trend. It is clear that the model reaches an equilibrium faster with a lower time-step.

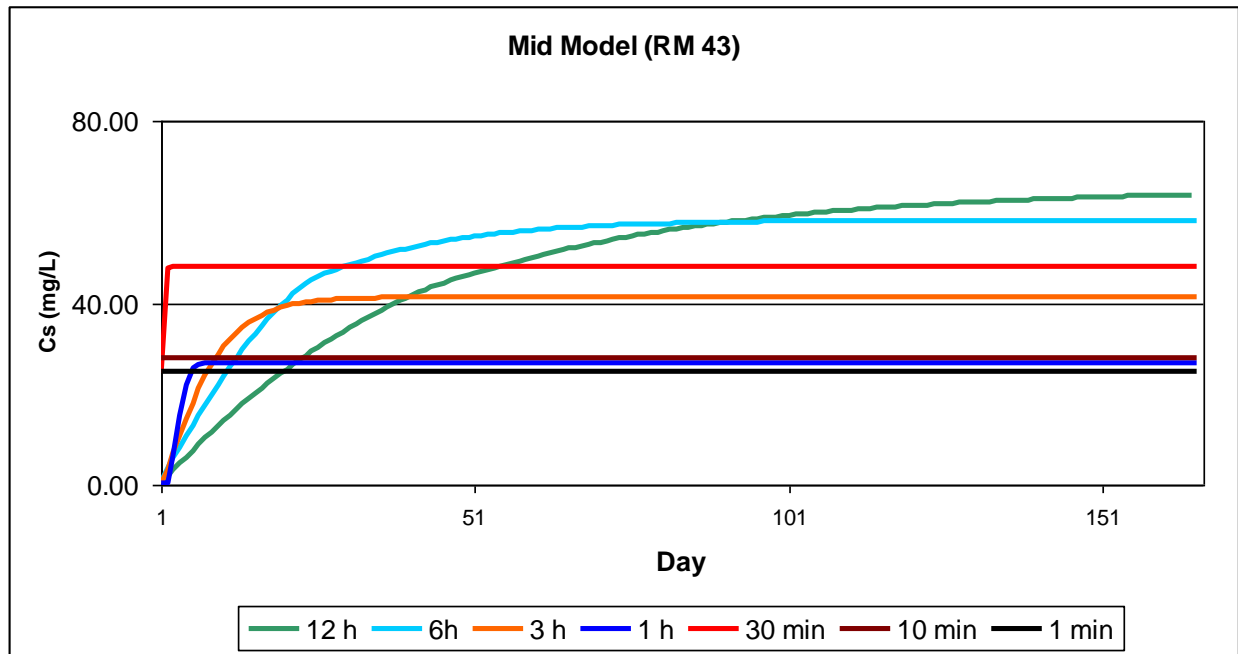


Figure 8.8 – Suspended Load Concentration for different time-steps (Rigid Bed)

The reason why the suspended-load results are time-step dependent is still not clear. There are several possible reasons. The first one could be the error introduced in the coefficients of the large matrices that must be inverted for the sediment variables in the Lower Mississippi River. There are between 37 and 40 nodes in one single node group, which could increase the error in the calculations. However, the model was tested with 5 node groups, meaning that each sub-matrix would only have to account for around 7 nodes and the results obtained were similar. In addition, the hydrodynamics calculation also involves the inversion of a matrix and no problems were found during the hydrodynamics simulations.

CHARIMA has been used very often for heat transport simulation and has been proved to perform well. Since the mechanisms are similar to those in the sediment transport (the same advection and diffusion subroutines are used), it is likely that the model would be time-step independent for these processes. On the other hand, the suspended-load calculations involve an interaction with the bed and if there is a strong non-linear interaction with the bed, some of the ad-hoc procedures applied while transferring the sediment variables from one node to another may possibly produce unexpected results.

After all the testing, several options were considered for sediment calibration. The application of the model with bedload only was considered but this option would require unrealistic small sediment sizes for calibration. The use of both suspended-load and bedload with smaller time-steps such as 10 minutes or even 1 hour caused the same problem: an underprediction of the sediment transport, meaning that an unrealistically low sediment-size would be necessary to calibrate the model. A wide range of specific diffusion coefficients for both horizontal and vertical sediment

transport was tested. In addition, the model was tested with the three available total-load predictors without achieving a satisfactory calibration: TLTM (Karim and Kennedy), Ackers-White and Engelund-Hansen.

The final sediment transport simulations were performed using a very large time-step (12 hours). Although, theoretically not the best option, this was the only time-step that permitted a calibration for suspended load while using a realistic sediment-size distribution and the Ackers-White formula. A time-step of 6 hours also gave reasonable results but for other time-steps lower than 12 hours, the only other option for calibration would be the use of unrealistically low sediment-sizes, as stated earlier.

The preliminary tests and the hydrodynamic simulations showed that the results obtained with $\Delta t=12$ hours are acceptable and in good agreement to the ones obtained with $\Delta t=1$ minute. The mobile-bed simulations also showed good agreement between the bedload and degradation results obtained with the whole range of time-steps. Thus, the use of a large $\Delta t = 12$ hours in the sediment calculations is a way of obtaining a good suspended-load calibration with realistic sediment-sizes and roughness coefficients. The use of such a high time-step appears to smooth the results and avoids some instabilities that make the model harder to calibrate. This makes it more of a quasi-steady state model for the sediment transport, rather than a real unsteady-state model. This calibrated sediment-transport model allows us to have an estimate of the sediment transport in the main channel and diversions for the calibration period but should be used with caution and its application for flows outside the calibration range is not guaranteed.

The tests described earlier showed that the bedload formulation used in CHARIMA is robust and the results obtained are consistent and time-step independent. Thus, it was decided that a good method to obtain a calibrated operational model for the Lower Mississippi River bed-material transport would be to develop a formulation that estimates the suspended-load as function of the bedload and the water discharge. To accomplish this, a Shocklitsch type formulation will be used, which is given as follows:

$$Q_{ss} = Q_b \left[1 + \left(\frac{Q - Q_{cs}}{Q_{cs}} \right)^\alpha \right] \text{ for } Q > Q_{cs}, \text{ with } \alpha = \frac{Q_{ref}}{Q} \quad (8.1)$$

where: Q_{ss} = suspended-load; Q_b = bedload; and Q = water-discharge.

By trial and error the following calibration was obtained for the study reach: Q_{cs} = critical sediment flow = 350,000 cfs; and Q_{ref} = 800,000 cfs \approx mean annual flood flow.

The critical sediment flow for sediment transport and the mean flood flow values used in this formulation are based on Lower Mississippi River main stem data. This formula is not applicable in any other reaches of the River or other alluvial Rivers.

This formulation was applied to the bedload results obtained with CHARIMA and the model calibrated for sediment measurements available for the Myrtle Grove and Scofield areas. A time-step of 10 minutes was used to retain the dynamic character of the model. Slight adjustments were made to the friction coefficients and a new calibration was obtained. The results are presented in Table 8-2. The calculated suspended sand concentration results at median and high flows are in good agreement with the field measurements but the calculations for lower flows are not. Nonetheless, most of the sand transport does not occur at low flows and the main goal of the formula is an accurate estimate of the transport at higher flows (Nittrouer *et al.* 2008; Allison, 2010; Allison and Meselhe, 2010).

Table 8-2 – Observed versus Modeled – 1-D Mobile-bed Simulations using the New Formulation

Date/Station	Suspended Sand Concentration (mg/L)			
	Myrtle Grove (RM 59)		Scofield (RM 16-24)	
	<i>Observed</i> ⁺ *	<i>Simulated</i>	<i>Observed</i> ⁺	<i>Simulated</i>
1/10/08 (Q = 420,000 cfs)	-	-	4.1	0.7**
3/10/08 (Q=790,000 cfs)	57.0*	52.7	-	-
4/15/08 (Q=1,150,000 cfs)	-	-	71.0	69.3**

+Data Collected by Allison (2010) *Value measured in April 2009 for a similar water discharge

** Arithmetic average of RM 24, RM 20 and RM 16 results

The new formulation was used to estimate the suspended-load as a function of the bedload given by the CHARIMA model using the Ackers-White method. It is important to verify if the new formulation can be a reasonable tool to estimate the suspended-load from available bedload field-measurements. The results showed that for main stem flows in the range of 500,000 to 600,000 cfs the concentrations of suspended and bedload are approximately the same and that the suspended load concentration can represent about 70% of the total bed-material load at peak flows (1,150,000 cfs). Nittrouer *et al.* (2008) showed that, under peak flow conditions, the suspended-load at may represent about 2/3 of the total bed-material load. Thus, the results obtained with the new formulation are consistent with field observations. However, the ratio between suspended-load and bedload may vary considerably along the Lower River.

8.2 Three-Dimensional Modeling

The 3-D modeling presented in this study was performed using ECOMSED. FVCOM was also tested and the initial plan was to use FVCOM as the main tool and have ECOMSED as a validation tool. FVCOM is a parallel code (more computationally efficient) and includes an

unstructured grid formulation. These are two features would make FVCOM a good option. Extensive trials were completed with FVCOM. The model was successfully applied to simulate the hydrodynamics in the Lower River for the Reach between Belle Chasse (RM 76) and Venice (RM 11) with two diversions. During this process, the FVCOM code was adapted to include time-variable friction, which in conjunction with the spatially-variable formulation coded by Retana (2008) permitted the use of the model for the hydrodynamic simulation of several months of the year 2008. Some of the results and an overview of the FVCOM work are presented in Meselhe *et al.* (2010).

ECOMSED was selected to model the sediment transport in the Lower River after testing of the FVCOM sediment transport module. During the FVCOM work, the van Rijn (1984) and the Ackers-White modified formulation (Profitt and Sutherland 1983) were added to the code because the only option available in the original code is the Meyer-Peter and Müller (1948) formulation, which is not intended to be used in alluvial rivers because it was developed for gravel beds. However, the testing showed that the FVCOM sediment module was not well parallelized; the model would run approximately ten times slower with the sediment options on. Also, there were insufficient information available on applications of FVCOM with non-cohesive sediment. As ECOMSED was a tested model for both cohesive and non-cohesive sediment transport and included the van Rijn formulation, it was adopted as a better option than FVCOM to be used in this research.

Boundary conditions play a key role in setting up a numerical model. A good model is only possible if appropriate boundary conditions are prescribed. The inconsistency of the available stage data for the modeled reach was the main reason to rely on the HEC-RAS results of Davis (2010) as the reference for calibration instead of using available data directly. The HEC-RAS model of Davis (2010) used the New Orleans-Carrollton station (RM 102.8) which had reliable and consistent data and adjusted the calibration parameters to obtain a best fit to the remaining stage gauges. The Davis (2010) model extended from Tarbert Landing (RM 306) to the Gulf of Mexico. Figure 8.9 shows some inconsistent stage measurements for 2008 and Figure 8.10 shows three examples of the inconsistencies found in the available stage data for different flow conditions. The stage values at Venice (RM 11) or Empire (RM 24) are higher than the stage at West-Pointe-À-La-Hache for low flow conditions, which is physically impossible.

Besides some obvious inconsistencies in the stages, the following issues were detected on the available stage measurements: 1) not all the stations use the same datum (NGVD29, NAVD88 or others); 2) for the same station, the datum used may vary with the time-period of the measurements; 3) in some cases, the conversion of measurements allocated to two different datums is not available; 4) the conversion between two different datums will depend on the location of the station. In addition, time dependent subsidence and sea-level rise impacts are hard to quantify and add uncertainty to the available measurements.

The upstream boundary of the model is at Belle Chasse (RM 76). There are no continuous flow records available for this station. To model the Lower Mississippi River it would be necessary to extend the domain to Tarbert Landing (RM 306) where there are flow measurements. However, it

would not be reasonable to have a 300-mile ECOMSED model for several reasons: 1) the model would run much slower than real time (10-day simulations would take around 1 month to run); 2) it would be necessary to have more sediment data for calibration of the reach between Tarbert-Landing and Belle Chasse; 3) most of the possible river diversions are located between Belle Chasse and the Head of Passes. Thus, the Belle Chasse inflow and the outflow water discharges were obtained from the model developed by Davis (2010) that extends from Tarbert Landing (RM 306, RK 492) to the Gulf of Mexico.

Another reason for using 1-D modeling results to obtain boundary conditions was the lack of information on distributaries. The total outflow for the modeled reach matches a quadratic function based on field measurements (ADCP) that were shown in Figure 6.17 but the outflow distribution is uncertain. ECOMSED does not offer the possibility of modeling hydraulic structures; it is necessary to prescribe the outflow as a boundary condition to emulate that behavior. In addition, the distributary channels that can theoretically be implemented in the model would require a much larger (and slower) model to resolve the total length of the channels modeled.

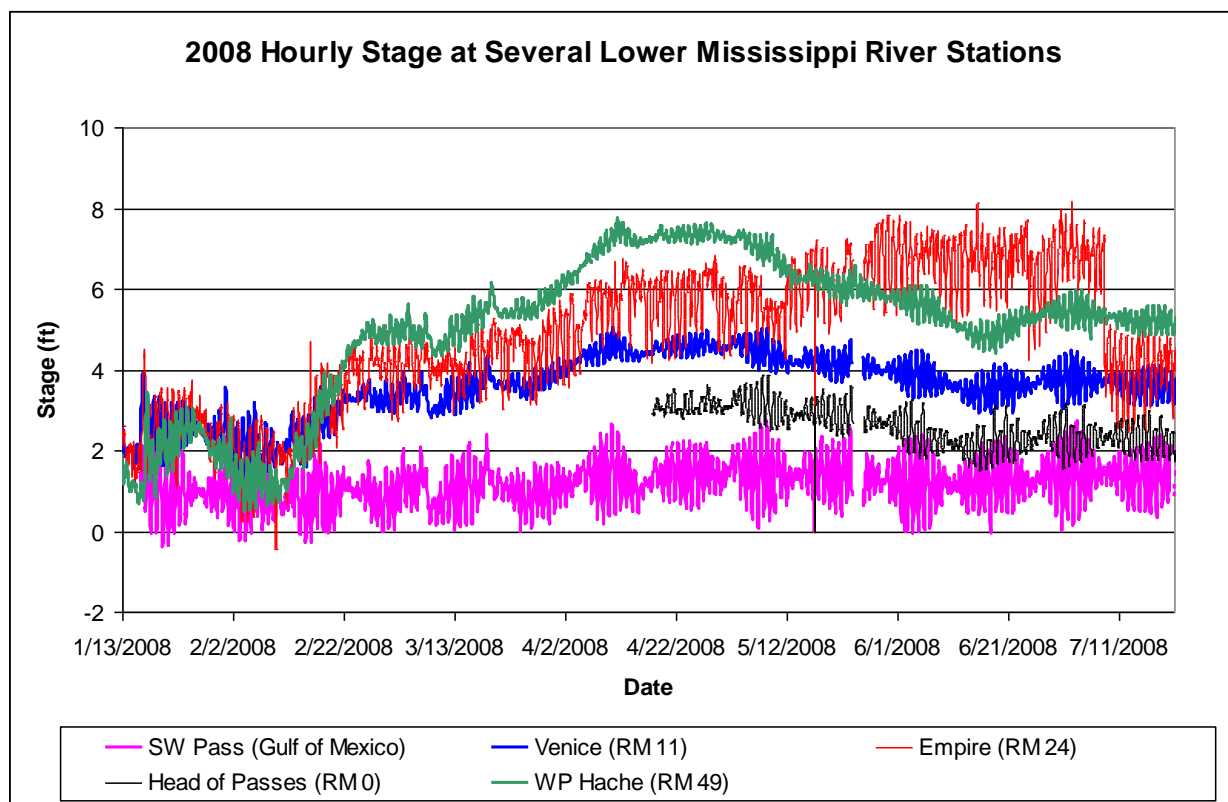


Figure 8.9 – 2008 Hourly Stage Data at Several Lower River Stations

ECOMSED has been applied in the past for modeling sediment transport but is a coastal and estuarine model. In addition, no applications to the Lower River are known. Thus, some work was necessary to adapt the original code to be applied to the Mississippi River. The ECOMSED code was

modified to allow the use of the Manning's formulation and of user defined spatially variable roughness coefficients, given as an input file. The latter feature was necessary for calibration of river hydrodynamics, where a constant roughness for the entire reach did not allow an accurate reproduction of the field data and 1-D model results; these changes were also needed for accurately reproducing and maintaining the observed flow and transport trends in the vicinity of the deep holes throughout the domain and to account for the additional energy losses due to bends and the flow expansions.

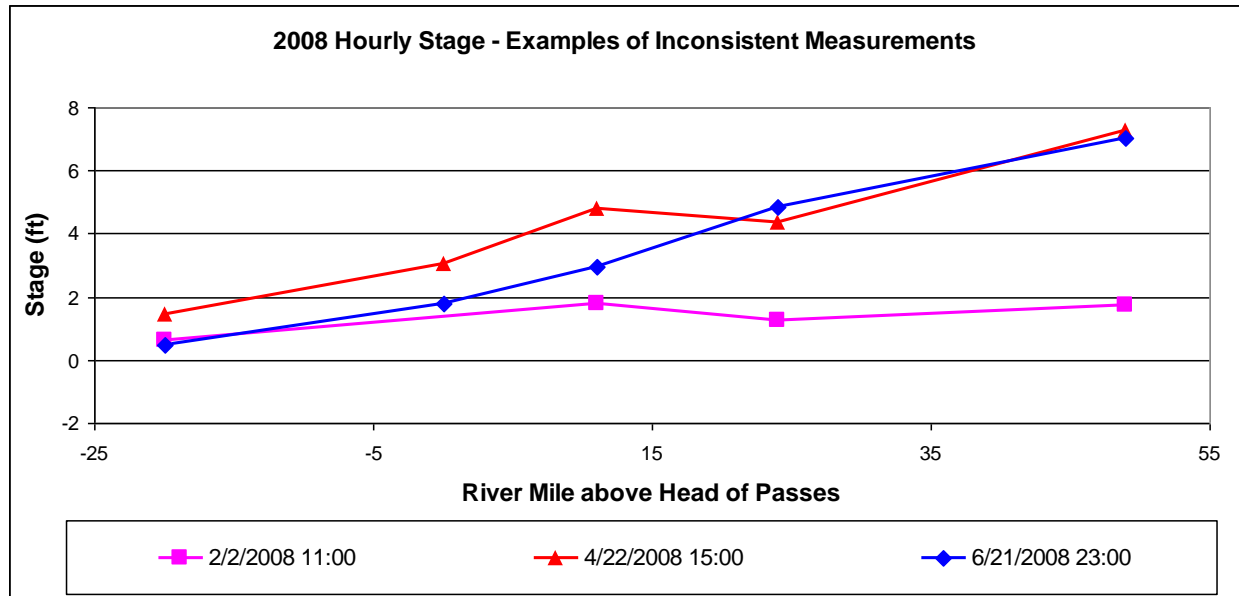


Figure 8.10 – 2008 Hourly Stage Data - Examples of Inconsistent Measurements

The ECOMSED initial tests with the Lower Mississippi River showed exaggerated erosion and bottom sand concentrations that resulted in numerical instabilities and/or unrealistic sediment transport results. Thus, some code changes were made to the original non-cohesive sediment load formulation. To calibrate the model, the code was modified to guarantee a minimum active layer volume of $1.0 \times 10^{-5} \text{ m}^3$ and a maximum of 1% change on bed-thickness in one time-step. The original formulation was also changed to set the reference height (3% of the flow depth instead of the original 1%) to reflect the dune height. This change is justified by the dimensions of the Lower Mississippi River bedforms as described by El Kheishy (2007).

To aid in the analysis of the model results, several new derived variables had to be computed through a post-processing subroutine. The subroutine used for this purpose was initially developed by Chilmakuri (2005) and was adapted to include variables relevant in riverine and sediment transport studies. The new variables were: water discharge (Q), sediment load (Q_s), discharge weighted averaged sediment concentration (C_s), total energy (E) and kinetic energy of the flow (ke), for both the main channel cross-sections and the River diversions. The formulations used the flow direction normal to the face of the element so that only one component of velocity was used. These assumptions may introduce some error in the results obtained for the new variables, particularly in

the distributaries or main channel cross-sections located in the vicinity of a distributary, where recirculation is more likely to occur.

The disturbances associated with the diversion of flow help explain why some slight flow oscillations and even water surface oscillations are visible in the main channel longitudinal profiles. Flow recirculation is the main reason for inconsistent sand concentrations such as those seen in the distributary modeled in the short reach test.

The implementation of large diversions in the system seems to be numerically simpler than the implementation of small diversions. The results showed that when the flow extracted at a diversion is too small (less than 1,000 cfs), it is hard to avoid very strong recirculation if the diversion is more than two elements wide. In addition, if a small diversion is implemented in an area where there is high-sediment transport, e.g., around RM 65 of the main channel, the sediment transport concentrations may become unrealistically high and the disturbance may propagate into the main channel leading to higher concentrations in the whole domain. Some tests were performed with small diversions at RM 75, where sediment transport is considerably lower and no excessive concentrations inside the distributary channels or in the main channel were detected. Nonetheless, it was decided to exclude the White Ditch and Naomi siphons from the final simulations because of their location (near RM 65).

Numerical modeling should always include a grid-dependency study. That was the main goal of the short reach tests. These tests showed that, overall, the grid resolution of 100 m by 50 m is acceptable, as the results were not significantly different from the ones obtained with a grid as fine as 25 m by 25 m. The model was capable of reproducing secondary flow patterns with the coarser grid and the sediment concentrations obtained are of the same order of magnitude and the hydrodynamic results (stage) were very similar. The grid-resolution effect is essentially visible closer to the boundaries. The results indicated that a lateral grid size of between 25 and 50 m is needed to best resolve the near bank effects.

The short reach tests and the final simulations show that the sediment concentrations prescribed as outlet boundary conditions do not have significant influence in the inner domain results; the effect is limited to neighboring elements.

The final simulations and the short reach tests revealed that the downstream sediment transport can significantly influence the upstream sediment transport results. This was unexpected but it is very clear from the results. For the existing conditions simulations that include the whole domain [Belle Chasse (RM 76) to downstream of Main Pass] the results show higher sediment concentrations for the Myrtle Grove area (RM 65 to RM 51) than the ones that were obtained with the shorter reach, although similar geometry data and appropriate boundary conditions were used. For this reason, additional simulations were performed for the following reaches: 1) RM 76 to RM 51; 2) RM 76 to RM 51; 3) RM 76 to RM 24. The sediment transport results obtained for the first two additional tests matched the short reach results while the results obtained for the third test (RM

76 to RM 24) matched the results obtained for the whole domain. Thus, the diversions located between RM 51 and RM 24 are possibly responsible for the higher concentration results in the main channel displayed upstream of that area. This fact shows that having an ECOMSED model calibrated for a certain domain doesn't mean that we can run part of the model domain without recalibrating it, or at least checking if the model is still calibrated. In the case of the short reach, a recalibration of the model for the Myrtle Grove area could be obtained, e.g., by reducing the fall velocity of the suspended sediment from 20 cm/s to 12 cm/s. It is important to state that the hydrodynamic results obtained for the different modeling domains were similar. It was therefore concluded that the difference was related to the sediment module only. To further investigate why the results were different while running the whole domain or just part of it, several variables used in the sediment transport calculations were analyzed, e.g., the bottom shear-stress, the friction coefficient, the bottom shear-velocity and bed-thickness change. None of these variables displayed results that were significantly different from one case to the other, although the final concentration results were significantly different. It is possible that the derivatives of the variables at the boundaries, which were not explicitly transferred, may account for the observed effect.

In ECOMSED, the Courant Friedrichs Lewy (CFL) condition for computational stability on the vertically integrated, external mode is given by:

$$\Delta t \leq \frac{1}{C_i} \left(\frac{1}{\Delta x^2} + \frac{1}{\Delta y^2} \right)^{-1/2} \quad (8.2)$$

where

$$C_i = 2(gH)^{1/2} + \bar{U}_{\max}$$

For a 100 m by 50 m grid, with a flow depth of 20 m, and a maximum velocity of 2 m/s, the external time-step (DTE) value should be equal to 1.5 s. The ECOMSED authors (HydroQual 2002) indicate that the model will likely be stable for 90% of that value (1.35 s). However, it was necessary to use a DTE of 0.4 s, around 25 % of the calculated value, and an internal: external time-step split of 4, to have a stable solution for a 100 m by 50m grid. The time-steps necessary for stable solutions with the finer grids are consistent with the results obtained with the coarser one. Doubling the resolution means cutting the time-step in half and increase the execution time by a factor of 8.

8.3 Results

The 1-D model was applied to simulate longer term (months to years) Lower River hydrodynamics and bed-material transport. The period of 01/01/2008 to 06/05/2008 was used for calibration of hydrodynamics and sand transport. The calendar year of 2007 was used for validation of hydrodynamics. Sediment data were obtained from Nittrouer *et al.* (2008) and Allison (2010). Hydrodynamic data were obtained from the Davis (2010) HEC-RAS study that covers the Lower River from Tarbert Landing (RM 306, RK 492) to the Gulf of Mexico.

Three different cases were tested: i) Existing outflows; ii) Myrtle Grove Diversion + Existing outflows; iii) Belair Diversion + Existing outflows. The existing case included 13 outflows divided into 5 distributaries and 8 man-made diversions. White Ditch and Naomi (RM 65) and West-Pointe-Á-La-Hache (RM 49) were treated as simple flow extractions meaning that the amount of flow to be extracted is prescribed directly to the model as a boundary condition. The rest of the outflows were modeled as distributaries and the stage at the Gulf of Mexico was given as the downstream boundary condition for these reaches. The Myrtle Grove and the Belair tests included 14 outflows (existing plus the diversion being tested.)

Table 8-3 shows the flow changes in the existing outflow channels with the introduction of the new diversions. The formulas used to calculate the flow changes were first given in Chapter 6 and are as follows:

$$Q_{average\ change Myrtle}(\%) = 100 \left[\frac{(Q_{average Myrtle} - Q_{average Existing})}{Q_{average Existing}} \right] \quad (6.4)$$

$$Q_{average\ change Belair}(\%) = 100 \left[\frac{(Q_{average Belair} - Q_{average Existing})}{Q_{average Existing}} \right] \quad (6.5)$$

The introduction of a medium-size diversion at Myrtle Grove (RM 59; 30,000 cfs or 2.5% of the maximum river flow at that location) did not affect greatly the flow in other diversions. The maximum change is registered at the Bohemia Spillway U/S structure, with a 15.8% decrease in the outflow. A reduction of more than 8% is registered for the Bohemia Spillway D/S structure. For the remaining cases, the flow reduction is under 4%. The downstream boundary outflow is reduced by only 2.35%. The results obtained with the introduction of the larger Belair diversion (RM 65; 200,000 cfs or 18% of the maximum river flow at that location) are considerably different from the ones obtained with the introduction of the Myrtle Grove structure. The maximum change occurs at the Bohemia Spillway D/S structure, with a 56% decrease in the outflow while there is a 50% decrease in the outflow at the Bohemia Spillway U/S structure. For the remaining cases the flow reduction ranges from 4% to 20%. The downstream boundary outflow is reduced by more than 14%.

For all tested scenarios, the sand concentrations at peak flow were about double of those at intermediate flows. In addition, the sand load is not directly proportional to the water discharge, e.g., an increase of around 50% in the water discharge can lead to an increase of more than 100% in the sand concentration. Increasing the water discharge increases the sand concentration and, thus the sediment load, which is a product of the concentration by the water discharge; this will be approximately three times higher for peak flows than for intermediate flows.

Table 8-3 – Change in the average flow with the introduction of the Myrtle Grove and the Belair Diversions – 1-D Calibration - 2008

Site	Q average Myrtle (m ³ /s)	Q average Belair (m ³ /s)	Q average Existing (m ³ /s)	Myrtle Change (%)	Belair Change (%)
Bohemia Spillway U/S (RM 34)	-1,530	-910	-1,817	-15.80%	-49.92%
Bohemia Spillway Int. (RM 32.5)	-283	-235	-292	-3.08%	-19.52%
Bohemia Spillway D/S (RM 31)	-325	-156	-355	-8.45%	-56.06%
Bayou Lamoque North (RM 33)	-39	-36	-40	-2.50%	-10.00%
Bayou Lamoque South (RM 32)	-26	-25	-27	-3.70%	-7.41%
Fort St. Philip** (RM 20)	-413	-382	-417	-0.96%	-8.39%
Baptiste Collette** (RM 12)	-3,243	-3,099	-3,258	-0.46%	-4.88%
Grand Pass** (RM 10)	-1,130	-1,075	-1,136	-0.53%	-5.37%
Tiger Pass** (RM 10)	-1,120	-1,069	-1,125	-0.44%	-4.98%
West Bay (RM 4)	-1,086	-1,041	-1,088	-0.18%	-4.32%
Main Pass** (RM 4)	-2,294	-2,185	-2,300	-0.26%	-5.00%
Downstream of Main Pass*** (RM 3)	+10,395	+9,135	+10,645	-2.35%	-14.19%

*Upstream Boundary

**Natural Outflows (Distributaries)

***Downstream Boundary

Note: Negative (-) signs denote distributary or diversion flow and positive (+) signs denote main channel flow

Figure 8.11 and Figure 8.12 show the tested scenarios main channel sand concentrations at Myrtle Grove (RM 59) and Scofield Intermediate (RM 20). The sediment transport results with the introduction of the Myrtle Grove diversion are not very different from the ones with the existing outflows only. The introduction of the Myrtle Grove diversion leads to slightly higher concentrations in the vicinity of the diversion (Figure 8.11) and slightly lower concentrations downstream (Figure 8.12). The results with the introduction of the Belair diversion are considerably lower than those obtained for the other scenarios. At peak flow, the main channel concentrations are reduced by about 15% with the introduction of the Belair diversion.

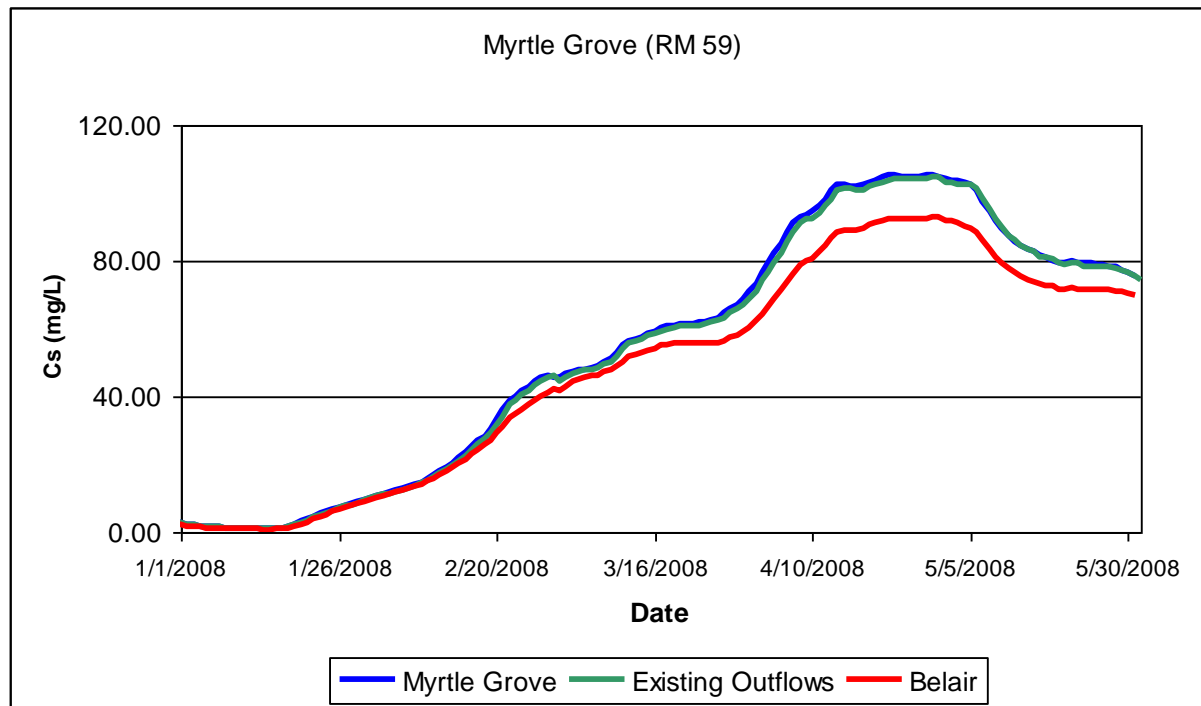


Figure 8.11 – 1-D Modeling – Main Channel Suspended Sand Concentration at Myrtle Grove (RM 59) for the Tested Scenarios – 2008 Calibration

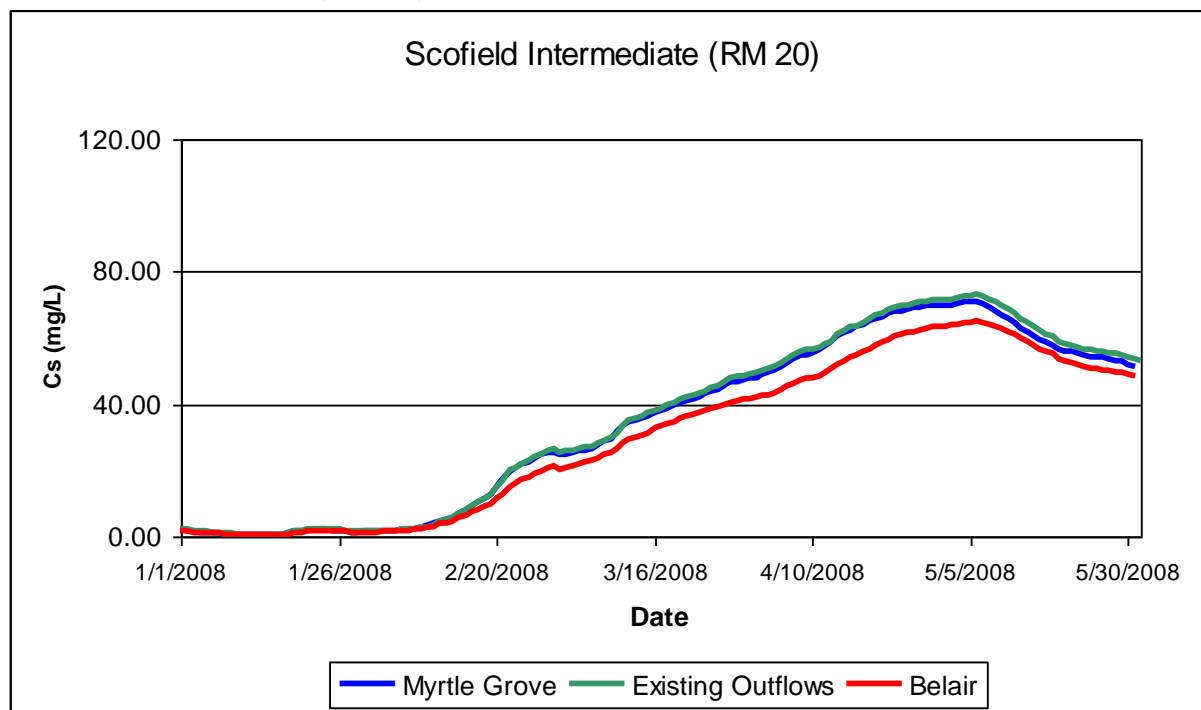


Figure 8.12 – 1-D Modeling - Main Channel Suspended Sand Concentration at Scofield Intermediate (RM 20) for the Tested Scenarios – 2008 Calibration

The 3-D model was applied to study the effects of the proposed Multiple Lines of Defense Strategy (MLODS) diversions and distributary modifications (Lopez and LPBF, 2008). The following simulations were carried out: 1) intermediate (Myrtle Grove) and large (Belair) diversions were separately modeled with no modifications to the Head of Passes; 2) all of the MLODS diversions were modeled with Southwest and South Passes closed and Pass a Loutr  dredged for navigation.

The Myrtle Grove (RM 59) simulation (30,000 cfs or about 2.5% of the maximum river flow at this location) at high River flow showed that this diversion would capture sand at close to the average sand concentration in the River at this location. The sand concentration upstream of the diversion showed a small increase while the downstream concentrations were almost unchanged. Except near the withdrawal, the river stages were not significantly lowered. Similarly, the sediment diversions at the existing diversions and distributaries were not dramatically changed.

The Belair diversion (RM 65) (200,000 cfs or about 18% of the river flow at this location) resulted in significant impacts in the River hydraulics and sediment dynamics. These impacts included:

1. a drop in the River stage throughout the study domain;
2. an increase in the energy gradient upstream of the diversion and a decrease downstream of the diversion;
3. an increase in the bed erosion at and upstream of the diversion with possible head-cutting;
4. an increase in the depositional areas downstream of the diversion, such as an increase in downstream shoaling;
5. a significant reduction in the flow to the existing diversions and distributaries; and
6. a significant decrease in the sand diversion loads at the downstream diversions and distributaries.

Figure 8.13 shows a comparison of the main channel energy head and Figure 8.14 shows a comparison of the kinetic energy term with the introduction of the Belair and Myrtle Grove diversions. A significant impact in the amount of energy available in the River due to the Belair diversion is evident. At the upstream boundary of the model, the total energy head is reduced by around 0.5 m with the introduction of the diversion, which corresponds to a 12% reduction. The kinetic energy downstream of the Belair diversion is reduced by values of the order of 0.03 m. These results are very different from the ones obtained with the Myrtle Grove diversion, which can be explained primarily by the difference in the amount of flow being extracted: 30,000 cfs at Myrtle Grove versus 200,000 cfs at Belair (almost seven times more).

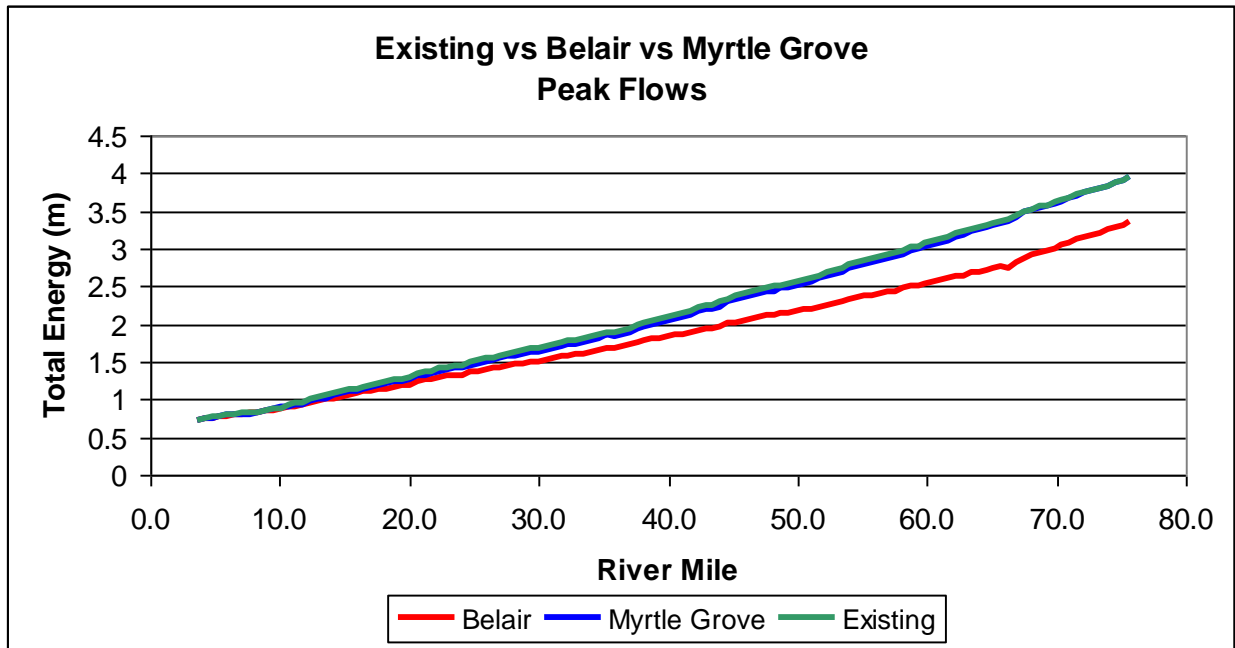


Figure 8.13 – 3-D Modeling - Comparison of Total Energy Line for Existing River alone, with an Intermediate Diversion and with a Large Diversion at High River Flows. Tested Diversions: Belair (RM 65, RK 105 and Myrtle Grove (RM 59, RK 94)

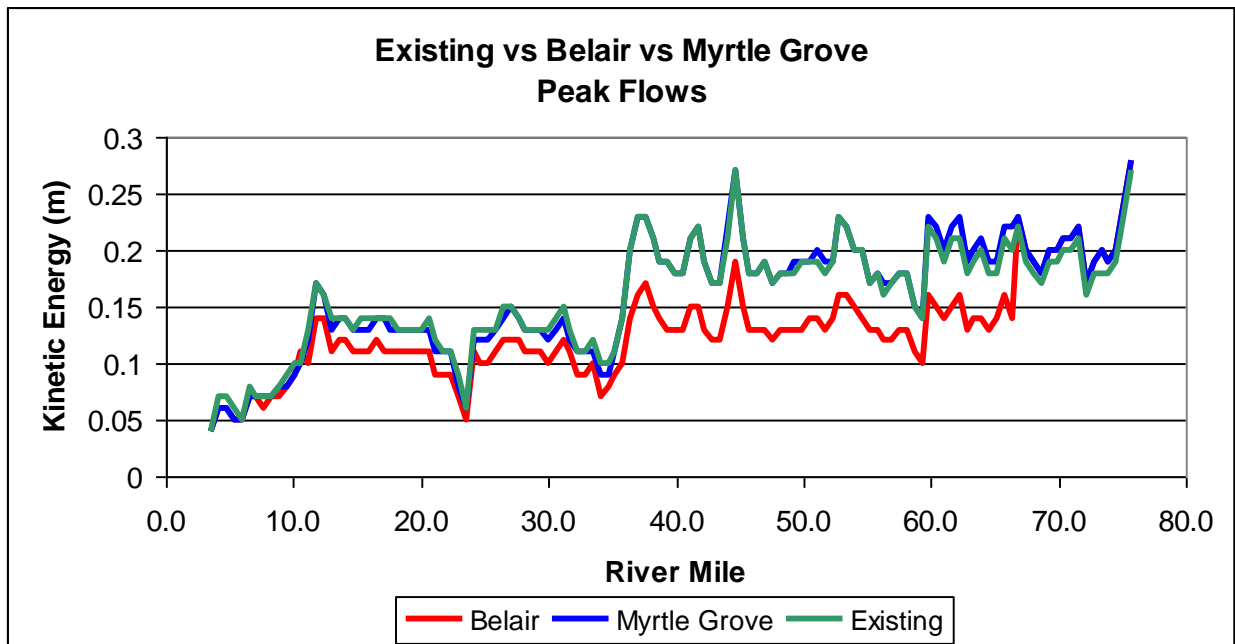


Figure 8.14 – 3-D Modeling - Comparison of Kinetic Energy Line for Existing River alone, with an Intermediate Diversion and with a Large Diversion at High River Flows. Tested Diversions: Belair (RM 65, RK 105 and Myrtle Grove (RM 59, RK 94)

Figure 8.15 shows a comparison of the sand load profiles obtained with the two new diversions. The significant impact of the Belair diversion on the sediment transport of the main channel is clear. A reduction of the energy leads to a reduction of the transported sand. The presence of the diversion contributes to an increase in the transport of bed material upstream (erosion) and an extraction of sediment at the diversion, which leaves the downstream area more starved of both material to be transported and of flow to transport the available material. Again, the medium-size diversion produces smaller changes than the large sediment-size diversion.

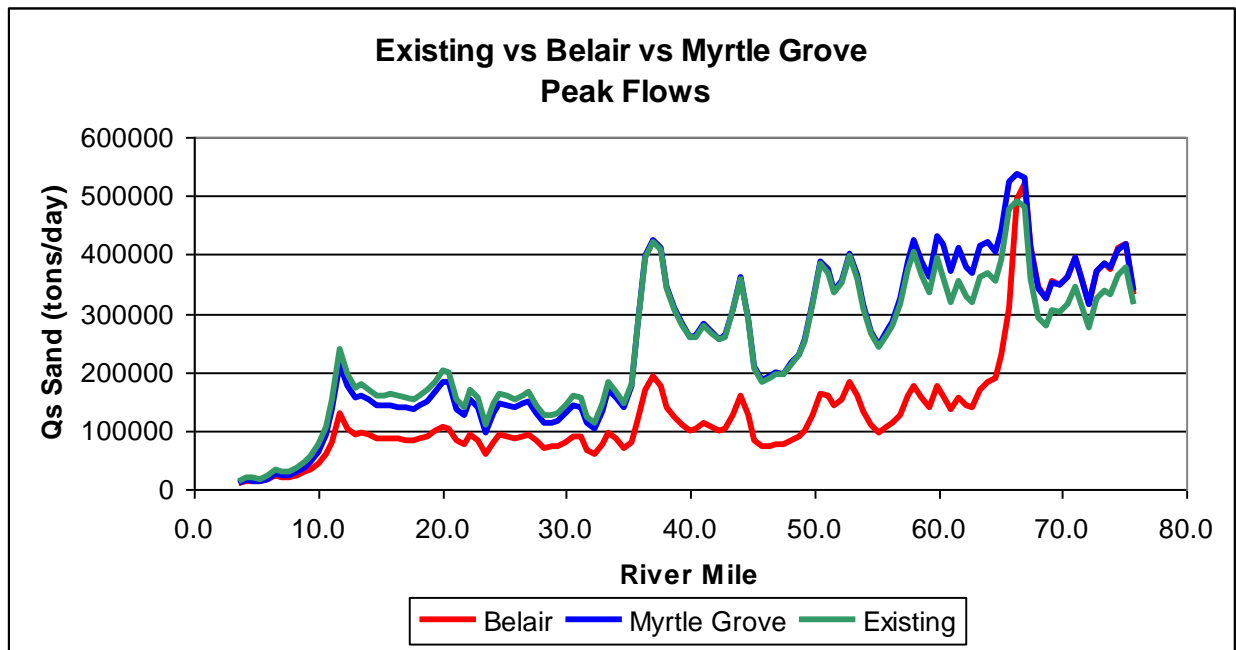


Figure 8.15 - 3-D Modeling - Comparison of Suspended Sand Load for Existing River alone, with an Intermediate Diversion and with a Large Diversion at High River Flows.
Tested Diversions: Belair (RM 65, RK 105 and Myrtle Grove (RM 59, RK 94)

The combination of closing Southwest and South Passes and dredging Pass a Loutr  with all of the MLODS diversions in place was simulated as an example of a fully developed River diversion plan. This simulation indicated that the large Belair diversion still dominated the River response. The HOP modifications raised the stage in the lower reaches which resulted in partially restoring the existing flows in the existing distributaries; however, due to the reduced sand transport capacities downstream of Belair, sand captured by diversions downstream of Belair was greatly reduced. The Buras diversion, which is also large, did not have as much effect on the stage as the Belair diversion; this is because it is near the downstream end of the domain. Nonetheless, the Buras diversion had a significant effect in the reduction of sediment transport downstream of Buras.

Figure 8.16 shows the sand concentration for the modeled diversions and distributaries at peak flows for the Tested Scenarios. It is evident that the Belair and the Proposed MLODS Diversions cases show similar results for the diversions between Belair (RM 65) and Buras (RM 25). The impact of the Buras diversion on the sediment transport downstream is clear. Figure 8.16 reveals the small impact of the Myrtle Grove diversion in the sediment transport of the existing distributaries and diversions.

The main channel sand concentration at peak flow for the tested scenarios is presented in Figure 8.17. It is evident that the Belair diversion (RM 65) is dominant over the remaining outflows located upstream of RM 30. The impact of the Buras diversion (RM 25), included in the Proposed Diversions scenario, is again visible, as there is almost no sediment transport downstream.

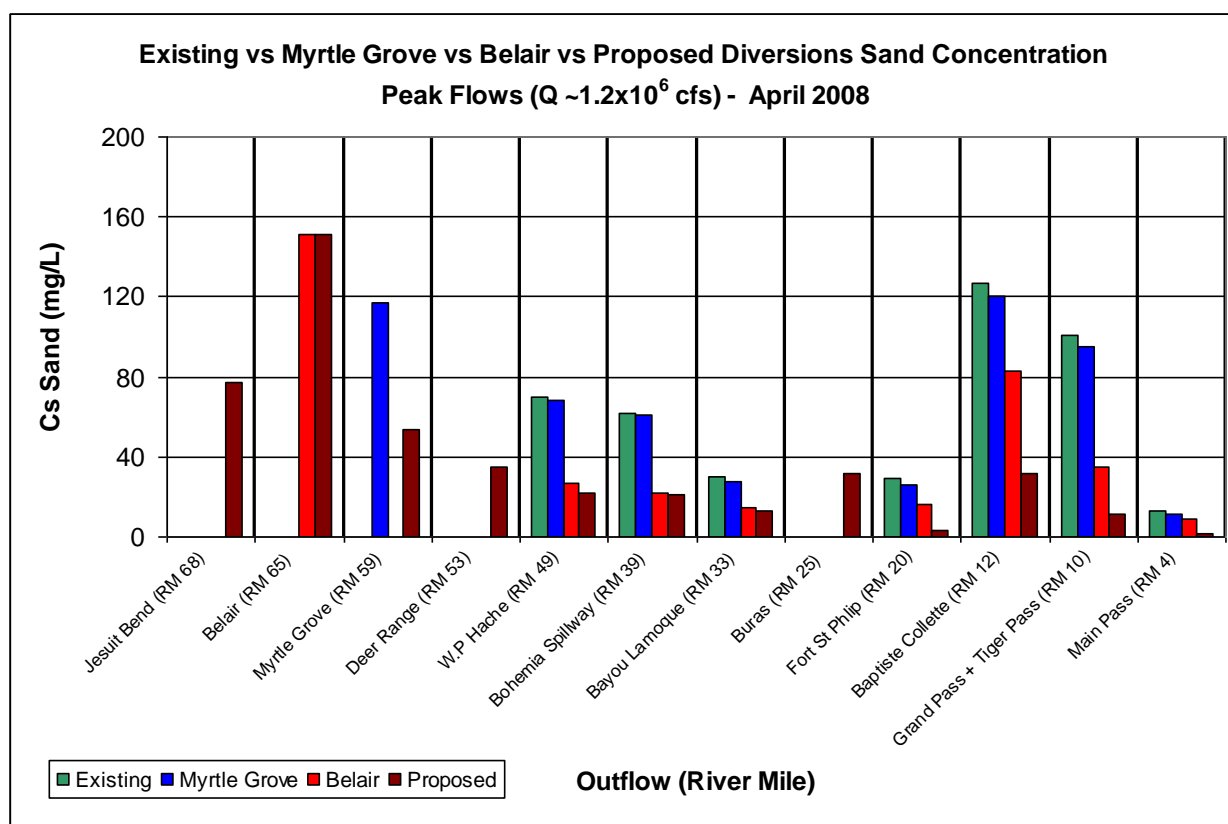


Figure 8.16 – 3-D Modeling - Outflows Suspended Sand Concentration at Peak Flows for the Tested Scenarios

The results obtained for different scenarios with ECOMSED and CHARIMA show the same general trends. The introduction of a large-size diversion (peak flow of 200,000 cfs) such as Belair contributes to a significant reduction in the sediment transport and concentration downstream. Nonetheless, the results obtained with ECOMSED for this particular case, show a higher amount of sediment being extracted at the diversion itself and, consequently, lower sediment available for

transport downstream. The introduction of a medium-size diversion such as Myrtle Grove (peak flow of 30,000 cfs) seems to have little effect in the sediment transport downstream. Once again, ECOMSED and CHARIMA results show agreement in the trend.

Aside from the limitations of 1-D versus 3-D, one of the causes of the difference between the 1-D and the 3-D results is the difference in the geometries used. In CHARIMA, the diversion of sediment and water is, in most cases, simulated with the use of hydraulic structures (weirs, gates) while in ECOMSED regular distributary channels without special internal boundary conditions are used. One of the effects that ECOMSED showed was that the presence of the large diversion caused local scour that contributed to the sand captured by the diversion. In the 1-D model, this localized erosion could not be simulated.

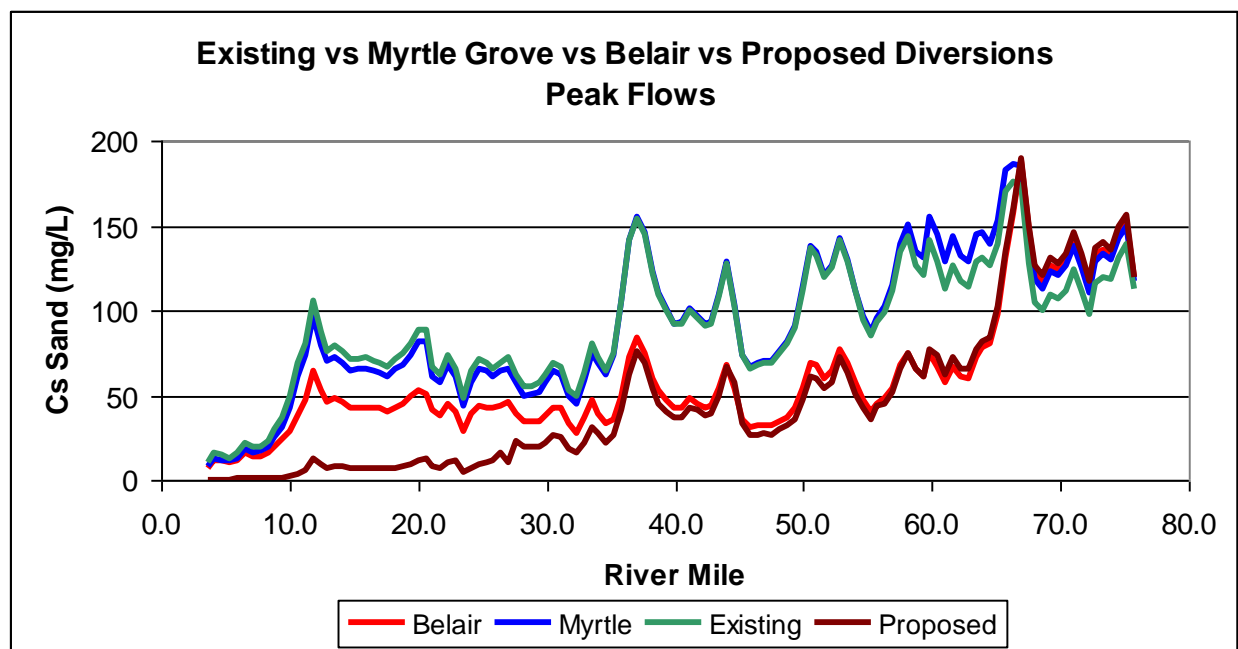


Figure 8.17 – 3-D Modeling – Main Channel Suspended Sand Concentration at Peak Flow for the Tested Scenarios. *Proposed Diversions: Jesuit Bend (RM 68, RK 109), Belair (RM 65, RK 105), Myrtle Grove (RM 59, RK 94), Deer Range (RM 54, RK 87) and Buras (RM 25, RK 40).*

9) CONCLUSIONS

The following conclusions can be made based on the research of this study:

9.1 One-Dimensional Studies

- CHARIMA was selected over HEC-RAS to be used for long term 1-D simulations because it is capable of modeling the split of both flow and sediment and is an unsteady-flow model. HEC-RAS does not automatically model the split of sediment at junctions.
- It was found that in CHARIMA the suspended load results are time-step dependent, which contradicts the theory. A smaller time-step tends to give a lower suspended-load concentration.
- Testing showed that the bedload formulation used in CHARIMA is robust and the results obtained are consistent and time-step independent.
- The use of a large-time step (12 hours) in the sediment simulations was a way of obtaining a good suspended-load calibration with realistic sediment-sizes and roughness coefficients. Nonetheless, the model should be used with caution for applications for flows outside of the calibration range.
- A calibrated operational 1-D model for the Lower Mississippi River bed-material was obtained by developing a calibrated Schocklitsch type formulation that estimates the suspended-load as function of the bedload and the water discharge for the study area.
- The new formulation was applied to CHARIMA bedload results. To retain the dynamic character of the model, a time-step of 10 minutes was used. The calculated concentration results at median and high flows are in good agreement with field measurements. The new formulation indicated that for main stem flows of about 500,000 cfs the concentrations of suspended and bedload are approximately equal, and that the suspended load concentration can represent about 70% of the total bed-material load at peak flows (1.2×10^6 cfs). These results are consistent with field observations.
- The 1-D model was applied to simulate long-term (months to years) hydrodynamics and bed-material transport of the Lower River [Belle Chasse (RM 76) to RM 3]. 2008 data was used for calibration of hydrodynamics and sand transport. The calendar year of 2007 was used for validation of the hydrodynamics.
- Three different cases were tested: i) Existing outflows; ii) Myrtle Grove Diversion + Existing outflows; iii) Belair Diversion + Existing outflows.
 - The introduction of a medium-size diversion at Myrtle Grove (RM 59; 30,000 cfs) did not affect greatly the flow in other diversions. Most outflows were reduced by less than 4% and the downstream boundary outflow was reduced by only 2.35%.
 - The introduction of the larger Belair structure (RM 65; 200,000 cfs) affected significantly the main channel and remaining diversions flows. Most outflows suffered a reduction that ranged from 4% to 20% but some were reduced by more than 50%. The downstream boundary outflow was reduced by more than 14%.
 - For all scenarios, the sand concentrations at peak flow were about double of the ones

at intermediate flows. The sediment load was approximately three times higher for peak flows than for intermediate flows.

- The introduction of the Myrtle Grove diversion leads to slightly higher concentrations in the vicinity of the diversion and slightly lower concentrations downstream.
- The addition of the Belair diversion leads to lower main channel and outflow sand concentrations than the ones obtained for the other scenarios. At peak flow, downstream of the large diversion, the main channel concentrations are reduced in about 15%.

9.2 Three-Dimensional Studies

- The ECOMSED model was selected over FVCOM for the 3-D studies because it had a robust sediment transport module. The FVCOM sediment module is not yet parallelized and there is insufficient information on its application with non-cohesive sediment.
- The FVCOM code was modified to include time-variable friction. It was successfully applied to simulate the hydrodynamics in the Lower River for the Reach between Belle Chasse (RM 76) and Venice (RM 11) with two diversions.
- Boundary conditions play a key role in setting up a numerical model. The inconsistency of the available stage data for the modeled reach was the main reason to rely on 1-D results for calibration instead of using available data directly. Another reason for using 1-D modeling results as boundary conditions was the lack of information on distributary flows. The total outflow for the modeled reach matches a quadratic function based on field measurements (ADCP) but the outflow distribution is uncertain.
- The Manning's formulation and user defined spatially variable roughness coefficients were implemented in the ECOMSED code to allow an accurate reproduction of the field data and 1-D model results, for accurately reproducing flow and transport trends in the vicinity of deep holes, and to account for additional energy losses due to bends and flow expansion-contraction.
- The River was discretized by a structured curvilinear grid with 50 m lateral and 100 m longitudinal planwise dimensions, and with 11 sigma levels in the vertical direction.
- The hydrodynamics module (stage and flow) of the ECOMSED model was calibrated for high, median and low River discharges. The sand transport and the River bed response at low, median and high flows were studied.
- The modified ECOMSED model was calibrated using suspended sand concentration and load measurements. A very good calibration was achieved. The model revealed that the sand transport capacity generally decreases from Belle Chasse to the Head of Passes. This is mainly due to the decreasing bed shear in the downstream direction. The outflows, especially on the East Bank, are a contributing factor in this decrease. This shear gradient tends to cause increased shoaling in the downstream direction.
- The model showed that at high flows there is a high spatial variability in the sand transport with zones of net erosion and net deposition; the general trend was for more erosion in the upper reach

of the study domain and more deposition in the downstream reach.

- The sand transport responds strongly to increasing flow with almost no transport of sand at flows of less than 400,000 cfs and of the order of 200,000 tons per day at flows of over 1,000,000 cfs.
- The model indicated that the deep holes generally were scoured at high flows and experienced a tendency for deposition at intermediate to low flows.
- Initial tests of ECOMSED for the Lower Mississippi River showed exaggerated erosion and bottom sand concentrations that resulted in numerical instabilities and/or unrealistic sediment transport results.
- The code was modified to guarantee a minimum active layer volume and a maximum change on bed-thickness in one time-step. The reference height was changed to better reflect the dune height of the Lower Mississippi River bedforms.
- New derived variables were computed through a post-processing subroutine: water discharge (Q), sediment load (Q_s), depth averaged sediment concentration (C_s), total energy (E) and kinetic energy of the flow (ke), for both the main channel cross-sections and the River diversions.
- It is hard to avoid very strong recirculation in small diversions (1000 cfs) if the diversion is more than two elements wide; if the diversion is implemented in an area where there is high-sediment transport, sediment concentrations may become unrealistically high and the disturbance may propagate into the main channel.
- The short reach grid-dependency study showed that a grid resolution of 100 m by 50 m is acceptable. The results were not significantly different from the ones obtained with a grid as fine as 25 m by 25 m. The model was capable of reproducing secondary flow patterns with the coarser grid, and mobile-bed and hydrodynamic results were similar for the tested resolutions.
- A lateral grid size of between 25 and 50 m is needed to best resolve the near bank effects, where the grid-resolution effect is more visible.
- It was revealed that the downstream sediment transport can significantly influence the upstream sediment transport results. Simulations that include the whole domain [Belle Chasse (RM 76) to downstream of Main Pass] gave higher sediment concentrations for the Myrtle Grove area (RM 65 to RM 51) than the ones that were obtained with the shorter reach, although similar geometry data and appropriate boundary conditions were used. Testing showed that the diversions located between RM 51 and RM 24 are possibly responsible for the higher concentration results in the main channel displayed upstream of the Myrtle Grove area. This fact shows that having an ECOMSED model calibrated for a certain domain or reach does not guarantee that a model of a sub-reach is calibrated.
- The 3-D model was applied to study the effects of the proposed MLODS diversions and distributary modifications. The following simulations were carried out: 1) intermediate (Myrtle Grove) and large (Belair) diversions were modeled with no modifications to the HOP; 2) all of the MLODS diversions were modeled with Southwest and South Passes closed and Pass a Loutr  dredged for navigation.
 - The Myrtle Grove simulation (30,000 cfs or 2.5% of the peak flow) showed that this medium-size diversion would capture sand at close to the average sand concentration in the River at this location. The sediment concentrations at the existing diversions and distributaries were not dramatically changed.

- The Belair large diversion (200,000 cfs or 18% of the peak flow) resulted in significant impacts in the River hydraulics and sediment dynamics: a drop in the River stage throughout the study domain; an increase in the energy gradient upstream of the diversion and a decrease downstream of the diversion; an increase in the bed erosion at and upstream of the diversion with possible head-cutting; an increase in the depositional areas downstream of the diversion leading to shoaling; a significant reduction in the flow to the existing diversions and distributaries; and a significant decrease in the sand diversion loads at the downstream diversions and distributaries.
- The combination of closing Southwest and South Passes and dredging Pass a Loutr  with all of the MLODS diversions in place was simulated as an example of a fully developed River diversion plan.
- This simulation indicated that the large Belair diversion dominates the River response. Due to the reduced sand transport capacities downstream of Belair, sand captured by diversions downstream of Belair was greatly reduced.
- The Buras diversion, which is also large, did not have as much of an effect on the hydraulic grade line compared to the Belair diversion but contributed for a significant reduction in the downstream sediment transport.

9.3 General

The model simulations support the concept that there are three inter-related resources that must be considered in optimizing the beneficial use of the Mississippi River; these are discharge, energy, and sediment transport. The multiple use of the Lower River for coastal restoration and navigation requires a plan that optimizes the benefits from these resources. The results of this study show the nature of the trade-offs as a function of the magnitude and location of the diversions.

10) RECOMMENDATIONS

The suspended load formulation used in CHARIMA was found to be time-step dependent, which contradicts the theory. A more detailed study of the model behavior and code will be necessary to correct this situation. Until the model is revised, it is suggested that CHARIMA should be applied for bedload transport only and that the suspended-load should be estimated as a function of the bedload simulation results through the use of a post-processing formulation (Power-Law, Schocklitsch-type, or other).

The recently released FVCOM code with the parallelized sediment module should be modified to include:

- 1) spatially and temporally varying friction,
- 2) the van Rijn sediment model from ECOMSED.

The new FVCOM model should be applied to the entire Lower River with the Gulf of Mexico as the open water boundary condition and should include: non-cohesive and cohesive sediment, tides and salinity. This model can run on a parallel machine (e.g. LONI) and discretized at a sufficient resolution to resolve the planwise recirculation at the inside of bends and sand transport within the diversions.

A systematic analysis of river diversions in the Lower Mississippi River should be conducted to quantify the effects of diversion size and location on the river resources. This study should lead to a methodology for optimum allocation of the River resources (flow, sediment and energy) for multiple uses. The modeling results show that the introduction of a large diversion (15 to 20% of the main stem flow at that location) can lead to a very strong downstream reduction of the three main resources available in the system: flow, energy and sediment. The introduction of a medium size diversion (2.5 % of the main flow at that location) has a mild impact in the resources available in the system. The introduction of several medium-size diversions should be favored over the selection of a sole large diversion.

One of the greatest needs, for advancing the sediment modeling of the Lower River, is more field data such as the data collected by Dr. Mead Allison's team and the West Bay Study.

11) REFERENCES

1. Ackers, P. and White, W.R., 1973. Sediment Transport: New Approach and Analysis, *J. of Hydraulics Division*, 99, No. HY11, 2041-2060, American Society of Civil Engineers (ASCE).
2. ADCIRC Development Group; 2005. *Quarter Annular Harbor with Tidal Forcing*. University of Notre Dame. <http://www.nd.edu/~adcirc/quater.htm>.
3. Allison, M. A., and E. A. Meselhe, 2010. The use of large water and sediment diversions in the lower Mississippi River (Louisiana) for coastal restoration, *J. Hydrology*, 387, 346-360, doi:10.1016/j.jhydrol.2010.04.001, #2289
4. Allison, M.A.; 2010. *Water and Sediment Surveys of the Mississippi River Channel Conducted at Myrtle Grove and Magnolia in support of Numerical Modeling (October 2008-May 2010)*. Report to the State of Louisiana of Coastal Protection and Restoration as subcontracted to C.H. Fenstermaker and Associates. October
5. Bamgboye, O.A.; and de Vries, J.J.; 1986. Physical and Mathematical Modeling of a River Diversion Scheme. *Water International*, 11, pp. 162-168, IWRA, USA.
6. Barbé, D.E.; Fagot, K. and McCorquodale, J.A., 2000. Effects on Dredging Due to Diversions from the Lower Mississippi River, *Journal of Waterway, Port, Coastal, and Ocean Engineering*, Vol. 126(3), 121-129
7. Barkdoll, B.D.; Duan, J.G., 2008. Sediment Modeling: Issues and Future Directions, *Journal of Hydraulic Engineering*, Vol. 134(3), pp. 285, American Society of Civil Engineers (ASCE).
8. Bray, D. I., 1979. Estimating Average Velocity in Gravel-Bed Rivers. *Journal of the Hydraulics Division*, ASCE Vol 105, No. HY9, Proceedings Paper 14810. pp. 1103-1122, September.
9. Burban, P.Y.; Xu, Y.J.; McNeil, J.; and Lick, W.; 1990. *Journal of Geophysical Research*, Vol. 95, No. C10, PAGES 18,213-18,220, October.
10. Chang, H.H., 1988. *Fluvial Processes in River Engineering*. Wiley-Interscience, United States of America.
11. Chen, C.; Beardsley, R.C. and Cowles, G.; 2006. *An Unstructured Grid, Finite Volume Coastal Ocean Model*. FVCOM User manual. School for Marine and Technology-University of Massachusetts-Dartmouth and Woods Hole Oceanographic Institution. Massachusetts.
12. Chen, C.; Huang, H.; Beardsley, R.C.; Liu, H.; Xu, Q. and Cowles, G.; 2007. A finite volume numerical approach for coastal ocean circulation studies: Comparisons with finite difference models. *Journal of Geophysical Research*, Vol. 112, C03018, doi:10.1029/2006JC003485
13. Chen, C.; Liu, H. and Beardsley, R.C., 2003. An unstructured, finite-volume, three-dimensional, primitive equation ocean model: application to coastal ocean and estuaries, *J. of Atmospheric and Oceanic Technology*, 20, 159-186.
14. Cheng, N.S.; 1997. Simplified Settling Velocity Formula for Sediment Particle, *ASCE Journal of Hydraulic Engineering*, 123, pp. 149-152.
15. Chilmakuri, C.S., 2005. Sediment Transport and Pathogen Indicator Modeling in Lake Pontchartrain. Ph.D. Dissertation, University of New Orleans, New Orleans, LA.
16. Chow, V.T., 1959. *Open-Channel Hydraulics*. New York: The Blackburn Press.
17. Chung, T.J.; 2002. *Computational Fluid Dynamics*, Cambridge University Press, United Kingdom, pp. 1012

18. Corti, S. and Pennati, V., 2000. A 3-D Hydrodynamics Model of a River Flow in a Delta Region, *Hydrological Processes*, Vol. 14(13), 2301-2309
19. Davis, M.A., 2010. *Numerical Simulation of Unsteady Hydrodynamics in the Lower Mississippi River*. M.Sc. Thesis, The University of New Orleans, Louisiana, May.
20. de Saint Venant, B. (1871) – *Théorie du mouvement non-permanent des eaux avec application aux crues des rivières et a l'introduction des marées dans leur lit*, Acad. Sci. Comptes rendus. Paris. Vol 73, pp. 148-154, 237-240.
21. Demuren, A.O, 1993. A Numerical Model for Flow in Meandering Channels with Natural Bed Topography, *Water Resources Research*, Vol. 29(4), 1269-1277
22. DHI, 2004. *Mike 11: A modeling system for rivers and channels*, User Guide, DHI Software.
23. Donnel, B.P. and Letter, J.V. Jr., 1991. *TABS-MD Numerical Investigation of Shoaling in the Mississippi River – Gulf Outlet*, Army Engineer Waterways Experiment Stations Vicksburg MS Hydraulics Lab
24. Einstein, H.A., 1950. The Bed-Load Function for Sediment Transportation in Open Channel Flows, Technical Bulletin No. 1026, Department of Agriculture, Washington, D.C., United States of America.
25. El Kheishy, K.; 2007. *Flow-Transport Modeling and Quantification of the Periodic Nature of Bed Forms in the Lower Mississippi River*. Ph.D. Dissertation, The University of New Orleans, Louisiana, May.
26. Engelund, F. and Hansen, E.; 1967. *A Monograph on Sediment Transport in Alluvial Streams*, Teknisk Vorlag, Copenhagen, Denmark
27. Ettema, R.; Arndt, R.; Roberts, P.; and Wahl, T. (2000). *Hydraulic Modeling: Concepts and Practice*, ASCE.
28. Ezer, T.; Arango, H. and Shchepetkin, A.; 2002. Developments in terrain-following ocean models: Intercomparisons of numerical aspects. *Ocean Modelling*, Elsevier, 4: 249-267.
29. Fofonoff, N.P., 1962. Physical Properties of sea-water. In: *The Sea*, edited by Hill, M.N., J. Wiley and Sons, 3-30.
30. Gailani, J.; Ziegler, C.K. and Lick, W.; 1991. The Transport of Sediments in the Fox River, *Journal of Great Lakes Research*, 17, pp. 479-494.
31. Garde, R.J. and Raju, K.R., 2000. *Mechanics of sediment transportation and alluvial stream problems*. 3rd Edition, Taylor & Francis, 686p.
32. Georgiou, I.Y.; McCorquodale, J.A.; Neupane, J.; Howee, N.; Hughes, Z.; Fitzgerald, D.; and Schindler, J. K., 2010. *Modeling the Hydrodynamics of Diversions into Barataria Basin*. Final Report submitted to the Lake Pontchartrain Basin Foundation (LPBF).
33. Graf, W.H.; 1998. *Fluvial Hydraulics – Flow and Transport Processes in Channels of Simple Geometry*. John Wiley & Sons, England.
34. Grant, W.D.; and Madsen, O.S., 1979. Combined Wave and Current Interaction with a Rough Bottom, *Journal of Geophysical Research*, 84(C4), pp. 1797-1808.
35. Guillot, M.; 2009. Personal communication. [Project in:] Course: Introduction to Computational Fluid Dynamics. Fall 2009. University of New Orleans.
36. Hawley, N.; 1982. Settling Velocity Distribution of Natural Aggregates. *Journal of Geophysical Research*, Vol. 87, No. C12, pp. 9849-9498, November.

37. Hey, R.D., 1979. Flow Resistance in Gravel-Bed Rivers. *Journal of the Hydraulics Division*, Vol. 105, No. 4, pp. 365-379, April.
38. Holly, F. M. Jr. 2009. *CHARIMA: Unsteady Hydrodynamics, Contaminant Transport and Mobile-Bed in One-Dimensional Channel Networks – Abbreviated User's Guide*. January
39. Holly, F. M. Jr; Yang, J. C.; Schwarz, P.; Schaefer, J.; Hsu, S. H.; Einhellig, R. 1990. *CHARIMA: Numerical Simulation of Unsteady Water and Sediment Movement in Multiply Connected Networks of Mobile-bed Channels*. IHHR Report No. 343, Iowa Institute of Hydraulic Research, Iowa, July.
40. Holly, F.M. Jr; and Rahuel, J.L.; 1990. New numerical/physical framework for mobile-bed modeling. Part 1. Numerical and physical principles, *Journal of Hydraulic Research*, Vol. 28, no. 4, pp. 401-416.
41. HydroQual, Inc.; 2002, A primer for ECOMSED. Users Manual, Ver. 1.3, HydroQual, Inc., Mahwah, New Jersey, pp. 188.
42. Iwagaki, Y., 1956. *Hydroynamical Study on Critical Tractive Force*, Trans. JSCE, No. 41
43. Karim, M. F.; and Kennedy, J. F. (1982) – *Computer-Based Predictors for Sediment Discharge and Friction Factor of Alluvial Streams*, IIHR Report No. 242, The University of Iowa, Iowa City.
44. Karim, M.F. (1985) – *IALLUVIAL: Analysis of Sediment Continuity and Application to the Missouri River*, Iowa Institute of Hydraulic Research, Report No. 292, The University of Iowa, Iowa City, Iowa, December.
45. Kim, J. and Nestmann, F.; 2009. Settling behavior of fine-grained materials in flocs. *Journal of Hydraulic Research*, Vol. 47, No.4, pp. 492-502, doi:10.3826/jhr.2009.3205.
46. Kobayashi, M; Pereira, J. M. and Pereira, J.C.; 1998. A second-order upwind least-squares scheme for incompressible flows on unstructured hybrid grids. *Numerical Heat Transfer, Part 2*. 34: 39-60.
47. Krone, R.B., 1962. Flume Studies of the Transport of Sediment in Estuarial Processes, Final Report, Hydraulic Engineering Laboratory and Sanitary Engineering Research Laboratory, University of California, Berkeley.
48. Lau, Y.L. and Krishnappan, B.G.; 1992. Size distribution and settling velocity of cohesive sediments during settling. *Journal of Hydraulic Research*, Vol. 30, 1992, No.5.
49. Liggett, J.A., and Cunge, J.A.(1975) – *Numerical Methods of Solution of the Unsteady Flow Equations*, Chapter 4, Vol.1, In: K. Mahmad and V.Yevjevich (eds.), *Unsteady flow in open channels*, Water Resources Publications, Fort Collins, Colorado, USA.
50. Limerinos, J.T.; 1970. Determination of the Manning Coefficient for Measured Bed Roughness in Natural Channels, *USGS Water Supply Paper 1898-B*.
51. Lopez, J.; Lake Pontchartrain Basin Foundation (LPBF) (2008) Comprehensive Recommendations Supporting the Use of the Multiple Lines of Defense Strategy to Sustain Coastal Louisiana 2008 Report (Version 1), Lake Pontchartrain Basin Foundation. Metairie, LA.
52. Lynch, D. R. and Gray, W. G.; 1978. Analytic Solutions for Computer Flow Model Testing. *Journal of the Hydraulics Division*, 10: 1409-1428.

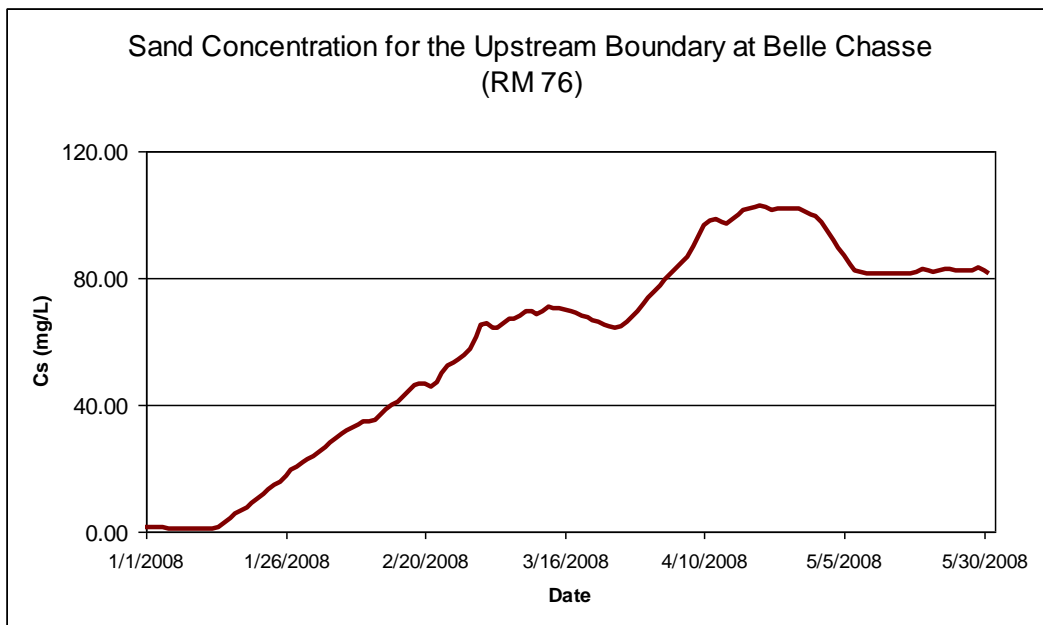
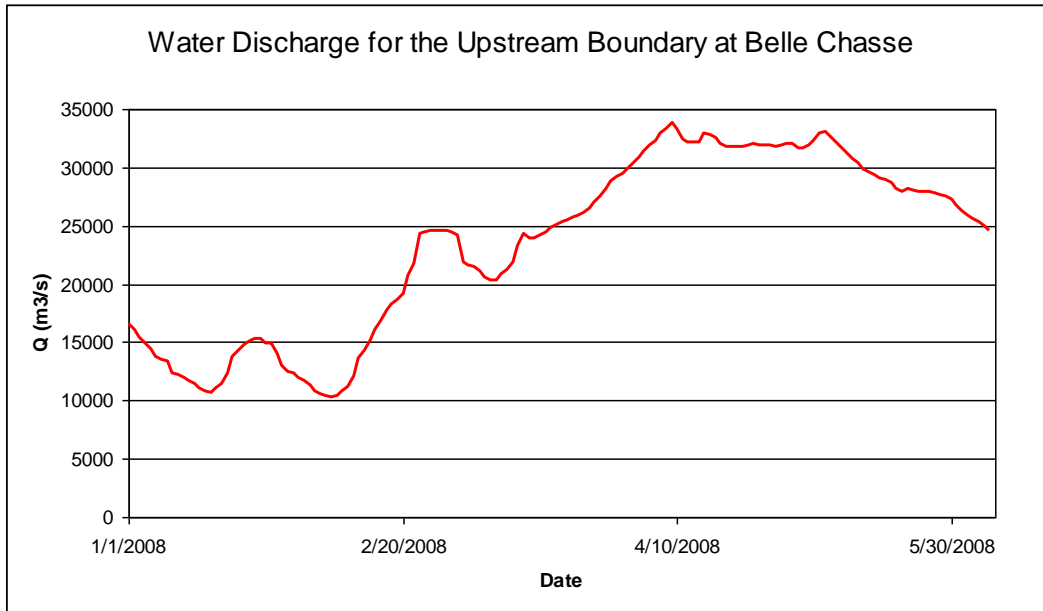
53. Maa, J.P., Kwon, J.I; Hwang, K.N.; and Ha, H.K.; 2008. Critical Bed Shear Stress for Cohesive Sediment Deposition under Steady Flows, *Journal of Hydraulic Engineering*, Vol. 134, No. 12, pp. 1767-1771.
54. McCorquodale, A. and Georgiou, I.; 2006. Evaluation of Water Quality Models for Ontario Receiving Waters. Report. University of New Orleans, New Orleans, LA. pp.127.
55. McCorquodale, J.A.; 2006. Sediment Transport and Erosion. In: Pfafflin, J. R. and Ziegler, E. N. (Eds.), *Encyclopedia of Environmental Science and Engineering*, Volume 2, pp. 1064-1081, Taylor & Francis, 5th Edition.
56. Mehta, A.J.; 1973. *Depositional Behavior of Cohesive Sediments*, Ph.D. thesis, Univ. of Fla., Gainesville.
57. Mehta, A.J.; 1989. On Estuarine Cohesive Sediment Suspension Behavior. *Journal of Geophysical Research*, Vol. 94, No. C10, pp. 14,303-14,314, October.
58. Mehta, A.J.; Hayter, E.J.; Parker, W.R.; and Teeter, A.M.; 1987. Cohesive Sediment Transport Processes, in *Sedimentation Control to Reduce Maintenance Dredging of Navigation Facilities in Estuaries*, National Academy Press, pp. 53-76, Washington, D.C., United States of America.
59. Mellor, G.L., 2003. *Users guide for a three-dimensional primitive equation, numerical ocean model*. Prog. In Atmos. and Ocean Sci., Princeton University, 53 pages, June.
60. Mellor, G.L.; Ezer, T. and Oey, L.Y.; 1994. The Pressure Gradient Conundrum of Sigma Coordinate Ocean Models. *Journal of Atmospheric and Oceanic Technology*, 11:1126-1134.
61. Mellor, G.L.; Oey, L.Y. and Ezer, T.; 1998. Sigma Coordinate Pressure Gradient Errors and the Seamount Problem. *Journal of Atmospheric and Oceanic Technology*, 15: 1122-1131.
62. Meselhe, E.A.; Habib, E.; Griborio, A.G.; Gautam, S.; McCorquodale, J.A. and Georgiou, I.Y., 2005. Hydro-Ecological Modeling of the Lower Mississippi River. *Proc. of the 14th Biennial Coastal Zone Conf.* (New Orleans, LA, USA).
63. Meselhe, E.A.; Habib, E.; Griborio, A.G.; Gautam, S.; McCorquodale, J.A. and Georgiou, I.Y., 2006. Multidimensional Modeling of the Lower Mississippi River. *Pro., of the 8th Federal Interagency Sedimentation Conference (FISC)*. (Reno, Nevada, USA).
64. Meselhe, E.A.; Pereira, J.F; Georgiou, I.Y.; Allison, M.A.; McCorquodale, J.A. and, Davis, M.A., 2010. Numerical Modeling of Mobile-Bed Hydrodynamics in the Lower Mississippi River, *Proc. of World Environmental & Water Resources Congress (EWRI) 2010*, A.S.C.E., Providence, RI
65. Meyer-Peter, E.; and Müller, R. (1948) – *Formulations for Bed-Load Transport*, Report on Second Meeting of International Association for Hydraulic Research, Stockholm, Sweden, pp. 39-64.
66. Nittrouer, J.A.; Allison, M.A. and Campanella, R., 2008. Bedform transport rates for the lowermost Mississippi River, *Journal of Geophysical Research Earth Surface*, 113 (F03004)
67. Papanicolaou, A.N.; Elkaheem, M.; Krallis, G.; Prakash, S. and Edinger, J., 2008. Sediment Transport Modeling Review – Current and Future Developments, *Journal of Hydraulic Engineering*, Vol. 134(1), 1-14, American Society of Civil Engineers (ASCE).
68. Parker, G. And Sequeiros, O., 2006. Large Scale River Morphodynamics: Application to the Mississippi Delta, *River Flow 2006 Proceedings*, Lisbon, Portugal, September 2006, Taylor & Francis Group, London.

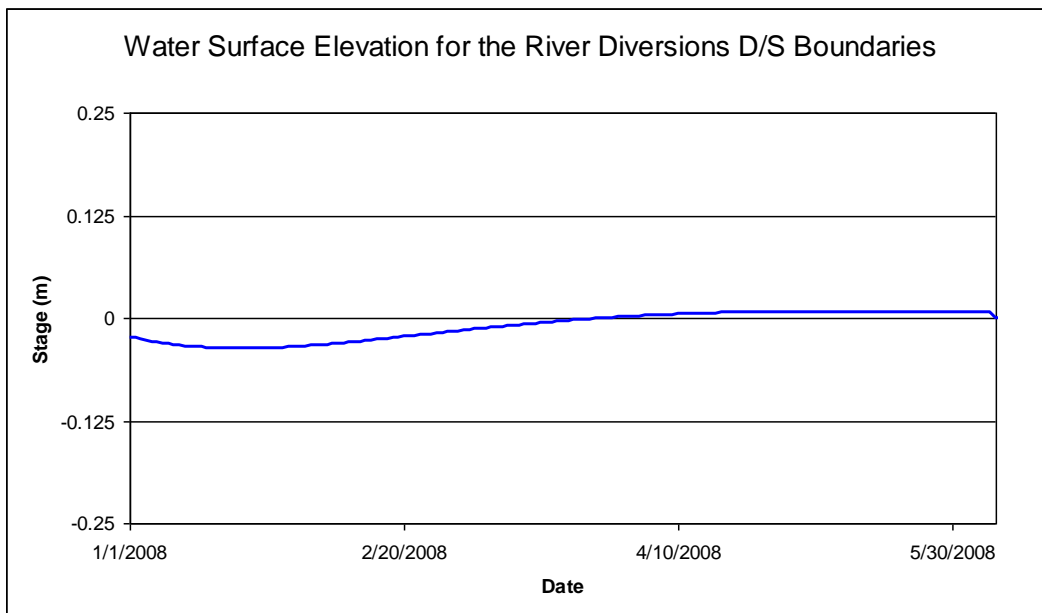
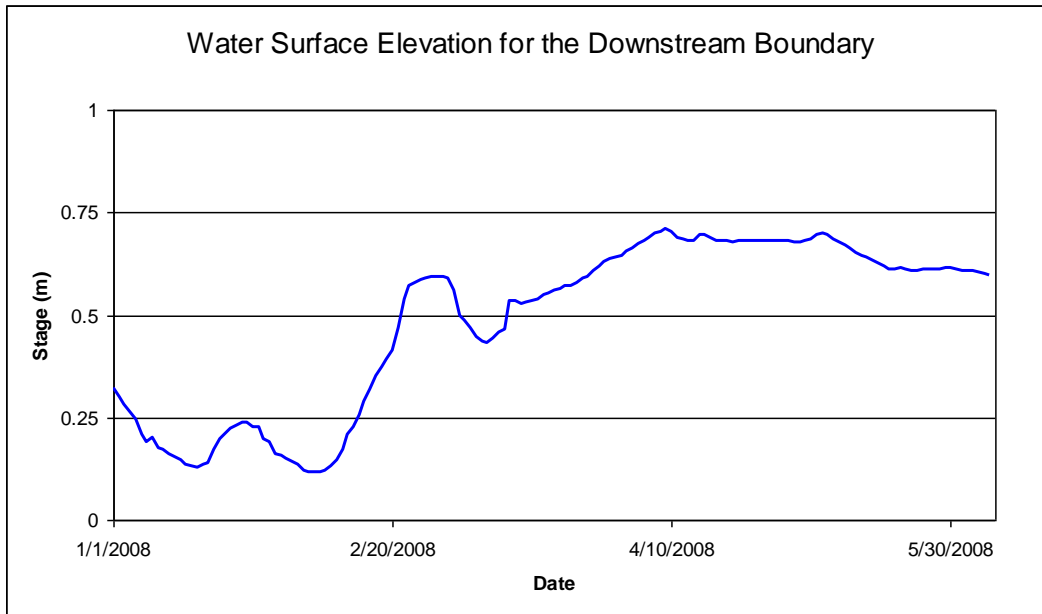
69. Partheniades, E., 1992. Estuarine Sediment Dynamics and Shoaling Processes, in Handbook of Coastal and Ocean Engineering, Vol. 3, J. Herbick, ed., pp. 985-1071.
70. Pereira, J.F., 2007. *Modelação Numérica de Escoamentos Variáveis em Leitos Móveis. Aplicação ao Rio Mondego*. M.Sc. Thesis, Instituto Superior Técnico (Technical University of Lisbon), Portugal.
71. Pereira, J.F.; Silva, J.M.; Holly, F.M., 2007. Numerical Simulation of Unsteady Mobile-Bed Hydrodynamics, with Application to Mondego River. International Association for Hydraulic Research (IAHR), Proceedings from the 32nd Congress. Spain.
72. Pereira, J.F; McCorquodale, J.A.; Meselhe, E.A.; Georgiou, I.Y. and Allison, M.A., 2009. Numerical Simulation of Bed Material Transport in the Lower Mississippi River, *J. of Coastal Research*, SI 56, 1449-1453. Lisbon, Portugal.
73. Pratt, T. (2009). West Bay Sediment Diversion Work Plan, Task 1: Data Collection and Analysis. U.S. Army Corps of Engineers (USACE), Engineer Research and Development Center, Vicksburg, MS.
74. Proffitt, G. T.; Sutherland, A. J., 1983. Transport of Nonuniform Sediments, *Journal of Hydraulic Research*, Vol. 21, No.1, pp. 33-43.
75. Reid, R.O.; and Bodine, B.R., 1968. Numerical Model for Storm Surges in Galveston Bay, ASCE, *J. Water. and Harb. Div.*, 94, 33-57.
76. Retana, A. G.; 2008. *Salinity Transport in a Finite-Volume Sigma-Layer Three-Dimensional Model*. Ph.D. Dissertation, The University of New Orleans, Louisiana, December.
77. Rouse, H., 1939. *An Analysis of Sediment Transportation in the Light of Fluid Turbulence*, Soil Conservation Service Report No. SCS-TP-25, United States Department of Agriculture, Washington, D. C.
78. Smagorinsky, J., 1963. *General Circulation Experiments with the Primitive Equations, I. The Basic Experiment*. Mon. Weather Rev, Vol. 91, pp. 99 to 164.
79. Spasojevic, M. and Holly, F.M., 1994. *Three-Dimensional Numerical Simulation of Mobile-Bed Hydrodynamics, Final Report*, New Orleans, LA: USCOE
80. Tambo, N.; and Hozumi, H.; 1979. Physical Characteristics of Flocs-II. Strength of Floc. *Water Research*, Vol. 13, pp. 421 to 427, Pergamon Press Ltd, Great Britain.
81. Torfs, H., 1997. Erosion of mixed cohesive/non-cohesive sediments in uniform flow. In: Burt, N., Parker, R., Watts, J. (Eds.), *Cohesive Sediments*, Wiley, Chichester, pp. 245-252.
82. U.S. Army Corps of Engineers, New Orleans District (USACE NOD), 2007. *Mississippi River Hydrographic Survey: 2003 – 2004; Black Hawk, LA to Gulf of Mexico*. Mississippi River Commission, Vicksburg, MS.
83. United States Army Corps of Engineers (USACE), 1993. *HEC-6, Scour and Deposition in Rivers and Reservoirs, User's Manual*, USACE Hydrologic Engineering Center, August.
84. USACE Staff, 2008. *HEC-RAS River Analysis System, User's Manual Version 4.0*. U.S. Army Corps of Engineers, Hydrologic Engineering Center (HEC) Publication, 733p.
85. van Rijn, L.C., 1984. Sediment Transport, Part II: Suspended Load Transport, *J. of Hydraulic Engineering*, 110(11), 1613-1638
86. Versteeg, H.K. and Malalasekera, W.; 2006. *An Introduction to the Computational Fluid Dynamics: The finite volume method*, 2nd Edition, Pearson Prentice Hall, England.

87. Visible Earth: Mississippi River Sediment Plume. (2001, March 15). *Visible Earth: Home*. Retrieved April 6, 2011, from http://visibleearth.nasa.gov/view_rec.php?id=1650.
88. Willis, D.H.; and Krishnappan, B.G.; 2004. Numerical modeling of cohesive sediment transport in rivers. *Canadian Journal of Civil Engineering*, No. 31, pp. 749-758.
89. Xue, P.; Chen, C.; Ding, P.; Beardsley, R.C.; Lin, H.; Ge, J. and Kong, Y., 2009. Saltwater intrusion into the Changjiang River: A model-guided mechanism study, *J. of Geophysical Research Oceans*, 114, C02006, doi: 10.1029/2008JC004831.
90. Zheng, L. and Chen, C., 2000. A 3-D modeling study of the estuarine system: an application to the Satilla River, Proc. 6th Inter. Conf. on Estuarine and Coastal Modeling, edited by Spaulding, A. S. C. E., New Orleans, LA, 1999, 1128-1149.

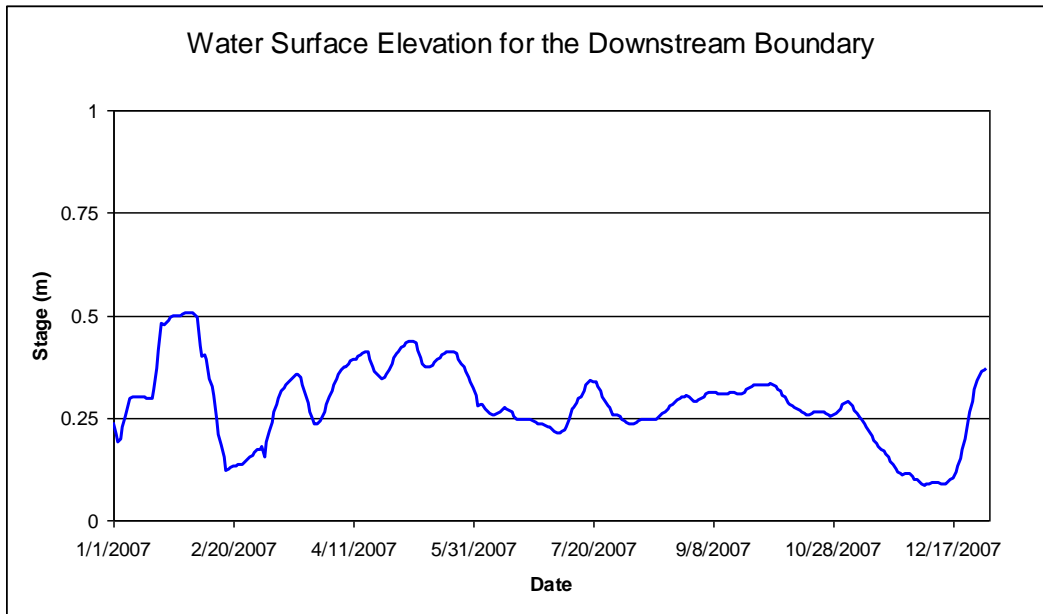
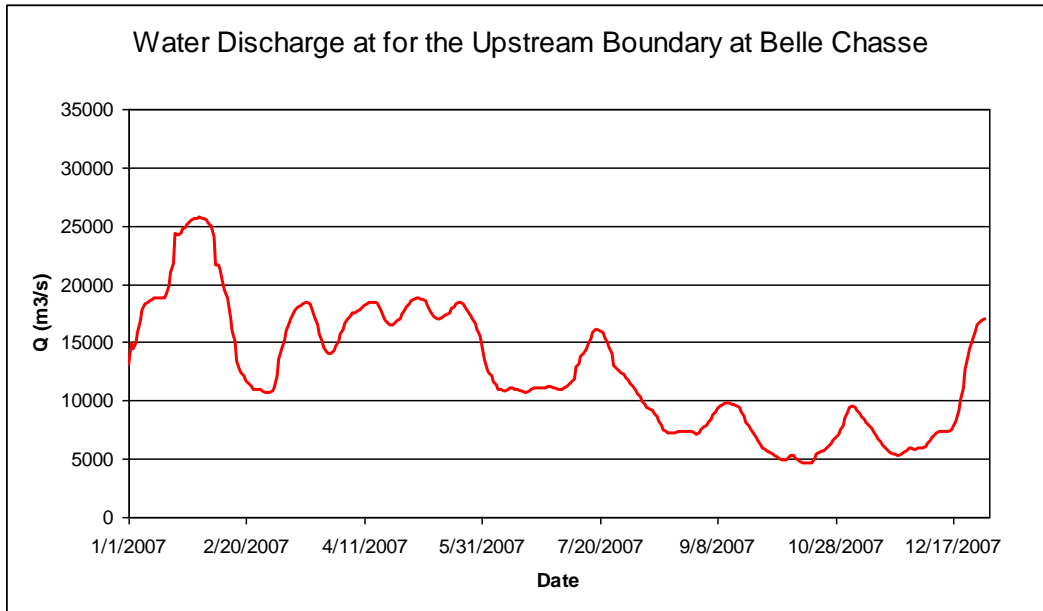
APPENDIX A: 1-D Modeling Boundary Conditions

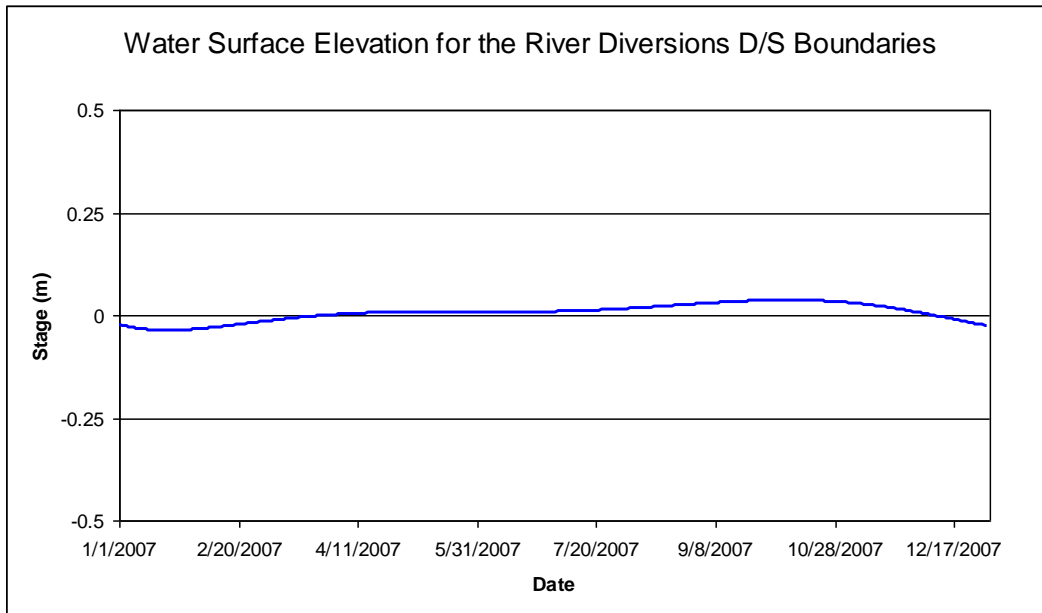
2008 CALIBRATION





2008 VALIDATION





APPENDIX B: Flow Roughness Coefficients (Ks and n) used in the 1-D Modeling

HYDRODYNAMICS CALIBRATION 2008

Mississippi River Main Channel

Mississippi River Main Channel				
Point	Link	River Mile	Ks	n
1	1	2.95	100.00	0.010
2	1	3.15	100.00	0.010
1	3	3.36	100.00	0.010
2	3	3.60	100.00	0.010
3	3	3.83	100.00	0.010
4	3	4.04	100.00	0.010
5	3	4.26	100.00	0.010
6	3	4.46	100.00	0.010
1	5	4.70	100.00	0.010
2	5	4.90	100.00	0.010
3	5	5.10	100.00	0.010
4	5	5.30	100.00	0.010
5	5	5.50	100.00	0.010
6	5	5.80	100.00	0.010
7	5	6.00	100.00	0.010
8	5	6.20	100.00	0.010
9	5	6.50	100.00	0.010
10	5	6.70	100.00	0.010
11	5	6.90	100.00	0.010
12	5	7.30	100.00	0.010
13	5	7.50	100.00	0.010
14	5	7.94	100.00	0.010
15	5	8.10	100.00	0.010
16	5	8.40	100.00	0.010
17	5	8.70	100.00	0.010
18	5	8.90	100.00	0.010
19	5	9.10	100.00	0.010
20	5	9.40	100.00	0.010
21	5	9.70	100.00	0.010
22	5	9.97	100.00	0.010
23	5	10.20	100.00	0.010
1	9	10.35	100.00	0.010

2	9	10.54	100.00	0.010
3	9	10.73	100.00	0.010
4	9	11.07	100.00	0.010
5	9	11.20	100.00	0.010
1	11	11.46	100.00	0.010
2	11	11.72	100.00	0.010
3	11	11.98	100.00	0.010
4	11	12.26	100.00	0.010
5	11	12.50	100.00	0.010
6	11	12.77	100.00	0.010
7	11	12.99	100.00	0.010
8	11	13.25	100.00	0.010
9	11	13.56	100.00	0.010
10	11	13.86	100.00	0.010
11	11	14.21	100.00	0.010
12	11	14.50	100.00	0.010
13	11	14.76	100.00	0.010
14	11	15.05	100.00	0.010
15	11	15.32	100.00	0.010
16	11	15.57	100.00	0.010
17	11	15.86	100.00	0.010
18	11	16.23	100.00	0.010
19	11	16.51	100.00	0.010
20	11	16.80	100.00	0.010
21	11	17.12	100.00	0.010
22	11	17.39	100.00	0.010
23	11	17.72	100.00	0.010
24	11	18.00	100.00	0.010
25	11	18.33	100.00	0.010
26	11	18.58	100.00	0.010
27	11	18.85	100.00	0.010
28	11	19.11	50.00	0.020
29	11	19.40	50.00	0.020
1	13	19.60	41.67	0.024
2	13	19.86	41.67	0.024
3	13	20.12	41.67	0.024
4	13	20.48	41.67	0.024
5	13	20.73	41.67	0.024

6	13	21.02	41.67	0.024
7	13	21.30	41.67	0.024
8	13	21.66	41.67	0.024
9	13	22.00	41.67	0.024
10	13	22.37	41.67	0.024
11	13	22.70	41.67	0.024
12	13	23.08	41.67	0.024
13	13	23.48	41.67	0.024
14	13	23.83	41.67	0.024
15	13	24.22	41.67	0.024
16	13	24.57	41.67	0.024
17	13	24.89	41.67	0.024
18	13	25.24	41.67	0.024
19	13	25.56	41.67	0.024
20	13	25.98	41.67	0.024
21	13	26.36	41.67	0.024
22	13	26.74	41.67	0.024
23	13	27.06	41.67	0.024
24	13	27.39	41.67	0.024
25	13	27.70	41.67	0.024
26	13	28.03	41.67	0.024
27	13	28.32	41.67	0.024
28	13	28.53	41.67	0.024
29	13	28.79	41.67	0.024
30	13	28.98	41.67	0.024
31	13	29.24	41.67	0.024
32	13	29.46	41.67	0.024
33	13	29.65	41.67	0.024
34	13	29.89	41.67	0.024
35	13	30.15	41.67	0.024
36	13	30.40	41.67	0.024
37	13	30.59	41.67	0.024
38	13	30.78	41.67	0.024
39	13	30.98	41.67	0.024
40	13	31.17	41.67	0.024
41	13	31.37	41.67	0.024
42	13	31.57	41.67	0.024
43	13	31.88	41.67	0.024

44	13	32.13	41.67	0.024
1	16	32.40	45.00	0.022
2	16	32.41	45.00	0.022
1	22	32.45	45.00	0.022
2	22	32.60	45.00	0.022
1	26	32.70	45.00	0.022
2	26	32.80	45.00	0.022
1	30	32.89	55.00	0.018
2	30	33.17	55.00	0.018
3	30	33.53	55.00	0.018
4	30	33.83	55.00	0.018
5	30	34.18	55.00	0.018
6	30	34.53	55.00	0.018
7	30	34.93	55.00	0.018
8	30	35.15	55.00	0.018
9	30	35.45	55.00	0.018
10	30	35.71	55.00	0.018
11	30	36.05	55.00	0.018
12	30	36.33	55.00	0.018
13	30	36.62	55.00	0.018
14	30	36.87	55.00	0.018
15	30	37.17	55.00	0.018
16	30	37.45	55.00	0.018
17	30	37.77	55.00	0.018
18	30	38.08	55.00	0.018
19	30	38.32	55.00	0.018
20	30	38.62	55.00	0.018
1	34	38.92	53.00	0.019
2	34	39.22	53.00	0.019
3	34	39.51	53.00	0.019
4	34	39.77	53.00	0.019
5	34	40.08	53.00	0.019
6	34	40.36	53.00	0.019
7	34	40.64	53.00	0.019
8	34	40.91	53.00	0.019
9	34	41.22	53.00	0.019
10	34	41.51	53.00	0.019

11	34	41.87	53.00	0.019
12	34	42.19	53.00	0.019
13	34	42.50	53.00	0.019
14	34	42.84	53.00	0.019
15	34	43.17	53.00	0.019
16	34	43.46	53.00	0.019
17	34	43.73	53.00	0.019
18	34	44.04	53.00	0.019
19	34	44.31	53.00	0.019
20	34	44.63	53.00	0.019
21	34	44.93	53.00	0.019
22	34	45.23	53.00	0.019
23	34	45.54	53.00	0.019
24	34	45.93	53.00	0.019
25	34	46.32	53.00	0.019
26	34	46.69	53.00	0.019
27	34	47.11	53.00	0.019
28	34	47.44	53.00	0.019
29	34	47.81	53.00	0.019
30	34	48.14	53.00	0.019
31	34	48.45	53.00	0.019
32	34	48.76	53.00	0.019
1	35	49.08	53.00	0.019
2	35	49.38	53.00	0.019
3	35	49.72	53.00	0.019
4	35	50.05	53.00	0.019
5	35	50.40	53.00	0.019
6	35	50.73	53.00	0.019
7	35	51.12	75.00	0.013
8	35	51.47	75.00	0.013
9	35	51.85	75.00	0.013
10	35	52.18	75.00	0.013
11	35	52.52	75.00	0.013
12	35	52.87	75.00	0.013
13	35	53.24	75.00	0.013
14	35	53.52	75.00	0.013
15	35	53.84	75.00	0.013
16	35	54.12	75.00	0.013

17	35	54.44	75.00	0.013
18	35	54.72	75.00	0.013
19	35	55.01	75.00	0.013
20	35	55.32	75.00	0.013
21	35	55.63	75.00	0.013
22	35	55.99	75.00	0.013
23	35	56.39	75.00	0.013
24	35	56.76	75.00	0.013
25	35	57.16	75.00	0.013
26	35	57.50	75.00	0.013
27	35	57.84	75.00	0.013
28	35	58.14	75.00	0.013
29	35	58.44	75.00	0.013
30	35	58.69	75.00	0.013
31	35	59.01	75.00	0.013
1	36	59.30	75.00	0.013
2	36	59.52	75.00	0.013
3	36	59.74	75.00	0.013
4	36	59.97	75.00	0.013
5	36	60.21	75.00	0.013
6	36	60.42	75.00	0.013
7	36	60.64	75.00	0.013
8	36	60.88	75.00	0.013
9	36	61.04	75.00	0.013
10	36	61.24	75.00	0.013
11	36	61.50	75.00	0.013
12	36	61.85	75.00	0.013
13	36	62.11	75.00	0.013
14	36	62.34	75.00	0.013
15	36	62.57	75.00	0.013
16	36	62.88	75.00	0.013
17	36	63.11	75.00	0.013
18	36	63.36	75.00	0.013
19	36	63.62	75.00	0.013
20	36	63.88	75.00	0.013
21	36	64.16	75.00	0.013
22	36	64.46	75.00	0.013
23	36	64.73	75.00	0.013

24	36	64.98	75.00	0.013
1	37	65.28	75.00	0.013
2	37	65.57	75.00	0.013
3	37	65.81	75.00	0.013
4	37	66.09	75.00	0.013
5	37	66.33	75.00	0.013
6	37	66.59	75.00	0.013
7	37	66.86	75.00	0.013
8	37	67.09	75.00	0.013
9	37	67.31	75.00	0.013
10	37	67.50	75.00	0.013
11	37	67.78	75.00	0.013
12	37	68.00	75.00	0.013
13	37	68.22	75.00	0.013
14	37	68.41	75.00	0.013
15	37	68.64	75.00	0.013
16	37	68.84	75.00	0.013
17	37	69.10	75.00	0.013
18	37	69.36	75.00	0.013
19	37	69.63	75.00	0.013
20	37	69.93	75.00	0.013
21	37	70.15	75.00	0.013
22	37	70.35	75.00	0.013
23	37	70.56	75.00	0.013
24	37	70.81	75.00	0.013
25	37	71.05	75.00	0.013
26	37	71.24	75.00	0.013
27	37	71.44	75.00	0.013
28	37	71.70	75.00	0.013
29	37	71.94	75.00	0.013
30	37	72.19	75.00	0.013
31	37	72.41	75.00	0.013
32	37	72.58	75.00	0.013
33	37	72.82	75.00	0.013
34	37	73.01	75.00	0.013
35	37	73.21	75.00	0.013
36	37	73.40	75.00	0.013
37	37	73.59	75.00	0.013

38	37	73.83	75.00	0.013
39	37	74.06	75.00	0.013
40	37	74.35	75.00	0.013
41	37	74.62	75.00	0.013
42	37	74.87	75.00	0.013
43	37	75.11	75.00	0.013
44	37	75.31	75.00	0.013
45	37	75.50	75.00	0.013
46	37	75.70	75.00	0.013
47	37	75.95	75.00	0.013
48	37	76.21	75.00	0.013

River Outflows

Main Pass (RM 4)				
Point	Link	River Mile	Ks	n
1	2	0.00	36.00	0.028
2	2	0.23	36.00	0.028
3	2	0.47	36.00	0.028
4	2	0.65	36.00	0.028
5	2	0.84	36.00	0.028
6	2	1.05	36.00	0.028
7	2	1.23	36.00	0.028
8	2	1.41	36.00	0.028
9	2	1.62	36.00	0.028
10	2	1.82	36.00	0.028
11	2	2.02	36.00	0.028
12	2	2.18	36.00	0.028
13	2	2.36	36.00	0.028
14	2	2.60	36.00	0.028
15	2	2.79	36.00	0.028
16	2	3.03	36.00	0.028
17	2	3.23	36.00	0.028
18	2	3.38	36.00	0.028
19	2	3.57	36.00	0.028
20	2	3.77	36.00	0.028
21	2	3.95	36.00	0.028
22	2	4.16	36.00	0.028
23	2	4.37	36.00	0.028
24	2	4.54	36.00	0.028
25	2	4.74	36.00	0.028
26	2	4.91	36.00	0.028
27	2	5.09	36.00	0.028
28	2	5.29	36.00	0.028
29	2	5.47	36.00	0.028
30	2	5.64	36.00	0.028
31	2	5.86	36.00	0.028
32	2	6.06	36.00	0.028
33	2	6.27	36.00	0.028
34	2	6.47	36.00	0.028

35	2	6.65	36.00	0.028
36	2	6.84	36.00	0.028
37	2	7.01	36.00	0.028
38	2	7.17	36.00	0.028
39	2	7.33	36.00	0.028
40	2	7.50	36.00	0.028
41	2	7.73	36.00	0.028
42	2	7.79	36.00	0.028
43	2	8.15	36.00	0.028
44	2	8.46	36.00	0.028
45	2	8.73	36.00	0.028
46	2	9.00	36.00	0.028
47	2	9.28	36.00	0.028
48	2	9.55	36.00	0.028
49	2	9.85	36.00	0.028
50	2	10.19	36.00	0.028

West Bay (RM 4)				
Point	Link	River Mile	Ks	n
1	4	0.00	4.70	0.213
2	4	1.00	4.70	0.213
3	4	1.89	4.70	0.213
4	4	2.10	4.70	0.213
5	4	2.21	4.70	0.213
6	4	2.23	4.70	0.213
7	4	2.24	4.70	0.213
8	4	2.28	4.70	0.213
9	4	2.32	4.70	0.213
10	4	2.34	4.70	0.213
11	4	2.36	4.70	0.213
12	4	2.38	4.70	0.213
13	4	2.40	4.70	0.213

Grand Pass & Tiger Pass (RM 10)				
Point	Link	River Mile	Ks	n
1	6	0.00	41.67	0.024
2	6	0.19	41.67	0.024
3	6	0.39	41.67	0.024

4	6	0.58	41.67	0.024
5	6	0.76	41.67	0.024

Grand Pass (RM 10)				
Point	Link	River Mile	Ks	n
1	7	0.00	35.00	0.029
2	7	0.13	35.00	0.029
3	7	0.32	35.00	0.029
4	7	0.53	35.00	0.029
5	7	0.73	35.00	0.029
6	7	0.90	45.00	0.022
7	7	1.09	45.00	0.022
8	7	1.29	45.00	0.022
9	7	1.47	45.00	0.022
10	7	1.68	45.00	0.022
11	7	1.83	45.00	0.022
12	7	2.04	45.00	0.022
13	7	2.22	45.00	0.022
14	7	2.44	45.00	0.022
15	7	2.65	45.00	0.022
16	7	2.81	45.00	0.022
17	7	2.96	45.00	0.022
18	7	3.15	45.00	0.022
19	7	3.37	45.00	0.022
20	7	3.54	45.00	0.022
21	7	3.77	45.00	0.022
22	7	3.93	45.00	0.022
23	7	4.10	45.00	0.022
24	7	4.31	45.00	0.022
25	7	4.53	45.00	0.022
26	7	4.69	45.00	0.022
27	7	4.89	45.00	0.022
28	7	5.05	45.00	0.022
29	7	5.20	45.00	0.022

Tiger Pass (RM 10)				
Point	Link	River Mile	Ks	n
1	8	0.00	43.00	0.023

2	8	0.19	43.00	0.023
3	8	0.35	43.00	0.023
4	8	0.54	43.00	0.023
5	8	0.71	43.00	0.023
6	8	0.92	43.00	0.023
7	8	1.10	43.00	0.023
8	8	1.28	43.00	0.023
9	8	1.48	43.00	0.023
10	8	1.69	43.00	0.023
11	8	1.86	43.00	0.023
12	8	2.02	43.00	0.023
13	8	2.24	43.00	0.023
14	8	2.43	43.00	0.023
15	8	2.63	43.00	0.023
16	8	2.80	43.00	0.023
17	8	2.99	43.00	0.023

Baptiste Collette (RM 12)				
Point	Link	River Mile	Ks	n
1	10	0.00	48.00	0.021
2	10	0.18	48.00	0.021
3	10	0.37	48.00	0.021
4	10	0.54	48.00	0.021
5	10	0.70	48.00	0.021
6	10	0.91	48.00	0.021
7	10	1.14	48.00	0.021
8	10	1.35	48.00	0.021
9	10	1.52	48.00	0.021
10	10	1.72	48.00	0.021
11	10	1.92	48.00	0.021
12	10	2.10	48.00	0.021
13	10	2.24	48.00	0.021
14	10	2.43	48.00	0.021
15	10	2.61	48.00	0.021
16	10	2.80	48.00	0.021
17	10	3.00	48.00	0.021
18	10	3.18	48.00	0.021
19	10	3.36	48.00	0.021

20	10	3.51	48.00	0.021
21	10	3.70	48.00	0.021
22	10	3.84	48.00	0.021
23	10	4.04	48.00	0.021
24	10	4.22	48.00	0.021
25	10	4.42	48.00	0.021
26	10	4.56	48.00	0.021
27	10	4.79	48.00	0.021
28	10	4.95	48.00	0.021
29	10	5.12	48.00	0.021
30	10	5.30	48.00	0.021
31	10	5.54	48.00	0.021
32	10	5.76	48.00	0.021
33	10	5.95	48.00	0.021
34	10	6.14	48.00	0.021
35	10	6.27	48.00	0.021

Fort St. Philip (RM 20)				
Point	Link	River Mile	Ks	n
1	12	0.00	6.00	0.167
2	12	0.09	6.00	0.167
3	12	0.19	6.00	0.167
4	12	0.28	6.00	0.167
5	12	0.38	6.00	0.167
6	12	0.47	6.00	0.167
7	12	0.57	6.00	0.167
8	12	0.66	6.00	0.167
9	12	0.76	6.00	0.167
10	12	0.85	6.00	0.167
11	12	0.95	6.00	0.167
12	12	1.04	6.00	0.167
13	12	1.14	6.00	0.167
14	12	1.23	6.00	0.167
15	12	1.33	6.00	0.167
16	12	1.42	6.00	0.167
17	12	1.52	6.00	0.167
18	12	1.61	6.00	0.167
19	12	1.70	6.00	0.167

20	12	1.80	6.00	0.167
21	12	1.89	6.00	0.167
22	12	1.99	6.00	0.167
23	12	2.08	6.00	0.167
24	12	2.18	6.00	0.167
25	12	2.27	6.00	0.167
26	12	2.37	6.00	0.167
27	12	2.46	6.00	0.167
28	12	2.56	6.00	0.167
29	12	2.65	6.00	0.167
30	12	2.75	6.00	0.167
31	12	2.84	6.00	0.167
32	12	2.94	6.00	0.167
33	12	3.03	6.00	0.167
34	12	3.12	6.00	0.167
35	12	3.22	6.00	0.167
36	12	3.31	6.00	0.167
37	12	3.41	6.00	0.167
38	12	3.50	6.00	0.167
39	12	3.60	6.00	0.167
40	12	3.69	6.00	0.167
41	12	3.79	6.00	0.167
42	12	3.88	6.00	0.167
43	12	3.98	6.00	0.167
44	12	4.07	6.00	0.167
45	12	4.17	6.00	0.167
46	12	4.26	6.00	0.167
47	12	4.36	6.00	0.167
48	12	4.45	6.00	0.167
49	12	4.55	6.00	0.167
50	12	4.64	6.00	0.167
51	12	4.73	6.00	0.167
52	12	4.83	6.00	0.167
53	12	4.92	6.00	0.167
54	12	5.02	6.00	0.167
55	12	5.11	6.00	0.167
56	12	5.21	6.00	0.167
57	12	5.30	6.00	0.167
58	12	5.40	6.00	0.167

59	12	5.49	6.00	0.167
60	12	5.59	6.00	0.167
61	12	5.68	6.00	0.167

Bohemia Spillway Downstream (RM 31)				
Point	Link	River Mile	Ks	n
1	17	0.00	5.00	0.200
2	17	0.10	5.00	0.200
1	14	N/A	N/A	N/A
2	14	N/A	N/A	N/A
1	15	0.00	55.00	0.018
2	15	1.00	55.00	0.018

Bayou Lamoque South (RM 32)				
Point	Link	River Mile	Ks	n
1	18	0.49	55.00	0.018
2	18	0.50	55.00	0.018
3	18	0.54	55.00	0.018
4	18	0.57	55.00	0.018
1	19	N/A	N/A	N/A
2	19	N/A	N/A	N/A
1	20	0.00	55.00	0.018
2	20	0.05	55.00	0.018
3	20	0.09	55.00	0.018
4	20	0.13	55.00	0.018
5	20	0.18	55.00	0.018
6	20	0.22	55.00	0.018
7	20	0.28	55.00	0.018
8	20	0.33	55.00	0.018
9	20	0.38	55.00	0.018
10	20	0.42	55.00	0.018
11	20	0.46	55.00	0.018
12	20	0.47	55.00	0.018

Bohemia Spillway Upstream (RM 34)				
Point	Link	River Mile	Ks	n

1	31	0.00	55.00	0.018
2	31	0.10	55.00	0.018
1	32	N/A	N/A	N/A
2	32	N/A	N/A	N/A
1	33	0.00	50.00	0.020
2	33	0.10	50.00	0.020

Bohemia Spillway Intermediate (RM 32.5)				
Point	Link	River Mile	Ks	n
1	23	0.00	55.00	0.018
2	23	0.10	55.00	0.018
1	24	N/A	N/A	N/A
2	24	N/A	N/A	N/A
1	25	0.00	55.00	0.018
2	25	0.10	55.00	0.018

Bayou Lamoque North (RM 33)				
Point	Link	River Mile	Ks	n
1	27	0.52	55.00	0.018
2	27	0.53	55.00	0.018
3	27	0.55	55.00	0.018
4	27	0.59	55.00	0.018
1	28	N/A	N/A	N/A
2	28	N/A	N/A	N/A
1	29	0.00	55.00	0.018
2	29	0.05	55.00	0.018
3	29	0.01	55.00	0.018
4	29	0.19	55.00	0.018
5	29	0.25	55.00	0.018
6	29	0.31	55.00	0.018
7	29	0.37	55.00	0.018
8	29	0.40	55.00	0.018
9	29	0.44	55.00	0.018
10	29	0.47	55.00	0.018
11	29	0.50	55.00	0.018
12	29	0.51	55.00	0.018

Bayou Lamoque North and South (RM 32.5)				
Point	Link	River Mile	Ks	n
1	21	0.00	55.00	0.018
2	21	0.34	55.00	0.018
3	21	0.63	55.00	0.018
4	21	0.92	55.00	0.018
5	21	1.22	55.00	0.018
6	21	1.50	55.00	0.018
7	21	1.76	55.00	0.018
8	21	2.01	55.00	0.018
9	21	2.21	55.00	0.018
10	21	2.40	55.00	0.018
11	21	2.48	55.00	0.018
12	21	2.55	55.00	0.018
13	21	2.63	55.00	0.018
14	21	2.70	55.00	0.018
15	21	2.77	55.00	0.018
16	21	2.84	55.00	0.018
17	21	2.90	55.00	0.018
18	21	2.96	55.00	0.018
19	21	3.03	55.00	0.018
20	21	3.09	55.00	0.018
21	21	3.13	55.00	0.018

MYRTLE GROVE TEST EXTRA CHANNEL

Myrtle Grove (RM 59)				
Point	Link	River Mile	Ks	n
1	38	2.13	65.00	0.015
2	38	2.84	65.00	0.015
1	39	N/A	N/A	N/A
2	39	N/A	N/A	N/A
1	40	0.51	65.00	0.015
2	40	0.71	65.00	0.015
3	40	1.42	65.00	0.015

BELAIR TEST EXTRA CHANNEL

Belair (RM 65)				
Point	Link	River Mile	Ks	n
1	38	2.00	65.00	0.015
2	38	2.50	65.00	0.015
1	39	N/A	N/A	N/A
2	39	N/A	N/A	N/A
1	40	0.50	65.00	0.015
2	40	1.00	65.00	0.015

MOBILE-BED CALIBRATION 2007/2008

Mississippi River Main Channel

Mississippi River Main Channel				
Point	Link	River Mile	Ks	n
1	1	2.95	65.00	0.015
2	1	3.15	65.00	0.015
1	3	3.36	65.00	0.015
2	3	3.60	65.00	0.015
3	3	3.83	65.00	0.015
4	3	4.04	65.00	0.015
5	3	4.26	65.00	0.015
6	3	4.46	65.00	0.015
1	5	4.70	65.00	0.015
2	5	4.90	65.00	0.015
3	5	5.10	65.00	0.015
4	5	5.30	65.00	0.015
5	5	5.50	65.00	0.015
6	5	5.80	65.00	0.015
7	5	6.00	65.00	0.015
8	5	6.20	65.00	0.015
9	5	6.50	65.00	0.015
10	5	6.70	65.00	0.015
11	5	6.90	65.00	0.015
12	5	7.30	65.00	0.015
13	5	7.50	65.00	0.015
14	5	7.94	65.00	0.015
15	5	8.10	65.00	0.015
16	5	8.40	65.00	0.015
17	5	8.70	65.00	0.015
18	5	8.90	65.00	0.015
19	5	9.10	65.00	0.015
20	5	9.40	65.00	0.015
21	5	9.70	65.00	0.015
22	5	9.97	65.00	0.015
23	5	10.20	65.00	0.015
1	9	10.35	65.00	0.015

2	9	10.54	65.00	0.015
3	9	10.73	65.00	0.015
4	9	11.07	65.00	0.015
5	9	11.20	65.00	0.015
1	11	11.46	65.00	0.015
2	11	11.72	65.00	0.015
3	11	11.98	65.00	0.015
4	11	12.26	65.00	0.015
5	11	12.50	65.00	0.015
6	11	12.77	65.00	0.015
7	11	12.99	65.00	0.015
8	11	13.25	65.00	0.015
9	11	13.56	65.00	0.015
10	11	13.86	65.00	0.015
11	11	14.21	65.00	0.015
12	11	14.50	65.00	0.015
13	11	14.76	65.00	0.015
14	11	15.05	65.00	0.015
15	11	15.32	65.00	0.015
16	11	15.57	65.00	0.015
17	11	15.86	65.00	0.015
18	11	16.23	65.00	0.015
19	11	16.51	65.00	0.015
20	11	16.80	65.00	0.015
21	11	17.12	65.00	0.015
22	11	17.39	65.00	0.015
23	11	17.72	65.00	0.015
24	11	18.00	65.00	0.015
25	11	18.33	65.00	0.015
26	11	18.58	65.00	0.015
27	11	18.85	65.00	0.015
28	11	19.11	65.00	0.015
29	11	19.40	65.00	0.015
1	13	19.60	41.67	0.024
2	13	19.86	41.67	0.024
3	13	20.12	41.67	0.024
4	13	20.48	41.67	0.024
5	13	20.73	41.67	0.024
6	13	21.02	41.67	0.024

7	13	21.30	41.67	0.024
8	13	21.66	41.67	0.024
9	13	22.00	41.67	0.024
10	13	22.37	41.67	0.024
11	13	22.70	41.67	0.024
12	13	23.08	41.67	0.024
13	13	23.48	41.67	0.024
14	13	23.83	41.67	0.024
15	13	24.22	41.67	0.024
16	13	24.57	41.67	0.024
17	13	24.89	41.67	0.024
18	13	25.24	41.67	0.024
19	13	25.56	41.67	0.024
20	13	25.98	41.67	0.024
21	13	26.36	41.67	0.024
22	13	26.74	41.67	0.024
23	13	27.06	41.67	0.024
24	13	27.39	41.67	0.024
25	13	27.70	41.67	0.024
26	13	28.03	41.67	0.024
27	13	28.32	41.67	0.024
28	13	28.53	41.67	0.024
29	13	28.79	41.67	0.024
30	13	28.98	41.67	0.024
31	13	29.24	41.67	0.024
32	13	29.46	41.67	0.024
33	13	29.65	41.67	0.024
34	13	29.89	41.67	0.024
35	13	30.15	41.67	0.024
36	13	30.40	41.67	0.024
37	13	30.59	41.67	0.024
38	13	30.78	41.67	0.024
39	13	30.98	41.67	0.024
40	13	31.17	41.67	0.024
41	13	31.37	41.67	0.024
42	13	31.57	41.67	0.024
43	13	31.88	41.67	0.024
44	13	32.13	41.67	0.024
1	16	32.40	45.00	0.022

2	16	32.41	45.00	0.022
1	22	32.45	45.00	0.022
2	22	32.60	45.00	0.022
1	26	32.70	45.00	0.022
2	26	32.80	45.00	0.022
1	30	32.89	55.00	0.018
2	30	33.17	55.00	0.018
3	30	33.53	55.00	0.018
4	30	33.83	55.00	0.018
5	30	34.18	55.00	0.018
6	30	34.53	55.00	0.018
7	30	34.93	55.00	0.018
8	30	35.15	55.00	0.018
9	30	35.45	55.00	0.018
10	30	35.71	55.00	0.018
11	30	36.05	55.00	0.018
12	30	36.33	55.00	0.018
13	30	36.62	55.00	0.018
14	30	36.87	55.00	0.018
15	30	37.17	55.00	0.018
16	30	37.45	55.00	0.018
17	30	37.77	55.00	0.018
18	30	38.08	55.00	0.018
19	30	38.32	55.00	0.018
20	30	38.62	55.00	0.018
1	34	38.92	50.00	0.020
2	34	39.22	50.00	0.020
3	34	39.51	50.00	0.020
4	34	39.77	50.00	0.020
5	34	40.08	50.00	0.020
6	34	40.36	50.00	0.020
7	34	40.64	50.00	0.020
8	34	40.91	50.00	0.020
9	34	41.22	50.00	0.020
10	34	41.51	50.00	0.020
11	34	41.87	50.00	0.020
12	34	42.19	50.00	0.020
13	34	42.50	50.00	0.020
14	34	42.84	50.00	0.020

15	34	43.17	50.00	0.020
16	34	43.46	50.00	0.020
17	34	43.73	50.00	0.020
18	34	44.04	50.00	0.020
19	34	44.31	50.00	0.020
20	34	44.63	50.00	0.020
21	34	44.93	50.00	0.020
22	34	45.23	50.00	0.020
23	34	45.54	50.00	0.020
24	34	45.93	50.00	0.020
25	34	46.32	50.00	0.020
26	34	46.69	50.00	0.020
27	34	47.11	50.00	0.020
28	34	47.44	50.00	0.020
29	34	47.81	50.00	0.020
30	34	48.14	50.00	0.020
31	34	48.45	50.00	0.020
32	34	48.76	50.00	0.020
1	35	49.08	50.00	0.020
2	35	49.38	50.00	0.020
3	35	49.72	50.00	0.020
4	35	50.05	50.00	0.020
5	35	50.40	50.00	0.020
6	35	50.73	50.00	0.020
7	35	51.12	65.00	0.015
8	35	51.47	65.00	0.015
9	35	51.85	65.00	0.015
10	35	52.18	65.00	0.015
11	35	52.52	65.00	0.015
12	35	52.87	65.00	0.015
13	35	53.24	65.00	0.015
14	35	53.52	65.00	0.015
15	35	53.84	65.00	0.015
16	35	54.12	65.00	0.015
17	35	54.44	65.00	0.015
18	35	54.72	65.00	0.015
19	35	55.01	65.00	0.015
20	35	55.32	65.00	0.015
21	35	55.63	65.00	0.015

22	35	55.99	65.00	0.015
23	35	56.39	65.00	0.015
24	35	56.76	65.00	0.015
25	35	57.16	65.00	0.015
26	35	57.50	65.00	0.015
27	35	57.84	65.00	0.015
28	35	58.14	65.00	0.015
29	35	58.44	65.00	0.015
30	35	58.69	65.00	0.015
31	35	59.01	65.00	0.015
1	36	59.30	65.00	0.015
2	36	59.52	65.00	0.015
3	36	59.74	65.00	0.015
4	36	59.97	65.00	0.015
5	36	60.21	65.00	0.015
6	36	60.42	65.00	0.015
7	36	60.64	65.00	0.015
8	36	60.88	65.00	0.015
9	36	61.04	65.00	0.015
10	36	61.24	65.00	0.015
11	36	61.50	65.00	0.015
12	36	61.85	65.00	0.015
13	36	62.11	65.00	0.015
14	36	62.34	65.00	0.015
15	36	62.57	65.00	0.015
16	36	62.88	65.00	0.015
17	36	63.11	65.00	0.015
18	36	63.36	65.00	0.015
19	36	63.62	65.00	0.015
20	36	63.88	65.00	0.015
21	36	64.16	65.00	0.015
22	36	64.46	65.00	0.015
23	36	64.73	65.00	0.015
24	36	64.98	65.00	0.015
1	37	65.28	65.00	0.015
2	37	65.57	65.00	0.015
3	37	65.81	65.00	0.015
4	37	66.09	65.00	0.015
5	37	66.33	65.00	0.015

6	37	66.59	65.00	0.015
7	37	66.86	65.00	0.015
8	37	67.09	65.00	0.015
9	37	67.31	65.00	0.015
10	37	67.50	65.00	0.015
11	37	67.78	65.00	0.015
12	37	68.00	65.00	0.015
13	37	68.22	65.00	0.015
14	37	68.41	65.00	0.015
15	37	68.64	65.00	0.015
16	37	68.84	65.00	0.015
17	37	69.10	65.00	0.015
18	37	69.36	65.00	0.015
19	37	69.63	65.00	0.015
20	37	69.93	65.00	0.015
21	37	70.15	65.00	0.015
22	37	70.35	65.00	0.015
23	37	70.56	65.00	0.015
24	37	70.81	65.00	0.015
25	37	71.05	65.00	0.015
26	37	71.24	65.00	0.015
27	37	71.44	65.00	0.015
28	37	71.70	65.00	0.015
29	37	71.94	65.00	0.015
30	37	72.19	65.00	0.015
31	37	72.41	65.00	0.015
32	37	72.58	65.00	0.015
33	37	72.82	65.00	0.015
34	37	73.01	65.00	0.015
35	37	73.21	65.00	0.015
36	37	73.40	65.00	0.015
37	37	73.59	65.00	0.015
38	37	73.83	65.00	0.015
39	37	74.06	65.00	0.015
40	37	74.35	65.00	0.015
41	37	74.62	65.00	0.015
42	37	74.87	65.00	0.015
43	37	75.11	65.00	0.015
44	37	75.31	65.00	0.015

45	37	75.50	65.00	0.015
46	37	75.70	65.00	0.015
47	37	75.95	65.00	0.015
48	37	76.21	65.00	0.015

River Outflows

Main Pass (RM 4)				
Point	Link	River Mile	Ks	n
1	2	0.00	44.00	0.023
2	2	0.23	44.00	0.023
3	2	0.47	44.00	0.023
4	2	0.65	44.00	0.023
5	2	0.84	44.00	0.023
6	2	1.05	44.00	0.023
7	2	1.23	44.00	0.023
8	2	1.41	44.00	0.023
9	2	1.62	44.00	0.023
10	2	1.82	44.00	0.023
11	2	2.02	44.00	0.023
12	2	2.18	44.00	0.023
13	2	2.36	44.00	0.023
14	2	2.60	44.00	0.023
15	2	2.79	44.00	0.023
16	2	3.03	44.00	0.023
17	2	3.23	44.00	0.023
18	2	3.38	44.00	0.023
19	2	3.57	44.00	0.023
20	2	3.77	44.00	0.023
21	2	3.95	44.00	0.023
22	2	4.16	44.00	0.023
23	2	4.37	44.00	0.023
24	2	4.54	44.00	0.023
25	2	4.74	44.00	0.023
26	2	4.91	44.00	0.023
27	2	5.09	44.00	0.023
28	2	5.29	44.00	0.023
29	2	5.47	44.00	0.023
30	2	5.64	44.00	0.023
31	2	5.86	44.00	0.023
32	2	6.06	44.00	0.023
33	2	6.27	44.00	0.023
34	2	6.47	44.00	0.023

35	2	6.65	44.00	0.023
36	2	6.84	44.00	0.023
37	2	7.01	44.00	0.023
38	2	7.17	44.00	0.023
39	2	7.33	44.00	0.023
40	2	7.50	44.00	0.023
41	2	7.73	44.00	0.023
42	2	7.79	44.00	0.023
43	2	8.15	44.00	0.023
44	2	8.46	44.00	0.023
45	2	8.73	44.00	0.023
46	2	9.00	44.00	0.023
47	2	9.28	44.00	0.023
48	2	9.55	44.00	0.023
49	2	9.85	44.00	0.023
50	2	10.19	44.00	0.023

West Bay (RM 4)				
Point	Link	River Mile	Ks	n
1	4	0.00	4.80	0.208
2	4	1.00	4.80	0.208
3	4	1.89	4.80	0.208
4	4	2.10	4.80	0.208
5	4	2.21	4.80	0.208
6	4	2.23	4.80	0.208
7	4	2.24	4.80	0.208
8	4	2.28	4.80	0.208
9	4	2.32	4.80	0.208
10	4	2.34	4.80	0.208
11	4	2.36	4.80	0.208
12	4	2.38	4.80	0.208
13	4	2.40	4.80	0.208

Grand Pass & Tiger Pass (RM 10)				
Point	Link	River Mile	Ks	n
1	6	0.00	41.67	0.024
2	6	0.19	41.67	0.024
3	6	0.39	41.67	0.024

4	6	0.58	41.67	0.024
5	6	0.76	41.67	0.024

Grand Pass (RM 10)				
Point	Link	River Mile	Ks	n
1	7	0.00	35.00	0.029
2	7	0.13	35.00	0.029
3	7	0.32	35.00	0.029
4	7	0.53	35.00	0.029
5	7	0.73	35.00	0.029
6	7	0.90	48.00	0.021
7	7	1.09	48.00	0.021
8	7	1.29	48.00	0.021
9	7	1.47	48.00	0.021
10	7	1.68	48.00	0.021
11	7	1.83	48.00	0.021
12	7	2.04	48.00	0.021
13	7	2.22	48.00	0.021
14	7	2.44	48.00	0.021
15	7	2.65	48.00	0.021
16	7	2.81	48.00	0.021
17	7	2.96	48.00	0.021
18	7	3.15	48.00	0.021
19	7	3.37	48.00	0.021
20	7	3.54	48.00	0.021
21	7	3.77	48.00	0.021
22	7	3.93	48.00	0.021
23	7	4.10	48.00	0.021
24	7	4.31	48.00	0.021
25	7	4.53	48.00	0.021
26	7	4.69	48.00	0.021
27	7	4.89	48.00	0.021
28	7	5.05	48.00	0.021
29	7	5.20	48.00	0.021

Tiger Pass (RM 10)				
Point	Link	River Mile	Ks	n
1	8	0.00	41.00	0.024

2	8	0.19	41.00	0.024
3	8	0.35	41.00	0.024
4	8	0.54	41.00	0.024
5	8	0.71	41.00	0.024
6	8	0.92	41.00	0.024
7	8	1.10	41.00	0.024
8	8	1.28	41.00	0.024
9	8	1.48	41.00	0.024
10	8	1.69	41.00	0.024
11	8	1.86	41.00	0.024
12	8	2.02	41.00	0.024
13	8	2.24	41.00	0.024
14	8	2.43	41.00	0.024
15	8	2.63	41.00	0.024
16	8	2.80	41.00	0.024
17	8	2.99	41.00	0.024

Baptiste Collette (RM 12)				
Point	Link	River Mile	Ks	n
1	10	0.00	45.00	0.022
2	10	0.18	45.00	0.022
3	10	0.37	45.00	0.022
4	10	0.54	45.00	0.022
5	10	0.70	45.00	0.022
6	10	0.91	45.00	0.022
7	10	1.14	45.00	0.022
8	10	1.35	45.00	0.022
9	10	1.52	45.00	0.022
10	10	1.72	45.00	0.022
11	10	1.92	45.00	0.022
12	10	2.10	45.00	0.022
13	10	2.24	45.00	0.022
14	10	2.43	45.00	0.022
15	10	2.61	45.00	0.022
16	10	2.80	45.00	0.022
17	10	3.00	45.00	0.022
18	10	3.18	45.00	0.022
19	10	3.36	45.00	0.022
20	10	3.51	45.00	0.022

21	10	3.70	45.00	0.022
22	10	3.84	45.00	0.022
23	10	4.04	45.00	0.022
24	10	4.22	45.00	0.022
25	10	4.42	45.00	0.022
26	10	4.56	45.00	0.022
27	10	4.79	45.00	0.022
28	10	4.95	45.00	0.022
29	10	5.12	45.00	0.022
30	10	5.30	45.00	0.022
31	10	5.54	45.00	0.022
32	10	5.76	45.00	0.022
33	10	5.95	45.00	0.022
34	10	6.14	45.00	0.022
35	10	6.27	45.00	0.022

Fort St. Philip (RM 20)				
Point	Link	River Mile	Ks	n
1	12	0.00	6.20	0.161
2	12	0.09	6.20	0.161
3	12	0.19	6.20	0.161
4	12	0.28	6.20	0.161
5	12	0.38	6.20	0.161
6	12	0.47	6.20	0.161
7	12	0.57	6.20	0.161
8	12	0.66	6.20	0.161
9	12	0.76	6.20	0.161
10	12	0.85	6.20	0.161
11	12	0.95	6.20	0.161
12	12	1.04	6.20	0.161
13	12	1.14	6.20	0.161
14	12	1.23	6.20	0.161
15	12	1.33	6.20	0.161
16	12	1.42	6.20	0.161
17	12	1.52	6.20	0.161
18	12	1.61	6.20	0.161
19	12	1.70	6.20	0.161
20	12	1.80	6.20	0.161
21	12	1.89	6.20	0.161

22	12	1.99	6.20	0.161
23	12	2.08	6.20	0.161
24	12	2.18	6.20	0.161
25	12	2.27	6.20	0.161
26	12	2.37	6.20	0.161
27	12	2.46	6.20	0.161
28	12	2.56	6.20	0.161
29	12	2.65	6.20	0.161
30	12	2.75	6.20	0.161
31	12	2.84	6.20	0.161
32	12	2.94	6.20	0.161
33	12	3.03	6.20	0.161
34	12	3.12	6.20	0.161
35	12	3.22	6.20	0.161
36	12	3.31	6.20	0.161
37	12	3.41	6.20	0.161
38	12	3.50	6.20	0.161
39	12	3.60	6.20	0.161
40	12	3.69	6.20	0.161
41	12	3.79	6.20	0.161
42	12	3.88	6.20	0.161
43	12	3.98	6.20	0.161
44	12	4.07	6.20	0.161
45	12	4.17	6.20	0.161
46	12	4.26	6.20	0.161
47	12	4.36	6.20	0.161
48	12	4.45	6.20	0.161
49	12	4.55	6.20	0.161
50	12	4.64	6.20	0.161
51	12	4.73	6.20	0.161
52	12	4.83	6.20	0.161
53	12	4.92	6.20	0.161
54	12	5.02	6.20	0.161
55	12	5.11	6.20	0.161
56	12	5.21	6.20	0.161
57	12	5.30	6.20	0.161
58	12	5.40	6.20	0.161
59	12	5.49	6.20	0.161
60	12	5.59	6.20	0.161

61	12	5.68	6.20	0.161
----	----	------	------	-------

Bohemia Spillway Downstream (RM 31)				
Point	Link	River Mile	Ks	n
1	17	0.00	5.00	0.200
2	17	0.10	5.00	0.200
1	14	N/A	N/A	N/A
2	14	N/A	N/A	N/A
1	15	0.00	55.00	0.018
2	15	1.00	55.00	0.018

Bayou Lamoque South (RM 32)				
Point	Link	River Mile	Ks	n
1	18	0.49	55.00	0.018
2	18	0.50	55.00	0.018
3	18	0.54	55.00	0.018
4	18	0.57	55.00	0.018
1	19	N/A	N/A	N/A
2	19	N/A	N/A	N/A
1	20	0.00	55.00	0.018
2	20	0.05	55.00	0.018
3	20	0.09	55.00	0.018
4	20	0.13	55.00	0.018
5	20	0.18	55.00	0.018
6	20	0.22	55.00	0.018
7	20	0.28	55.00	0.018
8	20	0.33	55.00	0.018
9	20	0.38	55.00	0.018
10	20	0.42	55.00	0.018
11	20	0.46	55.00	0.018
12	20	0.47	55.00	0.018

Bohemia Spillway Intermediate (RM 32.5)				
Point	Link	River Mile	Ks	n
1	23	0.00	55.00	0.018
2	23	0.10	55.00	0.018
1	24	N/A	N/A	N/A

2	24	N/A	N/A	N/A
1	25	0.00	55.00	0.018
2	25	0.10	55.00	0.018

Bayou Lamoque North (RM 33)				
Point	Link	River Mile	Ks	n
1	27	0.52	55.00	0.018
2	27	0.53	55.00	0.018
3	27	0.55	55.00	0.018
4	27	0.59	55.00	0.018
1	28	N/A	N/A	N/A
2	28	N/A	N/A	N/A
1	29	0.00	55.00	0.018
2	29	0.05	55.00	0.018
3	29	0.01	55.00	0.018
4	29	0.19	55.00	0.018
5	29	0.25	55.00	0.018
6	29	0.31	55.00	0.018
7	29	0.37	55.00	0.018
8	29	0.40	55.00	0.018
9	29	0.44	55.00	0.018
10	29	0.47	55.00	0.018
11	29	0.50	55.00	0.018
12	29	0.51	55.00	0.018

Bayou Lamoque North and South (RM 32.5)				
Point	Link	River Mile	Ks	n
1	21	0.00	55.00	0.018
2	21	0.34	55.00	0.018
3	21	0.63	55.00	0.018
4	21	0.92	55.00	0.018
5	21	1.22	55.00	0.018
6	21	1.50	55.00	0.018
7	21	1.76	55.00	0.018
8	21	2.01	55.00	0.018
9	21	2.21	55.00	0.018
10	21	2.40	55.00	0.018
11	21	2.48	55.00	0.018

12	21	2.55	55.00	0.018
13	21	2.63	55.00	0.018
14	21	2.70	55.00	0.018
15	21	2.77	55.00	0.018
16	21	2.84	55.00	0.018
17	21	2.90	55.00	0.018
18	21	2.96	55.00	0.018
19	21	3.03	55.00	0.018
20	21	3.09	55.00	0.018
21	21	3.13	55.00	0.018

Bohemia Spillway Upstream (RM 34)				
Point	Link	River Mile	Ks	n
1	31	0.00	55.00	0.018
2	31	0.10	55.00	0.018
1	32	N/A	N/A	N/A
2	32	N/A	N/A	N/A
1	33	0.00	50.00	0.020
2	33	0.10	50.00	0.020

MYRTLE GROVE TEST EXTRA CHANNEL

Myrtle Grove (RM 59)				
Point	Link	River Mile	Ks	n
1	38	2.13	65.00	0.015
2	38	2.84	65.00	0.015
1	39	N/A	N/A	N/A
2	39	N/A	N/A	N/A
1	40	0.51	65.00	0.015
2	40	0.71	65.00	0.015
3	40	1.42	65.00	0.015

BELAIR TEST EXTRA CHANNEL

Belair (RM 65)				
Point	Link	River Mile	Ks	n
1	38	2.00	65.00	0.015

2	38	2.50	65.00	0.015
1	39	N/A	N/A	N/A
2	39	N/A	N/A	N/A
1	40	0.50	65.00	0.015
2	40	1.00	65.00	0.015

APPENDIX C: Changes Made to the Original ECOMSED Code

Note: This Appendix presents only changes and additions to the ECOMSED code. It does not present the complete subroutines or code. Some of the lines of code shown had to be repeated several times in the same subroutine but are only presented once.

MANNING's FORMULATION AND SPATIALLY VARIABLE FRICTION

COMDECK

! Declaration of Manning's n Reference Value now given in "run_data" file
REAL MANNG

! Declaration of BFRIC as a 2-D array instead of a constant and declaration of spatially
! variable roughness factors given in new input file "manng_coeff"
COMMON/BLK2D/

. BFRIC(IM,JM), COEFF(IM,JM),

COMMON /ZWAVE/Z0WAVE,BFCOH,NWAVE !BFRIC deleted

SUBROUTINE ECOM3D.F

! BFRIC replaced by MANNG in "run_data"; Z0B replaced by BNK in "run_data"
READ(IURUN,3) MANNG,BNK,NU,THETA,ALPHA,TLAG,NWAVE,BCTYPE

! Calculation of BFRIC for each element as function of Manning's n Reference Value
! (MANNG) and element friction factor (COEFF(I,J))
$$BFRIC(I,J) = GRAV * ((MANNG * COEFF(I,J))^{2.0} / (D(I,J)^{(1/3.))})$$

CBC(I,J)=BFRIC(I,J)*FSM(I,J) !BFRIC replaced by BFRIC(I,J)

SUBROUTINE EXTRNL.F

WUBOT(I,J)=-BFRIC(I,J) !BFRIC(I,J) instead of BFRIC

WVBOT(I,J)=-BFRIC(I,J) !BFRIC(I,J) instead of BFRIC

! Calculation of BFRIC for each element as function of Manning's n Reference Value
! (MANNG) and element friction factor (COEFF(I,J))
$$BFRIC(I,J) = GRAV * ((MANNG * COEFF(I,J))^{2.0} / (D(I,J)^{(1/3.))})$$

CBC(I,J)=BFRIC(I,J)*FSM(I,J) !BFRIC replaced by BFRIC(I,J)

SUBROUTINES PROFU.F and PROFV.F

! Calculation of BFRIC for each element as function of Manning's n Reference Value

! (MANNG) and element friction factor (COEFF(I,J))

BFRIC(I,J)=GRAV*((MANNG*COEFF(I,J))**2.0)/(D(I,J)**(1./3.))

CBC(I,J)=BFRIC(I,J)*FSM(I,J) !BFRIC replaced by BFRIC(I,J)

SUBROUTINE SETDOM.F

C----- SPATIALLY VARIABLE FRICTION by Pereira -----!

!Input File with Spatially Variable Roughness Coefficients Added by Pereira 07/23/2010

OPEN(IUCOEFF,FILE='manng_coeff')

DO I=1,IM

DO J=1,JM

READ(IUCOEFF,1997) ICOEFF, JCOEFF, COEFF(I,J)

C 1979FORMAT(F5.2)

1997 FORMAT(2I5,F10.2)

ENDDO

ENDDO

C----- End of SPATIALLY VARIABLE FRICTION by Pereira -----!

SUBROUTINE STRESS.F

CBC(I,J) = AMAX1(CDE,BFRIC(I,J)) !BFRIC replaced by BFRIC(I,J)

EXAMPLE OF NEW INPUT FILE WITH VARIABLE ROUGHNESS FACTORS "manng coeff:"

1	1	1.00
1	2	1.10
1	3	1.00
1	4	1.20
1	5	1.00
2	1	0.95
2	2	1.00
2	3	1.30
2	4	1.00
2	5	1.10

EXAMPLE OF LINE OF "run data" file including Manning's n as an input:

MANNG	BNK	NU	THETA	ALPHA	TLAG	NWAVE	BCTYPE
0.0290	1.0000	0.10	0.225	0.	10.	10	CLAMPED

SEDIMENT MODULE

SUBROUTINE ECOM3D.F

! Limit bottom concentration to a maximum of 500 mg/L
CSED2(I,J,KBM1)=MIN(0.0005,CSED2(I,J,KBM1))

SUBROUTINE SUSLOD.F

c NIKURH=11.*Z0B !Turned off

! Use D50 instead of Z0B to calculate Nikuradse ks grain equivalent roughness
NIKURH=0.05*D50VAR(1,1)

! (0.01*DT(I,J),NIKURH) replaced by MAX(0.030*DT(I,J),NIKURH)
AREF=MAX(0.030*DT(I,J),NIKURH)

! Active Layer volume limited to a minimum value to avoid division by very small
! numbers

ACTLAY(1,I,J)=MAX(0.00001,CARMOR(I,J)*TAU(I,J,KB)*SUSARM)

! Change set not to exceed 1% to avoid coefficients growing out of control
FTEMP=MIN(1.01,FTEMP)

! Change set not to exceed 1% to avoid coefficients growing out of control
FPBED(K,I,J)=MIN(1.01,FPBED(K,I,J))

FALAY(K,I,J)=FTEMP

FALAY(K,I,J)=MIN(1.01,FALAY(K,I,J))

VITA

João Miguel Faísca Rodrigues Pereira was born in Lisbon, Portugal on September 10, 1979. In 1997, he graduated from High School. In September 2002 he obtained a 5-year degree of Bachelor in Territorial Engineering at the *Instituto Superior Técnico* (Technical University of Lisbon) in Lisbon, Portugal. In January 2007 he obtained the degree of Master of Science in Hydraulics and Water Resources also at the *Instituto Superior Técnico* (Technical University of Lisbon) in Lisbon, Portugal. In January 2008 he enrolled in the University of New Orleans Doctoral program in Engineering and Applied Science.

During graduate school while pursuing his master's degree, and after graduation, he worked as a research assistant in the Department of Civil Engineering and Architecture of the *Instituto Superior Técnico*. His research involved fluvial and environmental hydraulics, hydrodynamic numerical and physical modeling.

During his doctoral program, he has been working as a research assistant at the Department of Civil and Environmental Engineering of the University of New Orleans. The focus of his research has been the multidimensional coastal and fluvial hydrodynamic numerical modeling applied to the Lower Mississippi River and Lake Pontchartrain.